Exotic Kondo Effects in Metals: Magnetic Ions in a Crystalline Electric Field and Tunneling Centers

D.L. Cox,
Department of Physics,
The Ohio State University,
Columbus, Ohio, 43210
and
Department of Physics,
University of California,
Davis, California, 95616

and

A. Zawadowski,
Institute of Physics,
and
Research Group of Hungarian Academy of Sciences,
Technical University of Budapest,
Budafoki ut 8,
H1521,
and
Research Institute for Solid State Physics,
Hungarian Academy of Sciences,
P.O.B. 49, H-1525,
Budapest, Hungary

January 24, 2002

Abstract

The ordinary single channel Kondo model consists of one or more spin 1/2 local moments interacting antiferromagnetically with conduction electrons in a metal. This model has provided a paradigm for understanding many phenomena of strongly correlated electronic materials, ranging from the formation of heavy fermion fermi liquids to the mapping to a one-band model in the cuprate superconductors. The simplest extension of this ordinary Kondo model in metals which yields exotic non-Fermi liquid physics is the multichannel Kondo impurity model in which the conduction electrons are given an extra quantum label known as the channel or flavor index. In the overcompensated regime of this model non-Fermi liquid physics is possible, in contrast to the single channel model. We overview here the multichannel Kondo impurity model candidates most extensively studied for explaining real materials, specifically the two level system Kondo model relevant for metallic glasses, nanoscale devices, and some doped semiconductors, and the quadrupolar and magnetic two-channel Kondo models developed for rare earth and actinide ions with crystal field splittings in metals. We provide an extensive justification for the derivation of the theoretical models, noting that whenever the local impurity degree of freedom is non-magnetic a two-channel Kondo model must follow by virtue of the magnetic spin degeneracy of the conduction electrons. We carefully delineate all energetic and symmetry restrictions on the applicability of these models. We describe the various

methods used to study these models along with their results and limitations (multiplicative renormalization group, numerical renormalization group, non-crossing approximation, conformal field theory, and abelian bosonization), all of which provide differing and useful views of the physics. We pay particular attention to the role that scale invariance plays in all of these theoretical approaches. We point out in each case how various perturbing fields (magnetic, crystalline electric, electric field gradients, uniaxial stress) may destabilize the non-Fermi liquid fixed point. We then provide an extensive discussion of the experimental evidence for the relevance of the two-level system Kondo model to metallic glasses, nanoscale devices, and of the quadrupolar/magnetic two-channel models to a number of heavy fermion based alloys and compounds. We close with a discussion of the extension of the single impurity models which comprise the main focus of this review to other sytems (Coulomb blockade), multiple impurities, and lattice models. In the latter case, we provide an overview of the relevance of the two-channel Kondo lattice model to non-fermi liquid behavior and exotic superconductivity in heavy fermion compounds and to the theoretical possibility of odd-frequency superconductivity, which is realized (for the first time) in the limit of infinite spatial dimensions for this model.

Contents

1 Introduction

Since the great success of the many body theory of metals and superconductors developed in the 1950's, it had been generally believed that the theory of metals is well understood and the only exception is in magnetic properties. It was accepted that perturbation theory works well for ordinary clean and dirty metals and no one expected any deviation from the Landau theory at low temperature. Then in 1964 Kondo [Kondo, 1964] discovered a logarithmic divergence in the scattering of electrons by magnetic impurities in metals. This invoked extensive research since that time using very different tools of theoretical physics including K.G. Wilson's work on the renormalization group [Wilson, 1975] honored by the Nobel Prize in 1982. Indeed, the Kondo effect has become one of the most extensively studied many body problems in the field of theoretical solid state physics for the last three decades.

In the last 15 years several other problems related to the original Kondo problem have showed up in the literature, and the present review's main goal is to summarize the progress on the multi-channel Kondo model. The possible physical realizations of this model generally depend on local orbital degrees of freedom as opposed to the local magnetic moment considered originally by Kondo.

Before 1964, the electron-impurity interaction in metals with magnetic impurities had been studied by calculating the electrical resistivity in the second order of perturbation theory assuming simple effective Heisenberg exchange interactions between the local moments and the conduction electron spins. The contribution of the magnetic impurities to the residual resistivity was similar to that of non-magnetic impurities except in the magnetoresistance. This was despite the very early observation by W.J. de Haar, J. de Boer, and G.J. Berg in 1933 [de Haar *et al.*, 1933] that in some cases the resistivity of gold shows a minimum at around 3-4K (Fig. 1) and it was remarked that "...it is of course very interesting to investigate the influence of the purity of the metals on this minimum." At that time very little attention was paid to the observation and only the latter extensive studies in the 1960s clarified that different magnetic impurities contribute to the logarithmic temperature dependence of the electrical restivity with minima at different temperatures.

In the milestone work of Kondo in 1964 [Kondo, 1964], the calculation of the electrical resistivity was extended to third order in the local moment-conduction electron exchange coupling J of the form

$$H_{int} = J\vec{S}_I \cdot \vec{s}_c(0) \tag{1.1}$$

for a single impurity where $\vec{S}_I$ is the impurity spin and $\vec{s}_c(0)$ is the conduction electron spin at the impurity site. Note that positive J corresponds to antiferromagnetic coupling, and negative J to ferromagnetic coupling. Kondo's result was that the resistivity took the form

$$\rho(T) = \rho_0(T) + aN(0)J^2 + bN(0)^2J^3 \ln(\frac{D}{k_BT}) \tag{1.2}$$

where $\rho_0(T)$ is the resistivity of the pure metal, $N(0)$ is the conduction electron density of states at the Fermi energy, D is the bandwidth of the conduction electron system (of the order of the Fermi energy), T is the temperature, and a, b are constants proportional to the impurity concentration. The origin of this logarithmic term, as we shall discuss in subsequent paragraphs, is the *non-commutative* scattering when the impurity has internal degrees of freedom.

Several interesting results can be inferred from Eq. (1.2). First, given that in a clean metal such as gold $\rho_0(T) \sim T^5$ at low temperatures, a resistivity minimum will appear when $J > 0$ (antiferromagnetic coupling) since the logarithmic term then grows as the temperature is diminished. As Kondo noted, this minimum temperature should go as $c^{1/5}$ where, c is the impurity concentration. Second, given $a \simeq b$, the logarithmic term grows to the order of the quadratic in J term at a characteristic "Kondo" temperature scale

$$k_BT_K \approx De^{-1/N(0)J} \quad . \tag{1.3}$$

Below this scale systematic weak coupling perturbation expansions must break down, and so it represents a crossover between a high temperature, high energy regime which may be treated perturbatively and

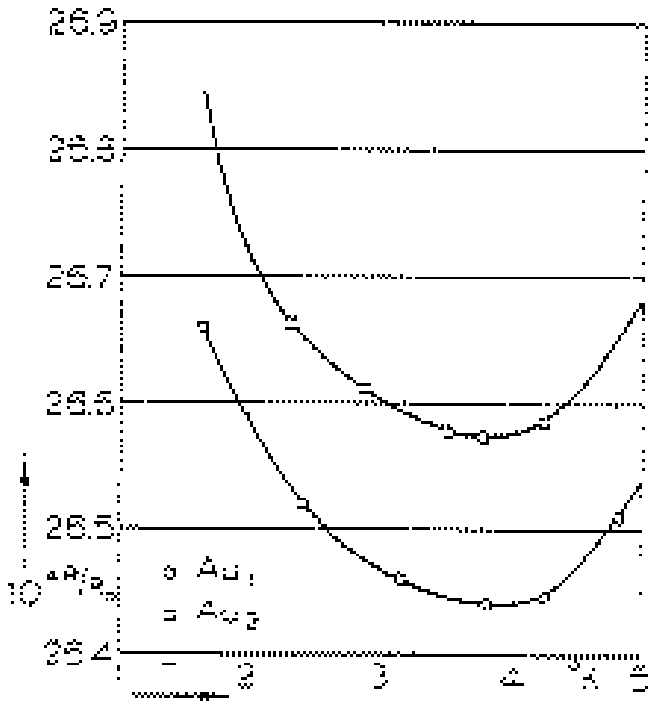

Figure 1: Early measurement of a resistivity minimum in metals.

a low energy regime of complex character which must be treated non-perturbatively. This makes the Kondo problem the first known example of an asymptotically free theory in physics, and the Kondo scale is analogous to the so-called QCD scale Λ_{QCD} at which perturbative quantum chromodynamics breaks down (see for example, Aitchison and Hey [1989], p. 298). Finally, it is clear from this remark and the restriction of unitarity on the scattering rate (a finite scattering probability must exist at the Fermi energy) that Kondo's theory is incomplete.

In order to resolve this latter problem, Abrikosov [1965] and Suhl [1965] introduced the concept of the Kondo resonance. The idea is that the appearance of the logarithm in Kondo's calculation signifies the development of a many body scattering resonance at the Fermi energy. These treatments summed up infinite numbers of diagrams diverging as powers of logarithms using building blocs with only one-electron or one-hole scattered states. While this led to a finite scattering rate at the Fermi energy, it did not lead to a complete solution of the problem.

A great boost in understanding the new phenomena came from studies on the x-ray absorption singularity worked out theoretically by Mahan ([1990], pp. 737-764), and more elaborately by Nozières and de Dominicis (Nozières and de Dominicis [1969]). The issue for this problem is how the conduction electrons react to the the appearance of a deep core hole created by x-rays and how this response affects the x-ray absorption spectrum. The problem can be formulated more generally in terms of how the conduction electrons relate to a change in a localized external potential. It is well known that in the electron screening of a localized potential a long range Friedel oscillation is induced with wave vector $2k_F$, where k_F is the Fermi wave vector. This oscillation signals the presence of a singular response for electronic states at the Fermi energy. Anderson reconceptualized this problem (Anderson [1967]) by pointing out that the ground state wave functions with two different localized potentials are orthogonal to one another in the thermodynamic limit. (This change of impurity potential can introduce a phase shift and amplitude modification to the Friedel oscillations about the defect site.) This phenomenon has been named the "Anderson orthogonality catastrophe". The relation of the Kondo

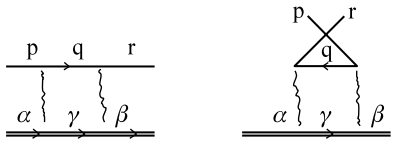

Figure 2: The two leading diagrams for the scattering of a light electron on a heavy object. The light electron is represented by the light line and the heavy object by the double line. The wavy lines indicate the interaction matrix element V. The quantum numbers characterizing the particles are also shown. The expression below gives the corresponding matrix elements of the interaction to this order and the minus sign arises from fermion anticommutation (the crossed lines in the second figure–Einstein convention applies to the indices): $V^{(2)}_{\beta\alpha rp} \sim V_{\beta\gamma rq}V_{\gamma\alpha qp} - V_{\gamma\alpha rq}V_{\beta\gamma qp}$.

effect to this problem is easy to see: whenever the local moment spin is flipped by interaction with the conduction electrons, a change in the scattering potential for up and down spins is the result. Hence, the orthogonality catrastophe arises for every single spin flip.

All these works made it obvious that the x-ray absorption problem and Kondo problem represent a new type of infrared divergence at low temperature and energy in which an infinite number of particle-hole pairs are involved on a scale extending to large distances away from the localized perturbation. On the other hand, there is a very essential difference between these two problems, which is related to the presence of internal degrees of freedom in the Kondo problem. The resulting scattering potential seen by conduction electrons is non-commutative in the Kondo case, while it is commutative in the x-ray core hole problem. In order to demonstrate this idea, we consider a simple scattering problem in which conduction electrons couple to a single heavy particle (e.g., a localized magnetic ion or a two-level system). The Hamiltonian is

$$H = \sum_{k\mu} \epsilon_k c^\dagger_{k\mu} c_{k\mu} + \epsilon_0 \sum_\alpha b^\dagger_\alpha b_\alpha$$

$$+ \sum_{k,k'} \sum_{\mu\nu\alpha\beta} V_{\mu\nu\alpha\beta} c^\dagger_{k\mu} c_{k'\nu} b^\dagger_\alpha b_\beta \tag{1.4}$$

where ϵ_k is the electron kinetic energy with momentum k in, e.g., an s-wave projection of plane wave states, $c^\dagger_{k\mu}$ creates an electron spherical wave with radial momentum k and internal quantum numbers μ, and $b^\dagger_\alpha$ creates a heavy particle with quantum numbers α. Note that the internal indices of the conduction electrons may represent magnetic spin or orbital indices or a combination of the two. The interaction potential is given by $V_{\mu\nu\alpha\beta}$. For the conduction electrons a band cutoff D is applied which is order of the Fermi energy. In the following remarks, the limit $\epsilon_0 \to \infty$ is taken to ensure that there is only single occupancy of the heavy particle.

In the second order of perturbation theory for the two-particle T-matrix describing electron scattering off the impurity, there are two diagrams shown in a time ordered way in Fig. 2. The direction of time corresponds to the directions of the lines on the heavy objects. As the interaction is assumed independent of k, k', the scattering amplitude for an incoming electron with energy ω is

$$V^{(2)}_{\mu\nu\alpha\beta}(\omega) = \sum_{\rho\gamma} [V_{\mu\rho\alpha\gamma}V_{\rho\nu\gamma\beta} - V_{\rho\mu\alpha\gamma}V_{\nu\rho\gamma\beta}] \ln(\frac{D}{\omega}) \tag{1.5}$$

where the quantum numbers of the internal lines are summed over and the negative sign arises from the fermion anticommutation relations (note the crossed lines in the second diagram) as the intermediate conduction state reflects a particle or hole, respectively. The logarithm is precisely that identified by Kondo.

Different localized perturbations can be classified by the value of the potential matrix "commutator" appearing in square brackets in Eq. (1.5):

(i) Commutative model: When

$$[V_{\mu\rho\alpha\gamma}V_{\rho\nu\gamma\beta} - V_{\rho\mu\alpha\gamma}V_{\nu\rho\gamma\beta}] = 0 \tag{1.6}$$

no Kondo logarithms appear. This occurs for a point like structureless interaction between the heavy object and conduction electrons which is diagonal in the internal indices.
(ii) Non-Commutative model: When

$$[V_{\mu\rho\alpha\gamma}V_{\rho\nu\gamma\beta} - V_{\rho\mu\alpha\gamma}V_{\nu\rho\gamma\beta}] \neq 0 \tag{1.7}$$

the model is non-commutative and logarithmic terms appear.

Case (i) applies to the x-ray absorption problem since the core hole has no internal degrees of freedom, and this also occurs in heavy particle motion of muons and protons in metals provided we neglect their spin degrees of freedom and focus only on the charge degrees of freedom. In these cases the couplings are not renormalized in second order and such theories have an energy and temperature independent coupling as a result.

Case (ii) is realized when the interaction depends, for example, on the spin variables or the pseudo-spin (position index) of a two-level system (TLS) describing an atom hopping between the lowest states of a double well anharmonic potential, or the orbital quadrupolar degrees of freedom of an open shell ion. In the latter two cases, the local orbital states of the conduction electrons are intrinsically involved as well. In these examples the effective coupling strength is strongly renormalized as a function of energy and temperature and can grow to infinity (antiferromagnetic Kondo problem), shrink to zero (ferromagnetic Kondo problem), or reach an intermediate coupling strength independent of the bare couplings (overcompensated multichannel Kondo problem).

The present review will be entirely devoted to non-commutative models. In order to clarify their solutions it is useful to look at the M-channel Kondo model. The interaction Hamiltonian for this model describes the interaction of conduction electrons living in M identical bands or channels with an arbitrary localized spin $\vec{S}_I$, and is given by

$$H_{int} = \frac{J}{2N_s}\sum_{k,k'}\sum_{\mu\nu}\sum_{\alpha=1}^{M}\vec{S}_I \cdot c^{\dagger}_{k\mu\alpha}\vec{\sigma}_{\mu\nu}c_{k'\nu\alpha} \tag{1.8}$$

where N_s is the number of atomic sites of the host metal responsible for the orbitals which form the conduction band, and $\vec{\sigma}$ is a Pauli matrix. The interaction Hamiltonian is diagonal in the channel index and an exact degeneracy of couplings is assumed. The original Kondo problem specified in Eq. (1.1) has $M = 1$. This multi-channel extension of the Kondo problem was first introduced by Nozières and Blandin [1980] and we follow their discussion here.

The ground state of the model with impurity S_I but different M can fall into three different classes for antiferromagnetic coupling $J > 0$, summarized in below and Fig. 3:
(i) Compensated ($M = 2S_I$) In this case the ground state is a singlet in which the impurity spin is completely screened by the conduction electron spins. The entropy tends to zero as the temperature tends to zero.
(ii) Undercompensated ($M < 2S_I$). In this case, there is not enough conduction spin to fully screen the impurity through the interaction of Eq. (1.8). $M/2$ units of spin are compensated, leaving behind a local moment of strength $S_I - M/2$ and a corresponding residual entropy at $T = 0$ of $R\ln(2S_I - M + 1)$ per mole of impurity ion (see (b) of Fig. 3). This residual entropy would appear to violate the third law of thermodynamics, but in the presence of more than one impurity intersite couplings will allow the possibility of spin-spin correlations or spin ordering to reduce the entropy. Note that this limit cannot be achieved with $S_I = 1/2$.
(iii) Overcompensated ($M > 2S_I$). In this case, there is an excess of conduction spin and depending on the boundary conditions for a finite size system, the ground state will have spin of either $M/2 - S_I$ or S_I with residual entropy $R\ln(M - 2S_I + 1)$ or $R\ln(2S_I + 1)$ (see (c) of Fig. 3). However, in the

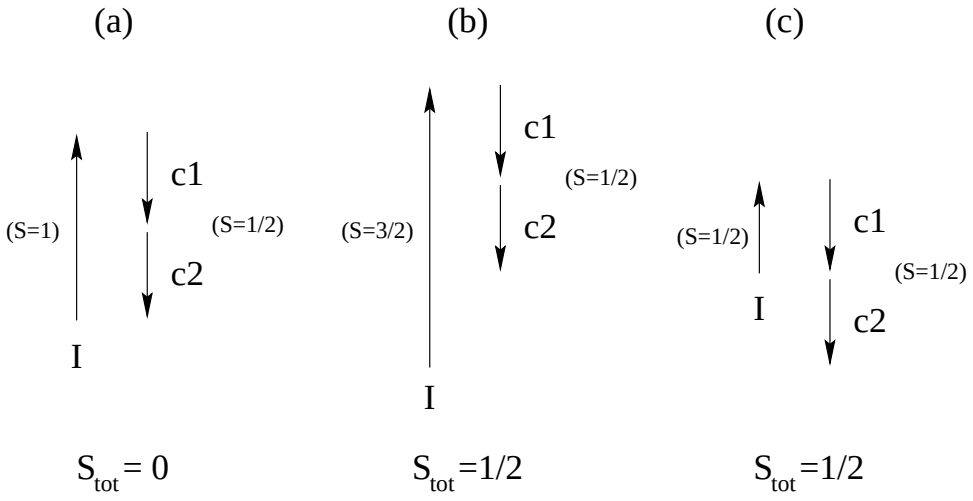

Figure 3: Compensated, Undercompensated, and Overcompensated multi-channel Kondo models. (a) shows an example of a compensated Kondo model. The two spin 1/2 conduction channels exactly cancel the spin 1 impurity to form a local singlet ground state. (b) shows an example of an undercompensated Kondo model. In this case, the two spin 1/2 conduction electrons cannot fully screen out the spin 3/2 impurity moment. The total ground state spin is determined by the residual, uncompensated impurity moment. The residual coupling of this to the conduction electrons is ferromagnetic and thus marginally irrelevant about the ground state. Finally, (c) shows an example of the overcompensated situation, in which the two spin 1/2 conduction channels over-screen the spin 1/2 impurity. In this case, the residual coupling of the bound spin 1/2 complex to conduction electrons at the next length scale is antiferromagnetic. This situation leads to a non-trivial fixed point.

thermodynamic limit the entropy tends to $R \ln g(M, S_I)$ where g is a universal non-integer number that we shall discuss in Secs. 6.3,7.2. The case $S_I = 1/2, M = 2$ is the marginal one, which still yields the non-trivial physics and appears to be the most realizable model in nature as we discuss in Sec. 2. This model has a residual entropy of $(R/2)\ln 2$. This residual entropy appears to have been observed in several uranium based alloys recently as we shall discuss later in the review (Sec. 8).

Let us specialize to the case $S_I = 1/2$ and discuss the thermodynamic properties at low temperatures which reflect the low energy excitation spectrum of the system. A convenient quantity to classify the behavior is the specific heat coefficient C_{imp}/T defined as the extra heat capacity per impurity induced by the impurities. In the case $M = 1$, the ordinary Kondo problem, C_{imp}/T tends to a constant value proportional to $1/T_K$, with T_K the Kondo temperature identified in Eq. (1.3). This describes a local Fermi liquid about the impurity with effective degeneracy temperature given by T_K. When $M = 2$, $C_{imp}/T \sim \ln(T_K/T)/T_K$, which illustrates the marginal nature of the $M = 2, S_I = 1/2$ overcompensated state. Finally, when $M > 2$, the specific heat coefficient shows a power law divergence given by $C_{imp}/T \sim T^{(2-M)/(2+M)}$. Clearly when $M \geq 2$ the excitation spectrum has a non-Fermi liquid character which thus places these models outside the Landau paradigm discussed at the outset of this introduction. The logarithmic behavior in C_{imp}/T has been recently observed in numerous materials as will be discussed in Sec. 8.

The scattering of an electron off the impurity in the low energy limit further reflects the breakdown of the Landau paradigm. We illustrate the scattering possibilities in Fig. 4. We show that for $M = 1, S_I = 1/2$, the $T = 0$ scattering is entirely one particle, reflecting the complete screening of the local moment into a simple charge scattering object. At elevated frequency and temperature some outgoing states can be dressed by multiple particle hole pairs giving rise to the familiar Landau

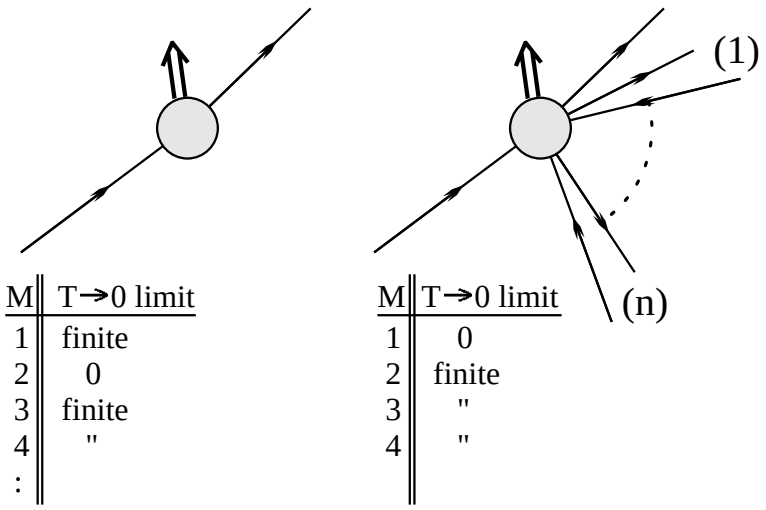

Figure 4: Fermi-level scattering states resulting from electrons incident on spin 1/2 Kondo impurities. For the $M = 1$ case, all outgoing scattered states at the Fermi energy is one-body in character, and hence can be parameterized in terms of a phase shift. For $M = 2$, all outgoing scattered states at the Fermi energy are *many-body* in character, and cannot be parameterized by a phase shift. For general M, the outgoing scattered states are a mix of one-body and many-body in character.

T^2 damping of the excited quasiparticles. In Fig. 4, we also show the case for $M = 2, S_I = 1/2$, in which single particle scattering is *completely* shut down on the Fermi surface. Indeed, the surprising result is that there is no S-matrix element to any outgoing state containing *arbitrary* finite numbers of particle-hole pair excitations; rather, as phrased in the original paper, there is a scattering to a "different Hilbert space hidden in the free field theory" but "opened up" by the impurity at the non-trivial fixed point (Maldacena and Ludwig [1996]). These fermionic excitations are non-local in the original variables. In the general case for $M > 2, S_I = 1/2$, the Fermi level scattering can be a mix of single particle and multiparticle scattering, as illustrated in Fig. 4. The outgoing scattering state may possibly be visualized as a "screening cloud" with one electron charge which is orthogonal to any states with finite numbers of simple particle-hole excitations, which phenomenon must be related to Anderson's orthogonality catastrophe (Anderson [1967]).

The consequence of these scattering properties on the electrical resistivity as $T \to 0$ is that in the $M = 1, S_I = 1/2$ case saturation to a value characteristic of the unitarity limit is accomplished with a regular T^2 behavior typical of a Fermi liquid. For $M \geq 2$, the low temperature resistivity goes as $\rho(T)/\rho(0) \simeq 1 - AT^{2/(2+M)}$ which is clearly non-Fermi liquid-like and related to the residual entropy and power law divergence of the specific heat coefficient. In the case of $M = 2$, the saturation to the low temperature limit follows a $T^{1/2}$ law which has been observed in recent point contact experiments to be discussed at length in Sec. 8.1.

A few words on notation. In the discussion of the quadrupolar and two-channel magnetic Kondo effects for rare earth and actinide ions, we have chosen to denote all crystal field states by the convention in the tables of [Koster *et al.*, 1963]. For irreducible representations of non-Kramers (non-double group) character, we also give the symbols used, e.g., in Tinkham's book on group theory[Tinkham, 1964]. Henceforth, we shall abbreviate "irreducible representation" by "irrep" following a common practice in group theory texts. Since the Two-Level-System (TLS) Kondo effects and those for rare earth and actinide ions "grew up" independently, there is not surprisingly a significant set of notational differences between papers on the two subjects. The TLS literature uses Pauli matrices to represent the local pseudo-spin variables, σ indices to represent the real conduction spin 1/2 indices, and $V^{x,y,z}$ to represent the couplings of the various pseudo-spin components to the conduction electrons. In the sections on quadrupolar and magnetic Kondo effects of actinide and rare earth ions, we shall use spin

Kondo Model	Local Pseudo-spin	Conduction Pseudo-spin	Conduction Channel
TLS	Atomic Position (Parity)	Orbital (Parity)	Magnetic
Quadrupolar	Quadrupolar (Orbital)	Quadrupolar (Orbital)	Magnetic
Magnetic Two-Channel	Magnetic	Magnetic	Quadrupolar (Orbital)

Table 1: Meaning of local spin and channel labels in real two-channel Kondo models.

Kondo Model	Local Pseudo-spin	Coupling Constants	Density of States
TLS	$\sigma^{x,y,z}$	$V^{x,y,z}$	ρ_0
Quadrupolar	$\tau^{1,2,3}$	$-J^{1,2,3}$	$N(0)$
Magnetic	$S^{1,2,3}$	$-J^{1,2,3}$	$N(0)$

Table 2: "Rosetta Stone" of notational correspondences between two-channel Kondo models. Note that the σ^i operators for the TLS model are Pauli matrices, while the τ, S operators for the quadrupolar and magnetic two-channel models are spin 1/2 matrices. Notice the relative minus sign between the couplings in the TLS models and the Quadrupolar and Magnetic Kondo models. Note that while the TLS literature consistently uses N_s to represent the number of conduction channels, we shall use this symbol for the number of sites in the lattice in our paper, and shall use M for the number of channels.

1/2 matrices throughout, with $\tau^{(1,2,3)}$ representing matrices in the quadrupolar pseudo-spin space, and $S^{(1,2,3)}$ representing matrices in the magnetic pseudo-spin space. Quadrupolar indices are represented by $\alpha = \pm$, and magnetic indices by $\mu = \uparrow, \downarrow$. The reason for the abstract $1, 2, 3$ labels on the pseudo-spin matrices is because they don't always have clear correspondence to symmetry directions of the crystal. All exchange couplings for the rare earth and actinide ion models will be labeled by J, not to be confused with angular momentum of ground state multiplets whose usage will be clear in the immediate context. Whenever an important formula is derived, such as a Kondo scale, we will report the results both for Pauli matrix and spin 1/2 form. The conduction density of states at the Fermi energy has been denoted ρ_0 in the TLS literature, and $N(0)$ in the rare earth/actinide papers. To avoid confusion to readers looking back at the literature, we shall use the same custom here. In either case, all excitations are measured with respect to the Fermi energy, which is therefore chosen as the zero of energy. A list of what local spin and channel labels mean in various models appears in Table 1. A "rosetta stone" clarifying the notational correspondences between the different two-channel Kondo models to be considered in this paper appears in Table 2. We will always use N to refer to pseudo-spin degeneracy of the impurity or conduction states; when it is necessary to distinguish the degeneracies, we will use subscripts I (impurity) and C (conduction). We will always use M to refer to channel degeneracy.

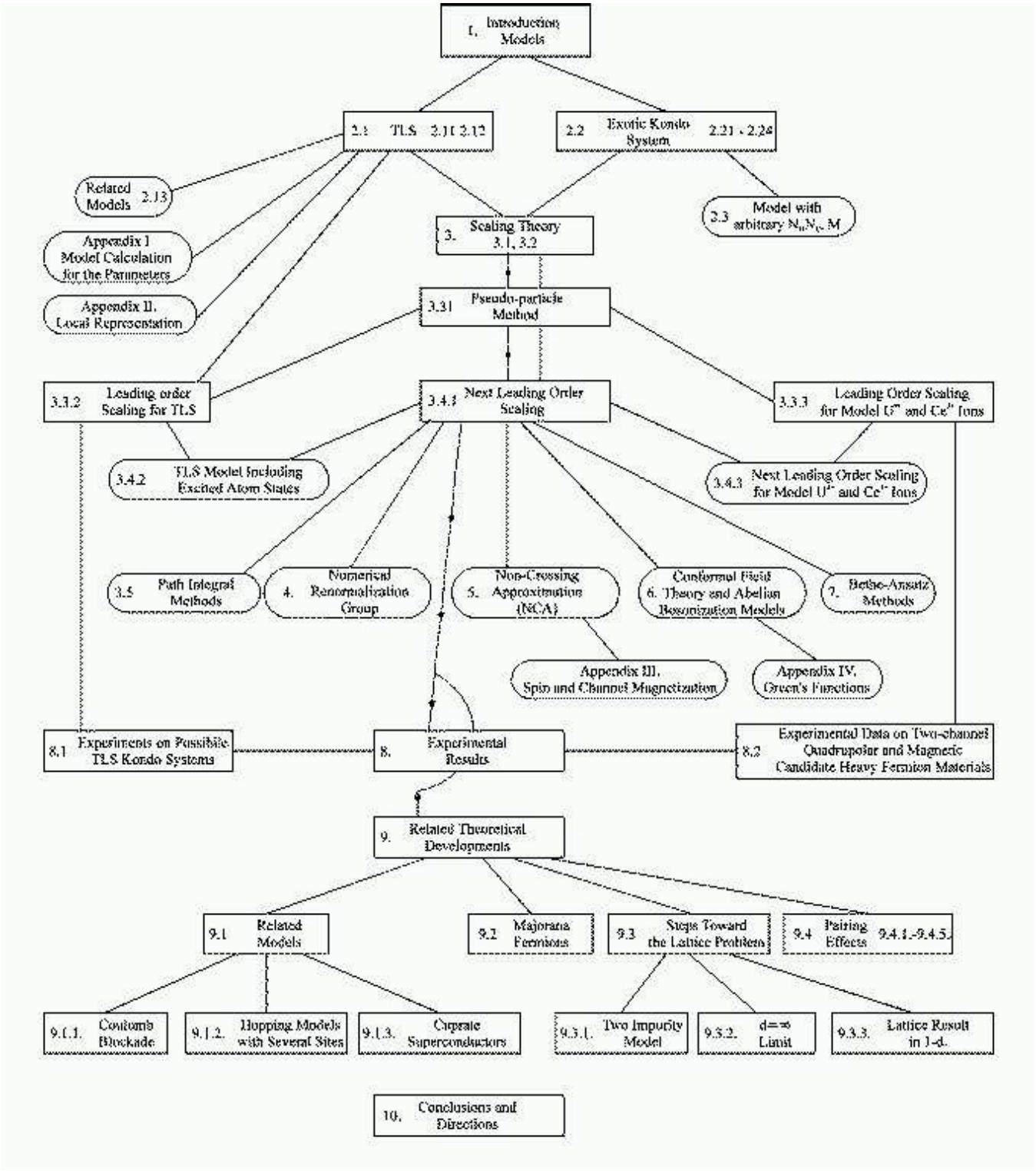

Figure 5: Guide to reading this review article

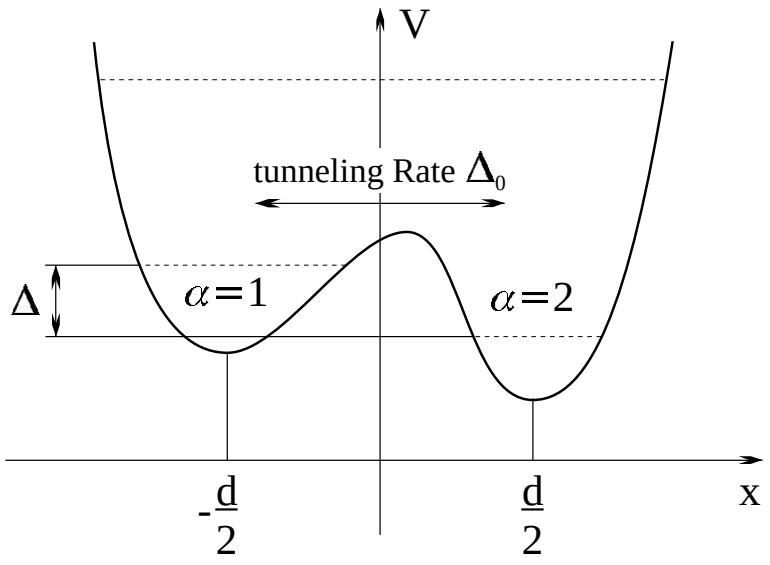

Figure 6: The potential for a single atom in a TLS is shown; this has two minima. The energies of the states localized at the minima and of the next excited state are shown by dashed lines. The energy splitting between the localized states is Δ. The minima are labeled by $\alpha = 1, 2$.

2 Model Hamiltonians

2.1 TLS Kondo Model and Related Hamiltonians

2.1.1 TLS Kondo Model: Physical Discussion

The simplest realization of a two-level system (TLS) is that of an atom which may sit in a double well potential, the two wells being localized along a line directed between their centers which are separated by a displacement vector $\vec{d}$. In the absence of coupling to a bath of excitations, the lowest two states of the atom are, approximately, the positional eigenstates associated with harmonic oscillations within either well. These are not exact eigenstates because of the overlap of their wave functions. The next level usually has energy above the barrier between the well minima, and therefore is not localized to either well. The basic picture for the atomic TLS is shown in Fig. 6.

To preview our discussion of the TLS Kondo effect, one should think of the position of the atom in one well or the other as an Ising spin variable. Electrons may "flip" the spin by assisting the tunneling between the wells. The usefulness of this spin description will depend upon the degree of splitting of the eigenstates in the absence of coupling to the electrons. If the splitting is too large, the ground state will be well separated from the first excited level, and the TLS will essentially possess a single degree of freedom leading to only potential scattering off the TLS site and no interesting many body phenomena. Hence, we shall pay close attention to the conditions which determine the splitting of the levels.

We note that the origin of the anharmonicity which produces the double well has not been extensively considered. It could derive from anharmonic coupling to vibrational degrees of freedom away from the TLS site [Sethna, 1981], or possibly from coupling to the electrons [Yu and Anderson, 1984]. The above model is certainly not exclusive in terms of the kinds of TLS which may occur in real materials; for example, one may imagine a local bistable breathing mode, a bistable librational mode for a cage of light atoms, such as may occur in doped perovskite conductors, or a vibronic TLS associated with the Jahn-Teller effect [Gogolin, 1995], for example. For further reading see Yu and Leggett [1989], and Burin and Kagan [1996].

An atomic tunneling TLS may also arise in a glass, due to positional disorder as sketched in

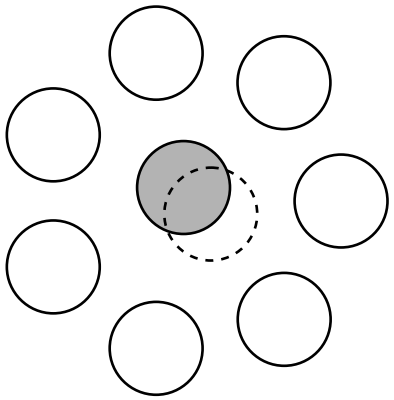

Figure 7: The atomic arrangement in the formation of a TLS is shown. The two positions belonging to the TLS are shown by the dashed and shaded circles.

Fig. 7 [Anderson, Halperin, and Varma, 1971; W.A. Phillips, 1972]. Indeed, the original motivation for studying such a model was the observation of logarithmic anomalies in the resistivity of metallic glasses [Cochrane *et al.*, 1975; Kondo, 1976(a); Vladár and Zawadowski, 1980]. There the positional disorder of the atoms could lead to a TLS for individual atoms. The complication with regard to the simple model presented here is that the TLS model must be concentrated (and disordered). For simplicity, we shall restrict attention to the simple model of a linear double well.

Given the TLS, in the absence of coupling to other excitations, the atom may move between the two positions one of two ways:

(i) Thermal Activation. To make thermally activated transitions between the two minima, the particle must make a real excitation to one of the higher levels within the double well potential. Roughly, one anticipates that the activated transition rate will be given by

$$\frac{1}{\tau_{thermal}(T)} \approx \omega_0 \exp(-E_{ex}/k_B T) \tag{2.1.1}$$

where the "attempt frequency" ω_0 is of order the characteristic vibration frequency in one of the well minima. The excitation energies for such processes have been directly measured in time resolved conductance experiments [Ralls and Buhrman, 1988; Zimmerman, Golding, and Haemmerle, 1991; Golding, Zimmerman, and Coppersmith, 1992] and are typically in the range of tens to hundreds of kelvin. Hence, these must eventually be frozen out at very low temperatures, certainly below 1-10K.

(ii) Quantum Mechanical Tunneling. In this process, the atom directly tunnels through the potential barrier between the wells. Given the freezeout of the thermally activated transitions, this process must dominate at sufficiently low temperatures. In this case, neglecting the coupling to the conduction electrons, the tunneling rate is given by

$$\frac{1}{\tau^s_{quantum}} \approx \omega_0 \exp(-w\sqrt{2MV_B}/\hbar) = \omega_0 e^{-\lambda} \tag{2.1.2}$$

where the superscript s stands for spontaneous tunneling, the barrier is approximated by a square well of width w and height V_B, and λ is the Gamow factor.

Based upon experimental results on mesoscopic devices, we may roughly distinguish between three regimes of quantum tunneling, depending upon the observed tunneling time:
(a) *Slow tunneling,* $(\tau^s_{quantum})^{-1} < 10^8 s^{-1}$. In this case the Gamow factor λ is large. The motion of the atom for such TLS has been measured by time resolved conductance experiments on nanometer scale point contacts [Ralls and Buhrman, 1988] and thin metallic films [Zimmerman, Golding, and

Haemmerle, 1991; Golding, Zimmerman, and Coppersmith, 1992]. The essential, and startling, idea is that each time the TLS hops between minimum, a measurable (order e^2/h) change δG in the device conductance G is observed, corresponding to an atomic scale change in the scattering cross section. Bistable switching corresponding to isolated TLS (of unknown character) has been observed directly! By producing histograms of the times between switching events, tunneling times can be determined. As our subsequent discussion will clarify, the spontaneous quantum mechanical tunneling rate is directly proportional to the electron assisted tunneling amplitude for the atom which is responsible for the TLS Kondo effect. When the TLS falls into this "slow" category, the TLS Kondo effect will occur at irrelevantly small temperature scales, if at all. This may be modified, however, with the consideration of excited states of the TLS, such as discussed by Zaránd and Zawadowski [1994(a,b)]. In this circumstance, it is possible to get an appreciable Kondo scale *without* a large splitting of the levels; see Sec. 3.4.2 for a discussion.

(b) *Fast tunneling,* $10^8 s^{-1} > (\tau^s_{quantum})^{-1} > 10^{12} s^{-1}$. In this case, the energy corresponding to the tunneling rate, determined by the uncertainty principle, is in the range of 1 mK to 10K. As we shall explain below, this energy determines the level splitting which we should like to have smaller than the Kondo energy scale $k_B T_K$. Given the typical estimates for electron assisted tunneling processes and the resulting T_K values, this range of tunneling times is the most probable for observing the TLS Kondo effect.

(c) *Ultrafast tunneling,* $10^{12} s^{-1} < (\tau^s_{quantum})^{-1}$. In this case, the splitting of the TLS ($\sim \hbar/\tau^s_{quantum}$) is so large that the ground state is uniformly spread in a bonding orbital between the two wells, and the Kondo effect never really happens. In this limit we may practically consider only the symmetric TLS, ($V(z) = V(-z)$). In the absence of coupling to the conduction electrons, the bonding level in this case is so well separated energetically from the anti-bonding level that description of the TLS states with a spin variable is essentially meaningless. Another way of putting it is that the pseudospin variable of the TLS is completely polarized.

Hence, for our purposes, since we are interested in a TLS Kondo effect, in the absence of excited states of the TLS, our attention will be directed to case (ii.b) of the above paragraph: fast quantum tunneling. With excited states included, we may very well obtain a reasonable Kondo scale while possessing neglibible splitting of the TLS. The reader is directed to 3.4.2 for an explanation.

2.1.2 Hamiltonian for TLS

(a) Non-interacting Hamiltonian

The atomic degree of freedom may be described as either bosonic or fermionic since we are discussing a single particle in motion. The creation operators at the lowest lying energy levels for the two minima are labelled by $b_1^\dagger$ and $b_2^\dagger$ and obey canonical commutation relations; e.g., taking the operators to be fermionic we have $\{b_i, b_j^\dagger\} = \delta_{ij}$. Since the Hilbert space is restricted, we are free to take these to be bosonic as well. The states $|+> = b_1^\dagger|0>$ and $|-> = b_2^\dagger|0>$, where $|0>$ is the particle vacuum for the TLS, may be regarded as pseudo-spin states, since we restrict our Hilbert space to these lowest two states. The importance of states with higher energies will be discussed in Sec. 3.4.2. Hence, the most general *noninteracting* TLS Hamiltonian is given by

$$H^0_{TLS} = \frac{1}{2}\sum_{i,\alpha,\alpha'} \Delta^i \sigma^i_{\alpha,\alpha'} |\alpha><\alpha'| = \frac{1}{2}\sum_i \Delta^i \sigma^i \tag{2.1.3}$$

where the σ^i are Pauli matrices ($i = x, y, z$). Δ^z measures the splitting between the levels in the two wells, while Δ^x and Δ^y are the *spontaneous tunneling* matrix elements which "flip" the spin with no assistance from other excitations in the system. If the wave functions of the atom in the two wells are chosen to be real, then the bare splitting Δ^y must vanish. The conventional notation in the TLS

literature is

$$\Delta^z = \Delta, \quad \Delta^x = \Delta_0, \quad \Delta^y = 0 \quad . \tag{2.1.4}$$

[Note that the correspondence to the spin Kondo problem is that Δ^z represents a local longitudinal magnetic field, while Δ^x represents a local transverse magnetic field. In the quadrupolar Kondo problem, Δ^z, Δ^x measure local stresses.]

It is straightforward to diagonalize Eq. (2.1.3) by rotating to a quantization direction $\tilde{z}$ in which one has a diagonal Pauli matrix only, and one finds energies $\pm E/2$ with the splitting E given by

$$E = \sqrt{\Delta^2 + \Delta_0^2} \quad . \tag{2.1.5}$$

The magnitude of the tunneling matrix element Δ_0 is approximately $\hbar\omega_0 e^{-\lambda}$ as determined by applying the uncertainty principle to the expression (2.1.2) for the spontaneous quantum tunneling time.

The use of projection operators in Eq. (2.1.3) automatically ensures we will not go outside the subspace of the lowest two levels. The price we pay is that the projection operators no longer obey standard commutation relations. This may be remedied by use of the Abrikosov pseudo-fermion method [Abrikosov, 1965], in which a fictitious chemical potential is inserted for the occupancies $b_i^\dagger b_i$ and taken to infinity at the end of all calculations. The effect of the projection is to remove all empty and doubly occupied states at the end of the calculation. This trick is particularly convenient for the scaling analysis (Sec. 3) and non-crossing approximation (NCA) integral equation analysis (Sec. 5), and we shall defer further discussion of the pseudo-particle method to that point in the article. On the other hand, it is convenient when one is implementing the path integral approach to retain the Hamiltonian in the spin representation, and it is typical to then split it into longitudinal and transverse terms.

(b) Coupling to Electrons

We model the conduction electrons as a free electron gas, with Hamiltonian

$$H_c = \sum_{\vec{k},\sigma} \epsilon_{\vec{k}} c^\dagger_{\vec{k},\sigma} c_{\vec{k},\sigma} \quad , \tag{2.1.6}$$

where $c^\dagger_{\vec{k},\sigma}$ and $c_{\vec{k},\sigma}$ create and destroy free electrons of wave vector $\vec{k}$ and *real (magnetic)* spin σ. We measure the excitation energies $\epsilon_{\vec{k}}$ from the chemical potential. While the real spin σ will play no direct role in the coupling to the TLS, it is crucial to retain it, for it plays the role of the channel index in the mapping of the TLS problem to a two-channel Kondo model.

The interaction Hamiltonian coupling the TLS and conduction electrons has the form

$$H_{int} = \frac{1}{N_s} \sum_{\vec{k},\vec{k}',\sigma} [V^0_{\vec{k},\vec{k}'} c^\dagger_{\vec{k},\sigma} c_{\vec{k}',\sigma} + \sum_{i=x,y,z} V^i_{\vec{k},\vec{k}'} \sigma^i c^\dagger_{\vec{k},\sigma} c_{\vec{k}',\sigma}] \tag{2.1.7}$$

where we have used the spin representation for the TLS. The first term in the interaction describes the scattering off of the average configuration of the TLS, and thus is simply a potential scattering term, of little importance unless the total scattering strength is large [Kagan and Prokof'ev, 1989]. The scattering form factors $V^i_{\vec{k},\vec{k}'}$ represent the following physical processes (see Fig. 8):
(i) The electrons scatter off of the atom sitting either in position one or two (V^z); this process induces *screening* of the TLS by the conduction electrons.
(ii) The electron scattering induces a transition between the two minima (denoted by matrix elements $V^{x,y}$ whose physical meaning shall be described later–see Fig. 9). This is what we mean by *electron assisted tunneling*, as opposed to the matrix element Δ_0 which we call *spontaneous tunneling*. (Recently, Moustakas and Fisher [1995] have noted that the V^0 term not only includes "ordinary" potential

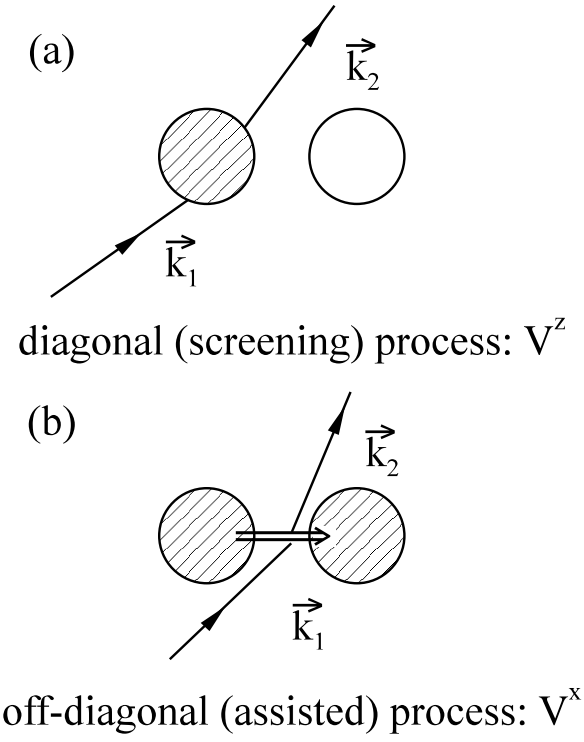

Figure 8: Visualization of screening (a) and assisted tunneling (b) of TLS by conduction electrons.

scattering, but potential scattering which transfers an electron from position 1 to position 2. This term modifies the physics somewhat as we shall discuss further in Secs. 2.1.2.c. and 3.5.)

The general properties of the scattering form factors $V^i_{\vec{k},\vec{k}'}$ are as follows:

(i) Since the Hamiltonian is Hermitian, we must have

$$V^i_{\vec{k}',\vec{k}} = (V^i_{\vec{k},\vec{k}'})^* \quad . \tag{2.1.8}$$

(ii) It is easy to determine the transformation properties under time reversal because of the absence of explicit dependence on the real conduction electron spin. Assuming we may describe the TLS states by real wave functions, then time reversal invariance implies that

$$< \vec{k}, \sigma, \alpha | H_{int} | \vec{k}', \sigma, \alpha' > = < -k', \sigma, \alpha' | H_{int} | -k, \sigma, \alpha > \tag{2.1.9}$$

where $|k, \sigma, \alpha >$ is a direct product state of a single electron with a state of the TLS. By comparison with (2.1.7), we see that

$$V^z_{\vec{k},\vec{k}'} = V^z_{-\vec{k}',-\vec{k}} \quad , \tag{2.1.10.a}$$

$$V^x_{\vec{k},\vec{k}'} = V^x_{-\vec{k}',-\vec{k}} \quad , \tag{2.1.10.b}$$

and

$$V^y_{\vec{k},\vec{k}'} = -V^y_{-\vec{k}',-\vec{k}} \quad . \tag{2.1.10.c}$$

(iii) In order to make explicit estimates of the matrix elements, we make the very reasonable assumption that the electrons couple to the TLS only through the local electronic density operator $\rho(\vec{r})$ given by

$$\rho(\vec{r}) = \frac{1}{N_s} \sum_{\vec{k},\vec{k}',\sigma} \exp(i(\vec{k}' - \vec{k}) \cdot \vec{r}) c^\dagger_{\vec{k},\sigma} c_{\vec{k}',\sigma} \quad . \tag{2.1.11}$$

This is an obvious coupling mechanism in the case of the diagonal matrix element V^z, since through Coulombic interactions or the pseudo-potential the electronic density is directly coupled to the density of the atom as it sits in either well. It is also quite reasonable for the off-diagonal (assisted tunneling) matrix elements, because fluctuations $\delta\rho$ in the electron density may modulate changes of the tunneling barrier height through the coupling of the atomic and electronic densities. Hence, one may envision expanding the Gamow factor in powers of the density fluctuations, i.e., we regard $V^i_{\vec{k},\vec{k}'}$ as a functional of $\rho(\vec{r})$. Since $\rho(\vec{r})$ depends only on the momentum transfer $\vec{k}-\vec{k}'$ for a given particle hole pair, we have that

$$V^i_{\vec{k},\vec{k}'} = V^i(\vec{k}-\vec{k}') \quad . \tag{2.1.12}$$

Property (iii) imposes a strong restriction on the TLS-electron interaction: by combining Eqs. (2.1.10.c) and (2.1.12) we see that

$$V^y_{\vec{k},\vec{k}'} = 0 \quad . \tag{2.1.13}$$

We stress that this is a property of the bare couplings; as we renormalize the interactions in the scaling theory and renormalization group calculations by integrating out virtual electronic excitations, we will generate couplings of V^y form because the higher order terms in $\delta\rho$ are not necessarily local in space [Kondo, 1976].

We are now in a position to explicitly estimate the matrix elements. The diagonal couplings $V^0 and V^z$ were first estimated by Kondo [1976] and Black, Györffy, and Jäckle [1979]. Denote the wave function for the atom in positions 1 or 2 by $\phi_{1,2}(\vec{r})$, and assume that the interaction between the electronic density and the atom at position $\vec{r}$ is given by $U(\vec{r})$. The potential scattering couples to the average of the atomic density over the two wells, while the V^z scattering couples to the density difference between the two wells. Hence

$$V^0_{\vec{k},\vec{k}'} = U(\vec{k}'-\vec{k}) \int d^3r \exp[i(\vec{k}'-\vec{k})\cdot\vec{r}] \frac{1}{2}[\phi_1^2(\vec{r}) + \phi_2^2(\vec{r})] \tag{2.1.14.a}$$

and

$$V^z_{\vec{k},\vec{k}'} = U(\vec{k}'-\vec{k}) \int d^3r \exp[i(\vec{k}'-\vec{k})\cdot\vec{r}] \frac{1}{2}[\phi_1^2(\vec{r}) - \phi_2^2(\vec{r})] \tag{2.1.14.b}$$

As mentioned earlier, the matrix element V^0 does not significantly impinge on the physics unless the scattering phase shift of the conduction electrons is near resonance; in particular, it cannot produce any logarithmic renormalizations in the scaling analysis.

Derivation of the assisted tunneling matrix element is more subtle. We follow Kondo [1976], who assumed the non-orthogonalized atomic wave functions at the two minima to be identical apart from displacement factors, i.e.,

$$\phi_{1,2}(\vec{r}) = \phi(\vec{r} \mp \frac{\vec{d}}{2}) \tag{2.1.15}$$

where the upper(lower) sign holds for well 1(2). The wave functions are assumed separable in cylindrical coordinates ($\phi(\vec{r}) = \chi(\vec{r}_{perp})\Phi(\theta)\zeta(z)$, where $\vec{r}_{perp}$ is the displacement transverse to the TLS axis and θ is the azimuthal angle about the TLS axis along the z direction). The wave function dependence along the axis of the TLS is taken to be the harmonic oscillator form

$$\zeta(z) \approx \frac{1}{\sqrt{\pi z_0}} \exp(-\frac{z^2}{2z_0^2}) \tag{2.1.16}$$

with z_0 the mean square displacement of the atom about the minimum due to zero point motion at frequency ω_0. Explicitly, assuming the atomic mass to be M, we have

$$z_0 = \sqrt{\frac{\hbar}{M\omega_0}} \quad . \tag{2.1.17}$$

If we consider atoms of intermediate mass $M \approx 50 m_p$ (m_p the proton mass), and with typical zero point energies of the TLS in the regime of 100-500K, we obtain z_0 values in the range of 0.03-0.1$\mathring{A}$.

Our evaluation of the coupling V^x borrows from the theory of inelastic tunneling formulated by Scalapino and Marcus [1967]. This derivation has the advantage of being physically transparent, and substantially correct quantitatively, in that a more formal derivation (using the Feynman-Hellman theorem based approach of Ngai *et al.* [1967] for the square barrier model and for a potential with quartic anharmonicity) yields the same answer to within factors of order unity. This will be elaborated in Appendix I. Recently Zaránd [1993] has pointed out that the accurate prefactor of the wave function given by (2.1.16) is also affected by the barrier fluctuation and it can be dropped only if the Gamow factor dominates, i.e., if $\exp(-\lambda) << 1$. The starting point of this analysis is to introduce the exact eigenstates of the atom in the double well potential extending over both minima but without interaction with the electrons. The potential $U_{ion,el}$ describing the interaction between the ion and the electrons induces the matrix elements. This method is suitable to include the higher atomic interaction levels in the potential in a straightforward manner (Zaránd and Zawadowski [1994(a,b)]) and the inclusion of those levels may lead to an increase in the Kondo temperature. See Sec. 3.4.2 for further details. The method of Zaránd is also applied to discusss the accuracy of the concept in which the treatment starts with the introduction of left and right states.

The idea of Scalapino and Marcus is illustrated in Fig. 9. The inelastic coupling to the conduction electron density fluctuations modulates the barrier height. Hence, inside the WKB exponent, we may expand the position dependent inverse decay length to linear order in the modulation. Explicitly, we take

$$V_B(\vec{r}) = V_B^0(\vec{r}) + U\delta\rho(\vec{r}) \tag{2.1.18}$$

where the coupling between electrons and atom is assumed to have a local pseudo-potential form

$$U_{ion,el}(\vec{r}_{el} - \vec{r}_{ion}) = v_0 U \delta(\vec{r}_{el} - \vec{r}_{ion}) \tag{2.1.19}$$

v_0 being the unit cell volume. The appropriate expression for $\delta\rho(\vec{r})$ is

$$\delta\rho(\vec{r}) \approx \rho(\vec{r}) - \frac{1}{2}[\rho(\frac{\vec{d}}{2}) + \rho(-\frac{\vec{d}}{2})] = \frac{1}{N_s}\sum_{\vec{k},\vec{k}',\sigma}[\exp(i(\vec{k}' - \vec{k})\cdot\vec{r}) - \cos((\vec{k} - \vec{k}')\cdot\frac{\vec{d}}{2})]c^\dagger_{\vec{k},\sigma}c_{\vec{k}',\sigma} \tag{2.1.20}$$

which is intuitively understood as the fluctuation relative to the averaged density at the minimum of the wells. This expression will be justified in detail in Appendix I. Because of the assumed axial character of the TLS, only the z dependence is relevant in Eq. (2.1.20). We note that the local potential approximation can in principle be dropped at the expense of complicating the formalism somewhat; see Vladár and Zawadowski [1983(a)] and Zaránd [1993] for details.

By approximating the tunneling matrix element in the WKB form we have, for the combined spontaneous and assisted tunneling Δ^x_{total}

$$\Delta^x_{total} = \Delta^x \exp[-\frac{U}{2\hbar}\int_{-d/2}^{d/2} dz \frac{\delta\rho(z)}{V_B^0(z)}\sqrt{2M_{ion}V_B^0(z)}] \tag{2.1.21}$$

which we may expand to linear order in the presumed small exponent to obtain

$$V^x = \Delta^x_{total} - \Delta^x = -\Delta^x \frac{\lambda U}{2dV_B}\int_{-d/2}^{d/2}\delta\rho(z)dz \quad . \tag{2.1.22}$$

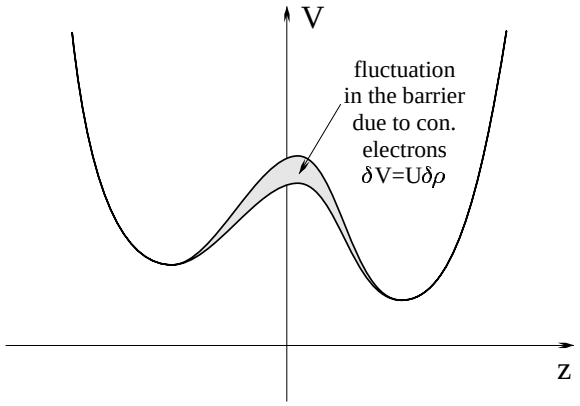

Figure 9: Fluctuation in the double-well potential for the TLS is shown. These fluctuations are produced by the density fluctuations $\delta\rho$ in the conduction-electron band. The shift of the potential is proportional to the pseudopotential U for the electron-atom scattering.

In Eq. (2.1.22) we have made a square barrier approximation, with the barrier height V_B and width d, so that the Gamow factor $\lambda = d\sqrt{2MV_B}/\hbar$. Substituting Eq. (2.1.20) for $\delta\rho$ and carrying out the resulting integration to lowest order in $(k'_z - k_z)d = \Delta k_z d$, we obtain

$$V^x_{\vec{k},\vec{k}'} = \Delta^x \frac{\lambda U}{24 V_B}(\Delta k_z d)^2 \quad . \tag{2.1.23}$$

The expansion in powers of $\Delta k_z d$ is justified for the intermediate mass atoms given $\Delta k_z \simeq k_F \simeq 1\mathring{A}^{-1}$, and our presumed value $d \simeq 0.1\mathring{A}$.

If we perform the small $\Delta k_z d$ expansion on V^z given by Eq. (2.1.14.b), we obtain

$$V^z \approx \frac{1}{2}(\Delta k_z d)U \tag{2.1.24}$$

so that the ratio V^x/V^z is roughly estimated as

$$\frac{V^x}{V^z} \approx \Delta^x \frac{\lambda(k_F d)}{12 V_B} \approx \frac{e^{-\lambda}(k_F d)}{3} \tag{2.1.25}$$

where we have used $\Delta^x \approx \hbar\omega_0 e^{-\lambda}$, $\lambda \approx d^2/4z_0^2$ as justified in Appendix I, and $\hbar\omega_0/V_B \approx 4z_0^2/(d/2)^2$ as justified in Appendix I. Taking $\lambda \approx 6$ so that $e^{-\lambda} \approx 10^{-3}$, we see that the order of magnitude for V^x/V^z is given by

$$\frac{V^x}{V^z} \sim 10^{-4} - 10^{-3} \quad . \tag{2.1.26}$$

Since these will play the role of bare exchange couplings in the mapping to the Kondo problem, and since V^y=0, we see that the initial coupling is extremely anisotropic! For further details, see Vladár and Zawadowski, [1983(a)]. A numerical study of the square potential model (Zaránd , [1993]) provides further justifications for the estimates presented above. The Hamiltonian with excited state will be given in Sec. 3.4.2.

(c) Angular Momentum Representation of H_{int}

The momentum dependence of the couplings V^x *and* V^z plays a crucial role in the development of the Kondo effect. The reason is that through the momentum dependence, or the form factors, the non-commutativity associated with the Kondo scattering as discussed in the introduction will develop.

The coupling can be expressed in partial waves. Let us first expand the coupling in a complete set of orthogonal functions $f_\alpha(\hat{k})$ depending only upon direction $\hat{k}$ so that

$$V^i_{\vec{k}',\vec{k}} \approx V^i_{\hat{k}',\hat{k}} = \sum_{\alpha',\alpha} f^*_{\alpha'}(\hat{k}') V^i_{\alpha',\alpha} f_\alpha(\hat{k}) \tag{2.1.27}$$

where we have assumed negligible dependence upon the magnitude of $\vec{k}, \vec{k}'$. The most convenient choice for the free electron gas is

$$f_\alpha(\hat{k}) = i^l \sqrt{4\pi} Y_{l,m}(\hat{k}) \tag{2.1.28}$$

where $Y_{l,m}$ is a spherical harmonic of indices l, m. Hence, the matrix elements of the couplings are given by

$$V^i_{l'm,lm} = \frac{i^{l-l'}}{4\pi} \int d\hat{k} d\hat{k}' Y^*_{l',m}(\hat{k}') V^i_{\hat{k}',\hat{k}} Y_{l,m}(\hat{k}) \tag{2.1.29}$$

where we have exploited the axial symmetry of the TLS in that the azimuthal quantum number m must be conserved in all transitions provided we choose our quantization axis along the direction $\hat{d}$. Using the previous approximation that the atomic motion is confined to the z-axis (or, more precisely, that the electronic scattering off of the atom is s-wave), we may neglect all but m=0 in the matrix elements of Eq. (2.1.29). This specifies spherical harmonics which are aligned along the tunneling axis $\hat{d}$. We shall henceforth suppress the m dependence.

Formally, the conduction "spin" in this model could have an arbitrarily large number of components N_c. This is seen from equation (2.1.29): partial waves with all orbital angular momentum values (the orbital index is the conduction pseudo-spin index) can be coupled to the impurity pseudo-spin. In practice, as we shall discuss in the scaling theory section, such a highly anisotropic model will always select out just two of this large number of conduction spin components as the temperature is lowered. Nevertheless, for various perturbative approaches, it is worth considering models in which N_c is allowed to be arbitrary.

It is clear from the considerations of the previous subsection that $V^z \sim (\vec{k}' - \vec{k}) \cdot \vec{d}$ is odd under inversion symmetry while $V^x \sim [(\vec{k} - \vec{k}') \cdot \vec{d}]^2$ is even. Hence,

$$V^x_{l',l} = 0, \quad l + l' \ \ odd \tag{2.1.30.a}$$

and

$$V^z_{l',l} = 0, \quad l + l' \ \ even \ \ . \tag{2.1.30.b}$$

In the approximation used in (2.1.19), $U(\vec{k}' - \vec{k}) = u_0$. We shall use this and employ the small $\Delta k_z d$ approximation. In view of the discussion of the previous paragraph, we then truncate the expansion at the level of s and p wave harmonics, yielding

$$V^z_{l',l} \approx \tilde{V}^z \begin{pmatrix} 0 & 1 \\ 1 & 0 \end{pmatrix} \tag{2.1.31}$$

with $\tilde{V}^z = k_F d u_0/2$, and

$$V^x_{l',l} \approx -\tilde{V}^x \begin{pmatrix} 1 & 0 \\ 0 & -1 \end{pmatrix} \tag{2.1.32}$$

with $\tilde{V}^x = -[(k_F d)^2/24][\lambda \Delta^x u_0/V_B]$, and where the matrix indices are $l' = 0, 1; l = 0, 1$ with m=0 as discussed above (see, for further discussion, Vladár and Zawadowski [1983a], and Zaránd [1994]).

The matrices in Eqs. (2.1.31,32) have the form of Pauli matrices, but they are rotated with respect to the Pauli matrices chosen for the TLS. We can remove this by performing a $\pi/2$ rotation

about the y axis of the space of conduction partial wave indices, taking the matrix for V^z to σ^z, and the matrix for V^x to $-\sigma^x$. In so doing, one effects a $\pi/4$ rotation in the space of orbital indices. Namely, if we denote the unit vectors in the restricted two-component orbital space of conduction states as $\hat{e}_0, \hat{e}_1$ for s and p wave components, respectively, then the rotated basis corresponds to

$$\hat{e}_\pm = \frac{1}{\sqrt{2}}[\pm\hat{e}_0 + \hat{e}_1] \quad . \tag{2.1.33}$$

We can now put everything together to make the mapping of the TLS model with coupling to conduction electrons to the $S = 1/2$ two-channel Kondo model. Within the restricted orbital basis,

$$H_{TLS} = \frac{1}{2}\sum_{i=x,z} \Delta^i \sigma^i + \sum_{i=x,z} \tilde{V}^i \sigma^i \sigma_c^i(0) \tag{2.1.34}$$

with

$$\sigma_c^i(0) = \frac{1}{N_s}\sum_{k,k',\alpha,\alpha',\sigma} \sigma^i_{\alpha,\alpha'} c^\dagger_{k,\alpha,\sigma} c_{k',\alpha',\sigma} \quad . \tag{2.1.35}$$

where N_s is the number of sites. Eq. (2.1.34) has the form of a two-channel Kondo model (the real spin of the electrons is a spectator to the scattering off the TLS) with the local $S = 1/2$ variable measuring the position of the atom in the TLS double well, and the corresponding index for the conduction electrons measuring the angular momentum.

In the introduction, where we discussed the isotropic two-channel Kondo model, we noted that antiferromagnetic coupling was required to produce a growth of coupling constants. In the present highly anisotropic model, independent of the signs of V^z, V^x we shall flow to strong coupling, as we will discuss in Section 3.3.1.

Note that without the inclusion of $\tilde{V}^x$, the model would correspond to an "Ising-Kondo" model, which simply has screening effects and a renormalized tunneling rate due to the orthogonality catastrophe associated with every spontaneous tunneling event (see, e.g., Kondo [1976(a)], Black and Györffy [1979], Black, Vladár , and Zawadowski [1982], Kagan and Prokof'ev [1986,1987,1989]).

We also note that the over-compensation of the two-channel Kondo model discussed in the introduction is not compromised by the various approximations used to cast (2.1.34) into a form which has pseudo-spin 1/2 conduction electrons. Were we to generalize to arbitary m values and not truncate the l expansion at the s, p level, we would simply have conduction states with larger effective spins and still have a two-channel model with the real conduction spin. In fact, the restriction to two-component conduction spins is thoroughly justified by the scaling analysis, which shows that only two dominant spin components are selected out in the absence of additional symmetries in the bare Hamiltonian (see Sec. 3.2 and Zaránd [1994]).

Hence, on quite general grounds, the TLS undergoing assisted tunneling maps to a highly anisotropic two-channel Kondo Hamiltonian in which the impurity spin is effectively 1/2.

2.1.3 Related lattice models with Kondo analogies

We will close this subsection with a discussion of two related lattice models in which assisted tunneling or hopping processes play a key role. The first is just the generalization of the TLS model to the situation where the atom or heavy particle (say, a muon) may move throughout a crystalline lattice. The second is the problem of electrons in two different bands, one heavy, one light, in which besides single particle hybridization between the bands one includes Coulomb assisted hopping between the bands.

(a) Lattice generalization of TLS with assisted hopping

The TLS model can be easily generalized in the case of a heavy particle hopping on a lattice. This could be, for example, either a muon or proton diffusing in a crystal where the massive particle jumps only on a lattice of interstitial sites (see Kondo [1984(a,b),1985,1986], Zawadowski [1987], Zimányi , Vladár , and Zawadowski [1987], and Kagan [1992]).

In the metallic environment, the conduction electrons form a degenerate gas which couples to the heavy particle. The non-interacting Hamiltonian is

$$H_0 = H_h + H_c \tag{2.1.36}$$

with H_c the free electron Hamiltonian discussed previously and

$$H_h = t \sum_{<\vec{R},\vec{R}'>} [h^\dagger_{\vec{R}} h_{\vec{R}'} + h.c.] \tag{2.1.37}$$

with $\vec{R}, \vec{R}'$ nearest neighbors on the lattice through which the heavy particle moves, and $h^\dagger_{\vec{R}}$ creating a heavy particle at site $\vec{R}$. Eq. (2.1.37) generalizes the non-interacting TLS Hamiltonian for the moving heavy particle. For convenience, we shall assume the heavy particles move about on a hyper-cubic lattice of dimension d, and we assume the spin of the particle has negligible coupling to the conduction electrons so we suppress that.

The screening interaction corresponding to V^z in the TLS case is local and the corresponding term in the Hamiltonian is

$$H_{int,z} = \frac{V}{N_s} \sum_{\vec{R},\sigma,} \sigma_{\vec{k},\vec{k}'} \exp(i(\vec{k}' - \vec{k}) \cdot \vec{R}) h^\dagger_{\vec{R}} h_{\vec{R}} c^\dagger_{\vec{k},\sigma} c_{\vec{k}',\sigma} \quad , \tag{2.1.38}$$

where V is the strength of the screening coupling. The simplest generalization of the electron assisted hopping V^x (see Fig. 9) in this context is when the hopping along a bond depends upon the conduction electron density at that bond, i.e., we have an interaction term

$$H_{int,x} = t_a \sum_{<\vec{R},\vec{R}'>} \sum_{\vec{k},\vec{k}',\sigma} \exp(i(\vec{k}' - \vec{k}) \cdot (\vec{R} + \vec{R}')/2) h^\dagger_{\vec{R}} h_{\vec{R}'} c^\dagger_{\vec{k},\sigma} c_{\vec{k}',\sigma} \quad , \tag{2.1.39}$$

where t_a is the strength of the electron assisted hopping (Zawadowski [1987]).

The problem described by the Hamiltonian $H_0 + H_{int,z}$ has been extensively studied in the literature for hydrogen and muon diffusion in metals. See, e.g., Kondo [1985,1986], Kagan [1992]. The physical relevance of the model when t_a is included is not yet clear. The model cannot be applied to the heavy fermion systems, for example, because they have only extremely weak direct hopping matrix elements for the f-electrons due to the small size of the f-orbitals. Moreover, the f-electron states hybridize with the conduction states, which are also the electrons that produce the screening. Finally, while the neglect of the muon or proton spin coupling is quite reasonable since no hybridization can occur so that only weak, ferromagnetic hyperfine coupling is possible and thus no Kondo effect, it is of course disastrous to ignore the internal degrees of freedom of the f-electrons in the heavy fermion systems.

(b) Occupation dependent hybridization between heavy and light electrons

The possible modification of the previous models for electronic systems with heavy and light electronic bands can be given in the tight binding formalism. The light electrons form a broad tight binding conduction band with large hopping rate while at certain sites there are heavy orbitals with site energy ϵ_h which have weak hybridization with the conduction orbitals but no direct overlap with heavy orbitals on other sites. It is assumed there is one heavy site per unit cell but possibly more than one light site per unit cell so that the corresponding creation operators are indexed by both unit cell vectors

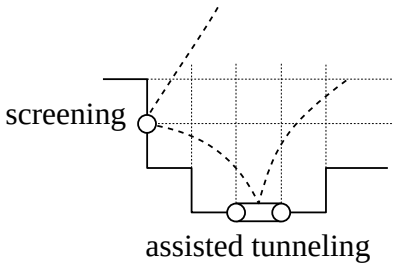

Figure 10: The path of a heavy particle moving on a square lattice is shown by the solid line. The electron (dashed line) is either scattered by the heavy particle sitting on a lattice position or just moving between two positions. The positions are represented by circles and the moving particle between two positions by a double line.

$\vec{R}$, basis vectors $\vec{\delta}$ which may extend into neighboring unit cells, and that there may be an internal orbital degeneracy to the heavy band.

Two physical systems to which such a model might apply are:
(i) Cuprate superconductors. Here the light carrier would be a mobile hole in the bonding oxygen bands residing in the CuO_2 planes, and the heavy carrier to holes in essentially filled non-bonding $\pi_{x,y}$ orbitals of the apex oxygen sitting above the copper sites. (See Fig. 10.)
(i) Heavy Fermion metals. In this case, considering for example UBe_{13}, the light carriers would derive from the Be $s-p$ bands, and the heavy carriers from the U $5f$ orbitals. In practice, the model will be more applicable to models where the physical f-level position (and not the renormalized or Kondo resonance position) is close to the Fermi level, which makes truly mixed valent Sm or Yb ions the most likely candidates. For further details we refer the reader to Zawadowski [1989(a,b,c)], Zawadowski, Penc, and Zimányi [1991], and Penc and Zawadowski [1994].

The unperturbed Hamiltonian is given by

$$H_0 = \epsilon_h \sum_{\vec{R},\gamma,\sigma} h^\dagger_{\vec{R},\gamma,\sigma} h_{\vec{R},\gamma,\sigma} + \sum_{\vec{R},\vec{\delta},\delta'\sigma} t(\delta,\delta') c^\dagger_{\vec{R},\vec{\delta},\sigma} c_{\vec{R},\vec{\delta}',\sigma} + \sum_{\vec{R},\vec{\delta},\gamma,\sigma} [t^\gamma(\vec{R},\vec{\delta}) h^\dagger_{\vec{R},\gamma,\sigma} c_{\vec{R},\vec{\delta},\sigma} + h.c.] \quad , \tag{2.1.40}$$

where $t(\delta,\delta')$ measures the direct light electron hopping and $t^\gamma_{\vec{R},\vec{\delta}}$ the heavy electron-light electron hybridization.

We assume that the heavy band is either completely empty or completely full, and thus there are only very few excited particles or holes. We may or may not assume a large on-site Coulomb interaction for the heavy band (large interaction can be dealt with via slave boson field theory techniques), and we shall discuss each case in later sections.

The term which we will add to H_0 which is analogous to the assisted tunneling interaction is an occupancy assisted hybridization term. Namely,, we assume that the heavy-light hybridization is modulated when the light orbital on the target site is simultaneously occupied with an electron of opposite spin. The corresponding interaction is

$$H_{\tilde{t}} = \sum_{\vec{R},\vec{\delta},\gamma,\sigma} [\tilde{t}^\gamma(\vec{R},\vec{\delta}) h^\dagger_{\vec{R},\gamma,\sigma} c_{\vec{R},\delta,\sigma} c^\dagger_{\vec{R},\vec{\delta},-\sigma} c_{\vec{R},\vec{\delta},-\sigma} + h.c.] \quad . \tag{2.1.41}$$

The coupling $\tilde{t}^\gamma(\vec{R},\vec{\delta})$ may arise in two different ways:
(i) We can assume that the radius of the light orbital depends upon whether the orbital is singly or doubly occupied. In this case the overlap and hopping rate is also modified [Zawadowski,1989].
(ii) Through the off-diagonal matrix elements of the Coulomb interaction [Hubbard, 1963; Kivelson, *et*

al., 1987; D. Baeriswyl, P. Horsch, and Maki, 1988; Gammel and Campbell, 1988; Hirsch, 1988] we may find a matrix element

$$\tilde{t}^{\gamma}(\vec{R},\vec{\delta}) = \int d^3r d^3r' (\phi^{\gamma}_{\vec{R},\sigma}(\vec{r}))^* \phi^*_{\vec{R},\vec{\delta},-\sigma}(\vec{r}') \frac{e^2}{|\vec{r}-\vec{r}'|} \phi_{\vec{R},\vec{\delta},-\sigma}(\vec{r}') \phi_{\vec{R},\vec{\delta},\sigma}(\vec{r}) \tag{2.1.42}$$

which clearly has the required form.

As we shall briefly discuss in the next section on scaling theory, when the complex character of the $\tilde{t}$ matrix elements is taken into account through momentum dependent form factors which reflect the intra-cell nature of the hopping, a Kondo like renormalization of two particle interactions between light electrons occurs. In this sense, there is a strong resemblance to the TLS and quadrupolar Kondo effects in which momentum dependent form factors drive the non-commutative algebra for interactions between the local pseudo-spin variables and the conduction electrons.

(c) Electric Dipole Kondo Model

Emery and Kivelson [Emery and Kivelson, 1992(a)] have considered the possibility of the electric dipole Kondo effect in the cuprate superconductors. The physical origin of the dipoles is through the formation of locally charge segragrated regions as has been argued to occur in the $t-J$ model at finite doping. Orbital coupling of itinerant electrons or holes to the extended electric dipoles maps onto the anisotropic two-level system Kondo problem discussed in this section. The real carrier spin is not involved in the coupling and so again serves as a channel index. Because of the electric dipole character of the effective impurity spin, the current operator is modified in this model and very different electrical conductivity results may be obtained in comparison with other physical realizations of the two-channel Kondo model. We defer a discussion to Sec. 9.3 where a one-dimensional concentrated system of electric dipole Kondo centers is discussed [Emery and Kivelson, 1993].

2.2 Exotic Kondo Models for Rare Earth and Actinide Impurities

2.2.1 Quadrupolar Kondo Model for U^{4+} ion in cubic symmetry

(a) Physical Discussion and Context

In this subsection, we shall derive the quadrupolar Kondo model for a uranium ion in a crystal field of cubic symmetry.

The idea of the quadrupolar Kondo effect was first proposed to explain the unusual magnetic field dependence of the heavy fermion superconductor UBe_{13}[Cox, 1987]. Subsequently, Barnes noted that the quadrupolar moments of Cu^{2+} ions in the cuprate superconductors could lead to such a Kondo effect as well [Barnes, 1988]. Later it was realized that tetravalent U ions in hexagonal symmetry with Γ_5 or Γ_6 doublets and in tetragonal symmetry with Γ_5 doublets will also be subject to a quadrupolar Kondo effect of slightly different character, as we shall discuss in more detail in Sec. 2.2.4 [Cox, 1993]. Finally, the suggestion of Cox [1987b] for UBe_{13} met some understandable skepticism, since in this material the putative quadrupolar Kondo sites are distributed on a periodic lattice. However, the discovery of the alloy $Y_{1-x}U_xPd_3$[Seaman *et al.*, 1991,1992; Liu, *et al.*, 1992; Andraka and Tsvelik, 1991], which for concentrations $x = 0.1, 0.2$ appears to display many of the features of the quadrupolar Kondo effect, has considerably strengthened the empirical basis for this theory.

The motivation for considering the quadrupolar Kondo effect in UBe_{13} was that in all properties except magnetoresistance, this material displays an extremely weak magnetic field dependence. However, the heavy fermion character is presumed to derive from a Kondo effect. It was noted that U^{4+} ions with a nominal configuration of $5f^2$ have a Hund's rule angular momentum of $J = 4$. In consequence, when placed on a site of cubic symmetry, as in UBe_{13}, the action of the crystal field lifting the full multiplet degeneracy could produce a non-Kramers Γ_3 or E doublet ground state, i.e., whose degeneracy is not guaranteed by Kramers' theorem. Kramers' theorem states that for an electronic configuration with an odd number of electrons, a minimal two fold degeneracy exists for each level due

Configuration	State	Parent J	Form	$< J_z >$	$< 3J_z^2 - J(J+1) >$
f^2	$\Gamma_3(+)$	$J = 4$	$\sqrt{\frac{5}{24}}[\|4> + \|-4>] - \sqrt{\frac{7}{12}}\|0>$	0	+8
f^2	$\Gamma_3(-)$	$J = 4$	$\sqrt{\frac{1}{2}}[\|2> + \|-2>]$	0	-8
f^1	$\Gamma_7(\uparrow)$	$J = 5/2$	$\sqrt{\frac{1}{6}}\|-5/2> - \sqrt{\frac{5}{6}}\|3/2>$	$+\frac{5}{6}$	0
f^1	$\Gamma_7(\downarrow)$	$J = 5/2$	$\sqrt{\frac{1}{6}}\|5/2> - \sqrt{\frac{5}{6}}\|-3/2>$	$-\frac{5}{6}$	0
c^1	$\Gamma_8(2)$	$J = 5/2$	$\sqrt{\frac{5}{6}}\|5/2> + \sqrt{\frac{1}{6}}\|-3/2>$	$+\frac{11}{6}$	+8
c^1	$\Gamma_8(\bar{2})$	$J = 5/2$	$\sqrt{\frac{5}{6}}\|-5/2> + \sqrt{\frac{1}{6}}\|3/2>$	$-\frac{11}{6}$	+8
c^1	$\Gamma_8(1)$	$J = 5/2$	$\|1/2>$	$+\frac{1}{2}$	-8
c^1	$\Gamma_8(\bar{1})$	$J = 5/2$	$\|-1/2>$	$-\frac{1}{2}$	-8

Table 3: Angular momentum character of states for two-channel Kondo models for U^{4+} and Ce^{3+} ions in cubic symmetry. The fourth column gives information about the states of definite azimuthal quantum number values which are mixed to form the state in cubic symmetry. The last two columns give information about the expectation values of magnetic and quadrupolar moments corresponding roughly to the $S^{(3)}$ and $\tau^{(3)}$ operators.

to time reversal symmetry that cannot by lifted by any crystalline anisotropy (see, e.g., Lax [1974]). No corresponding statement can be made for an ion with an even electron number configuration, though in some lower symmetries symmetry distinct singlet states may have enforced degeneracy through time reversal symmetry (see, for example, Tinkham [1964], p. 147).

The Γ_3 doublet is not the only possible ground state in the field of cubic symmetry for the U^{4+} ion, but will be over about half the crystal field parameter range. [See Lea, Leask, and Wolf, 1962, for a discussion of crystal field splittings in cubic symmetry. Some of the relevant states are listed in Table 3. Note that the sign of the W parameter in Lea, Leask, and Wolf must be negative to realize the stable $\Gamma_3(E)$ ground state. While this is excluded for a point charge model in simple coordination environments (e.g., octahedral), it is not excluded for complex coordinations such as in UBe_{13}, or for splittings induced by terms second order in the hybridization with conduction states, the most likely origin of the crystal field splittings in the heavy fermion materials. For a simple discussion of this latter idea, see Zhang and Levy, [1989].

Hence, since the two levels of the $\Gamma_3(E)$ doublet are not connected by time reversal, a magnetic field does not split the level, at least to linear order, and the field dependent properties will be correspondingly weaker than in a magnetic Kondo system. The double degeneracy of the ground level allows one to treat it as a two-level system, i.e., as a manifold with a pseudo-spin of 1/2. As we shall discuss in more detail, such a ground state is indeed susceptible to a Kondo effect when coupled to conduction electrons.

Any state with internal degrees of freedom must be characterized by a non-trivial multipole moment other than the simple occupancy or charge operator. The physical meaning of the $\Gamma_3(E)$ state is that it has a non-vanishing quadrupole moment. Recall from electrostatics that the quadrupole moment tensor describes the potential from an *aspherical* distribution of charge which appears in the energy through a coupling to the electric field gradient tensor. Given a charge distribution $\rho(\vec{r})$, the quadrupole tensor $\hat{Q}_{ij}$ is defined in cartesian form as

$$\hat{Q}_{ij} = \int d^3r \rho(\vec{r})[3r_i r_j - r^2\delta_{ij}] \quad . \tag{2.2.1}$$

Note that:
(i) The tensor $\hat{Q}_{ij}$ is symmetric and traceless, so that it has only five independent components.
(ii) For full rotational symmetry, these five components transform among one another like the elements

of the function $Y_{2,m}(\hat{r})$.
(iii) As the point symmetry is lowered to cubic, the case at hand, the tensor splits into a doublet of *tensors* (transforming according to a two-dimensional irreducible representation or "irrep" of the point group), which corresponds to the diagonal elements of Eq. (2.2.1) (in diad form, $\hat{Q}_{ii} \sim 3\hat{i}\hat{i} - 1\mathbf{I}$, where $\mathbf{I}$ is the identity tensor), and a triplet of tensors (transforming according to a three- dimensional irrep of the point group, which in diad form go as $\hat{Q}_{ij} = \hat{Q}_{ji} \sim 3\hat{i}\hat{j},\ i \neq j$), which corresponds to the off-diagonal elements of Eq. (2.2.1). The doublet tensor transforms according to the so called $\Gamma_3(E)$ irrep of the cubic point group, and the triplet tensor according to the so-called $\Gamma_5(T_2)$ irrep of the cubic point group. The reason for only two components in the $\Gamma_3(E)$ doublet tensor is the tracelessness of the quadrupolar tensor, *viz.*

$$\hat{Q}_{xx} + \hat{Q}_{yy} + \hat{Q}_{zz} = 0 \tag{2.2.3}$$

so that only two components are actually independent. It is convenient to write the two components as the two traceless combinations

$$\hat{Q}_{+} = \sqrt{3} q_{\Gamma_3} [\hat{x}\hat{x} - \hat{y}\hat{y}] \tag{2.2.4.a}$$

and

$$\hat{Q}_{-} = q_{\Gamma_3} [2\hat{z}\hat{z} - \hat{x}\hat{x} - \hat{y}\hat{y}] \tag{2.2.4.b}$$

where

$$q_{\Gamma_3} = \int d^3 r \rho(\vec{r}) x^2 = \int d^3 r \rho(\vec{r}) y^2 = \int d^3 r \rho(\vec{r}) z^2 \quad . \tag{2.2.5}$$

The equality of the three integrals above follows from the assumed cubic symmetry. Note that the diad forms to the tensors of Eqs. (2.2.4.a,b) explicitly demonstrate the tracelessness of Eq. (2.2.3).
(iv) The tensor pair $\hat{Q}_{\pm}$ will couple linearly to electric field gradients of the same symmetry applied to the crystal. The most practical way of effecting such gradients is through the application of external stresses $\hat{\eta}_{\pm}$ which will produce a coupling term in the energy of the charge distribution of the form

$$E_{stress} = A \sum_{a=\pm} Tr[\hat{Q}_a \hat{\eta}_a]. \tag{2.2.6}$$

The meaning of a pure stress of the form $\hat{\eta}_{-}$ is that the crystal is stressed either tensilely (elongated) or compressively (flattened) along one of the principal axes, in this case the z-axis. Such a uniaxial distortion lowers the crystal symmetry to tetragonal. This is clear because the stress will couple linearly to the corresponding strain tensor

$$\hat{\epsilon}_{-} = 2\epsilon_{zz} - \hat{\epsilon}_{xx} - \hat{\epsilon}_{yy} = 2\frac{\partial u_z}{\partial z} - \frac{\partial u_x}{\partial x} - \frac{\partial u_y}{\partial y} = 3\epsilon_{zz} \tag{2.2.7}$$

where $\vec{u}(\vec{r})$ is the atomic density displacement field at position $\vec{r}$, and where the far RHS of the above equation follows from the assumption of a pure stress, i.e., the uniform volume term $\epsilon_0 = \epsilon_{xx} + \epsilon_{yy} + \epsilon_{zz} = 0$. The meaning of a pure stress of the form η_{+} is that the crystal will distort orthorhombically since it will linearly couple to $\epsilon_{+} = \sqrt{3}[\epsilon_{xx} - \epsilon_{yy}]$ which will elongate(shrink) the x-axis as the y-axis is shrunk(elongated) while the z-axis is unchanged. Note that this discussion indicates the Γ_3 doublet tensor will linearly couple to a strain or vibration field of the same symmetry. A simple, useful visualization appears in Fig. 11

(v) Turning now to the quantum mechanical situation, we are interested in the charge distribution associated with a particular quantum mechanical angular momentum multiplet, in which case the quadrupolar tensor should be viewed as a representation of operators that act within the multiplet. The Wigner-Eckart theorem may be utilized to write this tensor purely in terms of the angular momentum

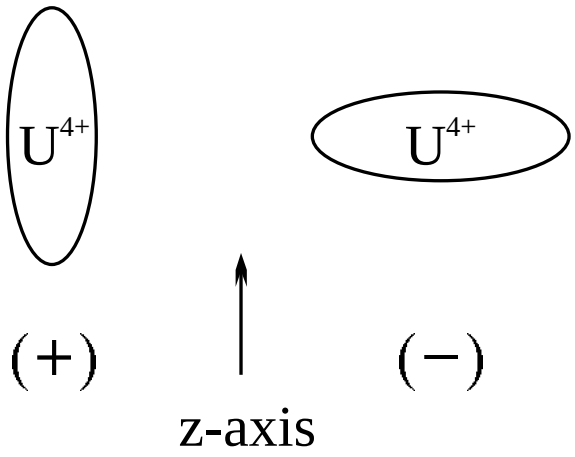

Figure 11: Mapping of Uranium quadrupole orientations to pseudo-spin variables in cubic symmetry. The Γ_3 quadrupole moment of the U^{4+} ion is quantized to two values. Choosing the quantization axis along the z axis, the stretched or prolate configuration maps to "up" or "+" pseudo-spin, and the squashed or oblate configuration maps to "down" or "-" variables.

operators $\vec{J}$; we follow the derivation of Slichter for nuclei [Slichter, 1989]. Because $\vec{r}$ transforms as a vector (rank 1 tensor), for an open shell ion with configuration f^n and angular momentum J in free space (full rotational symmetry) we may write

$$\hat{Q}_{ij} = q_{n\lambda J}[\frac{3}{2}(J_iJ_j + J_jJ_i) - J(J+1)\delta_{ij}] \quad , \tag{2.2.8}$$

where reduced matrix element $q_{n\lambda,J}$ is given by evaluation of the above equation in the stretched state $|n, \lambda, J, M_J = J>$; formally

$$q_{n\lambda J} = -e\frac{< n, \lambda, J, M_J = J| \sum_{i=1}^{n}[3z_i^2 - r_i^2]|n, \lambda, J, M_J = J >}{J(2J-1)} \tag{2.2.9}$$

where λ denotes the other quantum numbers of the system. The sufficiency of using $i = j = z$ and the stretched state in evaluating the reduced Matrix element is guaranteed by the rotational symmetry of free space; such tricks are customary in applying the Wigner-Eckart theorem. In principle, one should proceed by computing the one-particle matrix element and then using angular momentum algebra to compute the effective matrix element within the lowest multiplet. The idea is analogous to the calculation of the Landé g-factor. $q_{n\lambda J}$ measures the strength of the coupling to an applied field gradient, and thus for the quadrupolar system is analogous to the effective magnetic moment of a magnetic multiplet. Note that the above formula for $q_{n\lambda,J}$ only applies for $J > 1/2$.

Under the reduction to cubic symmetry, we will split the five dimensional tensor operator space of Eq. (2.2.9) into doublet ($\Gamma_3(E)$) and triplet ($\Gamma_5(T_2)$) spaces as in the classical discussion above. For the $\Gamma_3(E)$ space, the explicit operator forms are

$$\hat{Q}_+ = q_{n\lambda J}\sqrt{3}[J_x^2 - J_y^2] = q_{n\lambda J}\frac{\sqrt{3}}{2}[J_+^2 + J_-^2] \tag{2.2.11.a}$$

and

$$\hat{Q}_- = q_{n\lambda J}[3J_z^2 - J(J+1)] \quad . \tag{2.2.11.b}$$

In Eq. (2.2.11.a), $J_\pm = J_x \pm iJ_y$ are the angular momentum raising and lowering operators. Note that $\hat{Q}_-$ is diagonal in the J basis, while $\hat{Q}_+$ is off diagonal in the J basis.

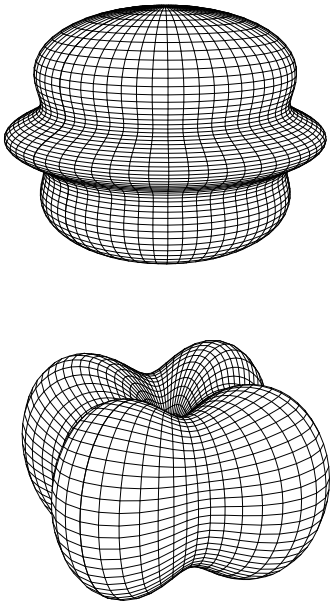

Figure 12: Actual orbital shapes for $4f$,$J = 5/2$,Γ_8 conduction electrons. The upper picture is for the elongated "+" orbital, the lower for the compressed "-" orbital. Each plot is a constant probability density contour. Taken from Kim [1995], and Kim and Cox [1997] (with permission).

Let us now connect these ideas to the $\Gamma_3(E)$ doublet on the U^{4+} site in cubic symmetry. The two states of the doublet are listed in Table 3. We see that under the action of the operator Q_- (apart from the proportionality factor of $q_{n\lambda J}$) the + state corresponds to a positive quadrupolar deformation, the − state to a negative quadrupolar deformation. In the plus state, for which $M_J = 0$ is the dominant component, we will measure an elongation along the chosen quantization axis in the z-direction. For the − state, with dominant $M_J = \pm 2$ components, the U^{4+} charge density will be squashed along the z direction. An over-simplified picture is shown in Fig. 11), where we view the ion as a "cigar" in the + state and a "pancake" in the − state. In fact, there is considerably more structure to the charge distribution as shown in the realistic depiction of Fig. 12

At this point, the reader might be confused as to why we don't have access instead to three "cigar"-shaped states along the three principal axes. The reason is that the ± states transform like a quadrupolar doublet themselves–while three cigars would be described by the 90^o rotation of the + state lined up along the z-axis to instead lie along the x- or y-axes, the x and y states are not in fact orthogonal to the original + state. This statement for the states is precisely analogous to the tracelessness condition for the tensors. Orthogonalization produces a linear combination of the x, y "cigar" orbitals which is overall flat.

Examining the forms of the states in Table 3, we see that the $\Gamma_3(\pm)$ states contain states of the original J manifold which differ by two units of angular momentum. Hence these two states will be connected by the operator $\hat{Q}_+$ which raises or lowers angular momentum by two units.

If we now recall Eq. (2.2.6) which describes the classical energy of a charge distribution with cubic symmetry under the influence of an external stress tensor field of $\Gamma_3(E)$ symmetry, we see that the external stress will have two possible effects on the $\Gamma_3(E)$ ground doublet of the U^{4+} ion:
(i) If $\hat{\eta}_-$ is non-zero, we will couple to $\hat{Q}_-$. Since $\hat{Q}_-$ linearly splits the ± states, this is analogous the

the effect of a longitudinal magnetic field applied to a spin-1/2 state. This corresponds to a uniaxial (tetragonal) distortion. The $\Gamma_3(+)$ state transforms as a $\Gamma_1(A_1)$ singlet in the tetragonal symmetry, while the $\Gamma_3(-)$ state transforms as a $\Gamma_3(B_1) \sim x^2 - y^2$ singlet in the tetragonal symmetry.
(ii) If $\hat{\eta}_+$ is non-zero, we will be allowed to mix the two doublet states. Recall that this corresponds to an orthorhombic distortion. Indeed, as we lower from cubic to orthorhombic symmetry, the $\Gamma_3(\pm)$ states both transform as $\Gamma_1(A_1)$ irreps since now there are no symmetry transformations of 90^o rotations about the principal axes to distinguish the two states.

Instead of using the representation of the impurity tensor operators in terms of the angular momentum, we may restrict our attention to the operator basis of the $\Gamma_3(E)$ doublet of states directly. Since the manifold is two dimensional, there are only four second rank tensor operators we may form. These operators are

$$\tau_I^{(0)} = \frac{1}{2}[|f^2\Gamma_3,+><f^2\Gamma_3,+| \; + \; |f^2\Gamma_3,-><f^2\Gamma_3,-|] \quad , \tag{2.2.12.a}$$

which describes just the charge (monopole) distribution of the U^{4+} ion,

$$\tau_I^{(1)} = \frac{1}{2}[|f^2\Gamma_3,+><f^2\Gamma_3,-| \; + \; |f^2\Gamma_3,-><f^2\Gamma_3,+|] \quad , \tag{2.2.12.b}$$

$$\tau_I^{(3)} = \frac{1}{2}[|f^2\Gamma_3,+><f^2\Gamma_3,+| \; - \; |f^2\Gamma_3,-><f^2\Gamma_3,-|] \quad , \tag{2.2.12.c}$$

and

$$\tau_I^{(2)} = \frac{1}{2i}[|f^2\Gamma_3,+><f^2\Gamma_3,-| \; - \; |f^2\Gamma_3,-><f^2\Gamma_3,+|] \quad . \tag{2.2.12.d}$$

The three operators $\tau_I^{(1)}, \tau_I^{(2)}, \tau_I^{(3)}$ clearly form a closed algebra in the $SU(2)$ space defined by transformations within the manifold of $\Gamma_3(E)$ states.

Clearly, $\tau_I^{(3)}$ which is diagonal and of opposing sign for the two states is proportional to $\hat{Q}_-$. Also, $\tau_I^{(1)}$ which "flips" between the two members of the doublet, is clearly proportional to $\hat{Q}_+$. Hence, the $\tau_I^{(1)}, \tau_I^{(3)}$ pair transforms as a doublet tensor of $\Gamma_3(E)$ symmetry which measures the corresponding $\Gamma_3(E)$ symmetry quadrupole tensor of the ion as restricted to the two lowest states. The action of a uniaxial stress $\hat{\eta}$ of pure $\Gamma_3(E)$ symmetry thus adds a term to the Hamiltonian of the quadrupolar doublet which has the form

$$H_{stress} = -\tilde{A}[\tau_I^{(1)}\eta_+ + \tau_I^{(3)}\eta_-] \tag{2.2.13}$$

where $\eta_\pm = \sqrt{Tr[\hat{\eta}_\pm]^2}/2$. Thus, the doublet external stresses $\eta_\pm$ for the quadrupolar Kondo model are analogous respectively to the spontaneous tunneling Δ^x and splitting Δ^z of the TLS model. This discussion is slightly over-simplified: the $\tau_I^{(1)}, \tau_I^{(3)}$ pair of tensors may also have components from all multipole moment tensors of even rank $\leq 2J$.

The operators $\tau_I^{(1)}, \tau_I^{(3)}, \tau_I^{(0)}$ clearly produce only real matrix elements. The operator $\tau_I^{(2)}$, just like the σ^y operator of the TLS discussion, is complex. The physical nature of this operator is made more clear by considering the commutation relation

$$[\tau_I^{(3)}, \tau_I^{(1)}] = i\tau_I^{(2)} \sim [\hat{Q}_-, \hat{Q}_+] \sim iJ_xJ_yJ_z \tag{2.2.14}$$

as may be readily verified by working out the commutators $[J_i^2, J_j^2]$ using Eqs. (2.2.11a,b). Thus the operator $\tau_I^{(2)}$ transforms as a $\Gamma_2(A_2)$ irrep of the cubic group. Since this tensor has three J_i operators, it is clearly odd under time reversal, and thus represents a magnetic octupole moment tensor.

The octupole tensor will couple to third order polynomials in the magnetic field, or alternatively, to the combined action of an applied magnetic field and an applied external stress that lowers the symmetry to rhombohedral . We may use this latter fact to understand the meaning of $\tau_I^{(2)}$ more deeply. First, apply a pure rhombic deformation (stress of $\Gamma_5(T_2)$ symmetry: $\hat{\eta} = \eta_0(\hat{x}\hat{y} + \hat{y}\hat{z} + \hat{z}\hat{x})$) along the body diagonal. This lowers the point symmetry of the uranium site from O to D_{3d}. Now apply a magnetic field along the body diagonal. The degeneracy of the Γ_3 doublet is now lifted. This lowers the symmetry from O to C_3, and breaks time reversal $\mathcal{T}$. The Γ_3 state transforms into a pair of singlets under C_3 which are however degenerate in the absence of a $\mathcal{T}$-breaking field; the applied magnetic field then splits these states. Thus, a term in the Hamiltonian arises of the form

$$H_{str.-field} = -\tilde{B}\tau_I^{(2)} \sum_{ijk} \hat{\eta}_{\Gamma_5,ij} H_k \quad (i,j,k\ cyclic) \tag{2.2.15}$$

where H_i is the i-th component of the applied magnetic field, and $\hat{\eta}_{\Gamma_5,ij}$ is the ij-th component of the Γ_5 symmetry external stress tensor. A magnetic field pointing along a body diagonal will also induce this coupling since the field will induce the equal magnetostriction induced strains tensors $\epsilon_{\Gamma_5 ij} \sim H^2 \hat{i}\hat{j}$, $i \neq j$.

It should be mentioned that the subject of crystal field levels in actinide intermetallics has been controversial [see, e.g., Ramakrishnan, 1988]. While $5f$ electrons have larger spatial extent should in general lead to larger crystal field splittings, sharp excitations attributable to crystal fields have been clearly seen only in a few uranium based compounds, most notably UPd_3 [Buyers *et al.*, 1980] and URu_2Si_2[Broholm *et al.*, 1992]. In contrast, relatively sharp crystal field excitations are frequently seen in rare earth intermetallics, e.g., in the heavy fermion superconductor $CeCu_2Si_2$[Horn *et al.*, 1981]. This situation will be discussed in somewhat more detail in Sec. 5.2.3, where the NCA equations are developed. Application of this theory to the appropriate model for a crystal field split uranium ion makes it clear that the excited crystal field level widths should be *generically* broader in the uranium materials [Cox, 1992a)]. This material shall be discussed in detail in the section on experimental manifestations of the two-channel models.

(b) Coupling to Conduction Electrons

Analogy to TLS model. In this subsection we shall develop the Kondo Hamiltonian for the coupling of the U^{4+} ions to the conduction states. We may think of the resulting coupling in a manner very similar to the TLS Hamiltonian. Namely, if the levels are polarized virtually so that $\tau_I^{(3)}$ would be non-zero, the electrons will attempt to relieve this polarization through a screening process producing a coupling J^3 analogous to V^z. Alternatively, we may view this screening term as representing the coupling of an electronic charge fluctuation of uniaxial (tetragonal) symmetry modulating the levels of the $\Gamma_3(E)$ doublet on the U^{4+} site. A fluctuation of the local electron charge density with orthorhombic symmetry coupled with strength J^1 will modulate the $\Gamma_3(E)$ states by producing transitions between them analogous to the assisted tunneling (V^x) term in the TLS model. Unlike the generic TLS model, the couplings $J^{1,3}$ are guaranteed to be equal due to the cubic point symmetry. Finally, a local octupolar distortion of the conduction electron charge density will modulate the $\Gamma_3(E)$ states by producing a mixing and an orbital magnetic moment. Since the $\tau_I^{(2)}$ operator transforms as a $\Gamma_2(A_2)$ irrep, nothing generically guarantees the equality of $J^{1,3}$ with J^2, though we shall see that a good starting model in fact yields isotropic bare coupling. In addition, in the absence of significant disorder or external stress, there will be no bare splittings or spontaneous tunneling terms in the quadrupolar Kondo model. Thus, we expect the quadrupolar Kondo models to typically be nearly isotropic in the starting Hamiltonian, and to possess no bare splittings or "spontaneous tunneling" terms.

Coupling to Conduction Electrons: Anderson Model The direct Coulombic couplings of the conduction electrons to the U^{4+} $\Gamma_3(E)$ doublet are likely to be much smaller than the effective couplings mediated through the hybridization of uranium $5f$ states with the conduction band. Thus

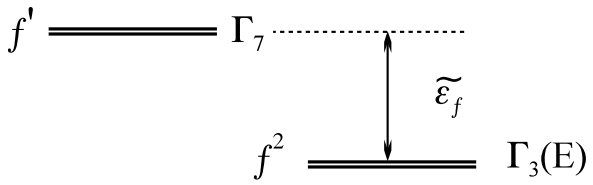

Figure 13: Simplified level scheme for U^{4+} ions in cubic symmetry undergoing quadrupolar Kondo effect. This simplest model involves a ground doublet in each of the two lowest lying configurations, with the f^2 having the quadrupolar or non-Kramers Γ_3 doublet, and the f^2 configuration having the magnetic or Kramers' Γ_7 doublet. Conduction electrons mix the two configurations through hybridization processes. Only a Γ_8 conduction state can couple these two doublets. Similarly, if f^3 rather than f^2 is presumed to lie lowest, the ground doublet of the excited configuration would be a Γ_6 Kramers' doublet, which can mix with the Γ_3 ground state of the f^2 again only through Γ_8 conduction states.

our derivation of the Kondo model must proceed in two steps here: first, we write down the relevant hybridization Hamiltonian which includes the strong atomic correlations on the U^{4+} site, and then we transform this model to the Kondo form.

In order to develop a Kondo effect, we must couple this quadrupolar moment to the conduction electrons. The appropriate framework for this is the Anderson Hamiltonian, in which atomic levels on the uranium site hybridize with the conduction states. The original paper by Anderson was motivated by a desire to understand the formation of local moments in solids, and assumed a single $s = 1/2$ electron present in an $s - wave$ impurity orbital [Anderson, 1961]. In order to provide realistical discussion of rare earth, actinide and transition metal impurity ions the model has been generalized to include orbital degeneracy by a number of workers [Coqblin and Schrieffer, 1969; Hirst, 1970, 1978; A. Yoshimori [1976]; L. Mihály and A. Zawadowski , [1978]]. A particularly helpful review of realistic, orbitally degenerate impurities was given by Nozières and Blandin [1980]. In this subsection we shall discuss the simplest model which gives rise to the quadrupolar Kondo effect. In fact, as will be justified in the sections of the paper discussing scaling theory (Secs. 3.3, 3.4) and the non-crossing approximation (NCA) integral equations (Sec. 5.3), this mapping is valid so long as the $\Gamma_3(E)$ level lies lowest in the f^2 configuration.

The picture of the level scheme for the Anderson model relevant for tetravalent uranium ions in cubic symmetry appears in Fig. 13. The most stable state is a $\Gamma_3(E)$ non-magnetic doublet of the f^2 configuration, and the first excited level is a Γ_7 magnetic doublet in the f^1 configuration. In fact, it is most likely that the f^3 configuration which has a Γ_6 magnetic doublet lies lower in energy, but the qualitative features will not depend upon this detail. We index the $\Gamma_3(E)$ states by the label

$$\alpha = \pm$$

and the Γ_7 excited states by the label

$$\mu = \uparrow, \downarrow \quad .$$

The promotion of $f^1 \rightarrow f^2$ by removing a conduction electron, or from $f^2 \rightarrow f^1$ by emitting a conduction electron specifies the symmetry of the conduction states about the impurity which may hybridize with the uranium $5f$ states. Group theoretically, since $\Gamma_3(E) \otimes \Gamma_7 = \Gamma_8$, only the Γ_8 conduction quartet partial waves may couple to the impurity through hybridization. These are derived from conduction partial waves with orbital angular momentum $l = 3$ spin-orbit coupled to produce $j = 5/2, 7/2$ manifolds, with each angular momentum manifold giving a Γ_8 partial wave quartet.

The projection to the $l = 3$ partial waves is implemented in terms of conduction electron annihilation operators, through the operation [Krishna-murthy, Wilkins, and Wilson, 1980a)]

$$c_{k3m\sigma} = \int \frac{d\hat{k}}{4\pi} Y^*_{3m}(\hat{k}) c_{\vec{k},\sigma} \quad , \tag{2.2.16}$$

and the coupling of these operators to produce $j = 5/2$ states is effected with standard Clebsch-Gordan technology, *viz.*

$$c_{k5/2m} = \sum_{\sigma} 2\sigma \sqrt{\frac{3 - 2\sigma(m-\sigma)}{7}} c_{k3,m-\sigma,\sigma} \quad . \tag{2.2.17}$$

The Γ_8 quartet from the $j = 5/2$ manifold will be retained for the discussion at hand; we defer a justification for this restriction to the later sections on scaling theory (Sec. 3) and NCA equations (Sec. 5). By looking at Table 3, we see that the combinations of states which produce the conduction Γ_8 creation and annihilation operators are written in the angular momentum basis as

$$c_{k8+,\uparrow} = c_{k8,2} = \sqrt{\frac{5}{6}} c_{k5/2,+5/2} + \sqrt{\frac{1}{6}} c_{k5/2,-3/2} \quad , \tag{2.2.18.a}$$

$$c_{k8+,\downarrow} = c_{k8,\bar{2}} = \sqrt{\frac{5}{6}} c_{k5/2,-5/2} + \sqrt{\frac{1}{6}} c_{k5/2,+3/2} \quad , \tag{2.2.18.b}$$

$$c_{k8-,\uparrow} = c_{k8,1} = c_{k5/2,+1/2} \quad , \tag{2.2.18.c}$$

and

$$c_{k8-,\downarrow} = c_{k8,\bar{1}} = c_{k5/2,-1/2} \quad . \tag{2.2.18.d}$$

The $2(\bar{2})$ and $1(\bar{1})$ subscripts in the middle part of the above equations gives the correspondence to the notation of Table 3 and the original paper [Cox [1987]]. The upper(lower) signs in the right hand side (RHS) of the above equations correspond to $\mu = \uparrow (\downarrow)$ The $\pm$ labels on the left hand side (LHS) correspond to the $\Gamma_3(E)$ index α.

The conduction electrons are assumed to reside in a broad band with a flat density of states $N(\epsilon)$ parameterized by a width D, which for convenience is typically taken to have the form

$$N(\epsilon) = \frac{1}{2D} \theta(D - |\epsilon|) \quad . \tag{2.2.19}$$

In order to implement this restricted Hilbert space, some appropriate limits of the atomic limit parameters must be taken. Essentially, we must take all crystal field, spin orbit, and exchange splittings to infinity. This done, we must take the limit of the direct $f - f$ repulsion U_{ff} to ∞ in a curious way. Denote the one-particle energy ϵ_f. To restrict to just the f^1 and f^2 configurations, we must have the energy difference $E(f^2) - E(f^1) = \tilde{\epsilon}_f = \epsilon_f + U_{ff}$ remain finite. Clearly this is achieved if $\epsilon_f = -U_{ff} + \tilde{\epsilon}_f$ and U_{ff} is taken to ∞. One may always restrict to just two configurations with similar tricks. However, to restrict to three or more configurations can only be done by hand and must be viewed as an approximation to the full Hilbert space, rather than an exact limiting case of the full model Hamiltonian with all configurations included. We remark that for 4f systems, $|\epsilon_f|$ is of the order of 2-4 eV, while U_{ff} is of the order of 6-10 eV [Herbst and Wilkins, 1987; Lang *et al.*, 1981]. In the actinide systems, the greater spatial extent of the 5f orbitals leads to correspondingly smaller values of 1-2 eV for ϵ_f and 3-6 eV for U_{ff} [Actinide Pars. Reference, :::].

With the above assumptions, the Anderson Hamiltonian in this restricted Hilbert space, which has been previously called the "3-7-8" model, may be written down as

$$H_{378} = \sum_{k\alpha\mu} \epsilon_{\vec{k}} c^{\dagger}_{k8\alpha\mu} c_{k8\alpha\mu} + \tilde{\epsilon}_f \sum_{\alpha} |f^2\Gamma_3, \alpha >< f^2\Gamma_3, \alpha| + H_{hyb} \tag{2.2.20}$$

$$H_{hyb} = -\frac{V}{\sqrt{N_s}} \sum_{k\alpha\mu} sgn(\mu) [|f^2\Gamma_3, \alpha >< f^1\Gamma_7, -\mu| c_{k8\alpha\mu} + h.c.] \tag{2.2.21}$$

where V is the hybridization strength and N_s is the number of atomic unit cells in the crystal. We have assumed the impurity to be located at the origin and have taken the f^1 configuration at the Fermi energy–clearly, this is sensible since energy differences between the configurations correspond to electron addition and removal energies which must be measured with respect to the Fermi energy. Note the presence of the phase factor $sgn(\mu)$ in the hybridization term. This arises because the Γ_3 doublet of the f^2 can mix with two particle states formed from a conduction electron and a single f electron which are a singlet in the channel variable μ and a doublet in the spin variable α.

The use of the "Hubbard" operators such as $|f^2\Gamma_3, \alpha >< f^1\Gamma_7, -\mu|$ in Eq. (2.2.19) is necessitated by the Hilbert space restriction. The advantage of using these operators is that strong correlations of atomic character are built in to the bare Hamiltonian, and the hybridization which is the smallest energy scale is to be viewed as the perturbation. The technical nuisance of these Hubbard operators is that they don't obey canonical commutation operator identities. Neveretheless, a direct perturbation theory may be developed [Keiter and Kimball, 1971; Inagaki, 1979; Grewe and Keiter, 1981; Grewe, 1983,1984; Coleman, 1983; Kuramoto, 1983; see also Bickers' review, 1987], or one may use pseudo-particle techniques to map the perturbation theory on to Feynman diagrams followed by a projection to the physical space [Abrikosov, 1965; Barnes, 1976; Coleman, 1983]. We shall implement the latter method in the NCA presentation later in the paper (see Secs. 3.3.1, 5).

Note that the general process to derive the Anderson Hamiltonian in the restricted subspace we have specified above requires explicit assumptions about the atomic states. This has been discussed in general detail by Hirst [1970,1978], and in detail for the problem at hand by Cox[1987b,1988a),1988b), 1991a),1992a)]. Specifically, while the single particle hybridization term may be written down independent of angular momentum coupling scheme (Russel-Saunders, intermediate, or $j-j$) when it is projected to the relevant many body states appropriate to the restricted set of configurations, then the strength of the matrix element depends upon which coupling scheme is used. However, the symmetry properties are unaffected by the choice of coupling scheme, as are the details about the ground state multiplets: $J=4$ is the ground multiplet in both extremes for Russell-Saunders *and* $j-j$ coupling. We shall assume that one or the other projection scheme has been employed, and incorporated into the overall magnitude of the hybridization matrix element.

The hybridization matrix element is more naturally parameterized through the "hybridization width" Γ, which measures the rate at which a single localized f-electron would tunnel off of the impurity site and into the electronic continuum. This level width is given by

$$\Gamma = \pi N(0) V^2 \quad . \tag{2.2.22}$$

Typically, for f-electron systems, this matrix element is in the range of 0.1-0.5 eV, with $4f$ electrons occupying the lower end of this range and $5f$ electrons the upper end of this range.

Mapping to Kondo model: Schrieffer-Wolff transformation. It has long been known that if charge fluctuations are rare, that is, if $\Gamma/|\tilde{\epsilon}_f| << 1$, then for low energy scales the Anderson Hamiltonian may map onto an effective exchange interaction for the lowest lying degenerate manifold. Physically, $\Gamma/|\tilde{\epsilon}_f|$ measures the deviation of the f-occupancy from 2, in this case, due to virtual fluctuations to the excited f^1 configuration. This mapping, under the name of the Schrieffer-Wolff [Schrieffer and Wolff, 1965; Schrieffer, 1967] transformation, for the non-orbitally degenerate Anderson model, or the Coqblin-Schrieffer transformation [Coqblin and Schrieffer, 1969], for the orbitally degenerate case, is by now well known. It may be implemented either through second order perturbation theory, or by applying a canonical transformation which eliminates the hybridization through second order. The strength of the effective exchange interaction is proportional to the square of the hybridization matrix element divided by the inter-configuration energy splitting. The most crucial result of the mapping, of course, is that the effective exchange interaction is *antiferromagnetic* as an example of the general ideas of superexchange formulated by Anderson [Anderson, 1950], and hence the Kondo effect is possible.

There are no subtleties in applying the canonical transformation to the current model, despite the fact that we are interested in an orbital doublet. The resulting exchange interaction in the space of

the $\Gamma_3(E)$ orbital degrees of freedom is

$$H_{Quad.Kondo} = \sum_{k\alpha\mu} \epsilon_{\vec{k}} c^\dagger_{k8\alpha\mu} c_{k8\alpha\mu} - J\vec{\tau}_I \cdot (\vec{\tau}_{c8\uparrow}(0) + \vec{\tau}_{c8\downarrow}(0)) \tag{2.2.22}$$

where $J = 2V^2/\tilde{\epsilon}_f < 0$ and, e.g.,

$$\tau_I^{(i)} = \sum_{\alpha,\alpha'} \tau^{(i)}_{\alpha,\alpha'} |f^2\Gamma_3, \alpha >< f^2\Gamma_3, \alpha'| \tag{2.2.23}$$

describes one of the multipole operators of the $\Gamma_3(E)$ doublet, $\tau^{(i)}_{\alpha,\alpha'}$ being one of the spin 1/2 matrices ($i = 1, 2, 3$), and

$$\tau^{(i)}_{c8\mu}(0) = \frac{1}{N_s} \sum_{k,k',\alpha,\alpha'} \tau^{(i)}_{\alpha,\alpha'} c^\dagger_{k8\alpha\mu} c_{k8\alpha'\mu} \tag{2.2.24}$$

describes the corresponding multipole operator formed from the conduction states. Note that the exchange interaction of Eq. (2.2.22) is isotropic, which is indeed expected from the 3-7-8 model. In general, the different symmetry properties of $\tau_I^{(2)}$ (which transforms as the $\Gamma_2(A_2)$ irrep) from the $\tau_I^{(1)}, \tau_I^{(3)}$ pair which forms a $\Gamma_3(E)$ tensor doublet will lead to *anisotropic* exchange, with $J^y \neq J^x = J^z$. Since this exchange anisotropy is irrelevant about the non-trivial fixed point, as will be discussed in subsequent sections, and since in no case is the exchange anisotropy expected to be as large as for the TLS case, we are certainly justified in writing down isotropic exchange in Eq. (2.2.22).

Koga and Shiba [1995] have studied a model which includes this exchange anisotropy together with scattering between Γ_8 and Γ_7 conduction states (cf. Sec. 4.1 of their paper). The latter scattering generates a coupling only to the $\tau_I^{(1)}, \tau_I^{(3)}$ operators since $\Gamma_7 \otimes \Gamma_8 = \Gamma_3 \oplus \Gamma_4 \oplus \Gamma_5$ and only the Γ_3 conduction tensors couple to the impurity. The resulting interaction takes the form

$$H_{ex,78} = \bar{J}(\tau_I^{(1)} \tau_{c78x} + \tau_I^{(3)} \tau_{c78z}) \tag{2.2.25}$$

where

$$\tau_{c78x} = \sum_{k,k',\mu} c^\dagger_{k'\Gamma_8,-,\mu} c_{k\Gamma_7,-\mu} + h.c. \tag{2.2.26}$$

and

$$\tau_{c78z} = \sum_{k,k',\mu} c^\dagger_{k'\Gamma_8,+,\mu} c_{k\Gamma_7,-\mu} + h.c. \quad . \tag{2.2.27}$$

They find (using the numerical renormalization group) that the low energy physics is still given by Eq. (2.2.22). Their results will be discussed in more detail in Section 4 of our paper.

We note here that the model of Eq. (2.2.22) has a counterpart for any non-Kramers doublet of U^{4+} ions in tetragonal or hexagonal symmetry. The differences are as follows: (i) first, the bare exchange is fully anisotropic for the tetragonal case, and has an Ising anisotropy in the hexagonal case; (ii) in each case, since the c-axis pseudo-spin of the U^{4+} ion couples linearly to the magnetic field, there is an unusual conduction channel spin-impurity pseudo-spin coupling for c-axis spins. This term appears to be irrelevant in renormalization group calculations. We discuss the origins of the hexagonal and tetragonal models below in Sec. 2.2.3.

The most notable thing about the Hamiltonian in Eq. (2.2.22) is that it has the two-channel Kondo form: two degenerate species of conduction electrons couple with identical exchange integrals to the local $S = 1/2$ object. In this case, the channel indices are the magnetic indices of the local conduction partial wave states, and hence the degeneracy is guaranteed by Kramers' theorem since

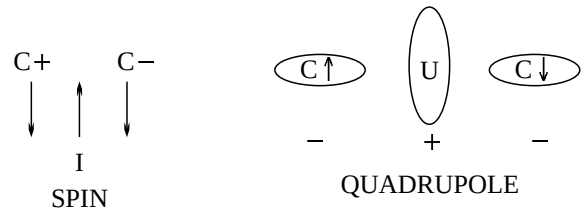

Figure 14: Mapping of the quadrupolar Kondo Hamiltonian to the two-channel Kondo model. At left is the standard picture of the two-channel model in spin space–two species of conduction electrons couple anti-parallel to the impurity spin at the center of the picture. In the quadrupolar Kondo case, "spin" is measured by quadrupolar or orbital deformations. The two-channels arise from the real magnetic spin of the conduction electrons (the Pauli principle allows a real-spin up electron and a real-spin down electron in the "negative pseudo-spin" squashed orbital of the conduction electrons.

this is a one electron state. Fig. 14 illustrates the principle and makes it clear why this is for very much the same reason as in the TLS case: the quadrupole moment, like the atomic position in the TLS, is invariant under time reversal. The pseudo-spin measures the shape of the local orbital. Hence, conduction electrons of opposite magnetic index must couple completely equivalently to the local quadrupole moment. In the limit of zero spin-orbit coupling, in fact, the Γ_7 index μ becomes the real spin index of the conduction electrons. The only complexity in this latter case is that it is impossible to achieve a pure orbital doublet ground state. We shall discuss this point in detail in one of the last sections.

Jahn-Teller effect. There is often considerable concern about the stability of the uranium ion against the Jahn-Teller effect [see for example, Fulde 1978]; ordinarily, an orbital doublet ground state will split spontaneously upon inclusion of the linear mixing to local nuclear coordinates. That will certainly happen here as well, but the Kondo effect provides a degree of stability against the Jahn-Teller effect in much the same way as the spin Kondo effect stabilizes against magnetism: the reduction of the on-site susceptibility by the Kondo effect from a Curie law form renders the ion stable against magnetic order below a critical strength to the intersite coupling of order T_K. Since the quadrupolar Kondo effect is of two-channel character, the susceptibility still diverges (logarithmically) but for a collection of such ions the collective Jahn-Teller instability is pushed to far lower temperature scales [Cox, 1987]. Similar conclusions have been reached about the single site Jahn-Teller effect by Gogolin [1995]. We shall discuss this point further in later sections of the paper.

Use of plane wave basis. The reader may be concerned about the use of plane wave states here when in many cases a tight-binding basis would be more appropriate. In this latter instance, one must only ensure that the ligand orbitals are not forbidden by symmetry from hybridizing with the uranium ion to write down an Anderson Hamiltonian. Even if the hybridization is symmetry forbidden, multipolar Coulomb coupling to the uranium ion can drive the quadrupolar Kondo effect through highly anisotropic bare couplings in precisely analogous fashion to the TLS example discussed in the previous subsection. Both possibilities have been discussed in detail in a tight binding basis using scaling theory [Deisz and Cox, 1995], and we shall outline some of these results in the next section. The main point is just this: given a local non-commutative algebra associated with the uranium ion, the Kondo effect will ensue, and it *does not* require two bands degenerate throughout the Brillouin zone.

2.2.2 Two-channel Magnetic Kondo effect for a Ce^{3+} impurity

(a) Physical Discussion and Context

The original work of Nozières and Blandin [1980] focussed on magnetic Kondo effects. The authors in fact concluded that realistic crystalline field anisotropy would make it unlikely to ever observe a multichannel magnetic Kondo effect: the anisotropies would always tend to make the system flow

eventually to the ordinary Kondo fixed point with a singlet ground state and Fermi liquid excitation spectrum.

The possibility of non-trivial two-channel physics has largely been overlooked in the last decade with the advent of expansion techniques based upon large orbital degeneracy N_I. Noting that Ce had a single f electron with total degeneracy of 14 neglecting spin orbit coupling, and 6 including spin orbit coupling, Anderson suggested that $1/N_I$ should serve as an expansion parameter [Anderson, 1981]. Subsequently, a number of workers developed approaches to and applications of the $1/N_I$ expansion [Ramakrishnan and Sur, 1982; Zhang and Lee, 1983; Read and Newns, 1983; Newns and Read, 1987; Coleman, 1983,1984,1987; Rasul and Hewson, 1984a,b; Kuramoto, 1983; Gunnarsson and Schonhammer, 1983,1984; Bickers, Cox, and Wilkins, 1985,1987; Auerbach and Levin, 1986; Millis and Lee, 1987]. Some efforts were also made to extend these ideas to models for uranium and thulium ions [Read *et al.* 1986; Nunes *et al.* 1986]. An extensive review of these methods appears in Bickers' article [Bickers, 1987].

In all of the above works, excepting the variational approaches of Gunnarsson and Schonhammer and the variational approaches to the uranium and thulium ions, the Coulomb repulsion U_{ff} was taken to be infinitely strong. In all cases, a non-degenerate singlet ground state is obtained meaning that the properties will be that of a Fermi liquid.

The point of this subsection will be to derive a Hamiltonian for Ce which indicates that in many cases, the considerations of Nozières and Blandin and the various large N_I efforts are entirely correct. Nevertheless, the possibility remains that Ce impurities may display a two-channel magnetic Kondo effect which lies outside the domain of $1/N_I$ theories. We shall see that the conditions allowing this physics are far more restrictive than for the quadrupolar Kondo effect. In particular:
(i) The ground state weight of fluctuations to the doubly occupied configuration must be higher than for fluctuations to the unoccupied configuration. For this reason, it is unlikely that Yb ions, the hole analogue to Ce, will ever exhibit two-channel physics.
(ii) Symmetry constrains the model to occur for only Kramers' doublets in cubic and hexagonal symmetry, and in the latter case only one such doublet exists [Cox, 1991,1992a)]

Ce ions are nominally trivalent in the metallic environment, and thus possess a single $4f$ electron with Hund's rule ground state angular momentum $J = 5/2$. The crystalline field will lift this degeneracy; in cubic symmetry, the ground state may be either a Γ_7 doublet or Γ_8 quartet [Lea, Leask, and Wolf, 1962]. Both ground states have been realized experimentally. For example, in $La_{1-x}Ce_xAl_2$ [see, for example, Maple, 1984] and $La_{1-x}Ce_xPb_3$ [Chen et al., 1987], the ground state is Γ_7, while in $La_{1-x}Ce_xB_6$, the ground state is Γ_8 [Winzer, 1975]. Unlike the non-Kramers' $\Gamma_3(E)$ doublet discussed in the previous subsection, the Γ_7 doublet must remain degenerate in the absence of a magnetic field, i.e., its degeneracy cannot be lifted by a Jahn-Teller effect.

(b) Couplings to conduction electrons

Anderson Model for Ce^{3+} ion in cubic symmetry. As in the case of the U^{4+} ion, we must derive the Kondo model by first developing the appropriate Anderson model which includes the $4f$-conduction hybridization and the strong electronic correlations on the $4f$ site.

We shall be concerned with the Γ_7 doublet in this subsection. The level scheme of the simplest model which can produce the two-channel Kondo effect is illustrated in Fig. 15. In this case, three configurations must be included, but in the spirit of simplicity the f^2 configuration is taken to have only the $\Gamma_3(E)$ ground doublet. Inclusion of higher levels can in principle produce new physics; see the last few paragraphs of this section (2.2.2.(b)), Sec. 2.2.4, and Sec. 5.2 for a discussion.

In this simple model, in essence, the level stability of the f^1 and f^2 have been inverted with respect to the model of the previous subsection. A simplifying feature of this model is that only Γ_7 symmetry partial waves of the conduction electrons will mix the f^1 doublet to the f^0 singlet, and only Γ_8 symmetry partial wave states will mix the f^1 and f^2 doublets.

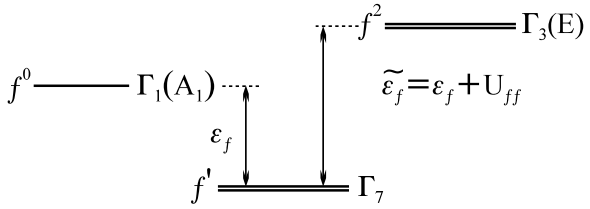

Figure 15: Simplest model for Ce^{3+} ions to produce the two-channel Kondo effect. This requires three configurations, since the $f^0 - f^1$ only model will always produce a single channel Kondo model. The virtual charge fluctuations to the Γ_3 doublet of the f^2 configuration induce a two-channel coupling of the ground Γ_7 doublet in the f^1 configuration to the Γ_8 conduction electrons. In that case, the spin index of the electrons is their magnetic spin, and the channel index is the quadrupolar/orbital pseudo-spin of the conduction states.

The Anderson Hamiltonian describing this restricted Hilbert space is much longer than for the uranium ion of the previous subsection, and is given by

$$H = H_{c7} + H_{c8} + H_{ion} + H_{771,mix} + H_{378,mix} \tag{2.2.28}$$

where

$$H_{c7} = \sum_{k,\mu} \epsilon_{\vec{k}} c^\dagger_{k7\mu} c_{k7\mu} \quad , \tag{2.2.29.a}$$

$$H_{c8} = \sum_{k,\alpha,\mu} \epsilon_{\vec{k}} c^\dagger_{k8\alpha\mu} c_{k8\alpha\mu} \quad , \tag{2.2.29.b}$$

$$H_{ion} = \epsilon_f \sum_\mu |f^1\Gamma_7, \mu >< f^1\Gamma_7, \mu| + (2\epsilon_f + U_{ff}) \sum_\alpha |f^2\Gamma_3, \alpha >< f^2\Gamma_3, \alpha| \quad , \tag{2.2.29.c}$$

$$H_{771,mix} = \frac{V_{17}}{\sqrt{N_s}} \sum_{k\mu} (|f^1\Gamma_7, \mu >< f^0, \Gamma_1| c_{k7\mu} + h.c.) \quad , \tag{2.2.29.d}$$

and

$$H_{378,mix} = \frac{-V_{37}}{\sqrt{N_s}} \sum_{k,\mu,\alpha} sgn(\mu) (|f^2\Gamma_3, \alpha >< f^1\Gamma_7, -\mu| c_{k8\alpha\mu} + h.c.) \quad . \tag{2.2.29.e}$$

Again, the phase factor which appears in the last equation derives from the proper admixture of f^2 states with states of one f and one conduction electron.

Schrieffer-Wolff transformation. Once again, we apply the Schrieffer-Wolff transformation [Schrieffer and Wolff, 1965; Schrieffer, 1967; Coqblin and Schrieffer, 1969] to convert the Anderson Hamiltonian of Eq. (2.2.29a-e) into a Kondo Hamiltonian. This transformation will produce a valid description of the low energy scale physics provided that $N(0)V_{17}^2/|\epsilon_f| = w_0 << 1$ and $N(0)V_{37}^2/\tilde{\epsilon}_f = w_2 << 1$, with $\tilde{\epsilon}_f = \epsilon_f + U_{ff}$ as in the previous subsection. The significance of the labels w_0, w_2 is that these are essentially the quantum weights of f^0, f^2 configurations in the ground state due to charge fluctuations. Provided the inequalities hold, we have the effective Kondo Hamiltonian

$$H_{Kondo} = H_{c7} + H_{c8} + J_7 \vec{S}_I \cdot \vec{S}_{c7}(0) + J_8 \vec{S}_I \cdot (\vec{S}_{c8+}(0) + \vec{S}_{c8-}(0)) \tag{2.2.30}$$

with $J_7 = 2V_7^2/\epsilon_f > 0$, $J_8 = 2V_8^2/\tilde{\epsilon}_f > 0$ and, e.g.,

$$S_I^{(i)} = \sum_{\mu\mu'} S_{\mu\mu'}^{(i)} |f^1\Gamma_7, \mu >< f^1\Gamma_7, \mu'| \quad , \tag{2.2.31}$$

$$S_{c7}^{(i)}(0) = \frac{1}{N_s} \sum_{k,k',\mu,\mu'} S_{\mu,\mu'}^{(i)} c_{k7\mu}^\dagger c_{k'7\mu'} \quad , \tag{2.2.32}$$

and

$$S_{c8\alpha}^{(i)}(0) = \frac{1}{N_s} \sum_{k,k',\mu,\mu'} S_{\mu,\mu'}^{(i)} c_{k8\alpha\mu}^\dagger c_{k'8\alpha\mu'} \quad . \tag{2.2.33}$$

Here, $S_{\mu,\mu'}^{(i)}$ are spin-1/2 matrices living in the Γ_7 space, with $i = x, y, z$. The exchange couplings in Eq. (2.2.30) are antiferromagnetic.

The first Kondo term in Eq. (2.2.30) involving J_7 is no surprise–it just reflects the effective exchange interaction mediated by virtual charge fluctuations to the excited empty configuration. This coupling yields the standard physics incorporated in the $U_{ff} \to \infty$ large N_I theories, with $N_I = 2$ here. This term, if J_8 were set to zero, would produce a singlet ground state and Fermi liquid excitation spectrum by the standard methods. The second term (J_8) is of course more interesting and has a two-channel character, with the channel indices here being the local $\Gamma_3(E)$ orbital labels. (Again, two degenerate bands throughout the Brillouin zone are not required–only local degeneracy is necessary to map to the two-channel Kondo effect.) As we shall show explicitly in later sections, provided $|J_8| > |J_7|$, which practically corresponds to $w_2 > w_0$, the two-channel physics will dominate the low temperature behavior. An intriguing third possibility exists when $J_8 = J_7$: the physics of the three channel Kondo model will be realized. While this requires fine tuning of the coupling strengths, it is in fact potentially realizable with the application of pressure, as we shall discuss in detail in the review of experiments (Sec. 8.2).

It is worth noting at this point that the two-channel behavior is unlikely for Yb^{3+} ions because of the requirement $|J_8| > |J_7|$. Yb^{3+} has a single $4f$ hole (f^{13}) and excited f^{14} (no hole) and f^{12} (two hole) configurations. Once the particle-hole mapping is effected, the physics is completely analogous to the Ce case. However, the details are different. First, since for Yb^{3+} the Hunds' rules ground state has angular momentum $J = 7/2$, either Γ_6 or Γ_7 doublets may lie lowest, besides the Γ_8 quartet [Lea, Leask, and Wolff, 1962]. This is not of concern, since $\Gamma_6 \otimes \Gamma_3(E) = \Gamma_8$ as well as if the Γ_7 doublet lies lowest in energy. More significant is that previous studies have indicated that $|\epsilon_f| << |\epsilon_f + U_{ff}|$ (these are now *hole* energies) for Yb [Herbst and Wilkins, 1987; Lang *et al.*, 1981], so that it will be difficult to ever realize $w_2 > w_0$.

Effects of excited states in the f^2 configuration

There are several consequences which arise from including excited states in the f^2 configuration. This discussion follows primarily the work of Kim [Kim, 1995; Kim and Cox, 1995; Kim and Cox, 1996; Kim and Cox, 1997; Kim, Oliveira and Cox, 1996] and Koga and Shiba [1995] who applied a similar analysis to a model with an $f^3\Gamma_6$ ionic ground state. The effects are as follows:

1) Enhancement of two-channel coupling. The two-channel antiferromagnetic coupling mediated by excited state Γ_3 states is enhanced when one accounts for the presence of nine such excited states. However, this can be reduced somewhat by the excited state triplets, which contribute negatively to the two-channel coupling. In the work of Koga and Shiba [1995] for the $f^3\Gamma_6$ ground state, it was found that the net two-channel coupling arising from the f^2 configuration is antiferromagnetic.

2) Reduction of one-channel coupling While excited state singlets contribute to an enhancement of the antiferromagnetic one-channel coupling that is already present due to $f^0 - f^1$ virtual charge fluctuations, the excited triplet states suppress this coupling strength. In their $f^3\Gamma_6$ model, Koga and Shiba [1995]

find a net ferromagnetic coupling of the Γ_6 pseudo-spin to the conduction Γ_7 states.
3) $\Gamma_7 - \Gamma_8$ *exchange coupling.* The presence of excited state Γ_4 triplet states can give rise to exchange interactions which scatter electrons between the Γ_7 and Γ_8 partial wave channels. The terms are rather complicated to write down.
4) Channel-spin/spin coupling in the Γ_8 *sector.* Both excited state Γ_4 and Γ_5 triplets can mediate a new coupling term in which the conduction spin and channel spin can couple. To understand why such a term exists, we note that $\Gamma_8 \otimes \Gamma_8$ tensor space of the conduction states contains two Γ_4 symmetry tensor triplets[Kim, 1994;Kim and Cox,1995a,1995b,1996; Kim, Oliveira, and Cox, 1996]. The first transforms as a scalar under quadrupolar indices and couples to the Γ_7 doublet with the usual two-channel form. The second transforms as an outer product of quadrupolar pseudo-spin and magnetic pseudo-spin operators. These operators have the form

$$\tilde{S}^i_{c8}(0) = \tilde{\tau}^i_{c8}(0) S^i_{c8}(0) \tag{2.2.34}$$

with $i = x, y, z$, the S^i_c being spin 1/2 magnetic pseudo-spin matrices for the Γ_8 states, and the $\tau^i_{c8}(0)$ are suitable combinations of quadrupolar spin 1/2 matrices given by

$$\tau^z_{c8}(0) = \tau^{(3)}_{c8}(0) \tag{2.2.35.a}$$

$$\tau^x_{c8}(0) = -\frac{1}{2}\tau^{(3)}_{c8}(0) + \frac{\sqrt{3}}{2}\tau^{(1)}_{c8}(0) \tag{2.2.35.b}$$

$$\tau^y_{c8}(0) = -\frac{1}{2}\tau^{(3)}_{c8}(0) - \frac{\sqrt{3}}{2}\tau^{(1)}_{c8}(0) \quad . \tag{2.2.35.c}$$

Note that these τ matrices obey a traceless condition, *viz.*, $\sum_i \tau^i_{c8}(0) = 0$. As an example of the tensor product, we write out $\tilde{S}^z_{c8}(0)$ as

$$\tilde{S}^z_{c8}(0) = c^\dagger_{8\uparrow+} c_{8\uparrow+} - c^\dagger_{8\uparrow-} c_{8\uparrow-} - c^\dagger_{8\downarrow+} c_{8\downarrow+} + c^\dagger_{8\downarrow-} c_{8\downarrow-} \quad . \tag{2.2.36}$$

For further purposes in Sec. 3, we note that these operators obey the commutation relations

$$[\tilde{S}^i_{c8}(0), \tilde{S}^j_{c8}(0)] = \frac{-i}{2}\epsilon_{ijk} S^k_{c8}(0) = \frac{-i}{2}\epsilon_{ijk} \sum_{alpha} S^k_{c8\alpha}(0) \tag{2.2.37}$$

and

$$[\tilde{S}^i_{c8}(0), S^j_{c8}(0)] + [S^i_{c8}(0), \tilde{S}^j_{c8}(0)] = -i\epsilon_{ijk}\tilde{S}^k_{c8}(0) \quad . \tag{2.2.38}$$

The latter relation, while not immediately evident, follows with application of the tracelessness condition on the τ^i_{c8} matrices. The corresponding coupling to the Γ_7 pseudo-spin has the form

$$\tilde{H}_{78} = \tilde{J}_8 \vec{S}_I \cdot \vec{\tilde{S}}_{c8}(0) \quad . \tag{2.2.39}$$

Koga and Shiba [1995] discuss a related model for f^3 states. Indeed, in Sec. 4.2 of their paper, the exchange Hamiltonian of Eqs. (4.19), (4.20) has the form of $H_{78} + \tilde{H}_{78}$ provided we neglect exchange interactions which scatter between Γ_7 and Γ_8 conduction states. Specifically, we replace our Γ_7 spin operators with Koga and Shiba's Γ_6 spin operators, and we can identify $J_7 = -J_0/3 - 19J_1/63$, $J_8 = 2J_0/3 + 49J_1/126$, and $\tilde{J}_8 = -10J_1/63$.

We will argue in Sec. 3.4.3 that provided $\tilde{J}_8$ is sufficiently small ($|\tilde{J}_8| < 2J_8$) it is irrelevant and the low temperature fixed point will still be that of the two-channel model when J_8 exceeds J_7. However, interesting new physics arises when $|\tilde{J}_8| > J_8$. Kim [1995] has observed that the special combination

of operators $I^{(i)}_{c8} = -\sum_\alpha S^{(i)}_{c8\alpha}(0) \pm 2\tilde{S}^{(i)}_{c8}(0)$ obey the standard $SU(2)$ angular momentum algebra [Kim, 1995; Kim, Oliveira, and Cox 1996]. Since they span a fourfold degenerate manifold, it is natural to guess that they serve as spin 3/2 operators. Indeed, with simple algebraic manipulations, one can show the $I^{(i)}$ operators are those of a spin 3/2 manifold. A combination of strong coupling perturbation theory, weak coupling scaling analysis, NRG calculations, and conformal field theory confirm that for $|\tilde{J}_8| > J_8$, the model flows to fixed points governed by an exchange coupling between the spin 1/2 impurity and spin 3/2 conduction electrons [Kim, Oliveira, and Cox, 1996]. Kim has observed that the form of this Hamiltonian can be obtained by keeping only an excited Γ_4 or Γ_5 triplet state in the f^2 configuration. While there is only a single channel of conduction spin, the ground state is overcompensated because of the large conduction spin. Hence, a different non-Fermi liquid fixed point is possible. We defer a more complete discussion of this issue to Sec. 6.3.2.

In summary, in this subsection we have demonstrated that when one includes the possibility of fluctuations to a realistic f^2 configuration which includes degenerate levels, a Ce impurity in cubic symmetry may have low temperature physics governed by the two-channel Kondo Hamiltonian (or, alternatively, a novel $S_c = 3/2$ model). However, to ensure this, the fluctuation weight of f^2 in the ground state must exceed that of f^0, so it is by no means the generic case.

2.2.3 Excited Crystal Field States

For both the Ce^{3+} and U^{4+} models discussed above, we have excluded excited crystal field levels in the lowest configurations. In fact, it is straightforward to include these in the Hamiltonian, and we shall show in detail that the low energy scale physics will still map onto the two-channel Kondo physics in the appropriate limit when we discuss the NCA approach to the problem (see Secs. 6.2,6.3). The situation is similar to the TLS with excited states which is discussed in detail in Sec. 3.4.2.

For the f^2 configuration, the additional states in the lowest $J = 4$ multiplet are $|f^2, \Gamma_4, \eta >$, $|f^2, \Gamma_5, \epsilon >, |f^2, \Gamma_1 >$. To the diagonal f^2 terms of Eqs. (2.2.19) and (2.2.29.c), we must add

$$\sum_{\Gamma_{cef},\eta_{cef}} (E(\Gamma_3) + \Delta_{\Gamma_{cef}})|f^2, \Gamma_{cef}, \eta_{cef} >< f^2, \Gamma_{cef}, \eta_{cef}| \tag{2.2.40}$$

where Γ_{cef}, η_{cef} run over the excited crystal field levels split from the ground $\Gamma_3(E)$ doublet by amounts $\Delta_{\Gamma_{cef}}$, and $E(\Gamma_3)$ is the energy of the Γ_3 level ($\tilde{\epsilon}_f$ for the U^{4+} model; $2\epsilon_f + U_{ff}$ for the Ce^{3+} model). η_{cef} indexes the states of any degenerate multiplets. The cef subscript is a reminder that these are states in the presence of the crystalline electric field (CEF). For the f^1 configuration, retaining only the $J = 5/2$ multiplet, the only excited level is a Γ_8 quartet, so to Eqs. (2.2.19) and (2.2.26.c) we must add

$$\sum_{\eta_8} (E(\Gamma_7) + \Delta_{\Gamma_8})|f^1, \Gamma_8, \eta_8 >< f^1, \Gamma_8, \eta_8| \tag{2.2.41}$$

where $E(\Gamma_7)$ is the energy of the Γ_7 level (0 for the U^{4+} model; ϵ_f for the Ce^{3+} model). In the above two equations, the η labels run over internal states of degenerate crystal field manifolds.

We must also generalize the hybridization term. Focussing only on the term which mixes f^1, f^2 configurations, the most general form is

$$H_{hyb} = \frac{V}{\sqrt{N_s}} \sum_{\Gamma(f^1),\eta(f^1)} \sum_{\Gamma(f^2),\eta(f^2)} \sum_{k,\Gamma_c,\eta_c} \Lambda(\Gamma(f^1)\eta(f^1); \Gamma(f^2)\eta(f^2); \Gamma_c\eta_c) \times$$

$$[|f^2, \Gamma(f^2), \eta(f^2) >< f^1, \Gamma(f^1), \eta(f^1)| c_{k\Gamma_c,\eta_c} + h.c.] \tag{2.2.42}$$

where the sums run over all states of the lowest $f^{1,2}$ multiplets ($\Gamma(f^{1,2}), \eta(f^{1,2})$) and all conduction partial waves (Γ_c, η_c), and $\Lambda(\Gamma(f^1), \eta(f^1); \Gamma(f^2), \eta(f^2); \Gamma_c, \eta_c)$ contains the Clebsch-Gordan coefficient for the cubic irreps and the reduced matrix element measuring the strength by which the f^1 may attach

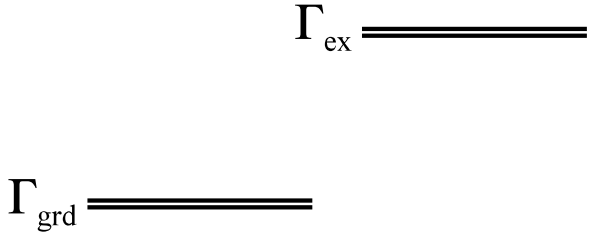

Figure 16: Simplest level scheme to produce a two-channel Kondo effect. The two-channel Kondo effect requires minimally that one have low lying configurations with doublets in each. These doublets may be magnetic (Kramers' doublet) or non-magnetic (non-Kramers' doublet) depending upon whether the configuration has an odd or even number of electrons.

to the $f^2, J = 4$ multiplet. This has been worked out extensively in the case of Russell-Saunders (LS) coupling of angular momentum, and the detailed presentation appears in Kim and Cox [1996].

Now, each crystal field level must be treated on equivalent dynamical footing, which means when we introduce Green's functions for the local levels, we must introduce a new Green's function for each excited crystal field level. We shall discuss in Sec. 3.4.2 how the excited states of the TLS corresponding to higher vibrational levels play a similar role to the crystal field levels here.

2.2.4 Group theory of two-channel Kondo models for Ce and U impurities

The purpose of this section is to state five selection rules which contain minimal necessary conditions requisite to have the low energy scale physics for a single U^{4+} or Ce^{3+} ion to be described by a two-channel Kondo model. We shall first produce a physical motivation for the selection rules, and then summarize the selection rules. This section is adopted from Cox [1993].

Fig. 16 displays the basic picture of the states of an impurity lanthanide/actinide ion and conduction electrons which are minimally required to achieve a two-channel Kondo model description of low energy scale physics. This restriction to two configurations is sufficient for $U^{4+}(5f^2)$ because the two lowest excited configurations must have odd numbers of electrons and therefore have at least doubly degenerate crystal field states. For definiteness, we assume the first excited configuration is f^1. For Ce^{3+}, we need to augment this picture to include three configurations as shown in Fig. 13 because the excited f^0 state must be a singlet.

Regardless, we see that two configurations of the impurity ion have doublets as the lowest crystal field states. These states span vector spaces which transform under the irreps $\Gamma_{grd}, \Gamma_{ex}$ of the group $\bar{G} \times \mathcal{T}$ where $\bar{G}$ is the double point group of the crystal and $\mathcal{T}$ is the group of time reversal (containing the identity and time reversal operators). The states in the $\Gamma_{grd,ex}$ spaces have labels $\alpha_{grd,ex}$. The extension to include $\mathcal{T}$ covers groups such as C_6 under which certain pairs of irreducible representations are complex singlets whose degeneracy is not assured by $\bar{G}$ but is assured by $\mathcal{T}$. The double group is required because one of the hybridizing configurations will always contain an odd number of electrons. The subscripts grd, ex refer to ground and excited configurations.

We express the conduction operator $c^\dagger_{\vec{k},\sigma}$ which creates a Bloch state of momentum $\vec{k}$, spin σ, and energy ϵ in a symmetry adapted basis around the impurity, i.e.,

$$c^\dagger_{\vec{k},\sigma} = \sum_{\Gamma_c,\alpha_c} a_{\Gamma_c,\alpha_c}(\epsilon_k) c^\dagger_{k\Gamma_c\alpha_c} \tag{2.2.43}$$

where Γ_c, α_c label irreps of $\bar{G} \times \mathcal{T}$ where the point group $\bar{G}$ is defined at the impurity site. The local conduction states are derived from partial waves in a plane-wave basis, or from suitable linear combinations of ligand orbitals in a tight-binding basis.

The Anderson Hamiltonian for U^{4+} ions then takes the form

$$H = H_{cond} + H_{grd} + H_{ex} + H_{mix} \tag{2.2.34}$$

with

$$H_{cond} = \sum_{k\Gamma_c\alpha_c} \epsilon_k c^\dagger_{k\Gamma_c\alpha_c} c_{k\Gamma_c\alpha_c} \tag{2.2.45}$$

$$H_{grd} = E(f^2) \sum_{\alpha_{grd}} |\Gamma_{grd}\alpha_{grd}><\Gamma_{grd}\alpha_{grd}| \tag{2.2.46}$$

$$H_{ex} = E(f^1) \sum_{\alpha_{ex}} |\Gamma_{ex}\alpha_{ex}><\Gamma_{ex}\alpha_{ex}| \tag{2.2.47}$$

and

$$H_{hyb} = \frac{1}{\sqrt{N_s}} \sum_k \sum_{\Gamma_c\alpha_c} \sum_{\alpha_{grd},\alpha_{ex}} V[\Gamma_c\alpha_c;\alpha_{grd};\alpha_{ex}][|\Gamma_{grd}\alpha_{grd}><\Gamma_{ex}\alpha_{ex}|c_{k\Gamma_c\alpha_c} + h.c.] \tag{2.2.48}$$

where $V[\Gamma_c\alpha_c;\alpha_{grd};\alpha_{ex}]$ includes the single particle matrix element, a reduced matrix element expressing the attachment probability for adding an f electron to get this f^2 state from this f^1 state, and a Clebsch-Gordan coefficient in the crystal field representation basis. Again, the restriction to f^1 for the excited configuration is purely a matter of convenience for the exposition purposes here. In fact it is sometimes more realistic to consider an excited f^3 configuration.

For the Ce^{3+} ions, we interchange ground and excited levels and (with $E(f^0)$ set at zero in this case) add the hybridization term

$$\frac{V_0}{\sqrt{N_s}} \sum_{\epsilon\alpha_{grd}} [|\Gamma_{grd}\alpha_{grd}><f^0|c_{\epsilon\Gamma_{grd}\alpha_{grd}} + h.c.] \quad . \tag{2.2.49}$$

In addition to discussing the symmetry properties of the states themselves, it is important to discuss the symmetry properties of the ground configuration tensor operators which live in the product space transforming according to $\Gamma^{ket}_{grd} \otimes \Gamma^{bra}_{grd}$. The superscripts are a reminder that the tensors are formed from outer products of the states. The form of the low energy scale interactions which will correspond to the two-channel coupling of Eq. (2.2.22) are entirely specified by the symmetry properties of these tensors. The interactions arise when we integrate out the virtual charge fluctuations to the excited configuration to derive an effective interaction between the conduction electrons and the ground configuration degrees of freedom of magnitude $\sim V^2/\Delta E$, where ΔE is the interconfiguration energy difference (Schrieffer and Wolff, [1966]). (Note: all notation for point group representations used in this paper follow those of Koster *et al.* [1963].)

We now state the *necessary* (and not sufficient) selection rules which will minimally ensure that the effective Hamiltonian at low energy scales derived from an underlying Anderson Hamiltonian has the two-channel $S = 1/2$ Kondo form:

Selection Rule 1 (Ground Doublet Selection Rule): Under the action of the crystal field, the lowest state of the lowest angular momentum multiplet of the ground configuration should be a degenerate doublet which transforms as the irrep Γ_{grd} of the group $\bar{G} \times \mathcal{T}$.

Selection Rule 2 (Excited Doublet Selection Rule): Under the action of the crystal field, the lowest state of the lowest lying angular momentum of the excited configuration must be a degenerate doublet transforming as a representation Γ_{ex} of the group $\bar{G} \times \mathcal{T}$.

Selection Rule 3 (Hybridization Selection Rule): The conduction band must contain states which, when projected to the impurity site, transform as the direct product representation Γ_c such that $\Gamma_c = \Gamma_{grd} \otimes \Gamma_{ex}$.

Corollary Selection Rule 4 (Tensor Selection Rule): When Γ_c is a reducible representation of the group $\bar{G}\times\mathcal{T}$ of the form $\Gamma_c = \Gamma_{c1}\oplus\Gamma_{c2}$ where $\Gamma_{c1,2}$ are irreducible doublet representations of $\bar{G}\times\mathcal{T}$, then the tensors $\Gamma^{ket}_{grd}\otimes\Gamma^{bra}_{grd}$ which are off diagonal in the Γ_{grd} space must be contained in the space of the product representation $\Gamma_{c1}\otimes\Gamma_{c2}$ and not in $(\Gamma_{c1}\otimes\Gamma_{c1})\oplus(\Gamma_{c2}\otimes\Gamma_{c2})$.

Selection Rule 5 (Dynamic selection rule): When Γ_{grd} is the lowest level of an odd number electron configuration, the exchange coupling generated by virtual excitations to Γ_{ex} must be larger than the coupling induced by virtual charge fluctuations to excited singlet states.

Selection Rule 1 ensures that the lowest impurity states have internal degrees of freedom so that a Kondo effect is possible. Selection Rules 2,3 are necessary for two-channel behavior in conjunction with Rule 1. The excited doublet state labels *are* the channel indices, and if the conduction band doesn't have local $\Gamma_c = \Gamma_{grd}\otimes\Gamma_{ex}$ symmetry states, no Kondo effect is possible.

The basis for Corollary Selection Rule 4 is an examination of the tensor operator structure. This rule is irrelevant for cubic structure because the irreducible Γ_8 representation is the only quartet of conduction states allowed for the Γ_3 and $\Gamma_{6,7}$ doublets of the different configurations. It is essential for the lower symmetry crystal syngonies. To see why, note that we form the exchange term of Eq. (1) by coupling tensors of the impurity states Γ_{grd} to those with the same symmetry derived from the conduction states $\tilde{\Gamma}_c$. In the lower symmetry syngonies of interest (hexagonal, tetragonal, rhombohedral) $\tilde{\Gamma}_c$ is reducible, decomposing into $\Gamma_{c1}\oplus\Gamma_{c2}$. The magnitude and antiferromagnetic sign are set by the integration out of virtual fluctuations to the Γ_{ex} states; hence, as in the conventional Anderson impurity, the exchange $J<0$ always. Now, the tensor operators forming the basis for $\Gamma^{ket}_{grd}\otimes\Gamma^{bra}_{grd}$ include two which are diagonal in the Γ_{grd} indices and two which are off-diagonal corresponding to $S_I^{(1,2)}$ in the pseudo-spin 1/2 space. The identity operator in the Γ_{grd} space gives charge scattering, while the other diagonal term corresponds to the $S_I^{(3)}$ component of the impurity pseudo-spin. This is always contained in both the tensor spaces $\Gamma^{ket}_{c1}\otimes\Gamma^{bra}_{c1}$ and $\Gamma^{ket}_{c2}\otimes\Gamma^{bra}_{c2}$. If the off-diagonal impurity operators were contained in these tensor product spaces, then no symmetry conditions would ensure the exact equality of exchange coupling constants between the channels (now indexed simply by the irreducible representation labels $\Gamma_{c1,2}$). This is *always* the case in rhombohedral symmetry, so that two-channel coupling will not be generically present in this case for f-ions. However, if the off-diagonal operators are contained in the mixed-direct product $\Gamma^{ket}_{c1}\otimes\Gamma^{bra}_{c2}$, then the "spin-flip" conduction tensors must mix states of the two doublets, and the channel degeneracy is automatically ensured.

With regard to the conduction tensor operators, we note that only the case of the Ce^{3+} ion in cubic symmetry gives rise to the additional pseudo-spin tensor, such as appears in Eq. (2.2.36). For all other cases, the relevant pseudo-spin tensors of the conduction electrons appear only once.

Strictly speaking, Corollary Section Rule 4 is redundant given rules 1,2, and 3 in that for the assumed ground doublets of the lowest configurations and appropriate conduction hybridization, the presence of the appropriate conduction tensors is guaranteed (Han [1995]). However, the physical importance of this rule leads us to state it precisely here as a corollary to these first three rules.

Table 4 specifies all the possible two-channel $S=1/2$ combinations of $\Gamma_{grd},\Gamma_{ex},\Gamma_c$ states for U^{4+} and Ce^{3+} ions. We note that a split doublet could display two-channel behavior above a crossover scale below T_0. Tables 5 and 6 summarize all the relevant tensor operators for impurity doublet states and conduction states together with their transformation properties in analogy to spherical harmonics. These tables give information about their multipole content as well.

Each of the tensors discussed in preceding paragraphs corresponds to some multipole moment tensors of the ion. Since the multipole formalism is very physical and familiar from electromagnetism and elementary quantum theory, it is worth exploring this connection further.

The matrix elements of multipole tensors of $l-th$ rank in first quantized notation are given by

$$<\eta|\hat{O}_{l,m}|\eta'>\sim\int d^3r\psi^*_\eta(\vec{r})r^lY_{l,m}(\hat{r})\psi_{\eta'}(\vec{r})$$

Ion	Ground Config.	Point Group	Γ_{grd}	Γ_{ex}	Conduction Quartet
U^{4+}	$5f^2(J=4)$	Cubic(O)	$\Gamma_3(E)$	Γ_7	$\Gamma_8=\Gamma_3\otimes\Gamma_7$
U^{4+}	$5f^2(J=4)$	Hexag.(D_6)	$\Gamma_5(E_1)$	Γ_7	$\Gamma_7\oplus\Gamma_9$
				Γ_8	$\Gamma_8\oplus\Gamma_9$
				Γ_9	$\Gamma_7\oplus\Gamma_8$
			$\Gamma_6(E_2)$	Γ_7	$\Gamma_8\oplus\Gamma_9$
				Γ_8	$\Gamma_7\oplus\Gamma_9$
				Γ_9	$\Gamma_7\oplus\Gamma_8$
U^{4+}	$5f^2(J=4)$	Tetrag.(D_4)	$\Gamma_5(E)$	Γ_6 or Γ_7	$\Gamma_7\oplus\Gamma_6$
U^{4+}	$5f^2(J=4)$	Tetrag.(D_4)	$\Gamma_1(A_1)\oplus\Gamma_3(B_1)$	Γ_7	$\Gamma_7\otimes(\Gamma_1\oplus\Gamma_3)$
Ce^{3+}	$4f^1(J=5/2)$	Cubic(O)	Γ_7	Γ_3	Γ_8
Ce^{3+}	$4f^1(J=5/2)$	Hexag(D_6)	Γ_9	Γ_5 or Γ_6	$\Gamma_6\oplus\Gamma_7$

Table 4: Symmetries of ground, excited, and conduction states for two-channel Kondo models of U^{4+} and Ce^{3+} ions. The ionic configuration is listed in the second column, with the Hunds' rules ground angular momentum in parentheses. The crystal point symmetry is in the third column; though we choose the most symmetric group from each syngony, equivalent results are found for all smaller point groups in the given syngony. The fourth column lists the ground doublet Γ_{grd}, the fifth column the doublet of the excited configuration in the simplest model Γ_{ex}, and the last column the symmetry of the conduction quartet which mixes the levels and screens the moment of the ground doublet.

Ion	Point Group	Γ_{grd}	(1)	(2)	(3)
U^{4+}			$\tau_I^{(1)}$	$\tau_I^{(2)}$	$\tau_I^{(3)}$
	O	$\Gamma_3(E)$	$\Gamma_3(+)[Y_{2,2}+Y_{2,-2}]$ $J_x^2-J_y^2$	$\Gamma_2[Y_{3,2}+Y_{3,-2}]$ $J_xJ_yJ_z$	$\Gamma_3(-)[Y_{2,0}]$ $3J_z^2-J^2$
	D_6	$\Gamma_5$orΓ_6	$\Gamma_6(1)[Y_{2,-2}+Y_{2,2}]$ $J_x^2-J_y^2$	$\Gamma_6(2)[Y_{2,2}-Y_{2,-2}]$ $J_xJ_y+J_yJ_x$	$\Gamma_2[\alpha Y_{3,0}+\beta Y_{1,0}]$ $\rho J_z^3+\gamma J_z$
	D_4	Γ_4	$\Gamma_3[Y_{2,-2}+Y_{2,2}]$ $J_x^2-J_y^2$	$\Gamma_4[Y_{2,2}-Y_{2,-2}]$ $J_xJ_y+J_yJ_x$	$\Gamma_2[\alpha Y_{3,0}+\beta Y_{1,0}]$ $\rho J_z^3+\gamma J_z$
	D_4	$\Gamma_1\oplus\Gamma_3$	$\Gamma_3[Y_{2,2}+Y_{2,-2}]$ $J_x^2-J_y^2$	$\Gamma_3[Y_{3,2}+Y_{3,-2}]$ $J_xJ_yJ_z$	$\Gamma_1[Y_{2,0}]$ $3J_z^2-J^2$
Ce^{3+}			$S^{(1)}$	$S^{(2)}$	$S^{(3)}$
	O	Γ_7	$\Gamma_4(1)[Y_{1,1}-Y_{1,-1}]$ J_x	$\Gamma_4(2)[Y_{1,1}+Y_{1,-1}]$ J_y	$\Gamma_4(3)[Y_{1,0}]$ J_z
	D_6	Γ_9	$\Gamma_3[Y_{3,3}-Y_{3,-3}]$ $J_y^3-3J_yJ_x^2$	$\Gamma_4[Y_{3,-3}+Y_{3,3}]$ $J_x^3-3J_xJ_y^3$	$\Gamma_2[Y_{1,0}]$ J_z

Table 5: Tensors of the local pseudo-spin for model U^{4+} and Ce^{3+} impurities. The operators indices correspond to the $1,2,3$ labels of the pseudo-spin operators. Their symmetry label for the appropriate group is the first label, and in square braces appears the "multipole content", i.e., which set of spherical tensor operators $Y_{l,m}(\vec{J})$ regarded as polynomials in the angular momentum corresponds to dominant term in the crystalline tensor. For the hexagonal and tetragonal cases involving Γ_5,Γ_6 (hex.) and Γ_4 (tet.) doublets, the $\tau^{(3)}$ operator is predominantly octupolar ($l=3$), with a weak dipolar admixture, so that $\beta >> \alpha$. Beneath each tensor symmetry, we display the corresponding cartesian form in polynomials of the angular momentum operator.

Ion	Pt. Group	Conduction Quartet	Conduction Tensors		
U^{4+}			$\tau_c^{(1)}(0)$	$\tau_c^{(2)}(0)$	$\tau_c^{(3)}(0)$
	O	$\Gamma_8 = \Gamma_7 \otimes \Gamma_3$	$\Gamma_1^{7\times7} \otimes \Gamma_3^{3\times3}(+)$	$\Gamma_1^{7\times7} \otimes \Gamma_2^{3\times3}$	$\Gamma_1^{7\times7} \otimes \Gamma_3^{3\times3}(-)$
	D_6	$\Gamma_7 \oplus \Gamma_8$	$\Gamma_6^{7\times8}(1) + h.c.$	$\Gamma_6^{7\times8}(2) + h.c.$	$\Gamma_2^{7\times7} + \Gamma_2^{8\times8}$
		$\Gamma_7 \oplus \Gamma_9$	$\Gamma_6^{7\times9}(1) + h.c.$	$\Gamma_6^{7\times9}(2) + h.c.$	$\Gamma_2^{7\times7} + \Gamma_2^{9\times9}$
		$\Gamma_9 \oplus \Gamma_8$	$\Gamma_6^{9\times8} \oplus (1) + h.c.$	$\Gamma_6^{9\times8}(2) + h.c.$	$\Gamma_2^{9\times9} + \Gamma_1^{8\times8}$
	D_4	$\Gamma_7 \oplus \Gamma_6$	$\Gamma_5^{7\times6}(1) + h.c.$	$\Gamma_5^{7\times6}(2) + h.c.$	$\Gamma_2^{7\times7} + \Gamma_2^{6\times6}$
		$\Gamma_7 \otimes (\Gamma_1 \oplus \Gamma_3)$	$\Gamma_1^{7\times7} \otimes \Gamma_3^{3\times1}$	$\Gamma_1^{7\times7} \otimes \Gamma_3^{3\times1}$	$\Gamma_1^{7\times7} \otimes (\Gamma_1^{3\times3} - \Gamma_1^{1\times1})$
Ce^{3+}			$S_c^{(1)}(0)$	$S_c^{(2)}(0)$	$S_c^{(3)}(0)$
	O	$\Gamma_8 = \Gamma_3 \otimes \Gamma_7$	$\Gamma_1^{3\times3} \otimes \Gamma_4^{7\times7}(x)$	$\Gamma_1^{3\times3} \otimes \Gamma_4^{7\times7}(y)$	$\Gamma_1^{3\times3} \otimes \Gamma_4^{7\times7}(z)$
	D_6	$\Gamma_7 \oplus \Gamma_8$	$\Gamma_3^{7\times8} + h.c.$	$\Gamma_4^{7\times8} + h.c.$	$\Gamma_2^{7\times7} + \Gamma_1^{8\times8}$

Table 6: Tensors of Conduction States. This table enumerates the symmetries of conduction tensors which may couple to the impurity (quadrupolar if U^{4+} , magnetic if Ce^{3+} ; see Table 2.3 for further information on the impurity tensors). The meaning of a superscript 3×3 for example, means that this operator is formed from the tensor (outer) product of Γ_3 bra and ket states.

$$\sim < \eta | [Y_{l,m}(\vec{J})] | \eta' > \tag{2.2.50}$$

where η, η' label states of the ion, and the second line follows from the Wigner-Eckart theorem. With regard to $[Y_{l,m}(\vec{J})]$, it is to be understood that: (i) the square braces indicate symmetrized combinations of the angular momentum operator components J^i, (ii) each time a particular direction cosine $\hat{i}$ appears in the explicit polynomial expansion of $Y_{l,m}$ one should insert J^i and properly symmetrize, and (iii) each time a power of $(J^i)^{l-p}$, with $p < l$ even, appears in the polynomial expansion of $Y_{l,m}$ one should multiply that term by a factor of factor of $[J(J+1)]^{p/2}$.

As an example of the use of multipole terminology, consider the $\Gamma_3(E)$ doublet of a U ion in cubic symmetry. The $\Gamma_1(A_1)$ tensor is of predominant monopole (charge, $l = 0$) character, but also contains components of fourth rank (hexadecapole, $l = 4$) as well as sixth rank (l=6) multipoles. The $\Gamma_3(E)$ doublet is of predominant quadrupolar ($l = 2$) character. It is a generic fact that one of the three non-trivial tensors formed from the quadrupolar doublets, in this case the $\Gamma_2(A_2)$ tensor, will be odd under time reversal. The predominant multipole character of the $\Gamma_2(A_2)$ singlet tensor is octupolar ($l = 3$). Hence, a non-zero expectation value to this operator will correspond to a combined lattice distortion and non-vanishing magnetic moment. The operator will couple to the third power of the magnetic field, or a combined product of electrical field gradient (uniaxial stress) and magnetic field.

The multipole character of the relevant tensor operators is summarized in Table 7.

In the lower symmetry cases, one can see that the diagonal pseudo-spin operator for the U ions has predominant octupole character, with a weak admixture of magnetic dipole character. The transverse operators, which are essential for the Kondo effect, have predominantly quadrupolar character. This justifies the labelling of the two-channel Kondo effect in these circumstances as quadrupolar. For the Γ_9 Ce doublet in hexagonal symmetry, it is interesting that the transverse operators must exchange three units of angular momentum and hence have predominantly octupolar character. Hence, it is perhaps most appropriate to label the Kondo effect in this case as an "octupolar" Kondo effect!

We now return to a discussion of the selection rules. Selection Rule 5 follows from scaling along the lines of Nozières and Blandin [1980], and from NCA analysis for the model Ce^{3+} ion (Cox [1993]; Kim, [1995]; Kim and Cox [1995a,b]). Specifically, we define two crossover temperatures $T_x^{(I,II)}$ where the superscript refers to single or two-channel crossover. Consider the case in cubic symmetry, with

Irred. Rep.	Dim.	Labels	J-basis	Spherical Basis
$\Gamma_1(A_1)$	1	-	$J(J+1)$	$Y_{0,0}$
$\Gamma_2(A_2)$	1	-	$J_xJ_yJ_z$	$Y_{3,3}(\vec{J})+Y_{3,-3}(\vec{J})$
$\Gamma_3(E)$	2	$\Gamma_3(+)$	$J_x^2-J_y^2$	$Y_{2,2}(\vec{J})+Y_{2,-2}(\vec{J})$
		$\Gamma_3(-)$	$3J_z^2-J(J+1)$	$Y_{2,0}(\vec{J})$
$\Gamma_4(T_1)$	3	$\Gamma_4(x)$	J_x	$Y_{1,1}(\vec{J})-Y_{1,-1}(\vec{J})$
		$\Gamma_4(y)$	J_y	$Y_{1,1}(\vec{J})+Y_{1,-1}(\vec{J})$
		$\Gamma_4(z)$	J_z	$Y_{1,0}(\vec{J})$
$\Gamma_5(T_2)$	3	$\Gamma_5(xz)$	$\{J_x,J_z\}$	$Y_{2,1}(\vec{J})+Y_{2,-1}(\vec{J})$
		$\Gamma_5(yz)$	$J_yJ_z+J_zJ_y$	$Y_{2,1}(\vec{J})-Y_{2,-1}(\vec{J})$
		$\Gamma_5(xy)$	$J_xJ_y+J_yJ_x$	$Y_{2,2}(\vec{J})-Y_{2,-2}(\vec{J})$

Table 7: Table of second rank tensor operators for U^{4+} and Ce^{3+} ions in cubic symmetry (point group O). The first column gives the label of the irreducible representation, the second column its dimensionality. The third column gives the label associated to the vectors spanning the space of the representation, and the fourth column gives a basis for the vector space in the Cartesian operator representation (or Qubic harmonics). Finally, the fourth column gives the corresponding basis in the spherical tensor language.

$\Gamma_{grd}=\Gamma_7$, $\Gamma_{ex}=\Gamma_3$, and $\Gamma_c=\Gamma_8$. Define dimensionless effective exchange coupling constants $\tilde{g}_7,\tilde{g}_8$ by

$$\tilde{g}_7=\frac{N(0)V_7^2}{E_0-E(f^0)} \quad ; \quad \tilde{g}_8=\frac{N(0)V_{37}^2}{E_0-E(f^2)} \tag{2.2.51}$$

where E_0 is the ground state energy, $N(0)$ is the conduction electron density of states, and $V_{17,37}$ the hybridization matrix elements with $\Gamma_{7,8}$ partial waves. The Kondo scale for the single channel model is $T_0^{(2)}\simeq D\exp(1/2\tilde{g}_7)$, and for the two-channel model is $T_0^{(2)}\simeq D\exp(1/2\tilde{g}_8)$ to leading exponential accuracy. As we shall explain in Sec. 5.2, for T below the crossover scale $T_{(1)}^x$

$$T_{(1)}^x\approx\frac{T_0^{(1)}}{3}|\frac{1}{\tilde{g}_8}-\frac{1}{\tilde{g}_7}|^{3/2} \tag{2.2.52}$$

single channel behavior will dominate for $|\tilde{g}_7|>|\tilde{g}_8|$. For T below the crossover scale $T_{(2)}^x$ given by

$$T_{(2)}^x\approx\frac{T_0^{(2)}}{2}|\frac{1}{\tilde{g}_7}-\frac{1}{\tilde{g}_8}|^2 \tag{2.2.53}$$

two-channel physics will dominate for $|\tilde{g}_8|>|\tilde{g}_7|$. Practically, this is tested by examining the sign of the thermopower, given the particle-hole asymmetry of the model. Dominant f^0-induced one-channel coupling will tend to produce positive thermopower, while dominant f^2-induced two-channel coupling will tend to produce a negative thermopower. For hexagonal symmetry, consider the D_6 point group for concreteness. Analogous arguments go through provided $\Gamma_{grd}=\Gamma_9\sim|\pm 3/2>$, and $\Gamma_{ex}=\Gamma_{5,6}$, with $\Gamma_c=\Gamma_7\oplus\Gamma_8$.

For Yb^{3+} ions with $\Gamma_{6,7}$ ground states in cubic symmetry or Γ_9 in hexagonal symmetry similar arguments go through, with $f^n\to f^{14-n}$. However, the very large $f^{12}-f^{13}$ splitting (order 10 eV) makes it unlikely that Selection Rule 5 can be satisfied (where we now require $w(f^{12})>w(f^{14})$).

U^{4+} ions with f^2 ground configurations have Hund's rules angular momentum $J=4$, so that non-Kramers doublets are possible. Consider the ground doublets for the hexagonal and tetragonal syngonies. All of these doublets have the property that the non-trivial diagonal operator transforms like the z-component of a real spin, while the off-diagonal elements are quadrupolar and contained only in direct products of two distinct irreps of local conduction states. The physical reason is simple, and

easily understood by considering states with $M_J = \pm 1$ pair of states in the presence of a crystal field Hamiltonian of pure axial character, viz $H_{cef} = \Delta_{cef}[3J_z^2 - J(J+1)]$. This term is even under time reversal and thus maintains doublet degeneracy of the ± 1 states. Hence, the non-trivial diagonal tensor is just $|1><1| - |-1><-1|$ which transforms like J_z as restricted to the doublet. The off diagonal tensor must change the angular momentum by two units, and hence must have quadrupolar character. Turning now to $\Gamma_{ex}, \Gamma_{c1,2}$ in the same axial field, we must have doublets of the form $\pm(2n+1)/2$, since the excited configuration has an odd number of electrons and the conduction states always transform as double valued representations which are descended from half integral angular momentum in the full isotropic symmetry. Hence, the off diagonal conduction tensors in a given representation can only change angular momentum by an *odd* number of units, and cannot 'flip' the impurity spin. However, it is possible to form tensors from the cross products $\Gamma_{c1} \otimes \Gamma_{c2}$ which can change the angular momentum index by two units. For example, for conduction states derived from $j = 5/2$ partial waves, the operator $|3/2><-1/2|$ changes the angular momentum by two units. Note that the results we have discussed are properties only of the representations, but easily illustrated in this pure axial limit.

From the discussion of the preceding paragraph it is apparent that any Kondo model derived from a degenerate doublet ground state of U^{4+} ions in hexagonal or tetragonal symmetry will be of the quadrupolar form, because the only degenerate levels in ground or excited states are doublets, time reversal guaranteeing the channel degeneracy (indexed by the excited state in effect). To make the idea more explicit, assume for definiteness that we have hexagonal D_6 point symmetry and $\Gamma_{grd} = \Gamma_5$, $\Gamma_{ex} = \Gamma_7$ in an excited f^1 configuration. This yields $\tilde{\Gamma}_c = \Gamma_5 \otimes \Gamma_7 = \Gamma_7 \oplus \Gamma_9$. Taking the simple axial crystal field model and using conduction plane waves in a $j = 5/2$ partial wave manifold, representative states in J, M_J form are $|\Gamma_5 \pm> = |4, \pm>$, $|\Gamma_7 \pm> = |5/2, \pm 1/2>$, and $|\Gamma_9 \pm> = |5/2, \pm 3/2>$. Let us reorganize the labelling of the conduction states. Define channel 1 as labelling the states created by the pair of operators $c^\dagger_{k\Gamma_7+}, c^\dagger_{k\Gamma_9-}$, and channel 2 as labelling the pair of states created by $c^\dagger_{k\Gamma_9+}, c^\dagger_{k\Gamma_7-}$. Now let α be the spin index, equal to $\pm$, and $\mu = 1, 2$ be the channel index. Denote channel spin operators by $\tau^{(i)}, i = 1, 2, 3$. Thus, for example, $c^\dagger_{k,+,1} = c^\dagger_{\Gamma_7+}$. By performing a Schrieffer-Wolff transformation, with the interconfiguration energy splitting given by $\epsilon_f = E(f^2\Gamma_5) - E(f^1\Gamma_7)$, we obtain the Kondo coupling

$$H_{Kondo} = -\frac{1}{N_s} \sum_{i,k,k',\alpha,\alpha',\mu} J^{(i)} S_I^{(i)} S^{(i)}_{\alpha,\alpha'} c^\dagger_{k\alpha\mu} c_{k'\alpha'\mu} - \frac{K}{N_s} S_I^{(3)} \sum_{k,k',\mu,\alpha} \tau^{(3)}_{\mu,\mu} c^\dagger_{k\alpha\mu} c_{k'\alpha\mu} \tag{2.2.54}$$

where $J^{(1,2)} = V_7 V_9/\epsilon_f$, $J^{(3)} = (V_7^2 + V_9^2)/2\epsilon_f$, and $K = (V_7^2 - V_9^2)/2\epsilon_f$. Here $V_{7,9}$ are the hybridization matrix elements coupling the $\Gamma_{7,9}$ conduction states to the impurity. Note that: i) this exchange Hamiltonian is intrinsically anisotropic but the diagonal ($J^{(3)}$) term is antiferromagnetic which is sufficient to ensure the Kondo effect, and (ii) this Hamiltonian has the peculiar term coupling diagonal spin and channel spin operators. These are not of concern, since it is now well established that exchange anisotropy is irrelevant in the $M = 2, S_I = 1/2$ model (Affleck, Ludwig, Pang, and Cox [1992]) and scaling calculations about the non-trivial fixed point indicate that the spin-channel spin coupling is marginally irrelevant (H.-B. Pang, [1992]). We note that for the case of tetragonal symmetry the spin-channel spin coupling again arises, and all bare exchange constants are generically unequal. Again, as we shall discuss in later sections the exchange anisotropy is irrelevant.

Koga and Shiba [1995] have studied a model related to Eq. (2.2.43) in which excited crystal field singlet states are retained in the f^2 configuration. The excited states yield a triplet when the crystal field splitting Δ is taken to zero. The idea of the study is that in the zero splitting limit the "triplet impurity" spin is exactly compensated, yielding a Fermi liquid fixed point at low temperatures, while for a range of finite splitting the two-channel fixed point is stable. In particular, the two-channel fixed point is found to be stable for all values of parameters in tetragonal symmetry, and for a wide range of parameters in the hexagonal crystal field. As the details of their model are rather technical, we refer the reader to section 3 of their paper for a complete discussion.

We note that the two-channel Kondo coupling for a Ce^{3+} ion in hexagonal symmetry has a precisely analogous form to Eq. (2.2.54).

A final comment on symmetry concerns the particle-hole transformation. Provided the conduction band of the host metal is symmetric about the Fermi energy, which it will always be for sufficiently small energy scales, and provided the exchange coupling is only easy axis-anisotropic in the case of the non-magnetic Kondo effects, the model Hamiltonians we have discussed in this section enjoy a discrete particle hole symmetry, which has a different meaning in the case of two-channel magnetic Kondo effects as opposed to the TLS and quadrupolar Kondo effects. No matter what the degree of exchange anisotropy, the particle-hole symmetry will be present in the asymptotic low energy spectrum, since, as we shall show, the exchange anisotropy is irrelevant about the non-trivial two-channel fixed point (and about the ordinary strong coupling Kondo fixed point as well).

For the spin Kondo models, the particle hole transformation is the usual charge conjugation operation. Suppressing all but magnetic labels μ on conduction states we map particle creation operators to hole annihilation operators according to

$$c_\mu^\dagger = i\sigma^y_{\mu,\mu'} h_{\mu'} \tag{2.2.45}$$

where summation convention has been used, and σ^y is the Pauli matrix introduced in Sec. II.A. This transformation reverses both charge and spin, and hence leaves the spin tensor operators unaffected in the Kondo coupling. This symmetry is present for magnetic Kondo effects even when one admits anisotropic exchange couplings.

For the non-magnetic Kondo effects, the transformation is different. We must first restrict our quantization axis in pseudo-spin space to the direction along which the lone octupolar operator points, and perform the usual particle hole transformation described above. The octupolar operator is odd under time reversal $\mathcal{T}$ and hence the coupling along that direction is invariant under the usual particle-hole transformation. However, the transverse operators, with this choice of quantization axis, have quadrupolar character and are thus even under time reversal but odd under the reversed sign of charge. Flipping the sign of transverse couplings does not remove the Kondo effect, as is well known, so that the spectrum will be unaffected by this transformation. However, to finish the transformation, we are free to follow the particle-hole transformation by a π rotation about the octupolar quantization axis. By the end of the procedure, we have performed the transformation

$$c_\alpha^\dagger = i\sigma^y_{\alpha,\alpha'} h_{\alpha'} \tag{2.2.46}$$

where we have suppressed all but the quadrupolar index of the conduction states.

To summarize the results of this subsection, we have demonstrated that the mapping of low energy scale properties to the two-channel quadrupolar Kondo model is robust for U^{4+} ions with doublet ground states in hexagonal and tetragonal symmetries in that *all* such doublets will be described by this model on coupling to the conduction states. We have also shown that under more restrictive conditions the model will apply to Ce^{3+} ions in cubic and hexagonal symmetry, but is unlikely to apply to Yb^{3+} ions.

2.2.5 Additional ions which may display two channel Kondo effects

Among the actinide ions, U^{4+} remains the best candidate for the two-channel quadrupolar Kondo effect. $Np^{2+}(5f^4)$ or $Np^{4+}(5f^2)$ would also have a $J = 4$ ground state and possibly the quadrupolar Kondo effect when one of the doublet levels lies lowest in cubic, hexagonal, or tetragonal symmetry. $Np^{3+}(5f^3, J = 9/2)$ and $Pu^{3+}(5f^5, J = 5/2)$ ions could display the two-channel magnetic Kondo effect in cubic or hexagonal symmetry provided they have the appropriate ground doublets. In the Np^{3+} case, the chances would be excellent since both the excited $5f^2$ and $5f^4$ configurations have $J = 4$ ground multiplets and thus possibly quadrupolar doublet ground states for Γ_{ex} as required by the selection rules. For the Pu^{3+} case, the ground multiplet of the f^4 excited configuration is $J = 4$, but for the

f^6 it is $J = 0$, so that a similar competition to Ce^{3+} models between single and two-channel Kondo effects arises. Heavy fermion like behavior has been reported in some concentrated Np and Pu based materials.

In the rare earth row, $Sm^{3+}(4f^5, J = 5/2)$ and $Yb^{3+}(4f^{13})$ could in principle exhibit two-channel magnetic Kondo effects, but unfortunately the very large energy splitting to excited configurations with degenerate ground multiplets ($4f^4(J = 4)$ for Sm^{3+}, $4f^{12}(J = 6)$ for Yb^{3+}) makes it far less likely than in the Ce case. With regard to the quadrupolar Kondo effect, $Pr^{3+}(4f^2)$ is the most direct analog to U^{4+} , and indeed shows valence fluctuation tendencies in some compounds [Cox, 1988b)]. Recent work on $PrInAg_2$ has renewed this promise (Yatskar *et al.* [1996]). $Tb^{3+}(4f^8, J = 6)$ and $Tm^{3+}(4f^{12}, J = 6)$ ions both display mixed valence tendencies and could exhibit the quadrupolar Kondo effect when the appropriate doublets lie lowest. Indeed, dilute Tb in cubic Th appears promising as a candidate [Sereni *et al.*, 1986; Cox, 1988b)]. A complication in cubic symmetry in this case is that for $J = 6$ the Γ_3 doublet has a much smaller window of stability, and when it is stable, the magnetic Γ_5 triplet tends to be very close energetically [Lea, Leask and Wolf, 1962]. That means the system will always be quite susceptible to magnetic ordering, or at the very least the magnetic excited state will obfuscate attempts to prove the quadrupolar ground state exists. For example, the low temperature susceptibility of Tb in Th at low concentrations is 2-4 emu/mole-Tb [Sereni *et al.*, 1986].

Generically, the odds of observing the two-channel behavior are higher for the actinide ions rather than the rare earth ions because of the greater extent of the 5f wave functions. This larger size of the orbitals both increases the hybridization and lowers the correlation energies, both of which serve to enhance the Kondo temperature. What allows the Kondo scale of the U^{4+} ions to be small (order 10-100K for the U^{4+} -based heavy fermion materials) in the actinide case is the multiplication of the hybridization by a fractional parentage coefficient (to project to the lowest states) which is a number smaller than unity. As a corollary, the effects of excited crystal field splittings are likely to be less, because the crystal field splitting in these intermetallics is expected to scale with the square of the hybridization [Zhang and Levy, 1988a,b)]. In $Y_{1-x}U_xPd_3$, for example, the first crystal field splitting appears to be 5-6 meV [Mook *et al.* 1993; Dai *et al.* 1995, McEwen *et al.*, 1995], while in UBe_{13} it appears to be 15 meV [Shapiro *et al.*, 1985; Cox, 1987]. In contrast, $PrPb_3$ is a collective Jahn-Teller system with an apparent Γ_3 ground doublet on the Pr sites, and the *overall* crystal field splitting there is of order 1 meV (Ott, [1982]).

2.3 Models with arbitrary N_I, N_C, M

.

We have now derived several model Hamiltonians which have the properties of spin 1/2 Kondo models possessing M=2 (or possibly 3) "channels" of electrons. As we have made clear in the introduction, by channel we mean those internal degrees of freedom of conduction electrons which are decoupled from the impurity. We are primarily interested in models in which the degeneracy of the conduction and impurity spins are $N_c = N_I = N = 2$, but we have encountered models in which $N_I, N_c > 2$ as well. Because these different degeneracy factors may serve as expansion parameters for organizing terms in perturbation theory, it is worth considering models in which we allow these parameters to acquire arbitrary values. We shall briefly list a few such models in this subsection.

$SU(N_c = 2) \otimes SU(M), N_I \geq N_c$ models. These are the "overscreened" models originally considered by Nozières and Blandin, and are specified in terms of a Kondo coupling

$$H_{Kondo} = -\frac{J}{N_s}\vec{S}_I \cdot \sum_{\alpha=1}^{M} \vec{S}_{c\alpha}(0) \tag{2.3.1}$$

where S_I is allowed to take any value and $S_{c\alpha}(0)$ is the conduction spin density in channel α at the impurity site, with all conduction electrons having $S = 1/2$.

$SU(N_c = N_I = N) \otimes SU(M)$ models. These are a straightforward generalization of Eq. (2.3.1) with the restriction of $N_I = N_c$. These models are amenable to the NCA treatment. In the Kondo form, the interaction Hamiltonian is given by

$$H_{Kondo} = -\frac{J}{2N_s} \sum_{k,k',\mu,\mu',\alpha} |\mu' >< \mu| c^\dagger_{k\mu\alpha} c_{k'\mu'\alpha} \tag{2.3.2}$$

where $|\mu >$ is one of the N_I states of the local "spin". One may also write an equivalent Anderson Hamiltonian, placing the local spin states at energy ϵ_f and introducing an excited state field indexed by label α, leading to the hybridization Hamiltonian

$$H_{hyb} = \frac{V}{\sqrt{N_s}} \sum_{k\alpha\mu} [-sgn(\alpha)|\mu >< -\alpha| c_{k\mu\alpha} + h.c.] \tag{2.3.3}$$

where the match to Eq. (2.3.2) is through the Schrieffer-Wolff transformation with $J = V^2/\epsilon_f$. This simple decoupling is only possible when $N_I = N_c$.

$SU(min(N_I, N_c)) \otimes SU(M)$ models. These models are the most general form and include couplings which are symmetric under unitary transformations of the smaller of the impurity or conduction spin degeneracy. They are difficult to write down, and probably of marginal relevance to real materials, except in the case $N_I = 2 \leq N_c$ in which case we can simply use Eq. (2.3.1) with $\vec{S}_{c\alpha}(0)$ being given by

$$S^i_{c\alpha}(0) = \frac{1}{N_s} \sum_{\mu,\nu} S^i_{\mu,\nu} c^\dagger_{k,\mu,\alpha} c_{k'\nu\alpha} \tag{2.3.4}$$

with $S^i_{\mu,\nu}$ being the i-th component of the $J_c = (N_c - 1)/2$ angular momentum representation of $SU(2)$. This model could be of possible relevance to the TLS theory, once the two-site problem is generalized to a multi-site problem, as discussed recently by Zaránd [1996]. As mentioned in Sec. 2.2, this model could also be of relevance for Ce^{3+} impurities.

3 Scaling Theory of Kondo Models

3.1 Overview of the Physics and Interelatedness of Methods

3.1.1 Concepts and Terminology of Scaling and Renormalization Group Theory

The basic philosophy of any renormalization group theory is to describe the physics of the problem in terms of an effective Hamiltonian at each length scale which is expressed in terms of a small basis set of operators multiplied by coupling constants which depend upon the length scale. Following the notions of Kadanoff and Wilson, we imagine integrating out variables on small length scales to derive Hamiltonians on large length scales. The first to apply such concepts to the Kondo problem in a straightforward manner was Anderson [1970]. Later this idea was formulated in the framework of the multiplicative renormalization group (Zawadowski and Fowler [1970]; Fowler and Zawadowski [1971]; Abrikosov and Migdal [1970]). In this subsection, we wish to lay out some of the relevant concepts and terminology.

Equivalence of Space and Time in Kondo models. We may interchange length scale with time scale in our impurity problems. The reason is simple: effectively, any impurity model presents a quantum problem in one spatial dimension equivalent to the radial direction away from the impurity. This is often called a "1+1" dimensional problem, where the "+1" refers to the time direction. The conversion factor between space and time or energy and momentum is simply the Fermi velocity v_F of the conduction electrons, which hinges on the fact that the dispersion of the electrons near the Fermi energy may always be linearized. In fact, the problem may be viewed as a Lorentz invariant model with speed of light equal to v_F. This simple idea underlies much of the physics of the Kondo model, and is essential for its solution using the the renormalization group theory (Sec. 4), conformal field theory (Sec. 6), and the Bethe-Ansatz (Sec. 7). Hence, our approach in the scaling and numerical renormalization group approaches shall be to determine the effective Hamiltonians describing the problem at different energy scales, which are set, for example, by the frequency of an external probe, the temperature, the magnetic field, or simply by the magnitude of the conduction bandwidth.

Appearance of Logarithms in Perturbation Theory. The methods we will employ in discussing the two-channel Kondo problems and Kondo analogues have features in common which derive from the appearance of logarithms in the high energy scale *(ultraviolet region)* perturbation theory which diverge upon approach to the low energy scales *(infrared region)*. As Wilson has noted, the appearance of logarithms indicates that all energy scales are of equal importance which strongly supports the relevance of a renormalization group approach. Practically, we will imagine accessing the infrared regime through the reduction of the temperature, frequency, magnetic field, or conduction bandwidth.

The individually logarithmically divergent terms in perturbation theory may be treated collectively by the various techniques to generate models characterized by renormalized couplings appropriate to whichever infrared energy scale we are sitting at in the calculation. The spirit here is very much the same as the "running coupling constant" scheme in quantum field theory. Unlike quantum field theory, the lattice always provides us with an ultraviolet cutoff (maximum energy scale) which will be the Fermi energy or conduction bandwidth in our work. Indeed, in those models where the coupling constants grow with reduced energy scale, we have in our hands a precise mathematical analogue of the asymptotically free models (such as quantum chromodynamics) studied in high energy theory.

Fixed Point Taxonomy. We are said to be at the *fixed point* of a renormalization group transformation if upon further rescaling the Hamiltonian remains unchanged. The fixed point may be characterized in terms of its *excitation spectrum* that may be either: (i) *Fermi-liquid-like* with a 1:1 map near the Fermi energy to the spectrum of one (or more) one-dimensional Fermi gases which have uniform level spacing $v_F\pi/L$, L the radial extent of the metal. A trivial modification of this spectrum occurs in the presence of an ordinary potential scattering center which imparts a phase shift δ to the conduction states; this phase shift manifests in the energy levels through an additional shift of the amount $-v_F\delta/L$ with respect to the free gas; (ii) *non-trivial* or *non-Fermi-liquid-like* in which case the excitations appear

at non-uniform, fractional spacings of the Fermi gas, and for which application of the phase shift concept δ is not meaningful. The states are characterized by separated spin, charge, and channel numbers, relative to the free fermion gas. (In between fixed points, the spectrum is a typically complex many body spectrum.)

We shall generically flow to four kinds of fixed points:

(1) Zero Coupling Fixed Point: This fixed point has precisely the free Fermi gas spectrum for each spin and channel of conduction electrons, and corresponds to an impurity uncoupled from the electrons, whence the phase shift $\delta = 0$. This is the stable infrared fixed point of the *ferromagnetic* isotropic Kondo model.

(2) Strong Coupling Fixed Point: As applied to some of the single channel Kondo models of interest here, at this fixed point, the effective coupling of the impurity to the conduction electrons is infinitely strong, and the excitation spectrum is Fermi liquid like with a phase shift fixed "universally" (i.e., independent of input parameters to the model) by the degeneracy of the impurity and conduction electrons. This is the infrared stable fixed point of the isotropic antiferromagnetic single-channel Kondo problem, where $\delta = \pi/2$.

(3) Intermediate Coupling Fermi-Liquid Fixed Point: These fixed points are Fermi liquid in character but possessed of non-universal phase shift values between 0 and $\pi/2$. Such fixed points typically arise when some low energy field is present in the problem that cuts off the scaling to strong or non-trivial fixed point, such as the level splitting and spontaneous tunneling in the case of the TLS model.

(4) Non-trivial intermediate coupling fixed point. This is the interesting fixed point of the multi-channel Kondo models first identified by Nozières and Blandin [1980]. At this kind of fixed point, the internal degrees of freedom of the impurity are never completely compensated, and the excitation spectrum is non-trivial. In consequence, instead of obtaining Fermi liquid properties at low T, one obtains critical phenomena: the incremental specific heat coefficient and susceptibility diverge as $T \to 0$. This divergence may be logarithmic ($n = 2$) or power-law in character ($n > 2$). Indeed, this fixed point is a true critical point–the impurity has driven the entire metal to the edge of a phase transition.

Stability of Fixed Points. A fixed point is also characterized by its stability properties: namely, if you begin with coupling constants arbitrarily close to the fixed point, will you flow into the fixed point with rescaling (lowering of energy) or will you flow away? The answer may be mixed–some couplings or parameters may drive you away, others towards the fixed point. Any coupling constant measured relative to the fixed point value which vanishes upon rescaling is said to be *irrelevant*, if the coupling difference grows, the coupling is *relevant*, and if the coupling to leading order is unchanged, it is *marginal*. Examination of next-leading order effects can further identify if a marginal operator is "marginally irrelevant" or "marginally relevant."

Universality. Asymptotically close to some of the above fixed points, properties may be *universal*, i.e., they can be expressed as universal functions of thermodynamic or dynamic variables measured with respect to a single energy scale that depend only upon properties of the fixed point and not the bare couplings. For example, at the strong coupling fixed point of the ordinary one-channel spin 1/2 Kondo problem, the phase shift of the conduction electrons is $\pi/2$, a universal number independent of the bare exchange value, and at low temperatures the susceptibility times the temperature with the non-universal effective magnetic moment divided out ($T\chi(T)/\mu^2$) is a universal function of temperature measured in units of the Kondo temperature T_K, a natural energy scale that divides high and low energy regimes and may be determined in the perturbative scaling analysis. When it is meaningful to use it, the effective scaled Fermi temperature T_0 differs from the Kondo scale T_K only by pure numerical factors of

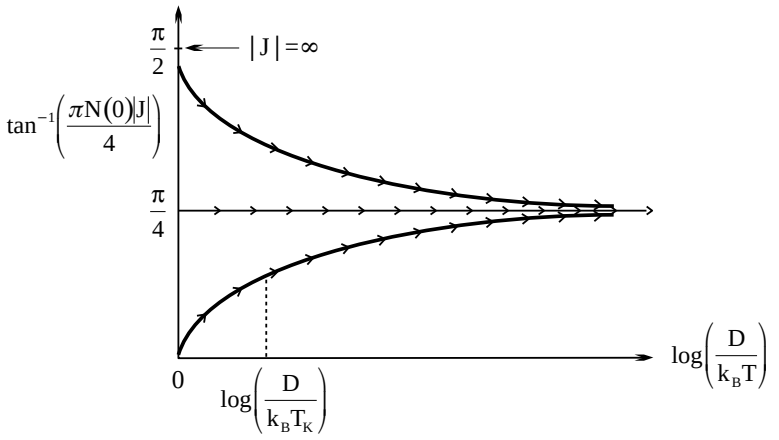

Figure 17: Scaling of dimensionless exchange coupling vs. logarithm of the bandwidth for the two-channel spin 1/2 Kondo model. Whether starting from initially strong ($J \to \infty$) or weak ($J \to 0$)coupling, the arctangent of the dimensionless exchange coupling scales to the fixed point value of $\pi/4$ as the bandwidth is reduced. The crossover scale for weak coupling is identified as the Kondo temperature. If one begins right at the fixed point, the coupling will be unchanged under renormalization.

order unity. However, independent of the properties of the infrared fixed point, the Kondo scale retains meaning as the boundary between high and low energy physics.

3.1.2 Illustrative Example: Two-channel model in applied spin and channel fields

The concepts discussed in the previous subsection have been discussed somewhat in the abstract. We would like to illustrate their meaning by providing an overview of the physics of the two-channel spin 1/2 Kondo model in applied spin and channel fields. The derivation of these results will follow in later sections. For the purposes of discussion, we shall assume the exchange interaction to be isotropic.

Zero Field Case. Fig. 17 displays the behavior of the effective exchange coupling as a function of the logarithm of the temperature beginning at high $T \sim D/k_B$ and flowing to low T (much smaller than the Kondo scale, T_K, in the case of initial weak coupling). The meaning of this plot is that the first few levels of the excitation spectrum can be fit by a simple model in which conduction electrons exchange couple to an $S_I^* = 1/2$ impurity. In fact, the "impurity" is a complicated bound object consisting of the original impurity at its core, but surrounded by shells of alternating conduction spin. (An amusing metaphor is to think of the impurity spin as the seed of a pearl, with the layers of conduction spin accreting like the layers of the pearl as the temperature is lowered [S. Williams, 1992].) At low temperatures (large values of $-\log(T/D)$) we "flow" to the fixed point coupling, regardless of the size of the initial, high temperature coupling. Nothing cuts off this scaling process, and the spin can never be compensated away as in the single channel Kondo effect, so that the properties of the system as the fixed point is approached are those of a critical point in which the system looks the same on all length scales.

Applied Spin Field. By applied spin field, e.g. in the Kondo problem, we mean a local field which couples to the impurity spin linearly, or a bulk field which also couples to the conduction spin. This could correspond to the spontaneous tunneling and level splitting terms in the TLS model, to a uniaxial stress in the quadrupolar Kondo model, or to an applied magnetic field in the magnetic two-channel model. The spin field cuts off the scaling process of the previous paragraph, so that below a "crossover temperature" T_{sp}^x determined by the field strength the system will behave like a Fermi liquid with energy scale set by the crossover temperature. If we begin from the physically relevant case of weak coupling, then assuming the spin field splitting $\Delta^z << T_K$, we will have $T_{sp}^x \approx (\Delta^z)^2/T_K$ (see Secs. 4.2.e, Sec.

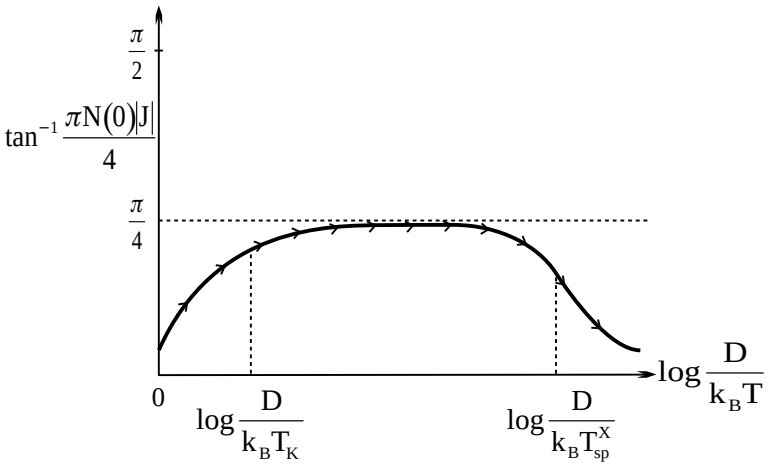

Figure 18: Scaling of the spin 1/2 two-channel Kondo model in the presence of a spin-field. In this case, where a field that linearly splits the spin of the local moment is applied, then provided the applied field is small compared to the Kondo scale, the system will first flow close to the fixed point coupling strength of the two-channel model, then flow to a value determined simply by the product of the bare exchange strength and the impurity spin as the system flows to the "polarized scatterer fermi liquid" fixed point. The crossover scale to the latter is $T^x_{sp} \sim H^2_{sp}/T_K$, where H_{sp} is the applied spin-field.

5.1.6, 6.1,7). This crossover effect on the effective coupling constant is illustrated in Fig. 18.

The low temperature fixed point in this case is of variety (3) (intermediate coupling, Fermi liquid) because the ground state phase shift will obtain a value determined by the magnetic field and the bare coupling constants. Because up and down spin electrons experience equal and opposite phase shifts, we must view the excitation spectrum as deriving from two independent Fermi gases. Fig. 19 illustrates how the spin field crossover manifests itself in the value of the conduction electron phase shift for up-spin electrons at the Fermi energy [Affleck *et al.*, 1992]. As we discuss in Sec. 7.2, this effect has a rather spectacular manifestation in the specific heat: above the crossover temperature, the specific heat displays the logarithmic behavior characteristic of the two-channel model, while below the ground state residual entropy is shoved out into a Schottky-like peak which for a range of temperatures is actually larger than the zero field specific heat by nearly an order of magnitude.

Applied Channel Field. By channel field, we mean an external probe which couples to the channel index of the conduction electrons and acts to lift the degeneracy of the exchange coupling. Practically, this is effected in the quadrupolar Kondo model by the application of a magnetic field, which splits the excited Γ_7 doublet and thus through the Schrieffer-Wolff mapping splits the exchange integrals for the different conduction channels by an amount $\Delta J \simeq (V/\tilde{\epsilon}_f)^2 \mu_{eff} H$ where μ_{eff} is the effective moment of the excited doublet and H the magnetic field strength. In the TLS model, magnetic field would also be a channel field in principle, but there is no obvious mechanism by which the couplings for up and down spin can be split. In the magnetic two-channel model, uniaxial stress will split the excited quadrupolar doublet and lift the channel degeneracy.

The channel field also cuts off the scaling of Fig. 17, but in a very different way than for the spin field, as made clear by Nozières [1980]. Assume initial weak coupling. Below a crossover temperature $T^x_{ch} \approx (\Delta J)^2/T_K$ (see Secs. 4.2.d,5.1.5,6.1,7), the more strongly coupled channel will tend towards the *strong coupling* ordinary single channel Kondo fixed point for which the phase shift is $\pi/2$, and the weakly coupled channel will tend towards the *zero coupling* fixed point with zero phase shift. Hence, as with the applied spin field, the excitation spectrum is composed of two fermi gas excitation spectra with different phase shifts. In this case This is illustrated in Fig. 20(a) where below T_{ch} the single line of high T scaling "bifurcates" with the upper branch corresponding to the strongly coupled channel, and the lower branch to the weakly coupled channel. In Fig. 20(b) we show the scaling flows in the space

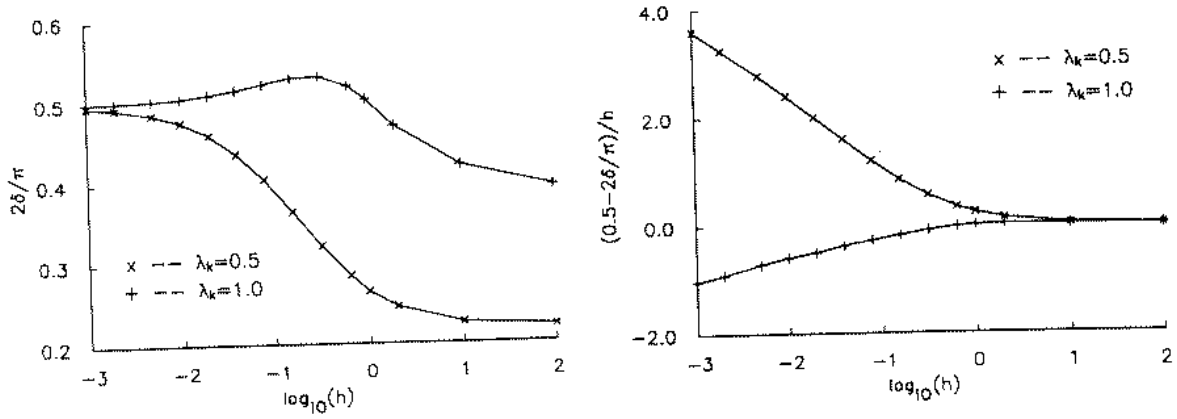

Figure 19: Physical effects of applied spin field on the two-channel spin 1/2 Kondo model. At left we display the phase shift as a function of field as determined by numerical renormalization group calculations (see Affleck *et al.* [1992]). As noted in the text, this may be used to calculate the magnetization. At right, we show that properly scaled this numerically calculated phase shift displays the logarithmic singularity expected in the differential susceptibility as a function of field.

of coupling constants, where the non-trivial fixed point of the flows is evident in the center. This fixed point is stable for $J_+ = J_-$, but unstable to any small differences. We note that in the case of the TLS Kondo model, the magnetic field splitting of conduction states will not induce a splitting of exchange integrals in the same way. The only possible influence on the fixed point is for physically irrelevant fields $\mu H \simeq D$ which cannot be realized experimentally.

A last point about the two-channel model is that it is stable with respect to anisotropy of the exchange integral while maintaining the channel degeneracy (see Secs. 3.4.1,4.2.c,6.1). Thus, while applied spin and channel fields destabilize the model and take it away from the non-trivial fixed point to one of the other three generic fixed points, the model enjoys stability against the realistic feature of exchange anisotropy.

3.2 Formal Development of Scaling Theory

3.2.1 Organization of Perturbation Expansion In Logarithms; Methods of Resummation

We have already pointed out in the introduction and elaborated above on the origin of logarithmic corrections in the perturbation expansion of the impurity models considered here due to the non-commutative character of the conduction electron scattering processes off the impurity. The logarithmic factor which occurs is

$$\mathcal{L}(max\{T,\omega,E\}) = \log(\frac{D}{max\{T,\omega,E\}}) \tag{3.2.1}$$

where D is the high energy cutoff which will always be the conduction bandwidth in the problems interesting us, and $max\{T,\omega,E\}$ is the largest of the other external parameters in the system, such as the temperature T, the driving frequency of an external probe ω, or the splitting of the TLS, $E = \sqrt{(\Delta^z)^2 + (\Delta^x)^2}$. E ultimately serves as the small energy infrared cutoff.

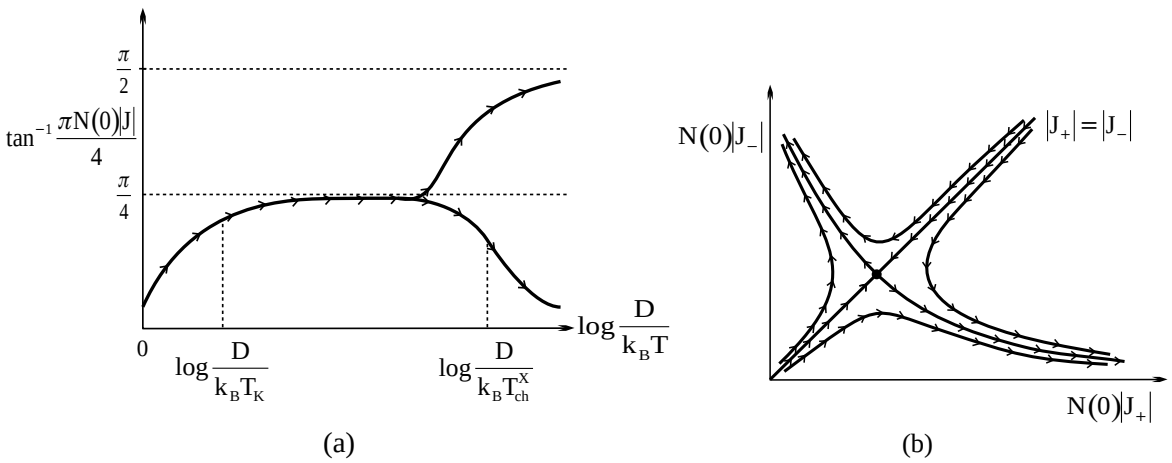

Figure 20: Scaling of the spin 1/2 two-channel Kondo model under application of a channel field. A channel field couples linearly to the conduction electron channel spin density and thus lifts the degeneracy of the two exchange integrals. (a) shows that one coupling will pass to strong coupling and the other to weak coupling at a crossover scale $T_{ch}^x \sim (\delta J)^2/T_K$, where ΔJ is the exchange integral splitting. (b) shows the corresponding flow diagram in the space of coupling constants. The flows are stable along the $J_1 = J_2$ separatrix, moving to the non-trivial fixed point. They are unstable away from this separatrix, moving the strong coupling fixed point of which ever exchange is initially stronger.

In the treatment of the models of interest in this Review, we may organize the perturbation theory for any quantity according to powers of the coupling g between impurity and conduction electron states, times powers of the logarithmic factor $\mathcal{L}$. Assuming a given quantity $\mathcal{Q}$ has a minimal power g^p of the coupling (e.g., for the resistivity in the Kondo problem, $p = 1$), we have the following hierarchy:

$$\mathcal{Q} = \begin{array}{cccc} g^p & & & \\ +g^{p+1}\mathcal{L} & +g^{p+1} & & \\ +g^{p+2}\mathcal{L}^2 & +g^{p+2}\mathcal{L} & +g^{p+2} & \\ +g^{p+3}\mathcal{L}^3 & +g^{p+3}\mathcal{L}^2 & +g^{p+3}\mathcal{L} & +g^{p+3} \\ .... & & & \\ .... & & & \\ .... & & & \end{array} \tag{3.2.2}$$

In this array, clearly the rows represent the order in a systematic expansion of the coupling constants. The columns give us the logarithmic hierarchy: since the logarithmic factors diverge as one tunes the infrared cutoff to zero, summing up the logarithms in the first column will produce a stronger singularity than summing up the logarithms in the second, third, fourth, etc. columns. We call the resummation of logarithms in the first column the *leading logarithmic approximation*, which sums one set of diagrams to all orders in perturbation theory of the coupling g. By including also the summed up logarithms of the second column, we include another set of diagrams to all orders in the perturbation expansion, and this is called the *next leading logarithmic* approximation.

We could of course proceed in this way through all the columns, which in principle would yield an exact calculation of the quantity $\mathcal{Q}$. In practice, however, a considerable amount of information may be obtained by considering only the first and second columns. (Indeed, in certain limits this approximation may be shown to be exact.) For example, the Kondo scale T_K is quite accurately estimated by the next leading logarithmic approximation; indeed, as shown by Wilson [1975] the next to leading order scaling theory determines the universal parts of the T_K expression. In the limit of large numbers of channels M, the non-trivial Nozières and Blandin fixed point is correctly uncovered by the next leading logarithmic approximation.

The systematic collections of terms in the logarithmic hierarchy may be accomplished by several methods. We shall discuss five strongly related methods here:
(i) Leading logarithmic order resummation of diagrams. This is equivalent to the direct diagrammatic summation methods of Abrikosov [1965], as well as to the "poor man's scaling" method of Anderson [1970]. In this case, the summation problem is cast in the form of a differential or integral equation for the relevant quantity (such as the conduction electron T-matrix describing scattering off of the impurity). This method is known as the "parquet" method, and is analogous to the lowest order RPA approximation in a metal, where one sums the diagrams built from spin-conduction particle/hole bubbles to all orders. We discuss this approach in section 3.3.
(ii) Multiplicative Renormalization Group in the Leading and Next Leading Orders of Diagrams. This method has been developed by Gell-Mann and Low, Bogulubov and Shirkov for treating infrared and ultraviolet divergences in field theory. This approach was first applied to the Kondo problem by Zawadowski and Fowler [1970] (see also Fowler and Zawadowski [1971]), and by Abrikosov and Migdal [1970]. The method was later simplified by Sólyom and applied for to the one-dimensional electron gas (Sólyom [1974,1979], Zawadowski [1973]). We shall discuss this in Sec. 3.4.
(iii) Path Integral Method. This approach used first by Anderson, Yuval and Hamann [1969] and subsequently by Zimányi ,Vladár , and Zawadowski [1988a,b]. We shall discuss this in Sec. 3.5.
(iv) Numerical Renormalization Group. This non-perturbative approach was developed by Wilson [1973,1975; Krishna-murthy, Wilkins, and Wilson, 1980a,b); Cragg and Lloyd, 1979; Cragg, Lloyd, and Nozières, 1980]. In essence, one solves the rescaled equations exactly on a cleverly discretized mesh by finding the lowest energy levels of the system at each renormalization step. It is possible to compute properties with this method if sufficiently many steps are retained. For example, Wilson provided the first calculation of the magnetic susceptibility which was accurate over the entire temperature range. We shall discuss this method in more detail in Sec. 4.
(v) Next-leading order resummation and NCA. As we shall discuss, this procedure sums a class of perturbation theory diagrams to all orders and includes to leading and next leading order the corrections to the vertex of the conduction electron-local spin scattering, and to leading order the corrections to the "self-energy" of the local spin variable, which shall be precisely defined in the next subsection. The resummation takes the form of coupled non-linear differential or integral equations. This approximation was first employed in the x-ray edge singularity problem by Moulet *et al.* [1969], and Nozières *et al.* [1969] where it was called the "self consistent parquet approximation." This method was first applied to the Kondo problem by Nozières [1969]. A somewhat different approximation appeared in the work of Keiter and Kimball [1971]. Subsequent use of the approximation as written by Keiter and Kimball for Anderson and Kondo models has gone under the name of the "NCA" or non-crossing approximation, since in the formalism of Keiter and Kimball, the diagrams retained have no crossed propagator lines. Although this approximation may seem crude, it in fact can be justified within a large N expansion. For all Kondo problems, it gives a good extrappolation of the high temperature physics into the low temperature regime, well below T_K (though it eventually fails to give the correct ground state for the single channel model). For the multi-channel model, it has been shown exact for the limit $N \to \infty$, M/N held fixed [Cox and Ruckenstein, 1993] and reproduces thermodynamic properties quite accurately even for $N = 2$ and $M = 2, 3$ [Kim, 1995; Kim and Cox, 1995,1997]. The NCA approach for the multi-channel Kondo problem is discussed in Sec. 5.
(vi) Conformal Field Theory and Bosonization Techniques. Conformal field theory may also be viewed in somewhat the same light as the scaling and renormalization methods, since it exploits a scale invariant critical point in $1 + 1$ dimensions which is also conformally invariant, and builds a description of the physics in terms of relevant and irrelevant operators about the conformal point. Conformal field theory is a kind of "non-Abelian bosonization" scheme, since the low lying excitations are written in terms of current operators which satisfy the Kac-Moody algebra commutation relations of non-Abelian symmetry groups. An extensive development of this theory for the Kondo problem has been carried out recently [Affleck and Ludwig, 1991a,b,c;1992;1993;1994a,b; Ludwig and Affleck, 1991; Ludwig, 1994].

We shall discuss this approach in Sec. 6.1. Separately, an Abelian bosonization scheme with ordinary harmonic oscillator operators has been developed by Emery and Kivelson [1992]. We shall discuss this approach in Sec. 6.2.

We note that methods (ii) and (v) are in fact similar, except that most formulations of (ii) have not included the imaginary part of the dressed exchange interaction and of the spin self-energy, while these are included in (v), so that all response functions have the appropriate analytic behavior. It is possible to apply (ii) in the energy region below the ground state threshold at zero temperature where all response functions are purely real (for negative energy, there are no allowed decay processes) and then to analytically continue the solution into the positive frequency region (Zawadowski, unpublished, [1970]; Sólyom [1971]). This appears to be substantially equivalent to the differential form of the NCA developed by Kuramoto and Kojima [1984] and Müller-Hartmann [1984].

The common feature in methods (i)-(iii) and (v) is that they are based on an expansion in the coupling which presumably should not be applied when the renormalized dimensionless coupling grows to order unity. Method (iv) does not suffer from this approach of course. In fact, method (v) appears to cross into the non-perturbative regime quite adequately as well, although the reasons are not completely clear as to why this works. What is useful about methods (i) and (ii) is that they correctly predict the growth of the couplings, and they can in some instances correctly predict other phenomena such as non-trivial fixed points.

In closing this subsection, we make two final observations:
(1) Absence of Asymptotic Freedom in commutative models. We still obtain logarithmic corrections in commutative models such as the x-ray edge singularity and the TLS model with $V^z \neq 0, V^x = 0$. However, in these cases, there is no renormalization of the bare coupling constant as we go to the infrared region. Nevertheless, power law singularities may result in physical quantities with the power laws related to the phase shift associated with the commutative coupling constants. As an example, in the commutative TLS model, for sufficiently large V^z, one finds that the spontaneous tunneling rate Δ^x is renormalized at low temperatures according to

$$\Delta^x(T) = \Delta^x(T = D)(\frac{T}{D})^K \tag{3.2.3}$$

where K is proportional to the square of the phase shift $\delta(V^z) = tan^{-1}(\pi V^z)$ (Kondo [1976], Libero and Oliveira [1991]).
(2) Conformal Field Theory Approach and Abelian Bosonization. Although we didn't include it in the list of methods based upon resumming logarithms, the conformal field theory approach first applied by Tsvelik [1990], and substantially evolved by Affleck [1990a,1995], Affleck and Ludwig [1991a,b,c;1992;1993], Ludwig and Affleck [1991,1994]; Ludwig [1994a,b], and Affleck *et al.*,1992] has a strong relationship to these other methods. This method exploits conformal invariance of the Kondo models at the fixed points to provide exact forms of universal functions (both thermodynamic and dynamic) and exact values for universal amplitudes (such as the residual ground state entropy). The method is very similar in character to the eigen-operator expansion of the renormalization group, but provides considerably more information due to the local character of the conformal invariance. The method can also be applied to the calculation of finite size excitation spectra, where detailed quantitative agreement with numerical renormalization group calculations has been found [Affleck *et al.*, 1992]. Unlike methods (i-v) above, however, the conformal theory is incapable of calculating full crossover behavior between fixed points. In principle, as well, the conformal theory requires additional confirmation that models displaying conformal invariance correspond to fixed point Hamiltonians of the original models. In practice, there no doubt that this is the case for the models considered by Affleck and Ludwig (Affleck [1990a], Affleck and Ludwig [1991a,b,c; 1992, 1993]; Ludwig and Affleck [1991]; Ludwig [1994a,b]). In addition, an approach based upon an Abelian bosonization of the anisotropic two-channel model has been introduced by Emery and Kivelson [1992] which reproduces many of the features of the conformal theory in perturbing around a special fixed point of the model. We shall discuss the conformal theory approach in some detail in Section 6.1, and the Abelian bosonization in Sec. 6.2.

Finally we must emphasize that the methods (i) and (ii) describe the high temperature results, and methods (vi) give the correct low temperature behavior in terms of non-universal amplitudes which can be determined by a match to other approaches (such as the numerical renormalization group). The NCA and NRG approaches are methods which also describe well the crossover regime between high and low energy scales.

3.2.2 Multiplicative Renormalization Group

The multiplicative renormalization group is based upon the following observation: let us consider an interaction between two different kinds of particles described by Green's functions $\mathcal{G}, G$ which are functions of frequency, temperature, field, momentum, etc. The $\mathcal{G}$ Green's function denotes a "heavy particle" which shall correspond to the localized pseudo-spin variables or mobile heavy particles in our models, and the G Green's function corresponds to a "light particle" which shall be the conduction electrons or light band electrons in our models. In the interaction terms of interest in our model Hamiltonians, a light particle is scattered by a heavy particle (Fig. 2). The bare scattering interaction between the particles (the coupling which appears in the Hamiltonian) is given by $V^{(i)}$, and the corresponding vertex which includes all multiple scattering processes is given by $\Gamma^{(i)}$.

Now, consider the following transformation of the Green's functions and couplings, where z_1, z_2, and $z^{(i)}$ are arbitrary numbers:

$$\begin{array}{c} G \to z_1 G \\ \mathcal{G} \to z_2 \mathcal{G} \\ \Gamma^{(i)} \to (z^{(i)})^{-1} \Gamma^{(i)} \\ V^{(i)} \to (z_1 z_2)^{(-1)} z^{(i)} V^{(i)} \end{array} \quad . \tag{3.2.4}$$

Then in any internal point of the general scattering diagram *beyond lowest (bare) order*, the z-factors cancel out because any higher than lowest order diagram may be expressed as powers of the factor

$$V^{(i)} G \mathcal{G} \Gamma^{(i)} \tag{3.2.5}$$

which is manifestly invariant under the above transformation. So far, this statement of the invariance under the rescaling specified by Eq. (3.2.4) is totally topological and general in character, and devoid of any specific contact to the problems of interest. What we shall proceed to demonstrate is that the rescaling of the conduction bandwidth in our models will generate a transformation of the form Eq. (3.2.4).

The main idea of the renormalization group, as emphasized in the previous subsection, is that the particle or hole excitations with large energy values do not directly participate in real processes at low energies. They only have an effect through virtual excitations of the low energy states to high energies through the scattering process. These high energy virtual processes may be taken into account for the low energy electrons by introducing renormalized parameters (or couplings $V^{(i)}$, Fermi velocities etc.) which sum up the high energy processes above a certain cutoff in energy. The goal will be to describe the model for all energies below a new cutoff D' instead of the bare cutoff D by integrating out the virtual excitations to states between D' and D and compensating by adjusting the couplings so that the same physics remains, i.e., Eq. (3.2.5) remains invariant.

It is useful to conceptualize the smaller bandwidth as proportional to the temperature T if that serves as the infrared cutoff in our perturbation expansion. As we lower the temperature of the system from order D, only those real excitations with significant Boltzmann weights, i.e., $E_{ex} \leq 10 k_B T \simeq D'(T)$, say, will contribute significantly to the low energy physics. On the other hand, through the scattering of Fig. 2, processes with energies above $D'(T)$ will contribute to the low energy physics. We are not free to simply include the real processes within $D'(T)$ to get the physics correctly, so we must adjust the Hamiltonian appropriate to computing properties from purely real processes within $D'(T)$

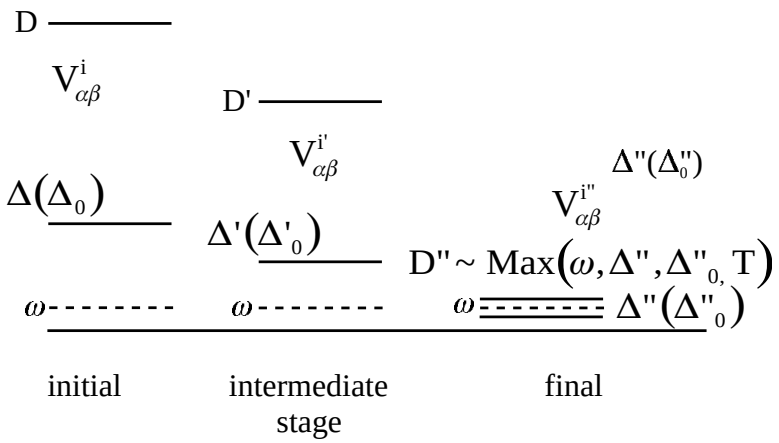

Figure 21: General scheme of the renormalization group. The bandwidth cutoff is reduced step by step. The parameters like Δ and Δ_0 must be changed also with the coupling. The procedure stops when the new cutoff reaches one of the parameters like ω, T or the renormalized Δ, Δ_0 values.

by adjusting the couplings to reflect the virtual excitations to higher energies. This general scheme is illustrated in Fig. 21.

We can illustrate this idea by considering what happens when we resum only leading logarithmic terms in the Kondo problem. The resummation, as is clear from Eq. (3.2.2), will simply result in a geometric series-like formula times the leading power g of the dimensionless coupling. Taking the temperature as the infrared cutoff, the factor obtained in the geometric series is $F(g, D, T) = (1 - g\log(D/T))^{-1}$. We may rewrite this expression in a trivial way that shows the effect of the bandwidth rescaling:

$$\frac{1}{1 - g\log(\frac{D}{T})} = \frac{1}{1 - g[\log(\frac{D'}{T}) + \log(\frac{D}{D'})]} \tag{3.2.6}$$

$$= z(g, \frac{D}{D'})\frac{1}{1 - g'\log(\frac{D'}{T})}$$

where

$$z(g, \frac{D}{D'}) = \frac{1}{1 - g\log(\frac{D}{D'})} \tag{3.2.7}$$

and

$$g' = z(g, \frac{D}{D'})g \quad . \tag{3.2.8}$$

Thus the original analytical form of $F(g, D, T)$ may be preserved with the new parameters g', D' instead of g, D, provided we multiply by the factor $z(g, D/D')$ which depends upon g, D but not T.

This behavior under bandwidth rescaling makes it possible to eliminate the virtual high energy phase space in the framework of the renormalization group and to introduce new effective couplings. Note that while the rescaling specified by Eqs. (3.2.4-5) is always possible, it is *not* always possible to find models which satisfy these properties in the multiplicative form manifest in Eqs. (3.2.6-8) characteristic of Kondo models. Thus, the ability to define and implement a multiplicative renormalization group transformation is only realizable for particular classes of models. In many problems, there are further parameters which might be changed as the width of the excitation spectrum is reduced (virtual excitations integrated out) such as the mass, Fermi velocity, etc.

Note that while the rescaling of the bandwidth corresponds to redefining the scale of energy on which we measure, we may also think of it as rescaling the length. This fact follows from the one-dimensional character of the impurity models we are considering in this paper, where only the radial direction is important, so that energy and momentum are related through the conversion constant v_F. Thus, when we talk about looking at problems on lower temperature or energy scales, we are equivalently talking about looking at longer length scales.

The change in effective coupling strength may be cast in the form of a differential equation by reducing the bandwidth $D \to D'$ infinitesimally. The general form of the differential equation is

$$\frac{\partial V^{(i)}}{\partial \log D} = \beta(V^{(i)}) \tag{3.2.9}$$

which defines the β-function of the multiplicative renormalization group. The β function will always vanish when the couplings vanish, and tend to infinity when the coupling strength tends to infinity, though it need not interpolate between these two points monotonically. Eq. (3.2.9) is quite general, but we shall typically approximate the β-function by a low order polynomial obtained from perturbation theory.

The perturbative approach breaks down when the couplings $V^{(i)}$ expressed in dimensionless form (measuring them in units of the bare conduction bandwidth D) grow to order unity. We define the value of the renormalized bandwidth D or the equivalent temperature T where the couplings grow to order unity as the Kondo Temperature, T_K. This is a kind of crossover temperature, which separates the high energy regime for which perturbation theory is valid, from the low energy regime where the electrons and heavy particles are strongly coupled.

If the β-function obtains zero for some value of couplings, $(V^{(i)})^*$, then under further rescaling at this value, the couplings will remain unchanged. That point in the space of couplings is called a *fixed point*, as we have discussed in Sec. 3.1.1. Usually, in the models of interest here, that point is outside the regime of perturbative scaling theory apart from the trivial fixed point where all $V^{(i)} = 0$ which corresponds to decoupled heavy and light particles. As an example, since the beta function diverges as $V^{(i)}$ diverge, infinite coupling strength will also always be a fixed point. We may artificially tune certain parameters, such as the channel number M, to bring the fixed points into the perturbative regime. In that case, as we shall demonstrate explicitly, for isotropic couplings (all $V^{(i)}$ equal) the β-function has the form (in terms of dimensionless couplings $g < 0$)

$$\beta(g) = g^2 + \frac{M}{2} g^3 + ... \tag{3.2.10}$$

so that a fixed point at $g^* = -2/M$ occurs in the perturbative regime for $M >> 1$. Wilson and Fisher introduced the $\epsilon = 4 - d$, d the spatial dimensionality, to obtain a similar perturbative control in problems where the renormalization group is applied to critical phenomena [K.G. Wilson and M.E. Fisher, 1969]. Otherwise *non-perturbative* methods must be employed to evaluate the β-function or perform equivalent calculations.

The crossover temperature scale calculated from the scaling equation depends upon the accuracy to which the β-function is estimated. For example, in the isotropic Kondo problem with antiferromagnetic exchange coupling J, we have

$$\begin{aligned} k_B T_K &= D \exp[\frac{1}{\rho_0 J} + \frac{1}{2}\log(|\rho_0 J|) + P(\rho_0 J)] \\ &\approx D|\rho_0 J|^{1/2} \exp[\frac{1}{\rho_0 J}] \end{aligned} \tag{3.2.11}$$

where $P(x)$ is a polynomial, so that for $|\rho_0 J| << 1$, we may neglect $P(\rho_0 J)$ compared to the singular terms in the exponent. These leading two terms will be shown to derive from the leading and next leading logarithmic approximations to the perturbation theory which provide terms of order J^2, J^3 in

the β-function. Thus, provided we begin with a small bare coupling strength meaning $|J| << D$, we need only the leading two orders in the perturbative expansion of $\beta(J)$ to obtain an accurate estimate of the Kondo scale.

3.3 Scaling in Leading Logarithmic Order

In this subsection, we shall present a number of results of physical interest readily derivable from leading logarithmic scaling. Since there are rather different physics issues to be addressed in each model case, we shall organize the derivations by reference to the Hamiltonian being studied. We shall spend the most time, however, on the TLS model which displays the broadest range of coupling space to which the method can be applied. We note that Anderson's "poor man's scaling" [Anderson, 1970] is entirely equivalent to the results presented here, and that this approach may be generalized beyond the leading logarithmic order (Sólyom and Zawadowski, [1974]). We also note that at this order, there is no distinction between single- and multi-channel Kondo models; the channel number M enters at next leading order. Before we begin discussing the physics of each model, we will introduce the Abrikosov pseudo-particle trick (Abrikosov, [1965]), together with the generalization by Barnes [1976], which is useful in evaluation of perturbation theory diagrams.

3.3.1 Pseudo-particle method

We wish to treat the dynamics of the local pseudo-spin variable as manifested in the Green's function $\mathcal{G}$ discussed in the previous subsection in a manner which as much as possible resembles that of mobile particles with access to the full range of occupancies. To do so, we follow Abrikosov [1965]. Namely, when dealing with a local spin variable, we choose to represent the spin in a fermionic form, *viz.*

$$\sigma^i = \sum_{\mu,\nu} \sigma^i_{\mu,\nu} f^\dagger_\mu f_\nu \tag{3.3.1}$$

where $f^\dagger_\mu$ creates a local fermion of spin index μ. However, the spin variable can only have two states, corresponding to the single occupied states of the local fermion. The correspondence of states is

$$|\mu >= f^\dagger_\mu |0_{ps}> \tag{3.3.2}$$

where $|0_{ps}>$ is the vacuum of the pseudo-fermion. Thus, to faithfully represent the Hilbert space of the local spin variable, we must add to our Hamiltonian a fictitious chemical potential term

$$H_{pseudo} = -\lambda_{ps}(\sum_\mu f^\dagger_\mu f_\mu - 1) \tag{3.3.3}$$

in which the chemical potential λ_{ps} is taken to $-\infty$ at the end of calculations to project to the physical subspace where the fermion occupancy is unity. In so doing, we must also shift the arguments of all pseudo-fermion frequencies to be measured with respect to the infinitely negative chemical potential λ_{ps}. The one pseudo-particle state has a statistical weight $(2S+1)\exp(\beta\lambda_{ps})$ with $S = 1/2$, and thus physical quantities should be normalized by this factor. The normalization factor is not affected by renormalization in low orders (Black, Vladár , and Zawadowski [1982]). Other than the minor nuisance of the projection, all the standard rules of Feynman perturbation theory in the interaction may be carried out since the bare Hamiltonian is quadratic in the fermion operators.

Thus, prior to projection, the pseudo-fermion propagator in Matusubara frequency has the form

$$\mathcal{G}^{(\lambda_{ps})}_\mu(\omega) = -\int_0^\beta d\tau e^{i\omega\tau} < T_\tau f_\mu(\tau) f^\dagger_\mu(0) >= \frac{1}{i\omega - E_\mu + \lambda_{ps}} \tag{3.3.4}$$

where $\omega = 2\pi k_B T(n+1/2)$ is a Fermion Matsubara frequency. The superscript on $\mathcal{G}$ is a mnemonic notation indicating that the projection and frequency shift have not yet taken place. We shall always drop these superscripts after projection.

For the purposes of discussing the rescaling of the one particle Green's function of the pseudo-fermion spin variable, and the two-particle Green's function describing the localized spin and the conduction electrons, this prescription alone is sufficient and has the effect of suppressing the unphysical states where the fermion level is empty or doubly occupied. However, when we wish to calculate measurable properties, we must explicitly project to the occupancy 1 subspace with a normalization factor that depends upon λ_{ps}. We defer discussion of this point to Section 4 where we discuss the NCA method.

In the case of the Anderson Hamiltonian, discussed in conjunction with the models for U^{4+} and Ce^{3+} ions, we have a larger local Hilbert space. For example, in the Anderson model for the U^{4+} ion, we may fluctuate between the f^1 states labelled by magnetic index μ and the f^2 states labelled by quadrupolar index α. In this case, we follow Barnes [1976], who pointed out that while you may retain the pseudo-fermion label for the ground configuration, you can generalize by describing the excited configuration by a bosonic variable so as to retain a net fermionic character to the change of configuration. Hence, in this example, we augment the pseudo-particle space by a pseudo-boson operator $b_\mu^\dagger$ with the state correspondence

$$b_\mu^\dagger|0_{ps}>=|f^1,\Gamma_7,\mu> \quad ; f_\alpha^\dagger|0_{ps}>=|f^2,\Gamma_3,\alpha> \quad . \tag{3.3.5}$$

Correponding to the pseudo-fermion occupancy in the previous paragraph, we define the "f-charge" as

$$Q_f=\sum_\alpha f_\alpha^\dagger f_\alpha+\sum_\mu b_\mu^\dagger b_\mu \tag{3.3.6}$$

which commutes with the Hamiltonian of Eq. (2.2.19), in which we write the hybridization term as

$$H_{hyb}=-\frac{V}{\sqrt{N_s}}\sum_{k\alpha\mu} sgn(\mu)[f_\alpha^\dagger b_{-\mu}c_{k,8,\alpha,\mu}+h.c.] \quad . \tag{3.3.7}$$

Physically this commutation is obvious, since each time we create a pseudo-boson, we destroy a pseudo-fermion, or vice versa. We then add a fictitious chemical potential term of the form

$$H_{pseudo}=-\lambda_{ps}(Q_f-1) \tag{3.3.9}$$

and take $\lambda_{ps}\to-\infty$ at the end of all calculations. As alluded to in the last part of Sec. 2, we may regard the pseudo-boson as being the boson mediating the exchange between the heavy particle and conduction electrons; in the Kondo form, its dynamics is completely generated by the states of the electronic system, while in the Anderson form it has independent meaning as an excited configuration state. The boson carries the labels of the channel index of the conduction electrons, the fermion the label of the spin index.

Thus, when working in the Anderson formulation where Eq. (3.3.7) specifies the perturbation term, we must also introduce the pseudo-boson Green's function

$$\mathcal{G}_\alpha^{(\lambda_{ps})}(\nu)=-\int_0^\beta d\tau <T_\tau b_\alpha(\tau)b_\alpha^\dagger(0)>=\frac{1}{i\nu-E_\mu+\lambda_{ps}} \tag{3.3.10}$$

where $\nu=2\pi k_BTn$ is a bosonic Matsubara frequency, and again the superscript means prior to any projection procedure.

Note that we are completely free to interchange the boson and fermion representations for the two configurations since on carrying out the projection only Boltzmann statistics remains. We must however always ensure that one configuration is fermionic and one bosonic to guarantee that the electron addition and removal processes are fermionic in character, i.e., so that each hybridization event conserves fermion number. We also observe that the extension to inclusion of higher fermion or boson excited levels is straightforward: we must simply add the occupancy factors for the new states to the conserved charge Q_f. This is true in the case of the excited states for the tunneling center as well (see Sec. 3.4.2).

3.3.2 Leading Order Scaling in the TLS Model

The idea of the leading order scaling is based upon the second order perturbation theory diagrams already discussed in the introduction and displayed in Fig. 2. Referring back to that figure, we see that the lowest order correction to the two-particle interaction between the local spin and conduction electrons is either of the form where the intermediate state includes an excited particle (Fig. 2(a)) or hole 2(b)). This holds for all of the models of interest in our review.

Turning to the TLS model with couplings specified by Eq. (2.1.7), we see that each of these diagrams contributes a logarithmic dependence. To evaluate, we represent the dashed line of the diagram by the pseudo-fermion propagator of Eq. (3.3.4). We see that the sign of the logarithmic corrections is different, and also the ordering of the spin matrices and momentum dependent couplings is different. The total coefficient of the diagram corresponding to Fig. 2(a) is

$$\sum_{i,j} V^i_{\vec{k}_2,\vec{k}} V^j_{\vec{k},\vec{k}_1} \sigma^i \sigma^j$$

where $k_{1,2}$ are the incident(outgoing) momenta, k is the internal momentum, and we see that the coefficient of the term corresponding to Fig. 2(b) is given by

$$\sum_{i,j} V^i_{\vec{k},\vec{k}_1} V^j_{\vec{k}_2,\vec{k}} \sigma^i \sigma^j$$

so that the conduction momentum indices are reversed on the second term. If we now evaluate the total two-particle scattering amplitude corresponding to Fig. 21 to second order, at zero temperature, we find

$$T^m_{\hat{k}_2,\hat{k}_1}(\omega, D, V^i) = V^m_{\hat{k}_2,\hat{k}_1} - 2i\rho_0 \sum_{i,j} \int \frac{dS_F(\hat{k})}{S_F} [V^i_{\hat{k}_2,\hat{k}} V^j_{\hat{k},\hat{k}_1} \epsilon^{ijm} \log(\frac{D}{\omega})] \tag{3.3.11}$$

where $dS_F(\hat{k})$ is an element of Fermi surface area in the direction of $\hat{k}$ of the total Fermi surface area $4\pi k_F^2$, we have neglected the radial dependence of the matrix elements upon k, and the Levi-Civitta symbol arises from the algebra of the Pauli matrices. We have taken the density of states to be constant within the band of full width $2D$.

The change in the bandwidth $D \to D'$ discussed in the previous subsection can be compensated by readjusting the couplings V^i. That scaling dependence may be written as

$$\frac{\partial T^m_{\hat{k}_2,\hat{k}_1}}{\partial D} dD + \sum_{i,\hat{k},\hat{k}'} \frac{\partial T^m_{\hat{k}_2,\hat{k}_1}}{\partial V^i_{\hat{k},\hat{k}'}} dV^i_{\hat{k},\hat{k}'} = 0 \tag{3.3.12}$$

which implies that the equation for the rescaled coupling constants is given by

$$\frac{\partial V^m_{\vec{k}_2,\vec{k}_1}}{\partial ln D} = 2i\rho_0 \sum_{i,j} \epsilon^{ijm} \int \frac{dS_F(\vec{k})}{S_F} V^i_{\hat{k}_2,\hat{k}}(D) V^j_{\hat{k},\hat{k}_1}(D) \quad . \tag{3.3.13}$$

The logic of (3.3.12) is that the physics may be specified in terms of the amplitudes of the T-matrices for 1,2,3,... particle scattering. Thus to ensure that the physics is unchanged, we must ensure that after renormalization we obtain the same T-matrix which means that in lowering the cutoff which explicitly affects the second term we must modify the couplings accordingly.

Following Zawadowski [1980], we may write this equation in a more convenient form by using the matrix representation $V^m_{\alpha,\alpha'}$ given in Eq. (2.1.27), and by introducing the dimensionless variable $x = \log(D_0/D)$ where D_0 is the original bare bandwidth and D the rescaled bandwidth. Then the leading order scaling equation is

$$\frac{\partial V^m_{\alpha,\alpha'}}{\partial x} = -2i \sum_{i,j} \epsilon^{ijm} \sum_{\gamma} V^i_{\alpha,\gamma}(x) V^j_{\gamma,\alpha'}(x) \tag{3.3.13}$$

subject to the boundary condition that we match the bare couplings at the original bandwidth, so that

$$V^i_{\alpha,\alpha'}(0) = V^i_{\alpha,\alpha'} \tag{3.3.14}$$

where the r.h.s. of the last equation just contains the couplings that appear in the Hamiltonian.

We shall now list several characteristic features of the equations for the leading order scaling:
(i) Lack of dependence on the channel number M. In the derivation of Eq. (3.3.13), we used the diagrams of Fig. 2. Notice that since these diagrams have no closed loops, all dependence on the channel index is through the label α which is conserved throughout the scattering. At next leading order, we will obtain a closed electron loop inside the diagram and thus pick up a dependence upon the number of channels.

(ii) Results for a two-dimensional subspace: irrelevance of anisotropy. Let us for a moment accept that the dominant space of conduction electron orbital indices will be two-dimensional as we scale from the band edge, a point we shall prove shortly. Given this assumption, we shall illustrate that exchange anisotropy is irrelevant as we scale, and that if we begin scaling in a subspace where just two couplings are non-zero, that independent of their sign we will ultimately flow towards the isotropic, antiferromagnetic coupling regime as we rescale.

As we have already seen in Sec. 2.1, even when restricted to the two component space of orbital indices, the quantization axis of the electron pseudo-spin need not align with the quantization axis of the TLS pseudo-spin. This means that the most general form of the coupling matrices in a two dimensional subspace is

$$V^i_{\alpha,\alpha'} = V^i_{\tilde{x}}\sigma^{\tilde{x}}_{\alpha,\alpha'} + V^i_{\tilde{y}}\sigma^{\tilde{y}}_{\alpha,\alpha'} + V^i_{\tilde{z}}\sigma^{\tilde{z}}_{\alpha,\alpha'} \tag{3.3.15}$$

where we remind the reader that $i = x, y, z$ are the directions in the TLS pseudo-spin space for quantization axis z, and $\tilde{x}, \tilde{y}, \tilde{z}$ are the directions in the conduction orbital pseudo-spin space for quantization axis $\tilde{z}$. Now the scaling equations will determine the nine coupling coefficients V^i_β. With this *Ansatz*, the leading order scaling equation has the form

$$\frac{\partial V^m_\gamma}{\partial x} = -2\rho_0 V^i_\alpha V^j_\beta \epsilon^{ijm}\epsilon_{\alpha\beta\gamma} \quad . \tag{3.3.16}$$

Let us now view the couplings as vectors in the space of conduction pseudo-spin. Thus, $\vec{V}^i = (V^i_{\tilde{x}}, V^i_{\tilde{y}}, V^i_{\tilde{z}})$ and, for example,

$$\vec{V}^p \cdot \vec{V}^s = \sum_\alpha V^p_\alpha V^s_\alpha \quad . \tag{3.3.17}$$

Using the properties of the Levi-Civitta symbols, it is straightforward to show that

$$\frac{\partial(\vec{V}^p \cdot \vec{V}^s)}{\partial x} = \delta_{ps}[-8\rho_0(\vec{V}^x \times \vec{V}^y)\cdot\vec{V}^z] \quad . \tag{3.3.18}$$

We should make a couple of notes about the derivation of Eq. (3.3.18):
(i) The factor of eight follows from one factor of two when differentiating for $p = s$, one factor of two already present in the scaling equation, and one factor of two for the two possible orderings of i, j in ϵ^{ijp} to give a non-vanishing contribution.
(ii) We used the invariance of $(\vec{V}^i \times \vec{V}^j)\cdot\vec{V}^k$ upon permuting i, j, k cyclicly to write the RHS of (3.3.18) in a form manifestly independent of the choice of p.

From Eq. (3.3.18), we may infer that the magnitude of each coupling constant vector is independent of its index in the TLS space. So long as the product $(\vec{V}^i \times \vec{V}^j)\cdot\vec{V}^k > 0$, the vectors $\vec{V}^p$ increase in length as D is reduced, and the ratio of the couplings $|\vec{V}^p|/|\vec{V}^s|$ tends to unity. Further, since the RHS of Eq. (3.3.18) vanishes if $p \neq s$ and since the lengths of the vectors grow towards ∞, we see that

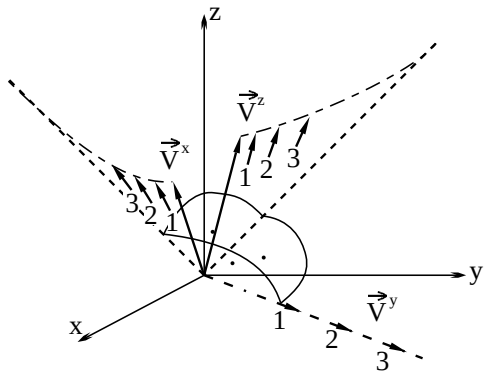

Figure 22: The scaling trajectories are depicted for Eq. (3.3.16) in the real space vaiable related to the lower indices. The starting vectors $\vec{V}^x$ and $\vec{V}^z$ are shown by solid lines, while $\vec{V}^y$ starst from $\vec{V}^y = 0$. $\vec{V}^x$ and $\vec{V}^z$ are scaled in the plane determined by them and $\vec{V}^y$ is moving in the normal direction to that plane. The scaling trajectories are depicted b dash-dotted lines, the asymptotes of vectors $\vec{V}^x$ and $\vec{V}^z$ are represented by dotted lines. The arrows indicatedthe vectors at different stages of the scaling, labeled by numbers. From Zawadowski [1980].

the vectors must become perpendicular upon scaling. If we start with $(\vec{V}^i \times \vec{V}^j) \cdot \vec{V}^k < 0$, the couplings tend towards zero, like the ferromagnetic Kondo model.

Hence, once we restrict the conduction orbital degrees of freedom to the two component space we see that the scaling drives the system towards isotropic coupling, allowing a simple rotation in the conduction orbital pseudo-spin space to give the Heisenberg form to the exchange coupling between the TLS and the electrons. Given the appropriate sign to the couplings, the effective Hamiltonian form at full strong coupling is ($V_{iso}(D) = |\vec{V}^p(D)|$)

$$H_{int}(D) = V_{iso}(D)\vec{\sigma}_{TLS} \cdot (\vec{\sigma}_{c\uparrow}(0) + \vec{\sigma}_{c\downarrow}(0)) \tag{3.3.19}$$

where the quantization axis of the conduction electrons has been rotated to line up with the TLS axis, and the real spin labels have been put on the conduction spin densities at the TLS site. Since the coupling is written without the conventional minus sign of the Kondo model, our positive choice of coupling coencides with the antiferromagnetic Kondo model. A schematic of the generic scaling trajectories in the coupling space for this antiferromagnetic case are illustrated in Fig. 22.

In the original TLS model, we have $|V^z| >> |V^x|, V^y = 0$. In this case, upon initially scaling we will generate $V^y \sim V^z V^x$. Thus the triple product $(\vec{V}^i \times \vec{V}^j) \cdot V^k \sim |V^x V^z|^2 > 0$ independent of the signs of V^x, V^z initially. That means we will *always* scale to strong coupling (towards the isotropic antiferromagnetic exchange model) in this extreme anisotropic limit.

(iii) Reduction to the two-dimensional subspace. The scaling equations themselves in the extreme anisotropic limit justify the restriction to the two-dimensional subspace of the conduction electron orbital pseudo-spin. This will hold provided the couplings $\vec{V}^{x,y}_{\alpha,\beta}$ in Eq. (3.3.13) have magnitudes much smaller than $V^z_{\alpha,\beta}$, as shown by Vladár and Zawadowski [1983(a)].

In order to prove this, we first perform a unitary transformation $V^z \to \tilde{V}^z$ in the conduction space such that

$$\rho_0 \tilde{V}^z_{\alpha,\beta}(0) = \tilde{v}^z_{\alpha,\beta}(0) = \tilde{v}^z_\alpha(0)\delta_{\alpha,\beta} \quad . \tag{3.3.20}$$

We now linearize the RHS of Eq. (3.3.13) in the small quantities v^x, v^z to obtain

$$\frac{\partial \tilde{v}^z}{\partial x} = 0 + \mathcal{O}(\tilde{v}^3) \tag{3.3.21.a}$$

(3.3.21.b) $$\frac{\partial \tilde{v}^x}{\partial x} = -2i[\tilde{v}^x(x), \tilde{v}^z(x)]_-$$

and

(3.3.21.c) $$\frac{\partial \tilde{v}^y}{\partial x} = 2i[\tilde{v}^x(x), \tilde{v}^z(x)]_-$$

where the $v's$ are understood to be matrices and the square brackets indicate commutators. We can separate the variables by differentiation with respect to x again, and for $i = x, y$ we find

(3.3.22) $$\frac{\partial^2 \tilde{v}^i(x)}{\partial x^2} = 4[[\tilde{v}^i, \tilde{v}^z]_-, \tilde{v}^z]_- \quad .$$

Using the diagonal form and the fact that $\tilde{v}^z$ is unchanged in this linearized form, we see that (putting matrix indices back in)

(3.3.23) $$\frac{\partial^2 \tilde{v}^i_{\alpha,\beta}}{\partial x^2} = 4\tilde{v}^i_{\alpha,\beta}(x)[\tilde{v}^z_\alpha(0) - \tilde{v}^z_\beta(0)]^2 \quad .$$

Given the boundary condition $\tilde{v}^y(0) = 0$, the solution to the linearized equations may be given as

(3.3.24.a) $$\tilde{v}^z_{\alpha,\beta}(x) = \tilde{v}^z_\alpha(0)\delta_{\alpha,\beta} \quad ,$$

(3.3.24.b) $$\tilde{v}^x_{\alpha,\beta}(x) = \tilde{v}^x_{\alpha,\beta}(0) cosh[2(\tilde{v}^z_\alpha(0) - \tilde{v}^z_\beta(0))x] \quad ,$$

and

(3.3.24.c) $$\tilde{v}^y_{\alpha,\beta}(x) = i\tilde{v}^x_{\alpha,\beta}(0) sinh[2(\tilde{v}^z_\beta(0) - \tilde{v}^z_\alpha(0))x] \quad .$$

What we learn from Eqs. (3.3.24.a-c) is that barring unforeseen degeneracies in the matrix v^z, whichever two elements of $\tilde{v}^z(0)$ which produce the largest difference $|\tilde{v}^z_\alpha(0) - \tilde{v}^z_\beta(0)|$ will produce the most rapid growth of the $\tilde{v}^{x,y}$ elements of the coupling. Because the functions grow *exponentially* with rescaling, any other splittings with even slightly smaller differences will grow negligibly fast upon scaling compared to the dominant subspace. In our TLS model, the axial character will always in practice restrict this dominant subspace to a linear combination of conduction orbitals with $m = 0$ and $l = 0, 1, 2$.

We stress that this argument depended upon the assumption of extreme anisotropy with zero initial coupling V^y, and that it has only been carried out so far in the context of second order scaling. We shall demonstrate that it is also valid if we go to all orders in V^z while remaining at lowest order in $V^{x,y}$. We conjecture that it is valid even in instances where the couplings are closer to isotropic and the perturbative approach breaks down, but this remains to be proven. As we shall explain, this result may have important implications for the Kondo models of U^{4+} and Ce^{3+} ions. In our discussion of these ions, we shall show that in the quadrupolar Kondo case the two-channel coupling to an additional symmetry allowed Γ_8 quartet is irrelevant through the two leading orders of scaling theory.

In fact, there is a symmetry based reason for this flow to a dominant two-dimensional subspace which holds at strong coupling. Namely, at strong coupling we have ample evidence that the exchange anisotropy vanishes. In this case, one can write down an $SU(2)$ invariant coupling deriving from the 2-dimensional manifold of the local pseudo-spin. We may then decouple this exchange via a Hubbard-Stratonivich transformation, as discussed in Sec. 2.3, and find that there are only two "exchange fluctuation" fields, indexed by the channel label, which are necessary to decouple the entire interaction. However, there is only a 1:1 match of the pseudo-spin index–a bonding combination of conduction operators will be selected which has a 1:1 match in pseudo-spin space with the labels of the TLS. The antibonding combination will decouple. We shall demonstrate this explicitly in the quadrupolar Kondo case.

(iv) General Form of the Fixed Point Hamiltonian. We will now offer some discussion of the form of the fixed point Hamiltonian for our two-channel Kondo models, although the discussion should be regarded as extrapolation at this point of the review, because the actual fixed point lies outside the perturbative regime. The point is that the perturbative scaling equations at lowest order provide considerable insight into the structure of the fixed point physics. This kind of analysis is supported in detail by the considerations of the numerical renormalization group and conformal field theory calculations.

Given the flow towards isotropy as the couplings grow, following Vladár and Zawadowski [1983(a)] we may write the couplings in the separated form

$$v^i_{\alpha,\beta}(x) = v^i(x)\tilde{V}^i_{\alpha,\beta} \tag{3.3.25}$$

where the first factor contains the scale dependence and the second factor the matrix structure which does not change upon further scaling. Then the scaling equations split into an equation describing the scaling, and one describing the operator algebra near the fixed point. The scaling equation is

$$\frac{\partial v^m(x)}{\partial x} = 2v^i(x)v^j(x) \quad , i,j,m \; cyclic \quad , \tag{3.3.26}$$

and the matrices are specified by the algebra

$$\tilde{V}^m_{\alpha,\beta} = \sum_{i,j,\gamma} \tilde{V}^i_{\alpha,\gamma}\tilde{V}^j_{\gamma,\beta}\epsilon^{ijm} \quad , \tag{3.3.27}$$

from which it is clear we simply scale to some irrep of $SU(2)$. Of course, it is possible that in the case of matrices of higher order, in a subspace the couplings follow $SU(2)$ symmetry while in the remaining subspace the coupling disappears. It has been shown by Zaránd [1995] that the representation of $SU(2)$ is always two dimensional for $M >> 1$ except in the presence of extra symmetry. We discuss this further in Secs. 3.3.3, 3.4.3 for rare earth and actinide impurity models. The analysis in the preceding note (iii) above makes clear we expect this to be generally a two dimensional representation to be dominant. The solution of Eq. (3.3.26) may be written as

$$v^i(x)^2 = \psi^2(x) + v^i(x_0)^2 \quad , \tag{3.3.28}$$

where

$$\frac{\partial \psi^2(x)}{\partial x} = 4v^x v^y v^z \tag{3.3.29}$$

with boundary condition $\psi^2(x_0) = 0$.

What is intriguing about this scenario is that we begin with an apparently artificial spin variable describing the TLS which is not conserved, even if we shut off the spontaneous tunneling terms. In examining the scaling of the exchange terms alone, we develop this picture that at the fixed point one has a full isotropy in the combined pseudo-spin space of the TLS plus conduction electrons, although this space has no obvious reason to become so symmetric from purely high energy considerations.

Thus, the Kondo effect serves to *restore* symmetries which are not present in the bare Hamiltonian, which is a fairly remarkable result. This contrasts with the usual scenario in high energy physics, in which symmetry is high at high temperatures and reduced as we lower the temperature.

This increase of symmetry on approach to the fixed point also holds for the quadrupolar Kondo effect, where generically only two of the local spin tensors should transform as an irrep of the point group that is quadrupolar in character, yet an extra tensor of octupolar character is generated and at the two-channel fixed point there is full isotropy in this unusual combined space.

We close this note on the general properties of the fixed point with an open question about the nature of the scaling. In the previous note we argued that when the bare couplings are extremely anisotropic, the scaling will preferentially select a two-dimensional subspace in the conduction orbital

pseudo-spin space as the dominant one. What is not clear is whether the couplings in the excluded space will grow or shrink as well when one moves out of the perturbative regime and into the fixed point region. This growth is ruled out by the arguments of Zaránd [1995] for $M >> 1$. While it is physically unlikely that such growth occurs for the physically relevant M=2 case, no rigorous proof yet exists to support this intuition.

(v) Leading order estimate of the Kondo scale.

If we first consider the fully isotropic limit, we will have to integrate the leading order differential equation

$$\frac{\partial v(x)}{\partial x} = 4v(x)^2 \tag{3.3.30}$$

and identify where the coupling strength grows unity. This yields the estimate

$$T_K^{(I)} \approx D_0 \exp(-\frac{1}{4v(0)}) \tag{3.3.31}$$

where the superscript (I) denotes leading order. If we were to use instead spin 1/2 matrices, we would replace the exponent by $-1/v(0)$.

In the TLS case where the starting parameters are extremely anisotropic, the perturbation theory will break down and the couplings grow to order unity when the energy scale from the leading order equations is such that $v^x(x) \approx v^z(0)$, which produces the leading order estimate for the Kondo scale, $T_K^{(I)}$ as

$$T_K^{(I)} \approx D_0(\frac{v^x(0)}{4v^z(0)})^{\frac{1}{4v^z(0)}} \tag{3.3.32}$$

when we use Pauli matrices (see Vladár and Zawadowski [1983(a)]). If we use spin 1/2 matrices, this expression changes only in that the singular exponent is modified according to

$$\frac{1}{4v^z(0)} \rightarrow \frac{1}{v^z(0)} \quad .$$

3.3.3 Leading Order Scaling for model U^{4+} and Ce^{3+} ions

Much of the work has already been done in the development of the equations for the TLS. We shall present some useful generalizations of these equations appropriate to the physics of the models for U^{4+} and Ce^{3+} ions.

(a) Leading order Kondo scale

This is the simplest modification to the TLS result. We utilize the isotropic result of Eq. (3.3.31) and replace $4v(0)$ by $|g(0)| = N(0)J$, where J is the maximum (in magnitude) of J_7, J_8 in the Ce^{3+} case. Hence

$$T_K^{(I)} = D_0 \exp(\frac{1}{g(0)}) \quad . \tag{3.3.33}$$

(b) Flow to two-dimensional subspace for U^{4+} ion in cubic symmetry

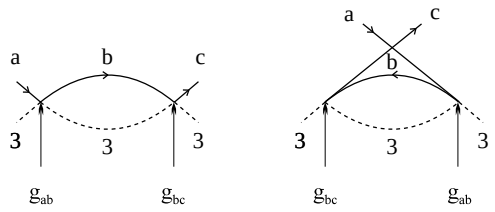

Figure 23: Leading order multiplicative renormalization group diagrams for the quadrupolar Kondo model with two conduction quartets. The lines marked with 3 are pseudo-fermion propagators for the non-Kramers Γ_3 doublet. The lines marked with a, b, c =8,8' are conduction electron lines which may come from either Γ_8 quartet (labeled by a, b, c =8,8' in the text and derived from the $j = 5/2, 7/2$ partial waves about the impurity). The vertices are coupling strengths g_{ab} which are symmetric in a, b and scatter from quartet a to quartet b. In the simplest model, $g_{88} > g_{88'} > g_{8'\,8'}$, and $g^2_{88'} = g_{88} g_{8'\,8'}$.

We could have generalized the discussion of the quadrupolar Kondo Hamiltonian in Sec. 2.2.1 to have allowed for exchange coupling to more than one Γ_8 quartet. What we shall demonstrate presently is that at leading order scaling, this produces a flow to a dominant two-dimensional subspace as has been found in the extremely anisotropic TLS case above. The interpretation is simply that one is selecting the relevant bonding combination of the Γ_8 states. Our scaling analysis follows similar reasoning developed for a different problem by Cragg, Lloyd, and Nozières [1980].

The physical source of the second Γ_8 state is the $j = 7/2$ angular momentum multiplet of the conduction electron partial wave states. Let us denote the Γ_8 level from the $j = 5/2$ partial wave manifold with no prime, and that from the $j = 7/2$ multiplet with a $'$. The exchange Hamiltonian of Eq. (2.2.6) is then generalized to

$$H_{ex} = \frac{-1}{N_s} \sum_{l,l'=8,8'} J_{l,l'} \vec{\tau}_I \cdot \sum_{k,k',\alpha,\alpha',\mu} \vec{\tau}_{\alpha,\alpha'} c^\dagger_{kl\alpha\mu} c_{k'l'\alpha'\mu} \quad , \tag{3.3.34}$$

where the couplings $J_{8,8'} = J_{8',8}$. In fact, since the bare couplings are determined by the Schrieffer-Wolff transformation, we may say more about the relative size of the bare couplings. Assume that the strength of hybridization of the 8 quartet with the excited Γ_7 and ground Γ_3 doublets is $a_8 V_0$, where the hybridization strength V_0 is independent of the labels $8, 8'$, and the corresponding hybidization strength for the $8'$ quartet is $a_{8'} V_0$. Then we have that

$$J_{l,l'} = a_l a'_l \frac{2V_0^2}{\tilde{\epsilon}_f} \tag{3.3.35}$$

so that, e.g, $J_{8,8'} = -\sqrt{J_{8,8} J_{8',8'}}$. Note that the appropriate way to think about the above exchange interaction is in terms of a conduction electron spin which is large, i.e., $N_c = 4$. The reason is that the channel index is still the two-dimensional magnetic index, and we have simply enlarged the space of orbital labels which couple to the impurity. Thus, this model is analogous to the TLS model with N_c actually arbitrary.

Using the diagrams shown in Fig. 23, we obtain the following leading order scaling equations for the three dimensionless couplings $g_{8,8}, g_{8,8'}, g_{8',8'}$:

$$\frac{\partial g_{8,8}}{\partial x} = -g^2_{8,8} - g^2_{8,8'} \quad , \tag{3.3.36.a}$$

$$\frac{\partial g_{8,8'}}{\partial x} = -g_{8,8'} [g_{8,8} + g_{8',8'}] \quad , \tag{3.3.36.b}$$

and

$$\frac{\partial g_{8',8'}}{\partial x} = -g^2_{8',8'} - g^2_{8,8'} \quad . \tag{3.3.36.c}$$

Notice that we lack a factor of four compared with TLS scaling from our use of $S = 1/2$ matrices here, and that the different sign convention has flipped the sign of the β-functions relative to the TLS case.

These scaling equations may be separated into soluble form in two stages. First, we identify a constant of the motion. By subtracting Eq. (3.3.36.c) from Eq. (3.3.36.a) and taking the ratio with Eq. (3.3.36.b), we see that

$$\frac{d(g_{8,8} - g_{8',8'})}{dg_{8,8'}} = \frac{(g_{8,8} - g_{8',8'})}{g_{8,8'}} \tag{3.3.37}$$

from which we infer that

$$g_{8,8'} = c_0(g_{8,8} - g_{8',8'}) \quad . \tag{3.3.38}$$

We may infer the constant c_0 from the initial conditions and Eq. (3.3.35) as

$$c_0 = \frac{a_8 a_{8'}}{(a_8^2 - a_{8'}^2)} \quad . \tag{3.3.39}$$

Next, we define the coefficients

$$\alpha_8 = a_8^2/(a_8^2 - a_{8'}^2) \tag{3.3.40.a}$$

and

$$\alpha_{8'} = -a_{8'}^2/(a_8^2 - a_{8'}^2) \quad . \tag{3.3.40.b}$$

Define the linear combinations of exchange couplings

$$\tilde{g} = \alpha_8 g_{8,8} + \alpha_{8'} g_{8',8'} \tag{3.3.41.a}$$

and

$$\tilde{g}' = \alpha_{8'} g_{8,8} + \alpha_8 g_{8',8'} \quad . \tag{3.3.41.b}$$

Note that $\alpha_8 + \alpha_{8'} = 1$, so that $\tilde{g}(0) = g_{8,8}(0) + g_{8',8'}(0)$. Then the scaling equations, with use of the constant of motion identified in the preceding paragraph, decouple giving

$$\frac{\partial \tilde{g}}{\partial x} = -\tilde{g}^2 \tag{3.3.42.a}$$

and

$$\frac{\partial \tilde{g}'}{\partial x} = -(\tilde{g}')^2 \quad . \tag{3.3.42.b}$$

In principle, both couplings will grow. However, with the use of the initial conditions, we see that $\tilde{g}'(0) = 0$, so that this set of couplings just drops out. This is not the case for $\tilde{g}$, and if we solve to estimate the leading order Kondo scale, we obtain

$$T_K^{(I)}(\tilde{g}(0)) \approx D_0 \exp(\frac{\tilde{\epsilon}_f}{2[a_8^2 + a_{8'}^2]N(0)V_0^2}) \quad . \tag{3.3.43}$$

Clearly, we can interpret the factor in square braces in this equation as simply representing the normalization of the "bonding combination" of Γ_8 orbitals. We shall show in the next subsection that this result also holds in next leading order scaling as well.

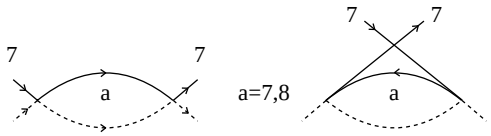

Figure 24: Leading order multiplicative renormalization group processes in the presence of excited crystal field levels for a Ce^{3+} impurity. The dashed line is a pseudo-fermion propagator for the impurity states. The label a refers to the intermediate states of both impurity and conduction electrons, which can be either Γ_7 (assumed to be the impurity ground state) or Γ_8 (assumed to be the impurity excited state). Assuming only $f^0 - f^1$ virtual charge fluctuations, all coupling strengths are equal.

(c) Effect of excited crystalline electric field levels

We may see using leading order scaling methods that excited crystalline electric field levels produce an enhancement of the Kondo scale estimated without the excited states. Our derivation is restricted to the rescaling of the J_7 exchange for the model Ce^{3+} ion, and follows the original analysis of Yamada, Yosida, and Hanzawa, [1984] and the analogous analysis for the TLS model of Zaránd and Zawadowski [1994(a),1994(b)] (see Sec. 3.4.2).

The idea is similar to the preceeding subsection. The diagrams are shown in Fig. 24. By virtually scattering into the Γ_8 conduction and f^1 manifolds through the coupling $J_{78} = J_7$ (due to the assumption of mixing only with f^0, Γ_1 excited configuration) we obtain the leading order scaling equation

$$\frac{\partial g_7}{\partial x} = -g_7^2[1 + 2\frac{D}{D + \Delta_8}] \tag{3.3.44}$$

where Δ_8 is the splitting between the $f^1\Gamma_7$ and $f^1\Gamma_8$ levels. The extra energy appears in the denominator due to the virtual excitation to the Γ_8 level, which is much larger than D when we shrink D to order $T_K^{(I)}$. The factor of 2 is the ratio of the degeneracies of the Γ_8 quartet to the Γ_7 doublet, which reflects the greater number of ways to scatter into the Γ_8 state.

It is straightforward to integrate these equations, and we find that

$$T_K^{(I)} = D_0(\frac{D_0}{T_K^{(I)} + \Delta_8})^2 \exp(\frac{1}{g_7(0)}) \quad . \tag{3.3.45}$$

This represents a self-consistent equation to solve for the Kondo scale. In the limit where $T_K^{(I)} << \Delta_8$, we obtain an enhancement over the Kondo scale without crystal field excitations by the rather large amount of $(D_0/\Delta_8)^2$. Given $D_0 \simeq 10^4 K$, $\Delta_8 \simeq 10^2 K$) this enhancement can be of order 10^4! This is obviously a significant effect. In the limit when $T_K^{(I)} >> \Delta_8$, we find that $T_K^{(I)}$ tends to the value of the six-fold degenerate multiplet obtained by forcing the Γ_8 level to be degenerate with the Γ_7 level. We will obtain the physics of the ground doublet provided that the Kondo scale of the full multiplet is smaller than Δ_8, because then the crystal field scale cuts off the logarithmic growth associated with the full multiplet.

Hence, the excited crystal field state produces a crossover between a high temperature Kondo effect associated with the entire multiplet and a low temperature Kondo effect associated with the ground multiplet, but significantly enhanced over the value with $\Delta_8 = \infty$. Within the NCA analysis of Sec. 5, it is easy to generalize this picture from the simple example treated here, and below all crossovers one generically finds a Kondo scale enhanced by factors of $\sim (D/\Delta_{cef})^{N_{cef}/N_{grd}}$ for all levels at energy Δ_{cef} with degeneracy N_{cef} (the ground level has degeneracy N_{grd}). Similar results obtain for each excited spin-orbit multiplet and LS term in multielectron configurations.

(d) Leading order scaling for a Ce^{3+} ion with spin/channel-spin coupling included

Following Kim [1995], Kim and Cox [1995,1996,1997], and Kim, Oliveira, and Cox [1996], we examine the effects of the channel-spin/spin coupling developed in Eqs. (2.2.34-2.2.38). We restrict ourselves to the space of Γ_8 coupling alone, i.e., neglect the scattering between Γ_8 and Γ_7 conduction partial waves. In this case, the coupled equations for the dimensionless interaction strengths $g_8 = N(0)J_8$ and $\tilde{g}_8 = N(0)\tilde{J}_8$ are

$$\frac{\partial g_8}{\partial x} = g_8^2 - \frac{1}{2}\tilde{g}_8^2 \tag{3.3.47}$$

and

$$\frac{\partial \tilde{g}_8}{\partial x} = -\tilde{g}_8 g_8 \quad . \tag{3.3.48}$$

These equations follow from the unusual commutation relations of the $\tilde{S}_{c8}$ operators specified in Eqs. (2.2.37) and (2.2.38). What can be verified from the above scaling equations are the following:
1) For $2g_8 > |\tilde{g}_8|$, g_8 grows and $|\tilde{g}_8|$ shrinks.
2) For $2g_8 = |\tilde{g}_8|$, both coupling strengths shrink to zero.
3) For $2g_8 < |\tilde{g}_8|$, $\tilde{g}_8$ grows without any sign change, and g_8 is driven towards the lines defined by $2g_8 = -|\tilde{g}_8|$.
4) For $\tilde{g}_8 = 0$ and $g_8 < 0$, there is no growth in $\tilde{g}_8$ and g_8 shrinks to zero. This is of course the usual ferromagnetic case.

Clearly the lines $2g_8 = \pm\tilde{g}_8$ occupy a special place in this scaling analysis, and the reason as indicated in Sec. 2.2 is that the tensors $I_{c8}^{(i)}(0) - S_{c8}^{(i)}(0) \pm 2\tilde{S}_{c8}^{(i)}(0)$ obey the ordinary angular momentum commutation relations and define a pseudo-spin 3/2 irrep. Along these lines the effective exchange coupling is $-J_8 \vec{S}_{I7} \cdot \vec{I}_{c8}(0)$. It is clear that for positive $g_8 = |\tilde{g}_8|/2$ one has ferromagnetic coupling of the pseudo-spin 3/2 conduction operators to the impurity spin, while when $g_8 = -|\tilde{g}_8|$ we obtain an antiferromagnetic coupling of the impurity pseudo-spin to the conduction pseudo-spin. Collapse to the line $g_8 = -\tilde{g}_8/2$ indicates dominant virtual fluctuations to the Γ_4 excited state, while collapse to the line $g_8 = \tilde{g}_8$ indicates dominant virtual fluctuations to the Γ_5 excited state. We note that the symmetry constraints along these lines imply that their special role in the coupling constant phase diagram will be maintained non-perturbatively.

3.4 Next Leading Order Scaling

The power of the multiplicative renormalization group equations is not evident at leading order scaling, because the most important corrections to the wave function renormalization factors z occur at next leading order. In this subsection, we shall explore the next leading order scaling equations for the Kondo models of interest using the multiplicative renormalization group equations. In parallel to the previous subsection on leading order scaling, we shall first present the results for the TLS model, which represents the most general formulation of the fully anisotropic Kondo model, and then present briefly results for the models of U^{4+} and Ce^{3+} ions. In the last part of this subsection, we will perform some stability analyses of the next leading order scaling equations about the non-trivial fixed point, to illustrate the destabilizing effects of channel fields, and the stability against exchange anisotropy in the simplest cases.

3.4.1 Next Leading Order Scaling for the TLS model

(a) Overview

What we seek are equations relating the original couplings V^i, Δ^i and Green's functions at bandwidth D to the rescaled couplings $V^{i'}, \Delta^{i'}$ and Green's functions at bandwidth D' using the multiplicative renormalization group formalism developed in Sec. 3.2.2. We will write all electron-TLS couplings in dimensionless form ($v^i = V^i \rho_0$). We shall perform the scaling analysis at zero temperature, with the external conduction electron frequency ω serving as the infrared cutoff in our equations.

The multiplicative renormalization group equations for the TLS model read (Vladár and Zawadowski [1983b])

$$G_k(\omega/D', v^{i'}, \Delta^{i'}) = G_k(\omega/D, v^i, \Delta^i) \quad , \tag{3.4.1}$$

$$\mathcal{G}(\omega/D', v^{i'}, \Delta^{i'}) = Z_2(D'/D, v^i)\mathcal{G}(\omega/D, v^i, \Delta^i) \quad , \tag{3.4.2}$$

$$\tilde{\Gamma}^i_{\alpha,\beta}(\omega/D', v^{i'}) = (Z^i_{\alpha,\beta}(D'/D, v^i))^{-1}\tilde{\Gamma}^i_{\alpha,\beta}(\omega/D, v^i) \quad , \tag{3.4.3}$$

and

$$v^{i'}_{\alpha,\beta} = (Z_2(D'/D, v^i))^{-1} Z^{(i)}_{\alpha,\beta}(D'/D, v^i) v^i_{\alpha,\beta} \tag{3.4.4}$$

where the functions $G_k, \mathcal{G}, \tilde{\Gamma}^i$ only depend upon dimensionful quantities. Note that: (i) the renormalization factor Z_1 has been dropped because corrections to the conduction electron Green's function in the dilute limit are of order $1/N_s$. This point will clearly need reexamination in lattice models. (ii) The meaning of $\tilde{\Gamma}^i$ is that the full interaction vertex is given by

$$\Gamma^i_{\alpha,\beta} = V^i_{\alpha,\beta}\tilde{\Gamma}^i_{\alpha,\beta} \tag{3.4.5}$$

so that $\tilde{\Gamma}^i_{\alpha,\beta}(D_0) = 1$. We use Γ^i when some of the V^i are zero, because then $\tilde{\Gamma}^i$ is not well defined. (iii) The pseudo-fermion Green's function $\mathcal{G}$ is generalized from the bare form of Eq. (3.3.4) to include a self-energy term. Written in matrix form for real frequencies at $T = 0$, we have

$$\mathcal{G}^{(\lambda_{ps})}(\omega/D, v^i, \Delta^i) = \frac{1}{(\omega + \lambda_{ps})\mathbf{I} - \Delta^i/2\sigma^i - \Sigma_{ps}(v, \omega)} \tag{3.4.6}$$

where $\mathbf{I}$ is the identity matrix in the 2×2 space, and Σ_{ps} is the pseudo-fermion self-energy.

(b) $\Delta^i = 0$ case

To proceed with these equations, let us start with the special case $\Delta^i = 0$. As mentioned, we needn't compute G_k beyond zeroth order in perturbation theory for the purposes of the scaling. We compute $\mathcal{G}, \tilde{\Gamma}^i$ in the leading two orders. We find that $\tilde{\Gamma}^i$ is already renormalized at first order in scaling; in fact, this is clear from the discussion surrounding Eq. (3.2.7), in which the renormalization factor z corresponds to Z^i in our present discussion. The renormalization of the pseudo-fermion Green's function occurs at next leading order, i.e., the leading order term in the perturbation expansion is order v^2 for Σ_{ps}.

The scaling transformation proceeds as follows:

(i) First the leading order term of the vertex are calculated and then Z^i is obtained in the leading logarithmic approximation; this corresponds to the diagram of Fig. 25(a). Self consistent determination of Z^i follows by inserting the unperturbed ($D = D'$) value of v for Γ^i. What we obtain is just (suppressing matrix indices)

$$(\delta v^i)^{(1)} = -2i \sum_{ij} v^j v^k \epsilon^{jki} \log(\frac{D}{D'}) \tag{3.4.7}$$

where the superscript (1) denotes leading order scaling. This is clearly just a repeat of the discussion in the previous subsection and if stopped at this point leads to precisely the same scaling equations.

(ii) At next leading order we compute Z_2, Z^i being careful not to include terms which will be obtained by the solution of the leading order order scaling equation. Since, as remarked earlier, solving that equation is equivalent to summing an infinite order of diagrams, we must take care order by order in the renormalized couplings that we generate unique *non-parquet* diagrams. Such a diagram is illustrated in Fig. 25(b). The test is simple: at a particular higher than leading order of the renormalized coupling, if the diagram can be cut in two by snipping one pseudo-fermion line and one conduction line, it is a *parquet* diagram. Once we compute the non-parquet third order diagram of Fig. 25(c) we must snip two pairs of conduction/pseudo-particle lines to break the diagram up, a test we can apply to higher order diagrams to determine if they are due to iteration of this diagram. Clearly the complexity of the procedure makes it unfeasible to apply beyond a few orders of perturbation theory. The lowest order self energy term for the pseudo-fermion is shown in Fig. 26. The corresponding renormalization factor Z_2 is given by

$$Z_2 \simeq 1 + (\frac{\partial[\Sigma_{ps}(\omega/D', v^{i'}) - \Sigma_{ps}(\omega/D, v^i)]}{\partial\omega})_0 \tag{3.4.8}$$

and is shown in Fig. 25(b). This figure makes it clear why it appears only at next leading scaling: we must multiply the second order correction coming from the frequency derivative of the self-energy times one factor of v^i to produce a third order renormalization of the v^i's. It is straightforward to show that the diagram of Fig. 25(c) is proportional to $\log(D/\omega)$, while the (shifted) pseudo-fermion self-energy goes as $\omega\log(D/\omega)$, so that the derivative in Eq. (3.4.8) produces a logarithm.

Note that the dividing out of Z_2 in the renormalization of V makes physical sense when viewed from the perspective of Landau's Fermi liquid theory. We are looking for the interaction between the conduction electrons and the fully dressed pseudo-fermion, or the pseudo-fermion "quasi-particle." Hence, since the quasi-particle has spectral weight Z_2, we should divide the relevant coupling by that quantity to correctly normalize in the quasi-particle space.

Since the next leading order term is more difficult to compute correctly than the leading order term, we will spell out a few details here. The changing of $D \to D'$ now leads to a total next leading order correction $(\delta v^i)^{(2)}$ to v^i which is given by (suppressing matrix indices)

$$\begin{aligned}(\delta v^i)^{(2)} &= v^i[(\mathcal{O}(v^i)^2\ from\ Z^i) - (\mathcal{O}(v^i)^2\ from\ Z_2)] \\ &= Mv^i[(Tr(v^i)^2 - \sum_{j\neq i} Tr(v^j)^2) - (\sum_j Tr(v^j)^2)]\log(\frac{D}{D'}) \\ &= 2Mv^i[Tr(v^j)^2 + Tr(v^k)^2]\log(\frac{D}{D'})\ \ ,\end{aligned} \tag{3.4.9}$$

where the terms in parentheses in the second line have a direct correspondence to the terms in parentheses immediately above. Notice the explicit appearance of the number of channels here, which derives from the closed conduction loop in Fig. 25(c) in which we may freely sum on channel index.

Putting (i),(ii) together, we see that through the leading two orders we have, putting all matrix indices back in, that

$$\frac{\partial v^m_{\alpha,\beta}}{\partial x} = -2i\sum_{i,j,\gamma} v^j_{\alpha,\gamma}(x)v^k_{\gamma,\beta}(x)\epsilon_{ijm} - 2Mv^m_{\alpha,\beta}(x)\sum_{l\neq m} Tr[(v^l(x))^2] + ... \tag{3.4.10}$$

which may be solved with the anticipation of flow to a two-dimensional subspace by substituting

$$v^i_{\alpha,\beta}(x) = v^i(x)\sigma^i_{\alpha,\beta} \tag{3.4.11}$$

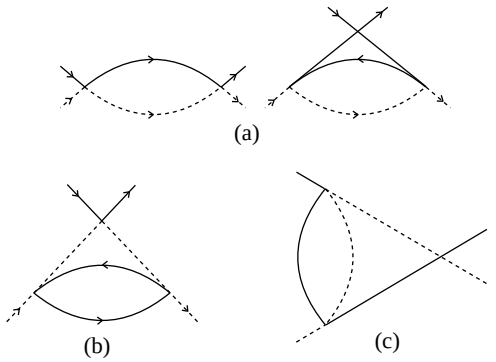

Figure 25: The vertex diagrams in the leading and next-leading logarithmic orders. The solid lines stand for the conduction electron and the dashed line for the heavy particle. Note that (c) is not an actual vertex correction.

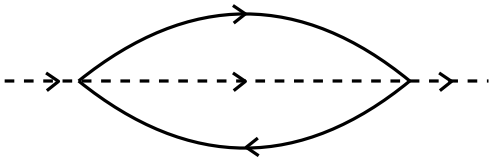

Figure 26: The first non-vanishing logarithmic self-energy diagram for the heavy particle. The solid line represents the electron and the dashed line the heavy particle.

which gives us (for $m \neq i \neq j$)

$$\frac{\partial v^m(x)}{\partial x} = 4v^i(x)v^j(x) - 4Mv^m(x)[(v^i(x))^2 + (v^j(x))^2] + \mathcal{O}((v^i)^4) \quad . \tag{3.4.12}$$

Note that if we had chosen to use spin 1/2 matrices instead of Pauli matrices, we would change the prefactor of the $\mathcal{O}(v^2)$ term to 1 from 4, and the prefactor of the $\mathcal{O}(v^3)$ term to 1/4 from 4. The flipping of sign between the TLS convention and the typical Kondo convention ($v^i > 0 \rightarrow J^i < 0$) would flip the sign of the first term and leave the sign of the second term which expresses the fact that the couplings grow *more negative* as you reduce the bandwidth (increase x).

(c) $\Delta^i \neq 0$ *case*

Now we are interested in deriving equations for the renormalization of the splitting Δ^i. In view of Eq. (3.4.2), we see that since Δ^i appears in $\mathcal{G}^{-1}$ that it must renormalize according to

$$\Delta^{i'}(D', v^i) = Z_2(D'/D, v^i)\Delta^i(D, v^i)$$

$$+ [\Sigma_{ps}(\omega = 0, D', v^{i'}, \Delta^{i'}) - \Sigma_{ps}(\omega = 0, D, v^i, \Delta^i)] \tag{3.4.13}$$

where we must include the latter term as a price for taking Z_2 independent of the splittings Δ^i. This term reflects the shifts of the splittings through self-energy effects. It is straightforward to estimate this by observing that the self-energy diagram of Fig. 26 vanishes when the combination $\omega + \lambda_{ps} - \Delta^i\sigma^i/2$ vanishes, so we may linearize the Green's function, and employ ω as the infrared cutoff of the resulting logarithmic divergence so that we find

$$\Sigma_{ps}(\omega, D, v^i, \Delta^i) \approx -M \sum_l Tr[(v^l)^2]\sigma^l[(\omega - \lambda_{ps})\mathbf{I} - \sum_i \Delta^i\sigma^i]\sigma^l \tag{3.4.14}$$

and thus with the use of Eq. (3.4.13) we obtain

$$\frac{\partial \Delta^i(x)}{\partial x} = -2M \sum_{j \neq i} \Delta^i Tr[(v^j)^2] \quad . \tag{3.4.15}$$

Note that: (i) The sign in front of the RHS for this equation: the fact that it is negative means that as we move in from the weak coupling fixed point, the splittings and spontaneous tunneling of the TLS actually renormalize downwards with reduced bandwidth. However, we shall see that this is not the correct interpretation overall: the dimensionless splitting Δ^i/D *grows* and is thus to be viewed as a relevant perturbation near the fixed point of Eq. (3.4.12). We shall elaborate on this point below. (ii) In this case where the impurity pseudo-spin is equivalent to spin 1/2, the rescaling cannot generate any splittings unless there is a bare splitting present. This corresponds to the fact that a real spin-1/2 doublet must remain degenerate in the absence of an applied magnetic field, i.e., it is not susceptible to quadrupolar splittings. If we were to allow for higher pseudo-spin, as in the generalized multi-channel models of Sec. 2.3, we would find quadrupolar splittings generated by anisotropic exchange couplings [H.B. Pang, 1992]. We shall return to this point in the numerical renormalization group (Sec. 4.2) and conformal field theory (Sec. 6.2) discussions and in the fixed point stability analysis below.

(d) Analysis of the Fixed Point

We note that the RHS (the β-function) of Eq. (3.4.12) vanishes when

$$v^x = v^y = v^z = v^* = \frac{1}{2M} \quad . \tag{3.4.16}$$

This is then a *non-trivial fixed point* of the fourth type, discussed in Sec. 3.1.1. Clearly the couplings are isotropic at this fixed point. However, caution is required in accepting the validity of this finding. Consider these cases:

M = 1. In this case, the fixed point occurs for $v^* = 1/2$ which is certainly outside the perturbative regime. We cannot trust the low order expansion of the β function. Strong coupling calculations first performed by Wilson [1973,1975] show that in this case, which corresponds to the single channel anisotropic Kondo model, the fixed point is of the strong coupling form, type (3) of Sec. 3.1.1.

M = 2. In this case, the fixed point occurs for $v^* = 1/4$, for which the perturbation expansion is still of questionable valididity. Nonetheless, the qualitative correctness of the fixed point is confirmed by non-perturbative methods such as the Bethe-Ansatz and NRG. In this case, the physical arguments presented in the beginning regarding the inability of the two conduction channels to exactly compensate the impurity pseudo-spin taken together with non-perturbative calculations confirm that the non-trivial fixed point is indeed obtained in the zero temperature limit, provided the splittings and spontaneous tunneling are zero. However, this is precisely the marginal case: rather than power law critical divergences in physical quantities, logarithmic divergences are obtained.

M >> 2. In this case, the fixed point is small and well within the bounds of the perturbative expansion of the β-function. In principle, all properties may be obtained as an expansion in powers of $1/2M$, the fixed point coupling strength, and therefore one has a clear hint of universality. For a more detailed discussion of this issue, we direct the reader to Sec. (3.4.3), which reviews the work of Muramatsu and Guinea [1986] and especially Gan, Andrei and Coleman [1993] on the calculation of physical properties at the nontrivial fixed point.

Note that a different kind of large M expansion is provided by the NCA analysis of the $SU(N) \otimes SU(M)$ multichannel model in which $N \to \infty$ while $M/N = \gamma$ is held fixed; see Sec. 5.1 for a review of this work.

(e) Linearized Stability analysis of the Fixed point

We may obtain further insight into the physics by linearizing the multiplicative renormalization group equations around the fixed point coupling. Such an approach will be valid for couplings $v^i(x)$ near v^*. This corresponds to an analysis of the stability of the fixed point against the introduction of various fields and couplings. We shall discuss, in order, exchange anisotropy, the relevance of the Δ^i about the fixed point, and channel field splitting.

Exchange Anistropy. We write $\delta v^i(x) = v^i(x) - v^*$ and expand the β-function to linear order in the deviations. We begin scaling at a bandwidth parameter value of x_0. The result is

$$\frac{\partial \delta v^i}{\partial x} = -\frac{2}{M}\delta v^i \tag{3.4.17}$$

which is readily solved to yield

$$\delta v^i(x) = \delta v^i(x_0)(\frac{x}{x_0})^{-\frac{2}{M}} \quad . \tag{3.4.18}$$

Clearly, the introduction of anisotropic couplings is completely *irrelevant* around the fixed point: as we increase x from our initial value of x_0, the couplings actually diminish. We note that Muramatsu and Guinea [1986] obtained the same scaling equations using a different diagrammatic technique.

It is worth noting in this context, following Affleck and Ludwig [1991a)], that while the fixed point coupling is *non-universal* (clearly we can insert an overall arbitrary scale factor in the energy) the slope of the β-function at the fixed point which determines the scaling exponent in Eq. (3.4.19) must be universal.

This argument is actually independent of the magnitude of the localized pseudo-spin [H.B. Pang, 1992]. In the special case of a spin 1/2 localized pseudo-spin, then when the Δ^i are set to zero, then no further splitting can be induced by the exchange anisotropy in this case. However, if we were to allow the impurity spin to be greater than 1/2, and keep M large, we would induce through the self-energy quadrupolar splittings of the pseudo-spin, and in this way the exchange anisotropy would generate a *relevant* perturbation.

Relevance of the splittings Δ^i about the fixed point. If we linearize the scaling equation for the renormalized splittings $\Delta^i(x)$ about the fixed point (Eq. (3.4.15)) we find that since the splittings are zero at the fixed point (this is the only way to make the RHS of Eq. (3.4.15) vanish) then

$$\frac{\partial \Delta^i}{\partial x} \approx -\frac{2}{M}\Delta^i \tag{3.4.19}$$

which is integrated to give

$$\Delta^i(x) = \Delta^i(x_0)(\frac{x}{x_0})^{\frac{-2}{M}} \quad . \tag{3.4.20}$$

If we were to stop the analysis here, we would incorrectly conclude that the splittings Δ^i are irrelevant about the fixed point. What is incorrect about this statement is that while the physical splittings do actually shrink, they do so (for $M >> 1$ where the perturbative analysis is valid) at a rate much smaller than the bandwidth itself shrinks. Hence, relative to the decrease of the bandwidth, the splitting actually grows. The dimensionless splitting $\delta^i = \Delta^i/D$ obeys the scaling equation

$$\frac{\partial \delta^i(x)}{\partial x} = (1 - 2\sum_{j \neq i} Tr[(v^i(x))^2])\delta^i(x) \tag{3.4.21}$$

which, when linearized about the fixed point, integrates to give

$$\delta^i(x) = \delta^i(x_0)(\frac{Max\{x, T/D, E/D\}}{x_0})^{1-\frac{2}{M}} \quad . \tag{3.4.22}$$

We can obtain the same result from Eq. (3.4.20) by simply dividing by D. As we have discussed in Sec. 3.2.1, all the logarithmic integrals have an infrared low energy cutoff which is either the temperature or the renormalized value of the splitting E.

We shall demonstrate using the NCA and conformal theory that Eq. (3.4.22) gives the correct scaling to leading order in $1/M$, as we would expect, for the local field Δ^i. This result may also be obtained within the Bethe-Ansatz approach.

Relevance of fields breaking channel symmetry. Channel symmetry breaking is practically effected by applying a field that couples to the electron channel index so that the exchange integrals are split, i.e., the couplings for different channels are no longer precisely identical. The magnetic field does not directly appear in the theory, but the magnetic field splits the Fermi energy for up and down spin electrons. Thus the densities of states at the Fermi energy for the different spins can differ by the scale of $\mu_B H/E_F \simeq 10^{-5}$ for a 1 T field, which results in an equal fractional difference in the dimensionless exchange couplings. Such a small change is practically negligible. Nevertheless, we shall investigate the effects here.

For simplicity, we shall present the stability analysis for this perturbation to next leading order in the M=2 isotropic case, although we realize that the analysis is somewhat questionable in this limit. We will obtain the correct qualitative results as will be demonstrated when we discuss the non-perturbative approaches, but our exponents characterizing the growth of the perturbation will be incorrect.

The equations in the isotropic limit for the couplings in the two channels are

$$\frac{\partial v_\sigma}{\partial x} = 4(v_\sigma)^2 - 8v_\sigma[(v_\uparrow)^2 + (v_\downarrow)^2] \tag{3.4.23}$$

where the coupling subscript is the channel label, which is the real spin of the conduction states. This equation follows from observing the decoupling of channel labels in the leading order diagrams, and the coupling of channel labels through the conduction electron intermediate state bubble in the next leading order diagram. Linearizing these scaling equations about the fixed point $v_\downarrow = v_\uparrow = v^* = 1/4$, we find the scaling equations

$$\frac{\partial(v_\sigma - v^*)}{\partial x} = -(v_{-\sigma} - v^*) = -\delta v_{-\sigma} \tag{3.4.24}$$

which are easily solved to give

$$\delta v_\pm = (\delta v_\uparrow(x) \pm \delta v_\downarrow(x)) \approx (\delta v_\uparrow(x_0) \pm \delta v_\downarrow(x_0))(\frac{x}{x_0})^{\pm 1} \tag{3.4.25}$$

where we have assumed that $\delta v_\uparrow(x_0) > 0, \delta v_\downarrow(x_0) < 0$. What this solution implies is that the sum of the linearized couplings tends to zero as we rescale, which implies that as $v_\uparrow$ grows (towards strong coupling, where the perturbative analysis surely breaks down) then $v_\downarrow$ shrinks towards zero. This picture is completely confirmed by the numerical renormalization group, conformal field theory, and NCA analyses. The physical view is that the stronger coupling tends towards an ordinary Kondo effect, while the weaker coupling tends towards the zero coupling fixed point. What we shall see is that at zero temperature, this rescaling behavior is discontinuous.

(f) Numerical integration of scaling equations

Fig. 27 illustrates the results for the solution of the next leading order scaling equations (3.4.12,15) with $v^z(0) >> v^x(0), v^y(0) = 0$ and $M = 2$. The right most curves in Fig. 3.11.a) which

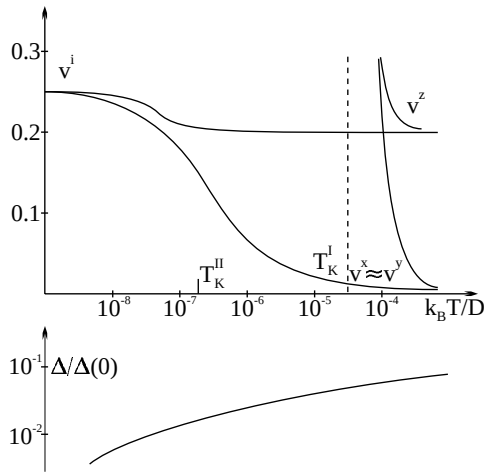

Figure 27: Scaled couplings v^i $(i = x, y, z)$ and energy splitting Δ as a function of k_BT/D for $M = 2$. The initial v^x coupling is 0.2 and the initial ratio v^x/v^z is 10^{-3}. The narrow (heavy) lines represent the first-(second-)order scaling. T_K^I and T_K^{II} are the Kondo crossover temperatures in the first- and second-order scaling, respectively. The dotted line is the asymptote of the coupling in the first-order scaling. The heavy lines for v^i are obtained analytically in second-order scaling. The region where $v^x \approx v^z$ does not hold is not represented. The ratio of the scaled and initial energy splitting $\Delta/\Delta(0)$ is calculated for the symmetridc TLS by using Eq. (3.4.13). The index of x for Δ^x is dropped. From Vladár and Zawadowski [1992].

blow up at the vertical line marked $T_K^{(i)}$ correspond to the leading order equations. The other two curves which show a rise to strong coupling on the next leading order Kondo scale

$$T_K^{(II)} \approx D_0 (\frac{v^x(0)}{4v^z(0)})^{\frac{1}{4v^z(0)}} [v^x(0)v^z(0)]^{\frac{M}{4}} \tag{3.4.26}$$

go all the way into the fixed point at $v^* = 0.25$ smoothly. In the vicinity of $T_K^{(I)}$, the couplings $v^x(x), v^y(x)$ are nearly equal in magnitude. We should contrast Eq. (3.4.26) which corresponds to the fully anisotropic Kondo limit solved by Shiba [1970] with the isotropic limit result

$$(T_K^{(II)})_{iso} = D_0 (v(0))^{\frac{M}{2}} \exp[-\frac{1}{4v(0)}] \quad . \tag{3.4.27}$$

The spontaneous tunneling matrix element in the extreme anisotropic limit is strongly renormalized downwards, as seen in Fig. 27(b). While the Δ^z value is also renormalized downwards, the reduction is less severe since the downward renormalization is driven by the weaker, planar couplings. In the limit of full isotropy, the downward renormalization would be independent of direction and Δ^z would thus be strongly reduced in absolute value.

(g) Dimensionality of the fixed point Hamiltonian

In Sec. 3.3.3, it has been shown using the leading logarithmic approxmiation that the structure of the matrices $V^i_{\alpha\beta}$ $(i = x, y, z)$ at the strong coupling fixed point is such that they are proportional to a representation of $SU(2)$. (Note that the leading logarithmic approximation generates a flow to the strong [infinite] coupling fixed point regardless of channel number since the channel number enters only at next leading logarithm level.) The following questions remain, however, without answers from this discussion:

1) Are these fixed point matrices reducible representations or always irreducible, and

2) Are there any restrictions on the dimensions of the irreducible matrices? It has been argued following

Vladár and Zawadowski [1983a] that at the beginning of scaling a two-dimensional subspace emerges due to the scaling. Nonetheless, it could still happen that going beyond the leading logarithmic order of scaling could lead to a larger relevant subspace. In the limit of large number of channels, this possibility has been ruled out by Zaránd [1995].

These questions cannot be generally answered from the scaling analysis and require non-perturbative resolution from such methods as conformal theory and Bethe Ansatz. To get at some more rigorous understanding, let us first assume that there is no additional symmetry which could influence the dimension of the subspace. Furthermore, in order to make a rigorous statement, let us (artificially) increase the channel number from $M = 2$ to $M >> 1$ so that the $1/M$ expansion is valid (this is discussed more extensively in Sec. 3.4.4). In this case the scaling equations given by (3.4.12) are correct and the higher order corrections on the RHS are controllably neglected as they contribute in higher powers of $1/M$. By proceeding in the scaling, the 2-D subspace bcomes dominant and contributed to the second term of Eq. (3.4.12), which slows down scaling. In this spirit, Zaránd [1995] was able to show that this next leading term suppresses the conduction orbital states with small amplitude coupling finally only a 2-D subspace remains.

This result can be summarized as follows: in the two-channel TLS Kondo problem we conjecture based upon the analysis of Zaránd [1995] that the original number of conduction orbitals in the matrices $V^i_{\alpha\beta}$ is reduced to 2 at the fixed point. Thus the orbital coupling matrices must be simple Pauli matrices at the fixed point. On the other hand, the impurity spin matrix usually is also reduced to a two-dimensional matrix. Thus we complete the mapping to the spin 1/2 two channel Kondo model for this TLS model given that the two-channel degeneracy is required by time reversal.

3.4.2 TLS Model Including Excited Atomic States

The TLS is defined by truncating the excitation spectrum of the atom in the double well keeping only the two lowest levels (see Fig. 6). This projection certainly gives the nature of the low temperature behavior correctly, but the higher level may contribute to the renormalization of the prameters of the truncated system. Similar renormalization has already been discussed for the original and orbital Kondo effect where the influence of the higher states split by the crystalline electric field is discussed in Sec. 3.3.c. Such renormalization can be crucial concerning the value of the Kondo temperature $T_K^{(II)}$ given by Eq. (3.4.26) which is very sensitive to the initial parameter values. We postpone a more detailed discussion related to the ex periments to Sec. 7.1. The following theoretical discussion is based on the work of Zaránd and Zawadowski [1994a,b].

For simplicity we treat the situation where all the higher excitations are extending over both minima of the double well. Instead of the left and right states, the exact states are introduced here which are symmetric and antisymmetric in the case of a symmetric double well. (See Fig. 28). All of these states are orthogonal, and thus there are no spontaneous transitions between them. The electron density interacting with them is not, however, homogeneous in real space and thus the interaction with the electrons can induce transitions between the states of the double well.

The wave functions and energies are denoted by ϕ_i and ϵ_i $(i = 1, 2, ...)$ with $\epsilon_1 < \epsilon_2 < \epsilon_3.....$ The generalized version of Hamiltonian (3.3.3) with creation operators $b_i^\dagger$ and pseudo-particle chemical pote ntial λ_{ps} is

$$H_0 = \sum_i (\epsilon_i - \lambda_{ps}) b_i^\dagger b_i \quad . \tag{3.4.28}$$

The electron-tunneling center interaction is

$$H_{int} = \sum_{i,j,k,k',\sigma} V^{i,j}_{k,k'} b_i^\dagger b_j a^\dagger_{k\sigma} a_{k'\sigma} \tag{3.4.29}$$

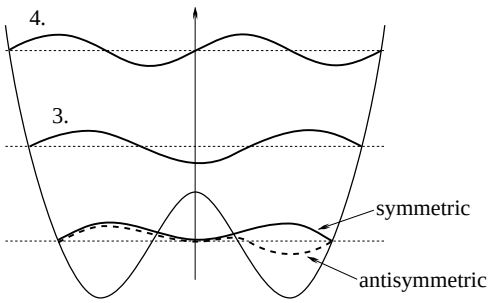

Figure 28: The double potential well is shown by the solid line. The linear combinations of the lowest left and right states are presented by heavy solid and dashed lines. Two further excited states labeled by 3 and 4 are also represented by heavy lines. The light lines represent the level of zero amplitudes of the wave function.

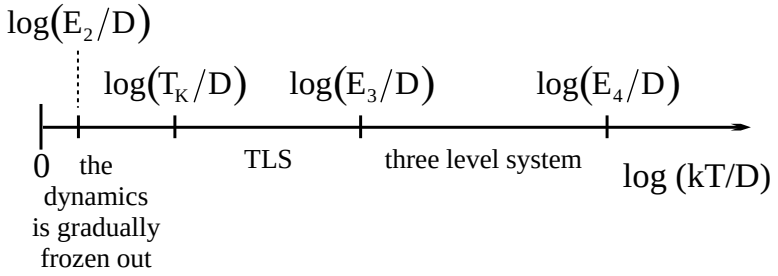

Figure 29: The different regions of the scaling. The excited states with energies E_3, E_4 are gradually frozen out.

where the matrix element in the scheme proposed by Zaránd [1993] is

$$V^{i,j}_{k,k'} = U(\vec{k}-\vec{k}')\int drexp[-i(k-k')r]\phi^*_i(r)\phi_j(r) \tag{3.4.30}$$

which is a generalization of Eq. (2.2.14.a,b). Later notation $\rho_0 V^{i,j}_{k,k'} = v^{i,j}_{\hat{k},\hat{k}'}$ is introduced indicating the dependence only on the direction of the momenta in the vicinity of the Fermi surface.

The first relevant vertex correction is just a straightforward generalization of Eq. (3.3.11) which has the form

$$T^{k,l}_{\hat{k}_1,\hat{k}_2} = v^{k,l}_{\hat{k}_1,\hat{k}_2} + \int \frac{dS_F(\hat{k})}{S_F}\sum_i \ln(\frac{max(|\epsilon_i|,T,|\omega|)}{D})[v^{k,i}_{\hat{k}_1,\hat{k}}v^{i,l}_{\hat{k},\hat{k}_2} - v^{i,l}_{\hat{k},\hat{k}_1} - v^{k,i}_{\hat{k},\hat{k}_2}] \quad . \tag{3.4.31}$$

Note that the factor of $2i$ is missing compared with Eq. (3.3.11) since we have not assumed a Pauli spin algebra here. The scaling equation is just a generalization of Eq. (3.3.13) given by

$$\frac{\partial v^{kl}_{\hat{k}_1,\hat{k}_2}}{\partial \ln(x)} = \theta(D'-|E_i|)\int \frac{dS_F(\hat{k})}{S_F}[v^{k,i}_{\hat{k}_1,\hat{k}}v^{i,l}_{\hat{k},\hat{k}_2} - v^{i,l}_{\hat{k},\hat{k}_1}v^{k,i}_{\hat{k},\hat{k}_2}] \tag{3.4.32}$$

where the θ-function assures that only those states contribute to the sum which are below the scaled bandwidth D' and $E_i = \epsilon_i - \epsilon_1$. As a result of these restrictions at a given energy or temperature only those states play a role in dynamics for which $E_i < k_BT$ and the others just contribute to the renormalization of the remaining effective coupling constants (see Fig. 29).

The solution of these scaling equations were studied numerically and analytically in great detail (Zaránd and Zawadowski [1994(a,b)]). The Kondo temperature can be enhanced or reduced depending on the values of the prameters, but for most of the physically interesting set of couplings, the Kondo temperature is enhanced by a factor of 2-3 orders of magnitude.

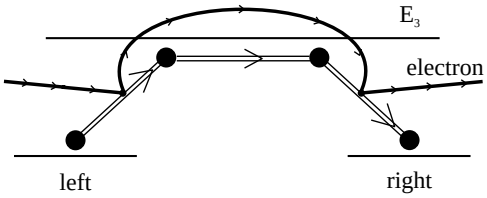

Figure 30: The left and right states of the TLS with the first excited state with energy E_3. The double line represents the heavy particle and the electron with solid line induces the transitions.

Just to emphasize the role of the excited states, the scaling calculations were performed under the fictitious assumption that the direct assisted tunneling between the left and right positions are zero, so that for the unrenormalized couplings $V^{12}(0) = V^{21}(0) = V^{12} = V^{21} = 0$ holds. Even in this case, the large enhancement of the Kondo temperature is reduced only by a factor of 0.6-0.7, which implies the excited levels are playing a crucial role in the dynamics.

This result is of special importance. To understand it, consider one of the dominant processes included in the scaling analysis in which the electron hits the atom, say, on the left and virtually excites the atom to, for example, the third level (see Fig. 30). That level covers both the left and right minima, so that from there the atom can fall into the right minimum with the assistance of the same electron. This result normally follows from the behavior of the matrix elements given by Eq. (3.4.29), which in the limit $k_F r << 1$ are the dipole matrix elements between the wave functions ψ_i of the atom. The interesting new feature is the following: Neglecting the overlap between the left and right wave functions, the induced effective electron assisted matrix elements are less sensitive on the distance despite the fact that the dipole matrix element even increases with the distance; for too large a distance the original expression must be used in favor of the dipole approximation. This has the great advantage that the direct hopping which is neglibible in this case does not split the ground state and first excited states; nonetheless, the excited state assisted tunneling is large enough and actually grows with distance as shown in Table 8. Previous to this analysis, any increase in the assisted matrix element was associated with the increase of the direct hopping and thus the splitting, which of course mitigates the possibility of observing the non-trivial fixed point physics. To obtain a sufficiently large Kondo scale together with a sufficiently small level splitting required in the most optimistic scenario a delicate balance of these effects. The inclusion of the excited levels now makes the observability of a TLS with sufficiently large Kondo scale and negligibly small splitting appear quite plausible.

The importance of the broad barrier is demonstrated by the data in Table 8, where the following parameters are chosen for the square well potential discussed in App. I and shown in Fig. 129: $1/2mR_0^2 = 50K$, $V_B = 490.5K$, and the width of the barrier is given by the parameter α as $d = 2r_0\alpha$. Table 8 clearly shows that the Kondo temperature in the leading order is strongly reduced in the next to leading order due to the factor $(v^x v^z)^{1/2}$ of Eq. (3.4.26). The enhancement due to the excited states is essential. The second excited state has a minor effect due to the reduced coupling strength arising from the presence of more wave function nodes. The splitting Δ is negligible in the broad barrier of interest here.

3.4.3 Formation of the TLS double well: Einstein phonon model

Concerning the anomalous behavior of the A15 compounds, P.W. Anderson and C.C. Yu proposed a model to clarify the role of the strong electron-phonon interaction in the formation of a double well potential for a TLS. The basic idea is similar to the physics of the Jahn-Teller distortion. A single well potential for a single atom can be deformed by the strong electron-phonon interaction to form a double well potential. Thus the coupling to the electronic heat bath is responsible for the TLS formation similar to the insulating case where the coupling to the phononic bath plays this role (Sethna [1981]).

The idea has recently been reinvestigated by H. Kusunose and K. Miyake [1996], where it is assumed the atomic motion is in a simple parabolic potential which can be regarded as a localized

α	1.0	1.5	2.0	2.5
E_1	331	277	255	245
E_2	540	406	337	330
Δ_0	4.47	0.53	0.063	0.0076
v^z	-0.061	-0.086	-0.112	-0.142
v^x	0.0005	0.0009	0.0013	0.0018
$\tilde{T}_K$	7.16×10^{-7}	0.00187	0.152	2.46
$\tilde{T}_K^{(1)}$	9.14×10^{-9}	0.00342	1.29	67.2
$\tilde{T}_K^{(2)}$	1.97×10^{-7}	0.005	1.29	65.1
$\tilde{T}_K^{(1)}\|_{v^x=0}$	2.3×10^{-7}	2.02×10^{-5}	0.41	44.9
T_K	4.13×10^{-9}	1.64×10^{-7}	0.00186	0.0343
$T_K^{(1)}$	3.05×10^{-11}	3.31×10^{-5}	0.026	2.76

Table 8: Kondo scales for a TLS model including excited states. Calculations are performed for a symmetric double square well potential (c.f. Appendix I) with a variable width following Zaránd and Zawadowski [1994a,b]. The width of the double well barrier is controlled by the parameter $\alpha = r_0/2d$, where r_0 is the width of an individual well and d the barrier thickness (See Fig. I.1). Plane wave conduction states are assumed. All energies are measured in K. The notation is as follows: $E_1(E_2)$ is the energy of the first (second) excited state. Δ_0 is the splitting of the lowest TLS states due to spontaneous tunneling through the square barrier. v^z, v^x are the bare dimensionless TLS coupling constants which measure the interaction strength with the ground doublet levels. $\tilde{T}_K$ is the Kondo scale in the leading logarithmic order neglecting excited states. $\tilde{T}_K^{(1)}$ is the Kondo scale in the leading logarithmic approximation including the first excited state, and $\tilde{T}_K^{(2)}$ includes both first and second excited states in leading logarithmic order. $\tilde{T}_K^{(1)}|_{v^x=0}$ is the leading logarithmic estimate with the first excited state kept but the bare v^x artificially set to zero; this illustrates the strong effect of assisted tunneling induced by virtual excitations to the first excited state. T_K is the next leading logarithmic approximation estimate without excited states, and $T_K^{(1)}$ is the next leading logarithmic estimate with the first excited state retained. We learn from these calculations that for sufficiently narrow barrier (relative to the square well width) the excited states enhance the estimated Kondo scales significantly (by as much as two orders of magnitude). and that the most crucial state to include is the first excited state–the second excited state has small additional effect. With the additional states Kondo scales within the correct order of magnitude of experiment to explain the resistance data on quenched metallic point contact devices (Ralph and Buhrman [1992,1995], Ralph *et al.* [1994,1995], Upadhyay, Louie, and Buhrman [1996]).

Einstein phonon described by the Hamiltonian

$$\mathcal{H}_{ph} = \Omega(b^\dagger b + 1/2) \tag{3.4.33}$$

on each site, where Ω is the phonon frequency and $b^\dagger$ is the phonon creation operator. The phonon operators are described alternatively in terms of a pseudo-fermion operator b_n which annihilates the state with n excitations, so we may write equivalently

$$\mathcal{H}_{ph} = \Omega \sum_n n b_n^\dagger b_n \quad . \tag{3.4.34}$$

Kusunose and Miyake truncated this model to the states $n = 0, 1$. For matrix elements involving the atomic coordinate Q in the direction along the possible deformation (Z-direction) then the harmonic oscillator wave functions for the $n = 0, 1$ levels are used. The atom electron interaction is similar to the one given by Eq. (3.4.30). The $n = 0, 1$ states are even and odd under z reflection ($z \to -z$). Then the Hamiltonian (3.4.3) is expanded in r (in the notation of Kusunose and Miyake, $Q = q(b + b^\dagger)$) keeping only the first and second order terms. In order to mimic the left and right states for this starting parabolic potential, the states with pseudo-spin $\uparrow, \downarrow$ are introduced as

$$b_\uparrow = \frac{1}{\sqrt{2}}(b_0 - b_1) \quad , b_\downarrow = \frac{1}{\sqrt{2}}(b_0 + b_1) \quad , \tag{3.4.35}$$

and then all the operations for the atomic states can be described by Paul operators acting in the pseudo-spin space. Using Eq. (3.4.30), the interaction $V_{kk'}^{ij}$ can be calculated and decomposed into Pauli matrices in the pseudo-spin states in the ij space of conduction partial waves. The Hamiltonian then takes the form described in Sec. (2.1.2)b, with a spcial initial value of the couplings v^z, v^x, with $v^y = 0$. Kusunose and Miyake then apply the renormalization group in the form described in Sec. 3.4.2. When the relatively large value of the initial splitting $\Delta^x \simeq \Omega$ scales to smaller values, this is interpreted as the formation of a TLS by effecting smaller direct coupling and overlap between the states with pseudo-spin $\uparrow, \downarrow$. It can be seen that the formation of the two-channel Kondo ground state requires very special initial parameters as has been discussed in Sec. 3.4.1.f. Kusunose and Miyake do not solve this problem by starting with larger overlaps.

This scheme represents a good starting point for further work, but for a more realistic and elaborate theory it will likely be necessary to include the higher excited states $n \geq 2$ and perhaps the continuum states must also be taken into account (see Sec. 3.4.2). More states may lead to better localization of the atom in the left and right wells and smaller overlap for the lowest left and right states.

3.4.4 Next Leading order Scaling for Model U^{4+} and Ce^{3+} Ions

(a) Kondo scale in the U^{4+} case

As derived above in the isotropic limit, the Kondo scale in this case where the bare couplings are isotropic is, for the quadrupolar Kondo model

$$T_K^{(II)} = D_0|g| \exp(\frac{1}{g}) \tag{3.4.36}$$

with $g = 2N(0)V^2/\tilde{\epsilon}_f$.

We shall consider the Ce^{3+} case separately.

(b) Stability analysis for U^{4+} ions

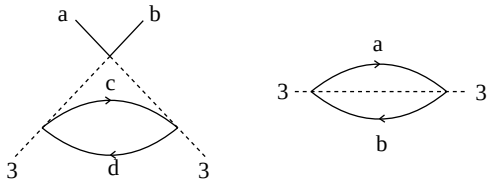

Figure 31: Next leading order scaling corrections to the quadrupolar Kondo model with two Γ_8 quartets. The indices a, b, c, d refer to the possible $8, 8'$ labels derived from the two conduction electron Γ_8 quartets which come from the $j = 5/2, 7/2$ partial waves (see 23 for the leading order diagrams). The diagram on the left is a vertex correction, while the diagram on the right gives the self energy renormalization which must be subtracted as discussed in Sec. 3.4.1.

As in the discussion above for the TLS, we anticipate a non-trivial fixed point for the quadrupolar Kondo effect of a U^{4+} ion. This fixed point is stable against anisotropic exchange, and destabilized by applied spin field (precisely analogous to the relevance of the TLS splitting and spontaneous tunneling discussed above) and applied channel field (splitting of the exchange integrals). In these cases, all of the analysis carries over completely from the TLS discussion, modulo the change of sign of coupling constants and the use of spin 1/2 matrices.

We also would like to show that the scaling to a two-fold degenerate conduction pseudo-spin space discussed in the leading order scaling analysis (Sec. 3.3.3.b) also carries through in next leading order. We employ the same notation as Sec. 3.3.3.b. The generalization of Eqs. (3.36.a-c) in next leading order follows from the renormalized parquet diagrams of Fig. 31 and gives

$$\frac{\partial g_{8,8}}{\partial x} = -[g_{8,8}^2 + g_{8,8'}^2] - g_{8,8}[g_{8,8}^2 + g_{8',8'}^2 + 2g_{8,8'}^2].... \tag{3.4.37.a}$$

$$\frac{\partial g_{8',8'}}{\partial x} = -[g_{8',8'}^2 + g_{8,8'}^2] - g_{8',8'}[g_{8,8}^2 + g_{8',8'}^2 + 2g_{8,8'}^2].... \tag{3.4.37.b}$$

$$\frac{\partial g_{8,8'}}{\partial x} = -g_{8,8'}[g_{8,8} + g_{8',8'}] - g_{8,8'}[g_{8,8}^2 + g_{8',8'}^2 + 2g_{8,8'}^2].... \tag{3.4.37.c}$$

By taking the difference of the first two equations and comparing to the third, we again conclude that

$$g_{8,8'}(x) = c_0[g_{8,8}(x) - g_{8',8'}(x)] \quad , \tag{3.4.38}$$

meaning that the integration constant $c_0 = a_8 a_{8'}/(a_8^2 - a_{8'}^2)$ once again. Now, with a little algebra it is possible to show that

$$[g_{8,8}^2 + g_{8',8'}^2 + 2g_{8,8'}^2] = [(\tilde{g})^2 + (\tilde{g}')^2] \tag{3.4.39}$$

so that the scaling equations for $\tilde{g}, \tilde{g}'$ are

$$\frac{\partial \tilde{g}}{\partial x} = -(\tilde{g})^2 - \tilde{g}[(\tilde{g})^2 + (\tilde{g}')^2] \tag{3.4.40.a}$$

and

$$\frac{\partial \tilde{g}'}{\partial x} = -(\tilde{g}')^2 - \tilde{g}'[(\tilde{g})^2 + (\tilde{g}')^2] + ... \tag{3.4.40.b}$$

These equations admit the non-trivial fixed points $\tilde{g} = -1, \tilde{g}' = 0$, $\tilde{g} = 0, \tilde{g}' = -1$ (both two-channel fixed points) and $\tilde{g} = \tilde{g}' = -1/2$ which is a new non-trivial fixed point, which is the four-channel

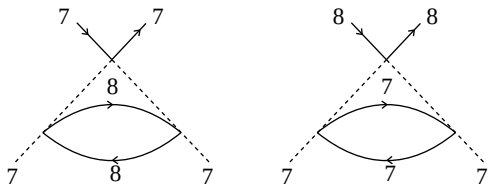

Figure 32: Next leading order vertex corrections for a Ce^{3+} ion with both $f^0 - f^1$ and $f^1 - f^2$ valence fluctuations. Corresponding wave function renormalization factors must be subtracted as per the procedure of Sec. 3.4.1, and in the case of Fig. 31.

Kondo model fixed point (the scaling equations and fixed point value are the same at this order). However, an analogous analysis to that of the channel field splitting applies here as well (see Sec. 3.3.3.b) and we see that that the new non-trivial fixed point is unstable so that whichever coupling $\tilde{g}, \tilde{g}'$ is larger, we will flow to the two-channel fixed point associated with that coupling. Then a linearized stability analysis around, e.g., $\tilde{g} = 1, \tilde{g}' = 0$ shows that an added perturbation in $\tilde{g}'$ is irrelevant. Hence, even if we begin with $\tilde{g}'(0) \neq 0$, if it is smaller than $\tilde{g}(0)$ we will quickly flow to the subspace where only $\tilde{g}$ is present. In the present model, since we begin with $\tilde{g}'(0)$ identically zero, we will always simply select out the bonding combination of Γ_8 orbitals and flow to the two-channel fixed point associated with that combination.

(c) Next leading order analysis for Ce^{3+} ions

For Ce^{3+} ions, the different exchange strengths for the Γ_7 partial waves and the Γ_8 partial waves couple at third order, as shown by the diagrams in Fig. 32, and the resulting scaling equations are (Kim [1995], Kim and Cox [1995,1996,1997])

$$\frac{\partial g_7}{\partial x} = -g_7^2 - \frac{1}{2} g_7 (g_7^2 + 2 g_8^2) \tag{3.4.41.a}$$

and

$$\frac{\partial g_8}{\partial x} = -g_8^2 - \frac{1}{2} g_8 (g_7^2 + 2 g_8^2) \quad , \tag{3.4.41.b}$$

with $g_{7,8} = N(0) J_{7,8}$.

These equations have three possible low temperature behaviors:(i) When $g_7 \to \infty, g_8 = 0$ then we get the normal Kondo behavior for the Ce^{3+} ion. (ii) When $g_7 = g_8 = -2/3$, we obtain the three channel Kondo fixed point. (iii) When $g_7 = 0, g_8 = -1$, we obtain the two-channel Kondo model fixed point. In case (i), we see from the lowest order results (quadratic term in Eqs. (3.4.38.a,b)) that if we start with $|g_7(0)| > |g_8(0)|$, g_7 will grow more rapidly than g_8 with initial scaling, so we conjecture that we will flow to the normal Kondo fixed point. This is substantiated by the non-perturbative NCA results we shall discuss in a later section. If we make $g_7 = g_8$ initially, we will remain on the $g_7 = g_8$ line throughout the scaling and thus flow to the three channel Kondo fixed point at low temperatures. This fixed point is unstable against any deviation from the equality of the couplings: the linearized stability analysis shows that if one applies $\delta g_7 < 0, \delta g_8 > 0$ one will begin to flow towards the normal Kondo fixed point, while reversing the inequality will drive one to the two-channel fixed point associated with the Γ_8 coupling. Finally, if we begin with initial couplings such that $|g_8(0)| > |g_7(0)|$, we will flow to the two-channel fixed point with $g_7 = 0$, and any added g_7 coupling is irrelevant about this fixed point within the linearized analysis. These results are summarized in the schematic flow diagram depicted in Fig. 33.

The dividing criterion on the dimensionless couplings corresponds to the comparison of the quantum fluctuation weights of f^0, f^2 in the ground state. Using second order perturbation theory, one

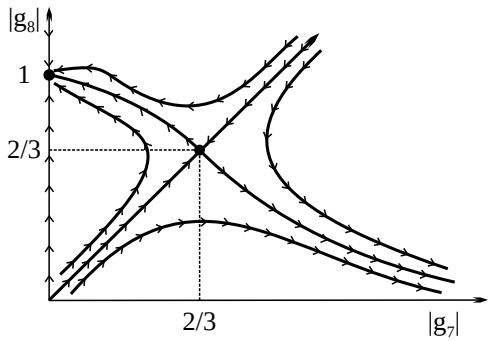

Figure 33: Multiplicative renormalization group flow diagram for the Ce^{3+} ion in next to leading order. The horizontal axis is the dimensionless coupling of the Γ_7 Ce^{3+} spin to the Γ_7 conduction states, and the vertical axis is the dimensionless coupling strength of the Γ_7 Ce^{3+} spin to the Γ_8 conduction quartet. Along the line $g_7 = g_8$, the three channel fixed point is stable. A slight deviation from this behavior gives rise to the two-channel fixed point (assuming $|g_7| < |g_8|$), or the single channel strong coupling fixed point ($|g_7| > |g_8|$). For more details, see Kim [1995], Kim and Cox [1995,1996,1997].

can easily show that the lowest order estimate for the occupancy deviation of f^1 towards f^0 is $\simeq g_7(0)$, and similarly for f^1 towards f^2 the occupancy deviation is $\simeq 2g_8(0)$.

(d) Next leading order scaling for Ce^{3+} ion with channel spin/spin coupling included.

Extending the leading order analysis of the last section, we follow Kim (Kim [1995]; Kim and Cox, [1996]; Kim, Oliveira and Cox, [1996]) and develop next leading order scaling equations for the Ce^{3+} model in which we set couplings to the Γ_7 partial waves to zero and retain only the J_8, $\tilde{J}_8$ couplings of Sec. 2.2. The development of the next leading equations follows precisely that of the preceding subsections, and we obtain

$$\frac{\partial g_8}{\partial x} = g_8^2 - \frac{1}{2}\tilde{g}_8^2 - g_8[g_8^2 + \tilde{g}_8^2] \tag{3.4.42}$$

and

$$\frac{\partial \tilde{g}_8}{\partial x} = -g_8\tilde{g}_8 - \tilde{g}_8[g_8^2 + \tilde{g}_8^2] \quad . \tag{3.4.43}$$

These equations have four fixed points:
(i) $g_8 = \tilde{g}_8 = 0$ (the weak coupling fixed point)
(ii) $g_8 = 1, \tilde{g}_8 = 0$ (the two-channel $S_I = 1/2$ fixed point)
(iii) $g_8 = -1/5, \tilde{g}_8 = 2/5$ ($S_I = 1/2, S_c = 3/2$ fixed point)
(iv) $g_8 = -1/5, \tilde{g}_8 = -2/5$ ($S_I = 1/2, S_c = 3/2$ fixed point)
A linearized analysis about the fixed points (ii-iv) confirms their local stability in the $\tilde{g}_8 - g_8$ plane, and the non-trivial character of the fixed points (iii, iv). As indicated in the discussion of leading order scaling, the special properties of the lines $g_8 = \pm\tilde{g}_8/2$ are maintained due to the special symmetry properties of the system along these lines. A complete schematic scaling diagram is displayed in Fig. 34
.

3.4.5 Physical Properties in the $1/M$ Expansion

According to the suggestion of Nozières and Blandin [1980], for large channel number $M >> 1$, the fixed point $v^x = 1/2M$ (see Eq. (3.4.16)) is in the weak coupling limit. As a result, the analytic renormalization group calculations based on a perturbative expansion will be perfectly adequate to treat

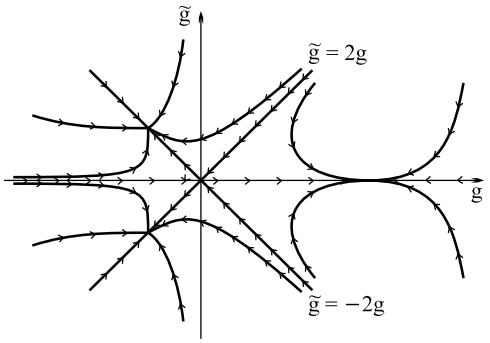

Figure 34: Multiplicative renormalization group flow diagram for Ce^{3+} ion when channel spin/spin coupling is included (and coupling to the Γ_7 conduction space is set to zero). In this case the Γ_8 conduction quartets can either couple as two-spin 1/2 objects to the Γ_7 Ce^{3+} conduction quartets (dimensionless coupling strength g_8), or can couple through a mixed spin/channel spin tensor (dimensionless coupling strength $\tilde{g}_8$). This leads to competing fixed points. The fixed point for positive g_8 and zero $\tilde{g}_8$ is the usual two-channel one. The fixed points for negative g_8 and finite $\tilde{g}_8$ are such that the Γ_8 manifold acts as a *single channel spin 3/2* band coupling to the spin 1/2 impurity. For further details, see Kim [1995], Kim and Cox [1996], and Kim, Oliveira, and Cox [1997].

the properties at all temperatures. The physics may be computed in an expansion of powers of $1/M$. This contrasts to the conformal field theory which is only applicable in the low temperature regime. Furthermore, within the perturbative renormalization group treatment, dynamical quantities may be computed as well which is beyond the scope of the Bethe-Ansatz method. (We remark that the large N, M NCA approach discussed in Sec. 5.1 also can treat all properties.) Thus, the $1/M$ expansion gives two different types of information:
(i) The result can be compared to the conformal field theory approach to check the assumed conformal invariance and related hypotheses;
(ii) The method can be used to evaluate physical properties in the entire temperature regime.

The actual performance of perturbation theory to higher orders in the coupling constant and the feedback into the renormalization group equations are very technically involved matters, and so we shall quote only some of the main results from the literature. The interested reader may turn to the original articles for further detail.

Muramatsu and Guinea [1986] were the first to make use of the $1/M$ expansion, and Gan, Andrei and Coleman [1993] carried out a more extensive set of calculations up to the next to leading logarithmic order The former work is based upon application of the bosonization technique developed by D.J. Amit, Y.Y. Goldschmidt, and G. Grinstein [1980], while the latter authors used a path integral method. The latter authors assumed an isotropic exchange and spin 1/2 impurity and conduction spins, as we shall throughout this subsection. We shall refer to the work of Gan, Coleman, and Andrei henceforth.

In the vicinity of the weak coupling fixed point, the effective exchange coupling g behaves as (see Eq. (3.4.18))

$$g(x) = \frac{1}{2M} + [g(0) - \frac{1}{2M}](\frac{x}{x_0})^{\Delta} \tag{3.4.44}$$

where

$$\Delta = \frac{2}{M}(1 - \frac{2}{M}) \tag{3.4.45}$$

as computed to the two leading orders by Gan, Andrei and Coleman [1993]. Assuming x measures the frequency, this equation may be rewritten

$$g(\omega) = g^* - \zeta(\frac{\omega}{T_K})^{\Delta} \tag{3.4.46}$$

where to leading order $\zeta = 4/eM^2$, e the natural log basis, and $T_K = Dg^{M/2}exp(-1/g)$. Making use of the linked cluster theorem, they obtain the free energy through order g^4 and from this compute the impurity contributions to the specific heat $C_{imp}(T)$, magnetic susceptibility $\chi_{imp}(T)$, and zero temperature residual entropy $S_{imp}(0)$. The results are

$$C_{imp}(T) = \frac{3\pi^2}{2}\zeta^2\Delta[\frac{T}{T_k}]^{2\Delta} \tag{3.4.47}$$

$$\chi_{imp}(T) = [\frac{M\zeta}{2}]^2\frac{1}{T}[\frac{T}{T_K}]^{2\Delta} \tag{3.4.48}$$

$$S_{imp}(0) = \ln 2 - \frac{\pi^2}{2M^2} \quad . \tag{3.4.49}$$

The resulting Wilson ratio (the dimensionless ratio of susceptibility to specific heat coefficient) depends on M as

$$R = lim_{T\to 0}\frac{\chi_{imp}}{C_{imp}}\frac{C_{bulk}}{\chi_{bulk}} = \frac{M^3}{36} \quad , \tag{3.4.50}$$

where $C_{bulk} = 2M\pi^2TN(0)/3$ and $\chi_{bulk} = 2MN(0)$. The Bethe-Ansatz and conformal theory exact results give $\chi_{imp}(T), C_{imp}(T)/T \sim T^{2/(M+2)-1}$, which clearly agrees to within leading order in $1/M$ in the exponent. For comparison of the amplitudes, Bethe-Ansatz and conformal theory give for the entropy

$$S_{imp}(0) = \ln[2\cos(\frac{\pi}{M+2})] \approx \ln 2 + ln[1 - \frac{\pi^2}{2M^2}] \approx \ln 2 - \frac{\pi^2}{2M^2},\ M \to \infty \tag{3.4.51}$$

and for the Wilson ratio

$$R = \frac{(4+M)(2+M)^2}{36} \approx M^3/36\ , M \to \infty \quad . \tag{3.4.52}$$

Gan, Andrei and Coleman also computed several dynamical quantities. The electrical resistivity is found to be

$$\rho(T) = [\frac{3\pi^2}{4M^2}]c\rho_U[1 - M\zeta[\frac{T}{T_K}]^{\Delta}] \tag{3.4.53}$$

where c is the impurity concentration and ρ_U corresponds to unitary scattering off of the impurity. The exponent of the next leading correction obtained by conformal theory is $2/(M+2)$ which agrees to leading order in $1/M$ with the above expression. Notice that the prefactor in square braces may be interpreted as spin disorder scattering–computing the spin disorder scattering from an impurity with dimensionless coupling strength $1/2M$ gives precisely this estimate. Clearly, this saturation of $\rho(T)$ contrasts with the T^2 saturation found in the conventional Kondo problem.

The lack of Fermi liquid behavior is made more concrete by studying the dynamic spin susceptibility χ''. It is found that the spin fluctuation power spectrum

$$\frac{\chi''(\omega,T)}{\omega} \approx \frac{3}{4T}[\frac{Max(T,\omega)}{T_K}]^{2\Delta}\frac{\Lambda(T)}{\omega^2 + \Lambda(T)^2} \tag{3.4.54}$$

where $\Lambda(T) = 4\pi T/M$. In the single channel Kondo problem, a Lorentzian form works rather well to describe χ''/ω, but $\Lambda \simeq T_K$. The vanishing width at low T found here contrasts with the local Fermi liquid theory of the single channel model, and agrees with results found for the two- and three-channel model using the NCA method (Kim [1995]; Kim and Cox [1995,1997]) (see Secs. 5.1,5.2).

We will further compare these large M results with the NCA (Sec. 5.1), Conformal Field Theory (Sec. 6.1), and the Bethe-Ansatz (Sec. 7) later in the paper.

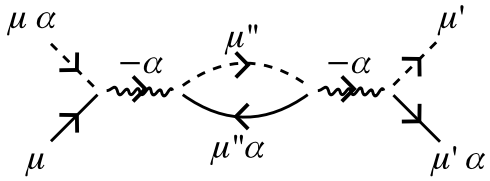

Figure 35: Leading order multiplicative renormalization group diagram for the $SU(N) \times SU(M)$ Coqblin-Schrieffer Model (N=spin degeneracy, M=channel degeneracy). The wavy line is an $SU(N)$ exchange vertex, the dashed line a pseudo-fermion line for the local $SU(N)$ impurity spin, and the solid line a conduction electron line (these carry both channel and spin).

3.4.6 Next Leading Logarithm Results in the $SU(N) \otimes SU(M)$ Coqblin-Schrieffer Model

In this subsection we wish to just briefly point out that with a Hamiltonian of the form in Eq. (2.3.2) is used, the origin of the next to leading order term in the β function has a different origin than in the spin exchange form.

The first point is that at second order in the coupling strength, the only diagram possible is that of Fig. 35. Note that we have drawn the exchange vertex as an extended wavy line. This diagram corresponds to a dynamical dressing of the exchange interaction through pseudo-fermion particle-conduction hole pairs. The contribution to the β function from this diagram is simply $-Ng^2$ where $g = N(0)J$ is the dimensionless coupling strength.

The next point is that at third order in the coupling strength, no vertex correction can be written down for the Coqblin-Schrieffer Hamiltonian. Thus, all corrections to third order arise solely from the pseudo-fermion self-energy [Coleman, 1983]. When this is evaluated for the Coqblin-Schrieffer model we find

$$\Sigma(\omega, T) \approx -MNg^2\omega \ln(\frac{D}{max\{\omega, T\}}) \tag{3.4.55}$$

and the resulting scaling equation for the coupling is

$$\frac{\partial g}{\partial x} = -N[g^2 + Mg^3 + ...] \quad . \tag{3.4.56}$$

If we solve for the Kondo scale at this order, we find

$$T_K = D|g(0)|^\gamma \exp(\frac{1}{Ng(0)}) \quad . \tag{3.4.54}$$

Eq. (3.4.57) gives the fixed point coupling strength $g^* = -1/M$; the slope of the β function at the fixed point is $\beta'(g^*) = -N/M$, so that $g(x) \approx g^* + \delta g(x/x_0)^{-N/M}$. Defining $\gamma = M/N$, we see that an expansion in $1/\gamma$ is possible about the fixed point. We see that the leading deviations from the fixed point are irrelevant, since as x grows the second term shrinks. Clearly this results agrees with Eq. (3.4.45) when $N = 2$, so the physics is the same as the more conventional Kondo exchange model in that case.

From this perspective, it is clear that the NCA to be discussed in Sec. 5, which produces self consistent analytic solutions for the self-energy of the pseudo-fermion and pseudo-boson of the $SU(N) \otimes SU(M)$ Anderson model is in some sense just the proper analytic continuation of the third order scaling theory. The pseudo-boson self-energy should just be viewed in the Coqblin-Schrieffer context as dynamical dressing of the exchange by pseudo-fermion particle, conduction-hole pairs (or particle-particle, depending on which configuration the pseudo-boson resides in).

3.5 Path Integral Approach to the TLS Problem

A separate approach which has been frequently used is the path integral method first pioneered by Anderson, Yuval and Hamann (Hamann [1970], Yuval and Anderson [1970], Anderson, Yuval, and Hamann [1970]). This approach yields renormalization group differential equations which have many of the features of the leading and next leading scaling theory but are different in a number of respects we shall make clear. The basic idea is to map the problem to a classical one dimensional Coulomb gas problem. Renormalization group equations are then derived for this Coulomb gas. The screening interaction V^z gives rise to phase shifts which will be expressed in terms of the "charges" of the Coulomb gas, while the tunneling processes give rise to "fugacities," and may make contributions to the charges as well. The contributins to the charges are determined by the electronic transitions combined with the tunneling processes. In making this mapping, the local conduction green's function is approximated with a long time form which allows one to pick up leading logarithmic behavior to all orders in V^z. Hence, the path integral approach allows the phase shift to be introduced in the place of V^z for terms that are of the leading logarithmic order. However, the tunneling terms which give the fugacity must still be treated perturbatively, and the long time approximation does not allow next leading logarithms associated with V^z to be picked up. Hence, the RG equations are something of a mix of leading and next leading log theory treated both perturbatively and non-perturbatively. While it is a great advantage to have V^z treated non-perturbatively at least in leading logs, the phase shift is ill defined at the non-trivial fixed point. Hence, the present method is useful for giving some overall view of the scaling flow tendencies, and is not to be relied upon in the vicinity of the non-trivial fixed point.

The path integral approach to the TLS model is very elaborate and cannot be followed without studying the original papers (Zawadowski and Zimányi [1985], Vladár , Zawadowski , and Zimányi [1988a,b]). The present section provides only a brief outline by pointing out some of the crucial steps and the additional complications in comparison to the treatment of the Kondo problem by Yuval and Anderson [1970].

In the previous treatment of Secs. 3.3 and 3.4, the renormalization group was constructed by determining the β-function up to the third order in perturbation theory. This is an internally consistent approach in the weak coupling limit. In physical applications, however, the screening coupling v^z can be large while the other two remain small $v^x, v^y << 1$. This situation is thus a hybrid of weak and strong coupling. A systematic treatment has been worked out in which the phase shift associated with an arbitrarily large v^z is combined with small v^x, v^y. The renormalization group is constructed by using the path integral method only in the leading order of v^x, v^y and thus the next leading results given by Eq. (3.4.12) cannot be reproduced exactly (the terms are similar, but there are differences in the coefficients).

We now describe the main procedure following Anderson, Yuval, and Hamann (AYH) (Hamann [1970], Yuval and Anderson [1970], Anderson, Yuval and Hamann [1970]). The TLS flips between two states. Following each flip the screening cloud starts to build up. If the flips are far enough apart in time (see Fig. 36), the the screening can be described by the long time shift. Assuming that the flips are spontaneous, the problem was solved by Yu and Anderson [1984] using the AYH method, where the free energy is constructed with the imaginary time path integral method. The electron variables are integrated out so that the free energy only depends on the classical path of the TLS on the time interval $(0, \beta)$ (see Fig. 36). The interaction along the time axis between the flips is logarithmic as in a one dimensional Coulomb gas. We note that Yu and Anderson also [1984] considered how the TLS forms beginning with a single well potential and assuming strong electron-phonon coupling.

The current problem is more complex than that considered by Yu and Anderson, as discussed by Vladár , Zawadowski , and Zimányi [1988a,b], since even if the electrons are integrated out the partition function still depends explicitly on the particular choice of the interaction at the different time points and the summation over the different realizations of those interactions cannot be given in a closed form. The problem without assisted hopping was studied by Black and Györffy [1978] using AYH techniques. In what follows, we will summarize some of the main ideas to give an overview to the

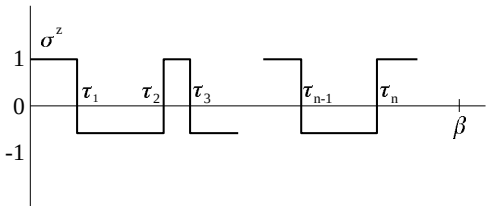

Figure 36: The classical path of the pseudo-spin σ^z is shown as a function of the imaginary time τ. τ_1, τ_2.... are the times of the jumps.

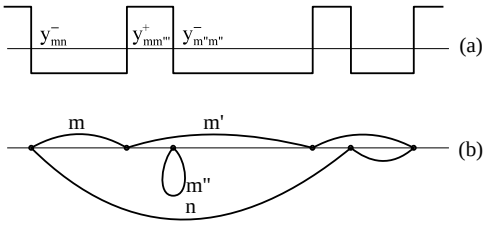

Figure 37: (a) The jumps of the quasi-spin are shown and the fugacities are also indicated. (b) A particular choice of the connecting of the different fugacities by electron lines is shown.

work in the original papers, leaving the technical details to those texts.

For the sake of simplicity, assume that a linear combination of angular momentum channels is used which diagonalizes the screening interaction so that $V^z_{mm'} = \delta_{mm'}$ (see Eq. 2.1.29 for the definition of $V^z_{mm'}$. Now, consider a the classical path $\sigma^z(\tau)$ of the tunneling atom shown in Fig. 36 where the states of the atom are characterized by the Ising variable $\sigma_z = \pm 1$. (We note that the representation in terms of these Ising variables may be effected directly by the discrete Hubbard-Stratonovich transformation introduced by Hirsch [1983] and Hirsch and Fye [1986] [Zhang, 1994]. If one considers only the V^z interactions, then different time dependent potentials $V^z_m(\tau) = V^z_m \sigma^z(\tau)$ are acting on the electrons of angular momentum m. This potential is shown in Fig. 37(a). Each flip of σ^z is associated with either a spontaneous flip or an assisted hopping process that turns the pseudo-spin either up or down, and which must also be characterized by the angular momentum channels of the incoming and outgoing electrons. In statistical physics, the probabilities of these hoppings are introduced as fugacities, which we define here as

$$y = \Delta_0 \tau_0, \quad y^+_{mm'} = V^+_{mm'} \rho_0, \quad y^-_{mm'} = V^-_{mm'} \rho_0 \tag{3.5.1}$$

where τ_0 is a short time cutoff replacing the bandwidth, i.e., $\tau_0 \simeq \hbar / D_0$. Notice that even if the interaction V^z is diagonal, the interactions $V^\pm$ need not be diagonal in the angular momentum indices. In Fig. 37(b), we illustrate the electron hops by projection of the Ising variable flips down to interaction points labelled by the angular momentum index. Note that the V^z interactions are not represented by points as they must be treated as time dependent potentials. These are constant between points along the projection line.

The continuous electron lines which connect the interaction points in Fig. 37(b) can have either up or down real spin. The continuous lines must form loops with the number of loops depending on the way the connections between points are made.

Let us first consider the effect of the time dependent field on an electron in angular momentum state m. In the presence of the potential $V^z_m(\tau)$, the Dyson equation of the one electron Green's function is solved. Applying the technique of Nozières and de Dominicis [1969], the Green's function depends on the time positions τ_i of flip i. The on-site Green's function in angular momentum state m has the

form for long times $|\tau - \tau'| >> \tau_0$ (where τ_0 is a short time cutoff)

$$G_m(\tau,\tau') = \frac{\rho_0}{\tau-\tau'}\cos^2\delta_\mu \exp[\sum_i c_i^m \ln|\frac{\tau_i-\tau'}{\tau_i-\tau}|] \quad . \tag{3.5.2}$$

The denominator $(\tau-\tau')^{-1}$ is due to the long time approximation of an unperturbed electron leaving and arriving at the TLS. The phase shift δ_m is used instead of V_m^z with

$$\delta_m = -tan^{-1}(\pi\rho V_m^z) \quad . \tag{3.5.3}$$

The coefficients of c_i^μ are introduced to indicate whether the spin flips up or down at flip time i, so that

$$c_i^\mu = \frac{\delta_\mu(\tau_i+O^+)}{\pi} - \frac{\delta_\mu(\tau_i-0^+)}{\pi} \quad . \tag{3.5.4}$$

Calculation of the part of the electron line contribution to the diagram of Fig. 37(b) from the exponential factor on the right hand side of Eq. (3.6.3) gives a result independent of the way in which the different interaction points are connected. This does not hold for the products of the first factor $1/(\tau-\tau')$. Anderson and Yuval [1970] noticed that for a given channel M the sum of the various contributions of the products of those factors forms a Cauchy determinant of order N which is

$$det(\tau_i - \bar\tau_j)^{-1} = \frac{\prod_{i<i'}(\tau_i-\tau_i')\prod_{j>j'}(\bar\tau_j-\bar\tau_j')}{\prod_{ij}(\tau_i-\bar\tau_j)} \tag{3.5.5}$$

where $\tau_1,\tau_2,....\tau_N$ and $\bar\tau_1,\bar\tau_2,...\bar\tau_N$ are the time orderings of the times where the electron is created and annihilated, respectively. This is valid only if the electrons are created and destroyed at different times which we assume for the time being.

With this assumption, the partition function can be written in the form of a sum over configurations which we explain presently. The interaction points τ_i are on the imaginary time axis in the interval $(0,\beta)$ as shown in Fig. 37(a) . Each point is associated with one of the fugacities $y, y_{mn}^{\pm}$. (There are other fugacities $y^z, y_\pm^z$ generated for technical reasons we shall not discuss here.) That association is called a configuration $\{\alpha\}$. If the fugacity descibes the assisted process, the the angular momentum indices of the outgoing and incoming electron lines (m,n) must also be added, which forms another configuration $\{m,n\}$. Finally we need a combinatorial factor $R=\pm1$ which is defined in the original paper of Vladár , Zawadowski , and Zimányi [1988a]. The resulting partition function is summed over loops of length N and the configurations, giving after much work the result

$$Z = \sum_{N=0}^{\infty}(-1)^N \sum_{\{\alpha\}}\sum_{\{m,n\}}\prod_{j=1}^{N} y_j Tr_\sigma \prod_{i=1}^{N}[\sigma(\alpha_i)] \tag{3.5.6}$$

$$\times\tau_0^{-N}\int_0^\beta d\tau_N ... \int_0^{\tau_{i+1}-\tau_0} d\tau_i ..... \int_0^{\tau_2-\tau_0} d\tau_1 R\exp[\sum_{i<j}\vec C_i\cdot\vec C_j \ln|\frac{\tau_i-\tau_j}{\tau_0}|]$$

where the real spin degeneracy has been set to 1 for the moment for simplicity. The time $\tau_0 \sim D^{-1}$ serves as a short time cutoff for the problem. The matrices $\sigma(\alpha_i)$ are $\sigma^+,\sigma^-,\sigma^z$ at a given time point for the fugacity configuration $\{\alpha(\tau_i)\}$ depend on whether the TLS pseudo-spin is flipped up,flipped down, or does not change. The vector "charge" $\vec C_i$ has components indexed by the angular momentum label m and is given by

$$C_{im} = \frac{[\delta_m(\tau_i+0^+)-\delta_m(\tau_i-0^+)]}{\pi} \tag{3.5.7}$$

for spontaneous tunneling, and

$$C_{im} = \frac{[\delta_m(\tau_i+0^+)-\delta_m(\tau_i-0^+)]}{\pi} + \delta_{m,m} - \delta_{m,n} \tag{3.5.8}$$

for assisted tunneling, with the index pair m, n associated to the charge. (For technical reasons in the initial papers of Vladár , Zawadowski , and Zimányi [1988a,b] charge matrices were used instead of vectors in order to avoid the diagonalization of V^z_{mn}.) The phase shifts are due to the exponents in Eq. (3.5.2), while the Kronecker delta terms take into account the determinants. Note the analogy to the 1D Coulomb gas with a logarithmic interaction; the vectors $\vec{C}_i$ take the place of the charges.

Clearly at this point a great complication has occured relative to the ordinary spin Kondo problem. In the latter case the configurations $\{\alpha\}$ and $\{m, n\}$ don't occur because the spin flips occur in a simple alternating way (+-+-+-....). Because of this, the more complex charge factor of Eq. (3.5.6) is simply replaced by $(-1)^{i-j}\delta/\pi$ in the ordinary Kondo problem.

A second complication is even more serious. It can happen that at a time point τ_i of an assisted tunneling process, the electron is annihilated and created with the same angular momentum index $m = n$. In that case, $\tau_i = \bar{\tau}_i$, so a divergence appears in the expression of the Cauchy determinant in Eq. (3.5.5). The divergence can be eliminated by the short time cutoff τ_0, by splitting the time of annihilation and creation by τ_0 (i.e., as $\tau_i = \bar{\tau}_i + \tau_0$). This complication results in a separate treatment of the Hartree-Fock (HF) terms in which a single electron line is attached to the aforementioned time point. This leads to the introduction of HF fugacities.

The main consequence of this complication is that a charge at time τ_j can interact with two charges at the points $\bar{\tau}_i$ and $\tau_i = \bar{\tau}_i + \tau_0$. Since the interaction of the 1D Coulomb gas is logarithmic, the following expression will appear in the sum over interaction terms:

$$\ln|\frac{\tau_j - \tau_i + \tau_0}{\tau_0}| - \ln|\frac{\tau_j - \tau_i}{\tau_0}| \approx \frac{\tau_0}{\tau_j - \tau_i} \tag{3.5.9}$$

where $|\tau_i - \tau_j| >> \tau_0$. Thus the charge at point τ_j interacts with the opposite charges forming a dipole at τ_i. Therefore, in the $m = n$ case, dipoles must be introduced which lead to charge-dipole interactions. For a complete discussion of all these complexities, we refer the reader to the original papers Vladár , Zawadowski , and Zimányi [1988a,b] where the complete expression for the partition function is given.

The derivation of the scaling equations follows a delicate and cumbersome procedure. The idea is to eliminate the short time behavior in small steps or in other words to replace τ_0 by $\tau_0 + d\tau_0$ where $d\tau_0$ is the increment in the short time cutoff. In that case if a pair of flips are eliminated they must be replaced by a single flip or an interaction without a flip. This leads to the essential renormalization of the fugacities and the phase shifts.

Restricting to the case when only two angular momentum states are important but the channel number (real spin here) is allowed to be arbitrary (M), the scaling equations are expressed in terms of the phase shift δ, the fugacity for spontaneous tunneling y and the fugacity for assisted tunneling y_a where the m, n dependence of Eq. (3.5.1) is now removed by decomposing the fugacities in Pauli matrices times the amplitude. The scaling equations are given by

$$\frac{d(\delta/\pi)}{d\ln\tau_0} = 4y_a^2(1 - 2M\delta/\pi) - 2y^2\delta/\pi \tag{3.5.10.a}$$

$$\frac{dy_a}{d\ln\tau_0} = 4y_a(\delta/\pi)(1 - M\delta/\pi) \tag{3.5.10.b}$$

$$\frac{dy}{d\ln\tau_0} = y(1 - 4M(\delta/\pi)^2) \quad . \tag{3.5.10.c}$$

These are similar to the scaling equations derived previously assuming noting that $v^x = v^y$ and the correspondence $\Delta_0\tau_0 \approx \Delta_0/D = y$, and that to linear order $\delta = -\pi v^z + O([v^z]^2)$. To within leading logarithmic order and the expansion of the phase shift, they agree with the results from the multiplicative renormalization group treatment (see Sec. 3.3.1). Considering the next leading order, some terms

are missing in the scaling equations presented above. This means that this derivation is not completely systematic, which can be traced back to the use of the long time approximation for the Green's function. The other main difference from the scaling equations derived previously is that the spontaneous tunneling occurs in (3.5.10.a) which describes the renormalization of the screening interaction. In the multiplicative renormalization group treatment, the electronic phase space is reduced and the spontaneous tunneling only occurs as an infrared cutoff in the logarithmic integrals. That is the origin of the difference in the scaling equations which has already occurred in the commutative model (see Black and Györffy) [1978], and Black, Vladár , and Zawadowski [1987]).

We now want to discuss the most interesting features of the scaling equations (3.5.10.a-c). First, ignoring the spontaneous tunneling in Eq. (3.5.10.a), we see that the phase shift renormalizes to the value

$$\delta^* = \frac{\pi}{2M} \tag{3.5.11}$$

which seems to have some connection to the fixed point given by Eq. (3.4.16) if we expand the phase shift to linear order in v^z. However, we must remind the reader that at the non-trivial fixed point the phase shift loses physical meaning since the projection to outgoing one particle processes is zero (see Fig. 4 in Sec. 1, and Sec. 6.1.3). Clearly, however, the flow to a non-trivial phase shift ($\delta \neq 0, \pi/2$) is indicated by this procedure. The same result emerges from a Friedel sum rule estimate of the number of electrons tied on average to the tunneling center, $Z = 1 = 2M\delta/\pi$. Indeed, for an infinitesimal applied spin field in the two channel problem, the phase shift experienced by up and down spin electrons is $\pm\pi/4$ (see Secs. 4.2,6.1.2). Next, if we consider the scaling of the fugacities, the primary results are that: (i)y_a increases if $\delta(0) < \pi/M$, which is always satisfied for $M = 2$ since $\delta(0) < \pi/2$ is assumed. (ii) y increases if $\delta(0) < \pi/(2\sqrt{M})$, but decreases otherwise hence giving localization to one well ($y = 0$) if the condition is reversed (see Yu and Anderson [1984]). For more channels ($M > 2$), $y_a \to 0$ may be the case so that localization in one of the potential wells occurs.

In a recent paper, Moustakas and D. Fisher [1995,1996] used the path integral approach to study the commutative model of TLS ($V^z \neq 0,\ V^x = V^y = 0$) with an additional potential scattering term at the TLS site (see $V^0_{\vec{k},\vec{k}'}$ in Eq. (2.17)). This problem has already been studied by Kagan and Prokof'ev [1983]. Suppressing the spin indices, the interaction part of the Hamiltonian is written as

$$H_1 = V_1(c_e^\dagger c_e + c_o^\dagger c_o) + V_1(c_e^\dagger c_e - c_o^\dagger c_o) + V_3\sigma^z(c_e^\dagger c_o + c_o^\dagger c_e) \tag{3.5.12}$$

where e, o refer to even and odd parity combinations of conduction states about the TLS center (see Appendix II for a discussion of how to generate these states). Moustakas and D. Fisher [1995,1996] pointed out that the presence of both V_1 and V_2 can be relevant in determining physical quantities through a modification of the local conduction density of states and in the modification of states near the band edges in the renormalization process. Indeed, one can sum up the diagrams involving the one particle Green's functions diagonal in the e, o indices (Zawadowski *et al.* [1997]). The associated two spectral functions are smooth, but the density of states is depressed by the increase in bandwidth. The remaining coupling V_3 can be treated in a rotated representation of the TLS where $-\sigma^x$ replaces σ^z. Application of the multiplicative renormalization group shows that the resulting model belongs to the commutative class, so that the coupling V_3 remains marginal after making it dimensionless by multiplying by the density of states that has been renormalized by V_1, V_2. In this formulation, no new coupling is generated. The formulation of Moustakas and D. Fisher [1995,1996] using the path integral approach derives a generalization of the scaling equations (3.5.a-c) by introducing an infinite number of new couplings. Among them the assisted tunneling coupling V^x is also generated by eliminating a close pairing of a V_2 potential scattering with a spontaneous hopping Δ_0 as shown in Fig. 38 . This generates an assited hopping term of the order of $V_2\Delta_0$ in lowest order. The serious consequence of this result is that the induction of this interaction V^x which fails to commute with V^z changes the universality class to the fully noncommutative model, away from the marginal line of fixed points associated with $V^x = V^y = 0$.

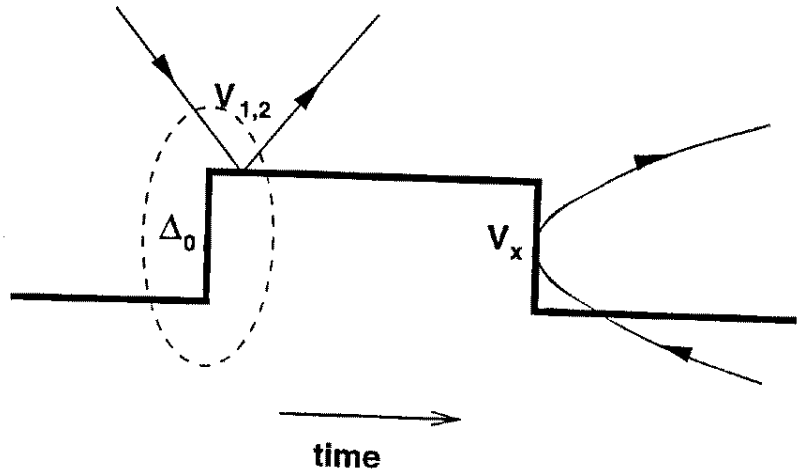

Figure 38: Diagram resulting in the generation of artificial interaction terms in the elimination scheme (i). The heavy line represents the motion of the heavy particle. The artificial interaction is genrated by the elimination of a spontaneous tunneling event Δ_0 and a potential scattering close to it ($V_{1,2}$). The lines with arrows represent the conduction electrons.

Considering that essential differences arise between the results obtained by the leading logarithms diagrammatic approach and the program of Moustakas and Fisher [1995,1996], the following questions are raised:
(i) The introduction of the coupling V_2 which breaks electron hole symmetry renders the $V^z = const.$, $V^x = V^y = 0$ line of fixed points unstable as mentioned above; assuming we start with bare $V^x = 0$, can we get close to the TLS two-channel Kondo fixed point?
(ii) There are two essentially different path integral approaches which may be adopted. In the space-time scaling, one integrates out short regions of time between interaction lines. In the first approach, only those times eliminated in the space-time scaling in which both ends are connected to electron lines (Vladár ,Zawadowski , and Zimányi [1988a,b,c]. In the second approach of Moustakas and Fisher [1995,1996], as discussed above, a spontaneous tunneling process combined with potential scattering at short times generates an effective V^x, even though there is an absence of interaction between the dynamical degrees of freedom of the TLS and the conduction electrons. The question is which approach generates the physical scaling equations, where the generated couplings can be directly used to calculate the quantities of physical interest (e.g., the resistivity), since at most one approach can be correct unless a mathematical equivalence is established.

We may answer the first question with assistance from symmetry considerations (Zawadowski *et al.* [1997]). Consider a commutative model with $V^x = V^y = 0$, $V^z \neq 0$, $\Delta^z = \Delta_0 \neq 0$, and $\Delta^z = \Delta = 0$. The Hamiltonian is invariant under the following combined symmetry operation:
$\rightarrow$ Interchange the L, R indices of the tunneling TLS.
$\rightarrow$ Apply electron-hole symmetry in both the e, o channels, *viz.*, $c_{e,o} \rightarrow c^{\dagger}_{e,o}$ (where we have suppressed spin indices). Note that without explicit spin dependence, we needn't introduce the customary $(-1)^{1/2-\sigma}$ factors because they cancel in pairs. (The electron-hole transformation is defined in this way where the electrons and holes are at the same sector of the Fermi surface, and the density of states and couplings are replaced by their values taken at the Fermi surface. That transformation is equivalent to one of the transformations used by Affleck, Ludwig, and Jones [1995] (see Sec. 9.3.1). An additional symmetry is that of time reversal, which gives $c^T_{e(o)} = c_{e(o)}$ and $d^T_i = d_i$, $i = 1, 2$, assuming that all the atomic wave functions are real. Furthermore, all c-numbers are replaced by their complex conjugates under time

reversal. The Hamiltonian of Eq. (3.5.12) is also invariant under that transformation. Finally, going over to the left and right states defined by Eqs. (A.2.7a-b) of App. II, the symmetries discussed above lead to the conservation of total number of electonrs separately for left and right states, as is pointed out by Mostakas and Fisher [1995].)
It is clear that the spontaneous hopping interaction and the V^z coupling are unchanged under this transformation, as is the conduction band provided it begins particle hole symmetric. However, the assisted hopping terms proportional to

$$\sigma^x(c_e^\dagger c_e + c_o^\dagger c_o)$$

and

$$i\sigma^y(c_o^\dagger c_e - c_e^\dagger c_o)$$

change sign under the transformation, as does any potential scattering (specifically the V^1, V^2 terms). A dependence of fixed point stability on particle-hole symmetry is also found in the two-impurity one- and two-channel Kondo models; see Sec. 9.3.1 and Affleck, Ludwig, and Jones [1995] for some details.

Now, clearly the marginal line of fixed points associated with this high symmetry Hamiltonian is unstable if small V^x and/or V^y couplings are introduced that generate a flow towards the TLS two-channel Kondo fixed point. We now demonstrate that any potential scattering leads to the same instability by breaking the same symmetry. This also hinges on the non-zero spontaneous tunneling term. A simple diagrammatic summation of multiple scattering processes results in the renormalization of the local electronic density of states in both the even and odd channels giving

$$\rho_{e,o} = \rho_0[1 + \alpha_{e,o}\frac{\epsilon}{E_0}] \tag{3.5.13}$$

where $\alpha_{e,o} \sim V_1$ and V_2 to leading order measures the asymmetry and E_0 is of the order of the bandwidth. We note that the e, o "bands" may have initial asymmetry as discussed in Appendix II (see also Sec. 9.3.2 on the two-impurity model).

In a diagrammatic renormalization group analysis the generation of the assisted hopping takes place as suggested by Moustakas and Fisher [1995,1996], but at a lower order than in their approach, namely, in the leading logarithmic order. Refer to the diagrammatic scaling analysis depicted in Fig. 39. which displays second order vertex corrections which include one spontaneous hopping renormalization of the internal TLS pseudofermion line. The contributions of the diagrams shown to the dimensionless coupling $v^x = \rho_0 V^x$ are

$$(v^z)^2\Delta^x\{\int_T^D \frac{d\epsilon}{\epsilon^2}\rho_0(1+\alpha\frac{\epsilon}{E_0}) - \int_{-D}^{-T}\frac{d\epsilon}{\epsilon^2}\rho_0(1+\alpha\frac{\epsilon}{E_0})\}$$

which leads to

$$\delta v^x \simeq (\rho_e\alpha_e - \rho_o\alpha_o)(v^z)^2\alpha(\frac{\Delta^x}{E_0})\ln(\frac{D}{T}) \tag{3.5.14}$$

where $\rho_{e(o)}, \alpha_{e(o)}$ may be calculated straightforwardly as an extension of App. II. The initial strength of this generated interaction is very weak, as typically $\Delta^x/E_0 \simeq 10^{-5}$, $v^z(0) \simeq 0.2$, and $\alpha << 1$. Hence, at $T \sim 1K$, the generated dimensionless coupling strength would be of order $v^x \simeq 5 \times 10^{-6}$, which is very small. Below this temperature the generation of the non-commutative couplings will be stopped due to the splitting $\Delta^x \simeq 1K$ which serves as an infrared cutoff (see Fig. 40).

Thus the breaking of the artificial combined particle-hole symmetry by introducing V_2 does indeed render the marginal line of fixed points of the commutative model unstable as suggested by Moustakas and Fisher [1995,1996]. However, we do not expect this symmetry breaking instability to lead in parameter space to the vicinity of the TLS two-channel Kondo fixed point. Thus even with the symmetry breaking present, it appears to be difficult to observe experimentally relevant consequences.

We now briefly return to question (ii) from above which concerns which path integral scaling approach is appropriate (for more details see Zawadowski *et al.* [1997]). The free energy which is the

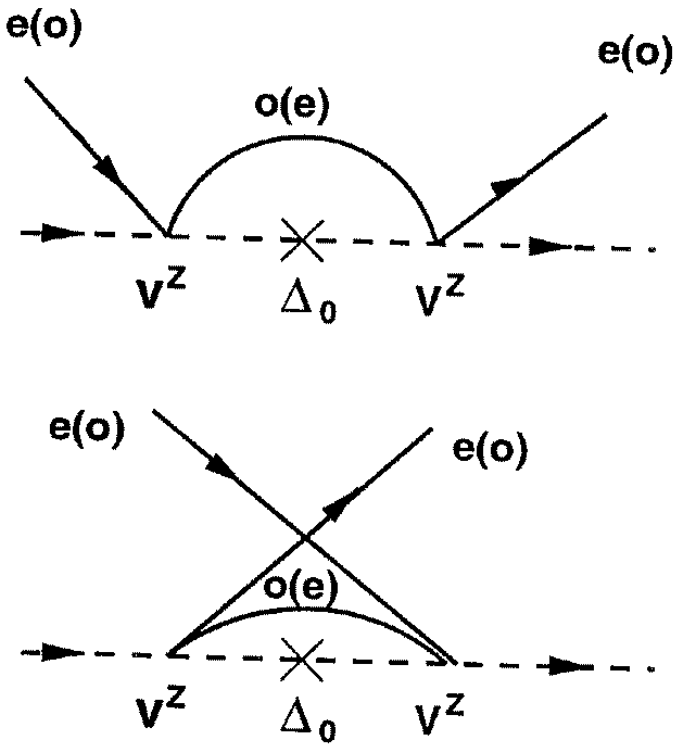

Figure 39: Time ordered diagrams generating the assisted tunneling process in the presence of appropriate electron-hole symmetry breaking. The cross indicates a spontaneous tunneling between the two positions of the heavy particle. The labels on the electron lines refer to the even and odd parity electron channels with repsect to reflection through the center of the system.

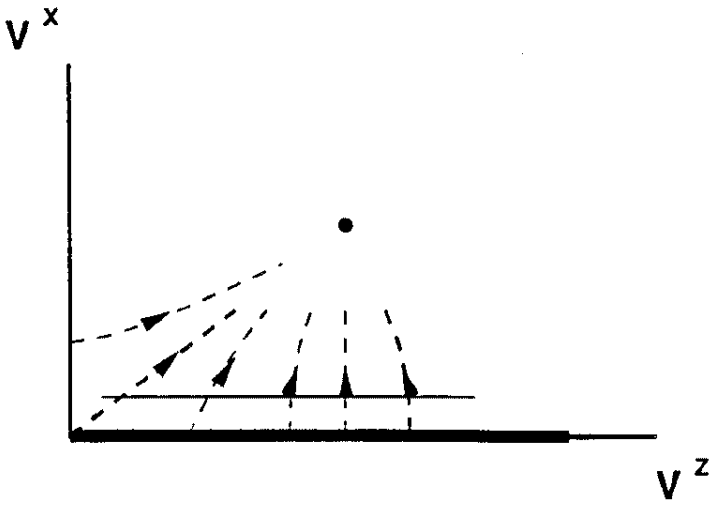

Figure 40: Sketch of the scaling trajectories of the TLS. The appropriate electron-hole symmetries drives the TLS away from the marginally stable fixed line $V_x = 0(\Delta_1 = 0)$ towards the two-channel Kondo fixed point. The scaling is stopped by the renormalized splitting, and the final ground state is a Fermi liquid. The freezing out of the TLS is indicated by a light continuous line.

logarithm of the path integral can be computed by either approach, and demanding invariance of the partition function (free energy) then leads to different scaling equations between the two methods. In principle this is not a problem as it may correspond to a simple reorganization of variables. However, when computing any physical quantity with the obtained renormalized couplings we must of course get equivalent physical results if each method is correct. A check is whether the scaling equations can be made to correspond to the diagrammatic method associated with the multiplicative renormalization group (leading logarithms approximation) at the appropriate level of approximation. In this way it has been shown that the approach in which only those time intervals are eliminated with endpoints connected to electron lines gives the same scaling as the multiplicative renormalization group; physically inequivalent scaling equations are generated by the second approach of Moustakas and Fisher [1995,1996]. The first space-time scaling method also has the feature in common with the multiplicative RG that in a noninteracting TLS-electron system no new couplings are generated.

A more general discussion of the scaling trajectories in the model of Moustakas and Fisher [1995,1996] was presented by Ye [1996e], applying bosonization methods to the problem. This will be briefly discussed in Sec. 6.3. His key finding is that all scaling goes finally to a Fermi liquid fixed point.

Finally, we close this section noting that as will be discussed in Sec. 6.2, the two-channel Kondo problem can, for a particular value of the coupling V^z (phase shift here) be mapped to a resonant level model as pointed out by Emery and Kivelson [1992]. That model has a strong similarity with the model suggested by Toulouse [1970]. In these works the mapping is established by bosonization. Recently, Fabrizio, Gogolin, and Nozières [1995] have established the mapping to the resonant level model by starting with the path integral formulation. They studied the partition function by studying its expansion in terms of the perpendicular coupling of the two-channel Kondo problem and compared with a similar expansion of the resonant level model of Emery and Kivelson [1992]. They have shown that the the two expansions agree term-by-term for the special value of the longitudinal coupling V^z (which corresponds to J^z in Sec. 6.2). The virtue of the path integral approach in this context is the

ability to study the cross-over regime from high to low temperatures as opposed to the asymptotic fixed point regime accessible with the bosonization approach.

4 Numerical Renormalization Group Approach

Our goal in this section will be to provide an overview of the NRG method pioneered by Wilson [1973,1975] for the ordinary Kondo model. We will stress the results obtained from this approach which provide insight on the two-channel Kondo model and the influence of symmetry breaking fields on that model. Specifically, we will consider the effects of exchange anisotropy, ($J^{(1)} \neq J^{(2)} = J^{(3)}$), the influence of local and bulk fields which couple to the spin, and the influence of a channel field which splits the exchange integrals for the electrons in the two different channels. We will also discuss a simple "shell model" approach which works remarkably well for characterizing the lowest few states of the non-trivial fixed point and appears to generalize to more complex models not treatable by the NRG.

The original NRG work on the two-channel model was performed by Cragg, Lloyd and Nozières [1980], who provided the first non-perturbative confirmation of the Nozières and Blandin arguments for a non-trivial fixed point in multichannel models with $M > 2S_I$. These calculations were performed for strong bare coupling values and for one case where the exchange in one channel differed from that in the other. Subsequent calculations have been performed by Pang and Cox [1991], and Affleck *et al.* [1992] to explore the weak coupling approach to the transition and the influence of exchange anisotropy, applied local and bulk spin fields, and channel fields (through the exchange splitting between channels) in greater detail.

4.1 Logarithmic Discretization, Hamiltonian, and Renormalization Group Transformation

(a) Logarithmic Discretization of the Hamiltonian

We begin with the two-channel Kondo model given by Eq. (1.1). As in the introduction, we label spin with $\mu = \uparrow, \downarrow$ and channel index with $\alpha = \pm$. Following the pioneering work of Wilson [1973,1975], we transform the Hamiltonian in the following ways:
(1) We logarithmically discretize the conduction band as shown in Fig. 41. This means we split the band up into a sequence of intervals between $\Lambda^{-n} D > |\epsilon_{\vec{k}}| > \Lambda^{-(n+1)} D$, with $\Lambda > 1$ the logarithmic discretization parameter.
(2) Within each logarithmic interval, we Fourier analyze the conduction states, but retain only the average components. There are two justifications for this seemingly gross neglect: (i) only the average states couple to the impurity spin given the assumed contact form of the Kondo exchange interaction, and (ii) in the full continuum limit ($\Lambda \to 1$) only these average states survive.
(3) For numerical convenience, we employ the Lanczos algorithm to convert the Hamiltonian to a tridiagonal basis which has a meaning in position space. The Lanczos states correspond to electron creation operators $f^\dagger_{n,\alpha,\mu}$ which have approximate radial extent of $\Lambda^{n/2}/k_F$ measured from the impurity. In order to get these wave functions the hoping amplitudes ϵ_n must also depend upon N. As the electronic energy grows, so does the energy spacing. Concommitantly, the amplitudes at the impurity site are increased due to localization of the electron into smaller volumes. The corresponding wave functions have higher numbers of nodes for higher n so that orthogonality holds. The state created by $f^\dagger_{0,\alpha,\mu}$ is just the on-site or Wannier orbital at the impurity position.

Following these steps, the two-channel Kondo Hamiltonian takes the form

$$\frac{H_{NRG}}{D} = \sum_{n=0,\alpha,\mu}^{\infty} \epsilon_n [f^\dagger_{n,\alpha,\mu} f_{n+1,\alpha,\mu} + h.c.] - \frac{J}{D} \vec{S}_I \cdot \sum_{\mu,\alpha,\alpha'} \vec{S}_{\alpha,\alpha'} f^\dagger_{0,\alpha,\mu} f_{0,\alpha,\nu} \quad , \tag{4.1.1}$$

where

$$\epsilon_n = \frac{\Lambda^{-n/2}(1+\Lambda^{-1})(1-\Lambda^{-(n+1)})}{2[(1-\Lambda^{-(2n+1)})(1-\Lambda^{-(2n+3)})]^{1/2}} \quad . \tag{4.1.2}$$

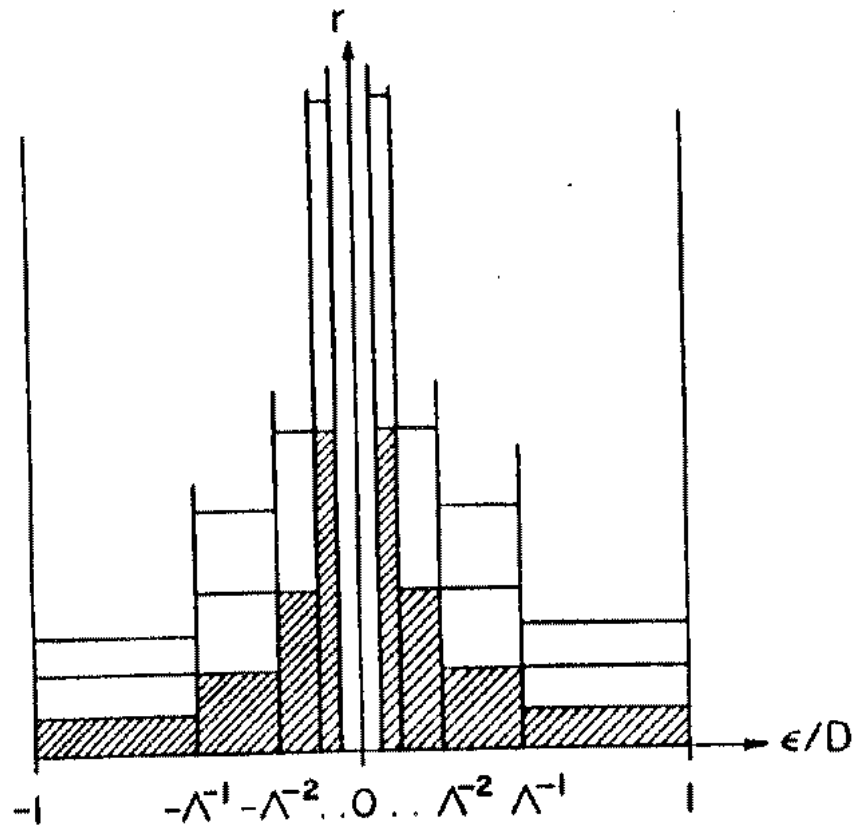

Figure 41: Logarithmic discretization of the conduction band for Numerical Renormalization Group (NRG) calculations. The conduction band is divided up into logarithmic bins $[\Lambda^{-(n+1)}, \Lambda^{-n}]$ for electrons and $-[\Lambda^{-n}, \Lambda^{-(n+1)}]$ for holes, with $0 < n < \infty$. The states are Fourier analyzed on each bin, and only the average Fourier components are retained (as only these couple to the impurity operators). After Krishna-murthy, Wilkins, and Wilson [1980].

The ϵ_n's correspond to the radial hopping matrix elements which transfer electrons from a state in "shell" n to "shell" $n+1$. Thus in a way rather different from the conformal field theory approach and Bethe-Ansatz approaches, we arrive at an effective one dimensional problem, with only the radial dimension being important.

(b) Renormalization Group Transformation

We can define a sequence of finite size dimensionless effective Hamiltonians which will reproduce H_{NRG} in the thermodynamic limit, and which define a renormalization group transformation. The discretized Hamiltonians are

$$\mathcal{H}_N = \Lambda^{N/2}\{ \sum_{n=0,\alpha,\mu}^{N} \epsilon_n [f^\dagger_{n,\alpha,\mu} f_{n+1,\alpha,\mu} + h.c.] - \frac{J}{D}\vec{S}_I \cdot \sum_{\mu,\alpha,\alpha'} \vec{S}_{\alpha,\alpha'} f^\dagger_{0,\alpha,\mu} f_{0,\alpha,\nu}\} \tag{4.1.3}$$

and the limit which reproduces H_{NRG} is

$$H_{NRG} = D \lim_{N\to\infty} [\Lambda^{-N/2}\mathcal{H}_N] \quad . \tag{4.1.4}$$

The renormalization group transformation is

$$\mathcal{H}_{N+2} = \Lambda\mathcal{H}_N + \Lambda^{N/2+1} \sum_{n=N+1,\alpha,\mu}^{N+2} \epsilon_n [f^\dagger_{n,\alpha,\mu} f_{n+1,\alpha,\mu} + h.c.] \quad . \tag{4.1.5}$$

Notice:
(i) The multiplication by $\Lambda^{N/2}$ in Eq. (4.1.3) has the effect of making the smallest hopping matrix element of order 1, which means the smallest resulting dimensionless excitation energy will be of order 1 in the corresponding spectrum.
(ii) The diagonalization of $\mathcal{H}_N$ corresponds to finding the effective Hamiltonian to describe the physics at length scale

$$L_N \approx \Lambda^{N/2} k_F^{-1} \tag{4.1.6}$$

and temperature scale

$$T_N \approx \Lambda^{-N/2} D \quad . \tag{4.1.7}$$

.
(iii) The need for a step size of 2 in the transformation (4.1.5) is because there are, generically, different fixed points for even and odd number of shells. Physically, we rescale the system size by an amount Λk_F^{-1} and inquire about the properties on that scale compared to the previous length scale.

The practical implementation of the RG transformation (4.1.5) is carried out by numerically diagonalizing the truncated Hamiltonians $\mathcal{H}_N$ for each N and using the states at level N to construct the basis for states at level $N+1$. The diagonalization process is repeated iteratively. A well defined procedure exists for the construction of these basis states using Clebsch-Gordan technology, and we refer the interested reader to Krishna-murthy, Wilkins, and Wilson [1980a)] and Jones [1988] for further details. A fixed point of the transformation (4.1.5) is obtained if the lowest lying spectrum of eigenvalues for the successive $\mathcal{H}_N$ is unchanged.

The approximation of logarithmic discretization thins out the number of states to keep for a particular system size quite substantially with respect to the customary exact diagonalization approaches. Taken together with block diagonalization using the symmetries we will discuss in the next subsection, the problem becomes considerably more manageable. Even still, the large degeneracy of states makes full diagonalization of $\mathcal{H}_N$ usually impossible for $N \geq 2$. Explicitly, the degeneracy is $\simeq 16^N$ at the

N-th shell, the factor of 16 deriving from the product of four conduction states for channel one times four conduction states for channel two including all occupancies. A practical way of implementing the transformation while keeping manageable numerics is to retain only the lowest few hundred states at each iteration. While there is no direct proof that this approximation is reliable, convergence tests in the original works [Wilson, 1973,1975; Krishna-murthy, Wilkins, and Wilson, 1980a),1980b)] and *a posteriori* comparison with other exact methods has confirmed the general validity of the method. In calculations for the two-channel model performed on a Sun workstation, typically the lowest 250 states were retained at each N value, while larger runs performed on a CRAY-YMP48 showed no significant difference from the runs with fewer states.

While the original efforts on the single channel Kondo model and s-wave spin 1/2 Anderson Hamiltonian had sufficiently many states within this space to reliably compute thermodynamic quantities, the higher degeneracy in the present problem means that practically we may only compute eigenvalues. Nevertheless, a considerable amount of information may be obtained from examining the spectrum of eigenvalues, as we shall discuss further below.

(c) Use of symmetry to reduce the basis size

For the isotropic model, one may obviously exploit the $SU(2)$ symmetry under spin rotations and use the total spin S^2_{tot} and z-component

$$S^{(3)}_{tot} = \sum_{n=1,\alpha,\mu}^{\infty} \mu f^{\dagger}_{n,\mu,\alpha} f_{n,\mu,\alpha} + S^3_I \tag{4.1.8}$$

as conserved quantities. $S^{(3)}_{tot}$ remains useful even in the presence of an applied spin field along the z-direction or an axial breaking of exchange isotropy $J^3 \neq J^1 = J^2$. In these cases the $SU(2)$ symmetry is broken down to a $U(1)$ symmetry for which S^3_{tot} is the conserved charge.

There are two ways to handle the charge and channel degrees of freedom of the conduction electrons. First, we have an obvious $SU(2)$ symmetry from rotations in channel space, and we could employ the total channel spin operators S^2_{ch} and $S^{(3)}_{ch}$

$$S^{(3)}_{ch} = \sum_{n,\alpha,\mu} \alpha f^{\dagger}_{n,\mu,\alpha} f_{n,\mu,\alpha} \tag{4.1.9}$$

as good quantum numbers. In addition, we can use the conduction charge operator

$$\hat{Q} = \sum_{\mu} Q_{\mu} = \sum_{n,\alpha,\mu} [f^{\dagger}_{n,\alpha,\mu} f_{n,\alpha,\mu} - \frac{1}{2}] \tag{4.1.10}$$

which is constructed to be zero in the ground state.

Alternatively, we may employ the "axial charge symmetry" or "isospin" symmetry first found by Jones [1988; Jones and Varma, 1988; Jones, Varma, and Wilkins, 1988]. Jones observed that the single channel particle-hole symmetric Kondo model enjoys an additional global $SU(2)$ symmetry specified by the "axial charge" generators

$$j^{+}_{\mu} = \sum_{n} (-1)^n f^{\dagger}_{n\uparrow\mu} f^{\dagger}_{n,\downarrow,\mu} \tag{4.1.11.a}$$

$$j^{-}_{\mu} = \sum_{n} (-1)^n f_{n\downarrow\mu} f_{n\uparrow\mu} \tag{4.1.11.b}$$

and

$$j^{(3)}_{\mu} = \frac{Q_{\mu}}{2} \quad , \tag{4.1.11.c}$$

where Q_μ is the charge in each channel. The total axial charge j_μ^2 and $j_\mu^{(3)}$ in each channel μ may be used as good quantum numbers. This has a clear numerical advantage over the use of the $SU(2) \times U(1)$ symmetry of channel spin times charge discussed in the previous paragraph because it leads to a greater reduction of basis size. Moreover, in the presence of channel symmetry breaking fields, this axial charge symmetry may still be used.

The axial charge operators, with the $(-1)^n$ generalized to $(-1)^{n_x+n_y}$ in two-dimensions are precisely the $SU(2)$ generators found later by Yang for the two-dimensional Hubbard Model [Yang, 1988] and employed by Zhang [1989], Yang and Zhang [1989], and Singh, Scalettar, and Zhang [1991] to speculate on the excitation spectra and "eta" pairing ($< j^+ > \neq 0$) in the Hubbard model away from half filling.

It is clear that the different symmetry choices of $SU(2)_{spin} \times SU(2)_{channel} \times U(1)_{charge}$ should we employ channel spin and charge or $SU(2)_{spin} \times SU(2)_{axial,1} \times SU(2)_{axial,2}$ if we use axial charge in each channel can only be compatible if these are subgroups of some larger group. Affleck *et al.* [1992] have noted that even in the logarithmically discretized form, the M-Kondo spin-1/2 model will have a full symmetry group of $SU(2)_{spin} \times Sp(M)$, where $Sp(n)$ is the so called symplectic group. This $Sp(M)$ symmetry is a hidden symmetry of the problem. (In the paper of Affleck *et al.* [1992], this is denoted $Sp(2n)$.) This is the group which results from the symmetry breaking of the $SU(2M)$ group of the free conduction electrons by the spin coupling to the impurity. It was noted that in the single channel Kondo model, $Sp(1)$ is isomorphic to $SU(2)$, which corresponds to the axial charge of the lone conduction channel. In the two-channel case, the only invariant subgroups of $Sp(2)$ (which is isomorphic to $SO(5)$) are $SU(2) \times U(1)$ which corresponds to the choice of channel spin and charge symmetries, and $SU(2) \times SU(2)$ which corresponds to the separate axial charge symmetries. In general, for M arbitrary, one always has $SU(M) \times U(1)$ and $[SU(2)]^M$ as invariant subgroups of $Sp(M)$ so that the channel spin/charge and axial charge symmetries may always be used. It was noted by Affleck *et al.* [1992] that the $Sp(M)$ symmetry holds for the generalization of the M model to a bipartite lattice form, which may be important for future work.

4.2 Overview of results from NRG studies

(a) Concepts and Reference Points

To orient the reader, in Fig. 42, we show the odd eigenvalues calculated by Krishna-murthy, Wilkins, and Wilson [1980a] for the single channel symmetric Anderson model in the Kondo limit beginning with an initial weak coupling $|J|/D << 1$. The lines connect the eigenvalues of the sequence of dimensionless Hamiltonians $\mathcal{H}_N$ for odd N. The labels reflect the spin and charge values of the many body states.

The reader should note the following features of these curves:

(i) Even-odd alternation. The spectra for an even number of shells differ from those for an odd number of shells. The reason is shown in Fig. 43 in the limit $J = 0$. When we have an even number of shells, we have an odd number of electrons at half-filling in the non-interacting limit and thus the Fermi level in the non-interacting limit cuts right through a level which is two-fold degenerate because of spin. For an odd number of shells, we have an even number of electrons, and the Fermi level passes through a gap above a non-degenerate Fermi sea.

(ii) Cross-over . There is a crossover evident in the spectra of Fig. 42 in that the spectra for even N crossover at large N to resemble the spectra for small odd N, while the spectra for odd N cross over at large N to resemble the spectra for small even N. The scale of this crossover is a measure of the Kondo temperature T_K. The reason is that in view of Eq. (4.1.6), we see that we may convert iteration

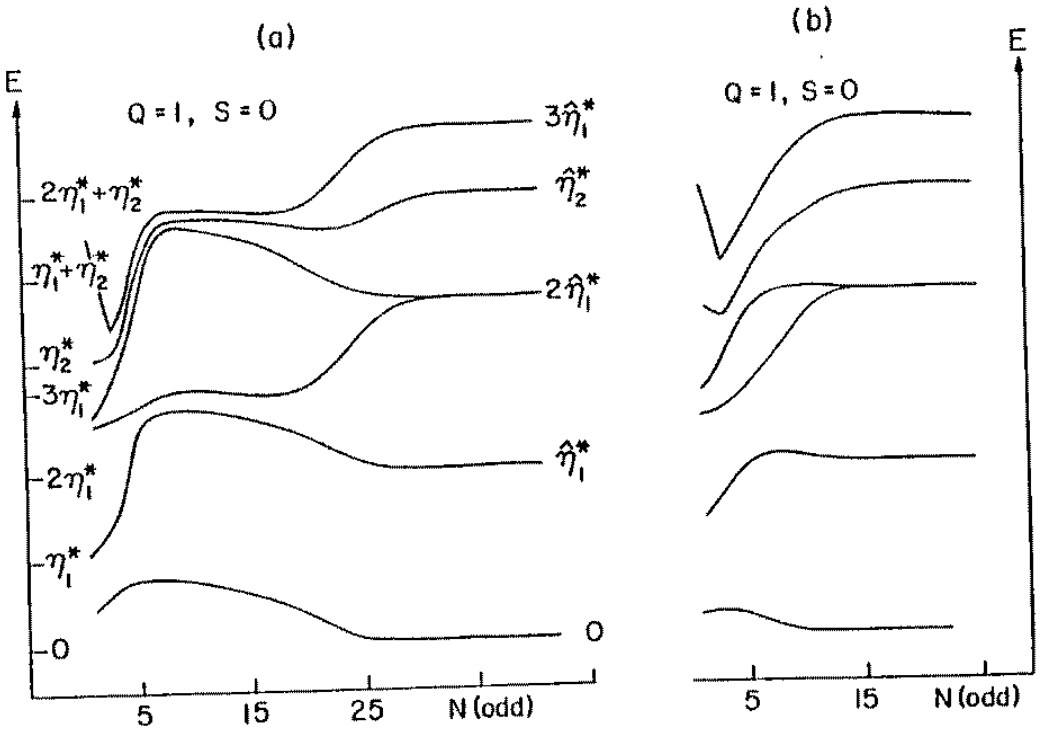

Figure 42: Odd spectra from the NRG calculations of the single channel spin 1/2 symmetric Anderson model for the charge 1 spin zero sector as a function of iteration number N. The levels begin near the free orbital fixed point, reach a plateau near the local moment fixed point, and finally approach the strong coupling Kondo fixed point for a ratio $U/\pi\Gamma = 5.63$ where U is the local Coulomb repulsion in the Anderson model and Γ is the hybridization width. The dimensionless exchange coupling is $N(0)J = 8\Gamma/\pi U$. Taken from Krishna-murthy, Wilkins, and Wilson [1980a].

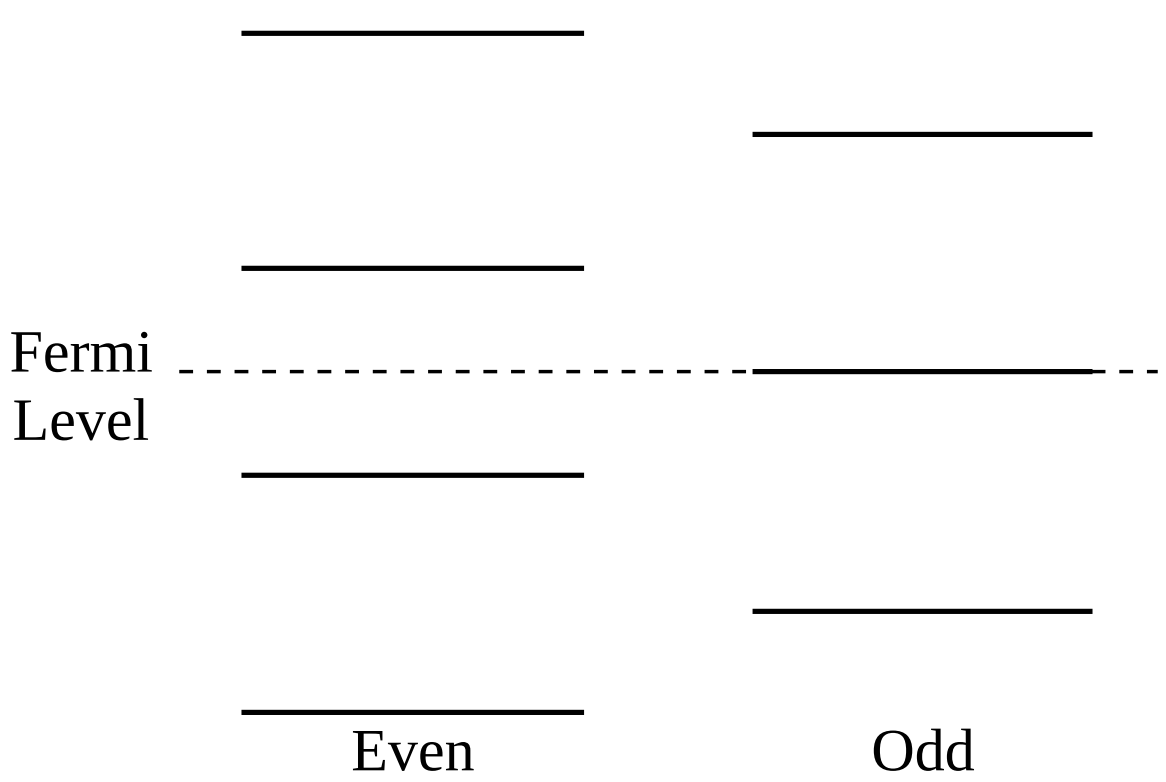

Figure 43: Even and odd energy levels for the noninteracting ($J = 0$) fixed point of the single channel Kondo model in the NRG logarithmically discretized scheme.

number N to temperature through

$$N(T) = 2\frac{\log(D/T)}{\log(\Lambda)} \tag{4.2.1}$$

so that the scale of the crossover N_K must correspond to a temperature T_K.

(iii) Equal level spacing: local Fermi liquid behavior. Provided we accept the reversal of spectra for even and odd N after the crossover, we see that there is a uniformity to the level spacing and a precise $1:1$ connection of large N even spectra to small N odd spectra and vice versa. This implies our low temperature spectrum is that of a Fermi liquid, since the electrons are essentially decoupled from the impurity at high T, and thus the high T spectrum is that of a free Fermi gas.

(iii) Meaning of the Large N/Low T spectra. The shifting of the low T spectra has a simple interpretation: due to the strong coupling to the impurity, each spin channel experiences a magnitude $\pi/2$ phase shift.

To elaborate, in the presence of a phase shift δ measuring scattering from a spherically symmetric target, radial quantization of the scattered waves on a sphere of size L implies a shift of wave numbers

$$k \to k - \frac{\delta}{\pi L} \quad . \tag{4.2.2}$$

For the linearized spectrum of conduction electrons near the Fermi energy, this implies a corresponding shift of energy levels by an amount

$$\delta E = -\frac{v_F \delta}{\pi L} \tag{4.2.3}$$

with the convention that an attractive potential gives a positive phase shift and thus shifts the levels down in energy.

Turning back to the Kondo problem, the sequence of Hamiltonians $\mathcal{H}_N$ is dimensionless, so the factor of v_F/L in δE is removed. The shift by $1/2$ unit of the fundamental spacing corresponds to exactly a $\pi/2$ phase shift of electrons with each spin value. This means the effective coupling is infinitely strong.

Note that this agrees with the Friedel sum rule also. The Friedel sum rule, valid for a Fermi liquid, relates the screening moments of the conduction electrons about an impurity to the scattering phase shifts. Since the impurity has only spin but no charge difference from the background, the sum rule insures that the screening charge around the impurity $\Delta Q = \delta_\uparrow/\pi + \delta_\downarrow/\pi = 0$. This implies $\delta_\uparrow = -\delta_\downarrow$. Imagine applying now an infinitesimal field in the positive z direction. For the ground state singlet case (N even) the total induced magnetization must be zero, but that results from a screening of the $S_I^z = 1/2$ contribution by the conduction electrons. Hence

$$S_{tot}^z = 0 = \frac{1}{2} + \frac{\delta_\uparrow - \delta_\downarrow}{2\pi} \quad .$$

Solving for δ_σ, we find

$$\delta_\sigma = -\sigma\pi \quad .$$

where $\sigma = \pm 1/2$.

(b) Isotropic Non-trivial Fixed Point

With the background of Wilson's calculations to guide us, we now turn to the more complicated spectra of the two-channel Kondo model. Fig. 44 shows the results of Pang and Cox [1991] for the approach to the non-trivial fixed point. What is plotted are the eigenvalues of $\mathcal{H}_N$ for sequential N connected by a line. In the case of the two-channel model, there is no even-odd alternation of energy levels in the region of the fixed point, and the curves in Fig. 44(a) displays the results for even N, the curves for odd N being in Fig. 44(b). The eigenvalues, are labeled by the quantum numbers (j_1, j_2, S) (see Eqs. 4.1.8,4.1.11). (Note that a very large Λ value was chosen to allow the weak-coupling crossover to occur in a manageable amount of computer time. The level spacings are Λ dependent for these spectra, though less dependent than in the Fermi liquid case.) The dashed curves are for an initial large value of J/D, while the solid curves are for an initial small value of J/D. In each case, the eigenvalues for large N tend to a fixed structure independent of the original coupling value. This confirms in a non-perturbative way that the two-channel spin $1/2$ model has a non-trivial fixed point which is stable in the absence of fields which break the full $SU(2)$ invariance of the exchange coupling. The rise of the low lying levels for the weak coupling starting case takes place on a crossover scale which corresponds to the Kondo temperature T_K. By studying a variety of couplings, we estimate, for $\Lambda = 3$, that $J_c \simeq -0.7D$. It is interesting that the eigenvalues for the initial strong coupling J/D value settle almost immediately to the fixed point value.

The other crucial point to notice in comparison to Wilson's spectra for the single channel model is that the spectra of the two-channel model have a non-uniform spacing. While it does not obviously follow from this that one has a non-Fermi liquid excitation spectrum, this is in fact the case. One may verify this by noting that the quantum numbers of the free states cannot be that of a Fermi liquid. Further discussion of this point is given in Sec. 6.1.2. (One could imagine a complicated combination of spectra from several independent Fermi gases producing the spectra for Fig. 44; this does not in fact work.) In fact, the concept of the phase shift used in the previous subsection is completely irrelevant here. The utility of the phase shift rests on the assumption that one has outgoing single particle states when incoming electrons scatter off the impurity which certainly holds in the ordinary Kondo model. However, as Ludwig and Affleck [1991] have emphasized, the projection of the full S-matrix on outgoing single particle states is identically zero for the two-channel Kondo model. Once a symmetry breaking field is applied to drive the system to a Fermi liquid fixed point, the phase shift analysis again becomes relevant.

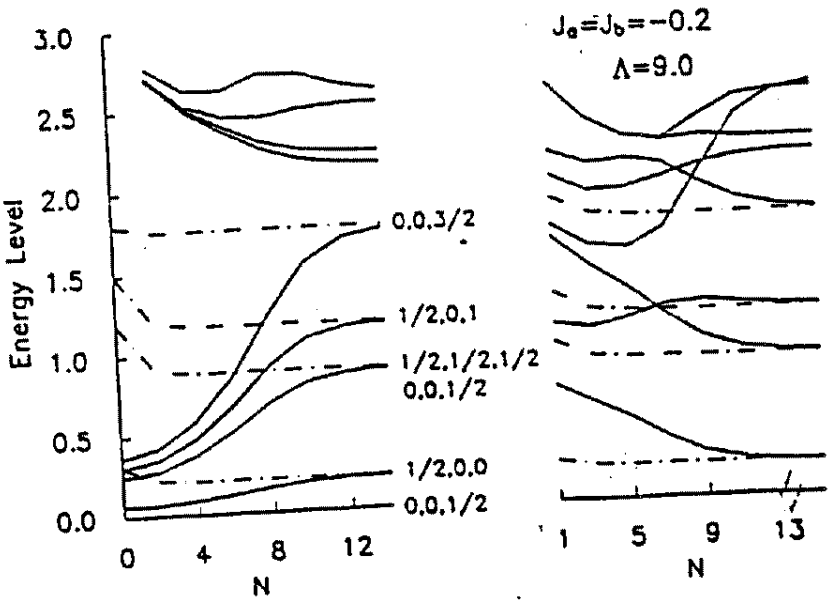

Figure 44: Lowest NRG energy levels for the weak-coupling isotropic two-channel spin 1/2 Kondo model, taken from Pang and Cox [1991]. The coupling strengths for the two-channels were taken equal to -0.2 and the logarithmic discretization parameter Λ was taken to be 9.0 for rapid convergence. There are discernible even-odd alternations for the first few NRG iterations, due to the proximity to the non-interacting fixed point, but the spectrum eventually goes to a single vixed point with increasing iteration number N. For comparison, the dashed line represents the energy levels for the case where the exchange coupling is set to -1.0 in each channel (also for $\Lambda = 9.0$). States are labeles by axial charge or isospin (one for each channel) and spin.

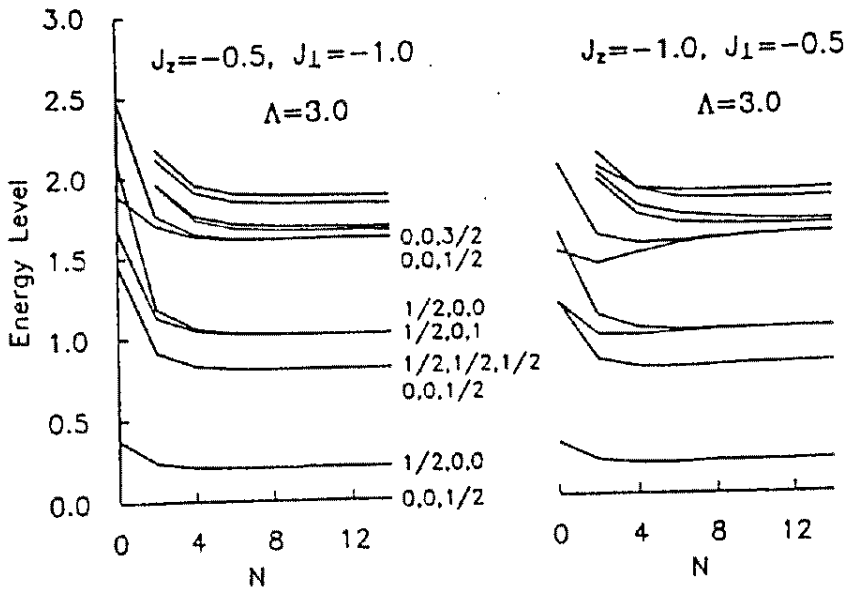

Figure 45: Irrelevance of exchange anisotropy for the two-channel spin 1/2 Kondo model. For both $J_z > J_\perp$ and $J_z < J_\perp$, the energy levels flow to the isotropic fixed point. The states here are labeled by axial charge or isospin for each channel (first two numbers) and total z-projected spin S_z (last number). Taken from Pang and Cox [1991]

The results for the non-trivial fixed point spectra are in quantitative agreement with conformal field theory finite size spectra. We postpone a discussion of that until the conformal field theory section (Sec. 6.1.2).

(c) Stability of non-trivial fixed point against exchange anisotropy.
Fig. 45 shows the NRG spectrum for the weak coupling side of the fixed point with an initial easy axis anisotropy in the exchange, such that $J^3 = 2J^1 = 2J^2$. The last label is now simply $S^{(3)}_{tot}$. The arrows mark the positions of the non-trivial fixed point eigenvalues. We see that the initial anisotropy does indeed relax away as anticipated from our scaling arguments in the previous section.

This irrelevance of exchange anisotropy has also been shown to work in strong coupling and for easy plane anisotropy ($|J^3| < |J^2 = J^1|$).

The NRG approach provides a way to understand this irrelevance of exchange anisotropy for the $M = 2$ case which generalizes to $M > 2$ as well, and we shall explore that picture in the last part of this subsection.

(d) Instability of non-trivial fixed point against application of a Channel Field.
We apply a channel field to the model through the perturbation

$$\mathcal{H}_{ch} = \Lambda^{N/2} - \frac{\Delta J}{D}\vec{S}_I \cdot \sum_{\alpha,\alpha',\mu} \vec{S}_{\alpha,\alpha'\mu} f^\dagger_{0,\alpha,\mu} f_{0,\alpha',\mu} \quad , \tag{4.2.4}$$

where the channel index $\mu = \pm 1$. As discussed in previous subsections, the origin of this symmetry breaking may be a magnetic field along a principal axis or a pure rhombohedral stress for the quadrupolar Kondo effect, and a uniaxial stress along a principal axis for the two-channel magnetic Kondo effect in cubic symmetry.

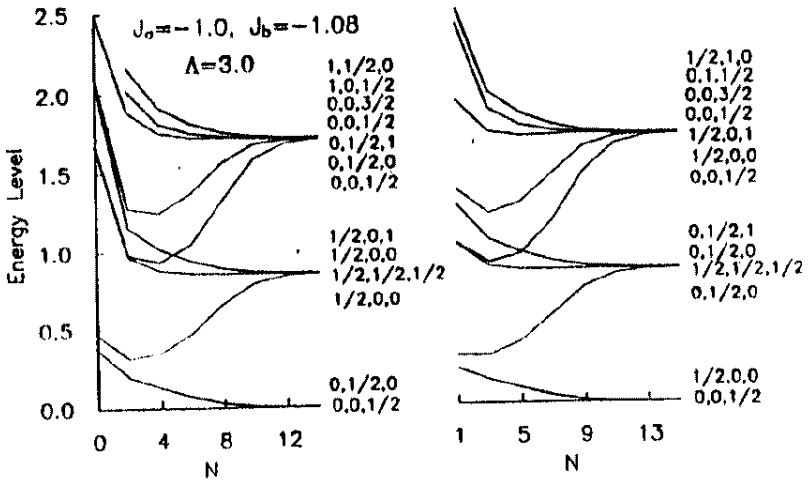

Figure 46: Lowest NRG energy levels for the case of channel anisotropy. Taken from Pang and Cox [1991]. States are labeled by axial charge for each channel (also known as isospin) and by total spin.

We have anticipated in our discussion of the next leading order multiplicative renormalization group equations that the application of channel symmetry breaking will produce a flow away from the non-trivial fixed point. We could not completely trust the scaling analysis in the two-channel case, however, since the fixed point coupling is of order unity. Hence the NRG provides a reliable non-perturbative approach for checking the scaling theory. The expectation of the scaling analysis was that the more strongly coupled channel (e.g., $\mu = +$ if $\delta J, 0$) will provide the ordinary Kondo effect, while the weakly coupled channel will produce a free Fermi gas (no phase shift).

Examination of the spectra in Fig. 46 shows that this expectation is precisely met. We see uniform level spacing characteristic of the Fermi liquid. There is no even-odd alternation, but that is because the fixed point spectra are formed from the vector space for both channels. For definiteness, assume $\Delta J > 0$. Then we expect a $\pi/2$ phase shift at the fixed point for $\mu = +$, so that even N correspond to zero coupling odd N, and vice versa. On the other hand, the μ=- spectra are zero coupling spectra. Hence the combined excitations for both even or odd N are the sum of even N and odd N spectra derived for a single fermi gas.

The NRG allows a determination of the crossover scale. We can define T_{ch} as that temperature where the first excited state shrinks to 1/10 of the splitting at the non-trivial fixed point value under application of the channel field splitting (Eq. (4.2.4)). (Recall that temperature and iteration number are related through Eq. (4.2.1).) By plotting $\Delta J/D$ vs. T_{ch}^x on a log-log plot and measuring the slope we get the crossover exponent. Pang and Cox [1991] found that $\Delta J \sim (T_{ch}^x)^{1/2}$. The third order scaling analysis of the previous section predicted $\delta J \sim (T_{ch}^x)^1$, but the exponent is expected to be correct only to leading order in $1/M$ which is 1/2 here. The exponent of 1/2 agrees exactly with conformal field theory and NCA arguments to be presented in subsequent sections.

Recently, some controversy has arisen over whether the fixed point in the presence of channel symmetry breaking is in fact a Fermi liquid based upon Bethe-Ansatz calculations (Jerez and Andrei, [1995]) and Majorana fermion techniques (Coleman and Schofield, [1995]); a bosonization method yields different results altogether, providing a Fermi liquid fixed point (Fabrizio, Gogolin, and Nozières [1995a,b]). We defer discussion of these issues to Secs. 6 and 7, and 9.2.

(e) Application of a local spin field.

If we apply a local spin field, we will also flow away from the non-trivial fixed point. The perturbation to be added to $\mathcal{H}_N$ is

$$\mathcal{H}_{sp} = -\Lambda^{N/2}\frac{H_{sp}}{D}S_I^{(3)} \quad . \tag{4.2.5}$$

This perturbation corresponds to the level splitting Δ^z in the TLS model, to an applied *local* magnetic field in the two-channel magnetic Kondo model, and to an applied *local* uniaxial stress in the cubic quadrupolar Kondo model, or an applied magnetic field along the c-axis for the tetragonal and hexagonal quadrupolar Kondo models.

For a particular choice of H_{sp} in the strong coupling limit, Fig. 47 shows the NRG flows obtained in the presence of the perturbation in (4.2.5) as obtained by Pang and Cox [1991]. The resulting spectra are rather mysterious and clearly spaced unevenly. However, a consistent analysis of the spectra may be performed by assuming that electrons have only an effective Ising coupling to the impurity so that the phase shifts for scattering are equal and opposite for the different spin values (for a complete test of this hypothesis, see Table VI of Affleck *et al.*, [1992]). The spectra are then the sum of excitations from up and down spin free Fermi gases scattering off a polarized impurity.

The phase shift, which determines the fixed point, may be computed in this manner as a function of magnetic field. This produced the curves in Fig. 19(a), taken from Affleck *et al.* [1992]. It should be noted that:

(i) For small field, the phase shift behaves as

$$|\delta(H_{sp})| = \frac{\pi}{4} - sgn(J-J^*)A\frac{H_{sp}}{T_K}\log(\frac{T_K}{H_{sp}}) \tag{4.2.6}$$

where J^* is the fixed point coupling strength and A is a pure number. The leading order term vanishes for $J = J^*$.

(ii) The value for $H_{sp} = 0^+$ of $|\delta(0^+)| = \pi/4$ may be understood from Friedel sum rule arguments [Pang, 1992]. The generalization from the single channel Kondo case is straightforward; taking $\delta Q = 0$ again demands $\delta_{\uparrow,\mu} = -\delta_{\downarrow,\mu}$, while in the absence of channel symmetry breaking the phase shifts for fixed spin and opposite channel must be equal. Hence the induced spin polarization in an infinitesimal positive field is given by

$$S_{tot}^{(3)} = 0 = \frac{1}{2} + \frac{2}{2\pi}(\delta_{\uparrow,+} - \delta_{\downarrow,+}) \tag{4.2.7}$$

where the 1/2 again reflects the induced $S_I^{(3)}$ value and the phase shift dependent term is due to the conduction electron polarization. This gives the $\pi/4$ phase shift on solution. The special value of $\pi/4$ was also singled out in the path integral approach to the scaling equations [Vladár , Zawadowski , and Zimányi , 1988a,b].

(iii) The phase shift dependence implies a $H_{sp}lnH_{sp}$ behavior to the low field magnetization, in agreement with exact Bethe-Ansatz and conformal field theory results, and a leading order $H_{sp}lnH_{sp}$ saturation to the magnetoresistance proportional to $sgn(J^* - J)$, which is quite different from the ordinary Kondo model which always produces an H_{sp}^2 saturation that is negative, i.e., saturates from below. Note that the phase shift is meaningful when used in the one-channel model and in the two-channel model with symmetry breaking fields, but not at the isotropic two-channel fixed point.

In analogy to the crossover study of the ΔJ perturbation, we may study the crossover exponents for the applied local spin field. Namely, we apply the local field and ask for the temperature T_{sp} (related to iteration number through Eq. (4.2.1)) when a certain set splitting has reached 10% of the splitting at the isotropic fixed point. Affleck *et al.* obtained the crossover behavior $H_{sp} \sim T_{sp}^{1/2}$, which agrees with conformal field theory and NCA results.

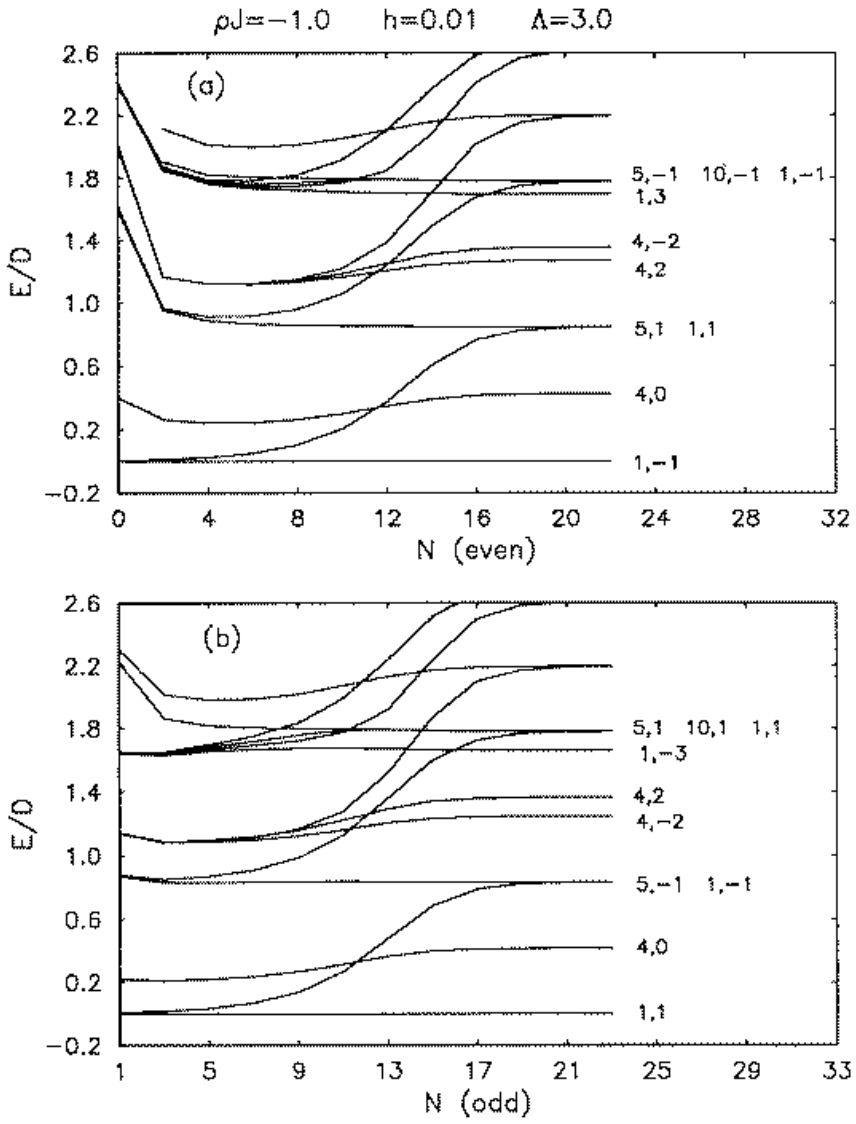

Figure 47: Lowest NRG energy levels in the presence of an applied spin field. From Pang and Cox [1991]. States are labeled by axial charge or isospin for each channel and by total z projected spin.

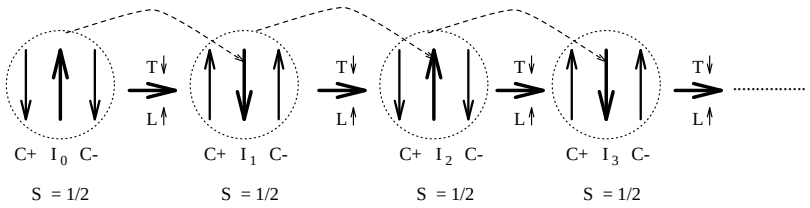

Figure 48: Cartoon visualization of the NRG process for the two-channel Kondo model. At high temperatures and short length scales L, the local moment (I) is weakly aligned antiparallel to the two conduction electron channels ($C\pm$) of spin. However, the binding process of Fig. 3 leads to another doublet which is antiferromagnetically coupled to the two channels of conduction spin outside that length scale. Eventually, this process continues till a fixed point finite coupling strength is attained. Taken from Cox and Jarrell [1996]

We may also apply a bulk magnetic field to the RG Hamiltonians, and provided the field is small compared with the bandwidth similar results are obtained [Pang 1992]. There are some technical issues involved for the NRG method in dealing with the bulk field, for which we direct the reader to the references.

The conformal field theory results for the analysis of these spectra are in excellent agreement with the NRG results, as we shall discuss in Sec. (6.1.2.c).

(f) Shell Model.

One can understand some of the physics shown in the NRG level spectra through a simple shell model. This picture is motivated by Fig. 48. Namely, suppose that we take seriously the idea that the physics at length scale is that of an effective spin-1/2 core object coupled to conduction electron states in the surrounding adjacent shell. We can readily find the energy by writing

$$S_{tot}^2 = S_I^2 + (\vec{S}_{c1} + \vec{S}_{c2})^2 + 2\vec{S}_I \cdot (\vec{S}_{c1} + \vec{S}_{c2})$$

where $S_I = 1/2$ is the effective spin of the impurity, and $S_{c1,2}$ is the spin of each channel. By solving for the dot product in terms of the total spin and the total spin in the conduction sector we can find the energy through

$$E = -\frac{J_{eff}}{2D}[S_{tot}^2 - S_I^2 - S_{cond}^2] \tag{4.2.8}$$

where S_{cond} is the total conduction spin. Clearly, we minimize the shell model energy of Eq. (4.2.8) by making the largest conduction spin S_{cond} for the smallest total spin S_{tot}.

The Shell Model exchange Hamiltonian gives the following results for the lowest few states listed in Table 9. Beyond this, we find detailed discrepancies with the NRG levels and with the conformal field theory finite size spectra, which is not surprising since the excited levels correspond to particle hole excitations which must take us outside the core shell. If we take $|J|/D \approx 0.8$, we get excellent agreement of these results with our first three splittings in Fig. 44 As we shall show, if we take $|J|/D$=0.5, we get perfect agreement with the lowest four states of the conformal field theory finite size spectra. The discrepancy here in the choice of normalization factors is likely a Λ dependent renormalization.

It also turns out that this gives good agreement with the lowest levels of the finite size spectra for conformal theory for three channels and spin 1/2 which is shown in Table 10.

The shell model is useful for understanding the irrelevance of exchange anisotropy which turns out to generalize to the $SU(2) \times SU(M)$ model with $S_I = 1/2, (M-1)/2$, and the relevance of exchange anisotropy for $S_I > 1/2$. To see this, start out with $S_I = 1/2$, M arbitrary. Then after one RG iteration

Q	S_{tot}	S_c	S_I	$E/\|g^*\|$	$\Delta E/\|g^*\|$	CFT
0	1/2	1	1/2	-1	0	0
± 1	0	1/2	1/2	-3/4	1/4	1/8
0	1/2	0	1/2	0	1	1/2
± 2	1/2	0	1/2	0	1	1/2
± 1	1	1/2	1/2	5/4	5/8	5/8

Table 9: Comparison of Shell Model Energies with Conformal Theory for $S_I = 1/2$, $M = 2$. The shell model exchange formula (Eq. (4.2.8)) reproduces the lowest three splittings of the conformal field theory finite size spectrum provided one takes the fixed point coupling $|g^*| = 1/2$, which agrees with the fixed point coupling $\lambda_K = 2/(M+2) = 1/2$ in the notation of Affleck and Ludwig [1991b)]. Energies above these in the table are not reproduced by the shell model.

Q	S_{tot}	S_{cond}	$E/\|g^*\|$	$\Delta E/\|g^*\|$	CFT
0	1/2	3/2	-5/2	0	0
± 1	0	1	-1	1/2	1/5
0	1/2	1/2	-1	3/2	3/5
± 1	1	1	-1	3/2	3/5
± 2	1/2	0	-1	3/2	3/5

Table 10: Comparison of Shell Model Energies with Conformal field theory finite size spectrum for $S_I = 1$, $M = 3$. The shell model exchange formula for the energy (Eq. (4.2.8)) agrees with the the lowest few splittings in the conformal field theory spectrum provided we take the fixed point coupling $|g^*| = 2/5$ which agrees with the non trivial fixed point coupling of the conformal theory $\lambda_K = 2/(M+2) = 2/5$. For higher energy states the shell model disagrees with the exact spectrum.

to the extent the shell model is correct, we will have a ground state with $S_{tot} = M/2 - 1/2$. At the next iteration, application of the shell model to the effective impurity spin equal to $(M-1)/2$ coupled to M electrons gives back an effective spin of $1/2$. Thus we alternate between these two spin values. Now, everytime we are on an iteration where the effective impurity spin is $1/2$, the lowest few states are either total spin zero or total spin $1/2$. Exchange anisotropy cannot lift the degeneracy of these levels. Hence, since these states are used to construct the spectrum for the next iteration, we expect the anisotropy to decay away with increasing iteration number.

On the other hand, consider for example $S_I = 1$, and four channels. In this case, the effective impurity spin will always be $S = 1 = 4/2 - 1$. Exchange anisotropy can generate a "crystal field" like splitting of the $S = 1$ state that will be propagated through the RG iterations. This is seen because the self-energy diagram corresponding to Figs. 26,31 will now have an induced splitting of the $S = 1$ levels through the quadrupolar field of the conduction electrons.

These simple ideas developed from the shell model turn out to be completely supported by conformal field theory, as we shall discuss in Sec. (6.1.2.c).

The shell model also provides the basis for a strong coupling expansion in the inverse exchange coupling, first discussed by Nozières [1974] and Nozières and Blandin [1980]. The idea is that the shell model gives the exact eigenvalues in the limit of infinite exchange coupling. One can then derive a perturbative expansion in powers of t/J where t is the hopping to the next Wilson onion-skin shell. In this way, one can determine that the $J = \infty$ limit is stable for the ordinary Kondo model, and unstable for the multichannel model, which together with the perturbative analysis from weak coupling assures the existence of a non-trivial, intermediate coupling fixed point.

5 Non-Crossing Approximation (NCA)

In this section, we survey some of the most important applications of the Non-Crossing Approximation, or NCA, to the multi-channel Kondo model. We shall first discuss application of the NCA to the $SU(M) \times SU(N_I = N_c = N)$ Anderson model for which the results are rigorous as $N \to \infty$ with $\gamma = M/N$ fixed. Despite the large N character to the theory, the physical properties computed for finite N, M are found to be in good agreement with exact results for most properties. Next, we shall discuss an application to a simple three configuration model for a Ce^{3+} ion which illustrates 1,2, and 3 channel Kondo physics in appropriate regimes. An important physical result which emerges from this analysis is that the sign of the low temperature thermopower is a diagnostic for the emergence of the two-channel ground state as required by the dynamic selection rule 5 of Sec. 2.2.4. Finally, we shall apply the NCA to a model for the U^{4+} ion which includes both ground state and excited state crystal field levels. These results show how the two-channel physics can emerge at low temperatures even with significant overlap between crystal field states due to conduction electron damping.

Since exact results, such as exist for the $SU(N) \otimes SU(M)$ model, are preferrable to approximate ones, the need for the NCA must be clarified. It has two principle virtues: First, it is quite simple to develop and use, and as a result the physical motivation is quite clear. Second, while the Bethe-Ansatz, conformal field theory, NRG, bosonization, and for the most part, Quantum Monte Carlo methods are currently limited to pristine models that lack much of the realistic physics such as crystal field excitations and interconfiguration fluctuations. The NCA is not limited in this way and still appears to give quite reasonable results and in some cases some useful new physics. Moreover, the NCA is able to calculate dynamics (such as the inelastic neutron scattering cross section) and transport properties over a much wider range of paramters and temperature regimes than any of the exact methds, and offers a ready extension to *non-equilibrium* properties which is still rarely possible for the exact methods. Hence, the first sub-section largely serves to calibrate the value of the method by comparing repeatedly to conformal field theory and Bethe-Ansatz results. This section also lays out the formalism and essential concepts of the NCA. The next two subsections are devoted to realistic applications to model Ce^{3+} and U^{4+} impurities. As we shall see, considerable new physics emerges from these applications.

5.1 $SU(M) \otimes SU(N)$ Model: The NCA as a Large N Limit

In this subsection, we shall follow the work of Cox and Ruckenstein [1993]. Following the discussion of Secs. 2.3 and 3.3, we write down an Anderson Model in the pseudo-particle representation as

$$H = \sum_{k\mu\alpha} c^\dagger_{k\mu\alpha} c_{k\mu\alpha} + \epsilon_f \sum_\mu f^\dagger_\mu f_\mu \tag{5.1.1}$$

$$- \frac{\tilde{V}}{\sqrt{NN_s}} \sum_{k\alpha\mu} sgn(\alpha)[f^\dagger_\mu b_{-\alpha} c_{k\mu\alpha} + h.c.] - \lambda_{ps}[\sum_\mu f^\dagger_\mu f_\mu + \mu_\alpha b^\dagger_\alpha b_\alpha - 1]$$

where we have anticipated the large N limit and normalized the hybridization such that $\tilde{V} = \sqrt{N}V$ is well defined in the $N \to \infty$ limit, and λ_{ps} is to be taken to $-\infty$ to project to the physical Hilbert space (c.f. Sec. 3.3.1, Eq. 3.3.3). The indices σ run from $-(N-1)/2, -(N-3)/2, ..., (N-1)/2$, and the indices α from $-(M-1)/2, -(M-3)/2, ..., (M-1)/2$. We have inserted the phase factor $-sgn(\alpha)$ relative to the hybridization term defined in Cox and Ruckenstein [1993], which will not alter the physics of the model. A Schrieffer-Wolff transformation on this model produces the $SU(M) \otimes SU(N)$ Coqblin-Schrieffer model discussed in Sec. 2.3, with exchange coupling $J = \tilde{V}^2/N\epsilon_f$ assuming $\epsilon_f < 0$ and large. We shall pass to $N \to \infty$ by holding the ratio $\gamma = M/N$ fixed.

We remark that a curious feature of the NCA is that it only appears to be useful for models which have the full $SU(N)$ symmetry so that a single boson is required to decouple each channel.

The leading order (order 1) diagrams for the self-energy of the pseudo-fermion and pseudo-boson propagators may be obtained now from the diagrams of Fig. 49. Each diagram is quadratic in

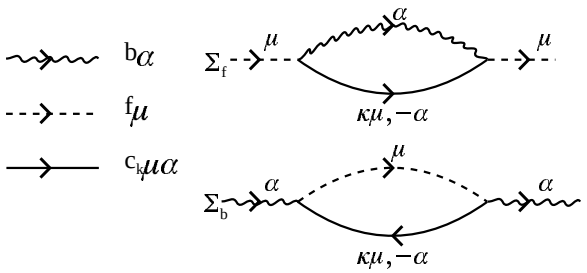

Figure 49: Order $(1/N)^0$ self-energy diagrams of the $SU(N) \times SU(M)$ multichannel Anderson model. The lowest ionic configuration is represented by a pseudo-fermion (dashed) line which carries spin index μ which runs over N values, and the excited ionic configuration by a pseudo-boson (wavy) line carrying channel index α which runs over M values. Conduction electrons carry both spin and channel (solid lines). Vertices represent the hybridization, which is scaled by a factor of $1/N^{.5}$ in this approach. Note that the $N \to \infty$ limit is taken by holding N/M fixed. As a result, the closed spin and channel loops in these diagrams give compensating factors of N, M to the $1/N$ from the vertices, rendering them order $1/N^0$. These self-energies (and the corresponding propagators) are not in themselves physically observable quantities. After Cox and Ruckenstein [1993]

the hybridization. The pseudo-boson self-energy Σ_b contains a sum over internal spin labels, and hence acquires a factor of N which cancels the $1/N$ in the denominator. The pseudo-fermion self energy Σ_f contains a sum over internal channel labels and hence acquires a factor of M which yields a net factor of γ out front when divided by N. Because each self-energy is $O(1)$, a self-consistent solution of the resultant coupled equations is required, since we can insert an infinite series of self-energy corrected propators into each of the diagrams. The leading order vertex corrections are shown in Fig. 5.1.b. These are down by order $1/N^2$ relative to the $O(1)$ diagrams, which is seen by counting vertices (6) giving a net count of $N \times (1/N)^3$ where the N comes from the sum over internal degrees of freedom.

Assuming we have particle-hole symmetry of the conduction band, the resulting $O(1)$ integral equations corresponding to the self-energy diagrams of Fig. 49 are given by

$$\Sigma_f(\omega) = \frac{\gamma\tilde{\Gamma}}{\pi}\int d\epsilon f(\epsilon)\frac{1}{\omega+\epsilon-\Pi_b(\omega+\epsilon)} = \frac{\gamma\tilde{\Gamma}}{\pi}\int d\epsilon f(\epsilon)\mathcal{G}_b(\omega+\epsilon) \tag{5.1.2.a}$$

$$\Sigma_b(\omega) = \frac{\tilde{\Gamma}}{\pi}\int d\epsilon f(\epsilon)\frac{1}{\omega+\epsilon-\epsilon_f-\Sigma_f(\omega+\epsilon)} = \frac{\tilde{\Gamma}}{\pi}\int d\epsilon f(\epsilon)\mathcal{G}_f(\omega+\epsilon) \tag{5.1.2.b}$$

where $\tilde{\Gamma} = \pi N(0)\tilde{V}^2$ and $f(\epsilon)$ is the Fermi-Dirac function. These equations also define the pseudo-boson and pseudo-fermion propagators $\mathcal{G}_b, \mathcal{G}_f$. We note that the conduction electron self-energy is of order $1/N_s$ for this single impurity problem.

These equations are called the "non-crossing approximation" (NCA) because the corresponding diagrams in a particular representation (diagrams on a cylinder) have no crossed conduction lines. See Bickers [1987] for an extended discussion of this diagrammatic approach. We observe that if the pseudo-boson propagator is viewed as a dynamically dressed exchange coupling, as is appropriate for the Coqblin-Schrieffer model, then these equations are none other than a fully self-consistent form of the third order scaling theory as discussed in Sec. (3.4.4). The scaling theory retains only leading logarithms (and thus neglects the imaginary parts of propagators), but the NCA retains the full analyticity of the various propagators. Note that: (i) the projection to $\lambda_{ps} = -\infty$ has taken place and so the superscripts of Eqs. (3.3.4) and (3.3.10) have been dropped; (ii) we are interested for the moment in the physical situation of zero spin and channel fields and so have dropped the spin and channel subscripts on $\mathcal{G}_b, \mathcal{G}_f$.

Alternatively, instead of a diagrammatic approach, one may derive Eqns. (5.1.2.a,b) from a path integral formulation as a saddle point condition. We sketch this derivation here. First, from the action

corresponding to the Hamiltonian of Eq. (5.1.1), the conduction electron fields are integrated out. This produces an effective interaction between the pseudo-boson and pseudo-fermion given by the term

$$S_{int} = -\frac{\tilde{V}^2}{N}\sum_{\sigma\alpha}\int d\tau \int d\tau' f^\dagger_\mu(\tau) f_\mu(\tau') G^0(\tau-\tau') b^\dagger_{-\alpha}(\tau') b_{-\alpha}(\tau) \tag{5.1.3}$$

where

$$G^0(\tau) = -\frac{1}{N_s}\sum_k \frac{1}{\partial/\partial\tau + \epsilon_k} \tag{5.1.4}$$

is the conduction green's function at the impurity site. This interaction term may be decoupled with collective Hubbard-Stratonovich fields$\Phi_b(\tau,\tau')$, $\Phi_f(\tau,\tau')$ which obey $\Phi_{f,b}(\tau',\tau) = \Phi^*_{f,b}(\tau,\tau')$. The resulting effective action term which is quadratic in the Φ fields is

(5.1.5)

$$\tilde{S}_\phi = -\tilde{V}^2 \int d\tau \int d\tau' G^0(\tau-\tau')[N\Phi_f(\tau',\tau)\Phi_b(\tau,\tau') - \sum_\mu f^\dagger)_\mu(\tau)\Phi_b(\tau,\tau')f_\mu(\tau') - \sum_\alpha b^\dagger_\alpha(\tau')\Phi_f(\tau',\tau)b_\alpha(\tau)] \ .$$

This may now be followed by an integration over the f, b fields to produce an effective action solely in terms of the Φ fields. Variation of $\Phi_{f,b}$ to determine the saddle point yields Eqs. (5.1.2.a,b) as the extremum conditions, provided we note that: (i) the Φ fields are time translation invariant at the saddle point, and (ii) $\Phi_{f,b}(\omega)$ are the projected λ_{ps} pseudo-fermion and pseudo-boson propagators in this limit.

The physical properties of the system can be expressed in terms of the spectral functions of the pseudo-particles. Keeping our notation here consistent with that of Cox and Ruckenstein [1993], we define

$$\mathcal{A}_{f,b}(\omega) = \frac{Im\Phi_{f,b}(\omega - i0^+)}{\pi} = \frac{Im\mathcal{G}_{f,b}(\omega - i0^+)}{\pi}. \tag{5.1.6}$$

At $T = 0$, these spectral functions vanish below the ground state energy E_0. We thus define occupied state spectral functions

$$\mathcal{A}^{(-)}_{f,b}(\omega) = e^{\beta(E_0-\omega)}\mathcal{A}_{f,b}(\omega) \ . \tag{5.1.7}$$

Upon multiplication of the exponential factor through Eqns. (5.1.2.a,b), it is seen that these occupied state spectral functions satisfy the self-consistency equations

$$\frac{\mathcal{A}^{(-)}_f(\omega)}{|\mathcal{G}(\omega)|^2} = \frac{\gamma\tilde{\Gamma}}{\pi}\int d\epsilon f(-\epsilon)\mathcal{A}^{(-)}_b(\omega+\epsilon) \tag{5.1.8.a}$$

$$\frac{\mathcal{A}^{(-)}_b(\omega)}{|\mathcal{D}(\omega)|^2} = \frac{\tilde{\Gamma}}{\pi}\int d\epsilon f(-\epsilon)\mathcal{A}^{(-)}_f(\omega+\epsilon) \ . \tag{5.1.8.b}$$

It is important also to keep track of the partition function which enters a calculation of all physical quantities. The total partition function factorizes into a product of the bare conduction band partition function times the pseudo-particle partition function $\mathcal{Z}_f$ given by

$$\mathcal{Z}_f = \int d\omega[N\mathcal{A}^{(-)}_f(\omega) + M\mathcal{A}^{(-)}_b(\omega)] \tag{5.1.9}$$

where we have assumed spin and channel isotropy for the moment.

The reason the partition function enters is due to the projection procedure: one assumes a Grand ensemble in the charge Q_f of Eq. (3.3.6), and then projects to the physical $Q_f = 1$ subspace. Practically, this means we must divide any observable quantity by the $Q_f = 1$ canonical partition

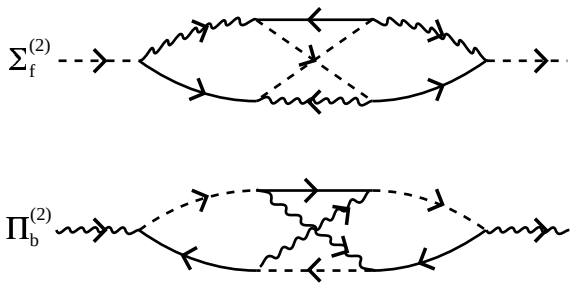

Figure 50: Order $1/N^2$ vertex corrections to self energy diagrams of the $SU(N) \times SU(M)$ Anderson model. Because there is only one closed loop for either spin or channel in each diagram, the presence of six vertices each scaled by $1/N^{1/2}$ leads to an overall suppression of these diagrams by order $1/N^2$ relative to the diagrams of Fig. 49.

function. We shall be interested in three quantities in this subsection, the physical one-particle spectral function $\rho_{\sigma\alpha}(\omega, T)$ which determines the conduction electron t-matrix, the spin susceptibility $\chi_{sp}(\omega, T)$, and the channel susceptibility, $\chi_{ch}(\omega, T)$. The leading order diagrams for these quantities within the NCA are shown in Fig. 50 (vertex corrections are down by $O(1/N^2)$. The diagram for $\rho_{\sigma\alpha}$ is the physical propagator $\mathcal{G}_{\sigma\alpha}$ with $\rho_{\sigma\alpha}(\omega, T) = Im\mathcal{G}_{\sigma\alpha}(\omega - i0^+, T)/\pi$ which measures the density of states for adding and removing electrons of spin σ and channel index α at the impurity site. When these diagrams are evaluated ($\rho(\omega, T)$ is the imaginary part of Fig. 51. divided by π) we obtain the expressions

$$\rho_{\sigma\alpha}(\omega, T) = \frac{1}{\mathcal{Z}_f} \int d\omega' [\mathcal{A}_f^{(-)}(\omega')\mathcal{A}_b(\omega + \omega') + \mathcal{A}_b^{(-)}(\omega')\mathcal{A}_f(\omega' - \omega)] \tag{5.1.10}$$

$$\tilde{\chi}''_{sp}(\omega) = Im\tilde{\chi}_{sp}(\omega - i0^+) = \frac{\pi N}{\mathcal{Z}_f} \int d\omega' [\mathcal{A}_f^{(-)}(\omega')\mathcal{A}_f(\omega + \omega') - \mathcal{A}_f^{(-)}(\omega')\mathcal{A}_f(\omega' - \omega)] \tag{5.1.11}$$

$$\tilde{\chi}''_{ch}(\omega) = Im\chi_{ch}(\omega - i0^+) = \frac{\pi M}{\mathcal{Z}_f} \int d\omega' [\mathcal{A}_b^{(-)}(\omega')\mathcal{A}_b(\omega + \omega') - \mathcal{A}_b^{(-)}(\omega')\mathcal{A}_b(\omega' - \omega)] \quad . \tag{5.1.13}$$

The tilde over the spin and channel susceptibilities signifies a definition wherein we assume a linear coupling of the form $-\mu_{sp}\sigma H_{sp}$ to a spin field and $-\mu_{ch}\alpha H_{ch}$ for the channel field with $\mu_{sp}^2(N^2-1)/12 = \mu_{ch}^2(M^2-1)/12$ set to unity. We shall employ these expressions in the following analysis. Note that the denominators of N and M in the corresponding definitions of Cox and Ruckenstein [1993] should be removed to obtain approximate equality in the RHS of Eq. (6) therein.

5.1.1 Differential Form of the NCA Equations at $T = 0$

As discussed by Kuramoto and Kojima [1984] and Müller-Hartmann [1984], the NCA equations may be converted to differential equations at zero temperature. The procedure is thoroughly discussed there and in the review article of Bickers [1987], and we shall simply outline it here. We note that these analyses were applied to the single channel Kondo model for which the NCA provides a pathological low temperature behavior that is non-Fermi liquid like in contrast to the known Fermi liquid excitation spectrum of the single channel Kondo model. It is amusing that the "pathology" obtained in applying the NCA to the single channel case is exactly what provides excellent results for the multi-channel model!

We assume the conduction electrons occupy a broad flat density of states from $-D$ to D and that this is half-filled. At zero temperature, Eqs. (5.1.2.a,b) may thus be rewritten as

$$\Sigma_f(\omega) = \frac{\gamma\tilde{\Gamma}}{\pi} \int_{-D+\omega}^{\omega} d\omega' \mathcal{G}_b(\omega') \tag{5.1.14.a}$$

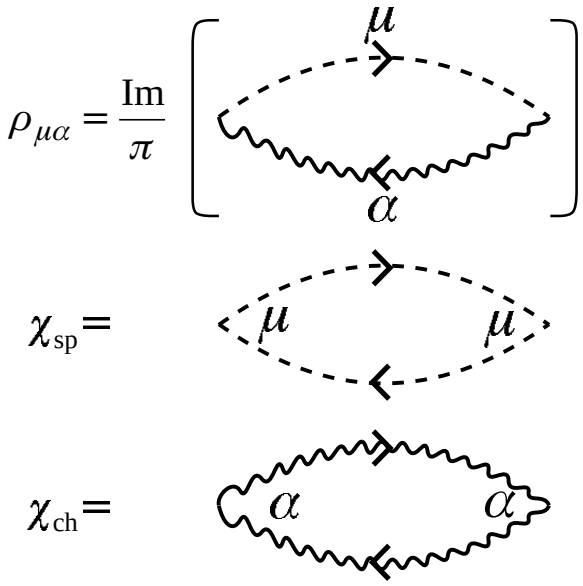

Figure 51: Leading order diagrams for physically measurable quantities in the $N \to \infty$ limit. Physically observable quantities are represented as convolutions of the pseudo-particle propagators. The local spin susceptibility to leading order is a self-convolution of the pseudo-fermion propagator. Likewise, the channel susceptibility is a self-convolution of the pseudo-boson propagator to leading order. The physical f-electron addition/removal propagator is a convolution of the pseudo-fermion and pseudo-boson propagators. Each physical quantity must be properly projected onto the constrained subspace as detailed in the text.

(5.1.14.b) $$\Sigma_b(\omega) = \frac{\tilde{\Gamma}}{\pi} \int_{-D+\omega}^{\omega} d\omega' \mathcal{G}_f(\omega') \quad .$$

Provided the bandwidth $D >> \tilde{\Gamma}$ which sets the scale of Σ_f, Σ_b over most of the frequency range, we may neglect the frequency dependence of the lower integration limit. The integral equations may then be differentiated with respect to ω to produce differential equations. It is most convenient to express these in terms of the inverse green's function variables

(5.1.15) $$g_f(\omega) = -\mathcal{G}_f(\omega)^{-1} \quad , g_b(\omega) = -\mathcal{G}_b(\omega)^{-1}$$

in terms of which the differential equations are

(5.1.16.a) $$\frac{dg_f}{d\omega} = -1 - \frac{\gamma\tilde{\Gamma}}{\pi g_b}$$

(5.1.16.b) $$\frac{dg_b}{d\omega} = -1 - \frac{\tilde{\Gamma}}{\pi g_f}$$

subject to the boundary conditions

(5.1.17) $$g_f(-D) = \epsilon_f + D, \quad g_b(-D) = D$$

which are compatible with the neglect of ω in the lower limit of Eqs. (5.1.14.a,b). We must also employ differential equations for the negative frequency spectral functions; by a similar analysis we obtain

(5.1.18.a) $$\frac{d}{d\omega}[\mathcal{A}_f^{(-)}(\omega) g_f^2(\omega)] = -\frac{\gamma\tilde{\Gamma}}{\pi} \mathcal{A}_b^{(-)}(\omega)$$

(5.1.18.b) $$\frac{d}{d\omega}[\mathcal{A}_b^{(-)}(\omega)g_b^2(\omega)] = -\frac{\tilde{\Gamma}}{\pi}\mathcal{A}_f^{(-)}(\omega)$$

subject to the boundary conditions

(5.1.19) $$[\mathcal{A}_f^{(-)}(E_0)g_f^2(E_0)] = [\mathcal{A}_f^{(-)}(E_0)g_b^2(E_0)] = 0 \quad .$$

To solve Eqs. (5.1.16.a,b), it is first important to note that they possess a constant of integration $\mathcal{C}$ that allows a connection to the Kondo scale. Namely, it is easy to verify by dividing the two equations and integrating that

(5.1.20) $$g_f + \frac{\tilde{\Gamma}}{\pi}\ln((\frac{g_f}{D}) - g_b - \frac{\gamma\tilde{\Gamma}}{\pi}\ln(\frac{g_b}{D}) = \mathcal{C} = \epsilon_f$$

provided we assume $\epsilon_f << D$. The equality on the far RHS of the above equation follows from the boundary conditions of Eq. (5.1.15). This equation may be rewritten in a form more convenient near E_0 as

(5.1.21) $$\frac{g_f/T_0}{(\pi g_b/\tilde{\Gamma})^\gamma} = \exp[\pi(g_b - g_f)/\tilde{\Gamma}]$$

with the Kondo scale T_0 defined by

(5.1.22) $$T_0 = D(\frac{\gamma\tilde{\Gamma}}{\pi D})^\gamma \exp(\pi\epsilon_f/\tilde{\Gamma}) \quad .$$

This agrees with the corresponding scale identified from third order scaling theory to within a factor of order unity (c.f., Eqs. 3.4.27, 3.4.48).

The NCA differential equations may now be solved in a power series expansion in the variable

(5.1.23) $$\Theta = \{[\frac{1+\gamma}{\gamma}]\frac{(E_0-\omega)}{T_0}\}^{\frac{1}{1+\gamma}} \quad .$$

The results are, for $\omega < E_0$,

(5.1.24.a) $$g_f(\omega) \approx T_0\Theta^\gamma + ...$$

(5.1.24.b) $$d_b(\omega) \approx \frac{\tilde{\Gamma}}{\pi}\Theta + ... \quad .$$

These expressions may be analytically continued above E_0 to give the positive frequency spectral functions, and may also be used to obtain the negative frequency spectral functions below E_0. The results for the positive frequency spectra are

(5.1.25.a) $$\mathcal{A}_f(\omega) = \theta(\omega - E_0)\frac{1}{\pi T_0}\sin(\frac{\pi\gamma}{1+\gamma})|\Theta|^{-\gamma} + ...$$

(5.1.25.b) $$\mathcal{A}_b(\omega) = \theta(\omega - E_0)\frac{1}{\tilde{\Gamma}}\sin(\frac{\pi}{1+\gamma})|\Theta| + ...$$

We need a couple of tricks to obtain the negative frequency spectra. First, an *Ansatz* is made that near threshold $\mathcal{A}_f^{(-)} \sim \alpha/g_f$, $\mathcal{A}_b^{(-)} \sim \alpha/g_b$. Because of the identity

(5.1.26) $$\frac{d}{d\omega}[M\mathcal{A}_b^{(-)}(\omega)g_b(\omega) + N\mathcal{A}_f^{(-)}(\omega)g_f(\omega)] = M\mathcal{A}_b^{(-)}(\omega) + N\mathcal{A}_f^{(-)}(\omega)$$

which follows from Eqns. (5.1.16.a,b), (5.1.18.a,b) with a little algebra, we have

$$\mathcal{Z}_f = [M\mathcal{A}_b^{(-)}(E_0)d_b(E_0) + N\mathcal{A}_f^{(-)}(E_0)g_f(E_0)] \quad . \tag{5.1.27}$$

From this it follows that $\alpha = \mathcal{Z}_f/(N+M)$; noting that $\mathcal{Z}_f$ at $T=0$ is none other than the expectation value of $Q_f = 1$, we see that $\alpha = 1/(N+M)$. In consequence,

$$\mathcal{A}_f^{(-)}(\omega) = \theta(E_0-\omega)\frac{1}{(N+M)T_0}\Theta^{-\gamma} + ... \tag{5.1.28.a}$$

$$\mathcal{A}_b^{(-)}(\omega) = \theta(E_0-\omega)\frac{\pi}{(N+M)\tilde{\Gamma}}\Theta + ... \quad . \tag{5.1.28.b}$$

(Note that $\mathcal{Z}_f$ may be normalized to unity by introducing a simultaneous chemical potential for the pseudo-particles prior to projection onto the physical subspace. This fixes the threshold energy of the auxiliary particle spectral functions to E_0=0 and greatly facilitates numerical evaluations [for a detailed discussion, see Appendix D of T.A. Costi *et al.*, 1996]. Note also that the exponents for the spectral functions may be evaluated numerically by application of the NRG, as shown T.A. Costi *et al.* [1994,1996].)

5.1.2 Scaling Dimensions

The scaling dimension of an operator O, denoted Δ_0, for a zero temperature impurity critical point as we have in the multi-channel Kondo model, indicates how the correlation function of the operator decays in the long time limit. Namely, $\mathcal{G}_O(\tau) = -<T_\tau O(\tau)O^\dagger(0)> \sim \tau^{-2\Delta_O}$, $\tau \to \infty$. This implies that the corresponding Green's function in the frequency domain will behave as $\mathcal{G}_O(\omega) \sim |\omega - E_0|^{2\Delta_O - 1}$ as may be readily verified through Fourier transformation. Alternatively, the scaling dimension tells us what scale factor to multiply the operator by under an arbitrary rescaling of time. The scaling dimension concept is particularly useful for connection to the Conformal Field theory work (Sec. 6.1), where the singular properties of various quantities are expressed in terms of the scaling dimensions of operators furnished by the theory.

We may read off the NCA expressions for the scaling dimensions of various operators straightforwardly from a knowledge of the above solutions to the zero temperature differential equations. If we express the frequency dependence of the pseudo-particle spectral functions as $\mathcal{A}_{f,b}(\omega) \sim |E_0 - \omega|^{2\Delta_{f,b}-1}$ we read off the scaling dimensions of the operators f_σ, b_α as

$$\Delta_b = \gamma\Delta_f = \frac{\gamma}{2(1+\gamma)} \quad . \tag{5.1.29}$$

The spin field, channel spin field, and physical fermion field are all quadratic in the f, b operators and so the corresponding scaling dimensions may be readily obtained as

$$(Spin): \quad \Delta_{sp} = 2\Delta_f = \frac{1}{1+\gamma} \tag{5.1.30.a}$$

$$(Channel): \quad \Delta_{ch} = 2\Delta_b = \frac{\gamma}{1+\gamma} \tag{5.1.30.b}$$

$$(Fermion): \quad \Delta_F = \Delta_f + \Delta_b = \frac{1}{2} \quad . \tag{5.1.30.c}$$

The latter result is consistent with unitarity, i.e., the conduction electron scattering rate which is proportional to the spectral function of the physical fermion operator ($\rho_{\sigma\alpha}$) must be bounded by unitarity

limit scattering at the Fermi energy. This implies that the low frequency leading behavior must be a constant, independent of N, M. Clearly, $\Delta_F = 1/2$ yields this result.

The crucial point we may take from the above paragraph is that the scaling dimensions $\Delta_{sp,ch,F}$ are correctly determined by the NCA for all $N \geq 1$ and $M \geq 2$ as may be determined from comparison with the conformal field theory, an exact approach that we discuss in detail in the next section. This is a remarkable result. It is diminished somewhat by the observation that if we take unitarity of the scattering matrix as a given constraint on the scaling dimensions, then the NCA determines really only one independent scaling dimension. As a result, certain operator scaling dimensions will not be correctly obtained by the NCA, a particular case of interest being the local pair field operators. These have an explicit N dependence unlike $\Delta_{sp,ch,F}$. Nevertheless, we shall see that the agreement of the NCA with exact results is remarkably good even in the unlikely region where $N = 2$!

5.1.3 Physical Properties at $T = 0$

We now summarize the results for calculation of physical properties.

One Electron Spectral Function. Substitution into the convolution formula of Eq. (5.1.9) gives

$$\rho_{\sigma\alpha}(\omega) \approx \frac{\pi}{(1+\gamma)^2 N\tilde{\Gamma}}[1 + \theta(\omega) f_+(\tilde{\omega}) + \theta(-\omega) f_-(\tilde{\omega}) + ...] \tag{5.1.31}$$

with $\tilde{\omega} = (1+\gamma)\omega/\gamma T_0$, and

$$f_\pm(\tilde{\omega}) = a_\pm |\tilde{\omega}|^{\Delta_{sp}} + b_\pm |\tilde{\omega}|^{\Delta_{ch}} \tag{5.1.28.a}$$

$$a_- = -\frac{4\gamma}{(2+\gamma)\pi} B(2\Delta_{sp}, \Delta_{ch}) \tag{5.1.28.b}$$

$$a_+ = -cos(\pi\Delta_{ch}) a_- \tag{5.1.28.c}$$

$$b_- = -\frac{4W_{ch}}{(1+2\gamma)\pi} sin(\pi\Delta_{ch}) B(2\Delta_{ch}, \Delta_{sp}) \tag{5.1.28.d}$$

$$b_+ = cos(\pi\Delta_{ch}) b_+ \quad . \tag{5.1.28.e}$$

Here $W_{ch} = \pi T_0/\tilde{\Gamma}$ measures the fluctuation weight of the channel configuration in the ground state, and $B(x, y)$ is the Beta function. In the case $M \geq N$, both the leading and next leading frequency dependence of Eq. (5.1.25.a,b) agree with the results obtained from conformal field theory. This spectral function explicitly breaks particle hole symmetry due to the non-particle hole-symmetric Hamiltonian.

Since the one-particle T-matrix describing scattering of conduction electrons off the impurity in an Anderson Hamiltonian is given by $t(\omega, T) = V^2 \mathcal{G}_{\sigma\alpha}$(Langreth, 1966), using the optical theorem we see that the conduction electron scattering rate is given by

$$\frac{1}{\tau(\omega, T)} = \frac{2\tilde{\Gamma}\rho_{\sigma\alpha}(\omega, T)}{N(0)N} \quad . \tag{5.1.33}$$

The electrical resistivity $\rho(T)$ may be obtained from the scattering rate assuming dominant scattering in the angular momentum channels corresponding to the pseudo-particles and using the standard transport theory formula (see, e.g., Bickers, Cox, Wilkins, 1987)

$$\rho(T) \sim [\int d\epsilon (-\frac{\partial f}{\partial \epsilon}) \tau(\epsilon, T)]^{-1} \quad . \tag{5.1.34}$$

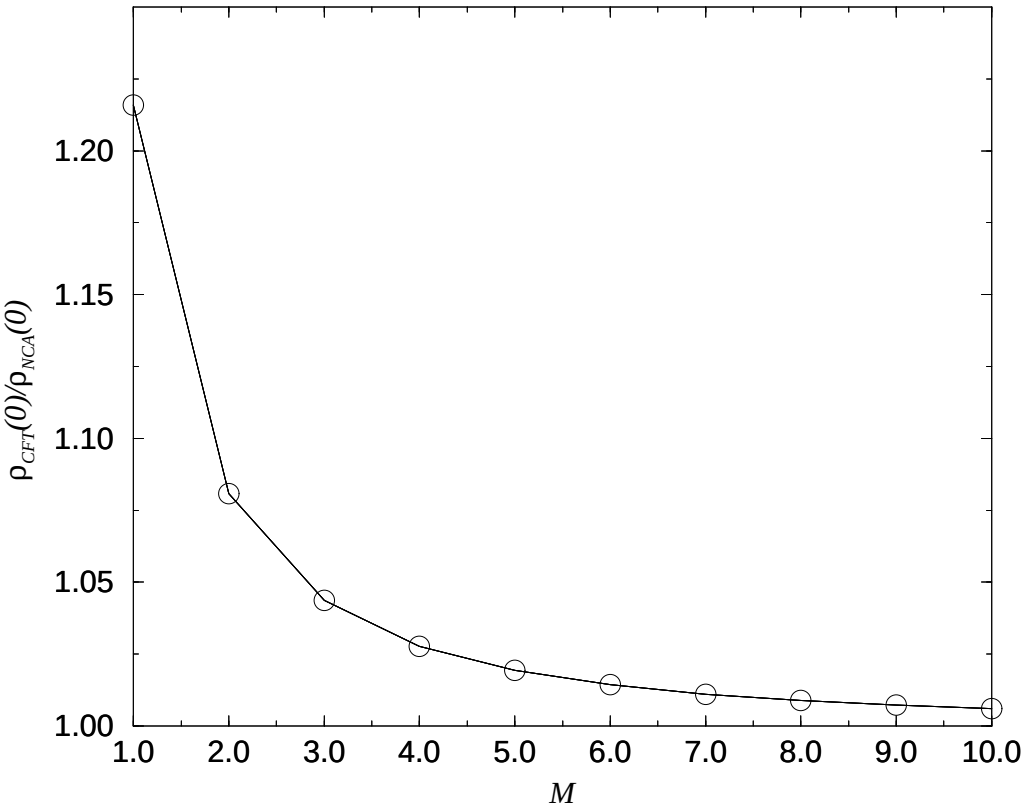

Figure 52: Ratio of NCA to Conformal Field Theory Resistivity vs. M for N=2 multi-channel Model in the Kondo limit. Potential scattering from the NCA has been subtracted. Although the NCA is strictly a large N limit, it clearly does well for $N = 2$ and arbitrary M, with agreement improving as $M \to \infty$.

On dimensional grounds, we can see that the NCA will give

$$\frac{\rho(T)}{\rho(0)} \sim 1 - c(\frac{T}{T_0})^{min(\Delta_{sp},\Delta_{ch})} + ... \tag{5.1.35}$$

where c is a pure number determined from the full temperature dependence of τ which is beyond the scope of the zero temperature NCA. This agrees with the conformal theory, in particular yielding a $\sqrt{T}$ correction for the special case $N = M$ in which $\Delta_{sp} = \Delta_{ch} = 1/2$. The two-channel spin 1/2 model is a special case of this limit ($N = M = 2$). Moreover, for $N = 2$, the zero temperature scattering rate (when corrected for potential scattering present in this model) gives

$$\frac{\pi N(0)}{2\tau(0,0)} = \frac{3\pi^2}{4(2+M)^2} \quad . \tag{5.1.36}$$

As may be seen from Fig. 52, this formula agrees with the exact result from conformal theory to within 8% for all $M \geq 2$. Clearly, it also agrees with Eq. (3.4.44) from the $1/M$ expansion when expanded to the leading order in $1/M$.

We note that because of the built in particle-hole asymmetry of our model Hamiltonian, the thermopower will also display a $\sqrt{T}$ behavior at low temperatures as has been found in the conformal theory.

Local Spin and Channel Susceptibilities The term local here means that the diagrams we keep from Fig. 51 correspond to applied fields coupling linearly only to the impurity spin and channel operators and not the conduction electron spin and channel operators. Using the results of the differential equation solutions together with Eqs. (5.1.10,11), we obtain

$$\tilde{\chi}''_{sp,ch}(\omega) \approx \frac{C_{sp,ch}}{T_0} sgn(\omega) |\tilde{\omega}|^{(\Delta_{sp,ch} - \Delta_{ch,sp})} \tag{5.1.37}$$

with

$$C_{sp} = \gamma \Delta_{sp}^2 \sin(\pi \Delta_{sp}) B(\Delta_{sp}, \Delta_{sp}) \tag{5.1.38.a}$$

$$C_{ch} = W_{ch}^2 \Delta_{ch}^2 \sin(\pi \Delta_{ch}) B(\Delta_{ch}, \Delta_{ch}) \quad . \tag{5.1.38.b}$$

Note that $\Delta_{sp,ch} - \Delta_{ch,sp} = 2\Delta_{sp,ch} - 1$ in view of Eq. (5.1.26.c). The leading behavior of $\tilde{\chi}''_{sp,ch}$ is in full agreement with conformal theory for all N, M. Next leading corrections to Eq. (5.1.36) go as $|\tilde{\omega}|^{(2\Delta_{sp,ch} - \Delta_{ch})}$. In the special case $N = M$ which includes the two-channel model, both susceptibilities reduce to the form $\tilde{\chi}''(\omega) \sim sgn(\omega)[1 - B\sqrt{\frac{|\omega|}{T_0}} + ...]$ which corresponds to a static susceptibility which is logarithmically divergent in temperature. This follows simply with the application of the Hilbert transform to χ''. This leading behavior in χ'', first noted by Cox [1988(a),1990,1994] may provide a link to the marginal Fermi liquid phenomenology [Varma *et al.*, 1989, Kotliar it et al., 1990] developed to understand the unusual normal states of the copper oxide superconductors.

The precise temperature dependence of $\chi_{sp,ch}$ must be determined numerically, but we can roughly estimate this along with relevant zero temperature values through Kramers-Kronig analysis, which implies ($\lambda = sp$ or ch below)

$$\tilde{\chi}_\lambda(T) = \frac{1}{\pi} \int_{-\infty}^{\infty} \frac{\tilde{\chi}''_\lambda(\omega, T)}{\omega} \quad . \tag{5.1.39}$$

We would like to put in the power law form of $\tilde{\chi}''$ from Eq. (5.1.32); this holds to an upper cutoff of order T_0 since the power law behavior only sets in below the Kondo temperature. The lower cutoff must be of order T since finite temperature will round the Fermi functions in the integral equations and hence round all power laws determined from these. With these limits of integration we see that

$$\tilde{\chi}_\lambda(T) \approx \frac{2C_\lambda}{\pi(2\Delta_\lambda - 1)T_0}[1 - (\frac{T}{T_0})^{2\Delta_\lambda - 1}] \quad for\ \Delta_\lambda \neq \frac{1}{2} \tag{5.1.40.a}$$

$$\tilde{\chi}_\lambda(T) \approx \frac{2C_\lambda}{\pi T_0} \ln(\frac{T_0}{T}) \quad for\ \Delta_\lambda = \frac{1}{2} \quad . \tag{5.1.40.b}$$

The above results for the spin and channel susceptibilities allow us to produce a phase diagram in the N, M plane, shown in Fig. 53. For $M > N$, which is the customary over-compensated situation shown by Nozières and Blandin [1980] to lead to a non-trivial fixed point, the spin susceptibility is divergent at $T = 0$, diverging with a power law that follows from Eq. (5.1.40.a). On the other hand, the leading singular behavior of $\chi_{ch}(T)$ vanishes as $T^{(\gamma-1)/(\gamma+1)}$ which implies a finite value to $\chi_{ch}(0) \sim W_{ch}^2/T_0$ as the leading term. In this region, all non-Fermi liquid response is driven dominantly by the spin fluctuations. For $N = M$, of which the two-channel spin 1/2 model $N = M = 2$ is a special case, we see that $\Delta_{sp} = \Delta_{ch} = 1/2$ so that each susceptibility diverges logarithmically. Both spin and channel fluctuations contribute to the non-Fermi liquid behavior at low temperatures, although the

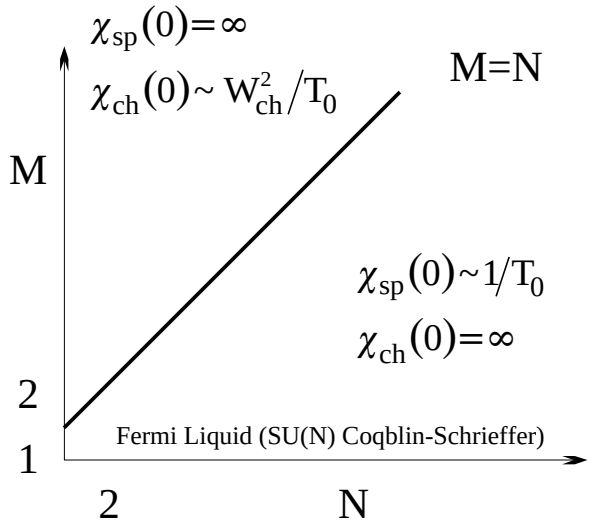

Figure 53: Phase diagram for $SU(N)\times SU(M)$ multichannel Kondo/Anderson Model. For $M > N$, spin fluctuations dominate, and the low temperature spin susceptibility is divergent. The only low energy scale is the Kondo scale. For $1 < M < N$, channel fluctuations dominate, and the low temperature physics has two scales, the Kondo scale and a final energy scale where channel fluctuations dominate. The low temperature channel susceptibility diverges in this case. For $M = N$, both channel and spin susceptibilities diverge logarithmically, and there is only one low energy scale (the Kondo scale). For $M = 1$, a Fermi liquid line results and there is only one low energy scale (the Kondo scale).

dominant effects are due to spin fluctuations due to the much smaller energy scale T_0 to be compared with $\tilde{\Gamma}$. This is reflected in the suppression of χ_{ch} by the factor $W_{ch}^2 \approx T_0^2/\Gamma^2$. For $N > M$, which is still overscreened, we are in a new physical situation, not discussed by Nozières and Blandin. In this case, Eq. (5.1.40.a) implies that $\tilde{\chi}_{ch}(T)$ diverges as $T^{(\gamma-1)/(\gamma+1)}$, while the spin susceptibility is finite at $T = 0$, $\tilde{\chi}_{sp}(0) \sim 1/T_0$. In this regime, the low temperature deviations from Fermi liquid behavior are ultimately driven by the channel spin fluctuations. However, this can only occur to the extent that their strength exceeds that of the spin fluctuations. This implies that a new temperature scale is present in the problem, which we shall call T_{ch}. This may be estimated by seeing where the leading channel driven term in $\rho_{\sigma\alpha}$ equals the leading spin driven term, yielding the energy scale

$$T_{ch} \approx T_0 W_{ch}^{\frac{1}{\Delta_{sp}-\Delta_{ch}}} \approx T_0 (\frac{\pi T_0}{\tilde{\Gamma}})^{\frac{1+\gamma}{1-\gamma}} \quad . \tag{5.1.41}$$

We note that T_{ch} evolves into the "pathology" temperature T_p discussed by Müller-Hartmann [1984] and Bickers [1987; c.f. Eq. (5.53)] when $M = 1$. This corresponds to the $SU(N)$ Anderson and Coqblin-Schrieffer model, designated by the horizontal $M = 1$ axis in Fig. 53. The low temperature physics here is of course Fermi-liquid like and beyond the scope of the NCA. However, as discussed extensively in Bickers, Cox, and Wilkins [1987] and Bickers [1987], the NCA does an excellent job on finite temperature properties provided $T_p << T << T_0$. Clearly the difficulty with applying the NCA in this context is in attempting to extrapolate to the line of zero slope; it does very well in describing the physics on all lines of non-zero slope in the N, M plane. Note that the scale T_{ch} is a real one provided $M > 1$. However, we know of no physical model for which $N > M > 2$ can be realized in practice.

5.1.4 Crossover Effects in Applied Spin and Channel Fields

The application of a spin or channel field will induce a crossover to new physics at low temperatures as discussed in previous sections. Specifically, we anticipate Fermi liquid behavior of two different sorts. For the applied spin field, at zero temperature, the physics becomes that of a Fermi gas interacting

with a polarized scattering center, so that Fermi liquid physics must set in below the crossover scale denoted as T^x_{sp}. For the applied channel field, the couplings to all but the lowest energy pseudo-boson are expected to become irrelevant, and this will lead to the $SU(N)$ Coqblin-Scrieffer model for that coupling with all other channels having zero scattering. The $SU(N)$ model will give a Fermi liquid excitation spectrum with a scale set by the crossover temperature denoted T^x_{ch}. The NCA cannot describe the low temperature physics well below the crossover scale well, since it cannot describe Fermi liquid physics. However, the crossover region will be well described and the NCA produces a correct estimate for the crossover scales $T^x_{sp,ch}$.

To estimate these crossover scales, consider first the case of an applied channel field. With the normalization $\mu_{ch} \sim 1/M$ to obtain a sensible large N, M limit, we see that the overall splitting of channel energies is of order H_{ch}, assumed to be small compared to the channel fluctuation scale $\tilde{\Gamma}$. Each of the pseudo-boson propagators now acquires a channel label α. The NCA differential equations (5.1.16.a,b) are modified to

$$\frac{dg_f}{d\omega} = -1 - \frac{\gamma\tilde{\Gamma}}{M\pi}\sum_{\alpha}\frac{1}{d_\alpha} \tag{5.1.42.a}$$

$$\frac{dg_{b\alpha}}{d\omega} = -1 - \frac{\tilde{\Gamma}}{\pi g_f} \tag{5.1.42.b}$$

with the new boundary conditions for the d_α

$$g_{b\alpha}(-D) = D - \alpha_L\mu_{ch}H_{ch} \quad . \tag{5.1.43}$$

Denote the α index corresponding to the lowest energy b state as α_L. It is easy to see that $dg_{b\alpha}/dd_{\alpha_L} = 1$, so that $g_{b\alpha} = g_{b\alpha_L} + |\alpha - \alpha_L|\mu_{ch}H_{ch}$. Hence, the spread of $g_{b\alpha}$ values is no more than order H_{ch}, given the above remarks. Now, at sufficiently high energies above the crossover scale, the lifting of the channel degeneracy should be irrelevant, meaning that all $g_{b\alpha}$ still go as $\sim \tilde{\Gamma}|(\omega - E_0)/T_0|^{1/(1+\gamma)}/\pi$ in this energy region. The crossover scale is determined by the equation

$$g^{>}_{b\alpha_L}(|\omega - E_0| = T^x_{ch}) = H_{ch} \tag{5.1.44}$$

where the superscript $>$ means we utilize the high energy form for the inverse propagator $g_{b\alpha}$. This gives

$$T^x_{ch} = \frac{\gamma T_0}{(1+\gamma)}\left(\frac{\pi H_{ch}}{\tilde{\Gamma}}\right)^{1+\gamma} \tag{5.1.45}$$

with the crossover exponent $1+\gamma$ in agreement with conformal field theory analysis, as we shall see in the next section. In particular, for the special case $N = M = 2$, we get $T^x_{ch} \sim H^2_{ch}$, which was also found in the NRG and Bethe-Ansatz treatments. We observe that we could also determine the crossover exponent from below, using the NCA forms for the one-channel $SU(N)$ Anderson model and an effective single channel Kondo scale given by the expression

$$T_0(H_{ch}) = D\left(\frac{\tilde{\Gamma}}{\pi D}\right)^{\frac{1}{N}}\prod_{\alpha\neq\alpha_L}\left(\frac{D}{|\alpha - \alpha_L|\mu_{ch}H_{ch}}\right)^{\frac{1}{N}}\exp\left(\frac{\pi\epsilon_f}{\tilde{\Gamma}}\right) \quad . \tag{5.1.46}$$

In this case, $g_{b\alpha_L} \simeq \tilde{\Gamma}|(\omega - E_0)/T_0(H_{ch})|^{N/(N+1)}$, and we would equate this expression to H_{ch} to obtain T^x_{ch}. Now, however, H_{ch} appears on each side of the equation through the functional dependence in $T_0(H_{ch})$. It may readily be verified that as a result we obtain the same estimate for T^x_{ch}.

We may follow a similar procedure for estimating T^x_{sp}. Here we assume H_{sp} to be smaller than the spin fluctuation scale T_0. We equate the high energy form for g_f to the spin field H_{sp} which gives

$$T^x_{sp} = \frac{\gamma T_0}{(1+\gamma)}\left(\frac{H_{sp}}{T_0}\right)^{1+1/\gamma} \quad . \tag{5.1.46}$$

This estimate agrees with NRG, Bethe-Ansatz, and conformal theory for $N = M = 2$, and in any case gives the right dependence on H_{sp} for all N, M.

From a knowledge of the crossover behavior, one can compute the spin magnetization M_{ch} and channel spin magnetization M_{ch}. For $\gamma > 1$, $M_{sp} \sim (H_{sp}/T_0)^{1/\gamma}$ as expected from conformal field theory and the Bethe-Ansatz. For $\gamma < 1$, $M_{ch} \sim (\pi H_{ch}/\tilde{\Gamma})^{\gamma}$ as can be inferred from conformal field theory. For $\gamma = 1$, $M_{sp} \sim (H_{sp}/T_0)\ln(T_0/H_{sp})$ and $M_{ch} \sim (\pi H_{ch}/\tilde{\Gamma})\ln(\tilde{\Gamma}/\pi H_{ch})$, both in agreement with conformal theory (sec 6.1.3.c). The method for computing the magnetization is based on a form for the ground state energy in terms of the inverse green's functions. We refer the reader to Appendix III for details.

5.1.5 Vertex Corrections

The success of the NCA in producing the critical exponents for $\rho_{\sigma\alpha}, \tilde{\chi}_{sp,ch}$ and the crossover exponents correct for all N, M, suggests that the vertex corrections are somehow unimportant in modifying the physics of the problem from these simple diagrams. The lowest order vertex corrections are illustrated in Fig. 50 for the pseudo-particle self-energies, and these are of order $1/N^2$ as argued previously. A little thought indicates the following scenario for the vertex corrections: since the exponents are obtained correctly for all orders in $1/N$ for the quantities considered, the most singular contribution from the vertex corrections cannot modify these exponents. The vertex corrections can, however, correct the *amplitudes* of the leading singular contributions by terms of order $1/N^2$ and higher.

Let us apply this reasoning to the self-energy equations, which, as we have seen, determine all the physics of the above quantitities. This scenario may be checked self-consistently by assuming the pseudo-particle propagators retain the same critical behavior at threshold E_0 as in the order 1 solutions. Explicit evaluation of the pseudo-fermion self-energy of Fig. 49 then shows that the dominant low energy contribution vanishes again as $|\omega - E_0|^{\gamma/(1+\gamma)}$. A detailed analysis is deferred to Appendix III.

With power counting arguments, we can see that this result is more general. Consider a generic contribution to Σ_f which has L loops and independent energy integrations, and hence contains L pseudo-boson propagators and $L-1$ pseudo-fermion propagators. By converting each energy integration to dimensionless form, we can read off the power law dependence on $\omega - E_0$. Each boson propagator diverges as $|\omega - E_0|^{2\Delta_b - 1}$, each fermion propagator as $|\omega - E_0|^{2\Delta_f - 1}$. From de-dimensionalizing the integrations we obtain L factors of $\omega - E_0$ from the differentials, L powers of $\omega - E_0$ from the boson propagators, and $L-1$ powers of $\omega - E_0$ from the fermion propagators. The net power is then $L + L(2\Delta_b - 1) + (L-1)(2\Delta_f - 1) = 2L(\Delta_b + \Delta_f) - 2\Delta_f - L + 1$ which, since $\Delta_f + \Delta_b = 1/2$, is just $1 - 2\Delta_f$. But this is precisely the leading order power of the self-energy, so we have self-consistently demonstrated the scenario.

This is analogous to result for the quasiparticle lifetime in a Fermi liquid– the correct $\omega^2 + \pi^2 T^2$ behavior can be found in a diagram second order in the interaction strength. Higher order diagrams may readjust the strength of the effective interaction– the amplitude of the leading order power–but will not modify the form of the lifetime, that is, the leading order power itself. As in Fermi liquid theory, where the renormalized interaction is of the order of the bandwidth and so no strict perturbation theory is applicable, we find ourselves in a situation here where the regime of strict validity of the theory (large N only) appears far smaller than its regime of applicability.

The observations of the last two paragraphs led Cox and Ruckenstein [1993] to speculate that in systems with non-Fermi liquid ground states which typically show some form of spin-charge separation, extended to spin-channel spin separation here, some form of self-consistent perturbation theory can capture the essential physics even when no obvious small parameters are available, barring some kind of phase transition which binds spin and charge (or spin and channel spin here).

In fact, there is evidence that just such a phase transition occurs in the Kondo problem between the overcompensated regime for which the NCA is obviously well suited to the single channel Fermi liquid line of Fig. 53. The work of Kroha *et al.* [1992,1996], together with that of Anders and Grewe [1994] and Anders [1995a,1995b] moves beyond the NCA to work on the single channel model. The work of Anders and Grewe [1994] and Anders [1995a,1995b] demonstrates that a tendency to restore Fermi liquid properties is indeed produced by a self-consistent inclusion of vertex corrections through order

$1/N^2$. Kroha *et al.* [1992,1996] demonstrate that the vertex corrections display a tendency towards bound state formation between the conduction electron and the pseudo-fermion state, closely related to the spin-screened Fermi liquid state. In particular, in a saddle point evaluation of the conduction electron-pseudo-fermion two-particle T-matrix, a pole is obtained on resumming an infinite number of repeated particle-particle interactions between the electrons and pseudo-fermions. However, due to fluctuations beyond this saddle point approximation, a true bound state is not in fact realized. Instead, the pole contribution serves to renormalize the threshold exponents of the pseudo-particle propagators from the NCA values of $\alpha_f = 1/(N+1) = 1 - \alpha_b$ to exact values which have been deduced both from a combined Bethe-Ansatz/Conformal Field Theory approach [Fujimoto *et al.*, 1996] and an analytic argument [Menge and Müller-Hartmann, 1988]. These exponents are dependent upon the occupancy of the pseudo-fermion level, in contrast to the NCA values, and are indeed characteristic of a Fermi-liquid ground state. Thus, the Fermi liquid ground state appears to be reinstated by an appropriate recombination of spin and charge degrees of freedom induced by complicated interactions between fermionic and bosonic degrees of freedom.

5.1.6 Properties at Finite Temperature

The NCA is not limited, of course, to zero temperature where the differential equation approach is applicable. The integral equations may be self-consistently solved at finite temperature and the properties calculated. In this subsection, we wish to point out that the comparison is astonishingly good of magnetic susceptibility, specfic heat, and entropy curves with exact calculations from the Bethe-Ansatz. In particular, the discrepancy for the susceptibility is barely visible, while a discrepancy with the $T = 0$ entropy at the several percent level is seen, but expected given the large N character of the analysis. The calculations are based on the Ce^{3+} model to be discussed in the next subsection, which has parameter regimes described by the two and three-channel spin 1/2 model.

In Fig. 54, we show results taken from Kim and Cox [1995,1997] for various parameter sets in the two-channel Kondo regime of the simplified model. What is apparent is that all the computed NCA $\chi(T)$ curves agree almost perfectly with the exact Bethe-Ansatz results of Sacramento and Schlottmann [1991]. Also shown in Fig. 54 is shown the corresponding calculation for the 3-channel regime. The agreement is clearly excellent. It needs to be mentioned that this is actually a two-parameter comparison; T_0 is adjusted to T_K from Sacramento and Schlottmann by sliding along the logarithmic temperature axis. A mild scale factor adjustment is also required to bring the vertical axis into alignment. Kim and Cox [1995,1997] argue that this scale factor is related to the crossover effects in the Ce^{3+} model they study.

Attempts to compute the specific heat have also proven successful. The only method developed to compute the specific heat from the NCA consists of numerical differentiation of $\mathcal{Z}_f$ (Bickers, Cox, and Wilkins [1987]). This works well for sufficiently large specific heat signal, but in the multichannel models, the residual entropy robs the finite temperature specific heat of considerable integrated intensity. As a result, it is essential to have high numerical precision to obtain the specific heat and entropy results. A recent numerical advance in the NCA codes by Kim [1995] allowed reliable computation of entropy and specific heat. The entropy curves for $N = 2$ and $M = 1, 2, 3$ are displayed in Fig. 55 [Kim and Cox, 1995,1997]. The $M = 1$ curve shows the expected extrappolation to $S = 0$ as $T \to 0$, although the NCA curve is not to be trusted in the low temperature region for this Fermi liquid case. The $M = 2, 3$ curves show temperature dependences in excellent agreement with Bethe-Ansatz. The residual entropies are within 10-15% of the expected values for $M = 2, 3$. We don't expect exact agreement of the residual entropy given the explicit N dependence found in Bethe-Ansatz [Tsevlik, 1985; Sacramento and Schlottman, 1991] and conformal theory treatments [Affleck and Ludwig, 1991c]. However, the overall agreement is clearly exceptional for this simple theory.

The specific heat curves for $N = 2$ and $M = 1, 2, 3$ are shown in Fig. 56 [Kim and Cox, 1995,1997]. Clearly, the $M = 1$ curve is in excellent agreement with the exact results. The slight underestimate of the magnitude for $M = 2, 3$ is understandable from the slight overestimate of the

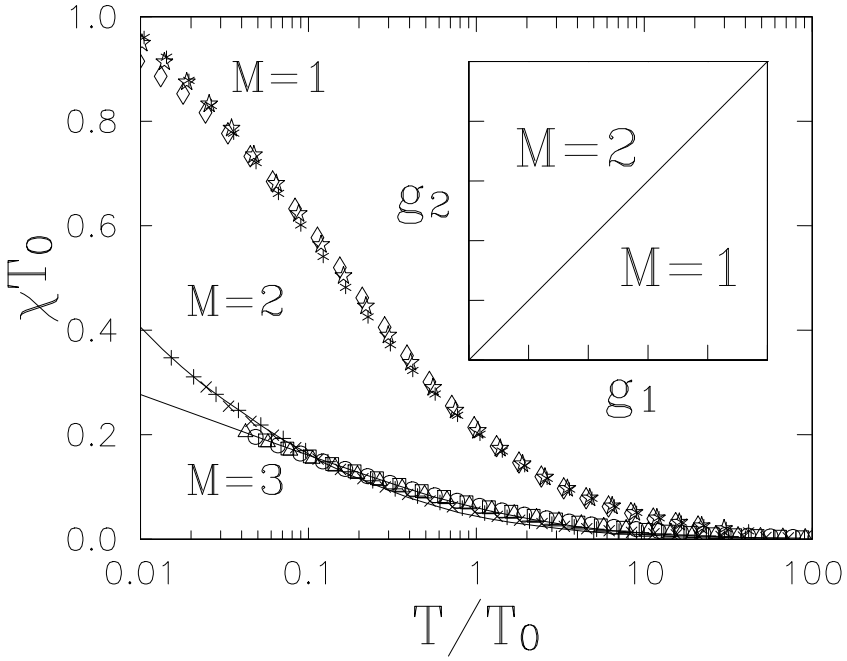

Figure 54: Spin susceptibility for $SU(2) \times SU(M)$ multichannel Anderson models in the Kondo regime obtained from the NCA. Of particular note here is the excellent agreement between the exact Bethe-Ansatz results for $M = 2, 3$ and the NCA results. From Kim and Cox [1997].

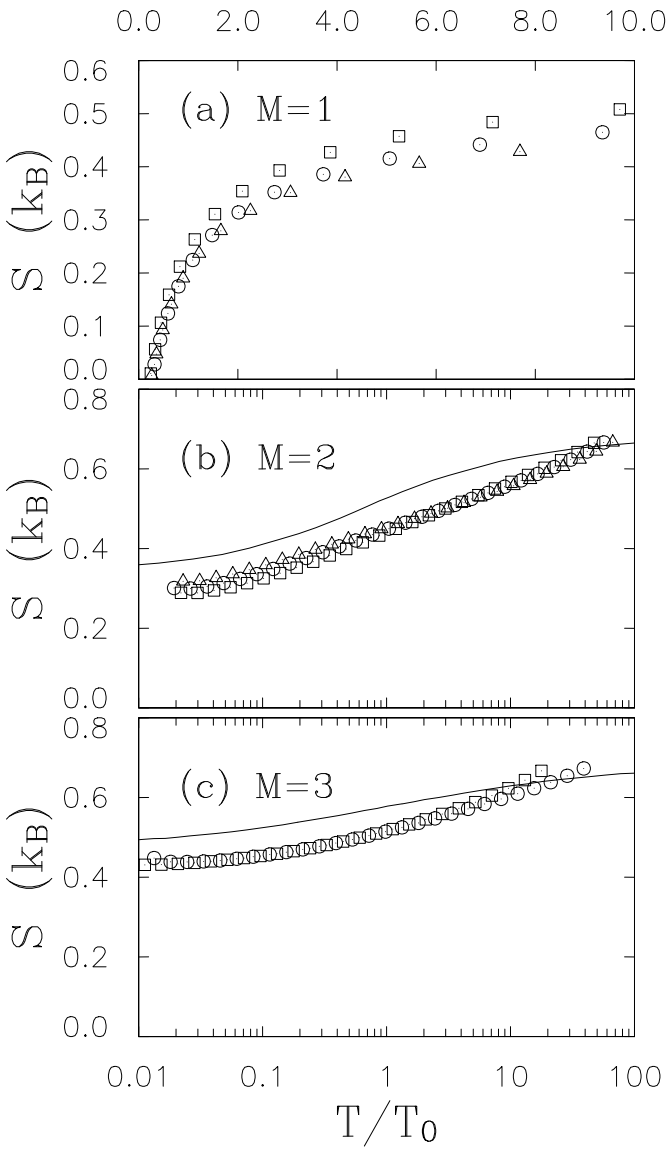

Figure 55: Numerically calculated entropy curves from the NCA for the $SU(2) \times SU(M)$ Anderson models in the Kondo regime. The $M = 1$ curve shows the clear (and expected) tendency towards $S(0) = 0$ as expected for the single channel model. The $M = 2, 3$ curves agree well with exact Bethe-Ansatz results (solid lines) and clearly display a tendency towards a finite residual entropy. Agreement for $S(0)$ is evidently at the 10-15% level. From Kim and Cox [1997].

residual entropy evident in Fig. 55, since the net high temperature entropy must be $R \ln 2$.

5.1.7 Alternative Large N formulation

Recently Parcollet and Georges [1997] have developed an alternative large N approach to the multi-channel model which represents the spins in terms of constrained Schwinger boson fields. This theory is able to treat overcompensated, undercompensated, and compensated cases exactly, and is expressed in terms of saddle point equations which are strongly reminiscent of the non-crossing approximation. The physical properties computed within this approach agree well with other methods, and in contrast to the NCA, an analytic formula for the zero temperature entropy is obtained for the over- and undercompensated models. The method would appear to hold considerable promise for a lattice generalization.

5.2 Application of the NCA to a model Ce^{3+} impurity

This subsection reviews the work of Cox [1993], Kim [1995], and Kim and Cox [1995,1997] in studying a model Ce^{3+} impurity which encompasses the possibilities of one, two, and three-channel spin 1/2 Kondo effects. The model is intended to be a simplified version of a more complete model for Ce in $LaCu_{2.2}Si_2$.

5.2.1 Pseudo-Particle Hamiltonian and NCA equations

The assumed level spectrum of the Ce^{3+} ion is shown in Fig. 57. The Hamiltonian is then given by Eqs. (2.2.25,26). We wish to rewrite this Hamiltonian in pseudo-particle form. We represent the f^1 doublet by a pair of pseudo-fermion operators $f_{7\mu}$, and the f^0, f^2 states by pseudo-bosons $b_1, b_{3\alpha}$ respectively. To enlarge the Hilbert space from the two-configuration model, the f-charge Q_f of Eq. (3.3.6) is modified to

$$Q_f = \sum_\alpha b^\dagger_{3\alpha} b_{3\alpha} + \sum_\mu f^\dagger_{7\mu} f_{7\mu} + b^\dagger_1 b_1 \tag{5.2.1}$$

The resulting pseudo-particle Hamiltonian is

$$\begin{aligned} H = & \sum_{k\Gamma_c\alpha_c} \epsilon_k c^\dagger_{k\Gamma_c\alpha_c} c_{k\Gamma_c\alpha_c} + \epsilon_1 \sum_\mu f^\dagger_{7\mu} f_{7\mu} \\ & + \epsilon_2 \sum_\alpha b^\dagger_{3\alpha} b_{3\alpha} + \frac{V_{17}}{\sqrt{N_s}} \sum_\mu [f^\dagger_{7\mu} b_1 c_{7\mu} + h.c.] \\ & - \frac{V_{37}}{\sqrt{N_s}} \sum_{\alpha\mu} sgn(\mu) [b^\dagger_{3\alpha} f_{7,-\mu} c_{k8\alpha\mu} + h.c.] - \lambda_{ps}(Q_f - 1) \quad . \end{aligned} \tag{5.2.2}$$

We denote the hybridization width corresponding to $V_{17}(V_{37})$ by $\Gamma_{17} = \pi N(0) V^2_{17} (\Gamma_{37} = \pi N(0) V^2_{37})$. Here $\epsilon_1 = \epsilon_f$ and $\epsilon_2 = \tilde{\epsilon}_f + \epsilon_f = 2\epsilon_f + U_{ff}$ where U_{ff} is the Coulomb repulsion.

As discussed in Sec. 2.2.2, for $\Gamma_{37}/\pi|\tilde{\epsilon}_f| < \Gamma_{17}/\pi|\epsilon_f|$, we anticipate a one channel Kondo effect. The NCA will correctly describe the approach to a Fermi liquid fixed point here, though not the actual fixed point. However, the scaling dimensions in this instance will be uniquely specified by the NCA and serve as a measure of the universality class within the method. For $\Gamma_{37}/\pi|\tilde{\epsilon}_f| > \Gamma_{17}/\pi|\epsilon_f|$, we anticipate a two-channel Kondo effect to describe the low temperature physics. This will be obtained essentially correctly through the NCA. For $\Gamma_{37}/\pi|\tilde{\epsilon}_f| = \Gamma_{17}/\pi|\epsilon_f|$, we anticipate the three-channel Kondo effect to regulate the low temperature physics, which again is obtained essentially correctly through the NCA. The above conditions on the dimensionless Schrieffer- Wolff coupling constants will be slightly modified in the full NCA analysis, but the essential physics is unchanged.

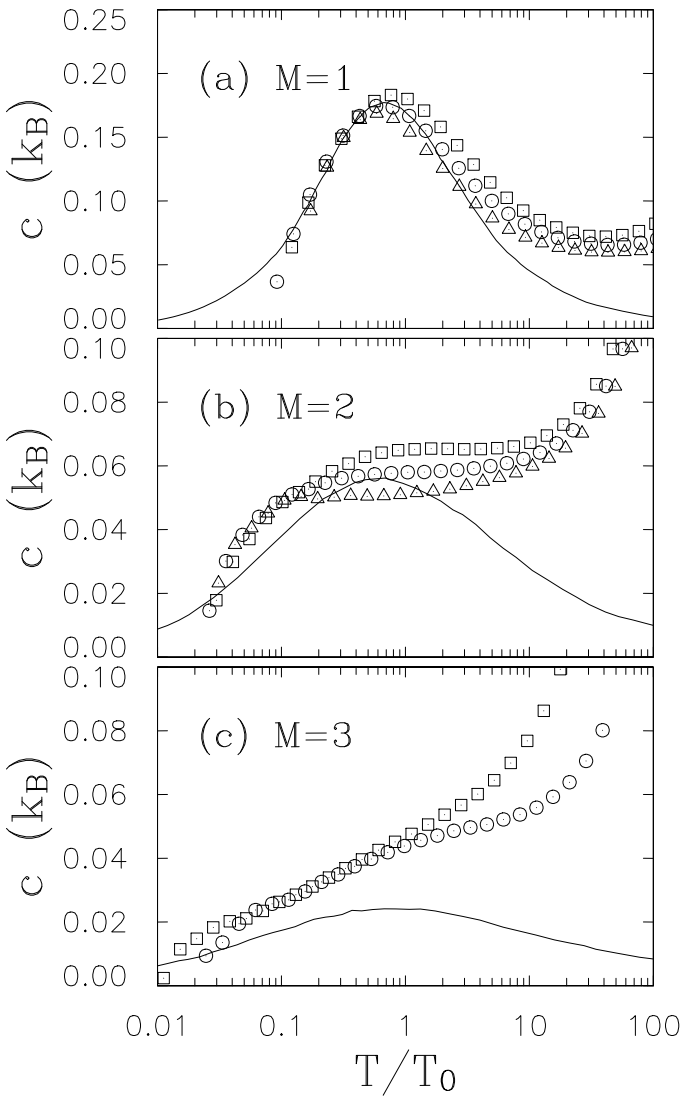

Figure 56: Specific heat for $SU(2) \times SU(M)$ Anderson models in the Kondo limit with $M = 1, 2, 3$ as calculated from the NCA. Points are from the NCA, lines are from exact Bethe-Ansatz results. The high temperature enhancements are due to the presence of the excited configurations in the model, which are not present in the Bethe-Ansatz model. From Kim and Cox [1997].

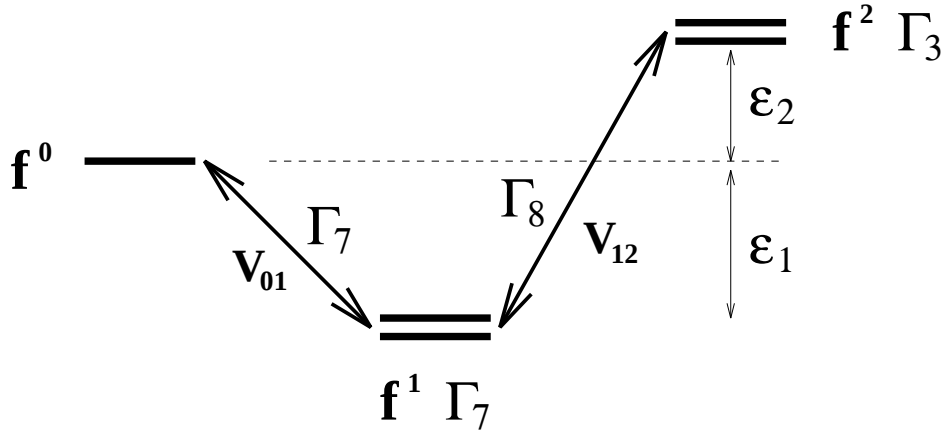

Figure 57: Energy levels of the f^0, f^1, f^2 states for the simplest Ce^{3+} ion Anderson model. Only a magnetic doublet is kept in the f^1 configuration, and only a non-Kramers' doublet is kept in the f^2 configuration. Taken from Kim and Cox [1997].

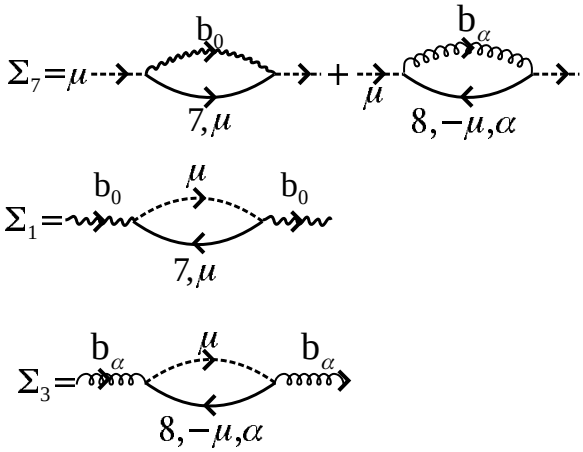

Figure 58: Pseudo-particle self energy diagrams for the simple Ce^{3+} ion Anderson model. Dashed lines are for the f^1 pseudo-fermion propagator which carries spin (magnetic) index μ. Wavy lines are for the f^0 pseudo-boson propagator. Curly lines are for the f^2 pseudo-boson propagator which carries channel (orbital) index α. Solid lines are for conduction electrons which may carry only spin (Γ_7, denoted by 7), or both spin and channel (Γ_8, denoted by 8). See Kim and Cox [1995,1997].

Fig. 58 illustrates the self-energy diagrams retained in the NCA. The resulting self energies are denoted Σ_7 for the f^1 doublet, Π_1 for the f^0 singlet, and Π_3 for the f^2 doublet. The corresponding propagators are

$$\mathcal{G}_7(\omega) = \frac{1}{\omega - \epsilon_f - \Sigma_7(\omega)} \tag{5.2.3}$$

$$\mathcal{G}_1(\omega) = \frac{1}{\omega - \Sigma_1(\omega)} \tag{5.2.4}$$

and

$$\mathcal{G}_3(\omega) = \frac{1}{\omega - \epsilon_2 - \Sigma_3(\omega)} \quad . \tag{5.2.5}$$

Assuming, for convenience, particle-hole symmetry to the conduction band, the integral equations of the NCA are

$$\Sigma_7(\omega) = \frac{\Gamma_{17}}{\pi} \int d\epsilon f(\epsilon) \mathcal{G}_1(\omega + \epsilon) \frac{2\Gamma_{37}}{\pi} \int d\epsilon f(\epsilon) \mathcal{G}_3(\omega + \epsilon) \tag{5.2.6.a}$$

$$\Sigma_1(\omega) = \frac{2\Gamma_{17}}{\pi} \int d\epsilon f(\epsilon) \mathcal{G}_7(\omega + \epsilon) \tag{5.2.6.b}$$

$$\Sigma_3(\omega) = \frac{2\Gamma_{37}}{\pi} \int d\epsilon f(\epsilon) \mathcal{G}_7(\omega + \epsilon) \quad . \tag{5.2.6.c}$$

Notice that $\Sigma_3 = (\Gamma_{37}/\Gamma_{17})\Sigma_1$.

This model has a special feature relative to other three configuration models studied previously with the NCA, such as the s-wave spin 1/2 Anderson Hamiltonian [Pruschke 1990,1992]. In the latter case, there is a vertex correction which in effect mixes the s^0, s^2 configurations. The origin of the simplification for this model is not mysterious when viewed from the standpoint of the Schrieffer-Wolff transformation: the s^0, s^2 states in the s-wave model each transform as fully symmetric representations and so contribute terms of the same form in the effective exchange Hamiltonian. Hence, there can be only one Kondo scale associated with the two excited configurations. The vertex corrections used by Pruschke have a direct corresondence to the scaling theory diagrams which couple the s^0-driven exchange to the s^2-driven exchange. In this model for a Ce^{3+} ion, however, the Schrieffer-Wolff exchange interactions induced by virtual f^0 and f^2 fluctuations have entirely different form and couple to different symmetry conduction partial wave states. Hence, there can be no such cross-couplings of effective exchange interactions in low order scaling theory, and no vertex corrections within the NCA analysis.

5.2.2 NCA Differential Equations

Following the same procedure of Sec. 5.1.1, and defining the inverse propagators $g_7 = -\mathcal{G}_7^{-1}$, $g_1 = -\mathcal{G}_1^{-1}$, and $g_3 = -\mathcal{G}_3^{-1}$ we obtain the following differential equations for the $T = 0$ NCA:

$$\frac{dg_7}{d\omega} = -1 - \frac{\Gamma_{17}}{\pi g_1} - \frac{2\Gamma_{37}}{\pi g_3} \tag{5.2.7.a}$$

$$\frac{dg_1}{d\omega} = -1 - \frac{2\Gamma_{17}}{\pi g_7} \tag{5.2.7.b}$$

(5.2.7.c)
$$\frac{dg_3}{d\omega} = -1 - \frac{2\Gamma_{37}}{\pi g_7}$$

subject to the boundary conditions

(5.2.8)
$$g_7(-D) = D + \epsilon_f, \quad g_1(-D) = D, \quad g_3(-D) = D + \epsilon_2 \quad .$$

These equations are clearly more complex than for the $SU(N) \otimes SU(M)$ model of the previous subsection. Indeed, if $\Gamma_{17} \neq \Gamma_{37}$, a complete low frequency analytic solution cannot be obtained, as we shall discuss below. The reason is that there is no integration constant corresponding to $\tilde{C}$ of Eq. (5.1.7) which connects low and high energy regimes. This does not prevent the derivation of some analytic results, nor does it prohibit a full numerical solution of the NCA equations.

5.2.3 Solution in the Special Case $\Gamma_{17} = \Gamma_{37}$

The special case $\Gamma_{17} = \Gamma_{37} = \Gamma$ is fully soluble in the spirit of the previous subsection, and provides considerable insight to the physics of the model (Kim [1994]). Accordingly, we shall devote most of our attention to this case. We can see immediately that the equality of Σ_3 and Σ_1 implies that $dg_3/dg_1 = 1$, so that $g_3 = g_1 + const.$. From Eq. (5.2.8), the integration constant is seen to be ϵ_2. We consider three separate cases, for $\epsilon_2 = 0, \epsilon_2 > 0$, and $\epsilon_2 < 0$.

(i) ϵ_2=0. In this case we anticipate the physics to be that of the three channel model. Clearly, the NCA differential equations imply $g_1 = g_3$. Substituting into Eqs. (5.2.7.a,b) we find the integration constant

(5.2.9)
$$\tilde{C} = \exp(\frac{\pi}{2\Gamma}[g_7 - g_1])(\frac{g_7}{D})^2(\frac{D}{g_1})^3 \quad .$$

Following the previous analysis for the $SU(N) \otimes SU(M)$ model, we evaluate this expression at $-D$ to obtain $\tilde{C} = \exp(\pi\epsilon_f/2\Gamma)$. This implies that at low energies approaching the threshold E_0,

(5.2.10)
$$1 \approx \frac{[g_7/T_0^{(3)}]^2}{[\pi g_1/\Gamma]^3}$$

with $T_0^{(3)}$ being the NCA estimate for the three-channel Kondo temperature

(5.2.11)
$$T_0^{(3)} = D(\frac{\Gamma}{\pi D})^{3/2} \exp(\frac{\pi\epsilon_f}{2\Gamma}) \quad .$$

Comparison with the previous section or direct substitution into Eqs. (5.2.7.a,b) confirms that the low temperature behavior is precisely that of the $N = 2, M = 3$ model. This means that $g_7 \sim T_0|\omega - E_0|^{3/5}$ and $g_1, g_3 \sim \Gamma|\omega - E_0|^{2/5}$ for $\omega \to E_0$.

(ii) $\epsilon_2 > 0$. We expect the low temperature physics here to be the same as in the three channel case. Now we eliminate g_3 in favor of g_1. Substituting into Eqs. (5.2.7.a,b) we find the integration constant $\tilde{C}$ given by

(5.2.12)
$$\tilde{C} = \exp(\frac{\pi}{2\Gamma}[g_7 - g_1])(\frac{g_7}{D})^2\frac{D^3}{g_1(g_1 + \epsilon_2)^2} \quad .$$

Following the previous analysis for the $SU(N) \otimes SU(M)$ model, we evaluate this at $-D$ to obtain $\tilde{C} = \exp(\pi\epsilon_f/2\Gamma)$. This implies that at sufficiently low energies when $g_1 << \epsilon_2$ as $\omega - E_0 \to 0$, we have the relation

(5.2.13)
$$1 \approx \frac{[g_7/T_0^{(1)}]^2}{\pi g_1/\Gamma}$$

where the Kondo scale $T_0^{(1)}$ is given by

$$T_0^{(1)} = D(\frac{\epsilon_2}{D})(\frac{\Gamma}{\pi D})^{1/2}\exp(\frac{\pi\epsilon_f}{2\Gamma}) \quad . \tag{5.2.14}$$

The low frequency relation of Eq. (5.2.10) implies asymptotically that $g_7 \sim |\omega - E_0|^{1/3}$ and $d_1 \sim |\omega - E_0|^{2/3}$. These are precisely the asymptotic forms expected for the single channel spin 1/2 model (see Müller-Hartmann [1984] and Bickers [1987]). The superscript (1) in the Kondo scale refers to the single channel character. T his implies further that $\mathcal{G}_7$ diverges as $|\omega - E_0|^{-1/3}$, and $\mathcal{G}_1$ diverges as $|\omega - E_0|^{-2/3}$. In contrast, $\mathcal{G}_3$ is finite at threshold, which implies that $\mathcal{A}_3(\omega) \sim |\omega - E_0|^{2/3}$ close to threshold. Since $\mathcal{G}_3$ corresponds to the dynamically screened exchange between the Γ_7 Ce^{3+} doublet and the Γ_8 conduction quartet, this vanishing corresponds to the irrelevance of that coupling when the bare $\Gamma_7 - \Gamma_8$ exchange is smaller than the bare $\Gamma_7 - \Gamma_7$ exchange.

We next identify the crossover energy scales at which the low temperature single channel behavior begins to dominate. This proceeds in much the same spirit as in the identification of crossover scales for applied spin and channel fields in the $SU(N) \otimes SU(M)$ model of the previous subsection. The relevant comparison here is between the magnitude of g_1 and $\tilde{\epsilon}_f$. The maximal scale of g_1 is set by Γ in the low energy region. Hence, if $\Gamma << \epsilon_2$, we will always pass to the single channel Kondo physics on lowering from high energy/temperature scales without seeing the three channel Kondo physics corresponding to essentially degenerate f^0, f^2 states. However, if $\epsilon_2 < \Gamma << |\epsilon_f|$, we have a more interesting situation. For $E_0 > \omega$, we have, following Müller-Hartmann [1984],

$$g_1(\omega) \simeq \frac{\Gamma}{\pi}[\frac{3(E_0 - \omega)}{T_0}]^{2/3} \tag{5.2.15}$$

which should be equated to $\tilde{\epsilon}_f$ to determine the crossover scale $T^x_{(1)}$. We thus find

$$T^x_{(1)} \simeq \frac{1}{3}T_0^{(1)}(\frac{\pi\epsilon_2}{\Gamma})^{3/2} \quad . \tag{5.2.16}$$

This clearly tends to zero as $\epsilon_2 \to 0$. For frequencies above this scale, g_1 exceeds ϵ_2 and the physics becomes that of the three channel model. An alternative approach is to compare the three channel form for g_1 above $T^x_{(1)}$ with ϵ_2. This yields

$$T^x_{(1)} \simeq \frac{3}{5}T_0^{(3)}(\frac{\pi\epsilon_2}{\Gamma})^{5/2} \quad . \tag{5.2.17}$$

Using the expression for $T_0^{(3)}$, we see that this result differs from that of Eq. (5.2.16) only by order unity.

The most interesting feature of the discussion in the preceding paragraph is that even for vanishingly small ϵ_2, the physics will ultimately be that of the single channel model at temperatures below $T^x_{(1)}$, with a Kondo scale fixed by $T_0^{(1)}$. Indeed, to cleanly see the single channel physics numerically, we infer that ϵ_2 must be at least of order Γ since $T^x_{(1)} \sim (\epsilon_2/\Gamma)^{5/2}$. Clearly more energy scales are present for a model Ce^{3+} ion than are evident from the bulk of theoretical approaches taking $U_{ff} \to \infty$!

(iii) $\epsilon_2 < 0$ In this case, we expect the low temperature physics to be governed by the two-channel spin 1/2 fixed point. Now we eliminate g_1 in favor of g_3 and obtain the integration constant

$$\tilde{C} = \exp(\frac{\pi}{2\Gamma}[g_7 - g_3])(\frac{g_7}{D})^2\frac{D^3}{g_3^2(g_3 + |\epsilon_2|)} \tag{5.2.18}$$

which now gives $\tilde{C} = \exp(-\pi[\epsilon_f + U_{ff}]2\Gamma)$ and implies near threshold

$$1 \approx \frac{[g_7/T_0^{(2)}]^2}{[\pi g_3/\Gamma]^2} \tag{5.2.19}$$

with

$$T_0^{(2)} = D(\frac{|\epsilon_2|}{D})^{1/2}(\frac{\Gamma}{\pi D})\exp(-\frac{\pi\tilde{\epsilon}_f}{2\Gamma}) \quad . \tag{5.2.20}$$

Notice the new exponential factor in this Kondo scale. Use of Eq. (5.2.19) in solving the NCA differential equations confirms that this is the $N = M = 2$ limit of the $SU(N)\otimes SU(M)$ model. Hence, each of g_7, g_3 vanish as $|\omega - E_0|^{1/2}$ near threshold, while $\mathcal{A}_1(\omega)$ vanishes as $|\omega - E_0|^{1/2}$ near threshold corresponding to the irrelevance of the single channel coupling in this instance.

We may discuss the crossover physics in exactly the same manner as for the single channel case. For $|\epsilon_2| >> \Gamma$, the three-channel fixed point is never approached from high energies and we simply flow directly to the physics of the two-channel fixed point. For $|\epsilon_2| < \Gamma$, we can determine the energy scale at which we crossover from three channel to two-channel physics by equating

$$g_3(\omega) \simeq \frac{\Gamma}{\pi}[\frac{2|\omega - E_0|}{T_0}]^{1/2} \tag{5.2.21}$$

to $|\epsilon_2|$ which yields

$$T^x_{(2)} \simeq \frac{1}{2}T_0^{(2)}(\frac{\pi|\epsilon_2|}{\Gamma})^2 \tag{5.2.22}$$

or by equating the three channel form for d_3 with $|\tilde{\epsilon}_f|$ that gives

$$T^x_{(2)} \simeq \frac{3}{5}T_0(\frac{\pi|\epsilon_2|}{\Gamma})^{5/2} \tag{5.2.23}$$

which agrees with Eq. (5.2.21) to within factors of order unity. Once again, even for vanishingly small ϵ_2, the low temperature physics below $T^x_{(2)}$ will be governed by the two-channel fixed point.

5.2.4 Remarks on the General Case $\Gamma_{17} \neq \Gamma_{37}$

As we mentioned in Sec. 5.2.2, when $\Gamma_{17} \neq \Gamma_{37}$, no integration constant can be found corresponding to $\tilde{C}$ and a full solution must be numerical. However, we can make some statements about universality classes with confidence since there are approximate integration constants there obtained by neglecting the -1 terms in Eqs. (5.2.6a,b). This is valid near threshold assuming g_7 diverges which in turn implies that at least one of d_1, d_3 diverge near threshold. Specifically, we see that $dg_3/dg_1 \approx \Gamma_{37}/\Gamma_{17}$. Thus

$$g_3 \approx (\frac{\Gamma_{37}}{\Gamma_{17}})g_1 + C \tag{5.2.24}$$

and C can be identified from the values at threshold to be

$$C = \epsilon_2^* = \epsilon_2 + (\frac{\Gamma_{37}}{\Gamma_{17}} - 1)E_0 \quad . \tag{5.2.25}$$

The meaning of ϵ_2^* is that this integration constant essentially plays the role of a hybridization renormalized value of ϵ_2 near the threshold. Clearly, the conditions of the previous section regarding the sign of ϵ_2 can now be replaced by the corresponding conditions on the sign of ϵ_2^*. Unfortunately, E_0 is not known *a priori*, so that this condition is not as useful in determining the low temperature physics.

The approximate integration constant relation of Eq. (5.2.24) will hold up to some energy cutoff D^*. Consider the case ϵ_2^*=0. Then in the same energy region we can identify a new approximate integration constant $\tilde{C}^*$ given by

$$\tilde{C}^* \approx (\frac{g_7}{D^*})^2(\frac{D^*}{g_1})^3 \tag{5.2.26}$$

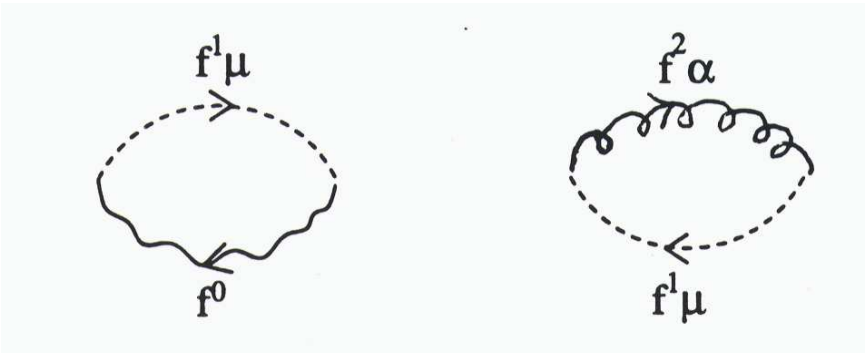

Figure 59: Diagrams for full $4f$ propagators for the simplest Ce^{3+} Anderson model. The diagram at left is for the Γ_7 symmetry full f propagator (which hybridizes with the corresponding conduction propagator), and the diagram at right for the Γ_8 symmetry full f propagator (which hybridizes with the conduction quartet propagator.

which implies

$$1 \approx \frac{[g_7/T_0^{(3)*}]^2}{[\pi g_1/\Gamma_{17}]^3} \tag{5.2.27}$$

with

$$T_0^{(3)*} \approx D^* \tilde{C}^* (\frac{\Gamma_{17}}{\pi D^*})^{3/2} \quad . \tag{5.2.28}$$

Note that Eq. (5.2.23) ensures that Γ_{37} cancels from dg_7/dg_1. Thus the form of the low temperature physics must be the same as in the simpler case with equal hybridizations, but the Kondo scale must be determined numerically for a given cutoff D^* through evaluation of $\tilde{C}^*$ at the cutoff. Similar analyses apply for the one and two channel limits. The crossover analysis can be done in terms of ϵ_2^* and $T^{(3)*}$ in the same way as discussed in Sec. 5.2.2.

Finally, we note that we can easily rewrite the condition $\epsilon_2^* >, <, = 0$ in terms of renormalized coupling constants $\tilde{g}_7, \tilde{g}_8$ given by

$$\tilde{g}_7 = \frac{\Gamma_{17}}{\pi |E_0|}, \quad \tilde{g}_8 = \frac{\Gamma_{37}}{\pi |E_0 - \epsilon_2|} \quad . \tag{5.2.29}$$

Let $\delta = \tilde{g}_7^{-1} - \tilde{g}_8^{-1}$. Then for $\delta > 0$, we will obtain two-channel physics, for $\delta = 0$ three channel physics, and for $\delta < 0$ we will obtain one channel physics at low temperatures. The estimates of the crossover temperatures are precisely those of Eqs. (2.2.40,41) discussed in Sec. 2.2.4. Clearly, if $\Gamma_{17} = \Gamma_{37}$, we revert to the sign of ϵ_2 determining the physics as in Sec. 5.2.2, and to the crossover scale formulae Eqs. (5.2.16,20).

5.2.5 Physical Properties at Finite Temperature

Kim and Cox [1995,1997] have evaluated the physical properties of this model at finite temperatures, and we shall survey their results here.

We shall focus on the magnetic susceptibility and the 4f spectral function here. The susceptibility diagram is precisely that of Fig. 51, with the Γ_7 propagators put in. The spectral function diagram includes two contributions show in Fig. 59. One term arises from Γ_7 symmetry interconfiguration transitions arising from $f^0 - f^1$ processes, and the other from Γ_8 symmetry transitions arising from $f^1 - f^2$ processes. Notice the reversed order of the Γ_7 propagator in the two diagrams.

The susceptibilities in the two- and three-channel regimes are shown in Fig. 54 . As discussed previously, these agree very well with the corresponding Bethe-Ansatz curves of Sacramento

and Schlottmann [1991]. There is however a necessary vertical scale adjustment which depends upon parameters. The origin of this scale factor, which is of order unity, is likely a residue of the crossover physics. Namely, the full one-parameter universality of the two-channel model, for example, may not show up until $\tilde{g}_8 >> \tilde{g}_7$. The dynamical spin susceptility in the three different regimes is shown in Fig. 60. In each case the inset shows the peak position as a function of temperature. This peak position is a rough measure of the spin relaxation rate, which is then illustrated in Fig. 61. For the one -channel case, this saturates to a constant value of order T_0 at low T, compatible with the Fermi liquid ground state (although χ'' is of course singular at lower frequency). For the two- and three-channel regimes, the effective relaxation rate vanishes as $T \to 0$, doing so linearly in the two-channel case. This is of course compatible with the marginal Fermi liquid hypothesis which postulates that T sets the low temperature energy scale (Varma *et al.*, [1989]).

The specific heat and entropy curves have already been discussed in Figs. 55,56 and section 5.1.6. Of importance in understanding the curves is the presence of the interconfiguration peak which gives a large background to the specific heat and entropy.

The most interesting new physics to emerge from this treatment concerns the transport coefficients, specifically the thermoelectric power. The temperature dependent spectral functions in the 1,2, and 3-channel regimes are shown in Figs. 62,63,64. For the 1 and 2-channel cases, the inset shows the separate contributions of the $f^0 - f^1$ and $f^1 - f^2$ diagrams at low temperatures. We notice that the contribution from either $f^1 - f^2$ transitions in the single channel case or $f^0 - f^1$ transitions in the two-channel case vanishes at zero frequency. This corresponds to the irrelevance of the smaller coupling constant in the renormalization group sense; the width of the region over which each spectral function vanishes is a measure of the corresponding crossover scale defined in the previous subsection.

What is quite clear from these figures is that in the one-channel regime is that the Kondo resonance weight is shifted predominantly to positive frequencies. For the two-channel regime, the Kondo resonance weight is shifted predominantly to negative frequencies. The physical origin is clear– in the one channel case, virtual charge fluctuations to the f^0 configuration dominate and so the f-occupancy is less than 1, meaning we should shift spectral weight above the Fermi energy relative to the $n_f = 1$ case. For the two-channel regime, virtual charge fluctuations to f^2 dominate, and hence we expect the f-occupancy to exceed one. Corresponding to this, we should shift spectral weight below the Fermi energy.

Since the scattering rate $1/\tau$ is proportional to to the full spectral function (modulo corrections from anisotropic hybridization matrix elements –see Kim and Cox [1995,1997] for a discussion), the discussion of the preceding paragraph has a direct bearing on the thermoelectric power which is proportional to the transport integral $I_1 = \int d\epsilon(-\partial f/\partial\epsilon)\tau(\epsilon)$. The one-channel regime scattering rate will lead to a stronger scattering of unoccupied (particle) states meaning that occupied(hole) states will dominate the heat transport in I_1 and hence we expect a positive sign to the thermopower in this regime. For the two-channel case, holes are scattered more strongly overall than particles, so we anticipate more effective heat transport by particles and a negative sign to the thermopower. In the three channel case, the scattering rate is approximately symmetric but slightly dominated by hole scattering since the excited f^2 state is a doublet. As a result we expect the thermopower to be slightly negative at low temperatures. The full numerical calculations bear out the physical discussion of the previous paragraph, as shown in Fig. 65. This implies that the thermopower is a sensitive probe of the possible *universality class* for Ce^{3+} impurities! As we have noted previously, $CeCu_{2.2}Si_2$ has a negative thermopower below 70K, well above any possible lattice coherence effects. This is strong support for a model in which the f^2 fluctuation weight in the ground state exceeds the f^0 weight. However, as discussed in Sec. 8.2, for dilute Ce in $LaCu_2Si_2$, the thermopower regains a positive sign, which is problematic for an interpretation in terms of the two-channel Kondo model.

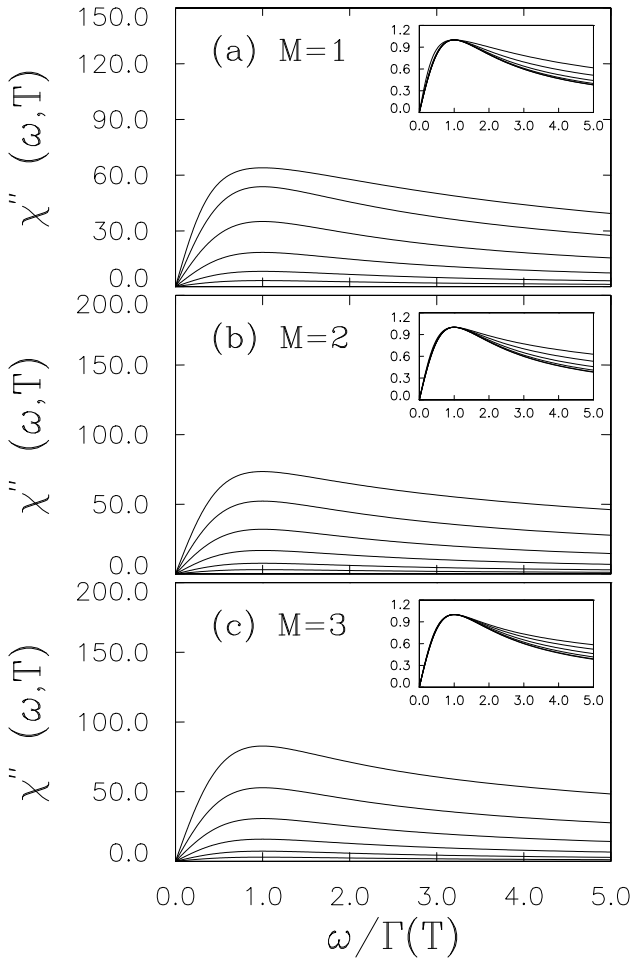

Figure 60: Dynamic susceptibility of the simplest Ce^{3+} Anderson model in the $M = 1, 2, 3$ channel regimes. The insets show scaling behavior in which the curves are divided by their maximum value and centered at their maximum position. The maximum position defines the linewidth Γ of Fig. 61. From Kim and Cox [1997].

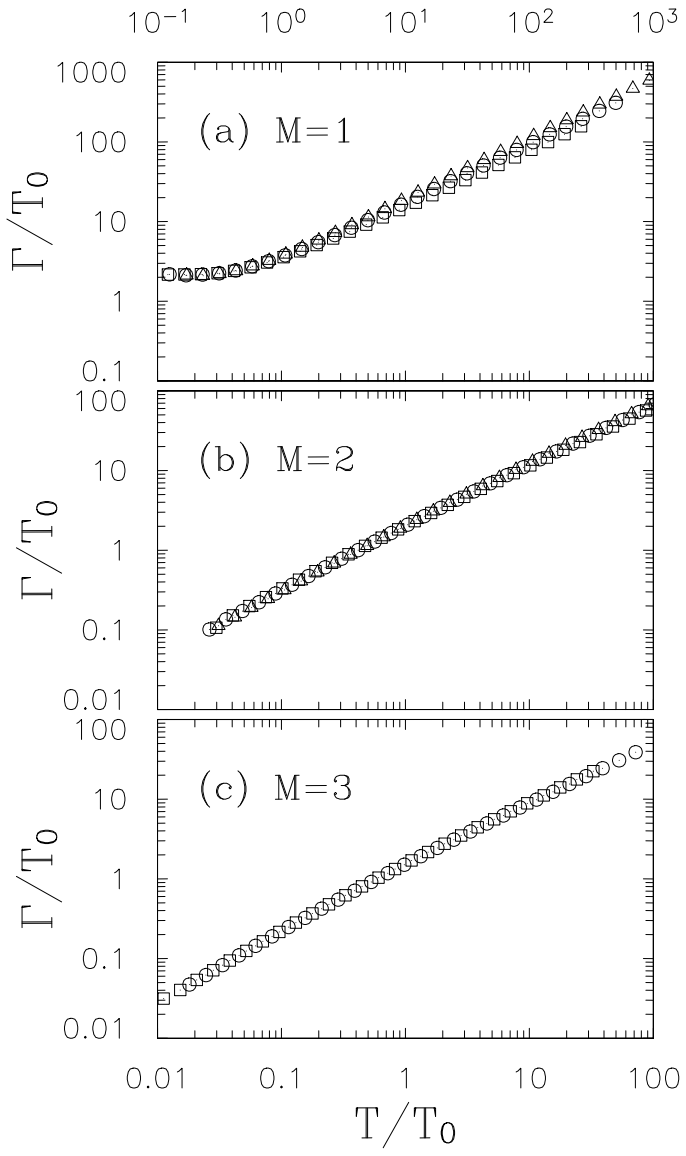

Figure 61: Magnetic relaxation rate of the simplest Ce^{3+} Anderson model in the $M = 1, 2, 3$ channel regimes. These rates are determined from the maximum position of the dynamic susceptibility curves in Fig. 60. Reflecting the residual ground state degeneracy ("degenerate spin screening cloud"), the linewidth vanishes linearly in temperature for $M = 2, 3$, whereas it is finite for $M = 1$, compatible with Fermi liquid behavior in that limit. From Kim and Cox [1997].

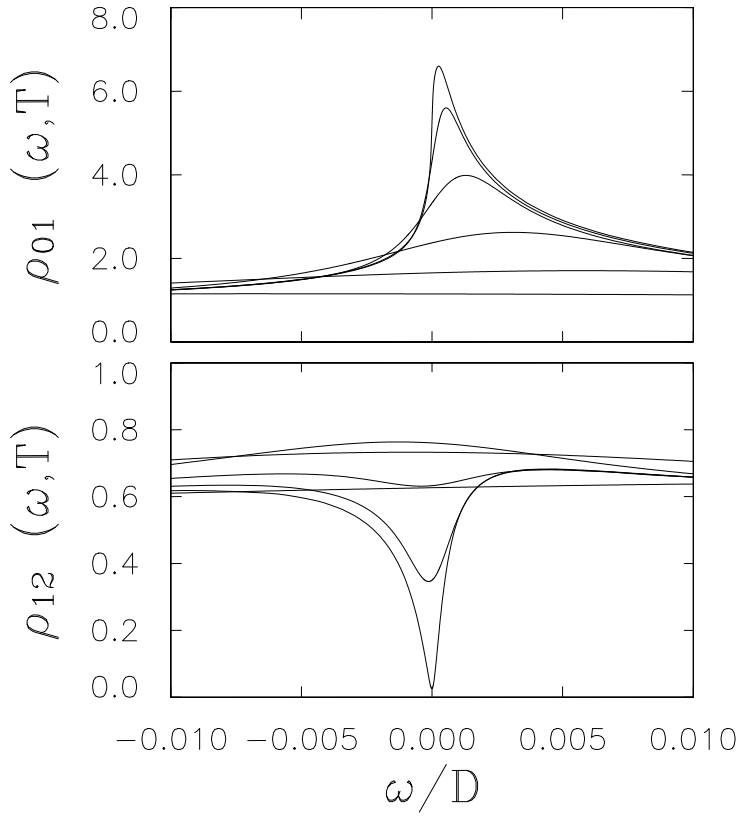

Figure 62: Atomic spectral functions in the one-channel regime of the simplest Ce^{3+} Anderson model. ρ_{01} is the interconfiguration spectral function which is obtained from the convolution between f^0 and $f^1\Gamma_7$ states. ρ_{12} is the interconfiguration spectral function which is obtained from the convolution between $f^1\Gamma_7$ and $f^2\Gamma_3$ states. The one-channel Kondo effect leads to the Kondo resonance development in ρ_{01} just above the Fermi level and the spectral depletion in ρ_{12} right at $\omega = 0$. Spectral functions are displayed for model set 8. The temperature variations are $T/D = 3.678 \times 10^{-2}$, 1.077×10^{-2}, 3.155×10^{-3}, 9.239×10^{-4}, 2.706×10^{-4}, 7.924×10^{-5}, 2.321×10^{-5}. From Kim and Cox [1997].

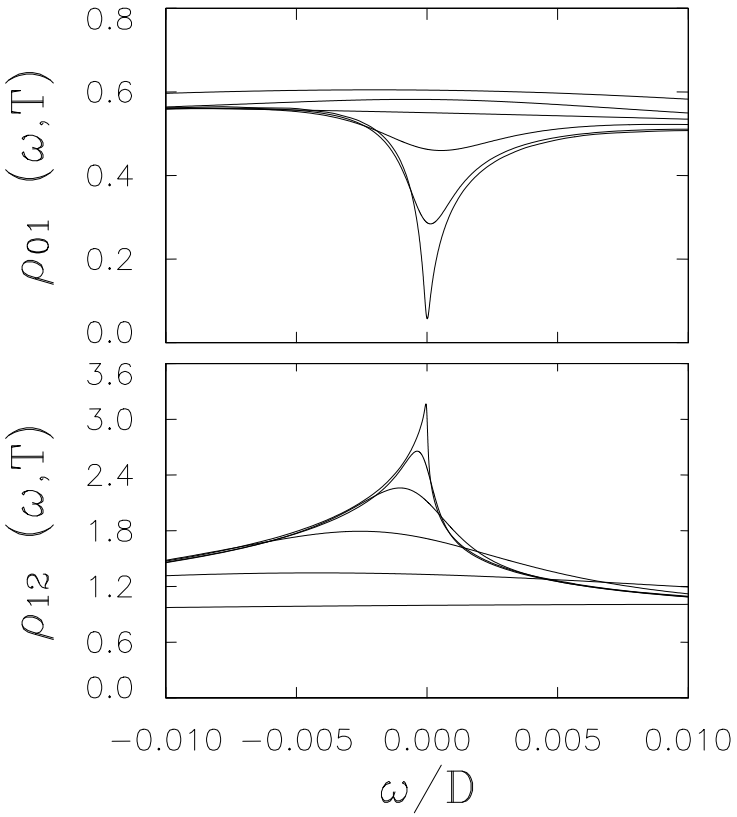

Figure 63: Atomic spectral functions in the two-channel regime for the simplest Ce^{3+} ion Anderson model. The two-channel Kondo effect leads to the Kondo resonance development in ρ_{12} at the Fermi level ($T = 0$) and the spectral depletion in ρ_{01} right at $\omega = 0$. Spectral functions are displayed for model set 1. The temperature variations are the same as in Fig. 62. From Kim and Cox [1997].

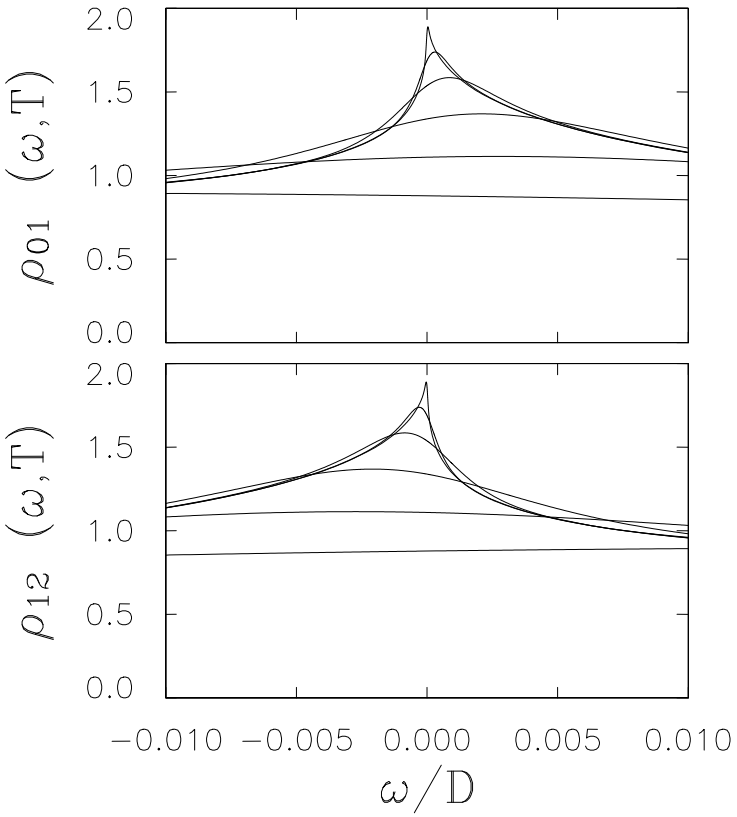

Figure 64: Atomic spectral functions in the three-channel regime of the simplest Ce^{3+} ion Anderson model. For this parameter regime (model set 4), the two spectral functions ρ_{01} and ρ_{12} are equivalent in the asymptotic limit after a particle-hole transformation. The temperature variations are the same as in Fig. 62. From Kim and Cox [1997].

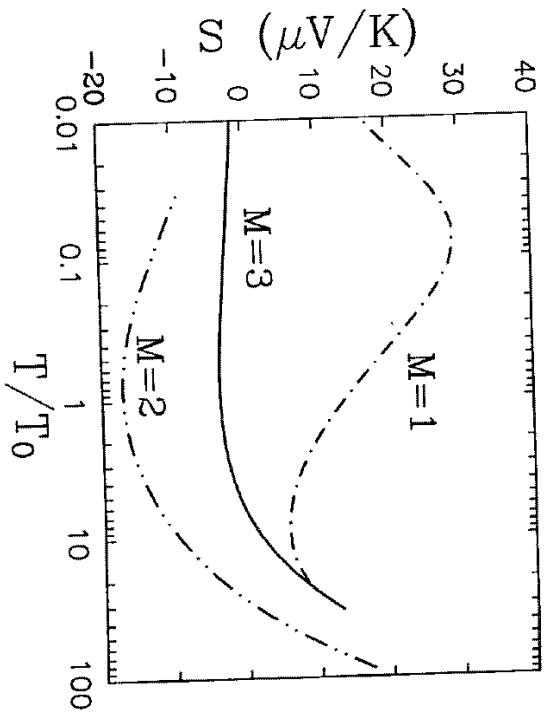

Figure 65: Thermopower $S(T)$ for the simplest Ce^{3+} ion Anderson model. The thermopower is positive at low T for the $M = 1$ parameter regime, strongly negative for the $M = 2$ parameter regime, and weakly negative for the $M = 3$ parameter regime. Dominant $f^0 - f^1(f^1 - f^2)$ virtual charge fluctuations give positive(negative) $S(T)$. From Kim and Cox [1995].

5.2.6 Critique and Directions

The simple model analyzed in this subsection may be criticized in its treatment of the f^2 configuration. Specifically, it is known for Ce^{3+} ions that $\epsilon_2 \approx +1 - 2\text{eV}$. On the other hand, Γ_{17} is known to be $\simeq 0.1 - 0.3eV$, and due to fractional parentage effects, we anticipate that for the lowest multiplet in f^2 that $\Gamma_{37} < \Gamma_{17}$. Thus, naively, unless it would seem that the two- and three-channel possibilities can never be realized in practice. Also, excited state $f^2\Gamma_4, \Gamma_5$ levels give rise to the additional $\tilde{J}$ coupling discussed in Sec. 2.2.2.

The NCA analysis can in principle be extended to include the lowest crystal field excitations of the excited configuration, but this will require inclusion of vertex corrections of the sort discussed by Pruschke [Pruschke, 1989] to reliably describe the low temperature physics. The effect here is not yet known, but given the scaling analysis of Sec. 3.4, we anticipate that the low energy scale physics will still be determined by the Γ_3 virtual charge fluctuations provided the coupling is sufficiently weak to the Γ_4, Γ_5 levels.

The first critique is more serious, but a possible answer is as follows: all the excited state Γ_3 levels will produce a contribution to the two-channel coupling. While the hybridization to any given Γ_3 is too weak to give an effective coupling exceeding the one-channel coupling driven by the f^0 charge fluctuations, we anticipate that the sum over the manifold of Γ_3 states may well produce a significantly larger coupling. Since this appears already at second order in the hybridization, we expect the NCA extended to the entire configuration to produce an answer to the question. The additional couplings will likely be brought in through admixture of all the d_3 propagators, which occurs at second order in the hybridization.

This argument can be made precise by considering a model with two excited state Γ_3 doublets and examining the first iteration of the NCA, which is sufficient to determine the Kondo temperature. Denote the corresponding hybridization matrix elements by $V_{37}^{(i)}$ and energies as $\tilde{\epsilon}_f^{(i)}$. Define the quantity $\tilde{\pi}(\omega) = \ln|(\omega - \epsilon_f)/D|/\pi$. Because the excited Γ_3 doublets can mix as shown in Fig. 5.12, the Γ_3 green's function is now a 2×2 matrix. The secular equation determining T_0 is found by requiring that the denominator of the inverse Green's function vanishes, which gives

$$[\omega - \tilde{\epsilon}_f^{(1)} - \Gamma_{37}^{(1)}\tilde{\pi}(\omega)][\omega - \tilde{\epsilon}_f^{(2)} - \Gamma_{37}^{(2)}\tilde{\pi}(\omega)] - \Gamma_{37}^{(1)}\Gamma_{37}^{(2)}\tilde{\pi}^2(\omega) \quad . \tag{5.2.29}$$

This function $\tilde{\pi}$ becomes large and negative near $\omega = \epsilon_f$, and to leading exponential accuracy we may thus rewrite this equation as (putting $\omega - \epsilon_f = -T_0$)

$$1 = [\frac{\Gamma_{37}^{(1)}}{\pi(\epsilon_f - \tilde{\epsilon}_f^{(1)})} + \frac{\Gamma_{37}^{(2)}}{\pi(\epsilon_f - \tilde{\epsilon}_f^{(2)})}]\ln(\frac{T_0}{D}) \tag{5.2.30}$$

so that the effective couplings driven by the different Γ_3 levels are clearly summed. This analysis may be readily extended to an arbitrary number of excited Γ_3 levels. Hence, the model with just one Γ_3 level captures the essential physics; the lone Γ_3 should just be taken as an effective representative of all the excited Γ_3 levels.

5.3 Application of the NCA to a Model U^{4+} Impurity

In this section we discuss results obtained from applying the NCA to a model U^{4+} impurity that have been reported in Cox[1987b], Cox [1988(a)], Cox and Makivik [1994], and Kim *et al.* [1997]. The most important physical conclusions are: (i) that even for arbitrarily small crystal field splitting in the ground $J = 4$ multiplet, when the Γ_3 level lies lowest the low temperature physics will be that of the two-channel Kondo model below a suitable crossover temperature. Hence, even when the crystal field levels overlap substantially, as appears to be the case for UBe_{13} to the extent that this model applies for this material, one may be confident of two-channel Kondo physics arising at low temperatures. (ii) the singular character of the ground non-magnetic doublet may reflect in the magnetic susceptibility

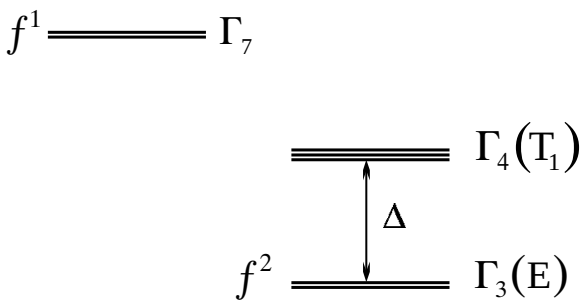

Figure 66: Level scheme for the simplest U^{4+} ion Anderson model studied within the NCA.

producing a $\sqrt{T}$ law. This result appears to be highly parameter dependent and most likely occurs in the regime where the crystal field levels overlap substantially.

5.3.1 Pseudo-particle model and NCA equations

We shall consider only a simple model in which we retain the lowest $J = 4\Gamma_3$ doublet of the ground configuration together with the first excited crystal field level (assumed to be a Γ_4 triplet) and the lowest $J = 5/2\Gamma_7$ doublet of the excited f^1 configuration. We will assume only $J = 5/2\Gamma_8$ conduction partial wave states. Additional crystal field states and conduction partial waves may easily be included with altering the essential conclusions. At the end of the section we shall briefly remark about the effects of including an excited

In this case, we simply introduce a pseudo-fermions for the Γ_3, Γ_4 states of the f^2 configuration, and a pseudo-boson doublet for the Γ_7 of the excited f^1 configuration. (Alternatively, we could assume a Γ_6 doublet in an excited f^3 configuration since $\Gamma_6 \otimes \Gamma_3 = \Gamma_7 \otimes \Gamma_3 = \Gamma_8$.) The level scheme is shown in Fig. 66. These are then put into the Hamiltonian in equations (2.2.30) and (2.2.32) in precisely the same manner we did for the Ce case. The reader should not be disturbed by the use of a pseudo-fermion operator for an even numbered configuration and a pseudo -boson operator for an odd numbered configuration since the statistics are lost once the full projection is made. The f charge is written as

$$Q_f = \sum_{\Gamma(f^2)\eta(f^2)} f^\dagger_{\Gamma(f^2)\eta(f^2)} f_{\Gamma(f^2)\eta(f^2)} + \sum_\mu b^\dagger_{\Gamma_7\mu} b_{\Gamma_7\mu} \tag{5.3.1}$$

and the full pseudparticle Hamiltonian is

$$H = \sum_{k\eta_8} \epsilon_k c^\dagger_{k8\eta_8} c_{k8\eta_8} + \sum_{\Gamma(f^2)\eta(f^2)} (\tilde{\epsilon}_f + \Delta_{\Gamma(f^2)}) f^\dagger_{\Gamma(f^2)\eta(f^2)} f_{\gamma(f^2)\eta(f^2)} + H_{hyb} - \lambda_{ps}(Q_f - 1) \tag{5.3.2}$$

with

$$H_{hyb} = \frac{V}{N_s} \sum_{k,\eta_8,\mu} \sum_{\Gamma(f^2)\eta(f^2)} \Lambda(\Gamma_7\mu; \Gamma(f^2)\eta(f^2); \Gamma_8\eta_8)[f^\dagger_{\Gamma(f^2)\eta(f^2)} b_{\Gamma_7\mu} c_{k8\eta_8} + h.c.] \quad . \tag{5.3.3}$$

Note that η_8 is shorthand for the spin/channel notation of Eqs. (2.2.18.a,b). We have taken $E(f^2) = \tilde{\epsilon}_f$, and shall denote henceforth $\Delta_{\Gamma_3} = 0, \Delta_{\Gamma_4} = \Delta$.

The NCA self-energy diagrams for this model are shown in Fig. 67. Prior to writing down the integral equations, it is useful to define the group theoretic coupling strengths

$$c(\Gamma(f^2), \Gamma(f^1)) = \frac{1}{\nu(\Gamma(f^1))} \sum_{\Gamma_c\eta_c\eta(f^1))} \Lambda^2(\Gamma(f^1)\eta(f^1); \Gamma(f^2)\eta(f^1); \Gamma_c\eta_c) \tag{5.3.4.a}$$

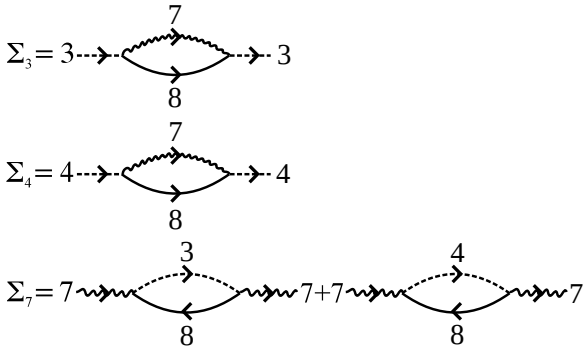

Figure 67: NCA pseudo-particle self energy diagrams for the simplest U^{4+} ion Anderson model.

and

$$(5.3.4.b) \qquad c(\Gamma(f^1),\Gamma(f^2)) = c(\Gamma(f^2),\Gamma(f^1)) = \frac{1}{\nu(\Gamma(f^2))} \sum_{\Gamma_c \eta_c \eta(f^2))} \Lambda^2(\Gamma(f^1)\eta(f^1);\Gamma(f^2)\eta(f^1);\Gamma_c\eta_c)$$

where $\nu(\Gamma)$ is the degeneracy of irrep Γ. For a given coupling model (LS, jj, or intermediate) and crystal field Hamiltonian, the c coefficients may be determined once and for all. Depending on the crystal field, the coefficients may also have to be recomputed in an applied magnetic field. This definition allows for a ready generalization of the NCA to arbitrary crystal field schemes. The definition is unmodified by the inclusion of all conduction partial waves. The hybridization factors appearing in the integral equations for the state indexed by irrep Γ_e and arising from a diagram with internal impurity irrep Γ_i will always just be of the form $\nu(\Gamma_i)c(\Gamma_e,\Gamma_i)\Gamma$. The coupling coefficients have an implicit dependence on the f^2 multiplet. They obey a simple sum sule

$$\sum_{\Gamma(f^1)} c(\Gamma(f^2),\Gamma(f^1)) = 2$$

independent of $\Gamma(f^2)$, where the sum includes the crystal field states of the $j = 7/2$ multiplet as well. This measures the total number of ways to make a transition from $f^2 \to f^1$, which is just two, since we may remove one or the other of the electrons. If we are instead considering a model with the f^3 excited configuration, the RHS of the above sum rule is changed to 12 provided we sum over *all* states of the excited f^3 configuration.

The integral equations of the NCA for this model are then

$$(5.3.5.a) \qquad \sigma_3(\omega) = \frac{2c(\Gamma_3,\Gamma_7)\Gamma}{\pi} \int d\epsilon f(\epsilon)\mathcal{D}_7(\omega+\epsilon)$$

$$(5.3.5.b) \qquad \sigma_4(\omega) = \frac{2c(\Gamma_4,\Gamma_7)\Gamma}{\pi} \int d\epsilon f(\epsilon)\mathcal{D}_7(\omega+\epsilon)$$

and

$$(5.3.5.c) \qquad \pi_7(\omega) = \frac{2c(\Gamma_3,\Gamma_7)\Gamma}{\pi} \int d\epsilon f(\epsilon)\mathcal{G}_3(\omega+\epsilon) + \frac{3\Gamma c(\Gamma_4,\Gamma_7)}{\pi} \int d\epsilon f(\epsilon)\mathcal{G}_4(\omega+\epsilon) \quad .$$

We have again assumed particle-hole symmetry to the conduction density of states.

Following the procedures of the previous two sections, we may convert these integral equations to differential form at $T = 0$ with the usual definition of inverse propagators, which gives

$$(5.3.6.a) \qquad \frac{dg_3}{d\omega} = -1 - \frac{2c(\Gamma_3,\Gamma_7)\Gamma}{\pi d_7}$$

(5.3.6.b)
$$\frac{dg_4}{d\omega} = -1 - \frac{2c(\Gamma_4,\Gamma_7)\Gamma}{\pi d_7}$$

and

(5.3.6.c)
$$\frac{dd_7}{d\omega} = -1 - \frac{2c(\Gamma_3,\Gamma_7)\Gamma}{\pi g_3} - \frac{3c(\Gamma_4,\Gamma_7)\Gamma}{\pi g_4}$$

subject to the boundary conditions

(5.3.7)
$$g_3(-D) = D + \tilde{\epsilon}_f, \quad g_4(-D) = D + \tilde{\epsilon}_f + \Delta, \quad d_7(-D) = D \quad .$$

5.3.2 Solution of the NCA equations for the Model U^{4+} Impurity

Clearly Eqs. (5.3.6a-c) have a very similar structure to Eqs. (5.2.7a-c). As in the case of those equations for the model Ce^{3+} impurity, we cannot solve Eqs. (5.3.6a-c) analytically without a further simplifying assumption. For convenience (and not reality) we shall take $c(\Gamma_3,\Gamma_7) = c(\Gamma_4,\Gamma_7)$. We shall then denote the product of the coupling coefficient and Γ by $\tilde{\Gamma} = \Gamma c(\Gamma_3,\Gamma_7)$. No qualitative differences arise in this modified model relative to the original one. Typically the coupling coefficients are of order unity; for the LS coupling scheme and all conduction partial waves included, $c(\Gamma_3,\Gamma_7) = 0.64$. This reflects fractional parentage coefficients. Notice that the effective reduction of the hybridization is important for understanding why we can get reasonably small Kondo scales in U materials when compared with Ce based materials despite the expectation of smaller interconfiguration energy differences and larger hybridization due to the greater spatial extent of the 5f wave-function.

With this simplifying assumption, we see that $g_4 = g_3 + C$, with the constant $C = \Delta$. This allows us to find the second integration constant $\tilde{C}$ given by

(5.3.8)
$$\tilde{C} = \exp[\frac{\pi}{\tilde{\Gamma}}(g_3 - d_7)](\frac{g_3}{D})^2(\frac{g_3+\Delta}{D})^{3/2}(\frac{D}{d_7})^2 \quad .$$

By evaluation at $-D$, as usual, we find $\tilde{C} = \exp(\pi\tilde{\epsilon}_f/2\tilde{\Gamma})$. In the low frequency limit for $g_3 << \Delta$, we can rewrite this as

(5.3.9)
$$1 \approx \frac{[g_3/T_0]^2}{[\pi d_7/\tilde{\Gamma}]^2}$$

with

(5.3.10)
$$T_0 = D(\frac{\tilde{\Gamma}}{\pi D})(\frac{D}{\Delta})^{3/2}\exp(\frac{\pi\tilde{\epsilon}_f}{2\tilde{\Gamma}}) \quad .$$

Notice the crystal field enhancement factor appears just as discussed in Sec. 3.3.3.c. Also, the hybridization multiplied by the coupling coefficient, $\tilde{\Gamma}$, appears, allowing in principle for a smaller Kondo scale despite increased Γ values as discussed previously.

In this low temperature region, it is clear that the physics is that of the $N = M = 2$ Kondo model. As a result, we expect the *quadrupolar* susceptibility and specific heat coefficient to diverge logarithmically, and the electrical resistivity to saturate with a $\sqrt{T}$ law as the temperature is lowered.

As the temperature or frequency is raised, a crossover can occur to the Kondo model corresponding to degenerate Γ_3, Γ_4 multiplets. The relevant comparison here is of $g_3 \sim T_0(2|\omega - E_0|/T_0)^{1/2}$ to Δ. If $\Delta >> T_0$, the crossover to the ground two-channel Kondo effect simply occurs at T_0. If on the other hand $\Delta \leq T_0$, then the crossover occurs when $g_3 \approx \Delta$. This occurs at an energy scale T^x_{CEF} given by

(5.3.11)
$$T^x_{CEF} \approx \frac{1}{2}T_0(\frac{\Delta}{T_0})^2 \quad .$$

What is important to notice here is that even for arbitrarily small crystal field splitting, the low temperature physics will still be that of the two-channel quadrupolar Kondo effect. This is important, since in UBe_{13}, for example, for which the quadrupolar Kondo effect was first proposed as a possible explanation for the heavy fermion behavior, the excited crystal field levels appear to be very broad and overlap strongly with the ground state. Nonetheless, a quadrupolar Kondo effect can still occur below a crossover temperature as defined above.

We briefly comment on two other issues before discussing physical properties:
(1) Inclusion of Excited Crystal Field States in the f^1 configuration. Here another kind of crossover can occur. Let us assume that the Γ_4 level is taken to ∞, for simplicity, and that a Γ_8 quartet is included at energy Δ' in the excited configuration. Maintaining the equal coupling coefficient limit, the relation between d_7 and g_3 at low energies is still given by Eq. (5.3.9), but with T_0 now modified to

$$T_0 = D(\frac{\tilde{\Gamma}}{\pi D})(\Delta'/D)^2 \exp(\frac{\pi\tilde{\epsilon}_f}{2\tilde{\Gamma}}) \quad . \tag{5.3.12}$$

Notice that excited state crystal field splittings *reduce* T_0. Arriving at the above equation required assuming $d_7 \approx (\tilde{\Gamma}/\pi)(2|\omega - E_0|/T_0)^{1/2} << \Delta'$. If $\Delta' >> \tilde{\Gamma}$, this is always satisfied and the crossover to the low temperature two-channel fixed point occurs at T_0. If $\Delta' \leq \tilde{\Gamma}$, then the crossover scale $T^x_{CEF'}$ below which the two-channel physics sets in is given by

$$T^x_{CEF'} \approx \frac{T_0}{2}(\frac{\pi\Delta'}{\tilde{\Gamma}})^2 \quad . \tag{5.3.13}$$

Clearly, the crossover physics of crystal field states in ground and excited configurations (together with the similar physics arising from all the higher lying angular momentum multiplets in ground and excited configurations) must be included in a complete treatment of the U^{4+} impurity and will produce a single crossover scale determined by the lowest energy scale determined from all the various crossover criteria. The Kondo scale will also require modification to respect all the excited levels in both the ground and excited configurations. Such a complete treatment has not yet been performed. Once any more excited crystal field levels are included in either configuration we must resort to full numerical solutions of the NCA equations.
(2) Effect of Non-equal Coupling Coefficients. As in the corresponding example for the Ce^{3+} impurity, we can no longer solve the model analytically if we relax the assumption of equal coupling coefficients. We can once more find approximate constants of integration at low frequencies since $dg_4/dg_3 \approx c(\Gamma_4,\Gamma_7)/c(\Gamma_3,\Gamma_7)$ so that

$$g_4 \approx \frac{c(\Gamma_4,\Gamma_7)}{c(\Gamma_3,\Gamma_7)}g_3 + \tilde{\Delta}, \quad \tilde{\Delta} = \Delta + (\tilde{\epsilon}_f - E_0)(\frac{c(\Gamma_4,\Gamma_7)}{c(\Gamma_3,\Gamma_7)} - 1) \tag{5.3.14}$$

which follows from requiring $g_3(E_0) = 0$. Depending on the ratio of coupling coefficients, the crystal field level may be renormalized upwards or downwards. When all states are included, we generically find a downward renormalization as expected on the basis of the orthogonality catastrophe (c.f. the discussion in Sec. 3.4.1.d). Then a the Kondo scale may be written in terms of a cutoff D^* over which the approximate integration constant relation holds (to be determined numerically) in a manner similar to that discussed in deriving Eq. (5.2.28). The crystal field crossover scale is changed to

$$T^{x*}_{CEF} = \frac{T_0}{2}(\frac{c(\Gamma_3,\Gamma_7)\tilde{\Delta}}{c(\Gamma_4,\Gamma_7)T_0})^2 \quad . \tag{5.3.15}$$

No qualitative modifications of the physics will emerge in the subsequent analysis.

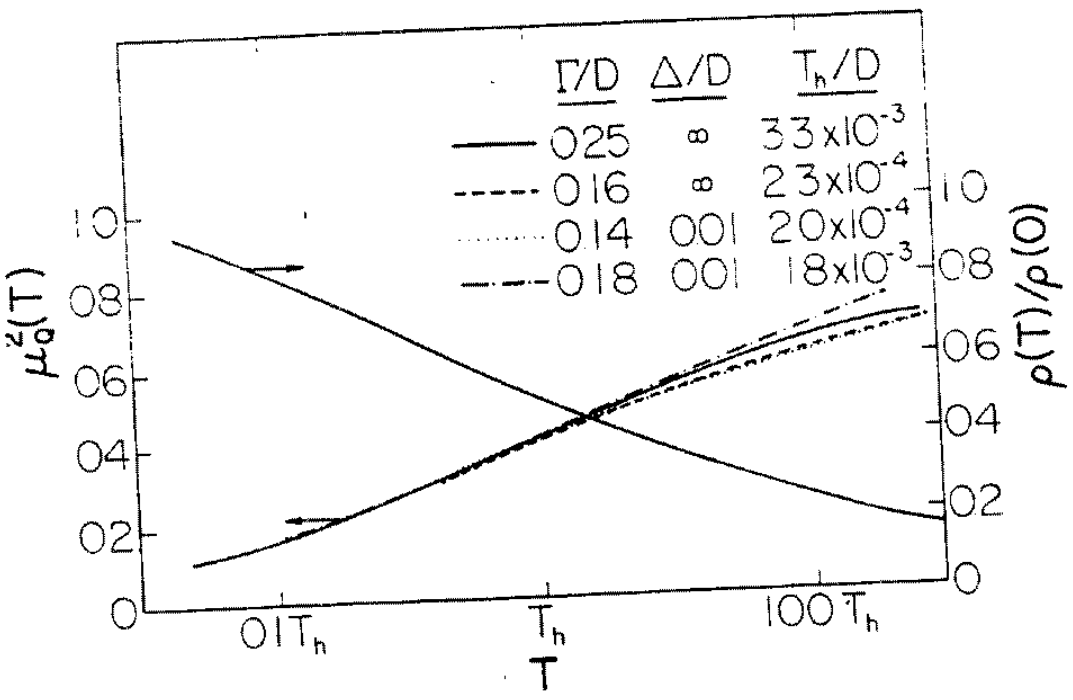

Figure 68: Static quadrupolar susceptibility vs. temperature for a U^{4+} ion model calculated by the NCA. Also shown (right hand axis) is the resistivity scaled by the appropriate zero temperature value obtained from an extrapolation. The temperature T_h is measured from the resistivity midpoint and is of order the Kondo temperature. From Cox [1987(b)].

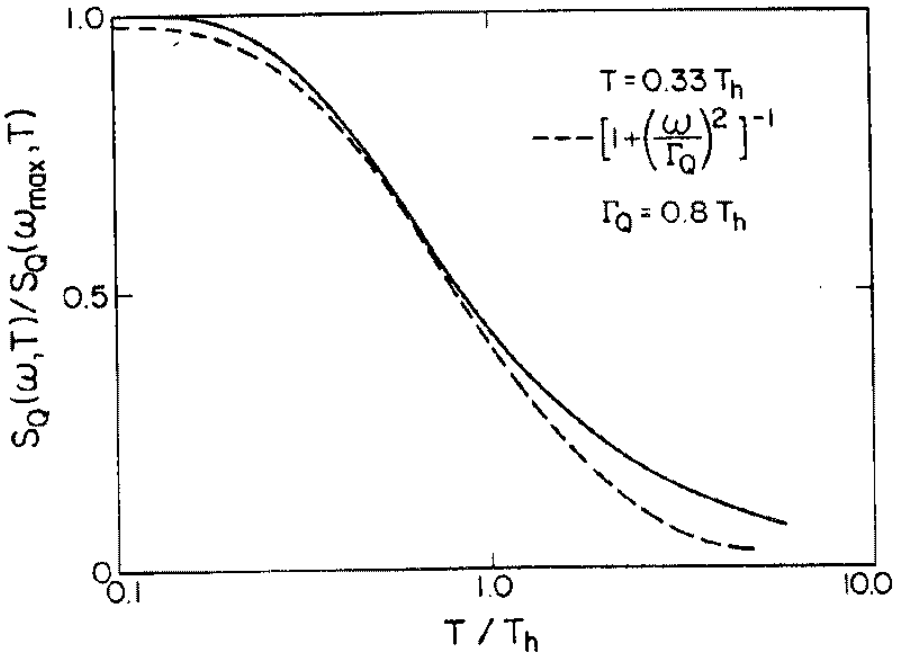

Figure 69: Quadrupolar dynamic structure factor of a model U^{4+} ion calculated within the NCA. For low T, this is the same as the positive frequency evaluation of the dynamic quadrupolar susceptibility. A Lorentzian fit to the structure factor works reasonably well, anticipating the Marginal Fermi Liquid theory of Varma *et al.* [1989], and the outcome of conformal field theory (Tsvelik [1990]; Ludwig and Affleck [1991,1994]) and bosonization results (Emery and Kivelson [1992]). From Cox [1988(a)].

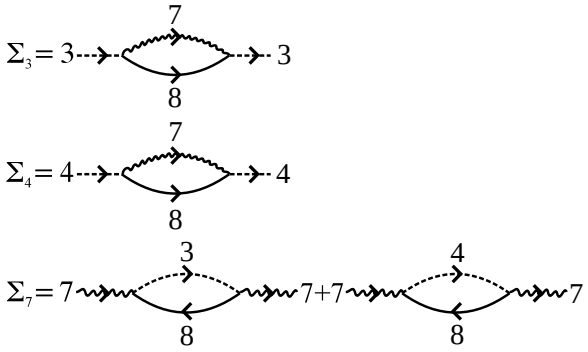

Figure 70: Van Vleck susceptibility diagrams within the NCA for the simplest U^{4+} Anderson model.

5.3.3 Physical Properties

In this subsection we will discuss those physical properties which are novel to the quadrupolar Kondo effect and for which the NCA gives useful information. An extensive review of calculations on model U^{4+} impurities appears in Kim *et al.* [1995].

Quadrupolar Susceptibility. Since the ground doublet is quadrupolar here, the strongly divergent susceptibility relevant for the Wilson ratio is the quadrupolar susceptibility χ_Q. This is obtained from the dashed bubble diagram of Fig. 51 with the Γ_3 propagators put in as pseudo-fermions. The calculated χ_Q curves from the NCA show a universality over a wide range of parameter sets as shown in Fig. 68 taken from Cox[1987b]. It is important that the Γ_3 occupancy must be divided out to produce the universality when excited crystal field levels are included. The data also agree well with the universal Bethe-Ansatz results of Sacramento and Schlottmann [1992]. The dynamic quadrupolar susceptibility shows the anticipated Marginal Fermi liquid form with a step function at the origin, and may be roughly fit to the form $sgn(\omega)T_0/(\omega^2 + T_0^2)$ as shown by Cox [1988(a)] and in Fig. 69.

Magnetic Susceptibility: van Vleck contribution. Given a quadrupolar doublet ground state, the dominant source of magnetic response must be of the type considered by van Vleck, namely, due to virtual transitions to excited crystal field levels. Considering only the excited Γ_4 state for the moment, in the ionic (zero hybridization) limit, this goes as $\chi_{vV}(0) \simeq g_J^2\mu_B^2| < \Gamma_3|J_z|\Gamma_4 > |^2/2\Delta$. As we shall discuss in Sec. 8.2, it was noted by Cox[1987b] that because of large magnetic moments the van Vleck susceptibility is sufficiently large to explain the measured $\chi(T)$ values in UBe_{13}. An open theoretical question is whether the form of $\chi_{vV}(T)$ is modified in an interesting (singular) way due to the singular character of the ground Γ_3 doublet. The temperature dependence in the ionic limit is exponential in that the saturation with diminishing T goes as $\exp(-\Delta/T)$. This is too weak a temperature dependence to fit any experiments on the relevant materials.

A qualified "yes" may be given as an answer to the question of whether χ_{vV} is modified in a singular way by the behavior of the Γ_3 ground doublet. To see why, we must delve in detail into the NCA diagrams for χ_{vV} which appear in Fig. 70. Using a $\tilde{\chi}_{vV}$ for the susceptibility with the magnetic matrix elements divided out, we have that

$$\tilde{\chi}''_{vV}(\omega,T) = \tilde{\chi}''_{vV,3\to4}(\omega,T) + \tilde{\chi}''_{vV,4\to3}(\omega,T) \tag{5.3.16}$$

with

$$\tilde{\chi}''_{vV,3\to4}(\omega,T) = \frac{\pi}{\pi\mathcal{Z}_f}\int d\epsilon \mathcal{A}_3^{(-)}(\epsilon,T)[\mathcal{A}_4(\omega+\epsilon,T) - \mathcal{A}_4(\epsilon-\omega)] \tag{5.3.17.a}$$

and

$$\tilde{\chi}''_{vV,4\to3}(\omega,T) = \frac{\pi}{\pi\mathcal{Z}_f}\int d\epsilon \mathcal{A}_4^{(-)}(\epsilon,T)[\mathcal{A}_3(\omega+\epsilon,T) - \mathcal{A}_3(\epsilon-\omega)] \quad . \tag{5.3.17.b}$$

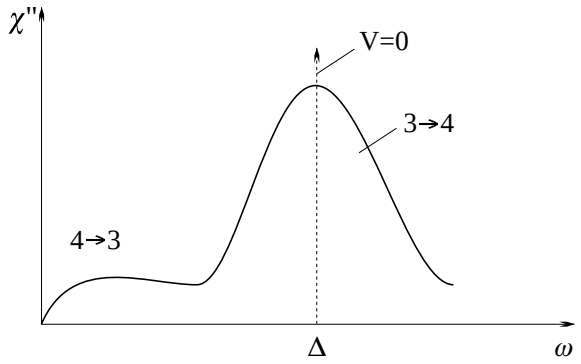

Figure 71: Schematic dynamic van Vleck susceptibility in the ionic and finite hybridization limits of the simplest U^{4+} Anderson model.

The first term corresponds to transitions from occupied Γ_3 states to Γ_4 states, while the second corresponds to transitions from occupied Γ_4 states to Γ_3 states. In the ionic limit, the former would give delta function absorption lines at $\omega = \pm\Delta$, while the latter would give no intensity at all since the Γ_3 state sits precisely at zero frequency. Moreover, the weight of Γ_4 in the ground state is zero since it may only be thermally occupied. This ionic limit result is sketched in Fig. 71..

The quantum broadening due to the Kondo effect allows for more interesting physics. As shown in Fig. 71, the delta-function lines of the ionic limit will be broadened out. These will still contain the bulk of the spectral response. However, since now the Γ_4 states acquire finite width, some quasielastic response due to the occupied $\Gamma_4 \rightarrow \Gamma_3$ transitions may now arise. The net weight in this quasielastic response will be proportional to the weight of Γ_4 in the ground state, as may be seen by integrating $(N_B(\omega)+1)\tilde{\chi}_{vV,4\rightarrow 3}(\omega,T)$ where $N_B(\omega) = (\exp(\omega/T)-1)$ is the Bose-Einstein factor. This gives the net spectral intensity in the dynamic structure factor for the $\Gamma_4 \rightarrow \Gamma_3$ transitions.

The question of the singularity in χ_{vV} now hinges on the behavior of the various spectral functions near to threshold. For simplicity, let us assume the limit of equal coupling coefficients. Applying the results of the $N = M = 2$ case from Sec. 5.1 together with $g_4 = g_3 + \Delta$, we see that the positive frequency spectral functions are

$$\mathcal{A}_3(\omega,0) \approx \theta(\omega - E_0)\frac{1}{T_0}\left(\frac{T_0}{2|\omega - E_0|}\right)^{1/2} \tag{5.3.18.a}$$

and

$$\mathcal{A}_4(\omega,0) \approx \theta(\omega - E_0)\frac{{T_0}^2}{\Delta}\left(\frac{2|\omega - E_0|}{T_0}\right)^{1/2} \quad . \tag{5.3.18.b}$$

Below E_0, the green's functions are purely real and given by

$$\mathcal{G}_3(\omega) \approx \frac{1}{T_0}\left(\frac{T_0}{2|\omega - E_0|}\right)^{1/2} \tag{5.3.19.a}$$

and

$$\mathcal{G}_4(\omega) \approx \frac{1}{\Delta} \quad . \tag{5.3.19.b}$$

What of the occupied state spectral functions? If we make Müller-Hartmann's *Ansatz* (Müller-Hartmann [1984]), then we have $\mathcal{A}_i^{(-)} = \alpha\mathcal{G}_i$ with $\alpha = \mathcal{Z}_f(0)/(2+3+2) = 1/7$ here, the denominator being the sum of all the level degeneracies. (see the discussion above Eq. (5.1.22)). With this *Ansatz*,

$$\mathcal{A}_3^{(-)}(\omega) \approx \frac{1}{7}\theta(E_0 - \omega)\frac{1}{T_0}\left(\frac{T_0}{2|\omega - E_0|}\right)^{1/2} \tag{5.3.20.a}$$

and

$$\mathcal{A}_4^{(-)}(\omega) \approx \frac{1}{7\Delta}\theta(E_0-\omega) \quad . \tag{5.3.20.b}$$

The applicability of the *Ansatz* is a crucial question. Clearly, it is nonsense for the *Ansatz* to apply to all excited levels because this would increase the denominator of α beyond any reasonable bound. Hence, it must fail for states which are too high in energy. Clearly it must work for the two propagators which are most divergent, since the model in that case is entirely equivalent to a multichannel model. It seems reasonable at least that it may apply to excited states which have sufficient overlap with the ground state in the sense of their quantum fluctuation induced occupancy.

If we accept the validity of the *Ansatz*, we obtain the following results for $\tilde{\chi}''_{vV}$:

$$\tilde{\chi}''_{vV,3\to 4}(\omega,0) \approx \frac{\pi^2\omega}{14\Delta^2} \tag{5.3.21}$$

$$\tilde{\chi}''_{vV,4\to 3}(\omega,0) \approx sgn(\omega)\frac{\sqrt{2}\pi}{7\Delta}\sqrt{\frac{|\omega|}{T_0}} \quad . \tag{5.3.22}$$

The $3 \to 4$ response is regular in ω, and if we calculate the corresponding $\chi(0)$ value, we obtain approximately $\tilde{\chi}_{vV,3\to 4}(0) \approx \sqrt{2}\pi/7\Delta$ which is very close to the ionic limit. The deviations at finite T are expected to go as T^2 since the dynamic response is analytic for $\omega \to 0$. If we roughly estimate the contribution from the $4 \to 3$ response, we obtain $\tilde{\chi}_{vV,4\to 3}(T) \approx (\sqrt{2}\pi/7\Delta)[1-\sqrt{(T/T_0)}]$. Hence, a $\sqrt{T}$ singularity seems to be observed which is a novel signature of the quadrupolar Kondo effect in the magnetic susceptibility.

The numerical evidence for the $\sqrt{T}$ behavior is mixed. For a set of calculations based on the present model with a single excited triplet level, the square root appears to be present in $\chi_{vV}(T)$ and $\lim_{\omega\to 0}(\chi''_{vV}(\omega,T)/\omega \sim 1/\sqrt{T}$. The latter quantity is important for an understanding of nuclear relaxation rates as we shall discuss further in Sec. 8.2. This is shown in Fig. 72 taken from Cox and Makivik [1994]. The model parameters for this run were chosen to give significant overlap between ground and crystal field levels in an effort to mock UBe_{13}, which we shall discuss further in Sec. 8.2. However, in runs with well separated crystal field levels, the static susceptibility appears to saturate as T^2 as shown in Fig. 5.23 from Kim *et al.* [1996]. The systematics of the $\sqrt{T}$ behavior remain unclear at the present time. Experimentally, the $\sqrt{T}$ form appears to describe the low temperature response in a number of materials as we shall discuss further in Sec. 8.2. It is quite clear that the quadrupolar Kondo effect does not substantially modify the zero temperature van Vleck susceptibility from the ionic limit.

Magnetic susceptibility: Contribution from the excited configuration. Because the excited configuration carries magnetic character, it will contribute a singular log-divergent term to the susceptibility. Of course, as we know from Sec. 6.1.4, this has a small pre-factor so that

$$\tilde{\chi}_7(T) \simeq \frac{W_{ch}^2}{T_0}\ln(T_0/T) \quad . \tag{5.3.23}$$

This must eventually overtake the leading constant behavior of the van Vleck susceptibility at sufficiently low temperatures. We can determine the temperature T_M^x at which this occurs by demanding $\tilde{\chi}_7(T) \approx \tilde{\chi}_{vV}(0) \approx 1/\Delta$. The result is

$$T_M^x = T_0\exp(\frac{T_0}{W_{ch}^2\Delta}) \approx T_0\exp(-\frac{\Gamma^2}{\pi^2 T_0\Delta}) \quad . \tag{5.3.24}$$

It would appear that unless Δ is quite large, this scale is too small to observe the expected logarithmic divergence. The only possible way out is if somehow W_{ch} is replaced by $\Gamma/\pi|\tilde{\epsilon}_f|$, the perturbative estimate which checks with the discussion of channel field splitting in the NRG analysis (c.f. Sec. 4.2.c.). Then the logarithmic divergence might be observable.

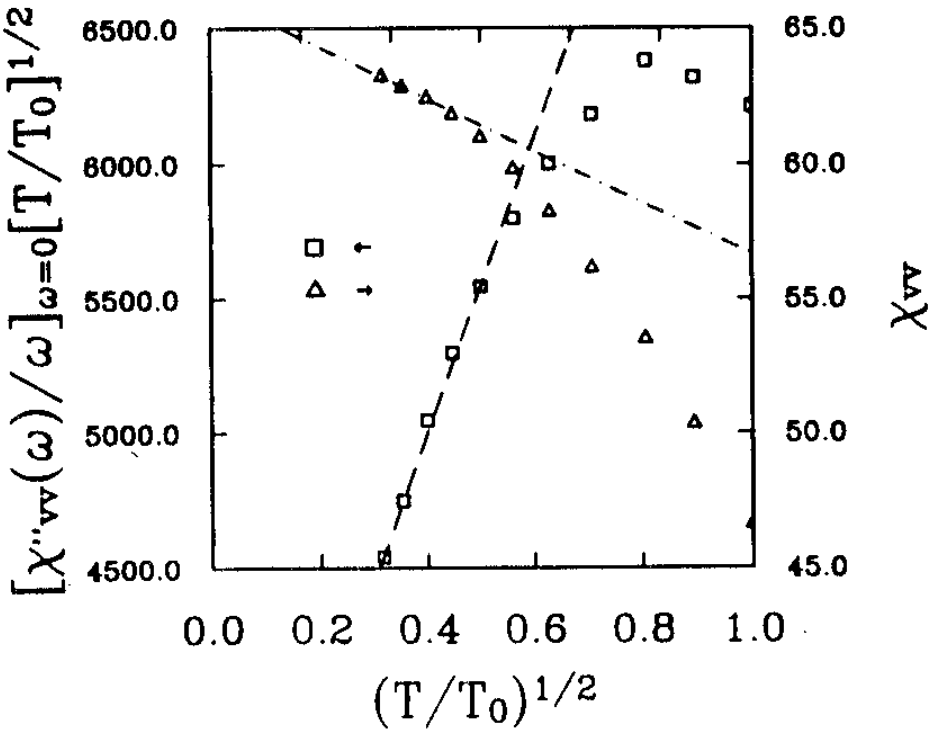

Figure 72: NCA calculations of χ_{vv} for the simplest U^{4+} ion model. Squares are the zero frequency limit of the imaginary part of the van Vleck susceptibility divided by frequency and multiplied by $(T/T_0)^{1/2}$, triangles are the static van Vleck susceptibility. Here the bare crystal field splitting is $\Delta(\Gamma_4) = 0.01D$ and $T_0 \approx 0.002D$. The matrix element coupling the Γ_3, Γ_4 states has been divided out. The dashed line is given by $(0.056/\Delta(\Gamma_4)k_BT_0)[1 + 1.95(T/T_0)^{1/2}]$ and the dash-dot line by $\chi_{vv}(0)[1 - 0.14(T/T_0)^{1/2}] = (0.66/\Delta)[1 - 0.14(T/T_0)]$. The ground state occupancies of the doublet and triplet are $n_3 = 0.56, n_4 = 0.23$. From Cox and Makivic [1994].

6 Conformal Field Theory and Abelian Bosonization Methods

In this section we shall discuss two powerful analytic methods for describing the low temperature physics of the multi-channel Kondo model. Both rely upon the ability to convert between bosons and fermions in 1(space)+1(time) dimensions. The spatial dimension here is the radial direction away from the impurity. The conformal field theory approach pioneered by Affleck and Ludwig in this context (Affleck [1990a]; Affleck and Ludwig [1991a,b,c;1992;1993]; Ludwig and Affleck [1991,1994]; Affleck *et al.* [1992]; Ludwig [1994a,b]; see also Tsvelik [1990]) is applicable to all versions of the Kondo model, Fermi liquid fixed point or not. This rests upon a description of low temperature states in terms of spin, channel, and charge degrees of freedom, and the ability to write conduction electron spin and channel operators in terms of "bosonic currents" which obey non-Abelian commutation relations (the Kac-Moody algebra). The charge operators are written in terms of conventional bosonic operators. The method may access both thermodynamic and dynamical quantities, but is restricted to low temperatures (asymptotically close to the critical point). We shall discuss this method in Sec. 6.1. A good review of the application of conformal field theory to a number of condensed matter problems is given in Affleck [1990b], and a recent review of the application to the Kondo problem may be found in Affleck [1995]. A recent reformulation of the problem by Maldacena and Ludwig [1996] in terms of Majorana fermions recovers the results of the previous work and makes explicit connection to the Abelian bosonization approach of Emery and Kivelson [1992] discussed in Sec. 6.2. We shall briefly discuss the Maldacena and Ludwig approach in Sec. 6.3.

For a particular highly anisotropic limit of the two-channel model, Emery and Kivelson [1992] (see also Sengupta and Georges [1994]) have shown that a purely Abelian bosonization scheme is possible to describe the physics. This approach leads to many results which overlap with the conformal theory, in particular providing a nice interpretation of the residual entropy and a simple expression for the dynamic susceptility of the impurity which agrees well with previous numerical NCA results [Cox, 1988(a)]. We shall discuss the abelian bosonization approach in Sec. 6.2. The application to transport coefficients is not transparent, but with the Majorana fermion formulation of the conformal theory produced by Maldacena and Ludwig [1996] the difficulties are resolved. We shall discuss this approach briefly in Sec. 6.3.

6.1 Conformal Field Theory Approach to the Kondo Model

Conformal field theory (CFT) has arisen in a number of contexts for describing two-dimensional critical phenomena, superstrings and other $1+1$ dimensional relativistic quantum field theories. Essentially, the theory exploits the absence of a length scale which occurs at critical points or in relativistic field theories together with the two dimensionality which assures invariance at the critical point under arbitrary conformal transformations which have spatially dependent scale factors. Hence, the conformal symmetry is much larger than the simpler dilatation invariance employed in the renormalization group. As a result, it can be used to fully specify critical exponents, correlation functions, and finite size spectra for a number of interesting models in field theory and two-dimensional critical phenomena. As shown by Cardy [1984,1986a,b], the CFT approach is not only useful for bulk problems, but also for problems with a boundary present. This is precisely the case for the Kondo model, which may be mapped to a $1+1$ dimensional relativistic field theory on the space+time half plane ($r > 0$, r the radial direction about the impurity site) where the 'speed of light' is the Fermi velocity v_F set by the linear dispersion of conduction electrons. The conformal invariance of the boundary condition (it is invariant under arbitrary conformal transformations with position and time dependent scale factors) assures the utility of the CFT technology. In a number of papers, Affleck and Ludwig (Affleck [1990a]; Affleck and Ludwig, [1991a,b,c]; Ludwig and Affleck [1991]; Affleck *et al.* [1992]; Affleck and Ludwig [1993]; Ludwig [1994a,b]) employed CFT in the presence of a boundary to work out the low temperature properties of the multi-channel Kondo model.

We shall divide our discussion of the conformal theory into three parts. First, in Sec. 6.1.1,

we lay out the ideas of bosonization and non-Abelian bosonization in particular and show how this leads to a complete if complicated description of free fermions. Next, in Sec. 6.1.2, we show how the complicated formulation for free fermions is quite natural for the Kondo problem, revealing in a remarkably simple way the "absorption" of the impurity spin into the many body spin density. Also, we show how finite size spectra and non-trivial operators at the impurity are readily generated within this approach through suitably chosen boundary conditions and "fusion" rules governing the absorption of the impurity spin into the many body spin density. Third, in Sec. 6.1.3, we outline how various thermodynamic quantities are obtained within the conformal theory approach. Finally, in Sec. 6.1.4, we focus on dynamical quantities such as the one-particle electron Green's function. Our intention in this section is to motivate the key ideas of the theory without reproducing in detail all the calculations presented in the papers of Affleck and Ludwig.

6.1.1 Non-Abelian Bosonization and Free Fermion Spectra

At the core of the conformal theory approach is the rewriting of the original Kondo Hamiltonian in terms of charge, spin, and channel-spin densities or "currents." This exploits the effective one-dimensional character of the problem. To review how this works, we follow Affleck [1990a] and Affleck and Ludwig [1991a] in the following order:
(a) First we review the mapping of three dimensions to one-dimension described in terms of left and right moving fermions on the half-axis (radial direction);
(b) We remind the reader of free fermion spectra in one-dimension for spinless and spin 1/2 one-channel fermions expressed in terms of the charge and spin of the excitations;
(c) Following Haldane [1981] we review how the spectrum of spinless one-dimensional fermions may be expressed in an Abelian bosonization approach;
(d) We then show how the spectrum of one dimensional spin 1/2 fermions may be recovered in a rather complicated way as a sum over commuting spin and charge Hamiltonians. The Kac-Moody algebra emerges naturally in this approach. In this free fermion case, spin and charge excitations are bound together in a way to reproduce free fermion excitations.
(e) We then outline how the multi-channel free fermion Hamiltonian may be written in terms of mutually commuting spin, charge, and channel Hamiltonians, where the spin and channel densities or currents both obey appropriate Kac-Moody commutation relations.
(f) Finally, we briefly comment on the generalization to arbitrary spin and channel degeneracy.

(a) Mapping of three-dimensions to one-dimension

This discussion follows closely Ludwig [1994a]. A similar discussion occurs in Krishna-Murthy, Wilkins, and Wilson [1980a], but here strict attention is paid to the boundary conditions and the appropriately defined one-dimensional fermion states. In the Kondo problem, only a particular set of conduction electron partial waves couples to the impurity spin or pseudo-spin. Although for real rare earth and actinide impurities these are likely to be dominantly of f symmetry about the ion, and for TLS sites they are considerably more complicated as indicated in Secs. 2 and 3, we shall make the simplifying assumption here that the impurity has an s-wave symmetry.

The s-wave projected part of a free electron annihilation operator with momentum $\vec{k}$ and spin and channel indices μ and α is given by

$$c_{k\mu\alpha} = \frac{k}{\sqrt{4\pi}} \int d\hat{k} c_{\vec{k}\mu\alpha} \quad . \tag{6.1.1}$$

The operators so defined obey continuum commutation relations. Corresponding to the momentum space operator is a real space operator

$$c_{\mu\alpha}(\vec{r}) = \frac{1}{i2\sqrt{2\pi r}} c_{\mu\alpha}(r) \quad . \tag{6.1.2}$$

The energy spectrum of the free electrons may be linearized about the Fermi momentum as is usual within some cutoff $\pm\Lambda$ about k_F so that $\epsilon_k = v_F(|k| - k_F)$. The physically relevant size of the cutoff scale is set by the Kondo temperature, *viz.*, $\Lambda \approx k_B T_K/\hbar v_F$. This reminds us that a continuum theory approach such as the CFT is useful only asymptotically below the low temperature energy scale.

We want to define left moving and right moving fields $\Psi_{p\mu\alpha}(r)$ (with "chirality index" $p = \pm$ for right or left) in the radial spatial dimension which have the rapid oscillations of order $\exp(\pm ik_F r)$ removed. Physically, a left-mover corresponds to an incoming spherical wave front, while a right mover corresponds to an outgoing spherical wave front. These operators are defined in terms of the $c_{k\mu\alpha}$ by

$$\Psi_{p\mu\alpha}(r) = \int_{-\Lambda}^{\Lambda} dk e^{-ipkr} c_{k_F+k,\mu\alpha} \quad . \tag{6.1.3}$$

In terms of these fields,

$$c_{\mu\alpha}(r) = e^{ik_F r}\Psi_{-,\mu\alpha}(r) - e^{-ik_F r}\Psi_{+,\mu\alpha}(r) \quad . \tag{6.1.4}$$

With this definition the free electron Hamiltonian near the Fermi energy can be written as

$$H_0 = \frac{iv_F}{2\pi}\int dr(\Psi^\dagger_{-,\mu\alpha}(r)\frac{d}{dr}\Psi_{-,\mu\alpha}(r) - \Psi^\dagger_{+,\mu\alpha}(r)\frac{d}{dr}\Psi_{+,\mu\alpha}(r)) \tag{6.1.5}$$

in position space and

$$H_0 = v_F \sum_{p,\mu\alpha}\int_{-\Lambda}^{\Lambda} dk pk \Psi^\dagger_{kp\mu\alpha}(r)\Psi_{kp\mu\alpha} \tag{6.1.6}$$

in momentum space.

Given the linear spectrum corresponding to massless fermions, the effective 'speed of light' of the problem is v_F. Moreover, the absence of a mass scale implies the absence of a length scale, which assures the equivalence of space and time axes and conformal invariance, the invariance of the system under arbitrary conformal transformations in the $1+1$ dimensional plane. We shall think of the time axis in terms of imaginary time, so that it becomes infinite only at $T = 0$. At first site it might appear that conformal invariance is violated by the boundary, (only positive r is allowed). However, the half-plane is indeed conformally invariant and may be mapped back to the full plane. Also, any finite strip may be mapped reversibly to the half plane, a fact which is useful for determining finite size spectra, allowed operators in the problem, and finite temperature correlation functions as we shall discuss in Secs. (6.1.2,3,4).

To specify the theory further it is necessary to introduce boundary conditions. First, the left and right moving fermions are not independent. At the origin, $\Psi_{+,\mu\alpha}(0) = \Psi_{-,\mu\alpha}(0)$. Thus one may eliminate the right moving fermions completely and express the physics in terms of the left movers by artificially extending to negative r and setting $\Psi_{+,\mu\alpha}(r) = \Psi_{-,\mu\alpha}(-r)$. Assuming the system to have a size l in the radial direction, Affleck and Ludwig [1991a,b] then typically assume

$$\Psi_{-,\mu\alpha}(l) = -\Psi_{-,\mu\alpha}(-l) \quad . \tag{6.1.7}$$

This boundary condition is typically denoted F^- by Affleck and Ludwig, and with the opposing sign on the right hand side the boundary condition is referred to as F (see Ludwig [1994a]). This specifies completely the effective one-dimensional theory. We may take as a convention that only the left moving branch couples to the impurity. We will typically write the momentum integral in discrete form to follow closely the conventions of Affleck and Ludwig. We depart from their convention on notating left and right movers slightly (they use simply L to denote left and R to denote right). This choice is of some convenience in the discussion of bosonization algebras that follows below. When we discuss the Kondo problem in more detail in Sec. 6.1.2, we will return to their convention.

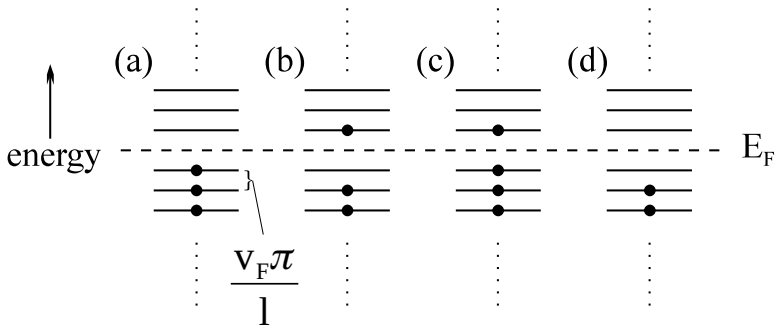

Figure 73: Low lying excitations of a single branch for a one-dimensional spinless Fermion gas. The shown levels are only for left (or right) moving electrons. The boundary conditions of Eq. (6.1.7) are chosen so that the ground state (filled Fermi sea) shown in (a) is non-degenerate. The excitations may be charge neutral, such as the particle-hole pair excitation of (b). The two lowest charge 1 excitations are shown in (c), where an electron is added, and (d) where a hole is added (electron removed).

Note that the linearization approximation is common in one-dimension. We shall usually not explicitly write the cutoff in which makes this treatment equivalent to the Luttinger model for the effective 1D system (Haldane [1981]).

(b) Spectrum of non-interacting spinless and spin 1/2 fermions in one dimension

The energy levels and states of one-dimensional free fermions may be specified completely in terms of the charge and spin relative to the ground state together with the number of excited electron hole pairs relative to the ground state. In the following discussion, we follow Affleck [1990a] and Affleck and Ludwig [1991a].

To remind the reader, we first focus on the case of spinless fermions. With the boundary condition of Eq.(6.1.7), the allowed k vectors for left moving fermions are given by $k_n = -\pi v_F/l(n+1/2)$ with $n = 0, \pm 1, \pm 2, ...$ The corresponding single particle energies are $\epsilon_n = -v_F k_n$. The ground state is obtained by filling all one particle levels below zero energy at which the Fermi level resides. This situation is shown in Fig. 73(a). We may excite relative to the ground state in two ways. First, we can create a particle hole excitation. This is shown in Fig. 73(b), where an electron below the Fermi energy is promoted above the Fermi energy. These excitations always raise the energy by integral multiples of $\pi v_F/l$. The second kind of excitation is effected by adding or removing charge from the Fermi sea. The simplest processes are shown in Figs. 73(c,d). The lowest energy to add or remove charge Q is obtained when states are sequentially filled, leading to an elementary sum for evaluation of the energy which gives $E(Q,0) = \pi v_F Q^2/2l$. Putting these two kinds of excitations together, we see that the energy spectrum for free left moving spinless fermions subject to the boundary condition Eq. (6.1.7) on a system size $2l$ are given by

$$E(Q, n_Q) = \frac{\pi v_F}{l}[\frac{Q^2}{2} + n_Q] \tag{6.1.8}$$

where Q counts the added charge (which may be positive or negative) and n_Q the number of particle-hole pairs. The states corresponding to these excitations are of course simple Slater determinants.

This kind of argumentation may now be straightforwardly extended to spin 1/2 fermions. Clearly, we can view the spectrum for spin 1/2 as a direct product of up- and down-spin electron spectra so that the energies add for the two independent branches. Hence we can define a charge Q_μ for each branch together with particle-hole excitation quantum numbers. Now, define the total charge of an excitation as $Q = Q_\uparrow + Q_\downarrow$ and the z component of the spin as $S_z = (Q_\uparrow - Q_\downarrow)/2$. Since $\sum_\mu Q_\mu^2/2 = Q^2/4 + S_z^2$, and $S_z^2 = S(S+1)/3$ for an excitation of spin S, we see that the total energy

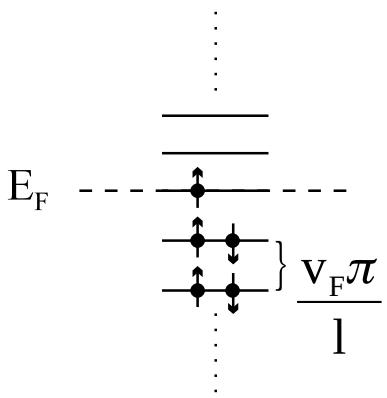

Figure 74: Ground state for spin 1/2 fermions in one-dimension for the boundary condition $\Psi_\mu(l) = \Psi_\mu(-l)$. In this case, the highest most occupied level is a zero mode, and we choose the charge reference to correspond to single occupancy of this level, whence charge and spin quantization conditions are reversed relative to the boundary conditions of Fig. 73.

can be written as

$$E(Q,S,n_Q,n_s) = \frac{\pi v_F}{l}[\frac{Q^2}{4} + \frac{S(S+1)}{3} + n_Q + n_S] \tag{6.1.9}$$

where $n_Q + n_s$ is a combination of particle hole excitations in the different spin branches. Note that not all values of Q, S are allowed. Strictly speaking, the S values must be restricted to 0,1/2. For integer spin, all other S_z^2 values can be reached from $S = 0$ by adding integers to zero spin, and all other S_z^2 values for half integer spin can be reached from $S = 1/2$ by adding integers. Hence, these are equivalent to particle hole excitations from the fundamental values. Also, there is a "gluing" condition on the excitations: if Q is even, then $2S_z$ must be an even integer, while if Q is odd, then $2S_z$ must be an odd integer.

For a different choice of boundary condition, $\Psi_\mu(l) = \Psi_\mu(-l)$, the k values are shifted to $-\pi n/l$ and now the upper most occupied energy is at zero. This corresponds to a $\pi/2$ phase shift of the levels considered in the previous paragraph. The corresponding level spectrum for the left moving branch is shown in Fig. 74. Note that there is a four fold degeneracy ($S = 1/2, Q = 0$ or $S = 0, Q = \pm 1$) to the ground state because of the presence of a zero energy state. The charge may be shifted by one unit to accomodate this phase shift, and the charge spin gluing conditions are reversed as a result. Even charge requires odd values of $2S_z$, and odd charge requires even values of $2S_z$. We note that the NRG free fermion Hamiltonians for odd N correspond to the boundary condition of Eq. (6.1.7) and for even N they correspond to the reversed boundary condition.

(c) Abelian Bosonization approach to the spinless fermion spectrum

The goal in this subsection is to show how the spectrum of Eq. (6.1.8) can be reproduced with an appropriate choice of bosonic operators which simply coincide with the momentum space charge density operators.

Here we closely follow Haldane [1981], who uses a system length L, to be compared with our $2l$. We now include both left and right moving fermions indexed by $p = \mp$, respectively. With k measured relative to the Fermi energy, the free Hamiltonian is given by

$$H_0 = \sum_{k,p} v_F p k \Psi^\dagger_{kp} \Psi_{kp} \quad . \tag{6.1.10}$$

We now introduce the density operators J_{qp} of momentum q and chirality index p which are

given by

$$J_{qp} = \sum_k [\Psi^\dagger_{k+q,p}\Psi_{k,p} - < \Psi^\dagger_{k+q,p}\Psi_{k,p} >_0] \tag{6.1.11}$$

where the second term "normal orders" the density operator, and refers to the ground state expectation value of the operator with respect to H_0. This term regularizes the density operator in such a way as to remove any divergences due to the occupied "positron sea" in our Luttinger model spectrum (the right and left movers are allowed to have positive and negative momenta). This particular regularization choice can be maintained at finite temperature and for an interacting model. Our notational choice of J to designate the density follows the convention of Affleck and Ludwig. The density operators in real space at $l, -l$ must have the same value and thus q runs over integer multiples of π/l. For q=0, J_{qp} is simply Q_p, the charge in each branch.

The density operators obey a simple commutation relation which is exact in this Luttinger formulation (though it will have band edge corrections in general–see Mahan [1990] pp. 324-343) which is

$$[J_{qp}, J_{q'p'}] = \delta_{p,p'}\delta_{q+q',0}\frac{pql}{\pi} \quad . \tag{6.1.12}$$

This relation is easily verified by considering simply the operator parts of (6.1.11) which give a sum that must be regularized due to the occupied sea, *viz.*

$$[J_{qp}, J_{q'p'}] = \delta_{p,p'}(J_{q+q',p} - J_{q+q',p}) + \delta_{p,p'}\delta_{q+q',0}\sum_k [< n_{k+q',p} >_0 - < n_{k,p} >_0] \tag{6.1.13}$$

The first term follows from the operator output of the commutator, and the second term from the regularization procedure. The expectation values simply give zero temperature Fermi functions, and the difference is non-vanishing only for a width q in momentum space, meaning that the sum gives pql/π, since the spacing between q points is π/l. Although the first term in Eq. (6.1.13) is clearly zero, we write it suggestively to indicate what will happen when the density operators involve internal degrees of freedom. In that case the second term will still arise but the first term will no longer cancel, and this is the source of the Kac-Moody algebra for the spin and channel degrees of freedom. The vanishing of this first term leads to the 'Abelian' nomenclature, while the non-vanishing of this first term when internal degrees of freedom are present is what leads to a 'Non-Abelian' label, corresponding to a Non-Abelian group symmetry for the Hamiltonian. The nomenclature is in precise accordance with that used in gauge field theories.

We note that Eq. (6.1.12) is reminiscent of the commutation relations for free bosons. To continue this observation it is straightforward to verify by use of (6.1.10), (6.1.11) that

$$[H_0, J_{qp}] = v_F pq J_{qp} \quad . \tag{6.1.14}$$

This is reminiscent of the commutation relation of a boson raising operator. In particular, if the product qp is positive, this is exactly the case. However, some normalization is required to define a suitable boson creation operator. Following Haldane, this is given for $|q| > 0$ as

$$a^\dagger_q = \sqrt{\frac{\pi}{|q|l}}[\theta(-q)J_{q,-} + \theta(q)J_{q,+}] \quad . \tag{6.1.15}$$

This operator satisfies $[H_0, a^\dagger_q] = v_F|q|a^\dagger_q$, and together with its Hermitian conjugate obeys the canonical boson commutation relation. Physically, these operators create particle-hole pairs of momentum q. This does not specify the energy due to addition or removal of charge with respect to the ground state. This can be written in terms of $J_{0,\pm}$. As a result, the now "bosonized" Hamiltonian can be written as

$$H_0 = \sum_{|q|>0} v_F|q|a^\dagger_q a_q + \sum_p \frac{v_F\pi}{2l}J^2_{0,p} \tag{6.1.16}$$

which can be rewritten as an unrestricted q sum

$$H_0 = \frac{\pi v_F}{2l} \sum_q [\theta(-q) J_{-q,-} J_{q,-} + \theta(q) J_{q,+} J_{-q,+}]$$

$$= \frac{\pi v_F}{2l} \sum_{q,p} : J_{qp} J_{-qp} : \tag{6.1.17}$$

which defines the "normal ordering" of the density operators. Clearly, the structure of this Hamiltonian reproduces faithfully the finite size energy spectrum of Eq. (6.1.8) for spinless fermions.

Strictly speaking, to prove that this is a faithful representation of the Hamiltonian, we need to prove that the states specified by the J_{qp} quantum numbers (occupancies of $q \neq 0$ states and charges Q_p) are complete. To do this, Haldane [1981] further introduces a ladder operator $U_p^\dagger$ which adds a unit of charge to Q_p each time it is applied. The states specified by Eqs. (6.1.12), (6.1.14), and (6.1.15) are then

$$|\{Q_p\}, \{n_{q,p}\}> \sim \prod_{qp>0} [J_{qp}]^{n_{q,p}} \prod_p [U_p^\dagger]^{Q_p} |0> \quad . \tag{6.1.18}$$

Haldane gives a simple and elegant proof of completeness by comparing the partition function for the free fermion case with that found from Eq. (6.1.17). They are in exact agreement indicating that no states are omitted from Eq. (6.1.18).

(d) Non-Abelian Bosonization of the Spin 1/2 Free Fermion spectrum

Now we follow the various papers of Affleck and Ludwig (particularly Affleck [1990a], Affleck and Ludwig [1991a,b], Ludwig [1994a]). Some key technical details of the decomposition are arrived at in the work of Altschüler, Bauer, and Itzykson [1990]. As in the previous section, we introduce left and right moving densities, now for both charge and spin:

$$J_{qp} = \sum_{k\mu} \Psi^\dagger_{k+q,p\mu} \Psi_{kp\mu} \tag{6.1.20}$$

$$\vec{J}_{qp} = \sum_{k\mu\nu} \frac{\vec{\sigma}_{\mu\nu}}{2} \Psi^\dagger_{k+q,p\mu} \Psi_{kp\nu} \quad . \tag{6.1.21}$$

Note that $[J_{qp}, \vec{J}_{q'p'}] = 0$, so the charge and spin degrees of freedom are decoupled in these densities. As in the spinless case, the operator $J_{0,p}$ simply counts the total charge in branch p, and the operator $J^c_{0,p}$ measures the total z component of spin in branch p.

Because of the spin degrees of freedom, the commutation relation (6.1.12) is modified to

$$[J_{qp}, J_{q'p'}] = \delta_{q+q',0} \delta_{pp'} \frac{2pql}{\pi} \tag{6.1.22}$$

where the factor of 2 arises from the spin sum in the ground state expectation value term of Eq. (6.1.13). On the other hand, the commutator with the Hamiltonian is unchanged, as may be verified by direct calculation with the free fermion form of Eq. (6.1.10) (augmented by a sum over spin degrees of freedom). Hence there is a charge term in the Hamiltonian still, but with a different normalization than Eq. (6.1.17) because of the factor of 2 in the commutation relation (6.1.22). We may write this as

$$H_{Q0} = \frac{\pi v_F}{4l} \sum_{qp} : J_{qp} J_{-qp} : \quad . \tag{6.1.23}$$

We note that the q=0 terms in this sum reproduce the Q_p^2 term in Eq. (6.1.9) for the energy of spin 1/2 free fermion excitations, and the $q \neq 0$ terms generate the particle-hole excitations corresponding to the n_Q term in (6.1.9).

Turning to the spin density, we may evaluate its commutation relation in a way precisely analogous to that of Eq. (6.1.13). However, in this case the operator dependent term does not cancel out because of the presence of the non-commuting Pauli matrix factors in Eq. (6.1.21). The result is (with Einstein summation convention on the spin components)

$$[J^a_{qp}, J^b_{q'p'}] = i\epsilon_{abc}\delta_{pp'}J^c_{q+q',p} + \delta_{ab}\delta_{pp'}\delta_{q+q',0}\frac{pql}{2\pi} \quad . \tag{6.1.24}$$

This is the so called 'level 1' $SU(2)$ Kac-Moody algebra. The 'level' is read off from the second term (which arises from the ground state subtraction) and is simply the overall numerical coefficient of the factor $\frac{pql}{2\pi}$. When we add channel degrees of freedom this will be modified to M due to the free sum over channel degrees of freedom in the ground state subtraction. The $SU(2)$ of course refers to the spin algebra of the density operators reflected in the first term of (6.1.24). (Note that the factor of 2 in Eq. (6.1.22) from the correponding ground state subtraction term is cancelled here by the factor of 1/4 from the product of spin matrices.)

Just as for the ordinary angular momentum algebra one can specify irreducible representations by the construction of raising and lowering operators, one can do the same with the Kac-Moody algebra. The irreducible representations of the $SU(2)$ level M Kac-Moody algebra specified by Eq. (6.1.24) consist of 'primary' states for each branch p with allowed spin s_p restricted by $0 \leq s_p \leq M/2$ along with 'descendants' which contain particle-hole pair excitations generated by acting on the primary states with operators J^a_{qp} where qp is positive. In the present case with $M = 1$, the allowed s_p values are $0, 1/2$, consistent with our discussion in Sec. (6.1.1.b). The set of a given primary state together with its descendants is known as a 'conformal tower.' High spin states can only be contained in the descendant sectors.

As with the charge density, one can compute the commutator of the current density with the free Hamiltonian to find if a bosonized structure is possible. By direct computation with the free fermion form of (6.1.10) (augmented by spin) one finds

$$[H_0, J^a_{qp}] = v_F qp J^a_{qp} \tag{6.1.25}$$

which suggests that the spin part of the free Hamiltonian can be written as a quadratic form $H_{sp,0} = A\sum_{qp} : \vec{J}_{qp} \cdot \vec{J}_{-qp} :$. As in the case of the charge, the $q = 0$ terms generate the added spin energy $\sim s(s+1)/3$ in Eq. (6.1.9), and the $q \neq 0$ terms generate the particle-hole pairs that carry net spin. The normalization A can be fixed by commuting this form with the spin density and matching to Eq. (6.1.25). This gives

$$[H_{sp,0}, J^a_{qp}] = A\{\frac{pql}{\pi}J^a_{qp} + i\epsilon_{bac}\sum_{q'} J^b_{-q'p}J^c_{q+q',p}[\theta(pq') - \theta(p[q'+q])\}$$

$$= A\frac{(1+2)pql}{\pi}J^a_{qp} = \frac{3Apql}{\pi}J^a_{qp} \tag{6.1.26}$$

where the '1' in the numerator follows from the ground state subtraction part of the Kac-Moody commutator in (6.1.24) and the '2' follows from the operator part. Note that $2\delta_{cd} = \epsilon_{abc}\epsilon_{abd}$ generates the '2'. This is important for Sec. (6.1.1.f) where we remark on the generalization to arbitrary spin and channel.

By comparing Eq. (6.1.26) with (6.1.25) we specify A and hence can write the free Hamiltonian as the sum of spin and charge parts with

$$H_0 = \frac{\pi v_F}{l}[\frac{1}{4}\sum_{qp} : J_{qp}J_{-qp} : + \frac{1}{3}\sum_{qp} : \vec{J}_{qp} \cdot \vec{J}_{-qp} :] \quad . \tag{6.1.27}$$

This representation of H_0 in terms of quadratic forms in the density operators is known as the 'Sugawara form' of the Hamiltonian. Clearly, these quadratic forms reproduce the energies of Eq. (6.1.9) obtained by elementary considerations, where the $q = 0$ terms generate the Q^2 and $S(S+1)$ terms in that equation, and the $q \neq 0$ terms generate the particle-hole pair excitations. Obviously the non-Abelian bosonization is not the easiest way to obtain these energies in the free case; its merit lies in the interacting case we discuss in Sec. (6.1.2). The corresponding states can be constructed in complete analogy with Eq. (6.1.18) for the spinless case, where we now have a direct product of boson Fock spaces spanned by the charge and spin excitations. The complete specification of allowed states must satisfy the fermion gluing rules discussed in Sec. (6.1.1.b), so that odd(even) Q is matched with odd(even) $2S_z$. This corresponds to the boundary condition of Eq. (6.1.7), and as remarked in Sec. (6.1.1.b) these are reversed if we change the sign in that boundary condition corresponding to a $\pi/2$ phase shift.

(e) Generalization to Include Channel Degrees of Freedom

If we now include channel degrees of freedom, we need to introduce additional density operators for these channel excitations. We now use a subscript s to denote spin density operators, and a subscript c for channel density operators. The definitions of the charge, spin, and channel densities become

$$J_{qp} = \sum_{q\mu\alpha} \Psi^\dagger_{k+q,p\mu\alpha} \Psi_{kp\mu\alpha} \quad , \tag{6.1.28}$$

$$\vec{J}_{sqp} = \sum_{q\mu\nu\alpha} \frac{\vec{\sigma}_{\mu\nu}}{2} \Psi^\dagger_{k+q,p\mu\alpha} \Psi_{kp\nu\alpha} \quad , \tag{6.1.29}$$

and

$$\vec{J}_{cqp} = \sum_{q\mu\alpha\beta} \frac{\vec{\sigma}_{\alpha\beta}}{2} \Psi^\dagger_{k+q,p\mu\alpha} \Psi_{kp\mu\beta} \quad . \tag{6.1.30}$$

The commutation relations for the operators amongst themselves are

$$[J_{qp}, J_{q'p'}] = \delta_{q+q',0} \delta_{pp'} \frac{4pql}{\pi} \quad , \tag{6.1.31}$$

$$[J^a_{sqp}, J^b_{sq'p'}] = i\epsilon_{abc}\delta_{pp'} J^c_{s,q+q',p} + \delta_{ab}\delta_{pp'}\delta_{q+q',0}\frac{pql}{\pi} \quad , \tag{6.1.32}$$

and

$$[J^a_{cqp}, J^b_{cq'p'}] = i\epsilon_{abc}\delta_{pp'} J^c_{c,q+q',p} + \delta_{ab}\delta_{pp'}\delta_{q+q',0}\frac{pql}{\pi} \quad . \tag{6.1.33}$$

Hence both the spin and channel densities satisfy level 2 $SU(2)$ Kac-Moody algebras. As such, the primary states of spin are restricted to values $S_p = 0, 1/2, 1 = M/2$ and those of channel spin (also an $SU(2)$ field) to $S_{cp} = 0, 1/2, 1 = N/2$ where $N = 2$ is the conduction spin degeneracy. The commutation relations of J_{qp}, J^a_{sqp} with the free particle Hamiltonian (6.1.7) (augmented to include spin and channel degrees of freedom) are unchanged from Eqs. (6.1.14) and (6.1.25). To this we add the commutation relation of J^a_{cqp} with the free Hamiltonian which has the same form

$$[H_0, J^a_{cqp}] = v_F qp J^a_{cqp} \quad . \tag{6.1.34}$$

Hence, proceeding along the lines of Secs. (6.1.1.c,d), we write the free particle Hamiltonian in terms of mutually commuting charge, spin, and channel quadratic forms (the 'Sugawara' representation) as

$$H_0 = \frac{\pi v_F}{l} \sum_{qp} [\frac{1}{8} : J_{qp} J_{-qp} : + \frac{1}{4} : \vec{J}_{sqp} \cdot \vec{J}_{s,-q,p} : + \frac{1}{4} : \vec{J}_{cqp} \cdot \vec{J}_{c,-q,p} :] \quad . \tag{6.1.35}$$

This creates free-fermion excitations which are tensor products of states in the charge, spin, and channel spin boson Fock spaces in each of the left and right moving branches, created from the primary states and descendants generated by application of density operators with positive qp values. The states are classified in terms of their primary charge (Q_p), spin S_p, and channel spin S_{cp} for each branch, along with integers characterizing the number of bosonic excitations, with energies give by

$$E = \frac{\pi v_F}{l} \sum_p [\frac{Q_p^2}{8} + \frac{S_p(S_p+1)}{4} + \frac{S_{cp}(S_c+1)}{4} + n_{Qp} + n_{Sp} + n_{Cp}] \tag{6.1.36}$$

which is an obvious generalization of Eq. (6.1.9). The spectrum is again subject to a fermion gluing condition and boundary conditions which can shift the spin/charge/channel gluing conditions.

Note that this representation of the free Hamiltonian is not unique. It is quite convenient for treating the Kondo problem, however. We could, for example, write down a Sugawara form for the larger $U(1) \times SU(4)$ symmetry deriving from overall rotations in spin and channel-spin space (Affleck and Ludwig, [1991b]). However, the coupling to the impurity will break this symmetry down into the $U(1) \times SU(2) \times SU(2)$ considered in Eq. (6.1.35). Obviously we could also write down an Abelian bosonization scheme for each branch, spin, and channel-spin index in terms of the charge densities restricted to each independent fermion branch. A different representation for the energies could then be generated by rewriting the charge for each value of spin and channel-spin indices in each branch p in terms of Q, S^z, S_c^z and the 'double-tensor' spin-channel operator $S^z S_c^z$. This scheme does not appear manifestly rotationally invariant in either the spin or channel spin sectors, however. The interesting thing is that this representation is closely related to the Abelian bosonization scheme developed by Emery and Kivelson. That approach has extra complications associated with 're-fermionization' as we discuss in Sec. 6.2.

(f) Generalization to Arbitrary Spin and Channel Degeneracy

If we now assume the fermion spins are N-fold degenerate and the channel spins are M fold degenerate, we must generalize our definitions of the spin and channel densities to $SU(N), SU(M)$ form. These are best specified in terms of the N^2-1 generators of $SU(N)$ $\mathcal{T}_N^a$, $a = 1, 2, ...N^2-1$ with normalization condition $Tr(\mathcal{T}_N^a \mathcal{T}_N^b = \delta_{ab}/2$ and commutation relations $[\mathcal{T}_N^a, \mathcal{T}_N^b] = i f_{abc}^{(N)} \mathcal{T}_N^c$ where $f_{abc}^{(N)}$ is the structure factor of the $SU(N)$ Lie algebra (see, for example, Hammermesh [1961]). Similar generators $\mathcal{T}_M^a$ should be introduced for the $SU(M)$ channel spin symmetry. Note that the structure constants satisfy $f_{abc}^{(N)} f_{abd}^{(N)} = N\delta_{cd}$. In the $SU(2)$ case, $f_{abc}^{(2)} = \epsilon_{abc}$.

The new density operators are thus defined as

$$J_{qp} = \sum_{q\mu\alpha} \Psi^\dagger_{k+q,p\mu\alpha} \Psi_{kp\mu\alpha} \quad , \tag{6.1.37}$$

$$J^a_{sqp} = \sum_{q\mu\nu\alpha} \mathcal{T}_N^a \Psi^\dagger_{k+q,p\mu\alpha} \Psi_{kp\nu\alpha} \quad , \tag{6.1.38}$$

and

$$J^a_{cqp} = \sum_{q\mu\alpha\beta} \mathcal{T}_M^a \Psi^\dagger_{k+q,p\mu\alpha} \Psi_{kp\mu\beta} \quad . \tag{6.1.39}$$

The commutation relations for the operators amongst themselves are

$$[J_{qp}, J_{q'p'}] = \delta_{q+q',0} \delta_{pp'} \frac{2MNpql}{\pi} \quad , \tag{6.1.40}$$

(6.1.41) $$[J^a_{sqp}, J^b_{sq'p'}] = if^{(N)}_{abc}\delta_{pp'}J^c_{s,q+q',p} + \delta_{ab}\delta_{pp'}\delta_{q+q',0}\frac{Mpql}{2\pi} \quad ,$$

and

(6.1.42) $$[J^a_{cqp}, J^b_{cq'p'}] = if^{(M)}_{abc}\delta_{pp'}J^c_{c,q+q',p} + \delta_{ab}\delta_{pp'}\delta_{q+q',0}\frac{Npql}{2\pi} \quad .$$

The spin(channel-spin) densities thus obey $SU(N)(SU(M))$ Kac-Moody algebras of level $M(N)$. There are restrictions on allowed primary states which are not however as readily written down as in the $SU(2)$ case described in Sec. (6.1.1.e).

The commutation relations of the charge, spin, and channel-spin densities with the suitably generalized free particle Hamiltonian are unchanged from the discussion in the preceding sections. The appropriately defined Sugawara Hamiltonian may be determined precisely as before, and the result is

(6.1.43) $$H_0 = \frac{\pi v_F}{l}\sum_{qp}[\frac{1}{2MN} : J_{qp}J_{-qp} : + \frac{1}{M+N} : \hat{J}_{sqp}\cdot\hat{J}_{s,-q,p} : + \frac{1}{M+N} : \hat{J}_{cqp}\cdot\hat{J}_{c,-qp} :]$$

where $\hat{J}_{sqp}(\hat{J}_{cqp})$ are vectors in the $N(M)$ dimensional tensor space transforming under $SU(N)(SU(M))$ rotations. The states are again tensor products of vectors from the charge, spin, and channel-spin boson Fock spaces for each branch p. These are subject to suitably generalized fermion gluing conditions. The single particle energies corresponding to Eq. (6.1.36) are exactly analogous except that the $S_p(S_p+1)$ and $S_{cp}(S_{cp}+1)$ terms are generalized to the quadratic Casimirs for each of the primary states. These may be worked out with suitable Lie group technology as has been done, for example, for the $M=3, N=2$ model (Affleck and Ludwig [1991b]).

6.1.2 Non-Abelian Bosonization Formulation of the Kondo Hamiltonian

In this subsection we shall review how Affleck and Ludwig developed a Non-Abelian bosonization formulation of the Kondo Hamiltonian. The outline of the subsection is as follows: in (6.1.2.a) we show how at special values of the exchange coupling, the impurity spin is 'absorbed' by the conduction electrons yielding a Hamiltonian which is still of the Sugawara form discussed in the previous subsection with new current operators which still obey the Kac-Moody algebra. The working hypothesis is that the special coupling values correspond to the low temperature fixed points of the Kondo model. The states however are subjected to new *non-fermionic* 'fusion' rules developed by Affleck and Ludwig [1991b; Ludwig, 1994] which precisely state how the spin, charge, and channel-spin degrees of freedom are restricted. While these quantum numbers are restricted to fermionic gluing conditions for exactly compensated $S_I = M/2$ models, they are 'freed up' in the overcompensated case, yielding a finite size spectrum which is no longer that of a Fermi liquid. Hence, as in the case of interacting one-dimensional metals which display non-Fermi liquid behavior, spin-charge-channel separation occurs in the multichannel overcompensated Kondo model. In Sec. (6.1.2.b) we discuss how the operator spectrum of the model may be determined by a finite size calculation with modified boundary conditions. This allows one to generate the allowed non-trivial operators which can effect the critical behavior on approach to the fixed point as well as cross-over phenomena in the presence of applied fields that break the spin and channel-spin symmetry. In Sec. (6.1.2.c), we discuss the effects of various perturbations on the finite size spectra following the work of Affleck *et al.* [1992].

(a) Sugawara form of the Kondo Hamiltonian: Absorption of the Impurity Spin

As discussed in (6.1.1.a), the lack of independence of left and right moving fermions in the one-dimensional radial half-space of the Kondo model means that we can eliminate the right movers from the problem with the suitable mirroring into the $r < 0$ half-plane. This means the Kondo exchange

interaction can be written solely in terms of the impurity spin together with the left-moving spin current. Restricting to spin 1/2 conduction electrons, the result is

$$H_K = \frac{\pi v_F}{l} \lambda \sum_q \vec{J}_{sqL} \cdot \vec{S}_I \tag{6.1.44}$$

where $\lambda = N(0)|J|$ is the dimensionless coupling constant. Note that we have now favored the L, R notation of Affleck and Ludwig over the p notation used in the previous subsection. Right movers will henceforth be dropped from the discussion. The free Hamiltonian for left movers is written in the Sugawara form discussed in the previous subsection.

Perhaps the most central component of Affleck and Ludwig's [Affleck, 1990a; Affleck and Ludwig, 1991a,b,c; Ludwig, 1994] work is the observation that for certain special values of λ, it is possible to 'complete the square' of the spin term in the free Hamiltonian to absorb the impurity term. leaving behind a trivial constant in the energy. Specifically, when $\lambda = 2/(2+M)$, we can write

$$H_{sp} = H_{0sp} + H_K = \frac{\pi v_F}{l} \frac{1}{2+M} \sum_q : \vec{\mathcal{J}}_{sqL} \cdot \vec{\mathcal{J}}_{s,-q,L} : \tag{6.1.45}$$

where the shifted spin density operator is simply

$$\vec{\mathcal{J}}_{sqL} = \vec{J}_{sqL} + \vec{S}_I \quad . \tag{6.1.46}$$

These new spin densities *still* obey the Kac-Moody algebra specified by Eq. (6.1.41) (with N=2). Because only the spin degrees of freedom are modified, the charge and channel parts of the free Hamiltonian in Eq. (6.1.43) are left unchanged.

Because the Hamiltonian with the absorbed impurity spin remains a quadratic form in the charge, spin, and channel-spin densities, the form of the energies is unchanged from Eq. (6.1.36) in the two-channel case ($M = 2$), and indeed in general from Eq. (6.1.43). However, what differs are the constraints on allowed states. Affleck and Ludwig [1991(b); Ludwig, 1994] made a "fusion rule" hypothesis to determine which states would be allowed in the new Hamiltonian with the absorbed spin. First, they apply a generalization of the $SU(2)$ triangle rule appropriate for adding spins in the Kac-Moody algebra. Restricting attention to $N = 2$, define S as the total spin of a primary state in a conformal tower in the shifted Hamiltonian specified by Eqs. (6.1.45,46), and S' as the conduction part of that spin. The generalized triangle rule is

$$|S' - S_I| \leq S \leq min\{S' + S_I, M - S' - S_I\} \quad . \tag{6.1.47}$$

Note that since the maximal primary spin in a conformal tower is $M/2$ that the right hand side of (6.1.47) assures that the primary spin in the new conformal towers of $\vec{\mathcal{J}}_{sqL}$ will not exceed $M/2$. Next, define the free fermion fusion factor $n_0^{QS'S_c}$ to be 1 if a free fermion primary state of charge Q, spin S', and channel-spin S_c is allowed in the free spectrum of Eq. (6.1.43), and zero otherwise. Define the corresponding quantity for the system with absorbed spin as $n_*^{QSS_c}$. The fusion rule of Affleck and Ludwig [1991b; Ludwig, 1994] states that

$$n_*^{QSS_c} = \sum_{S'} N^S_{S_I,S'} n_0^{QS'S_c} \tag{6.1.48}$$

where $N^S_{S_I,S'}$ is one if (6.1.47) is satisfied for S, S_I, S', and zero otherwise. Taking this fusion rule together with the general rules for constructing states within the Kac-Moody algebra allows a complete generation of the spectrum at the fixed point. Corrections to scaling arise as one moves away from the fixed point (by going to higher energies for example).

To understand how this fusion process works, the reader is directed to Tables 11 (free fermions for $M = N = 2, S_I = 1/2$) and 12 (spectrum of $N = M = 2, S_I = 1/2$ Kondo model). These are

Q	S	S_c	$SO(5)$	$(El/\pi v_F)$
0	0	0	1	0
±1	1/2	1/2	4	1/2
0	1	0	1	1
±2	1	0	5	1
0	1	1		1
±2	0	1		
0	0	0	10'	1
0	0	1		
±1	1/2	1/2'	4'	3/2
±1	1/2'	1/2	4	3/2
±1	3/2'	1/2	4	3/2
±3	1/2	1/2		3/2
±1	1/2	3/2'	16'	3/2
±1'	1/2	1/2		3/2

Table 11: Free fermion energy levels for the $M = 2$ channel model (c.f. sec. 6.1.d). The states are labeled by charge Q, spin S, channel spin S_c, and the combined Q, S_c indices are also designated by their $Sp(2) \sim SO(5)$ labels (which indicates the combined charge/channel degeneracy); different $SO(5)$ blocks are delineated by horizontal lines. Energies are measured in dimensionless units of $l/\pi v_F E$ and the F^- boundary condition $\Psi_L(l) = -\Psi_L(-l)$ is assumed so that the fermion wave functions are forced to zero at the boundary. (This is a combination of Tables I and III of Affleck *et al.* [1992].) Primes indicate descendant states generated by exciting particle hole pairs.

Q	S	S_c	$SO(5)$	$lE/\pi v_F$	E_{NRG}
0	1/2	0	1	0	0
±1	0	1/2	4	1/8	0.125
±2	1/2	0	5	1/2	0.505
0	1/2	1		1/2	0.505
±1	1	1/2	4	5/8	0.637
0	3/2'	0	1	1	1.013
±2	1/2	1		1	1.035
0	1/2	1	10'	1	1.035
0	1/2	0		1	1.035
±1	0	3/2'		9/8	1.147
±1	0	1/2	16'	9/8	1.147
±3	0	1/2		9/8	1.147
±1	1'	1/2	4	9/8	1.179
±1	0	1/2	4'	9/8	1.232

Table 12: Spectrum of the $M = 2, S_I = 1/2$ Kondo model. The notation is the same as for Table 11. The fifth column shows the energies generated by conformal field theory (CFT); the last column is the numerical renormalization group (NRG) energy (see Sec. 4.2) with appropriate normalization. This table is based on Table V of Affleck *et al.* [1992] and Table 1b of Ludwig [1994a]. As discussed in Secs. 4.2, 6.1.2.a, the NRG respects the $SO(5)$ symmetry but not the full conformal invariance. Hence, $SO(5)$ blocks all have the same energy as shown below. Spectra can be generated from Table 11 by using the single fusion rule (Eq. (6.1.48)) in conjunction with the Kac-Moody triangle rule (Eq. (6.1.47)).

constructed from corresponding tables in Affleck *et al.*[1992] and Ludwig [1994a]. Taking $S' = 0$ from the ground state $Q = S' = S_c = 0$ of the free fermion problem, it is easy to see from Eq. (6.1.47) that S is uniquely constrained to be $1/2$ and hence $n_*^{0,1/2,0} = 1$ by Eq. (6.1.48). Now at first one might think this corresponds to the spin charge reversal of the $M = 1$ model at the strong coupling fixed point as discussed in Sec. 4. However, the lone fermion with $S = 1/2$ would also have to have $S_c = 1/2$, which is clearly not the case. Next consider the first excited state of the free fermion spectrum with $Q = \pm 1(mod 4), S' = 1/2, S_c = 1/2$. The triangle rule (6.1.47) constrains S uniquely to zero, and yields an energy of $\pi v_F/8l$. This differs from a Fermi liquid theory in two key aspects. First, the level spacing relative to the ground state is a fraction of the minimum free fermion value of $\pi v_F/l$. Second, the quantum numbers cannot be that of free fermions with simple reversed spin and charge quantum numbers because the creation of a free $S_c = 1/2$ excitation would necessitate a spin $S = 1/2$ to accompany it.

Table 12 also contains a comparison with the lowest 76 NRG energy levels (Affleck *et al.* [1992]). It can be seen that the agreement is quite good, with discrepancies arising as one moves to higher energies. This disagreement can arise from three sources: (1) The logarithmic discretization of the NRG treatment breaks the conformal symmetry; (2) The numerical truncation procedure in the NRG can introduce systematic numerical error; (3) As one moves away from the low energy spectrum, corrections to scaling arise from the effects of the irrelevant operators. In practice, it is believed that (1,2) contribute more to the differences observed based upon an extrappolation of the NRG numerics to the continuum limit $\Lambda = 1$, where Λ is the logarithmic discretization parameter of the NRG. Notice that the NRG levels respect the $Sp(2) \sim SO(5)$ symmetry discussed in Sec. 4. The higher conformal symmetry renders a number of the $Sp(2)$ energy levels degenerate.

We end this subsection by noting that the fusion rule can be applied to exactly compensated and undercompensated models as well, as was discussed particularly clearly in Affleck [1990a]. As a couple of examples, consider first the $M = 1, S_I = 1/2$ model. The fusion rule then simply generates the reversed spin/charge relations corresponding to a $\pi/2$ phase shift as discussed in Secs. (4.1) and (6.1.1). For example, for the free fermion ground state with $S' = 0, Q = 0$, the fusion rule generates the state $S = 1/2, Q = 0$ (with energy zero, after effecting a shift of $\pi v_F/4l$ to the spectrum), and for the first excited free fermion state with energy $\pi v_F/2l$ and $S' = 1/2, Q = \pm 1$, the fusion rule generates the state $S = 0, Q = \pm 1$ with energy zero. The second excited state with $Q = \pm 2$, $S' = 0$, and energy $\pi v_F/l$ is mapped to the state $Q = \pm 2, S = 1/2$ with energy $\pi v_F/l$. These lowest two states correspond precisely to the spectrum of free fermions with the boundary condition $\Psi_{L\mu}(L) = \Psi_{L\mu}(-L)$ and reversed spin/charge relations, or equivalently to a $\pi/2$ phase shift. Affleck [1990a] also demonstrates that this simple absorption of the impurity spin holds for the $M/2 = S_I$ compensated Kondo model and the $SU(N), M = 1$ Coqblin-Schrieffer model which also has a compensated (singlet) ground state. For the undercompensated model with $S_I > M/2$, Affleck demonstrates that the absorption holds for $M/2$ of the impurity spin, leaving behind a local moment with net value $S_I - M/2$ and residual ferromagnetic coupling to the impurity spin. Hence, the fixed point spectrum is a direct product of a decoupled local moment with a Fermi liquid, as was suggested by Nozières and Blandin [1980]. Corrections to scaling from the marginally irrelevant ferromagnetic coupling can generate "non-Fermi liquid" thermodynamics which are related to those in the charge-only model discussed by Giamarchi *et al.* [1993].

(b) Relation of Boundary Operator Spectrum to Finite Size Spectra

One of the key features of boundary CFT as developed by Cardy [1984,1986a,1986b] is the existence of boundary operators with non-trivial scaling dimensions. The existence of these boundary terms gives rise to singular contributions to the free energy of the quantum impurity problem which are independent of l. These boundary operators live only at $r = 0$ and thus are dependent only upon the time variable.

Each boundary operator ϕ will have a distinct behavior under rescaling of space and time

coordinates, which is described in terms of the scaling index Δ_ϕ specified by its long time green's function, *viz.*

$$< \phi(\tau)\phi(\tau') > \sim |\tau - \tau'|^{-2\Delta_\phi} \tag{6.1.49}$$

for $|\tau - \tau'| \to \infty$. The scaling index also gives the renormalization group eigenvalue of the field h_ϕ conjugate to the boundary operator ϕ. This follows from adding to the Lagrangian $\mathcal{L}$ associated with the Sugawara Hamiltonian specified by Eqs. (6.1.43,45) a term of the form

$$\delta\mathcal{L}(h_\phi) = h_\phi \int d\tau \phi(\tau) \quad . \tag{6.1.50}$$

Consider a uniform rescaling of space and time by a factor b. Then from the integral we see that the field h_ϕ scales like $b^{1-\Delta_\phi}$ to leave the term scale invariant. Hence operators with scaling dimensions less than one have relevant conjugate fields. As we shall see below, this includes the primary spin and channel spin fields at the fixed point of the two-channel model.

Any operator with a scaling index $\leq 1/2$ may have a diverging susceptibility defined by the equation

$$\chi_\phi(T) = \int_0^\beta d\tau < \phi(\tau)\phi(0) > \sim T^{2\Delta_\phi - 1} \quad . \tag{6.1.51}$$

An exponent of 1/2 is a special case, clearly, and in this case one will either have logarithmic or constant behavior at long times and low energies. If the operator is bosonic in character, it will have a log divergence at low temperature because the spectral function of the ϕ green's function must change sign at zero frequency. If the operator is fermionic in character, it will be a constant at low temperature consistent with unitary bounds on the scattering amplitude for fermions. For a related discussion, see Sec. 5.1.2.

A key point made by Cardy [1986b] and utilized by Affleck and Ludwig [1991b], Affleck *et al.* [1992], and Ludwig [1994a] is that for a particular choice of boundary conditions on a finite strip, there is a one-to-one correspondence of the boundary operators to the low lying states and the corresponding energies (in units of $\pi v_F/l$) are precisely the scaling dimensions of the boundary operators. Let us briefly review the boundary conditions, referring to Figs. 75,76. In this section, we have described free left moving fermions which obey the F boundary condition at $r = 0$ and the F^- boundary condition at $r = l$ (*c.f.* Eq. (6.1.7). We refer to this as FF^- boundary conditions, following Ludwig [1994a], and represent this as the finite width strip in Fig. 75(a). Alternatively, given the mirroring of Ψ_L in the $r < 0$ plane, we may view this as a cylinder of circumference $2l$ with a 'seam' along which Ψ_L is forced to zero. In the presence of the impurity spin, the boundary conditions are shifted to KF^-, where the K denotes absorption of the impurity spin at the $r = 0$ boundary. This is represented in Fig. 75(b) .

According to the work of Cardy [1986], to obtain the scaling dimensions of the boundary operators we should look at the spectrum corresponding to the boundary conditions KK^-, namely, the non-trivial boundary is placed at each edge with a wall at the $r = l$ edge. It is important to note that this finite strip can be related back to the original half-plane with the conformal transformation shown in Fig. 76.

To implement this KK^- boundary condition, Affleck and Ludwig [1991b] (Ludwig [1994a]) hypothesized that the appropriate description was the 'double fusion rule'. Namely, first the impurity spin is absorbed at the K boundary, corresponding to the KF^- boundary conditions discussed in Sec. 6.1.2.a. Then the impurity spin must be absorbed at the far boundary $r = l$ *again*! In practice, this means that the conduction spin density for left movers is shifted (in real space) by $\vec{J}_{sL}(x) \to \vec{\mathcal{J}}^{op}_{sL}(x) + \delta(x)\vec{S}_{I1} + \delta(x-l)\vec{S}_{I2}$ and in k space to $\vec{\mathcal{J}}^{op}_{sqL} + \vec{S}_{I1} + (-1)^{lq/\pi}\vec{S}_{I2}$. Here we have included the superscript *op* to remind the reader this is for calculating the spectra of allowed boundary operators. It may be readily verified that this doubly shifted density operator still obeys the Kac-Moody algebra. Hence, the double fusion may be viewed first as conduction spin S'' absorbing impurity spin S_{I1} at $r = 0$

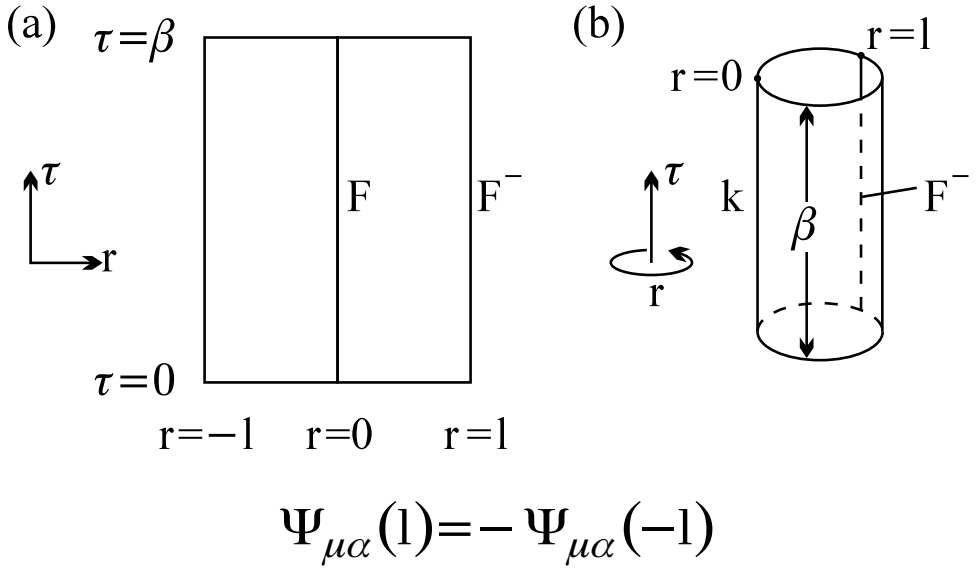

Figure 75: Boundary conditions for free fermions (a) and system with a Kondo impurity at the origin (b) for use in the conformal theory. After Affleck and Ludwig [1991a,b,c].

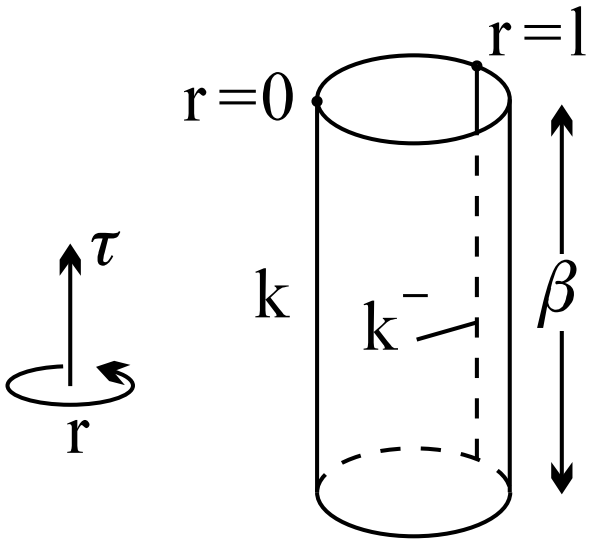

Figure 76: Boundary conditions for operator spectrum of Kondo impurity model. In this case a Kondo impurity is fused in at each boundary (KK^- boundary conditions). After Affleck and Ludwig [1991a,b,c].

Q	S	S_c	$SO(5)$	$\Delta = El/v_F\pi$
0	0	0	1	0
0	1	0	1	1/2
0	0	1	5	1/2
±2	0	0		1/2
±1	1/2	1/2	4	1/2
±1	1/2	1/2	4	1/2
0	1	1	5	1
±2	1	0		1
0	0	1		1
±2	0	1	10	1
0	0	0		1
0	0'	0	1	3/2
0	2'	0	1	3/2

Table 13: Operator spectrum of the $M = 1/2, S_I = 1/2$ Kondo model from the conformal theory double fusion rule (c.f. Sec. 6.1.2.b). Notation is the same as for Table 11. Here Δ is the scaling index of the operators. Table is adopted from Table 1.c of Ludwig [1994a]. Spectra can be generated from the free-fermion spectrum of Table 6.1 with the double fusion rule (Eq. (6.1.50)) or from Table 12 with the single fusion rule (Eq. (6.1.48)) in conjunction with the Kac-Moody triangle rule (Eq. (6.1.47)). The table is not complete for all operators with scaling index 3/2. The operators shown with scaling index 3/2 are the leading irrelevant operator about the fixed point (spin 0) and the quadrupolar spin operator (spin 2–see Sec. 6.1.2.c for discussion).

yielding composite spin S', with S' then absorbing S_{I2} at the boundary $r = l$ yielding spin S. Allowed states in the finite size spectra are characterized by integers $n_{KK^-}^{QSS_c} = 0$(unallowed) or 1(allowed) which are calculated from the rule

$$n_{KK^-}^{QSS_c} = \sum_{S'S''} N_{S_I,S'}^{S} N_{S_I,S''}^{S'} n_0^{QS''S_c} \tag{6.1.52}$$

where $n_0^{QSS_c}$ and $N_{S_I,S'}^{S}$ were defined in Sec. 6.1.2.a. Each generated state which is then a primary state of the Kac-Moody algebra correponds to a so-called primary field boundary operator. One may also generate descendants by operating with the charge, spin, and current densities for positive qp (i.e., negative q for left movers).

The lowest several states for the KK^- boundary conditions generated by the double fusion rule are displayed in Table 13. Again, the energies divided by $\pi v_F/l$ give the scaling dimensions, which may then be read off from Eq. (6.1.36) for non-zero values of $n_{KK^-}^{QSS_c}$. Note that the constraints of the Kac-Moody algebra imply that no primary fields can exist with S or S_c greater than one. From Table 13 we see that apart from the trivial constant operator there are four kinds of operators with scaling dimension 1/2. The physical meaning of each is as follows:
$Q = \pm 1, S = 1/2, S_c = 1/2$ *Operators*: These are the quantum numbers associated with a free fermion excitation, so the scaling dimension must be $\Delta_F = 1/2$ as discussed above and in Sec. 5.1.2. It is of interest that there are two such fields; the physical interpretation of this is unclear.
$Q = 0, S = 1, S_c = 0$ *Operator*: This is $\vec{\phi}_s$, a primary operator transforming as a vector triad of local spin tensors. This object describes the effective core spin at the fixed point. The scaling dimension of Δ_s=1/2 implies that this operator has a logarithmically divergent susceptibility which will be explicitly calculated in Sec. 6.1.3. The scaling dimension value of 1/2 also implies that the spin field (magnetic field for magnetic impurities, strain field for quadrupolar Kondo ions or TLS sites) is a relevant field

with renormalization group eigenvalue of 1/2.
$Q = 0, S = 0, S_c = 1$ *Operator*: This is $\vec{\phi}_{sc}$, a primary operator transforming as a vector triad of local channel spin tensors. The scaling dimension of Δ_c=1/2 implies that the corresponding channel spin susceptibility is logarithmically divergent at low temperatures, and the application of an external channel field (strain field for magnetic impurities, magnetic field for quadrupolar Kondo or TLS impurities) is a relevant perturbation.
$Q = \pm 2, S = 0, S_c = 0$ *Operator:* This is a primary operator describing an electron pair around the impurity site (Ludwig and Affleck [1991], Ludwig [1993]). The corresponding local pair field susceptibility is logarithmically divergent, and in principle a local source of such pairs is a relevant perturbation. This pair field is unusual, in that the antisymmetry of spin and channel spin labels implied by $S = S_c = 0$ means that something else must be done to the pair operator to render it antisymmetric under the Pauli principle. As discussed by Ludwig and Affleck [1991c], antisymmetrizing in the L, R indices between the electron fields will assure satisfaction of the Pauli principle. This is equivalent to odd-parity in the one-dimensional spatial index in view of the mirroring condition $\Psi_L(r) = \Psi_R(-r)$. After Emery and Kivelson [1992] noted the log divergence associated with an odd-in-time pair field in their Abelian bosonization approach, it was realized that antisymmetrizing in temporal arguments for $x = 0$ will do just as well (Ludwig [1993]) as a spatial gradient, given the equivalence of space and time axes in the conformal space. Alternatively, one may construct a dot product of the spin field $\vec{\Phi}_s$ with a local triplet pair field possessing quantum numbers $Q = \pm 2, S = 1, S_c = 0$. Although the triplet field by itself has scaling exponent 1 and thus has a non-diverging susceptibility, in combination with the local spin tensor a spin singlet is formed which has the same quantum numbers as those with inserted gradients. The equivalence is readily seen by explicitly carrying out the time and space derivatives. We postpone a more elaborate discussion of the pair fields until Sec. 9.4.

Some other interesting operators are: (1) the double tensor operator, with quantum numbers $Q = 0, S = 1, S_c = 1$, which is relevant to the generalized model considered by Pang [1992,1994] and Zaránd [1995], and which has scaling dimension 1; (2) the spin quadrupole operator (not shown in Table 13) which has $Q = 0, S = 2, S_c = 0$ and scaling dimension 3/2 (Affleck*et al.* [1992]). This operator is relevant to our discussion of perturbations about the fixed point, specifically exchange anisotropy, which we shall discuss in the next subsection 6.1.2.c.

Notice that no operators with $Q = 0, S = 1/2, S_c = 0$ or $Q = 0, S = 0, S_c = 1/2$ appear in the KK^- spectrum even though these are in principle allowed primary operators coming from the Kac-Moody algebras which permit, e.g., $S = 0, 1/2, ...M/2$ primary field spins for a level M spin algebra. The double fusion rule legislates against these possibilities.

Appliction of the Kac-Moody densities to the primary field operators generates the so called descendant operators with higher scaling dimensions. As an explicit example, put $q = n\pi/l > 0$ and consider the operator $\vec{\mathcal{J}}_{s,-q,L} \cdot \vec{\phi}_s$. This operator has $S = 0$ (since it is a scalar product of two spin operators) and scaling dimension $n + \Delta_{\phi_s} = n + 1/2$ for the two-channel case.

By way of slight generalization, we note that the primary spin and channel-spin operators transform as the fundamental representations of $SU(N)$ and $SU(M)$ for the generalization to the $SU(N) \times SU(M)$ model. The resulting scaling dimensions are $\Delta_s = N/(N + M)$ for the spin field, and $\Delta_c = M/(M + N)$ for the channel field, in precise agreement with Eqs. (5.1.30.a,b) (recalling that $\gamma = M/N$ is held fixed in the large N limit of Sec. 5.1).

(c) Perturbations about the Fixed Point

In this section we give an overview of the effects of various perturbations about the two-channel fixed point following the discussion in Affleck and Ludwig [1991c] and Affleck *et al.* [1992]. The point is that the conformal theory gives a natural basis for identifying relevant, irrelevant, and marginal operators about the fixed point. In order, we shall discuss perturbations due to: (1) The leading irrelevant operator; (2) an external spin field; (3) an external channel field; (4) exchange anisotropy.

(1) Leading Irrelevant Operator

As discussed by Affleck and Ludwig [1991b] and Affleck *et al.*, a central role is played by the leading irrelevant operator about the fixed point Hamiltonian. The restrictions on this operator are that it must be a singlet in spin and channel indices, so as to preserve the $SU(2) \times SU(2)$ symmetry, and must be chargeless to preserve the $U(1)$ symmetry. Finally, on physical grounds we expect this operator to involve only the primary spin field $\vec{\phi}_s$ since the non-trivial coupling induced by the Kondo impurity occurs only in the spin sector. By the remarks of the previous section, a reasonable candidate operator is $\vec{\mathcal{J}}_{s,-q,L} \cdot \vec{\phi}_s$ for $q = \pi/l$ which has scaling dimension $1 + \Delta_s = 1 + N/(N+M)$=3/2 when $N = M = 2$. In the case of $N = M$, the operator $\vec{\mathcal{J}}_{c,-q,L} \cdot \vec{\phi}_c$ also has the same scaling dimension, but since there is no impurity channel field is not a physically plausible candidate for the leading irrelevant operator.

The way this operator is added to the Hamiltonian is in the form $\delta\lambda = \lambda - \lambda^*$ where $\lambda^* = 2/(2+M)$ for $N = 2$ is the fixed point coupling. In the next section we shall see how this term enters into the calculation of the specific heat. (Note that in Affleck and Ludwig [1991b], the coupling λ used in the discussion of thermodynamics corresponds to $\delta\lambda$ here.)

(2) Application of a Spin Field

If we introduce a field $\vec{h}_s$ which couples linearly to the primary boundary spin operator $\vec{\phi}_s(\tau)$. Physically, this corresponds to a magnetic field for the magnetic impurity, and a stress field for the quadrupolar impurity or TLS impurity. Also, electric field gradients and magnetostriction induced stress fields (order H^2, H the magnetic field) will split the quadrupolar Kondo impurity, and the TLS impurity is subject to spontaneous tunneling matrix elements and well asymmetry which have the same effect. The presence of a spin field produces a term in Lagrangian of the form in Eq. (6.1.49) with $\vec{h}_s \cdot \vec{\phi}_s(\tau)$ inside the integral. Hence the spin field $\vec{h}_s$ is relevant with a renormalization group eigenvalue of 1/2. This implies that in the presence of a spin-field, there will be a crossover to a new fixed point with crossover exponent 1/2, i.e., low temperature properties will be universal functions of h_s^2/T. This implies the existence of a new energy scale in the problem given by h_s^2/T_K, as is verified in NRG and Bethe-Ansatz treatments. The conformal field theory cannot specify the nature of the new fixed point, but it is reasonable to guess that it is a free fermion fixed point in the presence of a polarized scatterer (the Zeeman split primary field). This is born out by the NRG calculations discussed in Sec. 4.2.e (see Fig. 19(a)). We note that the crossover physics is in precise agreement with the discussion of Sec. 5.1 where the large N NCA approach was used.

(3) Application of a Channel Field

A channel field $\vec{h}_c$ couples linearly to the primary channel spin operator $\vec{\phi}_c(\tau)$. This field corresponds to a stress field or electric field gradient for the magnetic impurity, and a magnetic field for the quadrupolar or TLS impurity. In practice, the channel field probably arises from a splitting of the exchange integrals in the presence of applied stress (magnetic impurity) or applied magnetic field (quadrupolar Kondo impurity). It remains something of a mystery how to effectively obtain a channel field splitting for the TLS since there is no obvious magnetic coupling to the impurity. By considering a perturbation to the Lagrangian of the form (6.1.49), with $\vec{h}_c \cdot \vec{\phi}_c(\tau)$ in the integrand, we see that the renormalization group eigenvalue of the field $\vec{h}_c$ is 1/2. This implies that the perturbation is relevant with a crossover exponent of 1/2, i.e., low temperature properties are universal functions of h_c^2/TT_K, and h_c^2/T_K is a new energy scale which sets the crossover temperature on passing first through the Kondo scale and then at lower temperatures to this new energy scale. The crossover behavior is in good agreement with that discussed in Sec. 5.1. The conformal theory again does not provide an answer as to what the crossover goes to, but the obvious guess in view of the analysis of Secs. 3.1.2, 4.2, and 5.1 is that the crossover is to the ordinary Kondo fixed point for whichever channel couples more strongly to the impurity and the weak coupling fixed point for the other channel. This is indeed seen in the NRG spectra, which suggest a direct product of phase shifted fermions with unshifted fermions at the fixed point. Jerez and Andrei [1995] and Coleman and Schofield [1995] have questioned the Fermi liquid character of the fixed point recently. Using a combination of Abelian bosonization and path integral methods, Fabrizio, Gogolin, and Nozières [1995a,b] have reasserted that the new fixed point is indeed a Fermi liquid.

(4) Exchange Anisotropy.

Exchange anisotropy breaks the $SU(2)$ spin rotational invariance to a $U(1)$ subgroup which is however *even* under spin reversal (time reversal for the magnetic impurity) unlike the magnetic field. If it is a relevant perturbation, there should be an appropriate primary field operator in the KK^- spectrum. The logical candidate is a spin quadrupole operator with quantum numbers $Q = 0, S = 2, S_c = 0$. This makes physical sense as argued by Pang [1992] and discussed in Sec. 3.3.1,3.4.1, since the exchange anisotropy will induce a local quadrupolar splitting of the impurity spin through the two-loop order contribution to the pseudo-fermion self energy. Thus, although the anisotropy term $\mathcal{J}^3_{s,-1,L}\phi^3_s$ has an irrelevant scaling dimension, it generates a relevant term in next order.

As noted by Affleck *et al.* [1992], the only primary operator with $Q = 0, S_c = 0$ for free fermions has $S = 0$. So it is logical to apply the double fusion rule to this state, which implies that the only primary field operator with $S = 2$ must satisfy the constraint implied by the Kac-Moody triangle rule, so that

$$2 \leq 2S_I, \quad 2 \leq M - 2S_I \quad . \tag{6.1.53}$$

This implies that $1/2 < S_I < M/2 - 1/2$. The scaling dimension is $\Delta_{quad} = 6/(M + 2)$, and so it is relevant for $M \geq 5$, and marginal for $M = 4$, provided $1/2 < S_I < M/2 - 1/2$. For $S_I = 1/2$ or $S_I = k/2 - 1/2$, the exchange anisotropy enters only through the perturbation $J^z_{s,-1,L}\phi^z_s$ which is part of the leading irrelevant operator about the fixed point and so cannot be relevant. In physical terms, as discussed in Secs. 3.3.1,3.4.1, and 4.2, one can understand this because for $S_I = 1/2$ or $k/2 - 1/2$ and $M > 2$, the ground state spin alternates between $k/2 - 1/2$ and $1/2$ for even or odd number of sites in the NRG, or alternatively one can always arrange to have a $S = 1/2$ ground state with appropriate boundary conditions in the CFT analysis. $S = 1/2$ states can never have a quadrupole moment; generically, the next few states in such a case have often $S = 1/2$ or $S = 0$ which also of course experiences no anisotropy to leading order.

6.1.3 Calculation of Thermodynamic Properties in the CFT Approach

In this subsection we show how Affleck and Ludwig [1991b,c] were able to compute various thermodynamic properties within the conformal theory approach. There are three parts. First, we identify the conformal transformation and mathematics which allows finite temperature calculations to be performed straightforwardly given a knowledge of the physics at the fixed point (Sec. 6.1.3.a). Next, we outline explicitly how the calculation of the specific heat and magnetic susceptibility with this finite temperature technology is carried out in Sec. 6.1.3.b, yielding an estimate of the Wilson ratio together with explicit confirmation of the singular behavior of the low temperature quantities. Finally, we switch to a discussion of how the ground state residual entropy is calculated which involves sophisticated use of the conformal invariance to relate spatial boundaries to temporal boundaries (Sec. 6.1.3.c).

(a) Conformal Mapping for Finite Temperature Physics

As noted by Affleck and Ludwig[1991b], the low temperature free energy of the continuum Kondo model can be written in two different ways, first as a trace over the exponential of the inverse temperature times the Hamiltonian living on the half plane $-\infty < \tau < \infty$, $0 < r$, and second in a Lagrangian formulation where the temperature explicitly enters the imaginary time integrals. Including a spin field h_s along the z axis, the Hamiltonian description gives

$$F(T, \delta\lambda, h_s) = \frac{-1}{\beta} \ln[Tr \exp\{-\beta(\hat{H}(\delta\lambda) - h_s\hat{\mathcal{J}}^3_{s0L})\}] \tag{6.1.54}$$

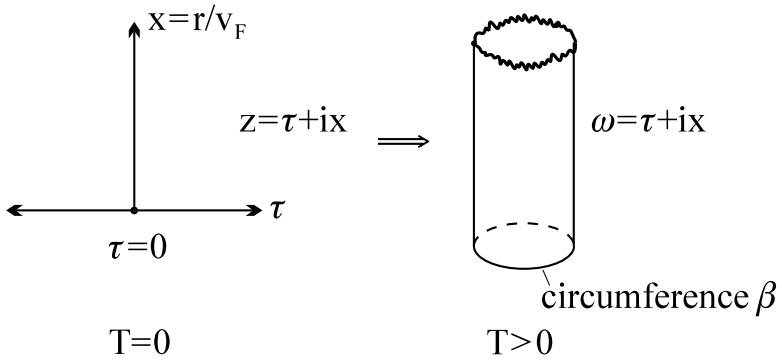

Figure 77: Conformal mapping of zero temperature half-plane to finite temperature cylinder. By applying this mapping of $z \to w$, one may straightforwardly evaluate finite temperature correlation functions in terms of zero temperature ones.

and in the Lagrangian formulation

$$F(T,\lambda,h_s) = F(T,0,0) - \frac{1}{\beta} ln < \exp\{\int_0^\beta d\tau [\delta\lambda(\tilde{\mathcal{J}}^a_{s,-1,L}\tilde{\phi}^a_s)(\tau) + h_s \tilde{\mathcal{J}}^3_{s0L}(\tau)]\} > \tag{6.1.55}$$

where the hat refers to the half plane geometry $\mathcal{G}_0$ with the Kondo impurity living at $r = 0$, and the tilde refers to the semi-infinite cylinder geometry $\mathcal{G}_T$ specified by $0 < \tau < \beta$, $0 < r < \infty$ where bosonic operators are periodic in β. Note that the spin field has been coupled to the total (conserved) spin operator $\mathcal{J}^3_{s0L}$. As in the discussion of Secs. 6.2.b,c, we put $q = n\pi/l$ and index the spin density operators by n rather than q. The above expectation value is with reference to the critical Hamiltonian ($\delta\lambda = h_s = 0$). These expressions have employed the identity $\mathcal{J}^3_{s0L} = (1/2\pi)\int \mathcal{J}^3_L(x)$ which is just the Fourier transform rule. Hence this treatment differs slightly from Affleck and Ludwig [1991b] where the spin density in real space is written down.

Affleck and Ludwig [1991b] point out that the free energy given by Eqs. (6.1.54,55) must obey standard finite size scaling relationships. Specifically, if we restrict the spatial dimension such that $0 < r < l$ and $l/v_F >> \beta$, then F separates into a bulk piece that scales with l, and an impurity piece independent of l, *viz.*

$$F(T,h_s,\delta\lambda) = \frac{l}{a} f_{bulk}(T,h_s) + f_{imp}(T,h_s,\delta\lambda) \tag{6.1.56}$$

where a is a minimum length scale (of order $\hbar v_F/k_B T_K$ here). The finite size scaling hypothesis (Barber, [1983]) says that the bulk and impurity parts may be written for $\beta \to \infty$ as

$$f_{bulk}(\beta,h_s) \approx E^{(0)}_{bulk} + \frac{1}{\beta^2} Q_{bulk}(\beta h_s) \tag{6.1.57}$$

and

$$f_{imp}(T,h_s,\delta\lambda) \approx E^{(0)}_{imp} + \frac{1}{\beta} Q_{imp}(\beta h_s; A\beta^{-\Delta}\delta\lambda) \tag{6.1.58}$$

where $\Delta = 1 + \Delta_s$ is the scaling dimension of the leading irrelevant operator. In principle, all bulk and impurity irrelevant couplings may be included in Eqs. (6.1.57,58), but these produce subleading corrections compared to the leading irrelevant operator. Our interest is in computing Q_{imp} which may be evaluated about the fixed point by expanding Eq. (6.1.55) in powers of h_s and $\delta\lambda$. This involves calculation of correlation functions between various combinations of $\mathcal{J}^3_{s0L}$ and $\mathcal{J}^a_{s,-1,L}\phi^a_s$ on the geometry $\mathcal{G}_T$.

To evaluate the finite temperature correlation functions one may exploit the conformal transformation shown in Fig. 77 which maps $\mathcal{G}_0$ into $\mathcal{G}_T$. Defining $z = \tau + ix$ in the half-plane and

$w = \tau + ix$ in the semi-infinite cylinder ($x = r/v_F$), the transformation is $w = (\beta/\pi)\tan^{-1}(z/\tau_0)$ where $\tau_0 = a/v_F \approx \hbar/k_B T_K$ sets the short time or high frequency cutoff of the model. (Note that Affleck and Ludwig [1991b] include the τ_0 factor in this transformation only implicitly.) As a result, at long times any boundary operator $\hat{O}$ in geometry $\mathcal{G}_0$ is related to the corresponding operator $\tilde{O}$ in geometry $\mathcal{G}_T$ by the identity

$$\tilde{O}(w) = (\frac{dw}{dz})^{-\Delta_O}\hat{O}(z) = (\frac{\beta}{\pi\tau_0}\frac{1}{1+(z/\tau_0)^2})^{-\Delta_O}\hat{O}(z) \tag{6.1.59}$$

where Δ_O is the scaling dimension of $\hat{O}$. This means that correlation functions in the long time regime which are simple power laws in geometry $\mathcal{G}_0$ may be related straightforwardly to correlation functions at finite temperature. For example,

$$< \tilde{O}(w_1)\tilde{O}(w_2) >= (\frac{\beta}{\pi\tau_0})^{-2\Delta_O}(1+(z_1/\tau_0)^2)^{\Delta_O}(1+(z_2/\tau_0)^2)^{\Delta_O} < \hat{O}(z_1)\hat{O}(z_2) >$$

$$\approx (\frac{\beta}{\pi\tau_0})^{-2\Delta_O}(1+(z_1/\tau_0)^2)^{\Delta_O}(1+(z_2/\tau_0)^2)^{\Delta_O}\frac{A_O\tau_0^{2\Delta_O}}{(z_1-z_2)^{2\Delta_O}} \tag{6.1.60}$$

where A_O is a normalization factor for the $O-O$ green's function. Through the conformal mapping the z variables on the right hand side can be related to the w variables on the left hand side in a straightforward manner. Specifically, repeated use is made of the relation

$$\frac{(1+(z_1/\tau_0)^2)(1+(z_2/\tau_0)^2)\tau_0^2}{(z_1-z_2)^2} = \frac{1}{\sin[\frac{\pi}{\beta}(w_1-w_2)]} \tag{6.1.61}$$

which follows from elementary trigonometric identities.

(b) Evaluation of the Specific Heat and Magnetic Susceptibility

The specific heat is calculated by evaluating the first non-vanishing term in the impurity free energy for $h_s = 0$ and $\delta\lambda$ finite. This term is of order $\delta\lambda^2$ because the expectation value of Eq. (6.1.55) is with respect to the fixed point Hamiltonian at which the average of the leading irrelevant operator is zero. Hence, the leading contribution to the free energy at zero field is

$$\delta f_{imp}^{(2)}(T) = -\frac{\delta\lambda^2}{2\beta}\int_0^\beta d\tau_1\int_0^\beta d\tau_2 < (\tilde{\mathcal{J}}^a_{s,-1,L}\tilde{\phi}^a_s)(\tau_1)(\tilde{\mathcal{J}}^b_{s,-1,L}\tilde{\phi}^b_s)(\tau_2) >$$

$$= -3(\frac{M}{2}+2)\delta\lambda^2(\frac{\pi\tau_0}{\beta})^{2(1+\Delta_s)}\int_{\tau_0}^{\beta/2}\frac{d\tau}{[\sin\frac{\pi\tau}{\beta}]^{2(1+\Delta_s)}}$$

$$= -3(\frac{M}{2}+2)\delta\lambda^2(\frac{\pi\tau_0}{\beta})^{2(1+\Delta_s)}I(2(1+\Delta_s),\beta) \tag{6.1.62}$$

where Eqs. (6.1.60,61) were used, $\tau_0 \approx \hbar/k_B T_K$ is a short time cutoff, and the factor $3[(M/2)+2]$ corresponds to A_O in Eq. (6.1.60). This factor corresponds to the usual green's function numerator for equal times and may be evaluated straightforwardly from the Kac-Moody algebra as noted by Affleck and Ludwig [1991a]. For the special case of $M = 2$ where , the integral in (6.1.62) is straightforwardly evaluated with the substitution $z = arsh[cot(\pi\tau/\beta)]$ to give

$$I(3,\beta) = \frac{\beta}{\pi}\int_0^{arsh[\beta/\pi\tau_0]} dz cosh^2 z$$

$$= \frac{\beta}{2\pi}[\frac{\beta}{\pi\tau_0/}\sqrt{1+(\frac{\beta}{\pi\tau_0})^2}+\ln(\frac{\beta}{\pi\tau_0})+\sqrt{1+(\frac{\beta}{\pi\tau_0})^2})] \quad . \tag{6.1.63}$$

As a result, for $\beta \to \infty$, we see that the impurity contribution to the specific heat goes as

$$C_{imp} = -T\frac{\partial^2 f_{imp}}{\partial T^2}$$

$$\approx k_B[9(\pi\delta\lambda\tau_0)^2\frac{T}{T_K}\ln(\frac{2T_K}{\pi\sqrt{e}T})] \ (M=2) \quad . \tag{6.1.64}$$

This displays the expected $T\ln T$ singular behavior. For $M > 2$, the specific heat behaves as $T^{4/(2+M)}$ as was earlier calculated by the Bethe-Ansatz (Andrei and Destri [1985], Wiegman and Tsvelik [1985]).

Turning now to the susceptibility, we wish to extract the leading impurity contribution to the free energy which is also order h_s^2. This must be quadratic in both $\delta\lambda$ and h_s because terms linear in h_s and $\delta\lambda$ have vanishing expectation values from the free Hamiltonian by construction. Hence the relevant term in the impurity free energy is found by the expansion of Eq. (6.1.55) to quadratic order in h_s and $\delta\lambda$ yielding

$$\delta f_{imp}^{(2,2)} = \frac{-1}{4\beta}\delta\lambda^2 h_s^2[\prod_{i=1}^{4}\int_0^\beta] < \tilde{\mathcal{J}}^3_{s0L}(\tau_1)\tilde{\mathcal{J}}^3_{s0L}(\tau_2)(\tilde{\mathcal{J}}^a_{s,-1,L}\tilde{\phi}^a_s)(\tau_3)(\tilde{\mathcal{J}}^b_{s,-1,L}\tilde{\phi}^b_s)(\tau_4) >_{conn} \tag{6.1.65}$$

which gives $\chi_{imp} = -(\partial^2 f_{imp}/\partial h_s^2)(h_s = 0)$ as

$$\chi_{imp} = \frac{1}{2\beta}\delta\lambda^2[\prod_{i=1}^{4}\int_0^\beta] < \tilde{\mathcal{J}}^3_{s0L}(\tau_1)\tilde{\mathcal{J}}^3_{s0L}(\tau_2)(\tilde{\mathcal{J}}^a_{s,-1,L}\phi^a_s)(\tau_3)(\tilde{\mathcal{J}}^b_{s,-1,L}\phi^b_s)(\tau_4) >_{conn} \quad . \tag{6.1.66}$$

The green's function in the above equation may be evaluated with the use of the operator product expansion (OPE) which pulls out the singular behavior in a product of operators. Heuristically, this amounts to a kind of generalized Wick's theorem in the following sense: the bare Hamiltonian in Eq. (6.1.55) is quadratic in the densities which obey (generalized) canonical commutation relations (the Kac-Moody algebra); hence, apart from possible non-trivial normalization factors for the Green's functions, we might expect Wick's theorem rules to hold. Thus we expect for the corresponding $\mathcal{G}_0$ Green's function to that of Eq. (6.1.66) that

$$< \hat{\mathcal{J}}^3_{s0L}(\tau_1)\hat{\mathcal{J}}^3_{s0L}(\tau_2)(\hat{\mathcal{J}}^a_{s,-1,L}\hat{\phi}^a_s)(\tau_3)(\hat{\mathcal{J}}^b_{s,-1,L}\hat{\phi}^b_s)(\tau_4) >_{conn} =$$

$$A[\frac{1}{(\tau_1-\tau_3)^2(\tau_2-\tau_4)^2}+\frac{1}{(\tau_1-\tau_1)^2(\tau_2-\tau_3)^2}]\frac{1}{(\tau_3-\tau_4)^{2\Delta_s}} \tag{6.1.67}$$

which follows by contracting the density operators together (they always give scaling dimension 1) and the two $\hat{\phi}^a_s$ operators together. This identity does indeed hold, and the normalization constant $A = (2 + M/2)^2$ may be fixed by a rigorous OPE calculation.

Employing Eq. (6.1.59) to convert the $\mathcal{G}_0$ correlation functions to $\mathcal{G}_T$ correlation functions, and shifting limits of integration, Eq. (6.1.65) may be manipulated into the form

$$\chi_{imp} = 8(2+\frac{M}{2})^2\delta\lambda^2(\frac{\pi\tau_0}{\beta})^{2(2+\Delta_s)}[I(2,\beta)]^2 I(2\Delta_s,\beta) \tag{6.1.68}$$

where

$$I(x,\beta) = \int_{\tau_0}^{\beta/2}\frac{d\tau}{[\sin(\pi\tau/\beta)]^x} \quad . \tag{6.1.69}$$

Let us specialize to $M = 2$. The relevant integrals here are, for large β,

$$I(2,\beta) \approx \tau_0 (\frac{\beta}{\pi\tau_0})^2 \tag{6.1.70}$$

and

$$I(1,\beta) \approx \frac{\beta}{\pi} \ln(\frac{2\beta}{\pi\tau_0}) \quad . \tag{6.1.71}$$

As a result, the estimate for the impurity susceptibility is, for $M = 2$ and large β,

$$\chi_{imp} \approx 72\delta\lambda^2\tau_0^3 \ln(\frac{2\beta}{\pi\tau_0}) \ (M = 2) \quad . \tag{6.1.72}$$

For $M > 2$, it is apparent that the integral $I(2\Delta_s, \beta)$ goes as β for large β, so that overall $\chi_{imp} \sim \beta^{1-2\Delta_s} \sim T^{4/(2+M)-1}$ in agreement with the Bethe-Ansatz.

Next we turn to a calculation of the Landau-Wilson ratio. Although the overcompensated model does not have a Fermi liquid fixed point, the fact that the specific heat coefficient and susceptibility have the same singular low temperature properties suggests that there should be a well defined Landau-Wilson ratio. Calculation of this ratio requires a knowledge of the normalization of the bulk Hamiltonian specific heat and susceptibility with no impurity present. Since there are M channels, the bulk specific heat follows from the usual Sommerfeld calculation for $\beta \to \infty$ as

$$C_{bulk} \approx \frac{2\pi^2 M k_B}{3} \frac{k_B T}{D} \tag{6.1.73}$$

where $D \simeq v_F k_F$ is the bandwidth of the conduction electrons. Note that the normalization of Eq. (6.1.73) follows the usual solid state physics conventions and not the conformal theory conventions (compare to eq. (3.6) in Affleck and Ludwig [1991b]; note also in their equation D is set to 1). The corresponding calculation for the Pauli susceptibility with the effective moment μ absorbed in h_s gives

$$\chi_{bulk} = \frac{2M}{D} \quad ; \tag{6.1.74}$$

again, this normalization differs slightly from Affleck and Ludwig [1991b] (compare with Eq. (3.7) of this reference). We can now specialize to the case $M = 2$ and find the Landau-Wilson Ratio as

$$R = \lim_{\beta\to\infty} \frac{(\chi_{imp}/\chi_{bulk})}{(C_{imp}/C_{bulk})} = \frac{8}{3} \ \ (M = 2). \tag{6.1.75}$$

This agrees with numerical results from the Bethe-Ansatz. Affleck and Ludwig [1991b] go further to note that for arbitrary M that

$$R_W = \frac{(2 + M/2)^2(2 + M)}{18} \tag{6.1.76}$$

which follows with explicit evaluation of the integrals in Eqs. (6.1.62) and (6.1.68).

To close this discussion of C_{imp} and χ_{imp}, we note that a diagrammatic view of Eqs. (6.1.62) and (6.1.65) for the free energy is possible. The conceptual point behind this is that it will illustrate a very close link to the discussion of these quantities within the Abelian bosonization approach discussed in Sec. 6.2.2.c. The appropriate diagrams are shown in Fig. 78, where solid lines represent density-density green's functions, and the dashed lines represent the ϕ_s green's function; dots represent the $\delta\lambda$ vertex, and crosses represent an h_s vertex. Fig 78(a) for the specific heat shows that the relevant free energy diagram is a bosonic 'bubble' with one line representing the ϕ_s propagator (which is the dynamic susceptibility for a localized magnetic field) and one line representing the conduction spin density propagator,

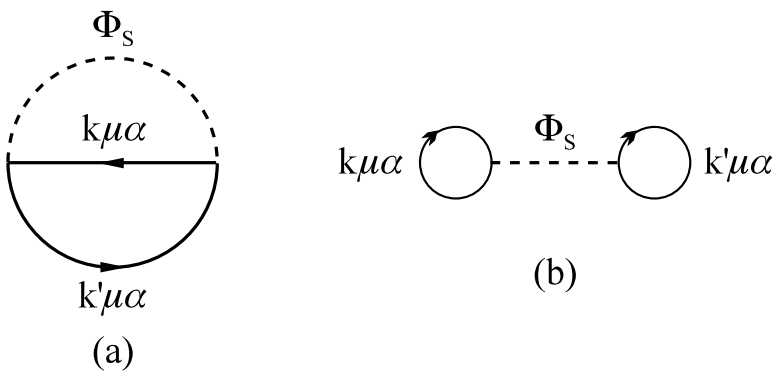

Figure 78: Diagrammatic visualization of free energy contributions yielding specific heat C_{imp} and susceptibility χ_{imp}. Solid lines are conduction electron propagators, dashed lines are local spin tensor Φ_s propagators. Dots are leading irrelevant operator vertices $\delta\lambda$, crosses are applied spin-field vertices h_s. Fig. (a) is in zero applied field and differentiated twice yields the specific heat. Fig. (b) is in finite applied field and differentiated twice yields the susceptibility. These diagrams have a close connection to the corresponding ones in the Abelian bosonization approach discussed in Sec. (6.2).

which in turn must be a continuum electron bubble for appropriately renormalized continuum fields. Fig. 78(b) for the susceptibility shows that the ϕ_s propagator gets two spin density bubbles attached at the end. Formally, these bubbles would have to correspond to double bubbles of suitably redefined continuum fermion fields.

(c) Residual Entropy

The calculation of the residual entropy requires different concepts from the conformal theory, drawing in particular on some mathematical properties of the so-called "modular S-matrix" worked out in the literature. We shall briefly outline the calculation here, as it appears in Affleck and Ludwig [1991c] and Ludwig [1994a].

The entropy of the multi-channel model in any finite size calculation will be the logarithm of an integer, where the integer represents the ground state degeneracy. Here finite size means effectively that we have lowered the temperature to be comparable to the level spacing so that $\beta v_F/l \geq 1$. For example, in the NRG spectra for the two-channel model displayed in Fig. 44, the degeneracy is always two, which would give an entropy or $R\ln 2$. In the continuum or "high temperature limit" where $\beta v_F/l << 1$ relevant to a macroscopic system, this is not the case any longer. In this case, by high temperature we only mean with respect to the quantum spacing of the levels, not to the Kondo scale itself (indeed we are interested in temperatures T satisfying $(\pi v_F/l) << k_B T << k_B T_K$).

The conformal theory provides an elegant approach for switching from the low temperature limit to the "high temperature limit" which was introduced first by Cardy [1989]. The idea is illustrated in Fig. 79. It goes as follows. We normally calculate the partition function by tracing over $exp(-\beta H_{AB})$ where A, B are the boundary conditions on the system at $r = 0, l$ in this one dimensional example. As is usual, this may be viewed as a path integral summing over imaginary time in a periodic way, namely we 'propagate' with $exp(-\beta H_{AB})$ around the cylinder of Fig. 79 in the time direction, always winding up back at the state at which we started. However, the conformal invariance implies that we can interchange space and time directions and that we must get equivalent physical results. Namely, we can interchange space and time axes, to get a new system 'length' equal to $v_F\beta$, and a new system 'time' of $2l/v_F$. The states are specified by a Hamiltonian H_P which has periodic boundary conditions in the new 'space' direction.

The partition function in the original case can be written in terms of 'characters' of the conformal

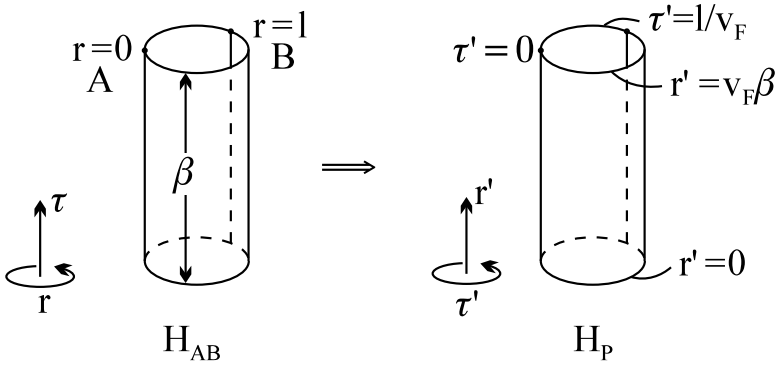

Figure 79: Conformal transformation exploiting the modular invariance of the partition function. To cross from the low temperature limit in which the temperature is less than the level spacing $v_F\pi/\ell$ to the "high temperature limit" in which $v_F\pi/\ell << k_BT << k_BT_K$, it is convenient to interchange space and Euclidean time coordinates. Because of the equivalence of space and Euclidean time coordinates, the transformation must preserve the partition function. This trick enables a calculation of the residual entropy for the thermodynamic limit.

towers in the following form

$$Z = Tr[e^{-\beta H_{AB}}] = \sum_{QSS_c} n_{AB}^{QSS_c} \chi_{QSS_c}(q) \tag{6.1.76}$$

where the sum is only over primary values of the spin, channel-spin, and charge, where $q = \exp(-\beta\pi v_F/l)$, and the character χ_{QSS_c} is given by

$$\chi_{QSS_c}(q) = q^{c/24} \sum_{m=0}^{\infty} d_m(QSS_c) q^{\Delta(QSS_c)+m} \quad . \tag{6.1.77}$$

In Eq. (6.1.77), c is the 'central charge' of the theory which for this model simply counts the degeneracy of the conduction electrons, i.e., $c = 2M$, and $d_m(QSS_c)$ is the degeneracy of the mth descendant of the primary state labeled by QSS_c. The character χ factorizes into a product of characters for the $U(1)$,$SU(2)$, and $SU(M)$ algebras of the charge, spin, and channel-spin sectors. The integers $n_{AB}^{QSS_c}$ have the same meaning as in Secs. 6.1.2.a,b.

In the basis where space and time are interchanged, the partition function propagates along the new 'time' axis from a state characterized by boundary condition A denoted $|A>$ to a state characterized by boundary condition B denoted $|B>$. This replaces the periodicity familiar from the standard trace formula of Eq. (6.1.75). The discrete spacing between states of H_P is now set by the scale $2\pi/\beta$ and as a result the partition function is given by

$$Z =< A|\exp(-2lH_P/v_F)|B >= \sum_{\tilde{Q}\tilde{S}\tilde{S}_c} < A|\tilde{Q}\tilde{S}\tilde{S}_c > \chi_{\tilde{Q}\tilde{S}\tilde{S}_c}(\tilde{q}^2) < \tilde{Q}\tilde{S}\tilde{S}_c|B > \tag{6.1.78}$$

where $\tilde{q} = \exp(-2\pi l/\beta v_F)$. Clearly, as $l/\beta \to \infty$, then only the lowest term of the above sum will remain, and if we set the ground state energy of H_P to zero, then we see that

$$S(0) = \ln Z(T=0) = \ln < A|0 > + \ln < 0|B > \tag{6.1.79}$$

and the calculation of the ground state entropy reduces to the calculation of the matrix elements in Eq. (6.1.79). Note that the mathematical transformation between Eq. (6.1.76) and (6.1.78) is reminiscent of a kind of generalized Poisson summation formula.

The characters for the different realizations H_{AB} and H_P are related by a linear transformation specified by the 'modular S-matrix'; here we restrict attention to just the spin sector which is all that is modified by the absorption of the impurity spin, and define the modular S-matrix by

$$\chi_{\tilde{S}}(\tilde{q}^2) = \sum_S S_s^{\tilde{S}} \chi_s(q) \quad . \tag{6.1.80}$$

In general, the modular S-matrix factorizes into products of S-matrices for the spin, charge, and channel-spin sectors. For an $SU(2)$ level M Kac-Moody algebra, the modular S-matrix is given by (Kac and Peterson [1984])

$$S_{j'}^{j} = \sqrt{\frac{2}{2+M}} \sin[\frac{\pi(2j+1)(2j'+1)}{2+M}] \quad . \tag{6.1.81}$$

A useful identity involving the modular S-matrix is

$$\sum_a S_a^{\tilde{a}} n_{AB}^a =< A|\tilde{a} >< \tilde{a}|B > \tag{6.1.82}$$

which follows straightforwardly from substitution of Eq. (6.1.74) on the left hand side of (6.1.78) and Eq. (6.1.80) for $\chi_a(\tilde{q})$ on the right hand side. Another important result is the Verlinde formula (Verlinde [1988])

$$\sum_j S_j^{\tilde{j}} N_{s,j'}^{j} = \frac{S_s^{\tilde{j}} S_{j'}^{\tilde{j}}}{S_0^{\tilde{j}}} \quad . \tag{6.1.83}$$

Armed with these mathematical results, it is now possible to obtain the ground state entropy.

The strategy is to pick $A = K$, the Kondo boundary condition, $B = F$, the free fermion boundary condition, and $\tilde{Q} = Q = 0$, $\tilde{S}_c = S_c = 0$, and $\tilde{S} = 0$. Then using the fusion rule of Eq. (6.1.48) together with Eqs. (6.1.82) and (6.1.83) allows one to show that

$$< K|000 >< 000|F >=< F|000 >< 000|F > (\frac{S_{S_I}^0}{S_0^0}) \quad . \tag{6.1.84}$$

The free fermion matrix element $< F|000 >$ is one, so in view of Eqs. (6.1.79), (6.1.81), and (6.1.84) we see that the residual entropy is given by

$$S(0) = \ln < K|000 >= \ln[\frac{\sin[\pi(2S_I+1)/(M+2)]}{\sin[\pi/(M+2)]}] \tag{6.1.85}$$

which is exactly the same result obtained from the Bethe-Ansatz (see Sec. 7).

6.1.4 Dynamical Properties

(a) One Electron Green's Function and T-matrix

We follow Ludwig and Affleck [1991c], Affleck and Ludwig [1993], and Ludwig [1994a] here. The T-matrix is useful in calculating the electrical resistivity since the scattering rate is related by $\tau^{-1}(\hat{k}, \omega, T) = -2c_i ImT(\hat{k}\hat{k}, \omega + i0^+, T)$, where c_i is the concentration of impurities and $\hat{k}$ is the propagation direction of an electron with momentum $\vec{k}$. This expression holds to leading order in the impurity concentration. For s-wave scattering as we have assumed here, the $\hat{k}$ dependence drops out. The T-matrix for an impurity at position $\vec{R}_i$ is defined by

$$G(\vec{r}_1, \vec{r}_2, \omega) = G_0(\vec{r}_1 - \vec{r}_2, \omega) + G_0(\vec{r}_1 - \vec{R}_i,)T(\omega)G_0(\vec{r}_2 - \vec{R}_i) \tag{6.1.86}$$

where G_0 is the unperturbed one-electron green's function and G is the perturbed one.

In terms of the effective one-dimensional problem, the T matrix arises from scattering of left moving electrons (incoming spherical waves) to right moving electrons (outgoing spherical waves) and thus shows up in the mixed LR electron green's function. The LL, RR electron green's functions are unperturbed by the impurity. Non-trivial physics shows up in the LR green's function due to the presence of the boundary at which the conduction operators mix with the local fermion operators discussed in Sec. 6.1.2.b.

At zero temperature and energy, where the effects of the leading irrelevant operator discussed in Sec. 6.1.2.c are unimportant, the LR green's function is also related to the S-matrix projected onto outgoing single particle states, denoted $S_{(1)}$. At the Fermi energy, $T(0,0) = (1 - S_{(1)})/2i\pi N(0)$ according to standard scattering theory, so that a calculation of $S_{(1)}$ gives the Fermi surface value of $T(0,0)$. In the case of trivial potential scattering, $S_{(1)} = \exp(2i\delta)$, where δ is the phase shift. This also goes through for the $M/2 = S_I$ compensated Kondo model, and the unit modulus of this says that any incoming single particle state has probability one of being scattered into an outgoing single particle state. In contrast, for the multi-channel model, $|S_{(1)}|$ is generally less than one, reflecting the unbinding of spin, charge, and channel degrees of freedom so that an incoming electron can generate outgoing many body states.

A formal definition of the one-particle projected S-matrix follows from the LR green's function. Put $z = v_F\tau + ir$,$\bar{z} = v_F\tau - ir$. Then

$$G^{LR}_{\mu\alpha}(z_1, \bar{z}_2) =< \Psi_{L\mu\alpha}(z_1)\Psi^{\dagger}_{R\mu\alpha}(\bar{z}_2) >$$

$$= \frac{S_{(1)}}{z_1 - \bar{z}_2} \tag{6.1.87}$$

where we have used the fact that left movers can only depend on z and right movers on $\bar{z}$. This follows from the fact that the electron fields are primary fields with scaling dimension $\Delta_F = 1/2$ together with the conformal invariance.

Eq. (6.1.85) is a special case of a more general boundary relation for primary fields. Consider a primary field operator O^a with quantum numbers specified by a. The green's function for a combination of left moving operators is

$$< O^a_L(z_1)O^a_L(z_2) >= \frac{1}{(z_1 - z_2)^{2\Delta_a}} \tag{6.1.88}$$

where Δ_a is the scaling dimension. On the other hand, the boundary A characterized by boundary state $|A>$ (c.f, Sec. 6.1.3.c) can mix left and right movers giving the green's function

$$< O^a_L(z_1)O^a_R(\bar{z}_2) >= \frac{< a|A >}{< 0|A >}\frac{1}{(z_1 - \bar{z}_2)^{2\Delta_a}} \tag{6.1.89}$$

where $< 0|A >$ is a normalization factor measuring the effect of the identity operator on the boundary state. Since a fermion operator has the quantum numbers $Q = 1, S = 1/2$ and transforms as the fundamental representation of $SU(M)$ which we denote simply M, then we see that for $A = K$, the Kondo boundary condition

$$S_{(1)} = \frac{< 1, 1/2.M|K >}{< 0, 0, 0|K >} \quad . \tag{6.1.90}$$

This ratio of matrix elements can be evaluated with the same kinds of methods employed to calculate the residual entropy of Sec. 6.1.3.c, and again Ludwig and Affleck [1991], Affleck and Ludwig [1993], and Ludwig [1994a] have employed the methods of Cardy [1986a,b;1989] for boundary critical

phenomena. Using the factorization of the modular S-matrix (not to be confused here with $S_{(1)}$), together with Eq.(6.1.80), we see that for $A = F$, $B = K$

$$\sum_{QSS_c} S^Q_{Q'} S^S_{S'} S^{S_c}_{S'_c} n_{FK}^{Q'S'S'_c} =< F|QSS_c >< QSS_c|K > \quad . \tag{6.1.91}$$

If we now substitute in the fusion rule of Eq. (6.1.48), and re-employ Eq.(6.1.82) together with the Verlinde formula Eq. (6.1.83) (Verlinde [1988]), we can obtain the relation

$$\frac{< QSS_c|K >}{< QSS_c|F >} = \frac{S^S_{S_I}}{S^S_0} \tag{6.1.92}$$

which generalizes Eq.(6.1.84) used for the entropy. We now note that for a free fermion boundary $S_{(1)} = 1$, so that the ratio $< 1, 1/2, M|F > / < 0, 0, 0|F >= 1$. In view of Eq. (6.1.91) this implies

$$\frac{< 1, 1/2, M|K >}{< 1, 1/2, M|F >} \frac{< 0, 0, 0|F >}{< 0, 0, 0|K >} = \frac{< 1, 1/2, M|K >}{< 0, 0, 0|K >} = \frac{S^{1/2}_{S_I} S^0_0}{S^{1/2}_0 S^0_{S_I}} \quad . \tag{6.1.93}$$

Employing the formula for the modular S-matrix of an $SU(2)$ level M Kac-Moody algebra given in Eq. (6.1.81) together with some minor trigonometric manipulations, we obtain

$$S_{(1)} = \frac{\cos[\pi(2S_I + 1)/(2 + M)]}{\cos[\pi/(2 + M)]} \quad . \tag{6.1.94}$$

As a result, the T-matrix at the Fermi level is purely imaginary and the zero temperature scattering rate is given by

$$\frac{1}{\tau(0, 0)} = -2ImT(\omega = 0^+, T = 0) = \frac{c_i(1 - S_{(1)})}{\pi N(0)} \tag{6.1.95}$$

We now consider this formula in some special cases:
(1) Compensated Kondo Problem ($S_I = M/2$). In this case it is easy to see that $S_{(1)} = -1$, corresponding to a phase shift of $\pi/2$ as expected from Sec. 4, Sec. 6.1.1,Sec. 6.1.2. Hence, $1/\tau(0, 0)$ obtains the unitarity limit of $1/\pi N(0)$.
(2) $M >> 1$. In this case, the perturbative treatment of Gan *et al* [1993] discusssed in Sec. 3.4.5 should hold. We expect that the T-matrix should just represent spin-disorder scattering off an effective impurity with spin S_I with dimensionless exchange coupling strength $N(0)J = 2/M$. If we expand Eq. (6.1.95) for large M, we obtain

$$\frac{1}{\tau(0, 0)} \approx \frac{\pi}{4N(0)} (\frac{2}{M})^2 S_I(S_I + 1) + O(\frac{1}{M^3}) \tag{6.1.96}$$

which fulfills our expectations. As noted in Sec. 5.1, the large N NCA restricted in an uncontrolled approximation to $N = 2$ and M arbitrary gives excellent agreement with Eq (6.1.95) for all values of M.
(3) M=2. In this case, $S_{(1)}$ vanishes, so $1/\tau(0, 0)$ reaches half the unitarity limit. What is remarkable, as stressed by Ludwig and Affleck [1991], is that this implies the strongest possible violation of Fermi liquid theory: an incoming single particle state is scattered completely into many body states!

In fact, the result is much stronger: scattering of an incoming particle(hole) into any state with $2n+1$ uncorrelated particles(holes) and $2n$ uncorrelated holes(particles) has zero amplitude (Maldacena and Ludwig [1996]). Thus, on the surface, unitarity of the scattering amplitude is completely violated. This "unitarity paradox" is resolved when a different basis for the conformal theory is chosen in terms of majorana fermions (Maldacena and Ludwig [1996]). The essence of the idea is that the Hilbert space

containing just physical particle/hole occupation is incomplete, and when extended, a new fermion arises into which a physical fermion my scatter with unit projection. This new fermion has fractional occupancy in terms of the physical states, and is thus not detectable with any external probes. We shall give a brief discussion of this approach in Sec. 6.3.

Affleck and Ludwig (Ludwig and Affleck [1991], Affleck and Ludwig [1993]) have also computed the leading corrections to the scattering rate in temperature and frequency. This calculation involves perturbing the one-electron green's function linearly in the leading irrelevant operators $\vec{\mathcal{J}}_{s,-1,L} \cdot \vec{\phi}_s$ (and, for $M = 2, S_I = 1/2$, $\vec{\mathcal{J}}_{c,-1,L} \cdot \vec{\phi}_s$). The full calculation is quite complex and exploits the operator product expansion (OPE) method extensively; since it is too long and involved to outline here, we refer the reader to Affleck and Ludwig [1991] for details. The main result is that the resistivity will experience a correction proportional to $\delta\lambda T^{\Delta_s}$ (which power law is in agreement with the NCA treatment of Sec. 5.1), so that the sign of the deviation is determined by whether one approaches the fixed point coupling strength from above or below. In the special case of $M = 2, S_I = 1/2$ they find that the resistivity is given by

6.1.97
$$\frac{\rho(T)}{\rho(0)} \approx [1 + 4\delta\lambda\tau_0\sqrt{\pi T\tau_0} + O(T)] \quad .$$

There is thus a universal amplitude relation between the square of $T^{1/2}$ term and the coefficient of the $\ln T$ divergence in C_{imp}/T.

Affleck and Ludwig [1993] also consider the effects of potential scattering, and show that while for the $M = 2, S_I = 1/2$ case it does not affect the zero temperature resistivity, it does affect the magnitude of the $\sqrt{T}$ term and can also induce a thermopower which goes as $\sqrt{T}$.

(b) Local Field Dynamical Susceptibility

Here we employ the conformal theory technique to calculate the local spin and channel spin susceptibilities for the $S_I = 1/2, M = 2$ case to confirm the suspicions that they have marginal fermi liquid form (Cox [1988]; Varma *et al.* [1989]; Tsvelik [1990]; Emery and Kivelson [1992]: Cox and Ruckenstein [1993]; Gan, Coleman, and Andrei [1993]). We simply show the calculations for the ϕ_s case; they are completely analogous for the channel field. This calculation has been carried out in Ludwig and Affleck [1994].

The idea is to consider a dynamical local field $h_s(\omega)$ which is coupled only to ϕ_s^3. At finite temperature, the response to this field will simply be the ϕ_s green's function given by

(6.1.98)
$$< \phi_s^3(\tau)\phi_s^3(0) >= \frac{\pi\tau_0}{\beta}\frac{1}{sin[\pi\tau/\beta]} \quad .$$

It is trivial to analytically continue this to real times, and if we Fourier transform to obtain the absorptive response function $\chi_s''(\omega, T)$ we obtain

(6.1.99)
$$\chi_s''(\omega, T) = \frac{2\pi\tau_0}{\beta}\int_0^\infty dt \frac{sin(\omega t)}{sinh[\pi t/\beta]} \quad .$$

This integral is easy to evaluate, and the result is

$$\chi_s''(\omega, T) = 2\tau_0 Im\psi(\frac{1}{2} - \frac{i\beta\omega}{2\pi})$$

(6.1.100)
$$= \pi\tau_0 tanh(\frac{\beta\omega}{2})$$

where $\psi(x)$ is the digamma function. This is precisely the marginal fermi liquid form of the local dynamic susceptibility (Varma *et al.* [1989]). When analytically continued to the real axis and set to zero

frequency it reproduces the log divergence of the static susceptibility.

(c) Other Dynamic Response Functions

In addition to the single electron green's function, Affleck and Ludwig (Ludwig and Affleck [1991], Affleck and Ludwig [1994a,b]) have computed a number of two-particle electron response functions. The functions have complicated and non-intuitive forms reflecting the non-trivial boundary condition and non-Fermi liquid fixed point. We simply survey the results here obtained for the $M = 2, S_I = 1/2$ case:
(1) Spatial-temporal dependent spin polarization response This function contains non-Fermi liquid response that could in principle be sampled by Knight shift measurements for a magnetic impurity and nuclear electric-field gradient measurements for a quadrupolar kondo impurity.
(2) Spatial-temporal dependent pair field response function. This function displays the expected singularities for the $Q = 2, S = 0, S_c = 0$ field obtained by antisymmetrizing in the spatial index r, which corresponds to antisymmetrizing in L, R indices near the impurity site in view of the mirroring condition $\Psi_L(r) = \Psi_R(-r)$. Equivalently we may go right to the impurity site and antisymmetrize in imaginary time in view of the conformal invariance. Specifically, in terms of the three dimensional field operators $\Psi_{\mu\alpha}(\vec{r})$, the full three dimensional pairing field is an orbital p-wave which is a singlet in spin and channel indices with

$$P^a = \sigma^{(2)}_{\mu\nu}\sigma^{(2)}_{\alpha\beta}\Psi_{\mu\alpha}(\vec{r})\frac{\partial}{\partial r_a}\Psi_{\nu\beta}(\vec{r}) = \frac{ik_F r^a}{8\pi^2 r^3}[\psi_{L\mu\alpha}(r)\psi_{R\nu\beta}(r) - \psi_{R\mu\alpha}(r)\psi_{L\nu\beta}(r)] \tag{6.1.101}$$

We shall provide a more complete discussion of pairing correlations in Sec. 9.4.

6.2 Abelian Bosonization Approach to the Two-Channel Kondo Model

In this subsection, we describe the Abelian bosonization approach to the two-channel Kondo model developed by Emery and Kivelson. The central idea which makes this work is that when using a spinless Fermion representation for the impurity spin, the x and y components corresponding to Majorana or "real fermions". The Kondo Hamiltonian becomes, for a special value of the longitudinal exchange coupling, a one particle resonant level model in the space of conduction electrons plus one of the Majorana variables. This model is exactly soluble. The other Majorana variable decouples. All singularities and anomalies in this approach are seen to be due to the presence of the uncoupled field. In a counting sense which can be made mathematically precise, each Majorana fermion is half a full fermion. This leads to a nice interpretation of the $R/2\ln 2$ entropy (this corresponds to the decoupled variable) and (possibly) of the scattering rate value at the Fermi energy to one half the unitarity limit (deriving from unitarity scattering from half a fermion!). However, as we shall discuss, a full interpretation of transport properties remains problematic in this approach. (Recently Fabrizio and Gogolin [1994] have applied similar ideas to the four channel spin 1/2 model to illustrate its equivalence to a model where two spin 1 conduction channels couple to the impurity and to calculate the low temperature properties.)

6.2.1 Model, Mapping to a Resonant Level Hamiltonian

Emery and Kivelson begin with the two-channel Kondo model in the anisotropic (xxz) limit, taking only left moving fermions living on $-\infty < x < +\infty$ (the incoming s partial wave states reflected about the origin) coupled to the impurity, following Affleck and Ludwig [1991(b)]. Thus, $x < 0$ is for incoming waves and $x > 0$ is for outgoing waves. Following their notation, the Hamiltonian is

$$H = iv_F \sum_{\mu\alpha}\int_{-\infty}^{\infty} dx \psi^\dagger_{\mu\alpha}(x)\frac{\partial\psi_{\mu\alpha}(x)}{\partial x} + \frac{1}{2}\sum_{\mu\nu\alpha\lambda} J_\lambda \tau^\lambda \sigma^\lambda_{\mu\nu}\psi^\dagger_{\mu\alpha}(0)\psi_{\nu\alpha}(0) \tag{6.2.1}$$

where μ, ν are conduction spin indices, α is the channel index, σ^λ are Pauli matrices, and the τ^λ are the spin 1/2 impurity operators. We assume $J_x = J_y$, $J_z > 0$ to ensure the Kondo effect (c.f. Sec. 3.3).

In the presence of a bulk magnetic field h, we add to this the term (Eq. 2.10 of Emery and Kivelson [1992] and Eq. (13) of Sengupta and Georges [1994])

$$H_{Zeeman} = -h\{\tau^z + \frac{1}{2}\sum_{\mu\alpha}\int_{-\infty}^{\infty} dx \sigma^z_{\mu\mu}\psi^\dagger_{\mu\alpha}(x)\psi_{\mu\alpha}(x)\} \quad . \tag{6.2.2}$$

We will also consider the possibility of an impurity field in which the second term of Eq. (6.2.2) is absent.

Now a sequence of transformations are applied to Eq. (6.2.1) to map this into a resonant level Hamiltonian, which go as follows:
(1) Bosonization. Following the conventions of Bander [1976], the "massless" (linear dispersion relation) fermion fields are replaced by bosons, through the relation

$$\psi_{\mu\alpha}(x) = \frac{1}{\sqrt{2\pi a}}\exp(-i\Phi_{\mu\alpha}(x)) \tag{6.2.3}$$

where

$$\Phi_{\mu\alpha}(x) = \sqrt{\pi}\int_{-\infty}^{x} dx'\{\Pi_{\mu\alpha}(x) - \phi_{\mu\alpha}(x)\} \tag{6.2.4}$$

and the Bose fields ϕ, Π obey canonical commutation relations

$$[\phi_{\mu\alpha}(x), \Pi_{\nu\beta}(x')] = i\delta_{\mu\nu}\delta_{\alpha\beta}\delta(x-x') \quad . \tag{6.2.5}$$

The length a appearing in Eq. (6.2.3) is essentially the lattice constant, which we take to zero in the full continuum limit. We shall look for physical quantities independent of a. The prescription of (6.2.3) should be familiar to any reader used to the Jordan-Wigner transformation. Using it, for example, it is easy to see that by applying the Baker-Hausdorff lemma (c.f., sec. 4.3 of Fradkin [1991]).

$$\psi_{\mu\alpha}(x)\psi_{\mu\alpha}(x') = \psi_{\mu\alpha}(x')\psi_{\mu\alpha}(x)e^{(-\pi[\Phi_{\mu\alpha}(x),\Phi_{\mu\alpha}(x')])} = \psi_{\mu\alpha}(x')\psi_{\mu\alpha}(x)e^{(i\pi[\theta(x'-x)-\theta(x-x')])} \tag{6.2.6}$$

so that the Fermion anticommutation relation is satisfied so long as $x \neq x'$; clearly from idempotence of the ψ fields, the ambiguity in the exponent for $x = x'$ is irrelevant in this case. However, for proper derivation of all the commutation relations we must take care at equal spatial separations as singular contributions will arise (Bander [1976]). Using the boson operators, the free Fermion hamiltonian becomes a free boson Hamiltonian (sum of harmonic oscillators),

$$H_{free} = \frac{v_F}{2}\sum_{\mu\alpha}\int dx[\Pi^2_{\mu\alpha}(x) + (\frac{\partial\phi_{\mu\alpha}(x)}{\partial x})^2] \tag{6.2.7}$$

and the exchange term becomes

$$H_{Kondo} = \frac{J^z}{2\pi}\tau^z\sum_{\mu\alpha}\sigma^z_{\mu\mu}[\frac{\partial\Phi_{\mu\alpha}}{\partial x}]_{x=0} + \frac{J_x}{4\pi a}\sum_{\lambda=x,y}\sum_{\mu\nu\alpha}\tau^\lambda\sigma^\lambda_{\mu\nu}\exp[i(\Phi_{\mu\alpha} - \Phi_{\nu\beta})] \quad . \tag{6.2.8}$$

The reason that the Φ gradient comes in the z-axis exchange coupling is because of the singularities in products of the exponential operators at zero separation (Bander [1976]). Specifically,

$$\lim_{x\to x'}\psi^\dagger_{\mu\alpha}(x)\psi_{\mu\alpha}(x') \sim \{\exp(i\sqrt{\pi}[\Phi_{\mu\alpha}(x) - \Phi_{\mu\alpha}(x')]) - 1\} \tag{6.2.9}$$

from which the origin of the derivative term is clear. All fermion number and current operators, in fact, can be expressed as linear forms of bosonic operators.
(2) Canonical Transformation to Collective Coordinates. Under a canonical transformation of boson coordinates that preserves the commutation relation structure of Eq. (6.2.5), the free boson Hamiltonian

will be unchanged. However, with a suitable transformation we may greatly simplify the interaction term H_{Kondo}. The choice made by Emery and Kivelson [1992] is to write the original bose fields in terms of "collective" coordinates describing charge (Φ_c), spin (Φ_s), channel or flavor (Φ_{sf}), and mixed spin/flavor degrees of freedom (Φ_{sf}). The definitions are

$$\Phi_c = \frac{1}{2}\sum_{\mu\alpha}\Phi_{\mu\alpha} \tag{6.2.10.a}$$

$$\Phi_s = \frac{1}{2}\sum_{\mu\alpha}\sigma^z_{\mu\mu}\Phi_{\mu\alpha} \tag{6.2.10.b}$$

$$\Phi_f = \frac{1}{2}\sum_{\mu\alpha}\sigma^z_{\alpha\alpha}\Phi_{\mu\alpha} \tag{6.2.10.c}$$

$$\Phi_{sf} = \frac{1}{2}\sum_{\mu\alpha}\sigma^z_{\mu\mu}\sigma_{\alpha\alpha}\Phi_{\mu\alpha} \tag{6.2.10.d}$$

which may readily be inverted to give

$$\Phi_{\uparrow+} = \frac{1}{2}[\Phi_c + \Phi_s + \Phi_f + \Phi_{sf}] \tag{6.2.11.a}$$

$$\Phi_{\uparrow-} = \frac{1}{2}[\Phi_c + \Phi_s - \Phi_f - \Phi_{sf}] \tag{6.2.11.b}$$

$$\Phi_{\downarrow+} = \frac{1}{2}[\Phi_c - \Phi_s + \Phi_f - \Phi_{sf}] \tag{6.2.11.c}$$

$$\Phi_{\downarrow-} = \frac{1}{2}[\Phi_c - \Phi_s - \Phi_f + \Phi_{sf}] \quad . \tag{6.2.11.d}$$

In terms of these operators, the conduction spin densities $s^\lambda(0)$ are given by

$$s^z(0) = \frac{1}{2}\sum_{\mu\alpha}\sigma^z_{\mu\mu}\psi^\dagger_{\mu\alpha}(0)\psi_{\mu\alpha}(0) = [\frac{\partial\Phi_s}{\partial x}]_{x=0} \tag{6.2.12.a}$$

$$s^x(0) = 2\cos(\Phi_s(0))\cos(\Phi_{sf}(0)) \tag{6.2.12.b}$$

$$s^y(0) = 2\sin(\Phi_s(0))\cos(\Phi_{sf}(0)) \tag{6.12.c}$$

so that

$$H_{Kondo} = \frac{J_z}{\pi}\tau^z[\frac{\partial\Phi_s}{\partial x}]_{x=0} + \frac{J_x}{\pi a}[\tau^x\cos(\Phi_s(0)) + \tau^y\sin(\Phi_s(0))]\cos(\Phi_{sf}(0)) \quad . \tag{6.2.13}$$

Notice that the sines and cosines in the above equation are already suggestive of "real" fermions, in that we know pure complex exponentials obey fermionic commuation relations, so the idea is to write, schematically, $\psi \sim \psi_R + i\psi_I$, which would correspond to the sine and cosine factors. Notice also that the transverse coupling in the above equation is in a position for simplification by a rotation about the z-axis, which in fact is the next step.

(3) Unitary Transformation. Φ_s can be eliminated from the transverse Kondo coupling by rotating the impurity pseudospin about the z-axis through the angle $-\Phi_s(0)$. This corresponds to applying the unitary transformation UHU^{-1} to the Hamiltonian with $U = \exp(i\tau^z\Phi_s(0)/2)$. When applied to the free particle term we obtain

$$UH_{free}U^{-1} = H_{free} - v_F\tau^z[\frac{\partial\Phi_s}{\partial x}]_{x=0} \tag{6.2.14}$$

$$UH_{Kondo}U^{-1} = -\frac{J_z}{\pi}\tau^z[\frac{\partial\phi_s}{\partial x}]_{x=0} + \frac{J_x}{\pi a}\tau^x\cos\phi_{sf}(0) \tag{6.2.15}$$

and when applied to the Zeeman energy we obtain (Sengupta and Georges [1994])

$$UH_{Zeeman}U^{-1} = -\frac{h}{2}\sum_{\mu\alpha}\int dx_{-\infty}^{\infty}\sigma^z_{\mu\mu}\psi^\dagger_{\mu\alpha}(x)\psi_{\mu\alpha}(x) = -\frac{h}{2\pi}\int_{-\infty}^{\infty}dx\frac{\partial\phi_s(x)}{\partial x} \tag{6.2.16}$$

so that the impurity coupling to the field ($-\tau_z$) drops out! This result shall be used below in discussing thermodynamics.

(4) Fermionization. Now the Hamiltonian can be "re-fermionized" in terms of the fermion operators corresponding to the collective coordinates, given by e.g., $\psi_c = \exp(-i\Phi_c)/\sqrt{2\pi a}$. The Hamiltonian may be written as a sum of terms from each of the c, s, f, sf sectors. The c and f sectors decouple from the impurity and are simply free fermion Hamiltonians. In addition to the re-fermionization of the conduction fields, the impurity spin field operators may be expressed in terms of a spinless fermion representation with creation and annihilation operators $d^\dagger, d$ such that the occupied fermion state corresponds to up spin and the empty state to down spin. In terms of these operators,

$$\tau^z = d^\dagger d - 1/2 \tag{6.2.17.a}$$

$$\tau^+ = d^\dagger \tag{6.2.17.b}$$

$$\tau^- = d \quad . \tag{6.2.17.c}$$

It is clear that the commuation relations $[\tau^i, \tau^j] = i\epsilon_{ijk}\tau^k$ are faithfully reproduced by this choice. The operators τ^x, τ^y are then proportional to the real or Majorana fermion variables $\hat{a}, \hat{b}$ given by

$$\hat{a} = \frac{1}{\sqrt{2}}[d + d^\dagger] = \sqrt{2}\tau^x \tag{6.2.18.a}$$

and

$$\hat{b} = \frac{1}{i\sqrt{2}}[d^\dagger - d] = \sqrt{2}\tau^y \quad . \tag{6.2.18.b}$$

The normalization conditions on $\hat{a}, \hat{b}$ are $\hat{a}^2 = \hat{b}^2 = 1/2$. In terms of these operators $\tau^z = -i\hat{a}\hat{b}$.

In terms of these new fermion operators, the sf, s sector Hamiltonians may be written as

$$H_{sf} = \int dx\psi^\dagger_{sf}(x)\frac{\partial\psi_{sf}(x)}{\partial x} + \frac{iJ_x}{\sqrt{\pi a}}[\psi_{sf}(0) + \psi^\dagger_{sf}(0)]\hat{b} \tag{6.2.19}$$

and

$$H_s = \int dx\psi^\dagger_s(x)\frac{\partial\psi_s(x)}{\partial x} - 2i(J_z - \pi v_F)\hat{a}\hat{b}\psi^\dagger_s(0)\psi_s(0) \quad . \tag{6.2.20}$$

We make three notes about Eqs. (6.2.19,20):
(i) If we work at the special point $J_z = \pi v_F$, the coupling of the impurity to $[\partial\phi_s/\partial x]_0]$ drops out (see eqns. (6.2.15,6.2.16)). As a result, only H_{sf} includes any coupling to the impurity, and at that only to the $\hat{b}$ Majorana fermion. Since this hamiltonian is a quadratic form (it is a particular realization of the resonant level model), the properties may be exactly solved for at this special point in coupling space. Nearby points in coupling space can be reached by performing perturbation theory in $\lambda = J_z - \pi v_F$.
(ii) A technical point about (6.2.19) which is glossed over by Emery and Kivelson [1992] is that to arrive at this properly Hermitian form, another unitary transformation $U = \exp(-i\pi\tau^z/4)$ must be performed, since $\hat{b} \sim \tau^y$, not τ^x. This unitary transformation doesn't affect any of the conduction fields. The need for this transformation is related to the desire for $\psi_{sf}, \hat{b}$ to anticommute. If instead we keep the $\cos\Phi_{sf}(0)$ term in Eq. (6.2.15), we would not need the additional unitary transformation. Eq. (19) of Sengupta and Georges [1994] must be amended in this regard.
(iii) The coupling to Majorana fermions is quite novel; one Majorana unit of Ψ_{sf} fermion is hybridized with the $\hat{b}$ fermion. In contrast, the single channel spin 1/2 model through similar tricks may be mapped to a spinless resonant level model with an ordinary hybridization term $\sim \Psi^\dagger(0)d + d^\dagger\Psi(0)$ (Toulouse [1970], Schlottmann [1979], Wiegman and Finkelshtein [1979]). All impurity degrees of freedom couple into the conduction electrons in this latter case, while the $\hat{a}$ field is left over in the two-channel case.

6.2.2 Thermodynamics

We now review the derivation of the thermodynamic properties within this approach.

(a) Green's Functions

The thermodynamics of the model to the extent that we perturb in powers of λ may be specified completely in terms of the Green's functions of H_{sf}. These may be obtained by equations of motion quite straightforwardly, which we present in App. IV. An important feature is that anomalous Green's functions appear for the ψ_{sf} fields because $\hat{b}$ couples to both $\psi_{sf}, \psi^\dagger_{sf}$. Also, the b fermion acquires a width $\Gamma = J_x^2/(\pi v_F a)$

(b) Entropy

A crucial point in dealing with the Majorana variables is that whenever we count their spectral weight we must include a factor of 1/2 relative to ordinary fermionic degrees of freedom. To understand this, we shall evaluate the the impurity free energy in the $J_x = J_z = 0$ limit by the complicated procedure of using the spinless fermion representation Green's functions. The imaginary time d fermion propagator is given by

$$G_d(\tau) = -\,<T_\tau d(\tau)d^\dagger(0)> = \frac{1}{\beta}\sum_{\omega_n}\frac{e^{i\tau\omega_n}}{i\omega_n} \tag{6.2.21}$$

where $\omega_n = (2n+1)\pi/\beta$ is a Fermionic Matsubara frequency, and from which we infer the spectral density $A_d(\epsilon) = \pi\delta(\epsilon)$ and the free energy

$$\begin{aligned} F_d &= -k_B T \int \frac{d\epsilon}{\pi} A_d(\epsilon)\ln(1+e^{-\beta\epsilon}) \\ &= -k_B T \ln 2 \quad . \end{aligned} \tag{6.2.22}$$

Now, on the other hand, G_d may be expressed in terms of the Majorana Green's functions $G_a(\tau) = -\,<T_\tau\hat{a}(\tau)\hat{a}>$, $G_b(\tau) = -\,<T_\tau\hat{b}(\tau)\hat{b}>$ we have $G_d = (G_a + G_b)/2$, so that each Majorana fermion contributes $(k_B/2)\ln 2$ of entropy to the free energy of Eq. (6.2.22).

Turning now to the case $\lambda = 0, J_x \neq 0$, we denote the spectral functions of the $\hat{a}, \hat{b}$ fields as $A_a(\omega) = \pi\delta(\omega)$, and $A_b(\omega) = \Gamma/(\omega^2 + \Gamma^2)$. Using fermion statistics and the weights identified above, we can write the impurity entropy as

$$S(T) = S_a(T) + S_b(T) = -k_B T \sum_{i=a,b} \int \frac{d\epsilon}{2\pi} A_i(\epsilon)[f(\epsilon)\ln f(\epsilon) + (1-f(\epsilon))\ln(1-f(\epsilon))] \tag{6.2.23}$$

$$= \frac{k_B}{2}\ln 2 - k_B \int \frac{d\epsilon}{2\pi}\frac{\Gamma}{\epsilon^2+\Gamma^2}[f(\epsilon)\ln f(\epsilon) + (1-f(\epsilon))\ln(1-f(\epsilon))] \quad .$$

The first term above is due to the $\hat{a}$ field, the second term from the $\hat{b}$ field. It is easy to see that for $T >> \Gamma$, the second term tends to $(k_B/2)\ln 2$, so the full $k_B \ln 2$ entropy of the impurity is recovered. On the other hand, for $T << \Gamma$, we rewrite the second term in a form amenable to the Sommerfeld expansion

$$S_b(T) = k_B \int \frac{d\epsilon}{2\pi}(\frac{-\partial f}{\partial \epsilon})(\beta\epsilon) tan^{-1}(\frac{\epsilon}{\Gamma}) \tag{6.2.24}$$

$$\approx \frac{\pi^3 k_B}{6}(\frac{k_B T}{\Gamma}), \quad T \to 0 \quad .$$

The above expression for the entropy may be obtained by differentiation of Eq. (3.5) in Emery and Kivelson [1992] with the field H set to zero.

Hence, for $\lambda = J_z - \pi v_F = 0$ we see that the unusual residual entropy of the two-channel model is understood as arising from the decoupled Majorana degree of freedom (S_a). However, the specific heat is analytic in the temperature, which will be remedied in Sec. 6.2.2.c by performing perturbation theory in λ.

An interesting question is the extent to which this idea can be pushed with other multichannel models to understand the residual entropy. It is clear that a Majorana representation alone will not be sufficient. For example, as mentioned previously, for the three channel spin 1/2 model the residual entropy is $-(R/2)\ln([\sqrt{5}+3]/8])$ which is not simply related to the entropy of a single Majorana field $R\ln\sqrt{2}$. However, it is conceivable that a different kind of composite field might be developed to describe the three channel case, which may give a description with a similar flavor to the above decomposition.

(c) Thermodynamics at $\lambda \neq 0$

The thermodynamics at $\lambda \neq 0$ has been considered by Emery and Kivelson [1993, see footnote [6]; 1994], by D. Clarke *et al.* [1993], and by Sengupta and Georges [1994]. We follow the more extensive discussion of the latter paper here. Now we include the bulk field term H_{Zeeman} and recall that after the unitary transformation only the coupling to the conduction degrees of freedom remains.

Using standard perturbation theory methods, two terms arise in the free energy to second order in λ. These are shown in Fig. 80, and are given by

$$\Delta F_{imp} = -\frac{\lambda^2}{2}[G_s^2(0,h)\int_0^\beta d\tau G_a(\tau)G_b(\tau) + \int_0^\beta d\tau G_s^2(\tau,h)G_a(\tau)G_b(\tau)] \quad . \tag{6.2.25}$$

It is easy to see that

$$G_s(0,h) = \frac{1}{\beta}\sum_\omega \int \frac{dk}{2\pi a}\frac{e^{i\omega 0^+}}{i\omega - v_F k - h} \approx \frac{h}{2\pi v_F}\int d\epsilon(\frac{-\partial f(\epsilon)}{\partial\epsilon}) = \frac{h}{2\pi v_F} \quad . \tag{6.2.26}$$

Note that $1/2\pi v_F$ is simply the Fermi level density of states $N(0)$. The first term in Eq. (6.2.25) will contribute the leading h dependence, while the second term will contribute the leading T dependence at $h = 0$; henceforth we set h=0 in the second term.

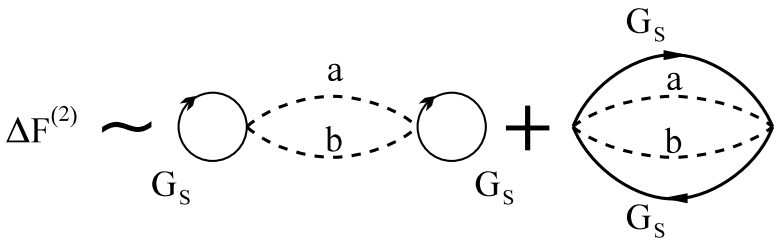

Fig. 6.8

Figure 80: Leading order in λ contributions to the impurity free energy in the Abelian bosonization scheme of Emery and Kivelson [1992,1993]. Solid lines are conduction "spin fermion" propagators, evaluated in the free ($\lambda = 0$) limit. Dashed lines are local Majorana fermion propagators. The first term is second order in the applied field and gives rise to the susceptibility (which is zero at the Emery and Kivelson point), while the second term gives the leading logarithmic contribution to the specific heat away from the Emery and Kivelson point. Since the convolution of the a, b Majorana propagators gives the local z-axis spin susceptibility, it is clear that these free energy diagrams have a close correspondence to those of the conformal theory (Fig. 78) modulo the assumed anisotropy here.

The first term in Eq. (6.2.25) is easy to evaluate in frequency space. Decomposing in Fourier modes, the integral can be written

$$\int_0^\beta d\tau G_a(\tau)G_b(\tau) = -\frac{1}{\beta}\sum_\omega \frac{1}{i\omega(i\omega + i\Gamma sgn\omega)} \tag{6.2.27}$$

$$= \frac{1}{2\pi\Gamma}[\Psi(\frac{1}{2} + \frac{\beta\Gamma}{2\pi}) - \Psi(\frac{1}{2})] \approx \frac{1}{2\pi\Gamma}\ln(1.13\beta\Gamma) \quad .$$

The second integral is easier to evaluate in the time domain (Sengupta and Georges [1994]), using

$$G_a(\tau) = -\frac{1}{2}sgn(\tau), \quad G_b(\tau) \approx \frac{1}{\beta\Gamma\sin(\pi\tau/\beta)}, \quad G_s(\tau) \approx \frac{1}{2\beta v_F \sin(\pi\tau/\beta)} \tag{6.2.28}$$

where the expressions for G_b, G_s are valid for $T << \Gamma$ and $\pi/\Gamma << \tau << \beta$. Clearly the expressions for G_b, G_s are symmetric about $\tau = \beta/2$, and so we cutoff at π/Γ below and $\beta - \pi/\Gamma$ above in the integral. This arbitrariness will not affect the amplitude of the most singular piece in the second term, but will affect the argument of the logarithm. The result is

$$I_2 = \int_0^\beta G_a(\tau)G_b(\tau)G_s^2(\tau,0) \approx \frac{(k_BT)^2}{4\pi v_F^2\Gamma}\int_{\pi/\beta\Gamma}^{\pi/2} dx \frac{1}{\sin^3(x)} \quad . \tag{6.2.29}$$

The latter integral may be evaluated using

$$\int_y^{\pi/2} \frac{dx}{\sin^3(x)} = \frac{1}{2}arsh[cot(y)] + \frac{1}{2}cot(y)csc(y) \tag{6.2.30}$$

to give

$$I_2 \approx \frac{1}{4\pi^3 v_F^2\Gamma}[\frac{\pi^2(k_BT)^2}{2}\ln(\frac{\Gamma}{k_BT}) + \frac{\Gamma^2}{2}] \quad . \tag{6.2.31}$$

Putting these results together, we see that the most singular terms in the impurity contribution to the free energy from the s sector to order λ^2 are given by

$$\Delta F_{imp} = -\frac{[N(0)\lambda]^2}{2\pi\Gamma}[h^2\ln(1.12\beta\Gamma) + \frac{\pi^2(k_BT)^2}{2}\ln(\pi\beta\Gamma)] \tag{6.2.32}$$

from which we may immediately read off the impurity susceptibility χ_{imp} and specific heat C_{imp} as

$$\chi_{imp}(T) = -\frac{\partial^2 \Delta F_{imp}}{\partial h^2} \approx \frac{[N(0)\lambda]^2}{\pi\Gamma} \ln(1.13\beta\Gamma) \tag{6.2.33}$$

and

$$C_{imp}(T) = -\frac{\partial^2 \Delta F_{imp}}{\partial T^2} \approx k_B \frac{[N(0)\lambda]^2}{2\pi\Gamma} k_B T \ln(\pi\beta\Gamma) \quad . \tag{6.2.34}$$

This allows us to compute the Wilson ratio; we see that

$$\lim_{T\to 0} \frac{T\chi_{imp}}{C_{imp}} = \frac{2}{\pi^2 k_B^2} \quad . \tag{6.2.35}$$

The corresponding bulk value which sets the free fermion scale is $3/4\pi^2 k_B^2$ (Affleck and Ludwig [1991(b)]). Hence, the Wilson ratio of the diverging susceptibility and specific heat coefficients is

$$R = \lim_{T\to 0} \frac{\chi_{imp}}{\chi_{bulk}} \frac{C_{bulk}}{C_{imp}} = \frac{8}{3} \tag{6.2.36}$$

in perfect agreement with the general results obtained by the Bethe-Ansatz and conformal field theory. Note that the present derivation is valid only for $\lambda/v_F << 1$ (see also Emery and Kivelson [1993]).

(d) Impurity Susceptibility

It is useful also to consider the case of a magnetic field which couples only to the impurity site, so the coupling is of the form $-H\tau^z = -iH\hat{a}\hat{b}$. We denote the corresponding susceptibility χ_I. Within linear response, we see that

$$\chi_I(T) = \int_0^\beta d\tau G_a(\tau) G_b(\tau) = \frac{1}{\pi\Gamma} \ln(1.13\beta\Gamma) \tag{6.2.37}$$

where we used the results of the previous subsection. Hence, the response to a purely local field is divergent as well for $T \to 0$.

6.2.3 Dynamical Properties

(a) Impurity Dynamic Susceptibility

A quantity which shall play a recurring role in discussion which follows is the dynamic susceptibility for an applied longitudinal magnetic field which couples only to the impurity. Following the discussion of Sec. 6.2.2.d, we may write down the dynamic susceptibility in Matsubara space as ($\nu = 2\pi n/\beta$ a bose Matsubara frequency, ω is a fermi Matsubara frequency)

$$\chi_I(\nu) = \frac{1}{\beta} \sum_\omega G_a(i\omega) G_b(\omega + \nu) \tag{6.2.38}$$

$$= \int \frac{d\zeta}{\pi} \frac{\Gamma}{\zeta^2 + \Gamma^2} \frac{1}{\beta} \sum_\omega \frac{1}{i(\omega - \nu)(i\omega - \zeta)}$$

$$= \int \frac{d\zeta}{\pi} \frac{\Gamma}{\zeta^2 + \Gamma^2} \frac{\tanh(\beta\zeta/2)}{i\nu - \zeta} \quad .$$

Analytic continuation of this result implies that the absorptive part of the dynamical susceptibility has the extremely simple form

$$\chi_I''(\omega) = \frac{\Gamma}{\omega^2 + \Gamma^2} \tanh(\beta\omega/2) \quad . \tag{6.2.39}$$

Given an identification of Γ with the cutoff ω_C this is precisely the form anticipated from Marginal Fermi liquid theory (Varma *et al.* [1989]), and identifying Γ with T_K, this also agrees with the form found numerically from NCA calculations by Cox [1988(a)], and with the form postulated from conformal field theory arguments by Tsvelik [1990]. Note that in Cox [1988(a)] a Lorentzian fit was made for positive frequencies to the dynamic spin structure factor $S_I(\omega) = (N_B(\omega) + 1)\chi_I''(\omega)$ at low temperatures with the understanding that this suffices to give $\chi_I'' \sim sgn(\omega)\Gamma/(\Gamma^2 + \omega^2)$ at zero temperature.

What is clear in χ_I'' is that the singular structure arises from the convolution of a regular Majorana field propagator G_b with the singular propagator of the decoupled field G_a. Hence again, as stressed in the previous subsection, it is the physics of coupling one of the two Majorana variables from the spinless fermion representation of the spin variable which gives rise to the interesting critical physics in this picture.

(b) Self-Energies

As remarked previously, after averaging over a random array of impurities, the self-energy of itinerant electrons to leading order in the impurity concentration c is given by the concentration times the one particle t matrix for scattering off a single impurity.

When the fermionic degrees of freedom are written in collective coordinates, only ψ_{sf} and ψ_s couple to the impurity, and so we can develop self energies only for these fields. We can obtain the retarded t-matrix for ψ_{sf} from Eqns. (A.4.4.a-c) as a Nambu matrix $\hat{t}$ with

$$\hat{t}(\omega) = \frac{1}{4\pi N(0)} \frac{\Gamma}{\omega + i\Gamma} [1 + \sigma^{(1)}] \tag{6.2.40}$$

where $\sigma^{(1)} = \delta_{i,-j}$ is a Pauli matrix in Nambu indices. From this we can see that the Fermi level scattering rate for the ψ_{sf} electrons is given by

$$\frac{1}{2\tau(0)} = c[-2Im(\hat{t}(+i\eta))_{11}] = \frac{c}{\pi N(0)} \tag{6.2.41}$$

which is precisely *half* the unitarity limit. The reduction from unitarity may be traced to the spectral weight factor of $1/2$ associated with the Majorana character of the b-field. It is very tempting to compare this with the result from the conformal field theory, which says that the total Fermi level scattering rate for an incoming electron scattering off a two-channel site is half the unitarity limit. However, the comparison is problematic, for reasons we shall discuss further below.

The coupling to the ψ_s field is perturbative in λ. Following the conformal theory, where the leading order imaginary part of the self-energy is, surprisingly linear in the deviation from the fixed point coupling, we can look for a term linear in λ. Because this has dangling $\hat{a}, \hat{b}$ legs, no such term exists (see Fig. 81(a)). The first non-vanishing diagram is shown in Fig. 82(b). This corresponds to the exchange of a local spin fluctuation boson with spectral weight χ_I''. This is precisely the kind of self-energy diagram considered in the Marginal Fermi liquid phenomenology (Varma *et al.* [1989]) and which was used by Cox to produce a heuristic estimate for linear in T scattering in interpreting the resistivity data for $Y_{1-x}U_xPd_3$ (Seaman *et al.* [1991]). It is straightforward to evaluate this diagram giving the imaginary part of the retarded s self-energy as

$$Im\Sigma_s(\omega, T) = -c\pi N(0)\lambda^2 \int \frac{d\zeta}{\pi} \chi_I''(\zeta, T)[N_B(\zeta) + 1 - f(\omega - \zeta)] \tag{6.2.42}$$

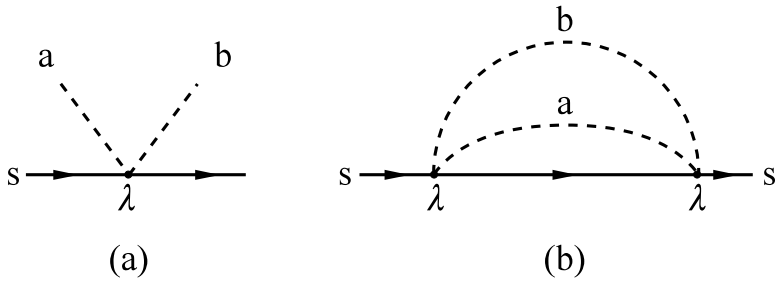

Figure 81: Leading order in λ self-energy diagrams for the conduction spin fermion of Emery and Kivelson [1992]. There is no self-energy correction which is linear in λ, since as shown in (a) this would yield unclosed Majorana fermion legs. There is a contribution at order λ^2 shown in (b), which has the marginal Fermi liquid leg. Suitable re-fermionization from the transformed fields may resolve this apparent discrepancy between the Abelian and non-Abelian bosonization approaches.

$$\approx -c\frac{\pi}{N(0)}[N(0)\lambda]^2\frac{1}{\pi\Gamma}[|\omega| + 2k_BT], \quad (|\omega|, k_BT << \Gamma) \quad .$$

Corresponding to this self-energy, the real part behaves as $Re\Sigma_s(\omega, T) \sim \omega \ln(max\{|\omega|, k_BT\}/\Gamma)$ which gives a logarithmically diverging effective mass for the s-fermions.

The difficulty in connecting these self energies to the self energies computed by, e.g., the NCA and conformal field theory, is that in the latter approaches the self energies are computed directly for the propagators of the original fermion fields. Loosely speaking, one of the original fermion fields is a square root of four collective fermion fields, as we can see by writing out $\psi^\dagger_{\uparrow +} \sim \exp(-i\Phi_{\uparrow +}) = \exp(-i[\Phi_c + \Phi_s + \Phi_f + \Phi_{sf}]/2)$, for example. Each of the exponentiated collective boson factors gives a "square root" of the corresponding collective fermion field operator because of the factor of 1/2 in the exponent. Thus, it is difficult to interpret the self energies of collective coordinate fermion fields in terms of physical self energies of electrons which scatter off of the impurity. This situation is reminiscent of the Bethe-Ansatz approach in which the wavefunctions of the real incoming and outgoing electrons cannot be easily constructed in terms of the exactly determined eigenstates.

(c) Conductivity

The Abelian bosonization scheme also produces a problematic interpretation of transport coefficients. First, as discussed in the previous subsection, there is no obvious way to go from a calculation of Σ_{sf}, Σ_s to a calculation of $\Sigma_{\mu\alpha}$ where $\mu\alpha$ are the original spin and channel labels. Thus we cannot immediately transcribe the self-energy results of the previous subsection to resistivity results through the transport integral formulae discussed in the NCA and conformal field theory reviews.

A second difficulty arises in the connection of the physical three dimensional current operator to the current operators of the effective one dimensional model. As discussed by Emery and Kivelson [1992], following Bander [1976], the collective fermion fields have currents which may be expressed by gradients of the corresponding collective bose fields. Thus, for example, the one dimensional charge current of left moving states is proportional to $\partial\Phi_c/\partial x$, the spin current to $\partial\Phi_s/\partial x$, the flavor current to $\partial\Phi_f/\partial x$, and the spin-flavor current to $\partial\Phi_{sf}/\partial x$. Of these, only $\partial\Phi_{s,sf}/\partial x$ couple to the impurity. This would suggest that the impurity cannot affect the electrical conductivity, because of the following argument: while the three dimensional current operator is not identical to $\partial\Phi_c/\partial x$, this is the only effective one dimensional current operator which is a singlet in spin and channel indices like the three dimensional current, and hence the only candidate effective one-dimensional current operator to match to the three dimensional one.

An exception to this identification is in the case when the local z-component of the impurity "spin" has the same transformation properties as the current operator under parity and time reversal,

which is the case for example in the electric dipole Kondo effect discussed by Emery and Kivelson [1993(a),1993(b)]. In that case, the contribution to the conductivity from the impurity is proportional to the spin conductivity, given by $Re\sigma_s \approx \chi_I''(\omega,T)/\omega$. This quantity behaves precisely as the marginal Fermi liquid phenomenology conductivity (Varma *et al.* [1989]). Emery and Kivelson [1993(a)] have shown that for a one dimensional array of such electric dipole Kondo scatterers, that there is no Drude contribution (following the discussion of the preceding paragraph) and that the above term gives a contribution to the electrical conductivity due to the bound dipole charge of the array.

As discussed in the next subsection, the difficulties can be reconciled conceptually, at least, by considering the Majorana fermion reformulation of conformal field theory introduced by Maldacena and Ludwig [1996]. This theory contains three eight dimensional fields which may be explicitly expressed in terms of the Abelian boson fields of Emery and Kivelson. The conductivity may be computed in terms of these fields, and there are no discrepancies between the results obtained in this method and those of the non-Abelian bosonization scheme discussed in Sec. 6.1.

6.2.4 Finite size spectra and scattering states

Recently von Delft and Zaránd [1997] have shown that the spectrum of states for the Emery-Kivelson of the two-channel model can be solved analytically for arbitary spin-flip coupling and magnetic field strength. Using this, they produced a complete spectrum of eigenvalues, states, and scattering states, and a new interpretation of the unitarity paradox (discussed more extensively in section 6.3.1 below). In particular, for zero magnetic field and infinite spin flip coupling, the fixed point spectrum of Affleck and Ludwig [1991c] is obtained, and this is taken to be an analytic confirmation of the fusion hypothesis, to be contrasted with the less direct confirmation obtained by comparison with NRG or Bethe-Ansatz spectra. It should be noted that the scattering states for the Emery-Kivelson line and its generalization to channel anisotropy were first constructed in a slightly different context by Schiller and Hershfield [1995,1997], who used the Emery-Kivelson approach to solve a nonequilibrium Kondo problem.

6.3 Additional Developments

6.3.1 Reformulation of the Conformal Theory with Majorana Fermions

In this subsection we will briefly review the results of Maldacena and Ludwig [1996] who reformulated the conformal theory in terms of Majorana fermions. As the work depends upon some rather technical aspects of Lie group theory, we will focus on summarising the philosophy and key results of the work.

Motivated in part by the success of the Abelian bosonization scheme of Emery and Kivelson discussed in the previous subsection and by the unitarity puzzle described in the introduction to Sec. 6 and in Sec. 6.1.4, Maldacena and Ludwig [1996] undertook to write the free Fermion hamiltonian in terms of eight Majorana fermion fields. The form is

$$\mathcal{H}_{free} = -\frac{i}{2\pi}\int dx \chi_a(x)\frac{d}{dx}\chi_a(x) \tag{6.3.1}$$

where a runs over the spin, channel, and complex (imaginary or real) indices of the Majorana fields. This Hamiltonian has a manifest $SO(8)$ symmetry under rotations in the space indexed by a. Rotations in the space are generated by currents

$$j^A(x) = \chi_a(x)(T^A)_{ab}\chi_b(x) \tag{6.3.2}$$

where T^A are appropriately defined 8x8 matrices associated with the generators of $SO(8)$. The currents obey a Kac-Moody algebra with four irreducible representations, a singlet, an eight dimensional vector representation, and two eight dimensional spinor representations. The Hilbert spaces of the representations are distinguished by the boundary conditions which must apply to the representations, namely, the singlet and vector representations are antisymmetric under $x \to x + l$, while the spinors are symmetric.

Similarly, under translation in imaginary time τ by β, the singlet and vector irreps are antisymmetric, while the spinors are symmetric. The free Hamiltonian is transparent to the two spinor irreps, but in principle they are present awaiting only some coupling to the free fermion space to make their presence felt.

To foreshadow the key results, we note that the $SO(8)$ set of eight dimensional representations obey a unique symmetry called 'triality' in which we can really flip around which of the three we choose as a fermionic vector and which two we choose as spinors. The bosonization scheme of Emery and Kivelson [1992] corresponds to one particular choice of fermionic vector. When we make this choice, the free fermion field becomes a spinor representation, and may in principle mix with the other spinor. The effect of the impurity at the boundary is to convert the free physical fermions with this other field. The scattering takes one free fermion incoming wave into precisely one outgoing spinor wave, which resolves the unitarity puzzle (the original Hilbert space was not the full Hilbert space of the problem). When the two point green's function is computed with this approach, the electron self energy acquires a $\sqrt{T}$ term. The problem with considering the self energies of the fermions in the Abelian bosonization scheme is that they have no simple relation to the original free fermions, as discussed in the previous subsection. A beautiful aspect of this approach is that no $SU(2)$ spin symmetry breaking is required, unlike the Emery and Kivelson [1992] expansion around the Toulouse limit.

The free fermion fields can be bosonized by writing the normal ordered products

$$\psi^\dagger_{\mu\alpha}(x)\psi_{\mu\alpha} := i\partial_x\phi_{\mu\alpha}(x) \tag{6.3.3}$$

so that

$$\psi^\dagger_{\mu\alpha}(x) = \exp[-i\phi_{\mu\alpha}(x)] \tag{6.3.4}$$

which is unchanged by a 2π rotation in phase, i.e., addition of 2π to the boson field. In contrast, the spinor fields written as exponentiated boson operators contain linear combinations of the ϕ fields multiplied by $\mp i/2$ ($-$ for a "creation" operator, $+$ for an "annihilation" operator) and hence change sign under the corresponding rotation.

Now, if we follow the Emery and Kivelson prescription to linearly transform to the $\phi_c, \phi_s, \phi_f, \phi_{sf}$ bose fields, what happens is that the original fermion field becomes a spinor while one of the original spinor fields (type II) becomes a fermion or vector irrep of $SO(8)$ in that it becomes expressed as simple exponentials of the transformed ϕ fields while the original fermion field and other spinor (type I) exponentials of linear combinations multiplied by $\pm i/2$. The impurity interaction basically becomes a boundary condition which expresses the interconversion of free fermion and type I spinor field interconvert. The type I spinor field has the same spin, channel, and charge quantum numbers as the original fermion fields, but fractional occupancy in terms of the original fields. In contrast, the type II spinor field has fractionalized spin, charge, and flavor quantum numbers and actually can be viewed as carrying the non-trivial primary fields discussed in Sec. 6.1.2 (spin, channel spin, and pair fields, a total of eight) when appropriately multiplied by grassman numbers.

Maldacena and Ludwig [1996] also show with this formalism that the two impurity one channel Kondo model and the Callan-Rubakov problem of four fermion species scattering off an $SU(5)$ magnetic monopole have equivalent non-trivial fixed points, and that the fixed point correlation functions of the three different models (two channel, two impurity one-channel, and Callan-Rubakov) may be mapped into one another. This latter trick employs the triality symmetry of the $SO(8)$ group explicitly.

Using a somewhat different approach with a Majorana fermion scheme similar to that of Coleman, Ioffe, and Tsvelik [1995], Zhang, Hewson, and Bulla [1997] have reached similar conclusions and presented an explicit realization of the finite size spectra and leading irrelevant operator in the Majorana fermion basis.

6.3.2 Conformal Theory of the Large Conduction Spin Single Channel Model

Fabrizio and Zaránd [1996], Sengupta and Kim [1996] and Kim, Cox, and Oliveira [1996] have studied the large conduction spin single channel model with conformal field theory techniques (Fabrizio and Zaránd [1996] have also employed $1/M$ and $1/S_c$ expansions, where S_c is the conduction spin, through the framework of the multiplicative renormalization group). In this model, the conduction electrons are allowed to have arbitrary spin j. The effective channel number which is read off as the rank of the spin Kac-Moody algebra is calculated to be $M(j) = 2j(j+1)(2j+1)/3$. (Fabrizio and Zaránd [1996] have established a more general correspondence allowing the channel number of the large spin electrons to vary; see the discussion in Sec. 7.1 for further details.) For example, when $j = 3/2$, $M(3/2) = 10$. This suggests that any spin satisfying $S_I < M(j)/2$ will be overcompensated in this problem. This model can arise as an unstable fixed point of the TLS Kondo effect and for Ce^{3+} ions in cubic symmetry as discussed in Secs. (3.3.3) and (3.4.3).

The simple physical reason for this overcompensation is as follows. (See also Secs. (3.3.3,3.4.3).) For definiteness, consider the $j = 3/2$ case. Proceed to the strong coupling limit, i.e., shut off the hopping. As shown in Fig. 82(a), it is energetically favorable about a single site to draw in *two* electrons with $j_z = +3/2, +1/2$, assuming the local moment to have down spin. From this simple picture, we would anticipate that for impurity spin up to $S_I = 3/2$ that an overcompensated ground state would result. For $S_I = 2$, exact compensation should occur, and for $S_I > 2$ undercompensation would occur. As in the arguments for the multichannel models, this strong coupling limit is unstable for $S_I \leq 3/2$, because a residual antiferromagnetic coupling will remain with electrons in the next spatial RG shell (Fig. 82(b)). For $S_I > 2$, the residual coupling is ferromagnetic, as illustrated in Fig. 82(c).

For general j, adding up only positive j_z values, we would expect the total screening spin to be $j_{max} = (j+1/2)^2/2$ for half integer j, And $j_{max} = j(j+1)/2$ for integer j. The condition in general for over-compensation is then $S_I < j_{max}$. This disagrees with the results of the conformal theory (Fabrizio and Zaránd [1996], Sengupta and Kim [1996], Kim, Oliveira, and Cox [1997]) as discussed below.

For the large j single channel model, the Hamiltonian written in terms of left moving fields is, in the position space domain,

$$\mathcal{H} = \sum_{\alpha} \int dx \psi^{\dagger}_{\alpha}(x) \frac{\partial}{\partial x} \psi_{\alpha}(x) + \mathcal{J} \vec{S}_I \cdot \vec{J}(x=0) \tag{6.3.5}$$

where $\psi^{\dagger}_{\alpha}(0)$ creates an electron with z-component spin $\alpha = -j, -j+1, ..., j$, and

$$\vec{J}(0) = \sum_{\alpha\beta} \psi^{\dagger}_{\alpha}(0) \vec{S}_{\alpha\beta} \psi_{\beta}(0) \tag{6.3.6}$$

with $\vec{S}$ spin matrices of the spin j representation of $SU(2)$.

Restricting attention now to just the $j = 3/2$ case, the Hamiltonian of Eq. (6.3.5) was cast by Sengupta and Kim [1996] and Kim, Oliveira, and Cox [1997] in Sugawara form for the generation of finite size spectra from conformal theory. As in the multichannel model analysis of Affleck and Ludwig [1991b], the single fusion hypothesis was assumed to generate finite size spectra relevant for comparison to the NRG, and the double fusion hypothesis was assumed for generating the operator spectrum and scaling indices.

The first observation is that the Kac-Moody algebra corresponding to the conduction spin current $\vec{J}(x)$ has a large rank. When written in momentum space, the commutation relation is

$$[J^a_q, J^b_{q'}] = i\epsilon_{abc} J^c_{q+q'} - \delta_{ab}\delta_{q+q',0} \frac{k(j) q l}{2\pi} \quad . \tag{6.3.7}$$

which follows from the fact that

$$\sum_{\alpha\beta} S^a_{\alpha\beta} S^b_{\beta\alpha} = \delta_{ab} \sum_{\alpha=-j}^{j} \alpha^2 = \delta_{ab} \frac{k(j)}{2} \tag{6.3.8}$$

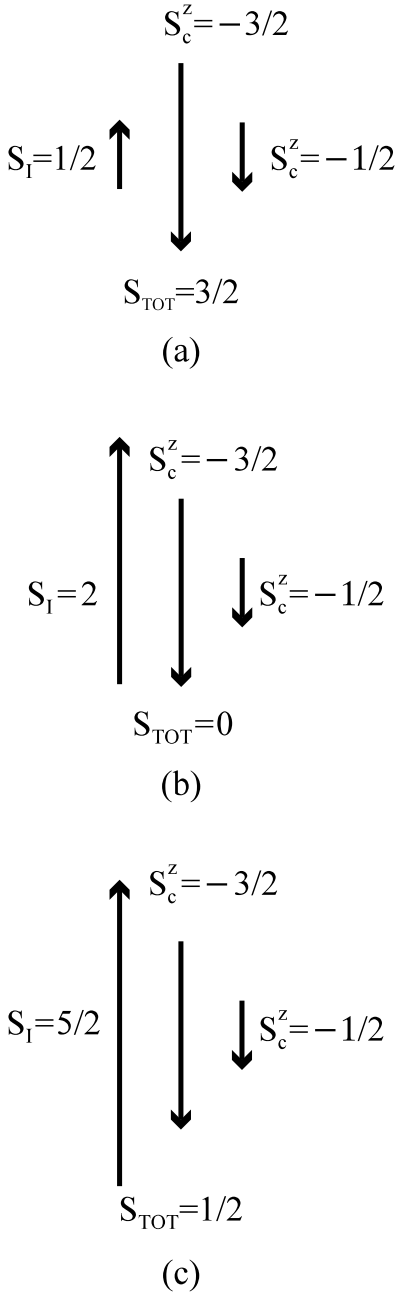

Figure 82: Strong coupling pictures for the single band $S_c = 3/2$ Kondo model. (a) displays an example of the overcompensated model when the impurity spin takes the value $S_I = 1/2$. In this case, the $S_z = -3/2, -1/2$ conduction channels overscreen the impurity, leading to an non-Fermi liquid fixed point. For $S_I = 2$, there is just enough conduction spin to compensate the impurity, as shown in (b), and this is expected to lead to a Fermi liquid fixed point. For $S_I = 5/2$, as shown in (c), there is too much impurity spin to be compensated by the conduction electrons, and we anticipate that an undercompensated fixed point will ensue.

as is familiar from $SU(2)$ spin algebra. Hence the rank of the spin current Kac-Moody algebra is given by $k(j)$ in contrast to the $j = 1/2$ case where it is the channel number M. For $j = 3/2$, $k(j = 3/2) = 10$. One has a choice of which quantum numbers to use here; we follow Kim, Oliveira, and Cox [1996], who used a generalized axial charge (Jones [1988]; Jones and Varma [1988]; Jones, Varma, and Wilkins [1988]), or isospin defined by (in their reference, Q is used in favor of I)

$$I_q^z = \sum_{k,\alpha} \left[c_{k,\alpha}^\dagger c_{k+q,\alpha} - c_{k7\mu} 1/2 \delta_{n,0} \right] \tag{6.3.9}$$

and

$$I_q^+ = \left(I_q^- \right)^\dagger = \sum_k \left(c_{k,3/2}^\dagger c_{-k-q,-3/2}^\dagger - c_{k,1/2}^\dagger c_{-k-q,-1/2}^\dagger \right) \quad . \tag{6.3.10}$$

$\vec{I}$ satisfies the Kac-Moody algebra ($I^x = (I^+ + I^-)/2$, $I^y = (I^+ - I^-)/2i$)

$$\left[I_q^a, I_{q'}^b \right] = i\epsilon^{abc} I_{q+q'}^c + \delta_{ab}\delta_{q+q',0} \frac{ql}{\pi} \tag{6.3.11}$$

from which we infer a rank $k_I = 2$. By following the same techniques to construct a Sugawara Hamiltonian as in Sec. 6.1, we obtain for the free $S_c = 3/2$ conduction electrons

$$\mathcal{H}_0 = \frac{v_F \pi}{\ell} \left[\sum_{q=-\infty}^{\infty} \frac{1}{12} : \vec{J}_{-q} \cdot \vec{J}_q : + \sum_{n=-\infty}^{\infty} \frac{1}{4} : \vec{I}_{-q} \cdot \vec{I}_q : \right] \tag{6.3.12}$$

and the impurity may be absorbed into new conduction spin currents

$$\vec{\mathcal{J}}_q = \vec{J}_q + \vec{S}_I \tag{6.3.12}$$

which obey the same Kac-Moody algebra as Eq. (6.3.8) provided the coupling strength $\lambda = N(0)\mathcal{J} = 1/6$ which we identify as the fixed point coupling within the conformal theory. In this case, the Sugawara Hamiltonian becomes

$$\mathcal{H} = \frac{v_F \pi}{\ell} \left[\sum_{q=-\infty}^{\infty} \frac{1}{12} : \vec{\mathcal{J}}_{-q} \cdot \vec{\mathcal{J}}_q : + \sum_{n=-\infty}^{\infty} \frac{1}{4} : \vec{I}_{-q} \cdot \vec{I}_q : \right] \tag{6.3.13}$$

(Sengupta and Kim [1996] choose a different basis with quantum numbers of spin, charge, and an Ising variable.)

In this basis, one can readily construct the spectrum of the system. For the free electrons, the primary (highest weight) states must have $i \leq k_I/2 = 1$, and $j \leq k(j)/10 = 5$ here. The spectrum of eigenvalues is then

$$E_0(i,j,m) = \frac{v_f \pi}{\ell} [\frac{i(i+1)}{4} + \frac{j(j+1)}{12} + m] \tag{6.3.14}$$

where m is an integer measuring the number of excitations induced by operating with I_{-q}^a, J_{-q}^b, $q > 0$ on the primary states. These states are constrained by the conditions that they correspond to excitations from the free fermi sea of $S_c = 3/2$ electrons. Note that one must construct different spectra for a system with a degenerate ground state (periodic boundary conditions in the continuum or even interation number in the numerical renormalization group) or a non-degenerate ground state (antiperiodic boundary conditions in the continuum or an odd NRG iteration number).

For the interacting system, we must apply the fusion rule of Affleck and Ludwig [1991b], which reads here, for those states satisfying fermion "gluing conditions" in the free spectrum, that

$$i \to i \quad , j \to j' \; with \; |j - 1/2| \leq j' \leq min\{j + 1/2, k(j) - j - 1/2\} \quad . \tag{6.3.15}$$

One may similarly generalize the double fusion rule for operator spectra. Kim, Oliveira, and Cox [1996] find excellent agreement between the conformal field theory spectrum generated in this way and the NRG energy levels, provided the CFT antiperiodic boundary conditions are identified with odd numbered NRG iterations, and periodic boundary conditions with even numbered NRG iterations. The inferred operator spectrum possesses a primary spin operator $\vec{\Phi}$ with a scaling dimension of 1/6, which will induce a $T^{-2/3}$ divergence in the spin susceptibility and the specific heat coefficient. (The leading irrelevant operator has a scaling dimension of 7/6.) This scaling dimension to $\vec{\Phi}$ produces a scaling exponent for the magnetic field of $\Delta_h = 5/6$, implying a crossover to Fermi liquid behavior in a polarized scattering potential in the variable $h^{6/5}/T$. Exchange anisotropy is relevant in this model. Sengupta and Kim [1996] reached the same conclusions about the lowest few energy levels and the leading irrelevant operator about the fixed point.

6.3.3 Conformal Field Theory Treatment of the Anisotropic Two-Channel Model, Spin-Flavor Two-Channel Model, and TLS Kondo model.

Recently, Ye has extended the applications of conformal field theory and abelian bosonization in a series of papers (Ye [1996a,b,c,d,e]). Among his accomplishments are: generalizing from the isotropic fixed point of Affleck and Ludwig to study the anisotropic "Emery Kivelson" line first identified in the work of Emery and Kivelson using Abelian bosonization (Ye [1996a]); a solution of the spin-channel Kondo model within conformal theory in which the impurity possesses both spin and channel degrees of freedom which couple to the electrons–in this work, the spectrum of Fermi liquid and non-Fermi liquid fixed points was worked out fully (Ye [1996b]); a general paper on the Abelian bosonization approach for quantum impurity problems (Ye [1996c]); a comparison of the two-channel Kondo and compactified one channel Kondo model (mentioned above and in Sec. 9.2 (Ye [1996d]) which leads to the conclusion that for channel anisotropy the resultant fixed point is a Fermi liquid one (in contrast to the claims of Andrei and Jerez [1995] and Coleman and Schofield [1995] but in agreement with Fabrizio, Gogolin, and Nozières [1995a,b]); and a paper (Ye [1996e]) which applies a combination of scaling theory, abelian bosonization, and conformal theory to study the two-level system Kondo model beginning from the framework of Moustakas and Fisher [1995,1996]. The latter paper concludes that the two-channel Kondo non-Fermi liquid fixed point is connected by a continuous line of unstable non-Fermi liquid fixed points to the new one of Moustakas and Fisher [1995,1996], and the latter is equivalent to the two-impurity single channel Kondo fixed point (discussed in Sec. 9.3.1). Any amount of spontaneous tunneling or TLS asymmetry will send the system to a Fermi liquid fixed point through the spin-field crossover described extensively in secs. 3,4,5,7 and above in this section. We refer the reader to these works for further details.

7 Bethe-Ansatz Method

The importance of the Bethe-Ansatz is not just for providing exact wave functions, spectra and thermodynamics for models to which it is applicable. As the energy spectrum is obtained for the entire energy range, the thermodynamic results are therefore valid for the entire range of temperature and magnetic field. The application of conformal field theory relies upon the hypotheses of conformal invariance (that the conformally invariant model corresponding to the special value of λ corresponds with the non-trivial fixed point of the multichannel Kondo model) and fusion rules, as discussed in Sec. 6.1, which are valid only at low temperatures and energies in contrast to the Bethe-Ansatz. Strictly speaking these cannot be proved *a priori*, but by making these assumptions and deriving results one can then compare to the exact Bethe-Ansatz results to verify the hypotheses. The conformal theory can then be extended to calculate dynamical properties for which the Bethe-Ansatz fails. Similar remarks apply to the NCA: as discussed in Secs. 5.1 and 5.3, the thermodynamic properties of the NCA are in good agreement with exact Bethe-Ansatz results for the overcompensated Kondo models, giving confidence in the dynamics results which are inaccessible to the Bethe-Ansatz. (The problem with dynamics is that while the Bethe-Ansatz provides exact many body wave functions, it is an unsolved problem to properly express the operators which couple to external probes, such as the electrical current, in terms of this diagonal basis. In particular, it is not known how to construct scattering state solutions for the Hamiltonian.)

In this section we present a brief overview of the Bethe-Ansatz approach to the multichannel Kondo model. Because there are extensive reviews available of the Bethe-Ansatz (Andrei, Furuya, and Lowenstein [1983], Wiegman and Tsvelik [1983b], Schlottman and Sacramento [1993], Hewson [1993]) we shall focus primarily on summarizing some of the key aspects of the method as applied to this problem together with some of the main results.

7.1 Methodology for the M-channel Kondo problem.

The Bethe-Ansatz method was originally used by Bethe to study the one-dimensional nearest neighbor antiferromagnetic spin 1/2 chain. It has also proven to be a powerful method for treating the electron gas in one-dimension and quantum impurities embedded in three dimensional hosts (where the mapping back to one dimension discussed in Secs. 4, Sec. 6.1.1.a is used). The essence of the Ansatz is to make a 'guess' for the many body wave function which is kind of determinant of generalized plane wave states. Clearly this can work only for interactions which are very short ranged so that the particles propagate rather freely between interactions. The Ansatz will not work for all models; an assessment of whether it will work rests upon testing it for 1,2, and 3 particles which is sufficient to prove that it will work for all particles.

The first applications were to spinless fermions and bosons (through the Jordan-Wigner transformation, clearly the spin 1/2 chain can be mapped to a spinless boson or fermion problem). Later came breakthroughs by Yang [1967] and Gaudin [1967] which allowed spin-ful particles to be treated: the 'plane wave' product terms acquire spin-matrix pre-factors which have certain consistency requirements. Yang and Gaudin showed that the consistency requirements map onto a separate Bethe-Ansatz solution for the spin 1/2 case. In general, spin S particles can be solved by $N = 2S + 1$ nested Bethe-Ansatz

The original $S_I = 1/2, M = 1$ Kondo model was solved with the Bethe-Ansatz independently by Andrei [1980] and Wiegman [1980]. Later, the multi-channel model was solved by Andrei and Destri [1984] and Wiegman and Tsvelik ([1983a], Tsvelik and Wiegmann [1984,1985], Tsvelik [1985]). In order for the Ansatz to work for the impurity models, one typically needs contact interactions together with a linear dispersion for conduction electrons.

Generalization of the original method for the $M = 1$ model to the arbitrary M case was not straightforward. Namely, as we discussed in the introduction (Sec. 1), the ground-state of the M channel spin S_I Kondo model consists of M electrons with parallel spin glued together to form a net spin $M/2$ which couples anti-parallel to the impurity spin S_I. Straightforward extension of the contact interaction picture with linear dispersion in this case leads to a bare S-matrix which is diagonal

in the channel indices. Clearly this cannot be true if the physical picture is to hold. Consider the $M = 2, S_I = 1/2$ example: in this case the 'big' spin one of the conduction electrons requires a channel spin antisymmetrization. Moreover, for large M this clearly contradicts the rigorous results computed perturbatively in the two-loop expansion of the beta function (see Sec. 3.4.5). This defect in the simple extension is due to the linear dispersion assumption, which implies the lack of a cutoff or short distance scale in the model.

In order to get physical results from the Ansatz for the multi-channel model, the different groups applied modifications to the original Kondo model. Andrei and Destri [1984] introduced a non-linear dispersion, $\epsilon_k = v_F[(k - k_F) + \Lambda^{-1}(k - k_F)^2]$ where Λ is a cutoff parameter. At the end of the calculation Λ is taken to ∞, and results are independent of Λ. To keep the model integrable, local counter-term potentials must be introduced into the Hamiltonian which follow the work of Rudin [1983]. The counterterm introduces coupling between the channels, but the strength of the counterterm drops out in the $\Lambda \to \infty$ limit and is therefore irrelevant. The presence of the cutoff allows the dynamic formation of the spin complex with spin $s_c = M/2$ ("dynamic fusion"). This dynamic fusion is observed both in the structure of the wave function and in the corresponding fused Bethe-Ansatz equations. In the former the momenta develop imaginary parts leading to the binding of M electrons to form a spin $s_c = M/2$ and flavor singlet, while the Bethe-Ansatz equations describbe the coupling of this composite spin to the impurity.

Tsvelik and Wiegmann [1984],[1985] use a different approach to resolve this difficulty. They first introduce a generalized M-channel Anderson Model with parameters for which a local moment of spin S_I is formed and for which the ground state is exactly compensated ($M = 2S_I$). The integrable M-channel Anderson model has the form

$$H = \sum_{k\sigma m} v_F(k - k_F) c^\dagger_{km\sigma} c_{km\sigma} + \sum_{m\sigma} \epsilon_d d^\dagger_{m\sigma} d_{m\sigma}$$

$$+\frac{U}{2} \sum_{mm'\sigma\sigma'} n_{dm\sigma} n_{dm'\sigma'} + V \sum_{km\sigma} (c^\dagger_{km\sigma} d_{m\sigma} + h.c.) \tag{7.1.1}$$

where m is the orbital index ranging from one to M, $\sigma = \uparrow, \downarrow$ is the spin index, and $d^\dagger_{m\sigma}$ creates a local electron of spin σ in orbital m. This model does not represent a realistic extension of the Anderson Hamiltonian since the Coulomb interaction is diagonal in the density operators (see Nozières and Blandin [1980] and Mihaly and Zawadowski [1978] for further discussion). This model, studied with diagrammatic methods by Yoshimori [1976] does give the correct universal behavior of the spin-compensated M-channel Kondo model at low temperatures and for large U, as can be expected from a Schrieffer-Wolff [1966] transformation to eliminate the hybridization at order V generating an effective exchange coupling.

Tsvelik and Wiegman [1984],[1985] then separately consider a generalized exchange model with arbitrary local spin S_I with electrons that have spin $M/2$. The Hamiltonian has the form

$$\mathcal{H} = \sum_{ka} v_F(k - k_F) c^\dagger_{ka} c_{ka} +$$

$$J \sum_{kk',aa'} c^\dagger_{ka} P(\vec{S}_I \cdot S_c, J)_{aa'} c_{k'a'} \tag{7.1.2}$$

where a indexes the conduction spin states and $P(x, y)$ is a polynomial of order $min(2S_I, M)$. This model is integrable (i.e., the Bethe-Ansatz works) if the polynomial has the explicit form

$$P(x, J) = \sum_{l=|M/2-S_I|}^{M/2+S_I} \prod_{k=0}^{l} \frac{1 - ikJ}{1 + ikJ} \prod_{p=0, p\neq l}^{min(M,2S_I)} \frac{x - x_p}{x_l - x_p} \tag{7.1.3}$$

where

$$x_p = \frac{p(p+1)}{2} - \frac{S_I(S_I+1)}{2} - \frac{M(M/2+1)}{4} \quad . \tag{7.1.4}$$

In the special case $S_I = 1/2$, the polynomial reduces to the form

$$P(\vec{S}_I \cdot \vec{S}_c, J) = a + b(\vec{S}_I \cdot \vec{S}_c) \tag{7.1.5}$$

where a, b are constants which may be determined from (7.1.4).

The claim of Tsvelik and Wiegman [1984,1985] is that the Hamiltonian of Eq. (7.1.2) is equivalent to that of Eq. (7.1.1) when charge fluctuations are projected out and $M = 2S_I$ as they have identical energy spectra. They further conjecture that the solution of the Bethe-Ansatz of Eq. (7.1.2) holds for the multichannel Kondo model for arbitrary S_I, M. The appealing feature of this picture is that it says one must simply form a large conduction spin as suggested by the Nozières and Blandin [1980] picture and the NRG results (Sec. 4) and solve the Bethe-Ansatz for one channel of electrons with that large spin. In contrast, Andrei and Destri [1984] do not assume the formation of the electron complex with total spin $M/2$, but it follows from their treatment. Tsvelik and Wiegman establish the equivalence of the different models by explicit Bethe-Ansatz solution (and exact comparison of the excitation spectra) which confirm that the results are identical for $M = 2S_I$. Also, for the overcompensated case $M > 2S_I$, they obtain indentical Bethe-Ansatz spectra as Andrei and Destri [1984]. As Tsvelik and Wiegman start with the electron complex with $s_c = M/2$, they do not therefore need the sophisticated cutoff scheme with counter term employed by Andrei and Destri [1984] which leads to the formation of the electron complex. For a full discussion of the different cutoff schemes, see Andrei, Furuya, and Lowenstein [1983].

For S_I=1/2, the conjectured mapping of Tsvelik and Wiegman [1984,1985] of the M channel model to the single channel, conduction spin $M/2$ model has been called into question by Fabrizio and Gogolin [1994], Fabrizio and Zaránd [1996], Kim and Cox [1996], and Kim, Oliveira, and Cox [1997]. Concretely, the conjectured mapping may be summarized in the form $MS_c = S_c^*$, where S_c is the conduction spin of the original multichannel model, and S_c^* is the conduction spin of the single channel large spin model. (This may be generalized to $MS_c = M^*S_c^*$ for effective models with arbitrary numbers of channels, as per Fabrizio and Zaránd [1996].) Explicitly, Fabrizio and Gogolin [1994], have shown that the $M = 4$, $S_c = 1/2$ model maps to the $M^* = 1$, $S_c^* = 1$ model, and Kim, Oliveira, and Cox have found that the critical properties of the single channel S_c=3/2 model are in complete disagreement with the $M = 3$,$S_c = 1/2$ model and rather agreed with the $M = 10, S_c = 1/$ model. Both of these results are in contradiction with the Tsvelik and Wiegman [1984,1985] conjecture. This latter result for $S_c^* = 3/2$ was also obtained within conformal theory by Sengupta and Kim [1996].

The most thorough treatment of this issue was given by Fabrizio and Zaránd [1996]. Utilizing $1/M$ and $1/S_c$ expansions as well as conformal field theory arguments, they have suggested that the correct equivalence mapping is summarized by

$$MS_c(S_c+1)(2S_c+1) = M^*S_c^*(S_c^*+1)(2S_c^*+1) \quad . \tag{7.1.6}$$

For the case $M^* = 1, S_c^* = 1$, the RHS of the above equation gives 6, while for $M = 4, S_c = 1/2$, the LHS gives 6 as well, in agreement with the findings of Fabrizio and Gogolin [1994]. For $M^* = 1, S_c^* = 3/2$, the RHS of Eq. (7.1.6) gives 15, while the LHS gives 15 also for the $M = 10, S_c = 1/2$ model, in agreement with Kim, Cox, and Oliveira [1997], and Sengupta and Kim [1996]. The origin of the discrepancy between the Bethe-Ansatz results and these other approaches will require further investigation.

Once the solubility of a model by the Bethe-Ansatz is established, physical properties can be computed. This is practically restricted to thermodynamic quantities (dynamical properties such as the electrical conductivity require a writing of, e.g, current operators in the diagonalized many particle basis which is a non-trivial and largely unsolved problem). The thermodynamic quantities are expressed in terms of excitation densities for spin(spinon), channel(channelon), and charge(holon) degrees of freedom

which are solutions to coupled non-linear integral equations. Note that the 'unbinding' of charge, spin, and channel degrees of freedom which arises naturally in the NCA (Sec. 5), Conformal Theory (Sec. 6.1) and Abelian Bosonization (Sec. 6.2) approaches arises quite naturally in the Bethe-Ansatz approach.

7.2 Results from the Bethe-Ansatz Method

7.2.1 Coupled Integral Equations and Numerical Procedure

In addition to the analytical expressions for various quantities at low and zero temperature, it is important for the computation of thermodynamics to understand the numerical results. Here we refer only to the final equations to be solved, and direct the reader to the original references for details. Our discussion here follows Sacramento and Schlottmann [1991]. One solves the Ansatz for arbitrary spin by flipping over electron spins from a fully polarized state. The ground state is given by a "sea of 2-strings" in the center of mass rapidity Λ. The resulting excitations are spin 1/2 'spinons' formed by creating holes in the ground state distribution and characterized by a one-particle rapidity λ which describes their momentum and energy. These spinons may form bound states with center-of-mass rapidity Λ (not to be confused with the above cutoff parameter in Eq. (7.1.1)) with population factors

$$\eta_l(\Lambda) = \exp(\epsilon_l(\Lambda)/T) \quad l = 1, 2, ... \tag{7.2.1}$$

where ϵ_l is the energy of a bound-state of l spin waves with rapidity Λ. These thermal occupancy factors obey an infinite recursion sequence

$$\ln(\eta_k(\Lambda)) = \int_{-\infty}^{\infty} d\Lambda' G(\Lambda - \Lambda') \ln[(1+\eta_{k-1}(\Lambda'))(1+\eta_{k+1}(\Lambda'))] - \delta_{kn} \exp(\pi\Lambda/2) \quad k = 1, 2, ... \tag{7.2.2}$$

with

$$G(\Lambda) = \frac{1}{4\cosh[\pi\Lambda/2]} \quad . \tag{7.2.3}$$

These recursion relations are completed by the boundary condition $\eta_0 = 1$ and the asymptotic requirement

$$\lim_{k\to\infty} [(\frac{1}{k}) \ln(\eta_k(\Lambda))] = \frac{H}{T} = 2x_0 \tag{7.2.4}$$

where H is the magnetic field (or the asymmetric level splitting in the TLS Kondo case). Physical properties can now be expressed by these quantities η_l. For example, the impurity contribution to the free energy is given by

$$F_{imp} = -T \int_{-\infty}^{\infty} d\Lambda G[\Lambda - (\frac{2}{\pi}) \ln(T_K/T)] \ln[1 + \eta_{2S_I}(\Lambda)] \tag{7.2.5}$$

where T_K is the Kondo temperature.

In the limit $\Lambda \to \pm\infty$, the asymptotic solutions as given by Andrei and Destri [1984], Desgranges [1985] and Sacramento and Schlottmann [1991] are

$$\ln[1 + \eta_k(\infty)] = 2 \ln\{sin[\pi(k+1)/(M+2)]/sin[\pi/(M+2)]\}, \quad k < M$$

$$= 2 \ln\{sinh[(k+1-M)x_0]/sinh[x_0]\}, \quad k \geq M \tag{7.2.6.a}$$

and

$$\ln[1 + \eta_k(-\infty)] = 2 \ln\{sinh[(k+1)x_0]/sinh[x_0]\} \tag{7.2.6.b}$$

which holds for all values of k. The $\eta_k(\Lambda)$ functions are monotonic decreasing, interpolating smoothly between the limits at $\pm\infty$. For the special case $k = M$, $\eta_M(\infty)$=0, which implies $\epsilon_M(\infty) = -\infty$, signalling the formation of a bound state of M spinons. For all other k values η_k is finite everywhere.

For finite Λ, the following numerical procedure can be used to solve Eq. (7.2.2). First, truncate the k values to some large discrete value k_c; typically, k_c of order 50 suffices. Above k_c, only the asymptotic solution given by Eq. (7.2.4) is employed. Further, truncate Λ (typically $|\Lambda| < 56$ is sufficient) and use the asymptotic forms specified by Eqs. (7.2.6.a,b) to characterize the large Λ behavior. The integral equations are then solved numerically on a discretized mesh, and thermodynamic quantities are obtained by taking numerical derivatives of the free energy. These numerical solutions are well controlled unless $H/T >> 1$, for which special care must be taken since the limits $T \to 0, H \to 0$ do not commute.

7.2.2 Thermodynamic Properties

We now summarize the various results. The low temperature thermodynamic properties may be extracted from the asymptotic behavior of the coupled integral equations.

(a) Residual Entropy

The residual entropy (with the limits $H \to 0$ then $T \to 0$ taken) is, for $S_I = 1/2$, (Andrei and Destri [1984], Tsvelik [1985])

$$S(0) = \ln\{2\cos[\pi/(M+2)]\} \quad . \tag{7.2.7}$$

This result can be obtained from the free energy of Eq. (7.2.5) where $\eta_{2S_I} = \eta_1$ when $S_I = 1/2$. In the $T \to 0$ limit, the large Λ values dominate the integral (see Eqs. (7.2.3) and (7.2.5)), so that $ln(1+\eta_1(\Lambda)) \approx 2\ln\{sin[2\pi/(M+2)]/sin[\pi/(M+2)]\}$ can be taken out of the integral. The remaining integral yields 1/2, so Eq. (7.2.7) results. This result agrees with the conformal theory result quoted in Eq. (6.1.83) and is non-zero when $M > 1$. With the limits taken in the order $T \to 0, H \to 0$, the entropy is zero, indicating that the external field generates a non-degenerate singlet ground state and hints at the return to Fermi liquid behavior discussed in Secs. 4,5, and 6. In general, the new scale $T_s = T_K(H/T_K)^{1+2/M}$ is introduced in the presence of field for $H << T_K$ which sets the scale of the crossover from non-Fermi liquid behavior to Fermi liquid behavior as the temperature is lowered through T_s. For the special case of $M = 2$, this scale is $T_s = H^2/T_K$. Clearly this scale definition agrees with the discussion of Sec. 4 (for $M = 2$), Sec. 5.1, and Sec. 6.1.2.c. In contrast, for the fully compensated model, the only scale is H itself. The crossover from non-Fermi liquid to Fermi liquid behavior is well illustrated in Fig. 83 which shows the entropy calculated by Sacramento and Schlottmann [1991] for a number of different M values. It can be seen that as M is raised so that $T_s \to H$ the range over which the non-Fermi liquid behavior is apparent shrinks relative to $M = 2$.

For $M = 2$, when one considers the TLS Kondo model, the level splitting Δ plays the role of H so that the crossover occurs at Δ^2/T_K. For splitting much smaller than T_K, the region over which non-Fermi liquid occurs is much smaller than the splitting itself, which may have considerable relevance to the experimental situation in small point contacts (Ralph and Buhrman [1988,1991], Ralph *et al.* [1994]).

An alternative approach to recovering the $T = 0$ entropy (and in principle the entire quasiparticle spectrum and thermodynamics) has been presented by Fendley [1993]. He solves directly for the S-matrix for scattering off of the impurity and interprets the entropy fractionalization in terms of "kinks" or solitons interpolating between $k+1$ degenerate minima of the ground state. A complete discussion is beyond the scope of this paper and we refer the reader to the original reference for more detail.

(b) Zero Temperature Magnetization

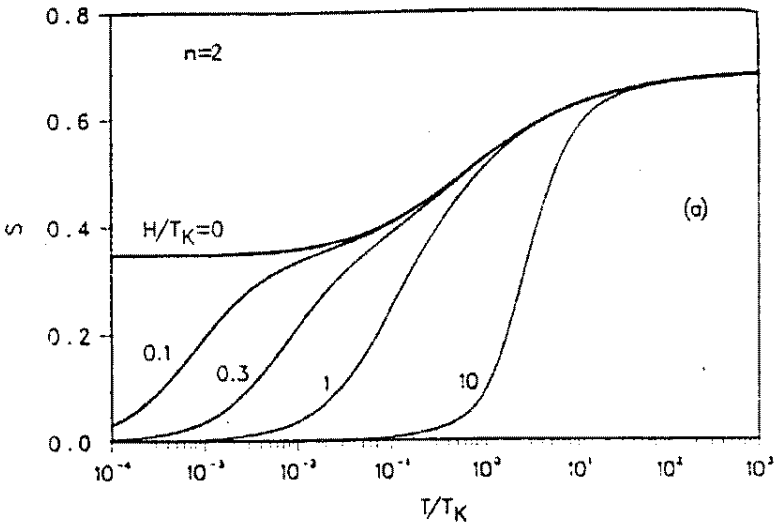

Figure 83: Entropy for two-channel Kondo models computed with the Bethe-Ansatz method, in zero and applied magnetic field. Note that n here corresponds to our M for channel number, and that H corresponds to the spin field H_{sp}. The magnetic field reduces the residual entropy to zero. From Sacramento and Schlottmann [1991].

The zero temperature forms of the magnetization and susceptibility for the $S_I = 1/2$ case are given by (Wiegman and Tsvelik [1983a], Andrei and Destri [1984], Tsvelik and Wiegman [1984])

$$M_{imp}(T=0,H) \sim (\frac{H}{T_K})^{2/M}, \quad \chi_{imp}(T=0,H) \sim (\frac{H}{T_K})^{2/M-1} \tag{7.2.9}$$

for $M > 2$, and for $M = 2$ (Sacramento and Schlottmann [1989])

$$M_{imp}(T=0,H) \sim (\frac{H}{T_K}) \ln(\frac{H}{T_K}), \quad \chi_{imp}(T=0,H) \sim \ln(\frac{H}{T_K}) \quad . \tag{7.2.10}$$

These results agree with the NRG results of Sec. 4.2 (for $M = 2$), the NCA results of Sec. 5.1.4, the CFT results of Sec. 6.1.3, and for large M with the $1/M$ expansion of Sec. 3.4.5.

(c) Low Temperature Specific Heat and Susceptibility

For $S_I = 1/2$, the heat capacity and susceptibility for $H = 0$ and low T are found to be (Andrei and Destri [1984], Tsvelik and Wiegman [1984])

$$\frac{C_{imp}}{T} \sim \chi_{imp}(T) \sim T^{4/(2+M)-1} \tag{7.2.11}$$

and for $M = 2$ (Sacramento and Schlottmann [1989])

$$\frac{C_{imp}}{T} \sim \chi_{imp}(T) \sim \ln(\frac{T_K}{T}) \quad . \tag{7.2.12}$$

These results are in agreement with the discussion of Secs. 5.1.3 (NCA), 6.1.3 (CFT), and 6.2.3 (Abelian bosonization, $M = 2, 4$ cases). For large M, the results also check with the large M expansion of Sec. 3.4.5. Note that the different power laws in χ at $T = 0, H \neq 0$ and $T \neq 0, H = 0$ are associated with the non-trivial scaling of H with T in the overcompensated model (for $M > 2$, $\chi(T, H = 0) \sim T^{4/(2+M)-1}$,

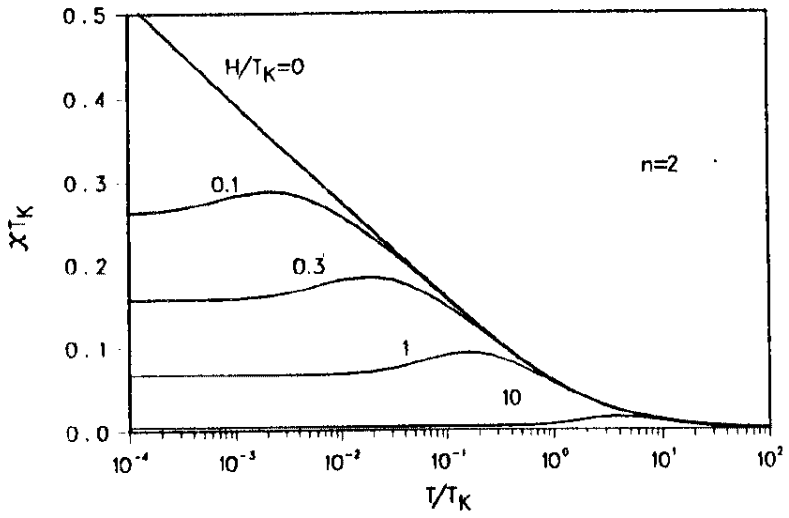

Figure 84: Magnetic susceptibility for the two-channel multichannel Kondo models in applied spin field computed with the Bethe-Ansatz method. Note that n here corresponds to our M for channel number, and that H corresponds to the spin field H_{sp}. The magnetic field removes the logarithmic singularity in the susceptibility. From Sacramento and Schlottmann [1991]

while ($\chi(0,H) \sim H^{2/M-1}$; for $M=2$, the behavior is logarithmic in both T, H).

(d) Full Numerical Solutions for C_{imp}, χ_{imp}

Desgranges [1985] and Sacramento and Schlottmann [1991] have solved for the thermodynamic properties over the full temperature range (above and below T_K). We display the χ_{imp} results from Sacramento and Schlottmann [1991] in Fig 84. The essential instability of the multi-channel fixed point is readily understood from the diverging χ_{imp} curves in this figure (for $H=0$). Namely, an arbitrarily small asymmetry in the TLS, electric field gradient or strain field in the quadrupolar Kondo model, or magnetic field in the magnetic impurity model will roll the divergence over below $T^x_{sp}(\approx H^2/T_K$ for M=2). to a Fermi liquid behavior. Heuristically, the presence of other impurities which produce a self-consistent molecular field due to the Ruderman-Kittel coupling mediated by the conduction electrons will also produce this kind of effect. This reasoning can be useful in interpreting features in the susceptibility data of $Th_{1-x}U_xRu_2Si_2$ (Amitsuka *et al.* [1993a,b]). See the discussion of Cox[1987b,1988a], Sacramento and Schlottmann [1989], and Gogolin [1995] for related remarks on the Jahn-Teller effect in the quadrupolar Kondo model. Note that the compensated Kondo model requires a 'critical' field strength to depolarize the impurity, of the order of T_K (Doniach [1976], Jayaprakash, Krishna-Murthy, and Wilkins [1981], Cox [1987a]).

The specific heat curves of Sacramento and Schlottmann [1991] are shown in Fig. 85 . Note the presence of the second peak below T^x_{sp} for the $H \neq 0$ case, which again indicates the crossover to the Fermi liquid. A heuristic interpretation of this peak is that it is a 'Schottky' like anomaly corresponding to the removal of the ground state residual entropy in the applied field. This appears to be useful in interpreting features in the specific heat data of $Y_{1-x}U_xPd_3$ (Seaman *et al.* [1991,1992]; Cox, Kim, and Ludwig [1995]).

The overall dependence of the specific heat and the susceptibility on the channel number in zero magnetic field is shown in Fig. 86.

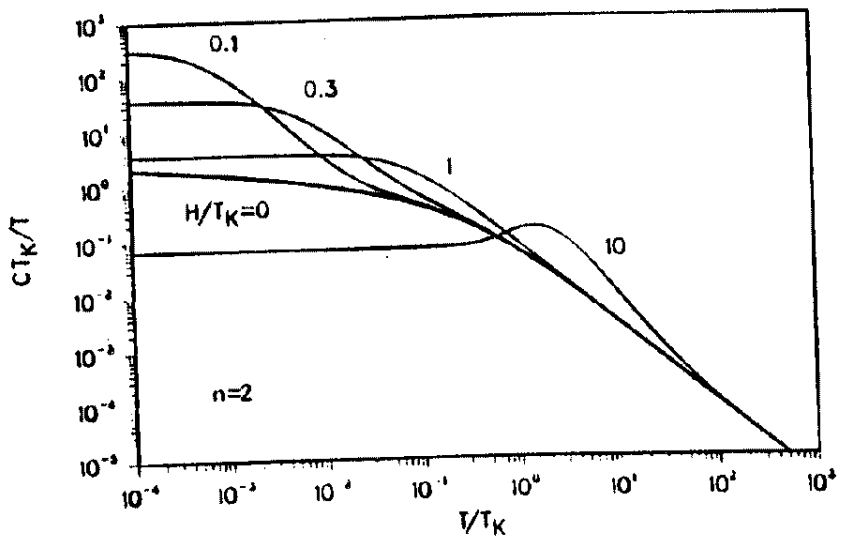

Figure 85: Specific heat for the two-channel multichannel Kondo models in applied spin field computed with the Bethe-Ansatz method. Note that n here corresponds to our M for channel number, and that H corresponds to the spin field H_{sp}. The applied field pushes out a Schottky anomaly seen very clearly as the peak in C/T here. From Sacramento and Schlottmann [1991]

(e) Electrical Resistivity: Magnetoresistance

The electrical resistivity cannot be calculated within the Bethe-Ansatz approach for arbitrary temperature. This requires a knowledge of cross sections for states with arbitrary numbers of excited particles and holes, and construction of the exact wave functions for outgoing many body states. This problem has not yet been solved.

At zero temperature, however, the Bethe-Ansatz can be used at least in the presence of finite magnetic field. For example, in the one-channel problem at zero temperature, the magnetic field excites a single spinon and holon which corresponds physically to a one fermion excitation. At zero temperature and arbitrary spin field, the scattering may be parameterized for both the compensated and over-compensated models in terms of phase shifts for each spin channel (Andrei [1982]). For example, for one channel $\delta_\uparrow(H) = -\delta_\downarrow(H) = \pi/2 - \pi M(H/T_K)$ where $M = (n_\uparrow - n_\downarrow)/2$ is the magnetization. The magnetoresistance is proportional to $\sum_\sigma \sin^2 \delta_\sigma(H)$. The situation for the two-channel model is different in that at least two spinons are generated (Andrei [1995]); nevertheless, a phase shift parameterization still holds allowing calculation of the magnetoresistance and magnetization (Jerez [1995]).

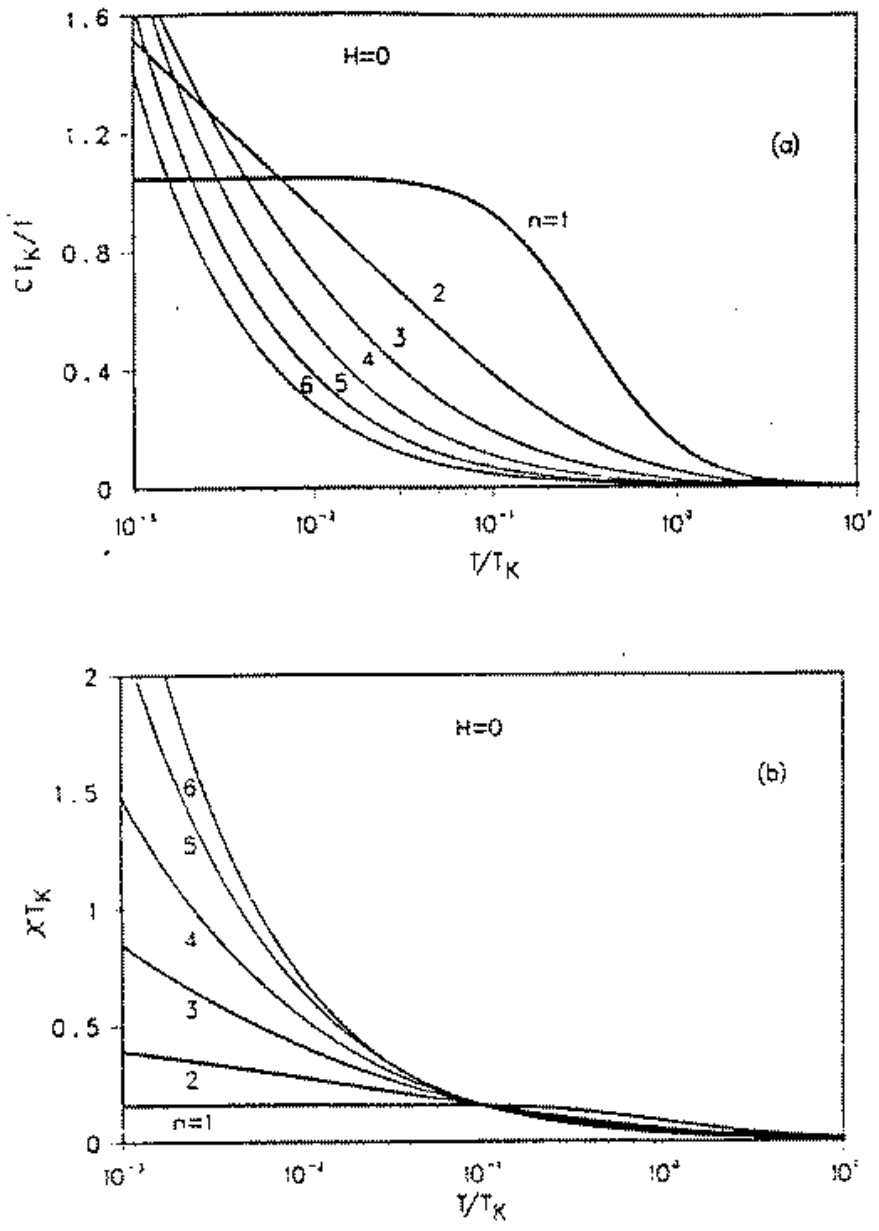

Figure 86: Dependence of zero field magnetic susceptibility and specific heat on channel number for overcompensated multichannel Kondo models computed with the Bethe-Ansatz method. Note that n here corresponds to our M for channel number. From Sacramento and Schlottmann [1991]

8 Experimental Results

In this section, we review the status of experimental understanding of possible TLS Kondo systems and two-channel spin and quadrupolar Kondo candidates among heavy fermion alloys and compounds.

A general comment is that the theory described in this paper is rigorous only for a single TLS site or U^{4+} or Ce^{3+} ion. Due to the divergent length scale about the multi-channel Kondo site, it is clear that there must always be some crossover away from the non-trivial fixed point for even two impurities (see sec. 9.3.1 for a discussion of the two impurity model). Hence the attitude here is that one may flow close to the non-trivial fixed point over some regime of temperature and other parameters at the finite concentrations which are always present in experiment, and then eventually will flow away. If the crossover regime occurs over an extended temperature range below the Kondo scale (which identifies the weak coupling to strong coupling crossover as the temperature is lowered) we may be confident that the physics is well described by the non-trivial fixed point.

8.1 Experiments on Possible TLS Kondo Systems

For this class of candidate systems, an excellent review of earlier experimental and theoretical work appears in J.L. Black [1981]. A more recent review of experimental work appears in von Delft *et al.* [1997a] for the specific results on copper nanoconstrictions.

The contributions of the TLS to the low temperature and low energy dynamics of amorphous materials and materials with defects are due to transitions between the ground state and the first excited state. Thus, according to the discussion of Sec. 2.1.1, the TLS must be slow or fast to have the energy splitting Δ of these TLS below or comparable to the characteristic energy of these experiments. The ultrafast TLS with large splittings are frozen out and those behave as rigid defect centers. The typical concentration of the TLS in amorphous materials is about $10^{18} - 10^{19}$ per cm^3, thus about 10-100 ppm.

Kondo type behavior only occurs in those cases where the Kondo temperature exceeds the TLS splitting ($T_K > \Delta$); the Kondo state does not form in the opposite case because the splitting "saturates" the pseudo-spin of the TLS. In the limit $\Delta = 0$ non-Fermi liquid behavior dominates the low temperature physics. For finite splitting, however, there is a crossover to Fermi liquid behavior as the characteristic energy of the experiment is reduced below $\sim \Delta^2/T_K$ (c.f., secs. 4.2,5.1.4,6.1.3.c,7.2), where Δ is the unrenormalized asymmetry splitting and $\Delta < T_K$ is assumed. In most of the samples, the parameters of the TLS, i.e., the splitting and the Kondo scale, are characterized by broad distributions. Thus the Fermi liquid and non-Fermi liquid behaviors are mixed in macroscopic samples where there are many TLS impurities. In principle, that can be avoided in two cases:
(i) materials with very well defined, uniform TLS's in a crystalline environment, and
(ii) small mesoscopic samples where there are only a few centers and by sample selection the two behaviors (Fermi liquid and non-Fermi liquid) can be separately studied.

In most instances, the TLS are formed in amorphous material or amorphous regions of the samples. The latter may also be represented by the vicinity of dislocations or by surfaces and interfaces between two different kinds of materials. The surfaces and interfaces are especially important in mesoscopic devices where they represent a large fraction of the samples.

There are however very few cases where the TLS are very well defined. The very well defined crystalline material $Pb_{1-x}Ge_xTe$ will be discussed below. This material shows Kondo like resistivity anomalies associated with the Ge atoms, which may hop between several quasi-equilibrium positions. A closely related and well defined problem is the diffusion of a light atom (e.g., hydrogen or a muon) through a metal. In this case, the interstitial sites between which the light atom moves are regularly distributed in the crystals. The hopping between two of those sites can be approximated by a TLS. A very extensive review of these phenomena has been given by Kagan and Prokofév [1992]. The most important process is the reconstruction of the electronic screening after the hopping which shows infrared divergent character. However, the non-commutative terms characterizing the Kondo effect do not play

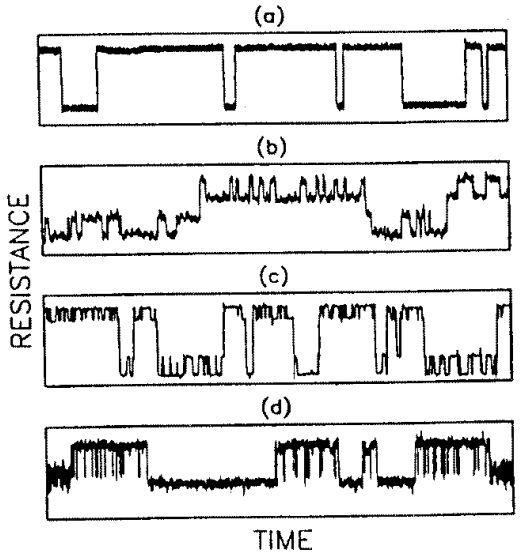

Figure 87: Telegraph noise displayed in time dependent resistivities of copper nanobridges for temperatures smaller than 150K (but still thermally activated) from Ralls and Buhrman [1988]. (a) shows the modulation of the resistance from a single TLS; (b) shows two independent TLS; (c) shows modulation of the amplitude by one TLS acting on another; (d) shows the modulation of the frequency by one TLS acting on another.

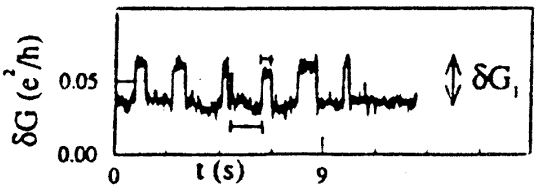

Figure 88: Time dependent electrical resistivity of a submicron bismuth sample near 1K where only tunneling is possible from Zimmerman, Golding, and Haemmerle [1991].

an important role, and so this fascinating area of research will not be discussed further in the present review.

The rest of the discussion in this section will focus on the electrical resistivity of bulk materials and the I-V characteristics of small mesoscopic devices, where the scattering rates of the electrons due to TLS's can be measured. The thermodynamic properties will be discussed only briefly, because in thsoe cases both the slow and fast TLS from the distribution of TLS sites play a role and as a consequence it is difficult to extract any reliable information about those sites which display a Kondo effect.

Slow Centers. For slow centers $V_x \approx V_y \approx 0$ and $V_z \neq 0$ characterizing the screening by conduction electrons. The slow centers show up in the fluctuations of the electrical resistivity (see Fig. 87,88). If there are several centers then they can modify each other's parameters, so that the average frequency of the transition and the amplitude depend on the states of the other centers, as measured on nanobridges at high temperatures by Ralls and Buhrman [1988,1991], where the transitions are thermally activated, and in the measurements of Zimmerman, Golding, and Haemmerle [1991], which were carried out at very low temperatures where only tunneling is possible. Such modulation of the conductance/resistance is called "telegraph noise". (For a review, see N. Giordano [1991].) The average

transition rate in metals is reduced by the screening of the electrons according to

$$\Delta_0(T) = \Delta_0(\frac{max\{T, \Delta_0(T)\}}{D})^{-K} \tag{8.1.1}$$

for a symmetric TLS, with splitting Δ_0 in the absence of TLS-electron interactions. This formula applies for thermally activated and tunneling induced transitions. The exponent K is, for weak coupling, quadratic in V_z and may be found through application of the renormalization group equation (3.4.15) to the commutative model which gives

$$K = 4v^z(0)^2 \quad . \tag{8.1.2}$$

More generally, K may be related to the phase shifts of the different angular momentum scattering channels off of the atom (Anderson [1967], Kagan and Prokofèv [1992]), *viz.*

$$K = \sum_l (2l+1)(\frac{\delta_l}{\pi})^2 \quad . \tag{8.1.3}$$

In most of the papers from the metallic theory side, the notation K is used for the exponent, while from the macroscopic quantum tunneling theory initiated by Caldeira and Leggett [1981,1983] K is denoted α. At low temperatures, the tunneling rate always exceeds T, and thus provided $K < 1$ the solution to Eq. (8.1.1) is

$$\Delta_0^* = \Delta_0(\frac{\Delta_0}{D})^{\frac{K}{1-K}} \quad . \tag{8.1.4}$$

This corresponds to a temperature independent hopping rate at low temperatures. In the case $K > 1$, the $\Delta_0(T) \to 0$ as $T \to 0$ and the particle localizes. Such a large value of K is not likely in a realistic system as the couplings are replaced by the phase shifts and K has an upper bound dependent on how many angular momentum channels participate in the screening (see, e.g., Kagan and Prokofèv [1992], Vladár [1993]).

Measuring the distribution of the time between two tunneling events K can be determined. A typical value is about $K = 0.2 - 0.3$, showing that the measured TLS are far from being localized (B. Golding *et al.* [1992], S.N. Coppersmith [1992], N.M. Zimmerman *et al.* [1991], K. Chun and N.O. Birge [1993]). These experiments can give information also about the asymmetric energy splitting of a particular TLS because the ratio of the time spent in the different states is determined by thermal equilibrium conditions.

Fast Centers. Eq. (3.4.26) gives the Kondo temperature for the two channel Kondo problem as

$$T_K^{(II)} = D_0(v^x(0)v^z(0))^{1/2}(\frac{v^x(0)}{4v^z(0)})^{\frac{1}{4v^z(0)}} \quad . \tag{8.1.5}$$

In order to estimate $T_K^{(II)}$, we take $D_0 \approx 10eV \approx 10^5 K$. A reliable estimate of $v^z(0)$ requires experimental input–it can be sampled through ultrasonic absorption or internal friction measurements (sound velocity shifts can provide further useful information). A TLS absorbs ultrasound and may be saturated for sufficiently high power (Golding *et al.* [1978], Black [1981]). The saturation power is much higher in metals than in insulators because the relaxation time characterizing the transition from the excited state of the TLS back to the ground state is much shorter due to the Korringa-type process relaxing the pseudo-spin by the creation of particle-hole pairs. This process for the TLS pseudo-spin is completely analogous to the Korringa relaxation of nuclear and electronic spins in metals. The Korringa process dominates over the channels existing in the insulator phase (e.g., phonon relaxation of the TLS). We discuss this in detail in the following paragraph. Most of the relevant experiments were performed over a decade ago and the results are summarized in Vladár and Zawadowski [1983(c)]. For more recent data, see Esquinazi *et al.* [1986], [1992] and references therein.

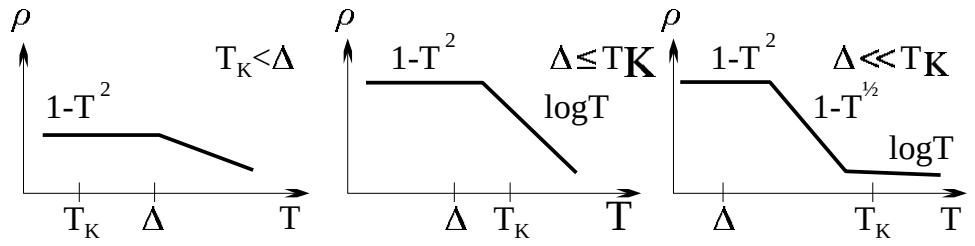

Figure 89: The temperature dependence of the electrical resistivity is shown in a schematic way for different cases $T_K < \Delta$ (left), $\Delta \leq T_K$ (center), and $\Delta << T_K$ (right).

Above T_K, the Korringa relaxation rate is proportional to the temperature times the renormalized coupling strength $v^2 = (v^z)^2 + (v^x)^2 + (v^y)^2$, which has a temperature dependence $v^2 \sim 1/\ln^2(T/T_K)$ in the vicinity of the Kondo temperature. If we go to sufficiently high temperatures, however, v^z dominates the coupling strength and is only mildly renormalized except in the most extreme cases. Hence, a rough estimate of $v^z(0)$ may be found by taking $v^2 \approx (v^z(0))^2$. The estimates found in this way give the range $v^z(0) \approx 0.02 - 0.25$, depending on the material (see Table I of Vladár and Zawadowski [1983(c)]). That estimate is in accordance with the value of $K = \alpha = 0.2 - 0.3$ measured for the slow center, since by Eq. (8.1.2) we see that $v^z(0) = (\alpha/4)^{1/2}$, which yields $v^z(0) \approx 0.2 - 0.3$.

If we consider the original TLS model with only the lowest two states of the TLS retained, Eq. (2.1.26) gives

$$\frac{v^x(0)}{v^z(0)} \sim 10^{-3} - 10^{-4} \quad . \tag{8.1.6}$$

Taking the largest value of this ratio (10^{-3}) and for $v^z(0)$ of 0.3, we come up with the most optimistic upper bound on $T_K^{(II)}$ of about 0.3K. Clearly, we can make this go down by orders of magnitude with the smaller estimates (and a smaller value for D_0). Experimental observability would require a larger T_K value. Recently, the work of Zaránd and Zawadowski [1994(a,b)] has solved this problem by taking into account the further excited states of the TLS, as discussed in Sec. 3.4.2. The essential point is that the higher levels induce a significant enhancement of the Kondo scale quite analogous to the enhancement of T_K for magnetic impurities by the presence of higher lying crystal field states and angular momentum multiplets. With realistic parameter choices, it was found that Kondo scales of the order of a few Kelvin were well within reach.

Electrical Resistivity. The electrical resistivity measures the electronic scattering rate off of the TLS. That subject has been first discussed by Cochrane *et al.* [1975] who introduced an ill-defined model with two sets of conduction electrons heuristically provided. The first calculation was performed by Kondo [1976(b)] up to fourth order introducing the assisted tunneling. Because $v^y(0) = 0$, and v^y is thus generated with a logarithmic factor at second order in perturbation theory (see Eq. (3.3.26)), the first non-vanishing logarithmic correction to the scattering rate is of order $(v^x v^z)^2 \ln^2(D/T)$. This contrasts, for the original Kondo problem where the leading log correction in the scattering rate shows up at third order (Kondo [1964]). The smallness of $v^x(0)$ led Kondo to conclude that no Kondo resistivity anomaly could be seen due to the TLS. Only the large renormalization discussed in Sec. 3 makes the effect observable. The resistivity behavior expected at different temperatures depends on the ratio of Δ_0/T_K, and this is illustrated in Fig. 89. In the left most curve of Fig. 89, $T_K < \Delta_0$ so that the Kondo correlated state is not developed and we pass to the Fermi liquid state. In the center and right hand curves of Fig. 89 we see the Fermi liquid behavior developing eventually below T_K, but with a non-Fermi liquid region possible provided $\Delta_0 << T_K$ (see the right hand curve of Fig. 89.

At high temperatures, summation of the logarithmically divergent terms gives the correct logarithmic rise in $\rho(T)$. A crude estimate for the incremental scattering strength per impurity $\Delta\tau^{-1}$ is provided by evaluation of the scattering rate at zero temperature and finite frequency using the coupling

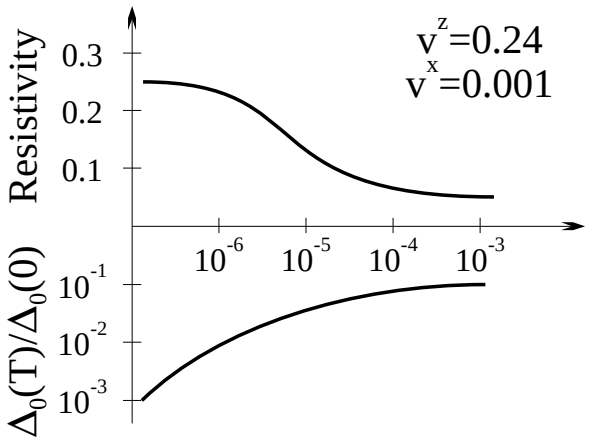

Figure 90: The resistivity and the renormalized tunneling rate are shown as a function of temperature in the next-leading logarithmic order of the renormalization group. The bare parameters are $v^z = 0.24$ and $v^x = 0.001$.

strengths evaluated at frequency scale $x = \omega/D$ in a golden rule estime. This gives

$$\Delta\tau^{-1}(\omega, 0) = \frac{4\pi}{\rho_0}[(v^z)^2 + (v^x)^2 + (v^y)^2]_{x=\omega/D} \quad . \tag{8.1.7}$$

We then estimate the additional resistivity due to the TLS as

$$\Delta\rho(T) \approx \frac{m}{ne^2} c_{TLS} \Delta\tau^{-1}(\omega)|_{\omega=k_BT} \tag{8.1.8}$$

where n is the electronic density, e the electron charge, m the electron band mass, and c_{TLS} the concentration of TLS. More appropriate formulae can be found in Vladár and Zawadowski [1983(c)] where the transport lifetime is properly evaluated. The result of the expression (8.1.8) is shown in Fig. 90 with the calculated TLS splitting Δ_0 for a symmetrical level using $\Delta = 0$ (c.f. Eq. (3.4.15)).

At low temperatures for zero splitting of the levels, the non-Fermi liquid excitation spectrum produces an anomalous saturation of the resistivity. According to conformal field theory [Ludwig and Affleck [1991], Affleck and Ludwig [1993]] and the NCA [Cox and Ruckenstein [1993]] $\delta\rho(T) \approx \Delta\rho(0)[1 - aT^{1/2}]$ in the weak-coupling limit $(v^x(0), v^z(0) << 1)$, where a is a pure number that may depend on the presence of ordinary potential scattering at the impurity site. So far, reliable calculation of the crossover from high to low temperatures can be done only with the NCA (a large N technique) or the direct $1/M$ expansion discussed in Sec. 3.4.5 (Gan *et al.* [1993]).

Examples of logarithmic resistivity signatures for TLS candidates. In amorphous materials, there are many experiments which show a logarithmic increase of the resistivity with decreasing temperature at low temperatures. The most convincing are those in which the amplitude of the maximum resistivity attained at low temperature decreases with sample annealing and disappears with re-crystallization. In order to rule out the spin Kondo effect as an origin for this anomaly, any dependence on applied magnetic field must be weak. Even in these cases, it is hard to rule out localization as a source of similar logarithmic temperature dependence. Typical resistivity data of this type are shown in Fig. 91, taken from Kästner *et al.* [1981] from a study of $Pd_{80}Si_{20}$ alloys.

A completely different example is the resistivity in highly doped conducting polymers at low temperatures studied by Ishiguro *et al.* [1992]. One example is highly doped polyacetylene. In this case, the authors argue against the competing localization mechanism mentioned above as a source for the logarithmic upturn in the resistivity. An alternative explanation in terms of magnetic impurities associated with certain carbon groups has been put forward (Cruz *et al.* [1995]).

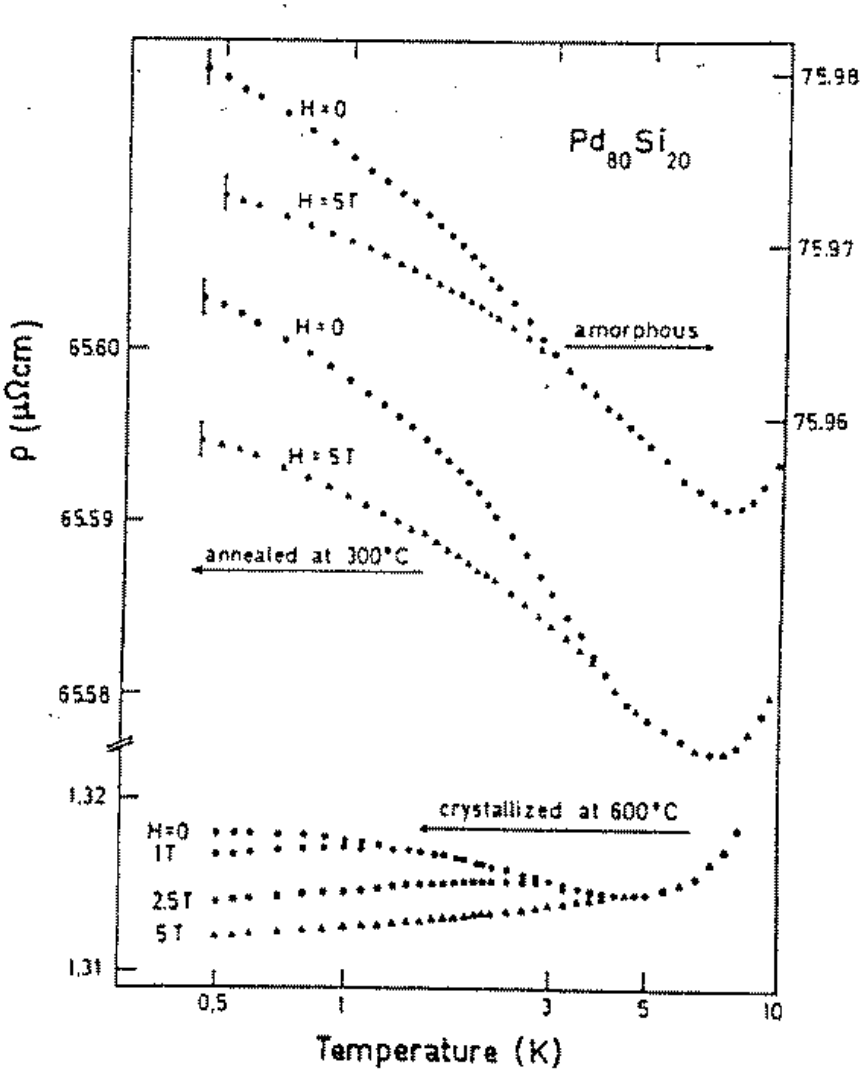

Figure 91: Resistivity vs. temperature of $Pd_{80}Si_{20}$ in the amorphous, annealed, and crystallized state for magnetic fields $0 \leq H \leq 5T$. The positive magneotresistivity has always been subtracted. From Kästner *et al.* [1981]

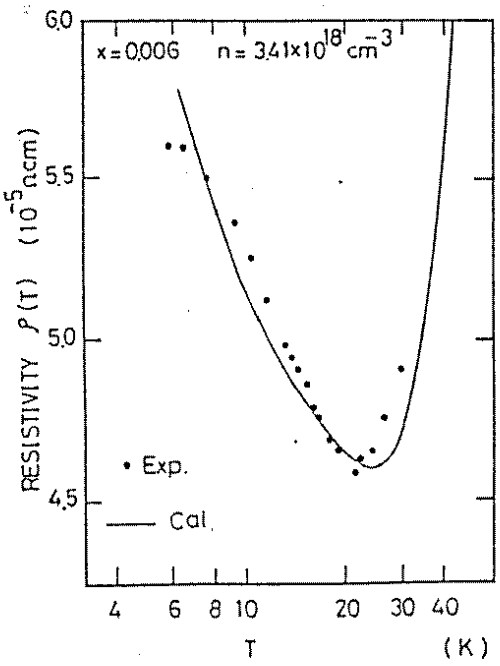

Figure 92: Total resistivity $\rho(T)$ vs. temperature for $Pb_{1-x}Gexe$Te. The closed circles correspond to the experimental results by Takano *et al.* [1989].

Resistivity of $Pb_{1-x}Ge_xTe$. PbTe is a type $II-VI$ crystalline semiconducting compound in which a small amount of Pb can be replaced by Ge. The material thus obtained is either a p-type or n-type degenerate semiconductor. The ambiguity arises because the concentration of charge carriers is different from sample to sample and cannot be controlled in a systematic way. Because the ionic radius of Ge^{2+} of $0.73\mathring{A}$ is much smaller than the $1.2\mathring{A}$ radius of Pb^{2+}, the Ge atoms do not stay at the lead positions, but slide around in the various body diagonal directions ([111]) giving rise to eight possible equilibrium positions. The randomness of the Ge atoms induces local strain fields that lift the eight-fold degeneracy, plausibly leaving only two close in energy at each Ge site and thus giving rise to a TLS. The relevant experimental work was performed by Takano *et al.* [1984].

The experimental data concerning resistivity minima was analyzed by Katayama *et al.*[1987]. The theoretical fit to the data of Takano *et al.* [1984] is based upon use of Eqs. (8.1.7,8), and is shown in Fig. 92. The curve clearly shows a logarithmic temperature dependence over about a decade of temperature. The composition of the sample for which the fit was performed has $x = 0.006$, a carrier density of $3.41\times10^{18}cm^{-3}$, an effective band mass of $m^* = 0.053$, a Fermi energy of $E_F = 718K$, and an estimated bandwidth of $D = 665K$. The coupling strength $v^z(0) = 0.33$ was estimated from a knowledge of the Ge positions, and $v^x(0)/v^z(0)$ was taken to be 0.001 in order to give the correct Kondo scale $T_K = 0.89K$. However, the leading logarithmic formulae were used to estimate T_K, and with this estimate for $v^x(0)$ the more correct estimate provided by $T_K^{(II)}$ will be too small. This can be remedied by making $v^x(0) = 0.01$, which seems perhaps too large. A more likely explanation is that the ratio of $v^x(0)/v^z(0)$ may be about right, but that the higher lying levels must be properly taken into account as per the discussion of Sec. 3.4.2 and the work of Zaránd and Zawadowski [1994(a,b)]. In order to get more accurate estimates, ultrasonic attenuation studies are needed in the future.

While this is a good material for study given that the exact source of TLS is known, there are complications. The random strain field induces a distribution of splittings, as discussed above. Also, the Ge ions not only introduce carriers and, apparently, the TLS Kondo effect, they also give rise at

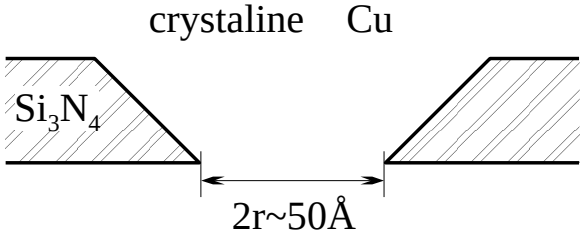

Figure 93: The point contact prepared by Ralph and Buhrman [1992,1994]. The gate (shaded) is made of Si_3N_4. The diameter of the orifice is $2r$. The contact is crystalline copper.

higher concentrations to ferroelastic transitions which intervene in the Kondo upturn. Thus there is practically no way to sample cleanly the non-Fermi liquid behavior at lower temperatures.

TLS at Dislocations TLS may be formed at dislocations. Endo *et al.* [1988] studied different dilute aluminum alloys where dislocations where introduced by shock loading or extension at different temperatures. The increase of the density of dislocations was associated with a logarithmic increase in the resistivity at low temperatures.

Point Contact Spectroscopy of Nanoscale Junctions. The most convincing measurement of TLS scattering amplitudes to date has been in the study of nanoscale junctions or gates through point contact spectroscopy sampling of dI/dV of the gates (Ralph and Buhrman [1992], Ralph *et al.* [1994], Ralph and Buhrman [1994]). The method of fabrication of such a junction is shown in Fig. 93. It starts with electron beam lithography as developed by Ralls and Buhrman [1988,1991] and reactive ion etching to make a hole in a silicon nitride membrane. The minimum size of the hole is 3-15 nm. Then the membrane is rotated and covered by different metals (Al,Ag,Pt,Ti,V and primarily Cu have been used) on both sides. The electron mean free path of the electrodes is about 180 nm at 4.2K. In the region of the gate very likely TLS are formed. The low frequency noise can be recorded by measuring the conductance of that gate as a function of time (Ralls and Buhrman [1988]). The recorded conductivity is similar to the one shown in Figs. 87,88 and those slow fluctuations are due to slow TLS.

The effect of the fast TLS cannot be seen through the resistivity fluctuations and can only be sampled by dI/dV characteristics. In that case there is a voltage difference between two electrodes attached on either side of the gate. On one side the Fermi energy is higher and thus the gate works something like a tunnel junction. Current is driven by electrons propagating ballistically through the small gate orifice. Because there is no barrier but actually a geometrically limited path for the electrons, the experiment is equivalent to point contact spectroscopy in which a sharp metal tip is placed against a material. In that case, the tip contact serves as the small orifice. Two reviews of point contact spectroscopy are Yanson and Shklyarevskii [1986] and Jansen *et al.* [1980].

The essential idea is as follows: even in the absence of scattering in the contact, the small orifice produces a geometrically limited resistance R_{B0} to the incoming electrons because not all the electrons can make it through the gate. In addition, the electrons experience scattering processes within the contact giving rise to a resistance electrons. To the extent these are frequency dependent, they will be sampled at a characteristic energy eV for each temperature because added electrons flying through the gate come with energy eV above the Fermi level. As a result, the dynamic resistance of the junction is given by (Jansen *et al.* [1980])

$$\frac{dV}{dI} = R(V) \approx \frac{h}{e^2}\frac{8}{(k_F d)^2}[1 + 0.4(\frac{d}{v_F \tau(ev)})] \tag{8.1.9}$$

where h is Planck's constant and d is the orifice diameter. This equation is actually the result for a circular hole in a membrane.

For the hypothesized TLS in Ralph and Buhrman's data, typical conductance curves $G(V,T) = dI(V,T)/dV$ are shown in Fig. 94. The conductance is minimum at $V = 0$ indicating a zero bias anomaly, and showing that the relaxation rate decreases with decreasing voltage. The conductance shows a clear

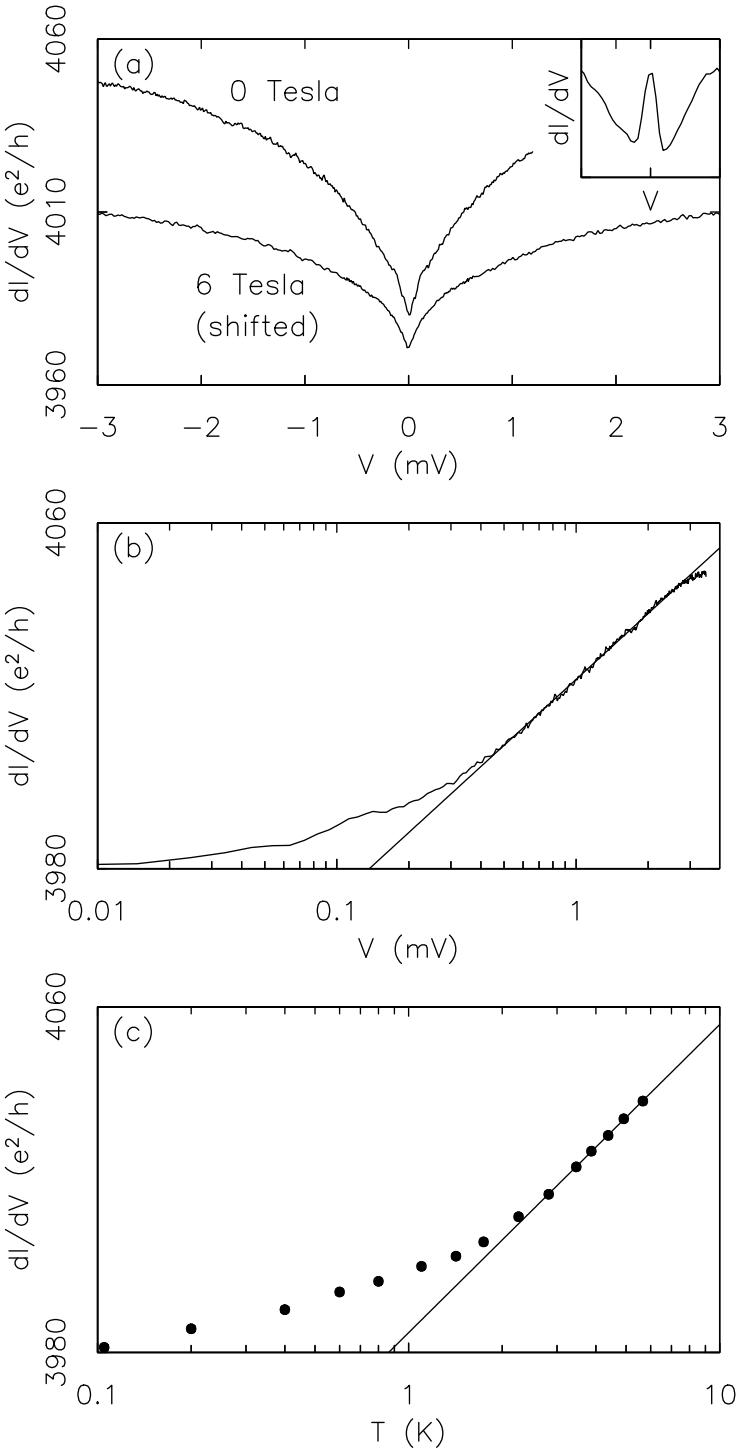

Figure 94: (a) Differential conductance of a Cu constriction at T=100mK. The curve measured in 6 T magnetic field is shifted down by $20e^2/h$ for clarity. (b) V dependence of the differential conducatance for $B = 0$ T and T=100 mK. (c) T dependence of th conductance for $B = 0$ T and V=0 mV. Straight lines illustrate regions of logarithmic V, T dependencees. Inset to (a): Conductance of Cu constriction with 200 ppm Mn at 100mK, 4 T, showing suppression of magnetic-impurity scattering by an applied magnetic field. From Ralph and Buhrman [1992].

region of logarithmic drop with voltage, indicative of a Kondo effect. To rule out a magnetic Kondo effect, applied magnetic field was also measured–a Zeeman splitting of the central zero bias anomaly would be expected, but none is observed in contrast to the devices controllably doped with magnetic impurities. The voltage dependence of the observed relaxation rate is similar to frequency dependent rate computed by Vladár and Zawadowski [1983(c)] for a TLS, and are also very similar to resistivity results of Fig. 89. In Fig. 94(c) the temperature dependence of the zero bias conductance is shown. This also shows a logarithmic temperature dependence with a break in that behavior at lower T that could was discussed in the original work as either a new $\ln T, \ln V$ dependence or a possible $\sqrt{T}, \sqrt{V}$ dependence at lower temeperature, which is characteristic of the low temperature two-channel Kondo model resistivity. At even lower temperature and bias, the two-channel Kondo scaling must be stopped by the presence of the renormalized TLS splitting. This occurs at a crossover scale we have denoted T_x in this review, and which is called T_Δ in the experimental paper of Upadhyay, Louie, and Buhrman [1997]. Fermi liquid behavior is recovered below this temperature scale. Thus, for $T < T_x = T_\Delta$, T^2 behavior should be seen in the zero bias resistance, and the $\sqrt{V}$ behavior saturates below $eV = k_B T_\Delta$. This crossover has been observed in Ti and V point contacts as we shall discuss further below (Upadhyay, Louie, and Buhrman [1997]).

In order to confirm the behavior arose from defects of the TLS variety, Ralph and Buhrman [1994] have performed a number of experimental tests. First, the effect is very reproducible–it shows up in half of the fabricated junctions and while initial studies focussed on Cu junctions, similar conductance curves have been found in silver, vanadium, titanium, and platinum devices. It is interesting that the effect of T_x is shown only by Ti and V samples (Upadhyay, Louie, and Buhrman [1997]). Furthermore, application of a high current to the junction leads to a shift of the TLS parameters measured after the high current is switched off and then used to fit the data, which strongly suggests that the current rearranges the atomic positions (electromigration) and modifies the TLS in the point contact (Upadhyay, Louie, and Buhrman [1997]). Second, the effect only arises in unannealed junctions, in which the samples are cooled to cryogenic temperatures hours after fabrication. Annealing removes the anomaly. Third, to rule out static disorder as a source of the anomaly, six percent Au was co-evaporated with Cu; no zero bias anomaly was found. (Moreover, it was observed that the conductance amplitude is too large to correspond to candidate energy dependent effects such as weak localization and disorder enhanced electron-electron scattering). Finally, to further rule out magnetic impurities as a source of the anomaly, small amounts of Mn and Cr ions were controllably co-deposited with the host junction metal. Not only do the Kondo anomalies associated with these impurities show a sizeable magnetic field dependence, the resulting conductance signals are stable over periods of months indicating that the magnetic impurities do not anneal away from the junction.

Ralph and Buhrman noted that the magnitude of the conductance anomaly indicated the presence of several scattering centers within the junction region (based upon the scattering being at half of the unitarity limit at $T = 0$ (c.f. Sec. 6.1.4) in conjunction with Eq. (8.1.9)) as the contribution to the conductance of a single scatterer in these junctions is of the order of e^2/h. They also ascribe the likely TLS sites to dislocation jogs or kinks. They observe that these same kind of zero bias conductance anomalies have been observed in many types of metal point contacts for many years and suggest the earlier measurements have also been of TLS Kondo scattering.

Perhaps the most compelling evidence that the observed anomalies correspond to TLS Kondo centers is a demonstration of non-Fermi liquid scaling behavior at low temperatures (Ralph *et al.* [1994]; Ralph and Buhrman [1994]). Ralph *et al.* focussed on the conductance in regions below the apparent Kondo scale inferred from the logarithmic regions seen first as voltage and temperature are lowered. Motivated by conformal field theory results for the electronic self-energy (Ludwig and Affleck [1991], Affleck and Ludwig [1993]), a scaling form for the conductance was assumed in which the conductance contributions from different TLS within the junction was assumed to be additive. This is reasonable

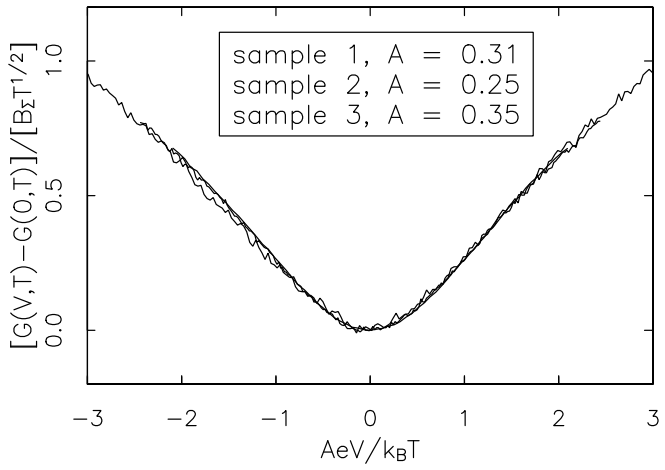

Figure 95: Scaling curves for the three Cu nanoconstriction samples of Ralph *et al.* [1994].

provided the different sites only interact weakly. The resulting scaling form is

$$G(V,T) - G(0,0) = T^{\alpha} \sum_i B_i \Gamma(\frac{A_i eV}{[k_B T]^{\alpha/\beta}}) \tag{8.1.10}$$

where the summation is over the TLS sites, $\Gamma(x)$ is a universal function, and B_i, A_i are non-universal amplitudes which may vary, for instance, as a function of the position of the defect from the narrowest point of the constriction. A test of this scaling for $\alpha = \beta = 1/2$ is shown in Fig. 95. The function $\Gamma(x)$ must go as x^{β} for $x \to \infty$ so that $G(V,T)$ is independent of T for $eV >> k_B T$. To normalize, $\Gamma(0) = 1$, and $d\Gamma(x)/dx^{\beta} \to 1$ for $x \to \infty$. We can immediately infer $\alpha = \beta$ since the voltage only enters in the Fermi functions of the leads in the combination V/T. Since the conformal theory gives $\alpha = 1/2$ in bulk, this is the expectation for the above scaling form; however, in attempting to describe the data, α was allowed to vary. We note that the above scaling must crossover to Fermi liquid behavior below $T_x = T_\Delta \approx \Delta^2/k_B^2 T_K$ for $\Delta < k_B T_K$ as discussed in Affleck *et al.* [1992] and in Secs. 4.2.e, 5.1.4, 6.1.2.c, and 7.2. No such deviations from *non Fermi liquid* behavior were found for the data of Ralph and Buhrman for Cu junctions, indicating very small splittings for the putative TLS in the junctions. Recently, a direct theoretical calculation of the scaling function was made using the NCA treatment of the two-channel Kondo model (Hettler *et al.* [1994]), while an extensive discussion of the corresponding effort based upon a conformal field theory approach appears in von Delft, Ludwig, and Ambegaokar [1997b]. We note that it is quite puzzling that order ten scattering centers exist in the sample with identical T_K values as evidenced by the scaling curves.

To test the scaling hypothesis, Ralph *et al.* manipulated Eq. (8.1.10) to eliminate $G(0,0)$ and considered

$$\frac{G(V,T) - G(0,T)}{T^{\alpha}} = \sum_i B_i [\Gamma(A_i x) - 1] \tag{8.1.11}$$

where $x = eV/k_B T$. The quantity on the left hand side of this equation may be plotted for different temperatures as a function of x with α varied. The result must be universal to the extent that A_i can be approximated as a single constant, which holds experimentally with $A_i \approx 0.25 - 0.35$. Then $\sum_i B_i$

can be found from scaling the curves together for large x and is found to be $\approx 10 - 30e^2/h$. The results normalized together are shown for several samples in Fig. 96, where different α values are used in a,b. The fit with $\alpha = 0.5$ looks perfect, while the universality is lost with $\alpha = 0.3$. The Fermi liquid value ($\alpha = 2$) is ruled out, as is apparently the possibility that $\alpha = 1$. Deviations from universal behavior are expected for $T, V \geq T_K$ (a range of T_K values of 0.6K$\leq T_K \leq$5K is suggested). Sample 2 data are shown in Fig. 96(c) for which $T_K \approx 0.5K$. For Sample 3 (Fig. 96(d)). at two different temperature ranges universality can be found indicating very likely that there is a distribution of parameters with two groups of TLS likely dominating. The idea is to determine α from those curves where universality is well satisfied so that the scattering centers have uniform parameters.

The scaling hypothesis is further tested in applied magnetic field $|H|$. Applied field serves as a channel field in this case, lifting the degeneracy of up and down spin electrons. In this case, the zero bias scaling function for a single TLS site must be generalized to the two parameter form $T^{1/2}\Gamma(V = 0, |H|/T^{1/2})$ which follows from the considerations of channel field scaling (see Secs. 4.2.c,5.1.4,6.1.2.c). Since this must be independent of T as $T \to 0$, we infer that $\Gamma(x = 0, y) \sim y, \quad y \to \infty$ so that the subtracted conductance should scale as $|H|$ for $H \to 0$. This is observed for small H and $T = 0.1K$. Nonlinear conductance spikes appear for fields above 1 Tesla which are clearly non-universal phenomena. In contrast, the ordinary Kondo resistivity would be expected to show scaling with H^2 for small H. At the theoretical level, the microscopic origin of the channel splitting in the TLS model is unclear, unlike the quadrupolar Kondo model for example. As discussed in Sec. 3.4.1.e, the Zeeman splitting of the conduction states alone cannot produce a discriminating channel asymmetry unless the applied field is of order the conduction bandwidth. Nonetheless, the observed field dependent scaling offers strong support for the applicability of the two-channel Kondo model description.

The success of the above scaling analysis places a constraint on the values of Δ for the TLS in the junction. Given the estimate for the crossover scale $T_x = T_\Delta = \Delta^2/k_B^2 T_K$ (for $\Delta < k_B T_K$), for T_K=5K, the absence of fermi liquid behavior down to $T = 0.4K$ implies $T_x = T_\Delta < 0.4K$ and $\Delta < 1.4K$.

The recent experiments by Upadhyay, Louie, and Buhrman [1996] on Ti and V point contacts appear to show the effect of the renormalized splitting below $T_\Delta = T_x$. For example, one Ti junction studied down to 76mK appears to have $T_\Delta = 1.4K$ and renormalized splitting $\Delta = 0.4$meV. In another junction, two such crossovers appear, very likely due to two different TLS, with $\Delta = 0.47$ meV and 1.6 meV. Here Δ is estimated from the formula $T_\Delta = T_x = \Delta^2/(k_B^2 T_K)$ with the two different T_K estimates of 6.2K and 28K and T_x read off from the crossover away from $\sqrt{V}$ behavior. To confirm the origin of these phenomena as arising from TLS Kondo scattering, it was observed that after the treatment of the junction with a large current flow for 10 seconds the inferred splittings were seen to change from 0.5$\to$ 0.7 meV, and 1.6$\to$ 1.54 meV. This is explainable by rearrangement of atomic positions and hence changed parameters of the TLS. We note that the alternative explanation of Altshuler, Wingreen, and Meir [1995] is unable to explain the crossover to T^2 behavior at a fixed temperature scale. The observation of the additional scale $T_\Delta = T_x$ gives us three distinct regions for the point contact resistance:

$\to T > T_K$, $\rho(T, V)$ is logarithmic in T, V
$\to T_K > T > T_\Delta = T_x$ $\rho(T, V)$ displays non-Fermi liquid $\sqrt{T, V}$ behavior
$\to T_x = T_\Delta > T$ $\rho(T, V)$ displays T^2, V^2 saturation (Fermi liquid)

We note that the inferred Δ values are relatively large. Since the distribution of TLS splittings is *apriori* flat in energy, it is more probable to observe TLS with higher Δ values. It remains still to explain the origin of the small (or zero) estimated splittings in Cu based junctions as compared to Ti and V based contacts. As mentioned above the overall size of the zero bias conductance is between 10-100 e^2/h. However, the current induced change is already about e^2/h indicating that the splitting of a single TLS plays the role.

Analogous phenomena (apart from the non-Fermi liquid behavior) should appear for magnetic

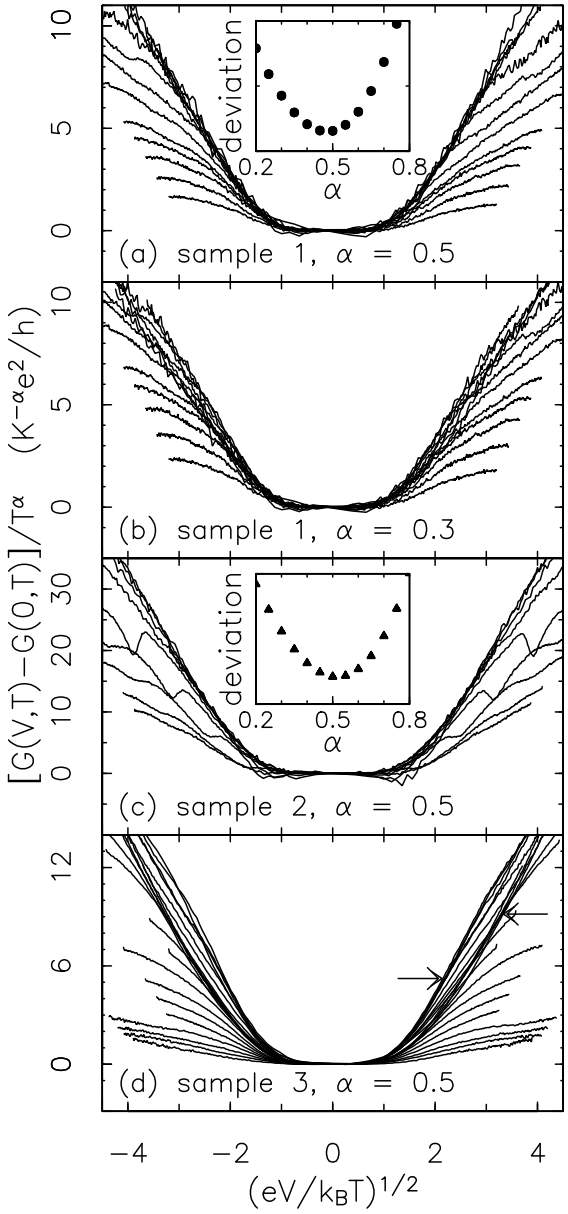

Figure 96: Scaling behavior of conductance for three different Cu nanoconstrictions at low voltage for $eV, k_BT < k_BT_K$. (a),(b) Rescaled conductance of sample 1 for (top to bottom) $T = 0.4, 0.6, 0.8, 1.1, 1.4, 1.75, 2.25, 2.8, 3.5, 3.9, 4.3, 4.9, and 5.6$K. (c) Rescaled conductance of sample 2 at same T values up to 4.3K. (d) Rescaled conductance of sample 3 from 125mK to 7.6K. Arrows show 2 separate scaling curves. Insets: Integrated mean square deviation from the average scaling curve for $T \leq 1.4$K and -8$\leq eV/k_BT \leq 8$. The scale of the deviation axis is in (a) from 0 to 4 $(e^2/h)^2$ and in (c) from 0 to $25(e^2/h)^2$. Residual deviations for $\alpha = 0.5$ are consistent with the amplifier noise. From Ralph *et al.* [1994].

impurities. Apart from the kind of controlled doping experiments with Mn and Cr impurities in the metal junctions described above that were performed by Ralph [1993], some early point contact experiments on Kondo alloys were performed (Jansen *et al.* [1980], Yanson [1995]) which showed characteristic logarithmic Kondo anomalies in the resistivity. Earlier experiments were performed with tunnel junctions. In this case, the magnetic impurities may reside either in the tunneling barrier or in the electrode near the barrier (on a scale less than $50\mathring{A}$. In the first case, the resonant density of states near the impurity induces near the Fermi energy actually assists the tunneling process and thus enhances the conductance, producing a maximum at zero bias (Wyatt [1964], Appelbaum and Shen [1972]). On the other hand, if the impurities are nearbye the interface, similar to the point contact configuration the junction resistance shows a maximum at zero bias (Bermon and So [1978], Mezei and Zawadowski [1971]). This can be understood because the electrode impurities backscatter incoming electrons away from the junction thus reducing the tunnel current.

Another interesting feature of the point contact experiment with magnetic impurities (Yanson [1995]) is that the intensity of the zero bias anomalies are larger by one or two orders of magnitude for small contact orifices. In a recent theory, Zaránd and Udvardi [1996a,b] have shown that the local density of states fluctuation for the electronic density is enhanced for reduced orifice size. Since $T_K \sim \exp(-1/J[\rho + \delta\rho])$ this will strongly enhance T_K for those centers for which the density of states is enhanced, and strongly suppress T_K (below observability) for other sites. According to that theory this enhancement must occur at the Femri energy in an energy range with width not more than about 10% of the Fermi energy or even less. Naturally, the enhanced T_K sites will be preferred. Obviously something similar can carry through for the TLS Kondo scale.

Another point contact experiment where the zero-bias anomaly is attributed to TLS is in the work of Keijsers *et al.* [1995]. In the original theory of Kozub and Kulik [1986] only the excitations of the TLS to higher states were taken into account, without Kondo corrections. However, it looks as though the TLS Kondo picture fits the data better as the temperature dependence looks predominantly like a thermal smearing in contrast to the other explanation (Zaránd and Zawadowski [1995]). In these experiments the apparent Kondo temperature (measured from the low temperature peak position of the derivative of the differential resistance) increases with decreasing contact size (larger contact resistivity) just like in the magnetic case discussed above (Yanson *et al.* [1995]). To the the large T_K values inferred from this interpretation requires the Zaránd and Zawadowski [1994a,b] enhancement arising from the excited states.

Finally, we mention that recently Wingreen, Altshuler, and Meir [1995] have criticized the TLS interpretation of the point-contact experiment by Ralph and Buhrman [1992] (Ralph *et al.* [1994], Ralph and Buhrman [1994]). They argue that in tunneling experiments with disordered material zero bias anomalies have been observed with square root behavior (for a review see Altshuler and Aronov [1985]) reflecting the renormalization of the local density of states and that similar density of states effects can occur in the present experiments. Ralph and Buhrman [1995] however presented evidence against that argument by introducing controlled disorder into their contacts as mentioned earlier.

Furthermore, Wingreen, Altshuler, and Meir [1995] challenged the TLS concept itself by considering the effect of extrinsic disorder from impurities on the TLS parameters through the couplings V^x, V^z (see sec. 2.1). In particular, they calculate the TLS self-energy diagrams of a Hartree type with the TLS on one end of a conduction electron bubble and a non-TLS impurity on the other end. Without the disorder interruption this diagram vanishes on tracing out the electron orbital pseudo-spin. This physically corresponds to a Ruderman-Kittel charge interaction between the TLS and non-TLS impurity. They then calculate the root mean square distribution of splittings Δ and find that it goes as $E_F v^z/\sqrt{k_F l}$ which is about 50-100K for the estimated mean free path in Ralph and Buhrman's experiments [1992,1994]. This same estimate for the magnitude of the splitting can be obtained by replacing the electron spectral functions in the Hartree diagram by the local density of states about the TLS site. Separately, one can estimate an upper bound on the contribution to the spontaneous tunneling matrix element Δ_0 as $\rho_0 \int V_x(\omega) d\omega \simeq 50K$(Zaránd and Zawadowski [1995]). This is easily renormalized down-

wards by scaling. (Calculating the root mean square spread in Δ_0 induced by the extrinsic impurities from the diagram considered by Wingreen, Altshuler and Meir [1995] produces a small estimate, of the order of a few tenths of a Kelvin.)

With regard to the large estimated RMS spread in Δ two remarks are to be made:
1) The modification of Δ corresponds to a modification of the *shape* of the potential and thus must influence Δ_0. The TLS of interest are only those few for which the the splitting Δ is small. The selection of these TLS must be made on the basis of the *renormalized* (by scaling) potential and is unrelated to the unrenormalized one. (An asymmetric potential may be made symmetric after the renormalization and vice versa.) The existence of TLS with small splitting and asymmetry is an experimental fact in amorphous materials. This most striking evidence for this is found in the existence of linear heat capacities in amorphous superconductors below the superconducting transition temperature (Graebner *et al.* [1977], Löhneysen *et al.* [1980], Lasjaunias and Ravex [1993]).
2) Recently Kozub [1995] has pointed out that in the argument of Wingreen, Altshuler, and Meir [1995], the largest contribution to the RMS splitting comes from those impurities close (i.e., nearest neighbor or next-nearest neighbor) to the TLS site (see also Smolyarenko and Wingreen [1997]). In a dilute case, most TLS do not have such a neighbor so that the actual splitting modification by the disorder is likely to be much smaller than reported. For those which do have a non-TLS impurity nearby, there will be a 'wipeout': the large splitting will destroy the TLS character and these simply will not be seen. Hence some more detailed consideration of the non-TLS impurity configurations is needed than provided by Wingreen, Altshuler, and Meir [1995].

Keijsers, Shklyarevskii, and van Kampen [1996] carried out another set of experiments using metallic glasses in break junctinos. At zero bias resistivity measurements revealed the same kind of telegraph nois due to a slow tunneling center as shown in Figs. 8788. When the slow center switches, then the zero bias anomaly is also changed, and actually two different curves are measured for the zero bias anomaly. This was interpreted as a demonstration of the interaction between a slow and a fast tunneling center. When the slow center changes then the parameters of the fast ones are also tuned, which results in a change of the zero bias anomaly. (Note that in Figs. 87,88 the interaction between two slow centers is displayed.)

The curve indicates that the low energy cutoff determined by the asymmetry Δ is tuned, and that the other parameters must have remained almost the same so as not to modify the width of the zero bias anomalies, which actually measure the Kondo temperature. This means that the v^α interactions are only very slightly tuned, which is the case when the assisted tunneling processes are induced via transitions through the excited states of the potential well. The first excited state overlaps with both minima of the TLS (see Sec. 3.4.2 and Zaránd and Zawadowski [1994a,b]). Assuming the orbital Kondo effect picture, the top of the anomaly is chopped off at different heights after the Δ parameter of the TLS is tuned. The difference in the conductance is shown in Fig. 98 for a single junction (curve (3) of Fig. 97). The theoretical fit, given by the solid line, assumes that the scattering resonance has the shape given by the second order renormalization group equations discussed in Sec. 3.4.1, and a sharp cutoff is used for $eV < \Delta$. The fit is remarkably good. On the other hand, the theory of Kozub and Kulik [1986] woudl provide the difference between two curves shown in the inset. The experimental data clearly does not show the long tail expected from the Kozub and Kulik [1986] theory, and thus offers strong support for the origin of the zero bias anomaly in terms of the orbital Kondo effect associated with TLS. An important feature of the experimetnal data is that the changes in the conductance are smaller than e^2/h which makes it possible to interpret them as arising from a single modulated TLS. In similar experiments, two such transitions are superposed, indicating that at least two fast TLS are affected by the slow TLS.

Recently a new experiment was performed by Balkashin *et al.* [1997] to distinguish between the TLS Kondo theory and the theory of Kozub and Kulik [1986] which includes direct excitation of the TLS without the Kondo effect. The two interpretations have two different characteristic energy scales, namely the Kondo scale T_K and, for Kozub and Kulik [1986], the Korringa-linewidth $\Gamma_K = (\rho V^z)^2(\Delta_0/E)^2 E$

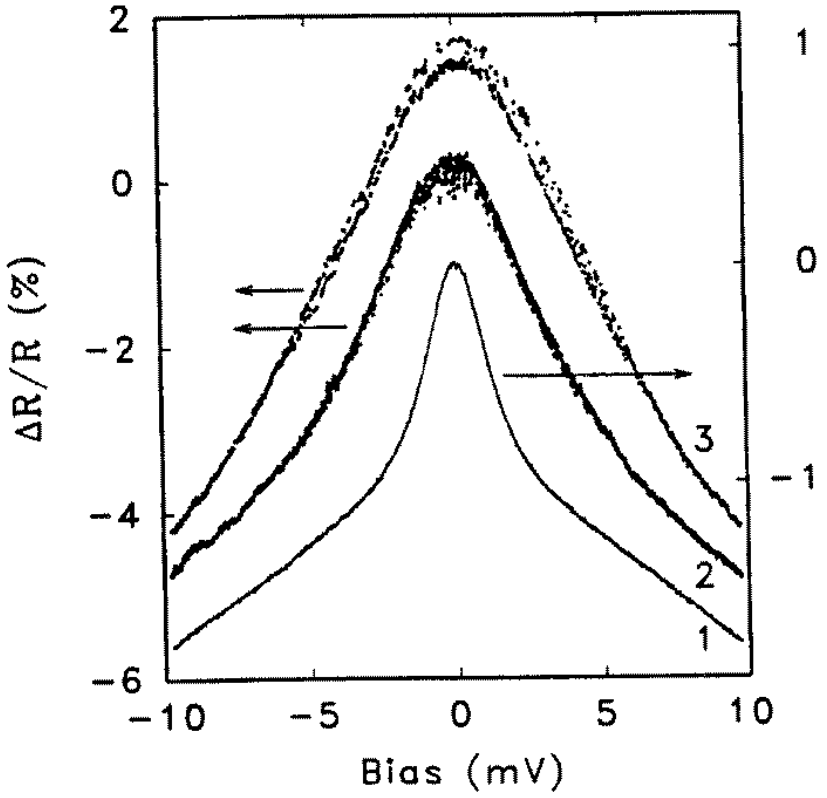

Figure 97: Experimental evidence for modulation of fast TLS by slow TLS (telegraph noise) in mechanically controlled metallic glass break junctions. The differential resistance R_d is measured as a function of bias voltage for $Fe_{80}B_{20}$ (1 and 2) and $Fe_{32}Ni_{36}Cr_{14}P_{12}B_6$ (3) break junctions at T=1.2K. (1) A 6.6ω contact, showing almost no noise. (2) A 366Ω contact that shows clear noise around zero bias. The noise amplitude decreases as the bias voltage increases. (3) A 145ω contact, showing a clear two-level switching behavior between two different R_d peaks. From Keijsers, Shklyarevskii, and van Kampen [1996].

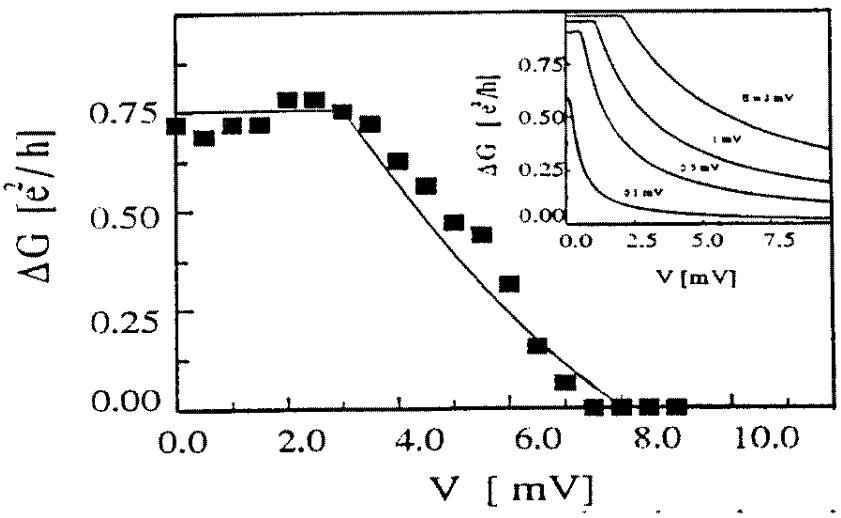

Figure 98: Conductance difference for mechanically controlled metallic glass break junctions. The dots are obtained from the measured resistance change values shown in curve (3) of Fig. 97, with uncertainties of order $0.1e^2/h$. The solid line is obtained from the theory of Vladár and Zawadowski [1983a,b,c] using a Kondo scale of $T_K \approx$35K, and two different splittings for the fast TLS of $E_1 = 3.5$meV, E_2=8meV, with the assumption that the modulation by the slow center induces these two different splitting values. The inset shows conductance difference curves generated by the theory of Kozub and Kulik [1986]. This figure is from Zaránd , von Delft, and Zawadowski [1997].

where $E = \sqrt{\Delta_0^2 + \Delta^2}$ is the full splitting of the two-level system including asymmetry and spontaneous tunneling. This latter result follows provided the temperature is low compared to E so that k_BT is replaced by E, and that $v^x = v^y = 0$ so the V^z interaction induces the transition in the presence of spontaneous tunneling and asymmetry (Vladár and Zawadowski [1983c]). To fit the zero bias anomalies, T_K or Δ_0 must be in the range of 1 meV. Thus, knowing that $(\rho_0 V^z)^2 \simeq 0.1$, the two characteristic frequencies are very different, of order 1 meV for the Kondo case, and 10^{-2} meV for the direct excitation model of Kozub and Kulik [1986].

In these more recent experiments, an a.c. bias was superimposed on a d.c. bias in the form

$$V = V_0 + V_1 cos(\omega t) \quad .$$

For $\omega << \omega_0$, where ω_0 is the characteristic energy of either theory, then at each time during the oscillation period the zero bias anomaly is determined by the instantaneous bias. Thus the time average of the current is

$$\bar{I} = I(V_0 + \bar{V}_1 cos\omega t) \approx I(V_0) + \frac{1}{4}\frac{\partial^2 I}{\partial V^2} V_1^2$$

provided that $V_1 << V$, and no significant frequency dependence is expected.

On the other hand, when $\omega > \omega_0$, the oscillating voltage averages out during the characteristic time scale $t_0 = 1/omega_0$, and the change in conductance must vary as $1/\omega$ with an amplitude proportional to V_1^2. The experiment was performed at two different frequencies, $\omega = 0.6GHz, 60GHz$, where the latter frequency corresponds to 0.25 meV. No significant dependence upon the amplitude or ω was found. Hence, the relevant energy scale must be significantly larger than 0.25 meV. As argued above, this can only be true for the Kondo effect, so the experiments offer further support for interpretation in terms of the TLS Kondo effect.

Summarizing, it can be claimed on solid ground that there are several cases where only the orbital Kondo effect of a TLS can explain the observed zero bias anomalies, and in several cases the

effect observed is of order e^2/h in the conductance, indicating that only one or at most a few TLS are playing the relevant role.

The above considerations notwithstanding, it remains an open question why several almost symmetric ($\Delta \leq$1.4K by estimates above) TLS with *identical* T_K values exist in the devices of Ralph and Buhrman [1992,1994].

Other Candidate Systems and Thermodynamics. Another promising candidate system of the mesoscopic variety has been studied by Gregory [1992] who finds Kondo anomalies which don't split in magnetic field in oxide coated tungsten wires in a crossed geometry.

Finally, we comment on the thermodynamics and other measurements on more concentrated systems such as the metallic glasses. In these the TLS have a broad distribution and for a large number of them the noncommutative terms can be neglected. Certainly the most important effect in this case is the renormalization of the splitting (see Eq. (8.1.4)). That downward renormalization may change an initially uniform distribution $P(\Delta) = constant$ to one which is peaked at low energy scales. The effect of the TLS on the electrons can also be probed in the superconducting states of amorphous metals where the conduction electrons and therefore the infrared divergences are cut off below by the superconducting gap. Tuning the gap by external magnetic field to smaller values will allow the suppressed infrared renormalization to return and the energies of the TLS to be pushed to smaller values. Such a renormalization effect has been observed, where the tunneling particle is atomic hydrogen in a superconducting metal (Yu and Granato [1985]). The splitting renormalization shown in Fig. 90 is enhanced by the noncommutative terms and that enhancement should be verified by further experiments.

8.2 Experimental Data on Two-Channel Quadrupolar and Magnetic Candidate Heavy Fermion Materials

Questions about the possibility of non-Fermi liquid physics in the heavy fermion materials are not new, and occurred concommitant with similar observations for the cuprate superconductors (on the theory side, see Cox [1987b]; on the experiment side see Ott [1987]).

Since 1991, a number of heavy fermion materials have come to light which display logarithmic upturns in the specific heat and more occasionally the susceptibility. Concommitant with these log upturns is usually a non-Fermi liquid resistivity. In Table 14, we summarize the results for various materials in which evidence exists for non-Fermi liquid behavior.

These non-Fermi liquid behaviors can be broadly summarized in three categories:

(1) Dilute or Local In this case doping on the rare earth/actinide sublattice away from a fully concentrated compound reveals the non-Fermi liquid behavior. The examples are: $Y_{1-x}U_xPd_3$ (Seaman *et al.* [1991], Andraka and Tsvelik [1991]), $Th_{1-x}U_xRu_2Si_2$ (Amitsuka *et al.* [1993,1994]), $Th_{1-x}U_xPd_2Si_2$ (Amitsuka *et al.* [1995]), $La_{1-x}Ce_xCu_{2.2}Si_2$ (Andraka [1994]), $Th_{1-x}U_xPd_2Al_3$ (Maple *et al.* [1994]), $Th_{1-x}U_xNi_2Al_3$ (Kim, Andraka, and Stewart [1993]), $Th_{1-x}U_xBe_{13}$ (Aliev *et al.* [1994]). It is of interest that all of these materials except $Y_{1-x}U_xPd_3$ are heavy fermion superconductors when $x = 1$. These are the systems for which the single impurity multi-channel Kondo model which is the focus of this paper have the best chance of working. Thus a compelling proof of single impurity behavior is important, and we shall discuss the evidence for this in each case.

(2) Concentrated and Ordered Two compounds appear substantially non-Fermi liquid like at the fully concentrated limit: the heavy fermion superconductors UBe_{13} (Aronson *et al.* [1989], McElfresh *et al.* [1994], Cox [1995]) and $CeCu_2Si_2$ (Steglich *et al.* [1995]). A third candidate has recently arisen, $PrInAg_2$ (Yatskar *et al.* [1996]) which has $4f^2$ Pr ions in a Γ_3 ground state (confirmed by neutron scattering studies). This material shows some behavior incompatible with a Fermi liquid. Two criteria specify the assignment of non-Fermi liquid behavior: (i) a continual rise of C/T at and below the superconducting transition (under application of a magnetic field (UBe_{13}: Steglich [1996]; $CeCu_2Si_2$: Steglich *et al.* [1995])– $PrInAg_2$ does not superconduct, but does show a region of logarithmic temperature dependence in C/T prior to a low temperature saturation; (ii) anomalously large residual resistivities and linear in

Alloy/Compound	T_K	C/T	$\chi(T)$	$\rho(T)$	Single Ion?
$Y_{1-x}(Th_{1-y},U_y)_xPd_3^{(*)}$	∼40K	$\ln T$	$1-aT^{1/2}$	$1-AT$	Yes
$Th_{1-x}U_xRu_2Si_2^{(*)}$	12K	$\ln T$	$\ln T$ $(H \parallel c)$	$1+BT^{1/2}$(?)	Yes
$Th_{1-x}U_xPd_2Si_2^{(*)}$	12K	$\ln T$	$\ln T$ $(H \parallel c)$	$1+BT^{1/2}$(?)	Yes
$La_{1-x}Ce_xCu_2Si_2^{(*)}$	∼10K	$\ln T$	$\ln T$	$1-AT$	Approx.
$Th_{1-x}U_xM_2Al_3$	∼ 20K	$\ln T$	$\ln T$(?)	$1-AT$	?
$Th_{1-x}U_xBe_{13}$	∼ 10K	$\ln T$	$1-aT^{1/2}$	$1+BT^{1/2}$ or $1+AT$	Yes($\chi(0)$) No(C/T)
UBe_{13}	10K	$\ln T$ at $H=12$T	$1-aT^{1/2}$	$1+AT$	-
$CeCu_2Si_2$	10K	$\ln T$	?	$1+AT$	-
$PrInAg_2$	2K	const.	?	AT?	-

Table 14: Non-Fermi Liquid Heavy Fermion Alloys and Compounds. This table lists the relevant properties of all non-Fermi liquid heavy fermion alloys and compounds for which a two-channel Kondo model description (in either dilute or concentrated limits) may be an appropriate starting place. The columns for specific heat, susceptibility, and resistivity indicate the low temperature behavior. All (but possibly $CeCu_2Si_2$ and $PrInAg_2$) have logarithmic in T specific heat coefficients over an extended temperature range. Those alloys marked with an asterisk show evidence for significant residual entropy at low temperatures. The coefficients A, B listed in the resistivity column are assumed positive, as is a in the susceptibility column. The column under 'Single Ion?' answers whether single ion scaling has been observed. Adapted from Cox and Jarrell [1996].

T resistivity behavior which is suppressed in magnetic field and pressure (for UBe_{13}) (UBe_{13}: Aronson *et al.* [1989]; $CeCu_2Si_2$: Steglich *et al.* [1995])–$PrInAg_2$ does not have a particularly large residual resistivity but never shows a region of Fermi liquid like T^2 behavior.
(3) Concentrated and Disordered Three systems, $UCu_{5-x}Pd_x$ (Andraka and Stewart [1992]), $U(Pt_{1-x}Pd_x)_3$ (Kim, Stewart and Andraka [1992]), and $CeCu6-xAu_x$ (Löhneysen *et al.* [1994]) fit into this category. Each is near an antiferromagnetic instability which is accessed by tuning the concentration of dopants off the rare earth/actinide sublattice. The non-Fermi liquid behavior appears closely associated with this proximity to a $T = 0$ magnetic transition, which has been extensively discussed recently by Millis [1994] (in an ordered system–the role of disorder in this theory requires further study). In the case of $UCu_{5-x}Pd_x$, the disorder may play a role in inducing a spread of Kondo temperatures which extends all the way down to T =0K based upon interpretation of inhomogeneous line broadening measurements in copper nuclear magnetic resonance lines (Bernal *et al.* [1995]; MacLaughlin, Bernal, and Lukefahr [1996]). These authors relied on the work of Dobrosavljević, Kotliar, and Kirkpatrick [1992] who argued that non-Fermi liquid behavior may be mimicked by this distribution of local fermi liquids in the vicinity of a metal insulator transition with a log normal distribution of the local conduction density of states about the impurity sites. An unusual *local* dynamic scaling of the neutron scattering cross section with frequency was observed by Aronson *et al.* [1995] over a wide range of x including $x = 1$ which is likely an ordered compound. This suggested that other mechanisms may be at work to induce the non-Fermi liquid behavior. The work of Miranda, Dobrosavljević, and Kotliar [1996,1997] has produced a different form of the probability distribution than Dobrosavljević, Kotliar and Kirkpatrick [1992], derived in infinite spatial dimensions, which holds away from the metal insulator transition. This form is in complete agreement with the form used by Bernal *et al.* [1995] in fitting experimental data. With this form, they reproduce the simple Gaussian distribution of coupling constants used by Bernal *et al.* [1995], and they are able with this distribution to (i) fit the linear temperature dependence of the resistivity, and (ii) the dynamic susceptibility of Aronson *et al.* [1995]. Hence, taken together with the experimental work of Bernal *et al.* [1995], it genuinely appears that the $UCu_{5-x}Pd_x$ system is described by the modified Kondo disorder theory as put forward by Miranda, Dobrosavljević, and Kotliar [1996,1997]. In related work, the optical conductivity of $UCu_{3.5}Pd_{1.5}$ has been studied (DeGeorgi and Ott [1996]). This can be fit with the same disorderd distribution of Kondo scales used by Bernal *et al.* [1995] (also MacLaughlin, Bernal, and Lukefahr [1996]) and Miranda, Dobrosavljević, and Kotliar [1996,1997] as was shown by Chattopadhyay and Jarrell [1996] (see also Jarrell *et al.* [1996c]).

Another material which defies the above categorization yet displays non-Fermi liquid behavior is $Ce_{1-x}Th_xRhSb$ (Andraka, [1994b]). This material is a Kondo insulator for $x \to 0$, but for the range $0.2 \leq x \leq 0.4$ shows possible non-Fermi liquid behavior in the form of a specific heat coefficient which appears logarithmically divergent over approximately a half decade of temperature.

Our attention shall focus here on a brief review of materials in categories (1) and (2) with regard to their possible explanation in terms of the two-channel Kondo effect. We discuss each system in order.

$\mathbf{Y_{1-x}U_xPd_3}$. The striking properties of this material have garnered considerable attention. Fig. 99(a) shows the specific heat for the composition $x = 0.2$ with the entropy shown in Fig. 99(b) as taken from Seaman *et al.* [1991]. The specific heat shows logarithmic behavior over about one-and-one-half decades of temperature, with an upturn clearly visible below 0.5K which we shall return to dicuss later in this subsection. The specific heat difference when integrated to yield the entropy difference has a clear shoulder near $R/2\ln 2$ per mole U near $T = 20$K. At higher concentrations apparent spin glass order sets in (evidenced by a hysteresis in the magnetization) and in the corresponding temperature range $R\ln 2$ entropy is recovered. This suggests that $R/2\ln 2$ entropy per U site should appear below the lowest temperature in $Y_{0.8}U_{0.2}Pd_3$. In addition, the resistivity in the same temperature range goes as $1-AT$ after showing a linear in $\ln T$ behavior at higher temperatures, and the magnetic susceptibility appears to go as $1 - BT^{1/2}$ (once a subtraction of apparent large moment paramagnetic impurities is made). Taken together, these data put forward a compelling view of this material as a non-Fermi liquid metal.

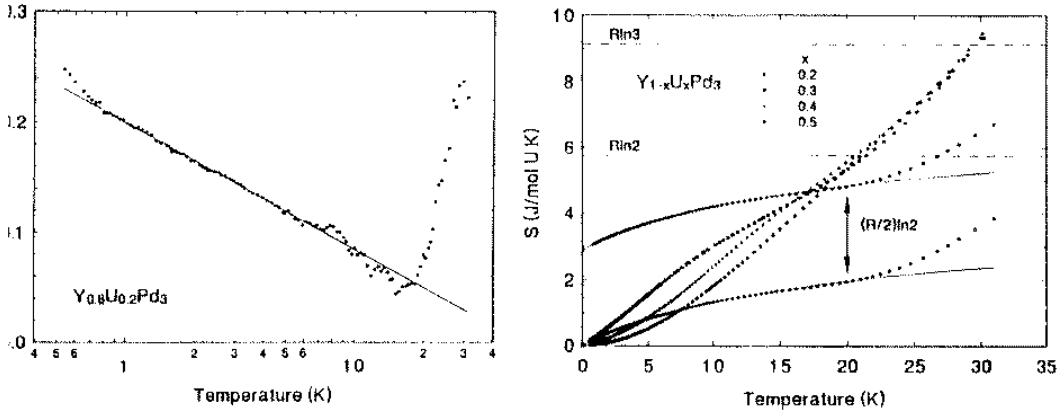

Figure 99: Specific heat and entropy of $Y_{1-x}U_xPd_3$. (a) shows the specific heat per mole for $x = 0.2$ (with YPd_3 subtracted off), and displays a $\ln T$ behavior over about a decade and a half of temperature. The specific heat integrated from the lowest temperature yields the entropy curve shown in (b); notice that for $x > 0.2$, of order $R \ln 2$ entropy is available below $T = 30K$; hence, entropy appears to be missing from the $x = 0.2$ curve. From Seaman *et al.* [1991].

A number of facts make the quadrupolar Kondo effect (Cox [1987b,d]) a worthwhile model to begin with to try to understand the physics of this system:

Tetravalence of U ions. The quadrupolar Kondo effect requires tetravalent U ions. From photoemission experiments clear evidence of "Fermi level tuning" is observed (Kang *et al.* [1992]). This means that the U 5f occupied peak shifts with doping. If the U ions were trivalent, they would not shift the occupancy because the Y ions are also trivalent. However, tetravalent U ions would shift the f-level provided the underlying density of states is small, which is the case for YPd_3. This Fermi level tuning complicates the proof of single ion behavior, though this may be remedied by combined Th,U doping as we discuss further below. The tetravalence is further supported by the absence of significant lattice constant change with doping; there is a very close size match between U^{4+} and Y^{3+} ions which is not the case for U^{3+} ions.

Cubic Symmetry The quadrupolar Kondo effect requires a site of either cubic, hexagonal, or tetragonal symmetry. Cubic symmetry is indeed maintained in this material. YPd_3 has a cubic Cu_3Au structure, as does antiferromagnetically ordered UPd_4 (which has 50/50 disorder of U and Pd ions on the Au sublattice of the Cu_3Au structure). It is also informative that UPd_3 has a dhcp structure with one site that is pseudo-cubic for the U ions. It is known in the UPd_3 case that the U ions are tetravalent and have well resolved crystal field splittings (Buyers *et al.* [1980], McEwen *et al.* [1994]; indeed, UPd_3 shows a complex triple-Q vector quadrupolar order–see Walker *et al.* [1995]).

Logarithmic behavior of C/T and residual entropy. The data obviously support the two-channel Kondo model in this case. For tetravalent U ions in cubic symmetry, only the non-magnetic Γ_3 doublet can provide the two-channel Kondo effect. The fact that order $R \ln 2$ entropy is available also points towards the Γ_3 doublet ground state. Employing the thermodynamics calculations of Sacramento and Schlottmann [1989,1991] yields an estimated Kondo scale of 40K for $x = 0.2$ and about 200K for $x = 0.1$. The increase is explainable in terms of the Fermi level tuning hypothesis.

Different temperature dependence to χ and C/T As discussed extensively in the Secs. 5,6, and 7, the susceptibility relevant to the impurity pseudo-spin must have the same temperature dependence if the two-channel Kondo effect is to prevail. The fact that the temperature dependence is significantly different argues for the quadrupolar Kondo effect.

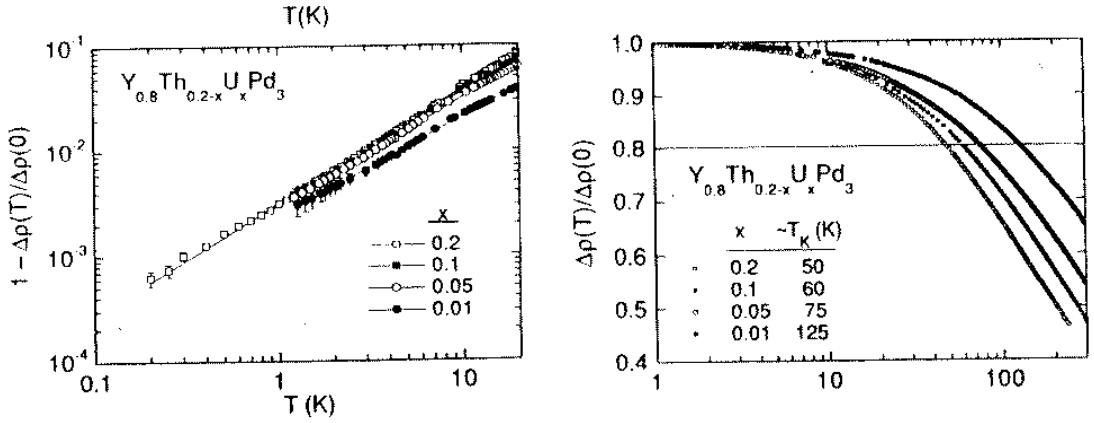

Figure 100: Resistivity of $Y_{1-x}(Th_{1-y},U_y)_xPd_3$, from Seaman and Maple [1994].

Low temperature upturn in C/T Below about 0.6K the specific heat rises above the logarithmic behavior, which has been studied more extensively by Ott [1993], who rules out a nuclear Schottky anomaly as an explanation (only small abundance Pd isotopes are candidates in zero magnetic field and there is simply too much entropy involved in the upturn). This upturn is quite reminiscent of the upturns visible in Fig. 85 in the calculations of Sacramento and Schlottmann [1991] representing the Schottky-like anomaly arising from the removal of ground state residual entropy. In the quadrupolar Kondo case the 'magnetic field' analogous to that of the pure spin Kondo model can either be strain fields or electric field gradients. The Y,U sizes are close which suggests little strain contribution; however, the charge difference can lead to sizeable random electric field gradients. An estimate of the mean electric field gradient splitting from Thomas-Fermi theory gives $\Delta \simeq 5K$ at $x = 0.2$ (Cox, Kim, and Ludwig [1997]). In conjunction with the spin crossover temperature $T_{sp}^x = \Delta^2/T_K$ discussed in Secs. 5.1,4.2, 6.1.3.c, and 7.2, this produces a crossover scale estimate of about 0.6K in good agreement with the location of the upturn.

Two crucial questions arise about the ground state of this system. First, is the non-Fermi liquid physics associated with collective effects associated with the proximity to antiferromagnetic and/or spin glass ordering, or with single ion physics? Second, is the identification of a ground state non-magnetic doublet on the U ions appropriate? Alloying experiments shed considerable light on these questions, strongly affirming the single ion picture and the doublet ground state assignment. There are two classes of alloying experiments:

1) $Y_{1-x}(U_yTh_{1-y})_xPd_3$ Alloys Seaman *et al.* [1994] have studied this system to shed light on whether the origin of the non-Fermi liquid behavior is to be found in single ion physics. The idea is that the Fermi level tuning introduces an intrinsic doping dependence to the Kondo scale through the f energy $\tilde{\epsilon}_f$ ($T_K \sim \exp(-\pi|\tilde{\epsilon}_f|/2\Gamma)$) and so simply reducing the number of U ions is insufficient to test the single ion hypothesis in this case. However, by introducing tetravalent Th ions of nearly the same size as the U ions, the f-level can be kept approximately constant and the U concentration can be diluted. In this way it is found that for $x = 0.1, 0.2$ very nearly the same Kondo scale and low temperature resistivity behavior are maintained down to low concentrations of U ions (order 1-5%). However, the distance from the spin-glass and/or antiferromagnetic ordering is increased. This provides strong support for a single ion interpretation. Resistivity curves for this system are shown in Fig. 100.

2) $M_{1-x}U_xPd_3$ alloys, M=Sc,Pr,La Here the trivalence of the M ions is kept fixed but the ionic volume is shifted systematically (Gajewski *et al.*[1994]). The volume primarily affects the hybridization: for the largest ion (La) the effect is to expand the lattice providing negative chemical pressure which would hypothetically drive down the hybridization width Γ and reducing the Kondo scale in turn relative to $Y_{1-x}U_xPd_3$ for a given x value. For the smallest ion (Sc, radius smaller than Y) the lattice would be compressed, which increases the hybridization width Γ, driving the Kondo scale up for fixed x. In the case of large ions, if T_K is sufficiently reduced it should be possible to see the full $R\ln 2$ entropy in the quadrupolar Kondo picture due to the random field gradient splitting of the non-magnetic Γ_3 doublet. These expectations are born out. For M=Sc, the region of non-Fermi liquid behavior is extended all the way out to $x = 0.3$, where the estimated Kondo scale is comparable to that of M=Y at $x = 0.2$, while for $x = 0.2$ the estimated Kondo scale for M=Sc is quite large (order 200K). For M=Pr, a mixed behavior is seen in the specific heat, as a pronounced peak in C/T is visible in the few K range. There is still a logarithmic upturn in the resistivity at higher temperatures but a downturn visible at low temperature in the same region where C/T peaks. For M=La, no Kondo anomaly is seen in the resistivity. At the same time, a clear peak arises in C at about 6K. This peak may be fit by a Gaussian broadened Schottky anomaly, and clearly has $R\ln 2$ entropy per U ion. We note that the peak position gives an estimated average splitting of the doublet ground state by $11K$ which is within a factor of two of the random field gradient estimate of Cox, Kim, and Ludwig [1997]. The size mismatch of the La and U ions will certainly induce random strain fields that can enhance the splitting above the random field gradient splitting. The specific heat curve for M=La and $x = 0.1$ is shown in Fig. 101.

Hence, there are a number of reasons to believe that the non-Fermi liquid physics of this alloy are driven by the one-impurity quadrupolar Kondo effect. However, a number of criticisms can be made of this interpretation based upon other experimental data:

Critique (1): Resistivity. The electrical resistivity shows a linear behavior even below 1K where, on the basis of NCA calculations one would expect a rollover to $T^{1/2}$ behavior (See Secs. 5.1 and 5.3 and Cox and Makivic [1994], Kim and Cox [1997]).

Critique (2): Field Dependent Specific Heat. Andraka and Tsvelik [1991] pointed out that the magnetic field dependence of the specific heat does not follow what would be expected for a quadrupolar Kondo system. At low fields, the magnetic field acts as a channel field which should produce a large increase of the specific heat coefficient as calculated by Andrei and Jerez [1995] (see Sec. 7.2 for a discussion). At higher values the Γ_3 level splits quadratically in the field which would also have the effect of increasing the specific heat coefficient. The detailed scaling function fit to $C(T,H)/T - C(0,T)/T$ is that it appears to go as $f(H/T^\beta)$ with $\beta = 1.3$ whereas the channel-field scaling would yield $\beta = 0.5$ and the spin-field scaling (through quadratic in H splitting of the Γ_3 doublet) would yield $\beta = 0.25$. Moreover, the specific heat coefficient pretty much just drops with magnetic field, whereas one would expect from the calculations of Andrei and Jerez [1995] an enhancement as the residual entropy is shoved out of the ground state. Similar behavior is seen in $U(Cu_{1-x}Pd_x)_5$ (Kim, Stewart, and Andraka [1992].) A possible complication with this picture is that in the quadrupolar Kondo picture there is a substantial background specific heat associated with excited magnetic triplet levels which would presumably drop in the applied magnetic field. Mysteriously, the magnetoresistance of this material is very small (Seaman and Maple [1994]). Only detailed numerical analysis within the NCA or other suitable method can be used to address this point on the theory side.

Critique (3): Neutron Scattering Cross Section. Unpolarized neutron scattering studies have been carried out by Mook *et al.* [1993] and McEwen *et al.* [1994] which subtract $Y_{1-x}Th_xPd_3$ as a reference. A subsequent polarized neutron study was carried out by Dai *et al.* [1995]. For high concentrations, the McEwen *et al.* [1994] and Dai *et al.* [1995] studies suggest that the U ground state

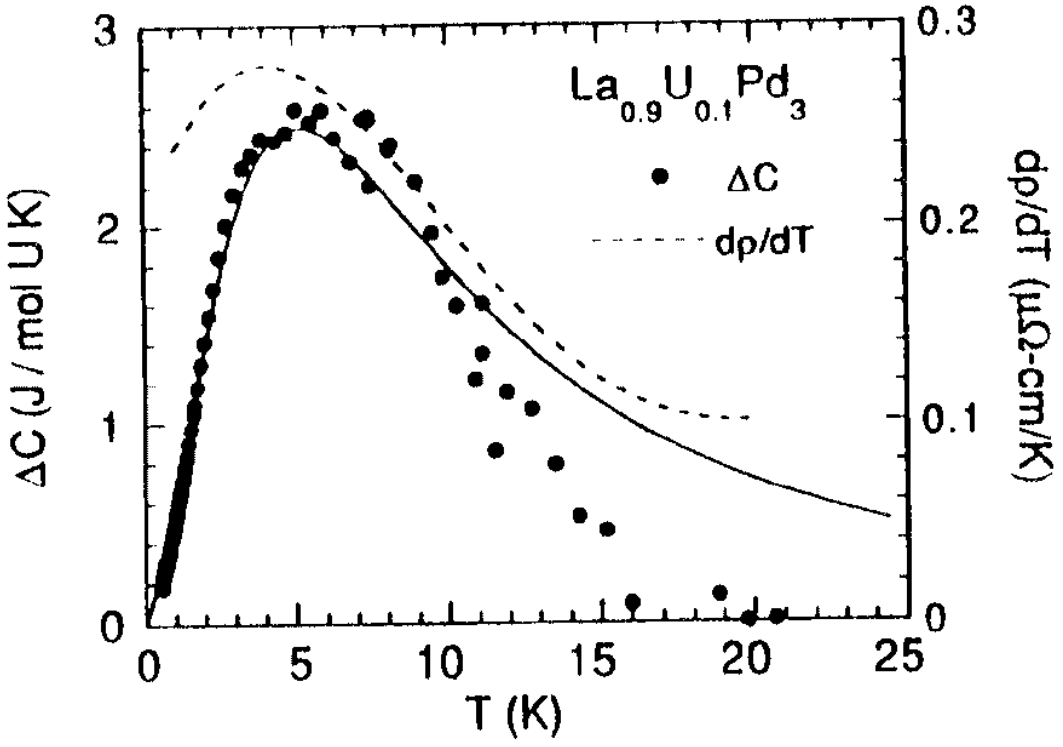

Figure 101: Specific heat of $La_{0.9}U_{0.1}Pd_3$ (from Seaman and Maple [1994]).

is a Γ_5 magnetic triplet level. Indeed, the Dai *et al.* [1995] study finds evidence for antiferromagnetic Bragg peaks at $x = 0.5$ which have the same structure as UPd_4. Moreover, for $x = 0.2$ they find evidence for near critical scattering in $S(\vec{q}, \omega)$ near these same Bragg peaks. For $x = 0.2$, both studies present evidence for two inelastic transitions which is compatible with the Γ_3 doublet ground state (this would have magnetic transitions to each of the excited triplets), at energies of about 6 meV and 39 meV. McEwen *et al.* [1994] take the Γ_3 interpretation. However, Dai *et al.* [1995] argue from the polarized data that significant quasielastic scattering exists below 1 meV in energy and have made a preliminary case for a Γ_5 ground state.

There are two difficulties with this assignment in reconciling with the experimental thermodynamics: (a) the intensity of this peak yields a $T \to 0$ magnetic susceptibility which exceeds the experimental value by a factor of at least 20, and a $T = 10K$ entropy which exceeds the experimental value by a factor of 3-5; (b) the energy scale associated with the peak is at most 10K, and the only characteristic energy scale from the data is 40K. Clearly more work is needed to understand the origin of this quasielastic scattering; the presence of concentration gradients in U ions and large moment paramagnetic impurities as evidenced in the magnetization need to be examined closely.

Critique (4): Ultrasonic Sound Velocity Measurements Sound velocity measurements on polycrystalline samples show no appreciable softening at any temperature (Amara *et al.* [1995]), which not only calls to question the quadrupolar Kondo effect (for which a logarithmic transverse anomaly would be expected at low temperatures) but also the Kondo effect itself (as most Kondo systems show a significant temperature dependence in the measured sound velocities due to the strong volume dependence of T_K– see Lüthi and Thalmeier [1988]). A possible drawback is the polycrystalline character of the samples measured thus far (Mandrus [1995]).

Critique (5): Concentration Gradients. The $Y_{1-x}U_xPd_3$ is subject to signficant concentration gradients (Mydosh *et al.* [1993], Seaman *et al.* [1993]) which may affect the ability to sort out single ion from concentrated physics effects. Recent studies show that this is a relatively small effect, in that the mean square concentration deviation is about 10near 0.2 the concentration would range from about 0.18 to 0.22–see Maple *et al.* [1996]).

Clearly an unambiguous assignment of the quadrupolar Kondo effect as the source of non-Fermi liquid physics cannot be made at this time, though there are a number of good arguments on behalf of this picture for this alloy system.

$Th_{1-x}U_xRu_2Si_2$ and $Th_{1-x}U_xPd_2Si_2$ Single crystals of tetragonal $Th_{1-x}U_xRu_2Si_2$ have been studied by Amitsuka *et al.* [1993a,b] from $x = 0.01 - 0.07$. The magnetic susceptibility, electronic specific heat, and electrical resistivity were measured. The magnetic susceptibility for $x = 0.01$ is shown in Fig. 102(a) , where it is clear that for in plane fields the susceptibility has weak temperature dependence, while for c-axis fields there is a logarithmic divergence apparent over about 2 decades of temperature. The solid curve is a fit of Sacramento and Schlottman's Bethe-Ansatz calculations for $M = 2, S_I = 1/2$ to the c-axis data, and the fit is quite good over four decades of temperature. The estimated Kondo scale is 11K. This is clearly a single site effect, as the c-axis concentration dependent susceptibility is shown in Fig. 102(b). Below about 0.5K, rounding is visible in the $\chi_c(T)$ curves, but above this temperature the curves are identical for four different concentrations up to $x = 0.07$. The rounding is reminiscent of that seen for applied field in Fig. 84 from Sacramento and Schlottmann [1991]. A heuristic interpretation is that interaction effects between the U ions are producing a self-consistent magnetic field that induces the crossover. Actually, only a self-consistent *fluctuation* is likely important since the crossover scale goes as H^2.

Taking the T_K value from the χ_c fits, Amitsuka *et al.* produce a satisfactory zero parameter fit to the $x = 0.07$ C/T data, which is shown in Fig. 103, where the solid curve is taken from Sacramento

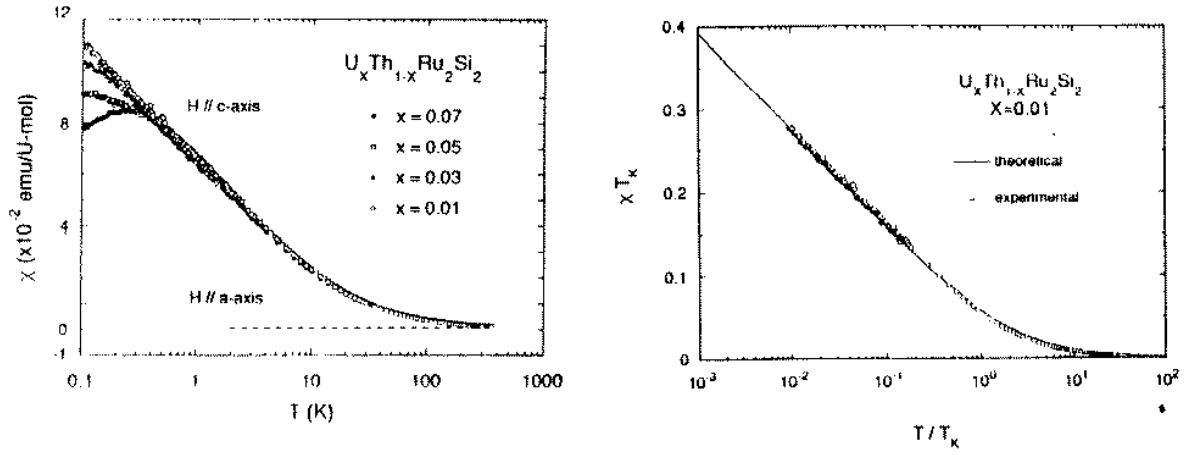

Figure 102: Magnetic susceptibility of $Th_{1-x}U_xRu_2Si_2$ for several values of x from Amitsuka *et al.* [1993]. The fit to the scaled curves is from the Bethe-Ansatz calculations of Sacramento and Schlottman [1991].

and Schlottmann [1989,1991]. Because the theory curve integrates to $(R/2)\ln 2$ entropy per mole U, that implies that a residual entropy of $(R/2)\ln 2$ remains below the lowest temperature measured which also fits with the $M = 2, S_I = 1/2$ theory.

Because the U ions are presumably tetravalent, the crystal symmetry is tetragonal, and the c-axis susceptibility obeys a Curie law well above T_K, it is reasonable to suggest that this physics arises from the quadrupolar Kondo effect in tetragonal symmetry as discussed in Sec. 2.2.3. This would arise from a non-Kramers doublet which can be Zeeman split by an applied field along the c-axis.

An experimental difficulty with this proposal is the resistivity, shown in Fig. 104. The shape of the resistivity curves for several different concentrations is clearly the same (the magnitude is subject to systematic correction from the different crystal geometry). While the magnitude is sufficiently large (order 40 $\mu-\Omega$-cm) to warrant consideration as a Kondo system, there are two differences from the two-channel Kondo theory: (1) There is no high temperature linear in $\ln T$ region present in the data; (2) There is a low temperature *downturn* below T_K, which, over limited regions, may be fit with T,$T^{1/2}$, or $\ln T$ behavior.

It is difficult to conceive of simple explanations for these resistivity discrepancies, but we do note a number of important considerations which could modify the behavior:
(i) The resistivity is significantly dependent on the details of the hybridization matrix elements between conduction states and the U $5f$ states. For example, in the simplest $M = 1, S_I = 1/2$ model for Ce^{3+} ions, a low temperature downturn in the resistivity is possible due to the "hot-spots" along principle axis directions at which the Γ_7 conduction partial wave states must have vanishing hybridization matrix elements (see Cox [1987c], and Trees [1993,1995] (Trees and Cox [1994]) for a discussion of the hybridization hot-spots and Kim and Cox [1995b] for a discussion of their influence on resistivity).
(ii) The $T^{1/2}$ coefficient expected at sufficiently low temperatures can experience a sign reversal for sufficiently large potential scattering on the U site which breaks particle-hole symmetry (Affleck and Ludwig [1993]–see eqn. (4.6)). If this is true there should be a substantial thermoelectric power present (this can only be non-zero for the $M = 2, S_I = 1/2$ model in the presence of particle-hole symmetry breaking).
(iii) A possible culprit for the potential scattering is excited crystal field levels, which will clearly break particle-hole symmetry, and which complicate the search for $\ln T$ upturns at high temperatures. (See

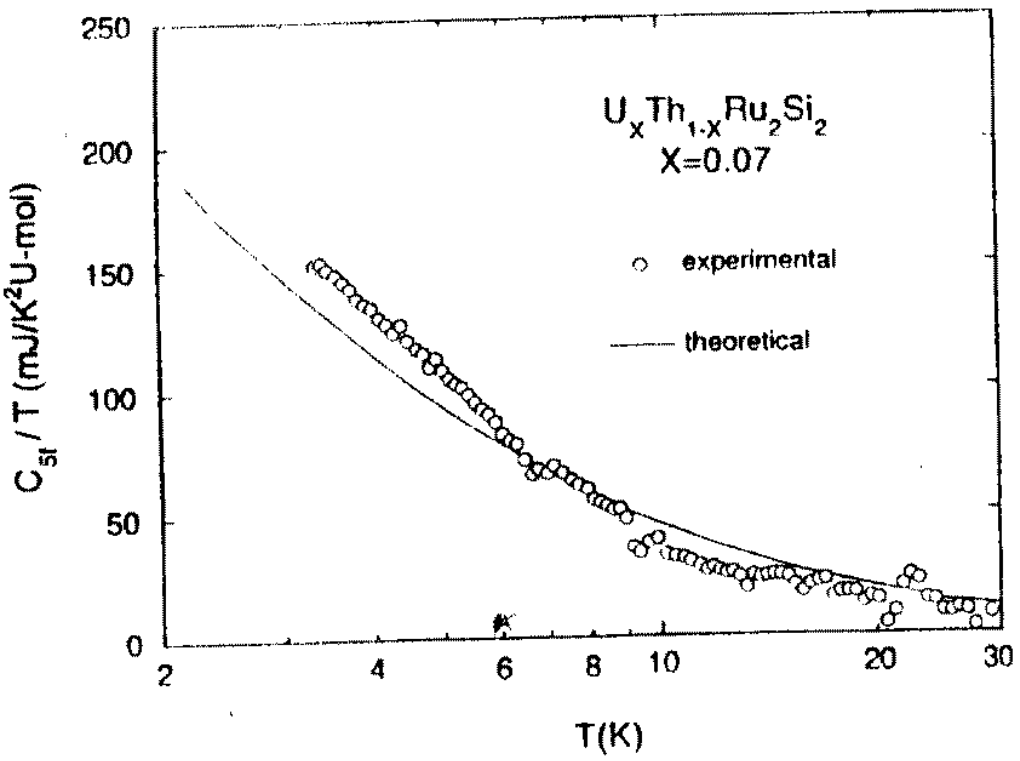

Figure 103: Specific heat of $Th_{1-x}U_xRu_2Si_2$ for x=0.07 from Amitsuka *et al.* [1993]. The fit is to the theoretical calculation of Sacramento and Schlottman [1991] with the value $T_K = 11K$ determined from the magnetic susceptibility.

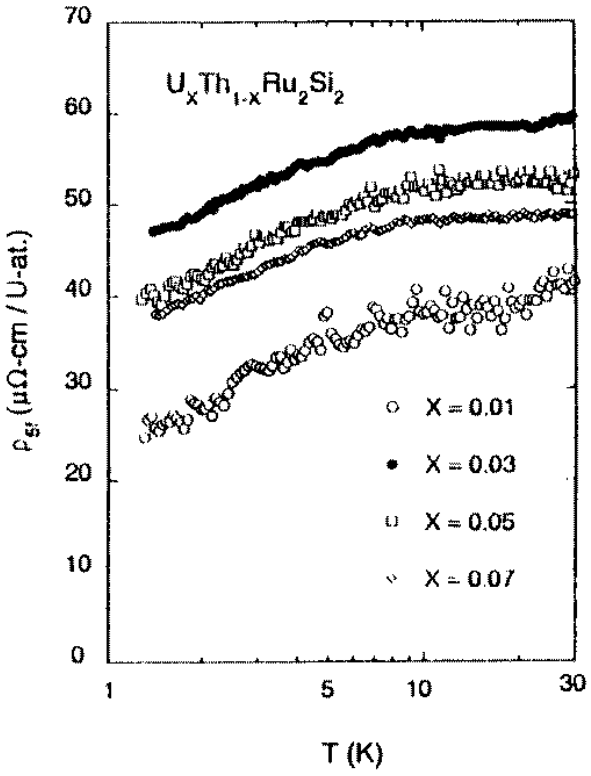

Figure 104: Resistivity of $Th_{1-x}U_xRu_2Si_2$ from Amitsuka *et al.* [1993].

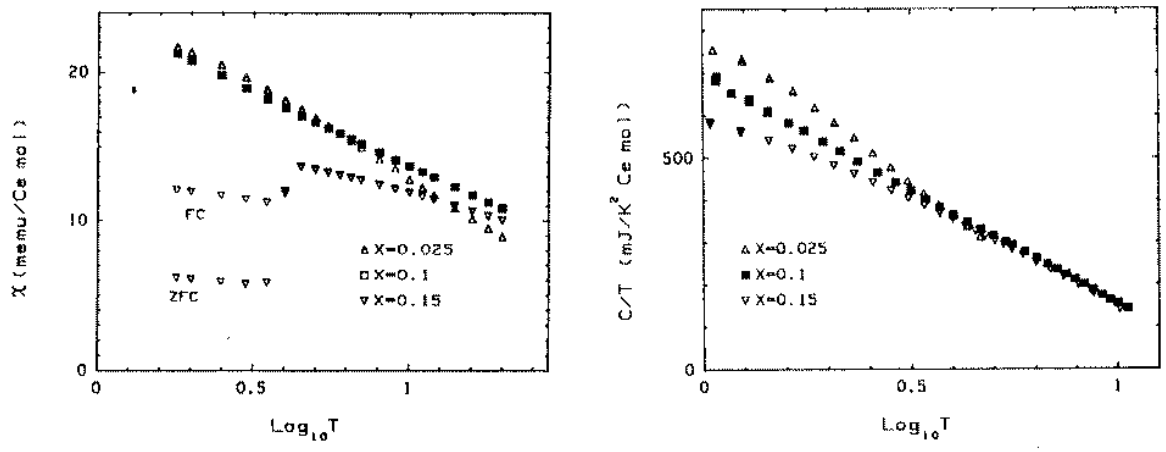

Figure 105: Susceptibility (left plot) and specific heat (right plot) per Ce for $La_{1-x}Ce_xCu_{2.2}Si_2$. From Andraka [1994].

Cox and Makivic [1994] for a discussion.)
(iv) The resistivity $\sqrt{T}$ coefficient can reverse sign in the strong coupling regime since the term is proportional to the leading irrelevant operator which is proportional to the deviation from the fixed point coupling. Arguing against this are the small Kondo scale and the excellent fits to Bethe-Ansatz results which are computed in the weak coupling limit.

In $Th_{1-x}U_xPd_2Si_2$ (Amitsuka *et al.* [1995]) the qualitative and quantitative features are similar. Again, in $\chi_c(T)$ (per U ion) a region of single ion behavior (overlapping curves for different concentrations) with a rounding of χ_c that increases with increasing x, and the in plane susceptibility has a smaller value and negligible temperature dependence. For the lowest concentration ($x = 0.03$) a fit to $\chi_c(T)$ with the Bethe-Ansatz results is similarly good. The specific heat per U ion shows a $\ln T$ behavior for low concentrations and drops as x is increased. This is actually mysterious since it is not clear where the entropy goes. The authors note that the estimated residual entropy for the $x = 0.03$ sample is actually somewhat larger than $R \ln 2/2$. The resistivity does show a Kondo like minimum at temperatures of order 20K, but below a maximum again drops in a manner that may be fit over limited regions by T, $T^{1/2}$, or $\ln T$ behaviors.

It should be mentioned that the dilute system $La_{1-x}U_xRu_2Si_2$ *does not* show any evidence for non-Fermi liquid behavior for $x \leq 0.15$ (Marumoto, Takeuchi, and Miyako [1996]).

Given the sheer number of details for these two materials which check with the $M = 2, S_I = 1/2$ model, further experimental investigation of these materials is clearly warranted despite the difficulties in understanding the resistivity. In particular, it would be desireable to have the specific heat measured under conditions of uniaxial stress in the basal plane and c-axis fields. This should shove out the residual entropy and confirm the assignment to a tetragonal quadrupolar Kondo model.

$La_{1-x}Ce_xCu_{2.2}Si_2$ This system has been studied by Andraka [1994] and shows great promise as a dilute $M = 2, S_I = 1/2$ *magnetic* Kondo system. The added magnetic susceptibility and specific heat per Ce ion for $x = 0.05, 1, 0.2$ are shown in Fig. 105. We note that there is rough single ion behavior in that the χ curves for $x = 0.05, 0.1$ are very close, and the specific heat curves are all close though deviations occur at lower T. For $x = 0.2$ there is hysteresis in χ which is taken as evidence for spin glass behavior.

We focus on $x = 0.1$ results. Clearly both χ and C/T exhibit a $\ln T$ behavior at low temperatures.

From a fit to the $\ln T$ slope of the C/T curve, one estimates $T_K \approx 12K$. Separately, one may compute the Landau-Wilson ratio. To do this requires a knowledge of the effective moment of the presumed doublet ground state of the Ce^{3+} ion. Fortunately we know from neutron scattering, susceptibility, and specific heat measurements (see Grewe and Steglich [1991] for details and references as well as Gorymychin and Osborne [1994]) that despite the tetragonal crystal structure, the crystal field on the Ce site is pseudo-cubic with a Γ_7 doublet ground state and excited Γ_8 quartet at about 360K. To then compute the Landau-Wilson ratio, we should compare the logarithmic slopes of the χ and C/T curves since there can be background constant terms in each quantity. Using the Γ_7 moment of $\mu_{eff} = 10\mu_B/7$ gives $R_W = 2.7(1)$, to be compared with the expected value of 8/3 from Secs. 6.1.3, 6.2.3, and 7.2. The agreement is obviously excellent.

The electrical resistivity appears to show linear in T behavior down to 1.4K, but in view of the results of Sec. 5 from the NCA (Cox and Makivic [1994], Kim and Cox [1995b]) a $T^{1/2}$ law should not be cleanly seen until about $0.05T_K$, which sits below 0.6K. Indeed the theory curve of Fig. 106 is a fit of the NCA calculations of Kim and Cox [1995b] to the $x = 0.1$ data, and it is credible given the limited range of the experimental data (about a decade). However, a clear break is seen in the data which takes it below the theory curve.

A separate qualitative confirmation of the validity of the $M = 2, S_I = 1/2$ model is that when magnetic field is applied, the specific heat coefficient shows a significant increase. In quantitative detail, it is not as large as for the $M = 2, S_I = 1/2$ model for the given field strengths, but the behavior sharply contrasts with the $M = 1, S_I = 1/2$ model where C/T should simply drop as the Kondo resonance Zeeman splits (Andrei, Furuya, and Lowenstein [1993]). We note that the presence of a sizeable background term in C/T of Fig. 105 likely corresponds to the tail of the lifetime broadened Schottky anomaly of the excited Γ_8 quartet. This should drop in magnetic field, which complicates the direct analysis of the data in terms of the $M = 2, S_I = 1/2$ model.

Clearly the material satisfies the requirement of cubic symmetry, and the question arises whether it satisfies the necessary requirement of greater fluctuation weight to f^2 than f^0 in the ground state. As discussed in Secs. 2.2.2,2.2.3, and 5.3, this is sampled by the thermopower which should be negative well above T_K (Cox [1993], Kim and Cox [1995,1997]). Early measurements of the thermopower on $La_{1-x}Ce_xCu_2Si_2$ by Aliev *et al.* [1984] revisited more recently by Buschinger, Geibel, and Steglich [1996] show that for low concentrations the thermopower goes positive. A complication is that the host system has a positive thermopower and so a proper way to isolate the Ce concentration must be worked out, which has not yet been done. For example, the Nordheim-Gorter correction has been used for the Kondo system $La_{1-x}Ce_xB_6$ to isolate the Ce ion induced thermopower (Winzer [1975]). According to the work of Buschinger, Geibel, and Steglich [1996], this correction actually enhances the positive peak in $S(T)$ for dilute samples.

The thermopower has not been measured for the $x = 0.1$ samples of Andraka [1994]. However, it has been measured for $x = 1$, and it is found that a sign change to negative thermopower occurs near $T = 70$K, which is so large compared to T_K that it is not attributable to lattice coherence effects. The thermopower in this case reaches a maximum amplitude of about -30μV/K, which is too large to be attributed to anything but resonant scattering, which the Kondo effect provides quite naturally. It is intriguing that a study of Ce based 1-2-2 compounds shows that the thermopower at 20K has a strong correlation with the unit cell volume, undergoing an abrupt change from negative to positive near the $CeCu_2Si_2$ unit cell volume. Based on the suggestions by Cox [1993] and Kim and Cox [1995a,b] that the $M = 3, S_I = 1/2$ Kondo effect can be realized with pressure, the crossing point is a promising region to look for three channel Kondo model candidate materials.

Andraka [1994] has argued that the quantitative discrepancies in the specific heat, and the apparent linear in T resistivity argue against the $M = 2, S_I = 1/2$ magnetic Kondo effect. However, as argued above, the resistivity actually is in good agreement with theory over the measured temperature range, and the specific heat coefficient increase is difficult to interpret given the large and possibly field dependent background term. Andraka [1994] also argues that $x = 0.1$ is a special concentration, since

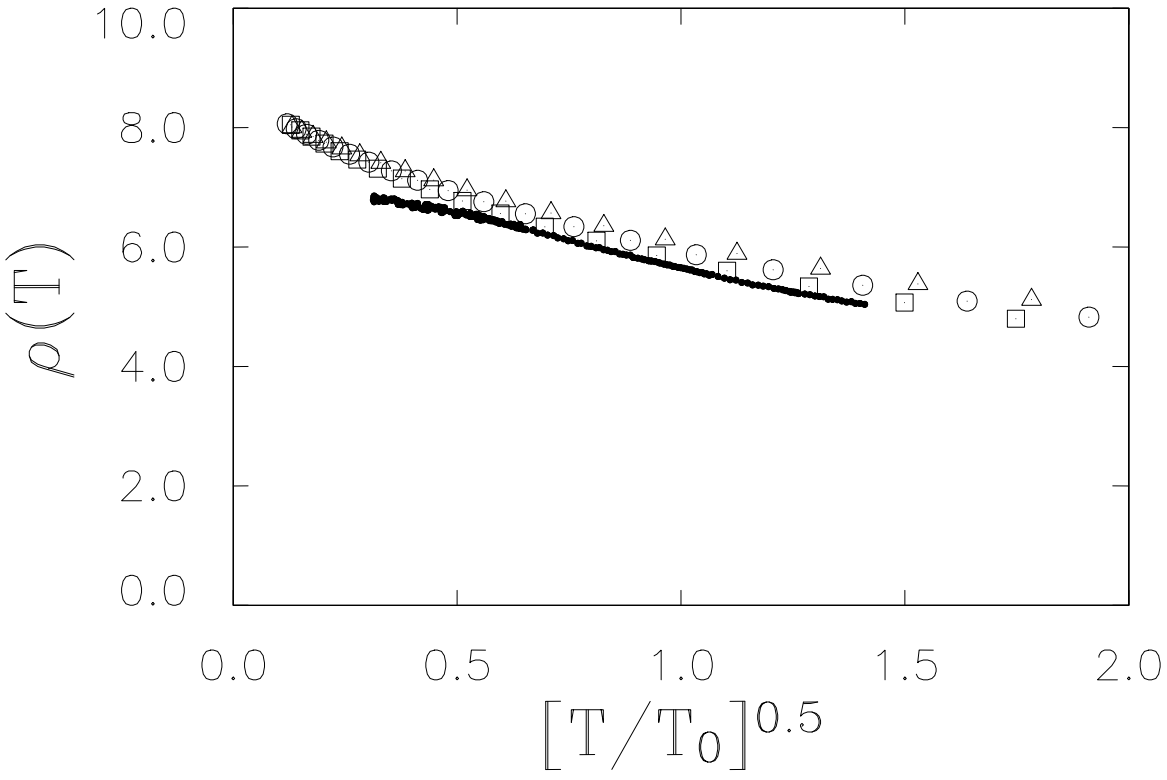

Figure 106: Fit to the resistivity of $La_{1-x}Ce_xCu_{2.2}Si_2$ by Kim and Cox [1997]. Theory (open symbols) is from an NCA calculation in the $M = 2$ channel Kondo limit using the NCA as discussed in Sec. 5.1.6; small dots are experimental points.

at $x = 0.05, 0.15$ the logarithmic anomalies are not seen. Moreover, the $x = 0.15$ sample is argued to possess a 'spin glass' transition due to irreversibility in the magnetization. Caution should be lent to accepting these arguments uncritically, however, because the $CeCu_2Si_2$ system is well known to be extremely sensitive to preparation conditions. After nearly twenty years of study for the concentrated case, only recently (Steglich *et al.*, 1995) has the ternary phase diagram been carefully worked out. It is found that the concentrated system has an extreme sensitivity to small variations (order percent) in the Cu concentration. The nominal 2.2 stoichiometry for Cu is based on starting composition during preparation and places the $x = 1$ samples in the slightly copper rich stoichiometry which leads to the most cubic crystal field scheme as well as superconductivity and lattice non-Fermi liquid behavior. Slight deficiency of Cu from this concentration leads to a still uncharacterized magnetic state. Hence, for a conclusive answer to the question of whether the $x = 0.1$ physics is or is not single ion in origin, we must await more careful studies of samples with well characterized Cu concentration.

$\mathbf{Th_{1-x}U_xBe_{13}}$ Aliev *et al.* [1992,1993,1994] have studied this system. extensively. At the value $x = 0.9$ which is certainly far from dilute, they find $C/T \sim -\ln T$, $\chi(T) \sim 1 - AT^{1/2}$, $\rho(T) \sim 1 + BT^{1/2}$ (with $B > 0$), all of which fit the two-channel cubic quadrupolar Kondo picture as discussed in Secs. 2.2.1, and 5.2. A complication is that in this crystal structure no dopants appear to leave the volume unchanged which means the hybridization is strongly affected by the doping. (Indeed, since the Th ions are larger they expand the lattice and diminish the hybridization which will lower T_K. The data appear to suggest this happens relative to the bulk $x = 1$ system.) An extensive study of $M_{1-x}U_xBe_{13}$ alloys by Kim *et al.* [1990] revealed that while the specific heat could be significantly altered by doping, the magnitude of the low temperature magnetic susceptibility was hardly affected. This suggests further that the origin of the specific heat and susceptibility are different, consistent with an interpretation in terms of van Vleck susceptibility which is important for the two-channel quadrupolar Kondo effect in cubic symmetry. Clearly it is desireable to dilute further.

A further consistency with the quadrupolar Kondo effect is the non-linear susceptibility (Aliev *et al.*, [1995a,b]). This was motivated in part by earlier measurements of Ramirez *et al.*[1994] on UBe_{13} which shall be discussed below. In theory, the non-linear susceptibility $\chi^{(3)}(T)$ defined from the magnetization via

$$\chi^{(3)}(T) = 6[M(H,T) - \chi(T)H]/H^3 \quad . \tag{8.2.1}$$

For a magnetic doublet ground state, $\chi^{(3)}$ is expected to be large and negative, as is easily seen from straightforwardly expanding the Brillouin function magnetization to obtain $\chi^{(3)} \sim 1/T^3$ for localized moments. This would be modified, at low temperature, to $\sim 1/T_0^3$ for a Kondo system. In a more general situation, $\chi^{(3)}$ depends upon the orientation of H. For a purely localized quadrupolar moment system with a cubic non-Kramers Γ_3 ground doublet, Morin and Schmitt [1981] have shown that for a field along a principle axis, $\chi^{(3)}$ will display a *positive* Curie law divergence, while for a field along a body diagonal $\chi^{(3)}$ will be of van Vleck character at low temperature and *negative*. This result is easily understood in terms of the magnetoelastic coupling of the Γ_3 ground state–principle axis fields induce tetragonal distortions which are quadratic in H and split the doublet. There is no linear coupling however to strains along the body diagonal (matrix elements do exist to excited states). Hence, the non-linear susceptibility for a principle axis field is essentially a measure of the quadrupolar susceptibility. While the quadrupolar Kondo effect would modify this from a $1/T$ divergence to $-\ln T$, the divergence would still be present, and the characteristic anisotropy provides an excellent test of the applicability of the quadrupolar Kondo model (Chandra *et al.*, [1993], Ramirez *et al.*, [1994]).

Aliev *et al.* [1995a,b] performed measurements only on polycrystalline samples. As shown in Fig. 107, for $x = 0.1$ they found that the powder averaged $\chi^{(3)}$ is predominantly negative at high temperatures but finds a minimum and changes sign as the temperature is lowered, which is in accord with the expectations of the previous paragraph. In contrast, when pure UBe_{13} is measured for similarly prepared polycrystalline samples, $\chi^{(3)}$ is relatively large, negative, and decreases with decreasing temperature, qualitatively in agreement with a magnetic ground state. Indeed, the polycrystalline data

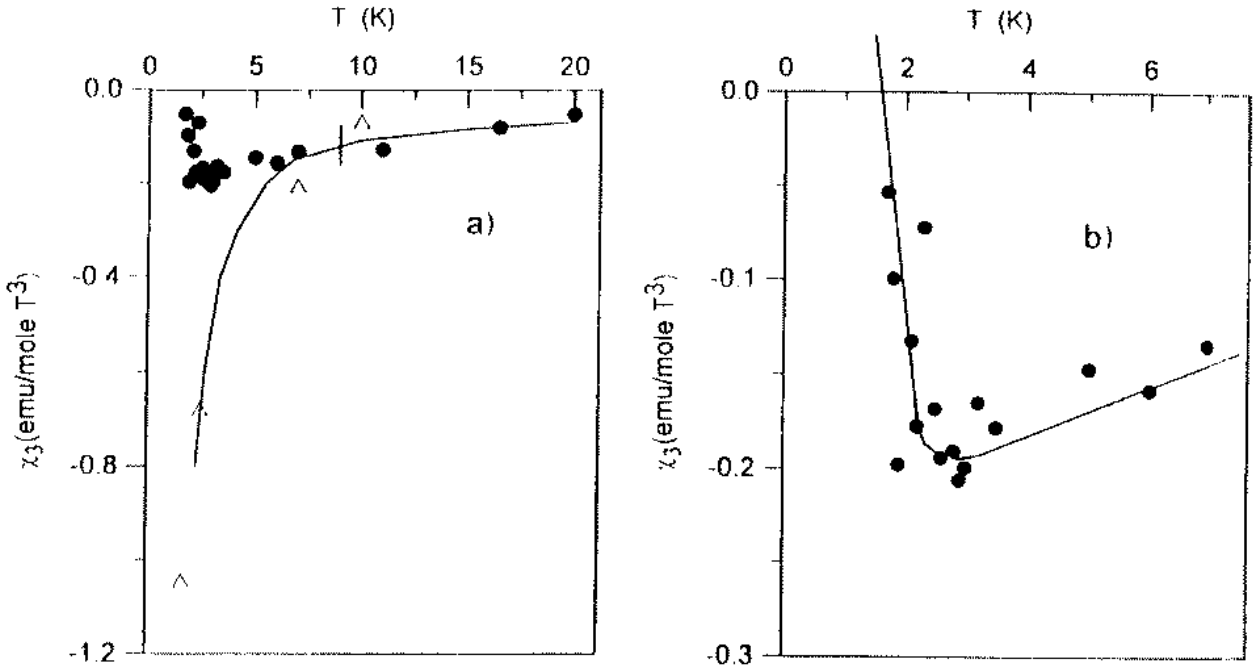

Figure 107: Non-linear susceptibility measurements on UBe_{13} and $U_{0.9}Th_{0.1}Be_{13}$ from Aliev *et al.* [1995a,b]. Triangles are measurements on a polycrystal of UBe_{13}, circles are measurements on a polycrystal of $U_{0.9}Th_{0.1}Be_{13}$. Line is taken from the data of Ramirez *et al.* [1994]. Right hand figure is a blow up of the low temperature region for $U_{0.9}Th_{0.1}Be_{13}$ indicating the tendency to a sign change expected for a quadrupolar Kondo material.

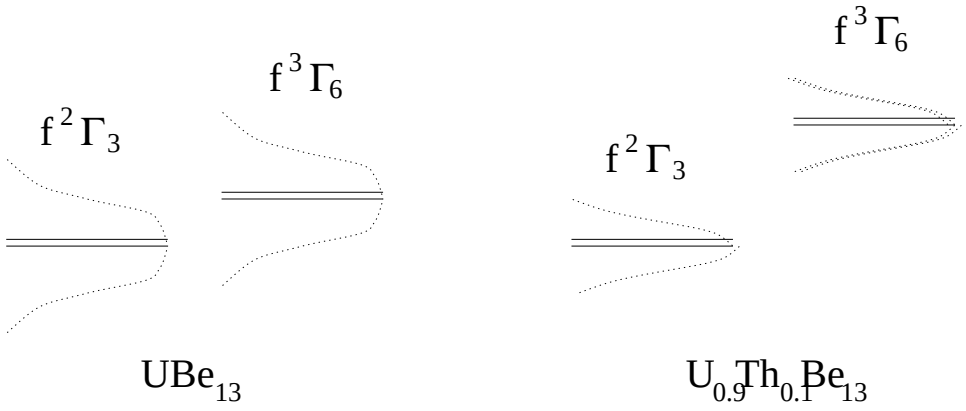

Figure 108: Mixed valence scenario for $U_{1-x}Th_xBe_{13}$ proposed by Aliev *et al.* [1995a,b]. For $x = 0$, the picture is one of almost complete mixed valence between f^2 and f^3 configurations. It is conjectured that the Th doping favors the f^2 energetically and diminishes the degree of valence mixing. This favoring could arise from a reduction in the hybridization broadening of the configuration energy levels. The broadening is indicated schematically by the dotted curves about each doublet level.

agrees excellently with Ramirez *et al.*'s [1994] single crystal data, which excludes the possibility of large moment paramagnetic impurities giving rise to the $x = 0$ $\chi^{(3)}$ results.

Based upon this work and the *positive* coefficient of $\sqrt{T}$ in the $x = 0.1$ resistivity, Aliev *et al.* [1995a,b] put forward an interesting set of hypotheses: first, the $x = 0.1$ samples are in the strong coupling regime. That is, the coupling strength exceeds that of the non-trivial fixed point. This can explain the positive coefficient of the resistivity. Second, the ionic ground state changes as a function of Th doping, being an $f^3\Gamma_6$ doublet for $x = 0$, and an $f^2\Gamma_3$ doublet for $x = 0.1$. This would require the U ions to be strongly mixed valent between 3+ and 4+, which is not implausible. This scenario is illustrated in Fig. 108. This second hypothesis checks with the first hypothesis because it is precisely in the mixed valence regime where strong coupling might plausibly occur (the dimensionless Schrieffer-Wolff exchange can grow to order unity). The hypotheses are very interesting because the different symmetry ground states would seem to imply a novel quantum critical point at the precise point in x where the levels cross.

There are three major concerns with the hypotheses:
1) Taking the Th ions as tetravalent, the substitution would add electrons, and this would actually drive the uranium ions more towards trivalence.
2) While the non-linear susceptibility for pure UBe_{13} is strongly temperature dependent, the susceptibility is not, and hence this interpretation is problematic.
3) It is not clear that a sufficiently small energy scale can be generated in the mixed valent regime for the uranium ions, though some variational treatments of the ion with full spherical symmetry suggest this is possible (Read *et al.*, [1986]; Nunes, Rasul and Gehring [1986]).

Nevertheless, the hypotheses of Aliev *et al.* are very intriguing and deserve further exploration.

$Th_{1-x}U_xPd_2Al_3$ and $Th_{1-x}U_xNi_2Al_3$ These two hexagonal systems reveal $-\ln T$ specific heat coefficients at low temperatures and low concentrations ($x \simeq 0.1$) (Maple *et al.* [1994] (Pd), Kim *et al.* [1993] (Ni)). The susceptibility in the Pd based system for a polycrystalline sample can be fit to either $-\ln T$ or $1 - A\sqrt{T}$ behavior at low temperatures. In each case the resistivity apparently saturates with a linear in T law. The U ions in these systems are likely tetravalent so that they are candidates for the quadrupolar Kondo effect in hexagonal symmetry arising from a non-Kramers doublet. The low concentration data clearly shows single ion scaling. Kim *et al.* [1993] argue that in the Ni case there is a proximity to a spin glass ordering. Nevertheless, given the same crystal structure and the single ion scaling observed in $Th_{1-x}U_xPd_2Al_3$, it is clear that these systems deserve further careful study as

quadrupolar Kondo candidates.

Concentrated non-Fermi liquid Compounds: UBe_{13}, $CeCu_2Si_2$, and $PrInAg_2$

UBe_{13}

UBe_{13} is certainly the most anomalous of the heavy fermion superconductors. We identify the following set:
(1) The specific heat is very weakly dependent upon magnetic field and highly sensitive to pressure. The low temperature value is of order 1000 mJ/mole-K^2, corresponding to an effective mass of several hundred free electron masses.
(2) The specific heat still rises with decreasing temperature on entering the superconducting state and with suppression of T_c by magnetic field continues to rise down to 0.3K (where measurements stop). This is clear evidence that the superconducting instability does not occur in a Fermi liquid normal phase.
(3) The magnetic susceptibility is weakly pressure dependent in comparison to the specific heat and under pressure has a completely different temperature dependence (McElfresh *et al.* [1993]).
(4) Doping on the U sublattice which drives away the specific heat anomaly leaves the low temperature susceptibility essentially unchanged.
(5) The magnetization is linear in field up to 20T.
(6) The dynamic magnetic susceptibility reveals no significant structure on the scale of 1 meV as is evidenced in C/T, and instead shows a broad 'quasielastic' response on the scale of 15 meV as evidenced both in neutron scattering and Raman spectra. Concommitant with the peak in χ'' is a Schottky anomaly in the specific heat, suggesting that the 15 meV peak represents highly damped crystal field levels for which further evidence appears in nuclear magnetic relaxation of the ^{9}Be sites. This dynamic susceptibility peak integrates to give 80% of the static susceptibilty up to the experimental cutoff. This places a stringent bound on any hypothetical moment carrying state in the low frequency region: given a 10K Kondo scale, to explain the residual susceptibility the effective squared moment must be less than $0.25\mu_B^2$ which would appear to rule out an interpretation in terms of a $5f^3\Gamma_6$ ground state.
(7) The electrical resistivity at the superconducting transition is reproducibly large (order 80-100$\mu-\Omega$-cm, and is reversibly suppressed by applied pressure and magnetic field (Aronson *et al.* [1989], Batlogg it et al. [1987], Andraka and Stewart [1994]). There is no region in ambient pressure or zero field in which a T^2 coefficient is visible in the resistivity (rather, a linear in T term is present). In applied magnetic field, there is some evidence that the resistivity obeys a scaling law $\rho(T,H)/\rho(T,0) \approx f(H/|T-T_0|^\beta)$ where $\beta = 1, T_0 = 0$ (Batlogg *et al.* [1987]) and $\beta = 0.7, T_0 = 0.5K$ (Andraka and Stewart [1993]) have been fit to the data.
(8) The muon Knight shift (Luke [1995]), ^{9}Be nuclear Knight shift (MacLaughlin *et al.* [1983]), and neutron scattering form factor (Stassis *et al.* [1985]) show no change upon entering the superconducting state.
(9) The upper critical field has a large low temperature limit which has been estimated above the Pauli paramagnetic value in at least one study (though not in others).

Different interpretations of these experimental data abound, most notably that the onset to superconductivity occurs above the coherence temperature which marks the beginning of well defined Fermi liquid behavior. We note that even if this is true, the superconductivity occurs in the absence of a well defined Fermi liquid state so that it is meaningless to use a quasiparticle picture for the description of the normal phase. We take points (1)-(9) to represent the following picture: heavy fermions arise in UBe_{13} in a non-Fermi liquid state (evidenced by points (2) and (6) particularly) which is likely not due to a magnetic lattice Kondo effect (evidenced by points (1),(3-5),(7,8)) but may potentially arise from a non-magnetic Kondo effect. The logical candidate is the quadrupolar Kondo effect (Cox [1987b], Cox [1988a,b], Cox [1993], E. Kim *et al.* [1996]; see also secs. 2.2.1, 2.2.3, and 5.2).

In this body of theory, it has been established that the quadrupolar Kondo effect can plausibly

explain the thermodynamic data and dynamic magnetic response measured in NMR, inelastic neutron scattering, and Raman spectroscopy. In particular, the susceptibility arises from vanVleck processes (virtual excitations to excited magnetic triplet levels) which have a different physical origin and overall energy scale than the specific heat coefficient. The low temperature relaxation of the NMR corresponds to the triplet to non-magnetic doublet peak shown in the schematic vanVleck response of Fig. 71. This peak has little overall spectral intensity and so is not clearly resolved in neutron scattering data (though the more recent data of Shapiro *et al.* [1993] may be showing some evidence for this behavior).

An interpretation of the unusual resistivity in terms of an infinite dimensional two-channel Kondo lattice picture is given in Cox [1996] (see also Sec. 9.3.2). In particular, it is argued that the finite resistivity is an intrinsic feature of the two-channel lattice in the absence of an ordering transition due to the 'spin-disorder' scattering off the degenerate many body clouds surrounding each Kondo site (see secs. 3.4.5, 5.1,6.1.4 for further discussion of this spin-disorder scattering). It is noted that ordinary Kondo lattice behavior cannot give the observed negative magnetoresistance at low temperature in this reference and in McElfresh *et al.* [1993] (where an interpretation of the pressure dependent $\chi(T)$ data in terms of the quadrupolar Kondo effect is given). It is possible that positive magnetoresistance expected for the ordinary Kondo lattice is obscured by the superconducting transition, but the large extrappolated residual resistivity goes against this interpretation (essentially the resistivity is already very close to its $T = 0$ value by any reasonable extrappolation scheme). The detailed scaling function predicted by the theory of Cox [1996] does not agree with the experimental data, but this may well be due to the oversimplifications induced by the infinite dimensional limit.

At this point, one main piece of experimental data is held up as an objection to this point of view: non-linear susceptibility measurements (Chandra *et al.* [1993], Ramirez *et al.* [1994]). response can be expected, and thus a low temperature *positive* susceptibility is anticipated which is non-divergent. The data of Ramirez *et al.* [1994] show apparently divergent $\chi^{(3)}$ curves for both body diagonal and principal axis fields. This would appear to rule out the quadrupolar Kondo effect. Three concerns may be raised about the data:
(1) $\chi^{(3)}$ measurements on Th doped samples by Aliev *et al.* [1995a,b] show the anticipated anisotropy and roughly correct temperature dependence.
(2) There is anisotropy in $\chi^{(3)}$ which goes the correct direction: if the body diagonal curve is subtracted from the principal axis curve, a weakly divergent response may remain.
(3) Points (1,2) suggest that an extrinsic origin to large negative non-linear susceptibility is possible. Contamination by large moment paramagnetic impurities such as Ho^{3+} ions can weakly affect the magnetic susceptibility (which scales as the effective moment squared times the concentration of impurities) while dominating the non-linear susceptibility (which would scale as the concentration times the fourth power of the effective moment). However, this scenario would produce significant sample dependence to $\chi^{(3)}$, while the polycrystalline data of Aliev *et al.* [1995a,b] fall right on top of that of Ramirez *et al.* [1994]. This would appear to argue against extrinsic origin to $\chi^{(3)}$.

$CeCu_2Si_2$

Careful recent studies of $CeCu_2Si_2$ coupled with attention to the ternary phase diagram show the following (Steglich *et al.* [1995]):
(1) In the slightly copper rich region which has only a superconducting phase at low temperature and magnetic field, the specific heat coefficient which has a large slope at the superconducting transition continues to rise on initial suppression of T_c with magnetic field. This, as for UBe_{13}, argues that the normal state from which the superconductivity occurs is not a Fermi liquid state.
(2) The normal state has a dominant linear in T resistivity with large (order 30-40 $\mu - \Omega$) residual value. The linear term goes to zero in applied magnetic field while a T^2 term grows, and an appreciable region over which T^2 behavior is seen in the resistivity opens up at precisely the region where some kind of field induced magnetic order occurs. The boundary of the T^2 region tracks the boundary of the

magnetic order. The linear term in $\rho(T)$ vanishes at precisely the field where the magnetic order first arises.

Given the data for $La_{1-x}Ce_xCu_{2.2}Si_2$ discussed earlier in this subsection, it is reasonable to propose $CeCu_2Si_2$ as a candidate magnetic two-channel Kondo lattice system. In terms of the infinite dimensional resistivity theory used to interpret UBe_{13} (Cox [1995]; see also Sec. 9.3.2), the low field behavior is compatible with the non-Fermi liquid behavior expected for the lattice. In higher fields, the combination of magnetic order with applied field induces a crossover to Fermi liquid physics associated with the same crossover in the impurity problem (c.f, Secs. 4.2, 5.1,6.1.2,7.2). The crossover scale in the infinite dimensional theory would track $(H_{mol}+H_{ext})^2/T_K$, where H_{mol} is the molecular field associated with the magnetic orderand H_{ext} is the applied field. This gives a rough interpretation of the high field T^2 region in the resistivity.

$PrInAg_2$

This is the first compound studied in a promising program to look for quadrupolar Kondo physics in lanthanide intermetallics (Yatskar *et al.*, [1996]). In this material, neutron scattering confirms that the Pr ions are in a Γ_3 ground state. The material shows anomalous properties, though not so unusual as UBe_{13}. The specific heat at low temperatures is large (C/T tends to a low temperature value of around 6 J/mole-K^2!) which is strongly indicative of Kondo effect physics. There is a pronounced region of $-\ln T$ behavior in the specific heat prior to saturation. However, the residual resistivity is clearly finite, although the low temperature behavior is not quadratic in the temperature. There is no evidence for long range quadrupolar or superconducting order.

The discovery of the first unambiguous quadrupolar Kondo lattice candidate presents reasons for theorists like the present authors to feel both excited and challenged. In particular, this result stands in stark contrast to the $d = \infty$ calculations discussed briefly above in relation to UBe_{13} and more in Sec. 9.3.2, where a residual resistivity is present for the lattice.

A tentative reconciliation of existing theory, data for UBe_{13}, and data for $PrInAg_2$ may rest upon "banding" effects which are excluded rigorously in infinite dimensions. Namely, for the quadrupolar(magnetic) two-channel lattice, inclusion of realistic inter-orbital hybridizations leads to a k-dependent splitting of the spin(channel) states in momentum space, except at special points in the Brillouin zone (only the Γ point and X point [zone-corner]) for the cubic lattice have degeneracy of the spin(channel) labels). As argued later in Sec. 9.3.2, these effects manifest in the k-dependence of the self energy which enters as a $1/\sqrt{d}$ correction. This splitting is of no concern in the conventional single-channel Kondo lattice where only one band plays a role in the physics. However, in this case, a new route to Fermi liquid physics is offered: if the self-consistent band splitting is small compared to the lattice Kondo scale, the system will pass close to the non-Fermi liquid fixed point prior to reaching a ground state which removes the residual degeneracy of the two-channel Kondo screening clouds. However, if the renormalized splitting exceeds the two-channel scale, a novel metallic state will be formed in which the finite paraquadrupolar susceptibility stabilizes the system against quadrupolar/collective-Jahn-Teller ordering. Of course, if the intersite coupling or strain-quadrupole coupling exceeds the Kondo scale and banding energy, this will separately cut off the non-Fermi liquid physics. If the Kondo scale exceeds the intersite strain-quadrupole coupling and banding energy, we create the situation most favorable for the formation of a heavy fermion superconducting state through odd-frequency staggered pairs.

Regardless, this is an exciting experimental development and offers a number of directions. For example, $PrPb_3$ is also a cubic system with a Γ_3 ground state, but in this case collective Jahn Teller order does set in at low temperature (Miksch *et al.* [1982]). However, only about $R/2\ln 2$ entropy is removed per Pr at below the ordering transition. Moreover, dilution studies might reveal a pure quadrupolar Kondo ground state in the impurity regime. The study of such Pr based compounds will be a very interesting new thrust to watch in the coming years.

Summary Six heavy fermion alloys show non-Fermi liquid behavior for which leading candidates models are the two-channel quadrupolar Kondo effect for the five U based alloys, and the two-channel magnetic Kondo effect for the Ce alloy. This picture explains most data but runs up against difficulties in explaining resistivity data for most of these systems. This picture naturally explains the **U**biquity of uranium based alloys, since the quadrupolar Kondo model is far easier to obtain than the two-channel magnetic model (c.f. Secs. 2.2, 3.4.4, 5.3). An intriguing experimental correlation is that five of these systems become heavy fermion superconductors when the U or Ce sublattice is fully occupied. This covers the known heavy fermion superconductors excluding UPt_3 for which no Th based reference compound exists (with the same crystal structure). Two of the heavy fermion superconductors (UBe_{13} and $CeCu_2Si_2$) have superconducting transitions which occur relative to normal phases which are not describable in terms of well defined Fermi liquid quasiparticle states. There are promising signs that UBe_{13} is describable as a two-channel Quadrupolar Kondo lattice, and $CeCu_2Si_2$ as a two-channel magnetic Kondo lattice. On the basis of the above discussion, all of these systems warrant further study to clarify the origin of the non-Fermi liquid behavior and whether its origin is in impurity or lattice versions of the two-channel Kondo model.

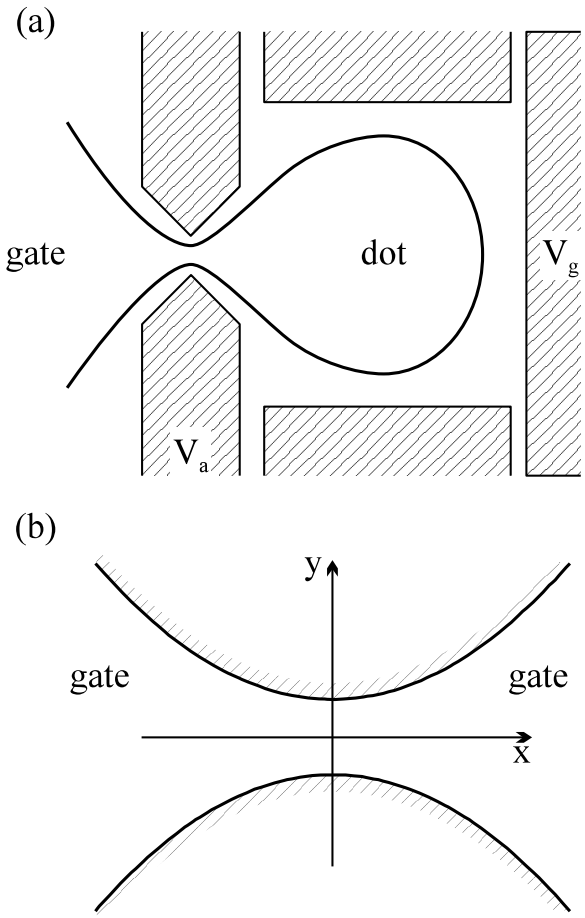

Figure 109: Quantum dot device (for coulomb blockade). (a) The voltage applied to the shaded areas localizes the electron states in the area of the dot and the electrode which are connected by the gate. The gate voltage V_g controls the charge in the dot, while the strength of the link between the electrode and the dot can be adjusted by the auxiliary potential V_a which controls width and the potential height of the gate. The electronic wave functions are appreciably non-zero only within the solid line. (b) The area of the gate is enlarged, and the wave function in this region has the form given by Eq. (9.1.2).

9 Related Theoretical Developments

9.1 Related Models

9.1.1 Connection to Coulomb Blockade Physics

The basic idea of the mapping of the coulomb blockade to a multichannel Kondo model hinges on the ability to view the charge variables as a pseudospin. The dynamical charge fluctuations in a small metallic particle can be described by a pseudospin if the number of electrons is fluctuating primarily between two integer values $N, N+1$ with all the other charging states neglected. It is precisely this situation which is called the "coulomb blockade". The origin of the restriction to two charge states arises from a proper setting of applied voltage to the metallic particle and a sufficiently small capacitance so as to create a large charging energy that effectively takes charge states $.., N-1, N+2, ...$ off to very large energies.

Such systems can be fabricated using nanotechnology methods. First, a two-dimensional electron gas is produced in a semiconductor through quantum well formation. Then additional electrodes are added on the top of the device to produce potential shifts in the quantum well and "pinch" the

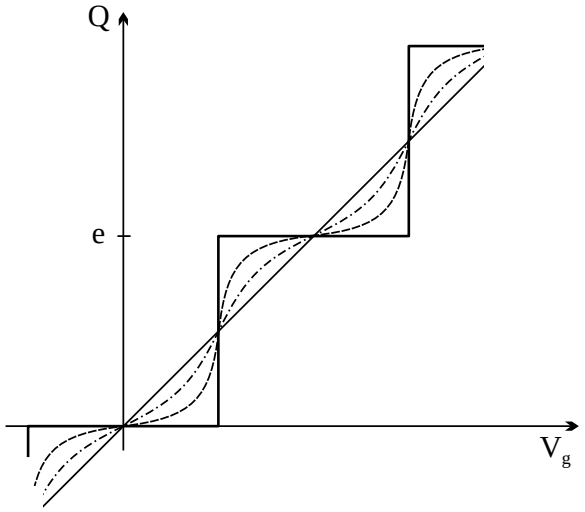

Figure 110: Average quantum dot charge as a function of bias number $N = CgV_g/e$ (c.f. Eq. (9.1.1)). The solid line is in the limit of zero transmission coefficient, indicating that in this limit where no charge leakage arises, the charge on the dot is quantized. If N is half-integer, then the charge is not well defined in this limit. For non-zero transmission amplitude, the number of electrons in the dot can fluctuate, so that the time average of the charge $< Q >$ deviates from an integer value (dotted line). Further increase of the transmission amplitude can lead to a complete washout of the charging steps (light solid line).

constriction through which electrons enter the blockade region, as shown in Fig. 109 . The Coulomb energy in the metallic particle or quantum dot may be expressed in terms of the capacitance C, gate voltage V_g, and dot charge Q as

$$E_c = \frac{Q^2}{2C} - gV_gQ = \frac{(Q - CgV_g)^2}{2C} - \frac{Cg^2V_g^2}{2} \tag{9.1.1}$$

where g is a geometric factor. By changing V_g the charge corresponding to the minimal energy is fixed. This procedure is unique except when $CgV_g = (N + 1/2)e$, where N is an integer. In this case the Coulomb energies of the $N, N + 1$ dot charge configurations are degenerate and this gives rise to strong charge fluctuations between these two states (see Fig. 110).

The coupling of the quantum dot to the external electrode is via the link of Fig. 109 which is characterized by the transmission amplitude T. The number of electrons can fluctuate on the dot, and if the amplitude T is gradually increased, the charging steps of Fig. 110 can be washed out. This has been seen experimentally (van der Vaart *et al.* [1993]; Pasquier *et al.* [1993]). More sophisticated arrangements have since been constructed by Molenkamp *et al.* [1995], Waugh *et al.* [1995,1996], Livermore *et al.* [1996], where two quantum dots connected by a weak are constructed in a similar manner to Fig. 109. In this case, the charge fluctuation between the two symmetrical dots can be studied in a very controllable way.

Now we turn to the connection of this system to the multi-channel Kondo model as discussed by Matveev [1991,1995] and Matveev, Glazman, and Baranger [1996a,b] (see also G. Falci, G. Schön, and G. Zimányi [1995], where a path integral method is applied). The key idea is again the mapping to the pseudospin as discussed above. The charge change about the biased value of $(N + 1/2)e$ is then analogous to the magnetic polarization of a spin impurity, and V_g is analogous to a magnetic field. The tunneling of electrons into and out of the dot which changes the charge states then plays the role of a transverse coupling in the spin model, or of the assisted hopping in the TLS Kondo model of Sec. 2. The capacitance C plays the role of the magnetic susceptibility. As in the TLS and quadrupolar Kondo effects, the real magnetic spin is a spectator field and gives rise to the channel index. In principle, by regulating the auxiliary gate voltage V_a of Fig. 109, the number of channels can increase beyond two by

allowing occupancy of more than one transverse sub-band. In this one assumes the wave functions on either side (electrode or dot) are given by

$$\psi(x,y) = \phi_n(y)e^{ikx} \tag{9.1.2}$$

with energy $E_n(k) = E_n + k^2/2m^*$. However, in practice the fillings of different sub-bands will not be identical, meaning that channel degeneracy between occupied sub-bands will not be satisfied. Hence, in contrast to Matveev [1991,1995] and Matveev, Glazman, and Baranger [1996a,b] one can expect that the condition $C_g V_g = (N + 1/2)e$ is satisfied for charge fluctuations only in one sub-band, so that the only stable fix point must be a two-channel one. See also Golden and Halperin [1996a,b].

The main goal of the theory is to calculate the profile of the charging steps shown in Fig. 110 as a function of the transmission coefficient T. Assuming just a single sub-band, the effective model Hamiltonian has been formulated in Matveev [1991], and is given by

$$\mathcal{H} = \mathcal{H}_0 + \mathcal{H}_T \tag{9.1.3}$$

where

$$\mathcal{H}_0 = \sum_{k,\sigma} \epsilon_k c^\dagger_{k\sigma} c_{k\sigma} + \sum_{k,\sigma} \epsilon_p c^\dagger_{p\sigma} c_{p\sigma} + \frac{Q^2}{2C} + \phi Q \tag{9.1.4}$$

and

$$\mathcal{H}_T = \sum_{kp\sigma} [t_{kp} c^\dagger_{k\sigma} c_{p\sigma} + h.c.] \tag{9.1.5}$$

with k indexing states on the left of the gate and p states on the right of the link. The matrix element t_{kp} describes the weak transmission rate across the gate in a way similar the classic tunneling Hamiltonian. All energies are measures with respect to the Fermi energy. ϕ in Eq. (9.1.4) is the energy shift due to the applied gate voltage. Q is the charge on the right hand side (in the dot) measured with respect to the occupied states, *i.e.*

$$Q = e \sum_{p\sigma} [c^\dagger_{p\sigma} c_{p\sigma} - \theta(-\epsilon_p)] \tag{9.1.6)]}$$

such that $< Q(\phi = 0) >= 0$.

To see the presence of Kondo like logarithms in this problem, it is sufficient to carry out perturbation theory in t_{kp} to second order. In that case one obtains a logarithmic singularity in $< Q >$ of the form

$$< Q^{(2)} > \approx N_e(0) N_d(0) t^2 \ln[\frac{|e/2C - \phi|}{|e/2C + \phi|}] \tag{9.1.7}$$

valid for $-e/2C < \phi < e/2C$, where t^2 is a suitably energy averaged matrix element, and $N_{e,d}(0)$ is the Fermi level density of states for the electrode (e) or dot (d). This result clearly demonstrates that the perturbation theory breaks down as the steps of Fig. 110 are approached.

Next, Matveev [1991] looked at the region $\phi = -e/2C + u$, with $u << e/C$. In this case higher energy charged states can be removed through the use of the projection operators P_0, P_1 which restrict to charge $Q = 0, 1$ (it is clear that an equivalent procedure can be followed for $N, N + 1$, with N arbitrary). Then the Hamiltonian becomes

$$\mathcal{H}_{01} = [\sum_{k,\sigma} \epsilon_k c^\dagger_{k\sigma} c_{k\sigma} + \sum_{k,\sigma} \epsilon_p c^\dagger_{p\sigma} c_{p\sigma}][P_0 + P_1] + euP_1$$

$$+\sum_{kp}[t_{kp}c^\dagger_{k\sigma}c_{p\sigma}P_1 + t^*_{kp}c^\dagger_{p\sigma}c_{k\sigma}P_0] \quad . \tag{9.1.8}$$

We distinguish two cases here:
(i) Point Contact In this case the transverse (y) dimension of the gate is comparable to the Fermi wave length $2\pi/k_F$ so that the transverse part of the wave function ϕ_n is always the same, e.g. ϕ_0. In this case a suitable dimensionless coupling is $g = N_e(0)N_d(0)|t|^2$, where t is the Fermi level value of t_{kp}.
(ii) Wide Junction Limit. In this case the dimension is large compared to the Fermi wavelength and a large number of transverse sub-bands can contribute (a number of order $M_{trans} \approx Ak_F^2$ where A is the transverse gate area). As mentioned above, however, the equivalence in this limit to a multi- channel Kondo model with $M = 2M_{trans}$ is questionable because the different sub-bands have very different transmission amplitudes and occupancies.

The Hamiltonian of Eq. (9.1.8) actually has the two-channel Kondo form, assuming just a single relevant sub-band, as we shall now demonstrate. Replace the indices k, p now by k, α $\alpha = \pm 1/2$ corresponding to the electrode momenta (+) or dot momenta (−). By restricting to just the $Q = 0, 1$ subspace the projection operators can be written in terms of 2×2 matrices, *viz.*

$$\mathcal{H}_{01} = \sum_{k\alpha\sigma} \epsilon_k c^\dagger_{k\alpha\sigma}c_{k\alpha\sigma} \begin{pmatrix} 1 & 0 \\ 0 & 1 \end{pmatrix} + eu \begin{pmatrix} 0 & 0 \\ 0 & 1 \end{pmatrix}$$

$$+t\sum_{kk'\sigma}[c^\dagger_{k,+,\sigma}c_{k',-,\sigma} \begin{pmatrix} 0 & 0 \\ 1 & 0 \end{pmatrix} + c^\dagger_{k,-,\sigma}c_{k',+,\sigma} \begin{pmatrix} 0 & 1 \\ 0 & 0 \end{pmatrix}] \tag{9.1.9}$$

where we have replaced t_{kp} by the constant value near the Fermi energy. Eq. (9.1.9) can be rewritten in terms of spin 1/2 or Pauli matrices in the conduction pseudospin space (electrode or dot index α, denoted by Pauli matrices σ^i) and the "impurity pseudospin" (charge Q denoted by spin 1/2 matrices S^i) to give the form

$$\mathcal{H}_{01} = \sum_{k\alpha\sigma} \epsilon_k c^\dagger_{k\alpha\sigma}c_{k\alpha\sigma} + eu(1/2 - S^z) + \frac{t}{2}\sum_{kk'\alpha\alpha'\sigma}[c^\dagger_{k\alpha\sigma}\sigma^+_{\alpha\alpha'}c_{k'\alpha'\sigma}S^- + c^\dagger_{k\alpha\sigma}\sigma^-_{\alpha\alpha'}c_{k'\alpha'\sigma}S^+] \tag{9.1.10}$$

which has the form of a purely transverse two-channel Kondo bare coupling in a magnetic field $h = eu$ and transverse coupling $J_\perp = t$. The channel index is the real magnetic spin index, as in the quadrupolar and TLS Kondo models. It is worth noting an oddity about this Hamiltonian, which is that the "impurity spin" enters solely through the Hilbert space restriction to the $Q = 0, 1$ subspace. This means that the "impurity" spin is composed from the same electrons which form the dot portion of the continuum states. This rather odd situation is certainly to be distinguished from TLS, magnetic, or quadrupolar Kondo effects where the continuum states and impurity pseudospin states form disjoint Hilbert spaces.

Starting with the planar $2M_{trans}$ Kondo model and using either multiplicative renormalization group methods (Matveev [1991]) or bosonization methods (Matveev [1995]), for $u \to 0$ one approaches an intermediate coupling fixed point at temperatures small compared to the Kondo scale

$$k_B T_K = D_0(N(0)J_\perp)^{M_{trans}} \exp[\frac{-\pi}{4N(0)J_\perp}] \tag{9.1.11}$$

where $N(0) = \sqrt{N_e(0)N_d(0)}$,$D = \sqrt{D_e D_d}$, D_i the bandwidth on the electron or dot side. Using the results from two-channel Kondo theory the average charge is

$$< Q > -e/2 \simeq e\frac{ue}{k_B T_K}\ln[\frac{k_B T_K}{eu}] \tag{9.1.12}$$

and the effective dot capacitance then

$$C_{eff} = \frac{-\partial^2 F_{ed}}{\partial u^2} \sim \frac{1}{T_K}\ln[\frac{T_K}{T}] \tag{9.1.13}$$

for temperatures $T \leq T_K$, where F_{ed} is the free energy per electron of the electrode-dot system.

In the latter paper (Matveev [1995]), the "tunneling" formulation is avoided by the introduction of a narrow conducting gate (see Fig. 109(b), where the electronic charge density is determined by the energy of the electrode and the dot. In this case, the electron energy varies continuously going through the gate, and therefore the bosonization technique can be applied. In this case the transmission coefficient can be large, with g of order unity, in which case the smeared step in Fig. 110 is replaced by a straight Ohmic line that is only slightly modulated near the special integer and half integer charging values. Considering the theory of the coupled dots studied by Waugh *et al.* [1995,1996] and Livermore *et al.* [1996] we refer to the works Golden and Halperin [1996a,b] and Matveev, Glazman, and Baranger [1996a,b].

9.1.2 Hopping Models with Several Sites

The concepts of the TLS Kondo model can be generalized to more than two sites, either with the sites forming a lattice or a cluster. In the first case, a proton or muon hopping between interstitial sites is a good candidate, while the second may be realized when in a crystalline solid a larger atom is replaced by a smaller one such that the substituent atom sits in a cavity where several equivalent potential minima are present. We believe the $Pb_{1-x}Ge_xTe$ described in Sec. 8.1 presents one such example. In amorphous metals, the formation of three or four almost degenerate sites can be ruled out by the stress due to the non-uniformity. In contrast, e.g., in $Pb_{1-x}Ge_xTe$, much less stress is expected because the substituent atoms provide the disorder (note the recent papers on more than two sites by Zaránd [1996] and by Moustakas and Fisher [1997]).

The Hamiltonian for the lattice system is given by Eqs. (2.1.37,38) and (2.1.39), where the heavy particle is created by $h^\dagger_{\vec{R}}$ at lattice position $\vec{R}$, and the conduction electrons form a band. The single heavy particle hops on a lattice, so that its dispersion in the absence of coupling to the conduction electrons is described by a tight binding band with width proportional to the one site hopping rate. We use the notation for the momentum space heavy particle operator $h^\dagger_{\vec{Q}}$ defined by

$$h^\dagger_{\vec{Q}} = \frac{1}{\sqrt{N}} \sum_{\vec{R}} e^{-i\vec{Q}\cdot\vec{R}} h^\dagger_{\vec{R}} \quad . \tag{9.1.14}$$

Electron assisted hopping (see Fig. 9) connects neighbors separated by displacement $a\vec{\delta}$ where a is the lattice spacing and $\vec{\delta}$ a unit vector assuming the heavy particle hops on a simple cubic lattice.

With this notation, the interaction Hamiltonian described by Eqs. (2.1.38) and (2.1.39) has the form (Zawadowski [1987])

$$\mathcal{H}_{int} \sim \sum_{\sigma,\vec{Q}'+\vec{k}'=\vec{Q}''+\vec{k}''+\vec{K}} [V + \frac{1}{2}u \sum_{\vec{\delta}} \cos(\frac{\vec{Q}''+\vec{Q}'}{2}\cdot\vec{\delta}a)] h^\dagger_{\vec{Q}''} h_{\vec{Q}'} c^\dagger_{\vec{k}''\sigma} c_{\vec{k}'\sigma} \quad . \tag{9.1.15}$$

The non-local nature of the assisted hopping shows up in the second term of that Hamiltonian as a form factor. The momentum is conserved to within a reciprocal lattice vector. The calculation of the two second order diagrams for the scattering amplitude shown in Fig 2. can be performed straightforwardly, and the diagrams to order u^2 don't cancel one another because of the presence of the form factor in Eq. (9.1.15). Actually, new form factors can be generated. The 2D and 3D cases are very complicated because an infinite set of couplings is produced in that way. The situation simplifies in 1D because only one new form factor is generated and the couplings correspond to forward and backward scattering in the problem of the 1D electron gas. The renormalization results in logarithmic terms where the low energy cutoff is due to the spontaneous hopping of the heavy particle on the lattice. From that work it is learned that the form factor of the assisted hopping makes the model non-commutative. The cluster problem has been discussed recently by Zaránd [1996].

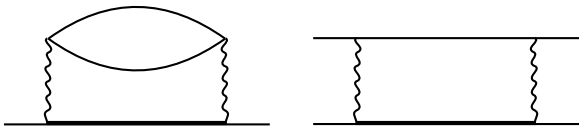

(a) (b)

Figure 111: Diagrams for Coulomb assisted hybridization of light and heavy particles. At left is the conduction electron self energy, where the wavy line is the interaction, light lines are conduction electron propagators, and the heavy line represents the heavy electron propagator. The diagram at right represents the induced electron-electron interaction brought about by this coupling.

In general, we expect these results to be most relevant to the finite cluster limit because the sites can be close to each other (on the scale of a lattice spacing) whereas in the lattice the overlap of the heavy particle wave function from site to site is apt to be very small. It is important to note that the low energy cutoff here is due do the spontaneous hopping, as mentioned above.

We now turn to the related problem of occupation dependent hopping. These models are given by the Hamiltonian of Eqs. (2.1.40) and (2.1.41) and by an additional heavy/light particle Coulomb interaction acting between the light and heavy particle on the same atomic site. The idea is that in the presence of a light particle, hybridization is assisted between light and heavy particles. The heavy particle is assumed to correspond to a weakly dispersed electronic band in this case as opposed to a muon or proton. The advantage of these models is that the heavy particle hybridizes with the conduction electrons so that the heavy particle wave function overlap does not appear and limit the physical relevance of the model. The model becomes noncommutative, because the light particle assisted hybridization has a form factor $t^{\gamma}(\vec{R},\vec{\delta})$ which has a simple Fourier transform proportional to

$$t(\vec{k}_1,\vec{k}_2;\vec{k}_3) = te^{i(\vec{k}_1+\vec{k}_2-\vec{k}_3)\cdot\vec{\delta}a} \tag{9.1.16}$$

if the light particle occupation with spin σ assisted a light particle of opposite spin to hop to a neighboring heavy site. In Eq. (9.1.16) the momenta $\vec{k}_1$ and $\vec{k}_2$ refer to the annihilated light particles and $\vec{k}_3$ to the created light particle.

It is quite easy to show that the number of newly generated form factors remains finite on renormalization, and that their form can be generated from Eq. (9.1.16) by omitting one, two, or all three of the momenta in that form factor. (The situation is somewhat different if the Coulomb interaction takes place on neighboring sites.) The vertex equation for this problem can be solved in the leading logarithm approximation, and results in an enhancement of the bare assisted hopping. There is a low energy cutoff in this problem set by the heavy particle energy ϵ_h (measured with respect to the fermi energy). This parameter is crucial, as it can be shown that is not renormalized to zero upon scaling of the bandwidth. This therefore cuts off the logarithmic divergence of the vertex function. The attractive feature of the model is that a mass enhancement of the conduction electrons together with a strong anisotropic pairing interaction are generated from this relatively simple source, namely, angular dependent form factors in the interaction matrix elements. Typical diagrams are shown in Fig. 111.

An interesting competition arises between the mass enhancement and the superconductivity. The highest T_c for superconductivity from this mechanism can be obtained when $m^* \simeq 2m_e$. Much higher mass enhancements can be obtained, but in that case the superconductivity is essentially suppressed to zero temperature as the wave fucntion renormalization $z << 1$ (Penc and Zawadowski [1994]). We note that these Coulomb assisted hopping models may be considered in dilute or lattice limits, and may be of relevance for those heavy fermion systems in which the f-level is close to the Fermi energy (on the scale of $\epsilon_h/E_F \leq 0.1$, say), or for those superconducting compounds in which atomic orbitals are near the Fermi energy and are weakly hybridized with the conduction electrons so that they form a heavy band (Zawadowski [1989b,c]).

Finally, we discuss the related impurity model proposed by Giamarchi *et al.* [1993]. The model Hamiltonian is

$$\mathcal{H} = \sum_{k,l} \epsilon_k c_{kl}^\dagger c_{kl} + \frac{t}{\sqrt{N_s}}(c_{ko}^\dagger h + h^\dagger c_{ko}) + \frac{1}{N_s}\sum_{kk'l} V_l (c_{kl}^\dagger c_{kl} - 1/2)(h^\dagger h - 1/2) \tag{9.1.17}$$

where the operator $c_{kl}^\dagger$ creates a spinless conduction electron in angular momentum state l about the impurity with radial momentum k, and $h^\dagger$ creates a "heavy" particle at the impurity site. The hybridization is assumed to occur only in one of the angular momentum channels ($l = 0$), but the Coulomb screening takes place between all the channels with the impurity. Because of the large number of channels, it turns out the an electron can be confined to the impurity orbital as $T \to 0$, and this gives rise to non-Fermi liquid behavior. Clearly this model is much simpler than the previous ones, because the interaction term has no form factors and is therefore commutative. The attractive feature of the non-Fermi liquid behavior is, however, limited to the situation when the localized orbital sits precisely at the Fermi energy. As soon as one shifts it off by energy ϵ_h, the logarithms are cut off and Fermi liquid behavior is recovered. Unfortunately, just as in the previous model, the energy ϵ_h is not renormalized upon scaling (Zawadowski and Zimányi [1995]). Physically it is hard to accept that accidentally small values of ϵ_h/E_F are likely to occur.

In conclusion, it can be said that the impurity models of this type are attractive only if the couplings are noncommutative so that they can be enhanced by the logarithmic terms in perturbation theory. However, due to the infrared cutoff imposed by ϵ_h, they are not good candidates to describe non-Fermi liquid systems.

9.1.3 Application of Two-Channel Models to the Cuprate Superconductors

Emery and Kivelson [1993,1994] have proposed a number of other models for realizing the two-channel Kondo effect in the context of explaining marginal fermi liquid theory in the cuprate superconductors. We shall briefly mention here two of them, both of which hinge critically upon the idea of phase separation in the cuprates.

First, the idea came of a quantized hole running in a bound state around the boundary of a region of short ranged magnetic order. The idea is to think of the orbital moment of the hole as the longitudinal component of the pseudo-spin. A counter-clockwise traversal of the boundary would count as an up-pseudo-spin, and a clockwise traversal would count as a down pseudo-spin. A mobile electron outside the domain can flip the orbital moment of the hole. Since the real spin of the electron is a spectator, this is argued to map to a two-channel Kondo problem.

A second realization is that of a small region of segregated holes. If a motion of the region can be triggered by a passing carrier, there will be a net flip of an electrical dipole moment. Because the electric dipole moment is independent of the magnetic spin of the carrier, this again is expected to map to a two-channel Kondo problem.

9.2 Majorana Fermion Approach to the Two-Channel Model

Coleman and Schofield [1995] and Coleman, Ioffe, and Tsvelik [1995] have developed an alternative approach to the two-channel model using Majorana fermions to represent the conduction electrons. The mapping to the two-channel model rests upon introducing a single channel model in which the impurity spin couples not only to the conduction electron spin but also their isospin or axial charge. This introduction of Majorana fermions has some of the same flavor as the approach of Emery and Kivelson [1992] and Sengupta and Georges [1994]; in particular, the residual entropy, logarithmically divergent specific heat and susceptibility, and marginal local dynamic susceptibility emerge from the presence of a decoupled local Majorana degree of freedom. However, in contrast to the bosonization route, (i) no exchange anisotropy is introduced, (ii) the Majorana fields emerge immediately at the initial

stages of calculation, and (iii) the non-trivial fixed point, rather than being at intermediate coupling strength, is shoved off to strong coupling. This has an advantage in that while the intermediate coupling fixed point is not accessible to any finite order perturbation theory schemes, an explicit perturbation theory may be set up about the strong coupling fixed point in powers of the hopping over the exchange integral.

The non-trivial physics then emerges from the undispersed local Majorana fermion, which may be viewed as a bound state of three other Majorana fermions. This method has been used to lend support to the idea that the channel anisotropic two-channel model is in fact a non-Fermi liquid in contrast to conformal field theory and numerical renormalization group results but in agreement with Bethe-Ansatz calculations. The particular representation of the model in terms of spin and isospin does not generalize to the two-channel Kondo lattice; however, a lattice extension does exist and we shall discuss that later in this subsection.

The primary approach is outlined in the paper by Coleman, Ioffe, and Tsvelik [1995] and we shall follow their arguments here. The first step is to write down the following Hamiltonian for a single channel of conduction states, restricted to a one-dimensional chain assumed to represent the radial quantization discussed for the NRG and CFT approaches:

$$\mathcal{H} = it \sum_{n,\sigma} [c^\dagger_\sigma(n+1) c_\sigma(n) - h.c.] + \mathcal{J} \vec{S}_I \cdot [\vec{\sigma}_c(0) + \vec{\tau}_c(0)] \tag{9.2.1}$$

where $\sigma_c(0)$ is the conduction spin density at the origin where the impurity sits, and $\tau_c(0)$ is the isospin density. Because the low energy spin and isospin degrees of freedom decouple, correlation functions of the two-channel model involving conduction spins from each channel are completely equivalent to correlation functions of the model specified by Eq. (9.2.1) where one of the channel spins is replaced by spin, the other by isospin. This equivalence may be established formally, and is done so in an appendix to Coleman, Ioffe, and Tsvelik [1995]. The authors call this a "compactified" Hamiltonian in that uncoupled degrees of freedom are removed; this jargon does not refer to the application of compactification of dimensions used in string theory.

An unusual aspect of Eq. (9.2.1) is that the analogue to overcompensation of the two-channel model is not possible at any finite coupling strength because in view of the Pauli principle it is impossible to have both maximal spin and isospin at a given site. As a result, the nontrivial coupling fixed point is pushed off to infinite coupling strength. Practically, this corresponds to a change of the cutoff procedure; because only the first two perturbative terms in the beta function are universal in form, higher order terms can shift the fixed point coupling around. The particular choice here shifts it to infinity.

The next step is to replace the conduction electrons by Majorana fermion variables. An explicit representation in terms of "scalar" and "vector" Majorana variables is

$$(c^\dagger_\uparrow(n) c^\dagger_\downarrow(n)) = (0i) \frac{1}{\sqrt{2}} (\Psi^{(0)}(n) - i\vec{\psi}(n) \cdot \vec{\sigma}) \tag{9.2.2}$$

where $\vec{\sigma}$ are Pauli matrices and the Ψ^i $(i = 0, 1, 2, 3)$ obey the Majorana anticommutation relations

$$\{\Psi^{(i)}, \Psi^{(j)}\} = 2\delta_{ij} \quad . \tag{9.2.3}$$

In terms of these Majorana variables, the spin plus isospin combination of Eq. (9.2.2) may be written as

$$\vec{\sigma}_c(n) + \vec{\tau}_c(n) = -i\vec{\Psi}(n) \times \vec{\Psi}(n) \quad . \tag{9.2.5}$$

The $i = 0$ Majorana component has the interpretation of a 'charge' degree of freedom, and the $i = 1, 2, 3$ components make up a 'spin' vector.

Since the coupling flows towards infinite strength, the fixed point Hamiltonian at zero temperature is simply

$$\mathbf{H}_\infty = -i\mathcal{J} \vec{S}_{imp} \times (\vec{\Psi}(0) \times \vec{\Psi}(0)) \tag{9.2.6}$$

which has a two fold degenerate ground state corresponding to either a net spin singlet or isospin singlet (in this model the impurity has the rather bizarre feature of either playing the role of spin or isospin). The degeneracy is implied by the presence of the Majorana fermion operators $\Psi^{(0)}$ and

$$\Phi = -2i\Psi^{(1)}(0)\Psi^{(2)}(0)\Psi^{(3)}(0) \quad , \tag{9.2.7}$$

both of which commute with the fixed point Hamiltonian. Application of the complex fermion combination $\zeta = (\Psi^{(0)}(0) - i\Phi)/\sqrt{2}$ will allow one to flip back and forth between the spin and isospin singlet states. The excited states of this Hamiltonian are spin and isospin triplet states.

Adding the hopping back in to the nearest neighbor site on the chain, one may admix singlet and triplet states of the strong coupling Hamiltonian. If one eliminates the virtual triplet fluctuations through a canonical transformation that projects to the singlet levels, the resulting effective Hamiltonian is, for the 'spin' sector

$$\mathcal{H}^* = it \sum_{n=1}^{\infty} \vec{\Psi}(n+1) \cdot \vec{\Psi}(n) + \alpha \Phi \Psi^{(1)}(1)\Psi^{(2)}(1)\Psi^{(3)}(1) \tag{9.2.8}$$

where $\alpha = 3t^3/4\mathcal{J}^2$, and the now strongly coupled state at the origin is explicitly excluded. The form of the interaction term in this Hamiltonian is very similar to that of Eq. (6.2.20) introduced by Sengupta and Georges [1994] within the Emery and Kivelson [1992] bosonization approach. The Φ fermion of Eq. (9.2.8) plays the same role as the $\hat{a}$ fermion of Sengupta and Georges [1994], and as a result contributes a residual 'half' degree of freedom to the entropy. Indeed, perturbation theory in α about the fixed point may be carried out, and the diagrammatics are precisely analogous to the work of Sengupta and Georges [1994], so that $\chi(T), C/T$ are second order in Φ and diverge logarithmically with the temperature, and have a Landau-Wilson ratio of 8/3. Moreover, (i) the mixed susceptibility in which one line is a Φ propagator and the other a Ψ propagator is marginal in form (Varma *et al.* [1989]), and the calculation is completely analogous to that of Eq. (6.2.38); (ii) the self energy of the Ψ fields is 'marginal' (Varma *et al.* [1989]) in that $\Sigma_\Psi(\omega, T) \sim -\omega \ln(\omega/\omega_c) + i \max \omega, T$ and the calculation is precisely analogous to that of the 'spin' fermion self energy of Emery and Kivelson [1992] (see Eq. (6.2.42)); (iii) the self energy of the Φ fermion is regular, with an imaginary part that vanishes as T^2. It is this quasiparticle-like sharpness to the Φ state which supports the marginal behavior at low temperatures.

Coleman, Ioffe, and Tsvelik [1995] then extend the model in two different ways. First, they notice that the original Hamiltonian enjoys an $O(3)$ symmetry. A well regulated large N expansion may be obtained when this is extended to $O(N)$. For even N, the Ψ self energies are analytic, while for odd N they are non-analytic. However, no divergent thermodynamic properties arise apart from the physical case $N = 3$.

Second, they extend the model specified by Eq. (9.2.8) to the lattice, and note that the Φ fermions of each site will acquire a dispersion in the lattice which will lift the residual entropy and induce a crossover from the non-Fermi liquid state; the estimated crossover scale is α^2/t which is of the order of the induced ϕ hopping through the Ψ fermions. This lattice generalization is *not* the same as the two-channel Kondo lattice model, but nonetheless offers a potential theoretical playground for understanding non-Fermi liquid behavior in a lattice model.

Coleman and Schofield [1995] have also considered the situation in which the spin and isospin channels of Eq. (9.2.1) are not identical, which then simulates the channel spin anisotropy of the original two-channel Kondo model. They find within this formalism that channel anisotropy may not drive the physics to a Fermi liquid fixed point. This possibility was anticipated by Andrei and Jerez [1995], who suggested that marginal operators could allow a flow to a line of Non-fermi liquid fixed points in the overcompensated model with exchange anisotropy, but called for further studies of asymptotic correlation functions to support or refute this conjecture. This consideration does not at all affect the thermodynamics presented by Andrei and Jerez [1995].

The parent $O(3)$ symmetric Anderson model which maps to this compactified Kondo model in the limit of large Coulomb repulsion has recently been studied with the numerical renormalization group

by Bulla and Hewson [1997]. They find that the calculated properties are indeed in agreement with those of the two-channel Kondo model, but rather than a non-Fermi liquid fixed point in the presence of spin/isospin symmetry breaking (analogous to channel anisotropy for the two-channel model) the crossover is to a Fermi liquid fixed point. These NRG results are independent of the Coulomb repulsion U in the $O(3)$ Anderson model, indicating that the correspondence to the non-fermi liquid fixed point has greater validity than anticipated by Coleman and Schofield [1995]. This has been further confirmed by weak and strong coupling perturbation studies by Bulla, Hewson, and Zhang [1997].

Finally, Schofield [1997] has shown that the Emery-Kivelson bosonization (Emery and Kivelson [1992]) can be easily extended to yield a description in terms of the compactified or $\sigma - \tau$ model, further cementing the equivalence of this formulation to the two-channel model.

9.3 Steps Toward the Lattice Problem

In this last subsection, we will briefly overview the steps made to extend the theory of impurity models to the lattice. These steps consist of studies of two impurity single- and two-channel Kondo models, which we discuss in Sec. 9.3.1, and approaching the problem from the $d = \infty$ limit (d the spatial dimensionality) which we discuss in Sec. 9.3.2.

9.3.1 Two Impurity Model

The two-impurity Kondo model has proven to be a source of non-Fermi liquid physics in both the one- and two-channel cases. It is of interest to review the one-channel model first, both to set the tone of the discussion and to note a strong similarity between a non-trivial fixed point of that model with the two-channel one-impurity model, first stressed by Gan [1995b]. Following that, we shall overview the more complex physics of the two-impurity two-channel Kondo fixed point.

For both the one- and two-channel models, a competition results between the Kondo effect and the intersite impurity coupling (RKKY interaction). For antiferromagnetic RKKY interaction, non-trivial non-Fermi-liquid fixed points develop for particle-hole symmetric limits of the models. For the one-channel model, a single (unstable) non-trivial fixed point emerges, while for the two-channel model an entire sheet of non-trivial fixed points emerge with continuously tuneable exponents. However, in the case of the single-channel model, the non-trivial fixed point is removed with particle-hole symmetry breaking associated with asymmetry of the density of states about the Fermi energy or the addition of potential scattering. It is not yet clear whether the manifold of fixed points is removed in the two-channel model, but the bias based upon the one-channel results is that it is removed.

(1) One-Channel Two Impurity Model

The Hamiltonian for this model is simply

$$\mathcal{H} = \sum_{\vec{k}\sigma} \epsilon_k c^\dagger_{\vec{k}\sigma} c_{\vec{k},\sigma} + J \sum_{j=1,2} \vec{S}_I(\vec{R}_j) \cdot S_c(\vec{R}_j) \tag{9.3.1}$$

where j indexes the site of the two impurities. Although at second order in J, RKKY interactions between the impurities will be generated, a "bare" interaction term $-I_0 \vec{S}_I(\vec{R}_1) \cdot \vec{S}_I(\vec{R}_2)$ is often added to Eq. (9.3.1) to allow for greater tuneability of the model parameters (with this convention, $I < 0$ is antiferromagnetic). This model possesses a non-trivial fixed point for suitably defined particle hole symmetry at antiferromagnetic RKKY coupling, as was first identified by Jones and Varma [1987,1989] and subsequently characterized by Jones, Varma, and Wilkins [1988].

It is convenient to project the conduction electrons into local channels which are of even and odd parity about the midpoint of the line between the two impurities. It is only these states which couple to the impurity. The projection allows for a reduction to an effective one-dimensional problem analogous to that of the two-channel model as outlined in Sec. 6.1. Assuming a symmetry conduction

band of width $2D$, the projected local annihilation operators are (Silva *et al.* [1996])

$$c_{0\sigma\pm} = A_\pm \int_{-D}^{D} d\epsilon \frac{1}{N_s} \sum_{\vec{k}} \delta(\epsilon - \epsilon_k)[e^{i\vec{k}\cdot\vec{R}_1} \pm e^{i\vec{k}\cdot\vec{R}_2}]c_{\vec{k}\sigma} \tag{9.3.2}$$

$$= A_\pm \int_{-D}^{D} c_{\epsilon\sigma\pm} \sqrt{1 \pm \frac{\sin kR_{12}}{kR_{12}}} d\epsilon$$

where $A_\pm$ is a normalization constant, $R_{12} = |\vec{R}_1 - \vec{R}_2|$ and +(-) indicates even(odd) parity about the inversion center. Note the correspondence to the operators for the TLS defined in Eq. (A.2.5a,b) of App. II (also, the $\pm$ corresponds to the $e(o)$ labels of Moustakas and Fisher [1995,1996]). Defining the square-root factor in Eq. (9.3.2) by $N_\pm(E)/A_\pm$, it is possible to write the exchange interaction term of Eq. (9.3.1) as (Affleck, Ludwig, and Jones [1995])

$$\mathcal{H}_{int} = \frac{J}{4}[\vec{S}_I(\vec{R}_1) + \vec{S}_I(\vec{R}_2)] \cdot (\sum_{p=\pm,\mu\nu} \vec{\sigma}_{\mu\nu}) \int_{-D}^{D} d\epsilon \int_{-D}^{D} d\epsilon' N_p(\epsilon) N_p(\epsilon') c^\dagger_{\epsilon\mu p} c_{\epsilon'\nu p} \tag{9.3.3}$$

$$+ \frac{J}{4}[\vec{S}_I(\vec{R}_1) - \vec{S}_I(\vec{R}_2)] \cdot (\sum_{p=\pm,\mu\nu} \vec{\sigma}_{\mu\nu}) \int_{-D}^{D} d\epsilon \int_{-D}^{D} d\epsilon' N_p(\epsilon) N_{-p}(\epsilon') c^\dagger_{\epsilon\mu p} c_{\epsilon'\nu -p} \quad .$$

As stressed by Affleck, Ludwig, and Jones [1995] and more recently, in the context of the TLS Kondo effect by Zawadowski *et al.* [1997], there are two kinds of particle-hole symmetry relevant to such a two-site quantum impurity problem. First (Type I), we require that

$$N_p(E) = N_p(-E) \;\; and \;\; c_{\epsilon\mu p} \to (-1)^{1/2-\mu} c^\dagger_{-\epsilon\mu p} \tag{9.3.4}$$

which preserves the parity index. This simply says that the local parity projected densities of states are invariant under inversion about the Fermi energy. Another kind of particle-hole transformation (Type II) corresponds to the mapping of electron minima to hole maxima for a nearest neighbor tight binding model (under which $\vec{k} \to \vec{k} + \vec{Q}/2$, where $Q = \pi(111)/a$ in three-dimensions). In this case, parity labels get interchanged and the symmetry is specified by

$$N_p(-E) = N_{-p}(E) \;\; and \;\; c_{\epsilon\mu p} \to (-1)^{1/2-\sigma} c^\dagger_{-\epsilon\mu -p} \quad . \tag{9.3.5}$$

It turns out that by considering, for example, a two-impurity Kondo model on a nearest neighbor lattice in one dimension, that if the two sites differ by an odd number of lattice spacings, the model is invariant under type II symmetry, while for an even difference in the number of sites, the model is invariant under type I symmetry (Fye and Hirsch [1989]; Fye [1994]; Affleck, Ludwig, and Jones [1995]). In this particular model, the induced RKKY couplings will be antiferromagnetic for odd separation and ferromagnetic for even separation. Affleck, Ludwig, and Jones [1995] further note that potential scattering will break Type I particle-hole symmetry but not type II particle-hole symmetry. In this sense, Type I particle-hole symmetry places a stronger constraint on the model.

In the presence of particle-hole symmetry of Type I, Millis, Kotliar, and Jones [1990] have given the following argument to explain the existence of a non-trivial fixed point: for zero total RKKY interaction strength (bare+induced), the ground state will be characterized by the independent impurity fixed point (two isolated and screened Kondo impurities). This is a stable fixed point (there are only irrelevant operators about it), and the phase shift in each parity channel is $\pi/2$. On the other hand, for infinite antiferromagnetic RKKY coupling, the local moments are quenched into a singlet with no dynamics remaining, and the phase shift for scattering off of the extended singlet is zero in each channel. This fixed point is also stable for Type I particle-hole symmetry (no relevant or marginal operators about the fixed point). They also showed that these two possible phase shift values, zero or $\pi/2$, are the only allowablve values in the presence of Type I particle-hole symmetry. In consequence, as a parameter

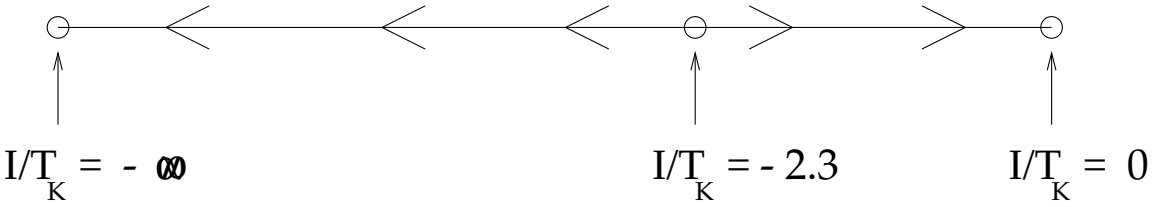

Figure 112: Phase diagram of the two-impurity Kondo model with full particle-hole symmetry. For $I \to -\infty$, the system goes to the local singlet fixed point, which is a Fermi liquid, in which the local moments just lock out in a singlet. For $I = 0$, the local moments each are Kondo compensated (this is actually extended to positive $I < \infty$). Most striking is the non-trivial unstable fixed point for antiferromagnetic RKKY interaction strength $I/T_K \approx -2.3$. After Jones and Varma [1987,1989].

such as the intersite coupling strength tunes one between the independent impurity fixed point and the antiferromagnetic singlet fixed point while Type I symmetry is enforced, there must be a point arising in which the phase shift jumps discontinuously between 0 and $\pi/2$. This implies a critical point separating the stability regimes of the two different fixed points along the axis of the intersite coupling (normalized to the one impurity Kondo scale). The renormalization group flow diagram for this model is shown in Fig. 112 in terms of the total intersite coupling $I = I(J) + I_0$ where $I(J)$ is the induced RKKY coupling strength (measured in units of the Kondo scale). (Note that for infinite ferromagnetic I the odd channel drops from the problem, and the model maps to the single channel spin 1 Kondo impurity model, while in general for ferromagnetic $I < \infty$, a two-stage Kondo quenching occurs of the net impurity spin (first even and then odd, or vice-versa), as first envisioned by Jayaprakash, Krishnamurthy, and Wilkins [1980]. The universality class of the successive quenching model is the same as the two isolated impurities fixed point.)

The original NRG work of Jones and Varma [1987,1989] and Jones, Varma, and Wilkins [1988] together with the CFT calculations of Affleck and Ludwig [1992] and Affleck, Ludwig, and Jones [1995] confirms that the critical point is characterized by a second order transition, at which the staggered susceptibility, specific heat coefficient, and local pair field susceptibility in the spin singlet sector diverge logarithmically. Moreover, the residual entropy is $(R/2)\ln 2$ and the Fermi level scattering rate is at half the unitarity limit. These results have a strong similarity to the results for the two-channel one-impurity model. It should be noted that the original NRG work was based upon an "energy-independent" coupling constants approximation. Namely, the coupling strengths in Eq. (9.3.3) were set to their Fermi level values and the energy dependence ignored. This manifestly introduces full particle-hole symmetry and thus to a critical point of some sort (as explained in the preceding paragraph), although the non-trivial fixed point was an unexpected result (instead a simple level crossing could have resulted).

Gan [1995b] has proposed that this critical point is very similar to the two-channel one-impurity non-trivial fixed point. The idea is that the critical point is identified by a doubly degenerate ground state in each case. For the two-channel fixed point, the ground state has a double degeneracy in spin. For the two-impurity one-channel fixed point, the double degeneracy corresponds to a level crossing in a finite size spectrum. The levels roughly are described by the isolated Kondo singlets on the one hand, and the extended singlet on the other hand. The level degeneracy is lifted by the deviation of the RKKY coupling from the critical value, and in this sense the RKKY coupling plays exactly the same role as a spin field in the two-channel Kondo model, so that for $I - I_c \neq 0$, the specific heat coefficient and staggered susceptibility diverge as $(I - I_c)^{-2}$, similar to the $1/H^2_{spin}$ divergence for the two-channel one impurity model.

To understand why the mapping breaks down, it is helpful to mention a few details of the CFT approach to the model as explained in detail in Affleck and Ludwig [1992], and Affleck, Ludwig, and Jones [1995]. They first consider a free fermion theory. For each parity channel of the free theory, when full particle-hole symmetry is maintained, there is a global conservation of $SU(2)$ axial charge or isospin

(as defined in Secs. 4 and 6.1) and the $SU(2)$ spin symmetry. Hence, the total free field symmetry group may be taken to be $SU(2)_{iso,+} \otimes SU(2)_{sp,+} \otimes SU(2)_{iso,-} \otimes SU(2)_{sp,-}$. The conformal charge of this theory provides a dimensionless measure of the numbers of degrees of freedom present in the Hamiltonian (it is technically defined in terms of the commutation relations of the Fourier transforms of the real space Hamiltonian density, which obey the so-called Virasoro algebra when conformal invariance holds–a complete discussion is beyond the scope of this paper–we refer the reader to Affleck, Ludwig, and Jones and references therein). Each of the $SU(2)$ spin and isospin currents obey the level $k = 1$ Kac-Moody algebra (c.f. the discussion of Sec. 1), and each has a conformal charge of $c = 1$, so that the total conformal charge of the effective one-dimensional model is $c_{tot} = 4$.

Now, the presence of the impurities breaks the $SU(2)_{sp,+} \otimes SU(2)_{sp,-}$ spin symmetry into a global $SU(2)$ spin symmetry. The impurities do nothing to the isospin symmetry, provided we maintain full particle-hole symmetry. If the Kac-Moody commutation relations are computed for these currents one finds that the level is $k = 2$. For a general k-level KM algebra, the conformal charge of the resulting Sugawara Hamiltonian density quadratic in the KM currents is $c = 3k/(k + 2)$. Thus for example, for $k = 1$ we recover $c = 1$ as claimed above, while for $k = 2$ we obtain $c = 3/2$. This means that the sum of conformal charges for isospin and global spin currents is $c' = 7/2$. However, the representation in terms of the global spin current can be done for the free Hamiltonian which implies that we are not counting all the degrees of freedom (or else we would obtain $c' = c_{tot} = 4$).

The missing conformal charge is $c = 1/2$. There is a unique, unitary conformal theory with conformal charge $c = 1/2$, and it is the Ising model. Hence, quite surprisingly, the remaining degrees of freedom obtained after coupling to the impurities and preserving maximal isospin and spin symmetry are that of the Ising model! As an example, in terms of the primary $i = 1/2$ field h_p of the $k = 1$ isospin algebra, the $j = 1/2$ field g_μ of the $SU(2)$ $k = 2$ spin algebra, and the order parameter field σ of the Ising model, the one-dimensional fermionic operators are given by

$$\psi_{\mu p}(x) \sim (h_p)_1 g_\mu \sigma \tag{9.3.6}$$

where the 1 on the h_p field denotes the first component of the spinor field and the i is the species label. The creation operator would pick out the second component of the isospin spinor doublet. This operator has a scaling dimension of 1/2 since $\Delta_h = 1/4$, $\Delta_g = 3/16$, and $\Delta_\sigma = 1/16$ add up to 1/2.

Affleck and Ludwig [1992] first noticed that the non-trivial fixed point of this model admits a very large $SO(7)$ symmetry. Gan [1995a], proposed that this $SO(7)$ symmetry can be understood from writing a Majorana fermion representation of the full model. The full free theory has an $SO(8)$ symmetry in this representation as discussed in Sec. 6.3 (Maldocena and Ludwig [1996]). In Gan's [1995a] approach, a single Majorana fermion is decoupled by the impurity leaving behind a global $SO(7)$ symmetry to the remaining free Majorana fields. It is apparent from the consideration of these paragraphs, that a full mapping of the two-channel one-impurity model to that of the two-impurity one-channel non-trivial fixed point (at particle-hole symmetry) cannot be established–the symmetries of the problems are simply too different.

It is unlikely that this non-trivial fixed point will be generically relevant to the understanding of experimental data for heavy fermion or TLS materials, although it is possible that for some systems a crossover region may exist regulated by the properties of this fixed point. As shown in detailed studies by Jones [1991], the addition of simple potential scattering induces a line of Fermi-liquid fixed points between the two isolated impurity fixed point and the antiferromagnetic fixed point, with continuously varying phase shifts. In extensive Quantum Monte Carlo studies, Fye [1994] found no evidence for the non-trivial fixed point in nearest neighbor tight binding models both in one- and three-dimensions. In retrospect, this is related to the breaking of Type I particle-hole symmetry in his calculations. Finally, Silva *et al.* [1996] have performed an extensive series of NRG calculations in which no approximation is made for the energy dependence of the couplings. They do not find the non-trivial fixed point when they consider only the two impurity Kondo model (with $I_0 = 0$), but they do find that they can get close to the non-trivial fixed point by shrinking the bandwidth parameter $\Delta = v_F k_F$; this has the effect

of dynamically restoring particle hole symmetry. Further, they find that they can scale all of their data for specific heat coefficient and uniform susceptiblity onto common curves as a function of the bandwidth parameter and fixed impurity separation. The specific heat curve is sharply peaked as a function of RKKY interaction strength (tuned by J and Δ) which indicates that at least for sufficiently small asymmetry, it is in principle possible to observe a specific heat peak due to the proximity to the non-trivial fixed point.

(2) Two Impurity Two-Channel Model.

To define the two-channel two-impurity model, we simply augment the conduction bands of Eqs. (9.3.1,9.3.2,9.3.3) by channel indices. The phase diagram for ground states of this model, obtained from NRG calculations under the assumption of energy independent coupling constants, is shown in Fig. 113., taken from Ingersent, Jones, and Wilkins [1992], and Ingersent and Jones [1994] (see also Jones and Ingersent [1994]). The most salient features are arguably:

(i) an unstable non-Fermi liquid fixed point at the origin, corresponding to the isolated impurities–we should not be surprised that the isolated impurity fixed point is unstable, as the Kondo spin clouds around each two-channel site must eventually feel each other for $T \to 0$ since the length scale of the two-channel clouds is divergent (this is not the case for the one channel model);

(ii) stable Fermi liquid fixed points for sufficiently large difference between even and odd exchange coupling strengths;

(iii) a complete manifold of non-Fermi liquid fixed points for antiferromagnetic intersite spin coupling, with a marginally stable line marking the leftmost boundary of this manifold.

We shall now discuss points (i-iii) in order.

The instability of the isolated two-channel one-impurity fixed point is often simplistically pointed to as evidence of the irrelevance of the single impurity model to any realistic description of heavy fermion or TLS materials. The difficulty with this simplistic argument is that it ignores the quantitative aspect of crossover: namely, while the fixed point is unstable, it may still regulate the physics over a large parameter range for sufficiently small values of the intersite coupling strength and even-odd coupling difference. Indeed, as discussed in Sec. 8.2, the apparent single ion physics present for $Th_{1-x}U_xM_2Si_2$ (M=Ru,Pd) suggests that over a wide temperature range the two-channel one impurity fixed point governs the low energy scale excitations until some interaction physics enters (in this case, well below 1K for the concentrations studied). At issue then is the need for *quantitative* estimate of the crossover temperatures and exponents for this model.

In addition to the intersite interaction strength, the two-impurity two-channel model has an additional relevant parameter, which is the asymmetry between even and odd coupling strengths, with $J_p(0,0) = JN_p(0),\ p = \pm$. The understanding of this is as follows, argued for the case of zero intersite spin interaction: if J_e differs from J_o, then there are sufficient conduction degrees of freedom to fully screen the spin for either channel, so whichever couples most strongly will simply drive the system to the stable isolated impurity fixed point of the single channel Kondo model, a Fermi liquid fixed point. We note that this crossover is related to the "banding" of the electrons, in that we cannot retain two-fold degenerate bands at all points of the Brillouin zone for the full two-channel lattice. Here we are seeing that fact reflected by the generic difference of even and odd coupling constants in the two-point Brillouin zone of the two-impurity model. As noted in Sec. 8.2, this banding effect may be relevant for understanding the unusual behavior of the quadrupolar Kondo lattice candidate $PrInAg_2$ (Yatskar *et al.* [1996]).

A fortunate point about the crossover to Fermi liquid behavior for non-zero $J_e - J_o$ is that the crossover exponent is extremely small. Specifically, the crossover temperature identified from the NRG (Ingersent and Jones, [1994b]) is found from $|J_e - J_o| \sim T^{\Delta_{eo}}$ which gives a scale $T_{eo} \sim |J_e - J_o|^{1/\Delta_{eo}}$. Numerically, it is found $\Delta_{eo} \approx 0.1$! This implies that unless $|J_e - J_o|/J_e \approx 1$, the crossover is *extremely* slow.

Finally, we turn to the manifold of fixed points. Georges and Sengupta [1995] have developed a

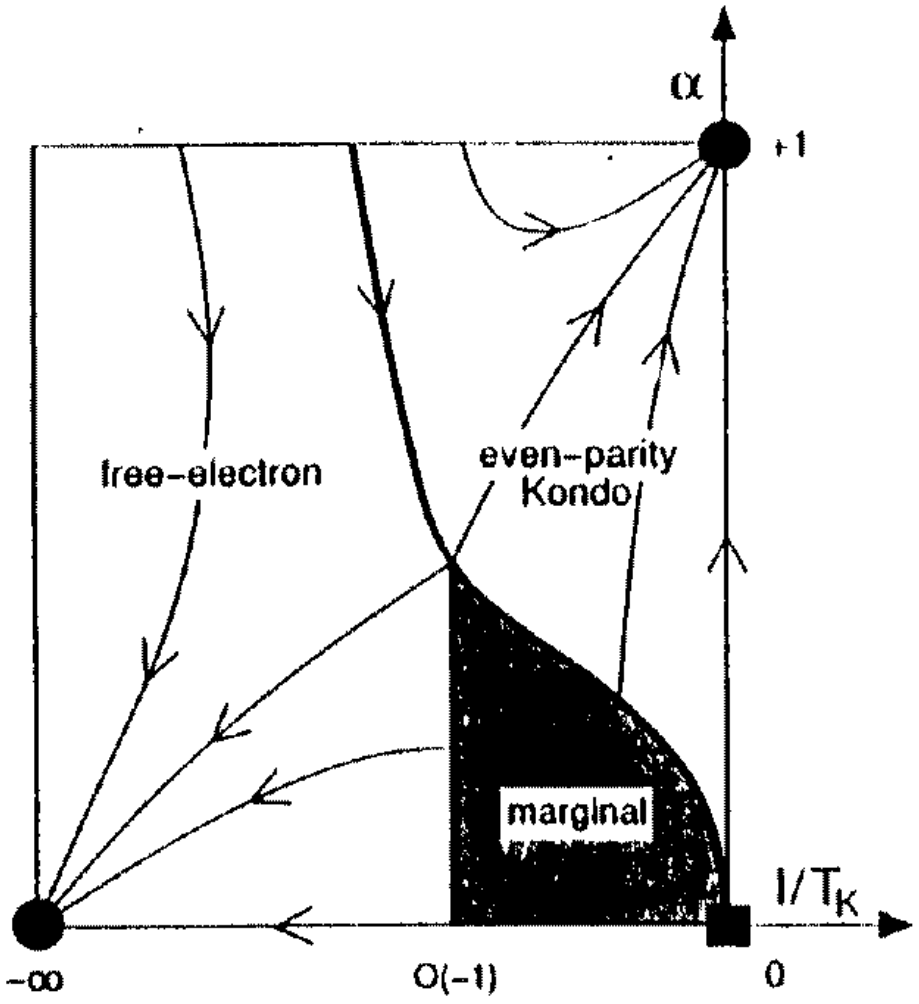

Figure 113: Phase diagram of the two-channel, two-impurity Kondo model. Relevant parameters are the RKKY coupling strength (measured in units of the Kondo scale) and the even-channel/odd-channel exchange asymmetry (vertical axis). Most striking is the marginal sheet for negative RKKY coupling. From Ingersent and Jones [1994].

complete conformal field theory (in concert with Abelian bosonization) for the particle-hole symmetric model, which properly displays continuously tuneable scaling dimensions to the primary field operators as the intersite coupling strength is tuned, indicating that the intersite interaction is a marginal parameter in the theory. This theory is considerably more complex than that of the one-channel two-impurity model, and we shall not go into details here. Suffice to say, as for the two-impurity one-channel model, it is a matter of concern whether the non-trivial fixed point manifold is robust to the lifting of particle-hole symmetry.

9.3.2 $d = \infty$ Limit

Given the very interesting data on UBe_{13} and $CeCu_2Si_2$, it is worth studying the properties of the two-channel Kondo lattice. One regime where this can be carried out rigorously is in the limit of infinite spatial dimensions where the lattice problem becomes a self-consistent impurity problem.

Key Ideas of the $d \to \infty$ limit

The procedure for going to the infinite dimension limit is by now well known and has been discussed extensively in the original works of Metzner and Vollhardt [1989] and Müller-Hartmann [1989] as well as two recent review articles by Pruschke *et al.* [1995] and Georges *et al.* [1996]. There are two key ideas, which we illustrate for simplicity on a hypercubic lattice assuming a nearest neighbor tight-binding model for the conduction electrons.

First, the energy dispersion relation in d dimensions is

$$\epsilon_{\vec{k}} = -2t \sum_{i=1}^{d} \cos k_i a \tag{9.3.7}$$

where t is the tight binding matrix element and a is the lattice constant. This can be viewed as a sum of random variables, each distributed on the interval $[-2t, 2t]$. Accordingly, the density of states must take a Gaussian form as $d \to \infty$ by the central limit theorem. The width of the Gaussian is $\sqrt{2d}t = t^*$. To have a sensible density of states in the limit, we obviously should hold t^* fixed, which means $t \sim 1/\sqrt{d}$.

This scaling immediately implies that the self energy becomes purely local in this limit, as we illustrate in Fig. 114 for the two-channel Kondo lattice model. This illustrates a contribution to the conduction electron energy in real space. If the sites i and j are identical, the diagram plus all higher order ones will be non-zero. However, suppose $i \neq j$. Then the real space conduction propagator $G(i, j, \omega) \sim t^{||i-j||}$, where $||i - j||$ measures the minimal number of nearest neighbor hops required to connect sites i, j. Because three intersite propagators appear in the diagram and $t \sim 1/\sqrt{d}$, then clearly this self energy contribution scales as $d^{-3||i-j||/2}$ as $d \to \infty$. Note that for when i, j are nearest neighbors we get the largest contribution, and when Fourier transformed this will give a momentum space contribution scaling as $1/\sqrt{d}$.

Because the self-energy becomes purely local, the problem is reduced to an effective impurity problem. Specifically, one picks a single site (say i) which is called the impurity. One makes an initial guess for the "medium" propagator $\tilde{G}_c(i, i, \omega)$, i.e., the conduction propagator for a lattice with this site plucked out. One solves then for the self energy of the conduction electrons by an appropriate impurity method (e.g., quantum Monte Carlo or the NCA), and constructs an estimate for the local propagator through

$$G_c(i, i, \omega) = \frac{1}{N_s} \sum_{\vec{k}} \frac{1}{\omega - \epsilon_k + \mu - \Sigma(\omega)} \tag{9.3.8}$$

where N_s is the number of sites, and μ is the chemical potential. This equation crucially illustrates the self consistency required to solve the lattice–the same self energy which enters the momentum space propagator enters the local propagator. The new estimate for the medium propagator is given by

$$\tilde{G}_c(i, i, \omega) = (G_c(i, i, \omega)^{-1} + \Sigma(\omega))^{-1} \tag{9.3.9}$$

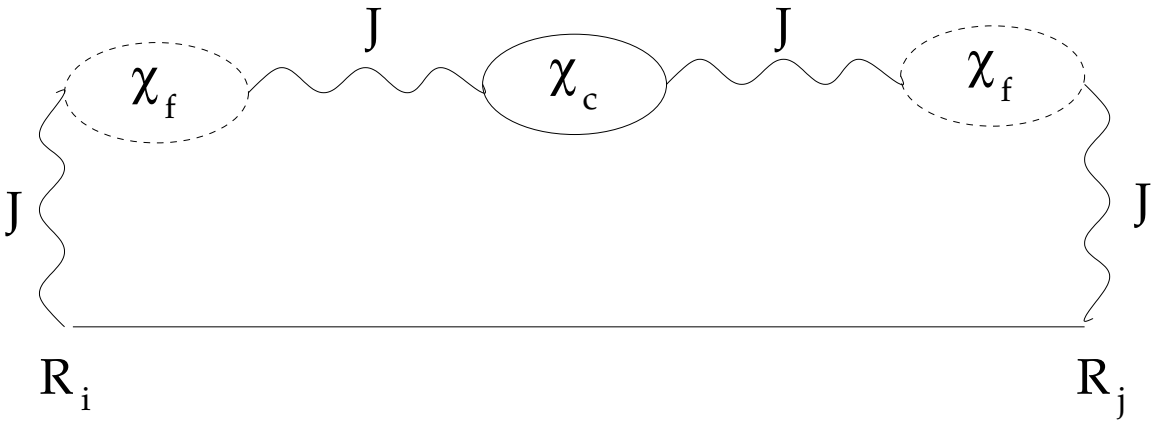

Figure 114: Self energy diagrams for the two-channel Kondo lattice for $d = \infty$. A dashed bubble represents a local moment susceptibility, a solid bubble represents a conduction electron susceptibility; wavy lines represent the exchange interaction. For site index $i = j$, the diagram is of order $1/d^0$, while for $i \neq j$, the diagram is at least of order $1/d^{3/2}$ which holds for nearest neighbor sites.

which is then used for the next iteration of the impurity problem. Iterations continue until self consistency of Eq. (9.3.8) is reached, or until the medium propagator, say, does not change from iteration to iteration.

Examples: Hubbard and Anderson Lattice Models

The mapping to an effective impurity model affords considerable qualitative insight into a number of problems. For example, the Hubbard model then becomes a self-consistent Anderson impurity model. This implies that the density of states should possess satellite peaks separated by the Coulomb interaction U and corresponding to transitions of the singly occupied state to empty and doubly occupied orbitals. In addition, in any metallic phase, a quasiparticle "Kondo resonance" will appear in the vicinity of the Fermi energy. The energy scale of this quasiparticle resonance is self-consistently determined and has no simple analytic form (Pruschke *et al.* [1993,1995], Georges *et al.* [1996]). For the single-channel Anderson lattice model, at particle-hole symmetry a band insulator forms with an indirect gap determined by the "coherently enhanced Kondo scale" (Jarrell [1995]). For sufficiently small hybridization (and therefore effective on-site exchange coupling) the band insulator may give way to an antiferromagnetic insulator, with the combination of intersite RKKY and superexchange coupling driving the formation of the antiferromagnetic state. Finally, the energy scale may in turn be coherently suppressed in the metallic phase (Tahvildar-Zadeh *et al.* [1996]).

Two-particle Properties

Because of the local character of the problem, great simplification also results for two-particle properties (Pruschke *et al.* [1995], Georges *et al.* [1996]). Specifically, the irreducible interaction functions for particle-hole and particle-particle propagators become momentum independent. This makes evaluation of the magnetic susceptibility and $s-wave$ pairing susceptibilities particularly straightforward. Any quantity which involves off-site vertices, such as the conductivity (current vertex) or a $d-wave$ pairing susceptibility will be formally of order $1/d$. In the case of the conductivity, the diagram can still be evaluated, but the local character of the interaction implies that no vertex corrections will arise to leading order in $1/d$. To see this, consider the lowest order vertex correction, illustrated in Fig. 115. Momenta which arise on each side of the diagram will be independently summed, and the interaction function entering the vertex correction is independent of momentum, so that factors of $\sum_{\vec{k}} \vec{k}$ will be present in the conductivity. This will vanish. Hence, only the bubble diagram need be retained in a calculation of the conductivity.

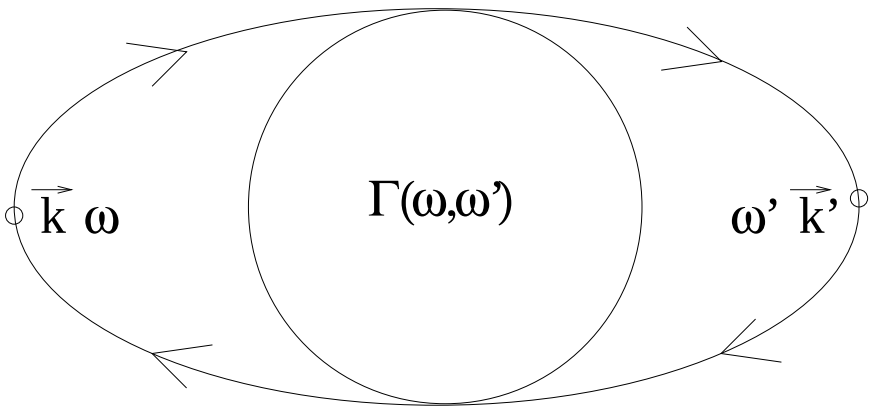

Figure 115: Conductivity vertex correction in $d = \infty$. The interaction vertex is momentum independent, and as a result, only the bubble diagram (with fully dressed electron propagators) need be retained.

Application to the Two-Channel Kondo Lattice Model

The two-channel Kondo lattice model is amenable to such a treatment in infinite dimensions. In the simplest form of this model we simply have two degenerate bands of electrons which have identical coupling to the local moments $\vec{S}_I(\vec{R})$ located on every site of the lattice $\vec{R}$, *viz.*

$$\mathcal{H} = \sum_{\vec{k}\sigma\alpha} \epsilon_{\vec{k}} c^\dagger_{\vec{k}\sigma\alpha} c_{\vec{k}\sigma\alpha} + \mathcal{J} \sum_{\vec{R}} \vec{S}_I(\vec{R}) \cdot \sum_{\vec{k}\vec{k}'\mu\nu\alpha} e^{i(\vec{k}-\vec{k}')\cdot\vec{R}} \vec{S}_c|_{\mu\nu} c^\dagger_{\vec{k}\mu\alpha} c_{\vec{k}'\nu\alpha} \tag{9.3.10}$$

where $\vec{S}_c$ are spin 1/2 matrices in the conduction space. This model is unrealistic in the sense that it is impossible for two spin 1/2 bands to be degenerate throughout the Brillouin zone; however, we will see that this lack of degeneracy is irrelevant in the infinite dimension limit.

In the two-channel Kondo model considerable attention has been paid to the conductivity, motivated in large measure by the data for UBe_{13} discussed in Sec. 8.2. An initial effort with a Lorentzian density of states for which self-consistency of Eq. (9.3.2) is trivial showed that the paramagnetic state of this model should be an incoherent metal. Namely, the resistivity would be finite and the density of states finite if the paramagnetic phase is extrapolated to $T = 0$ (Cox [1996]). Concommitant with this residual resistivity is a residual resistivity which may be shown to be $R/2 \ln 2$ per site at half filling of the conduction bands. It was further argued that application of a "spin field" (a field which couples linearly to the local moment spin operators) or a "channel field" (which linearly couples to the conduction electron channel spin) would restore a phase shift description at zero temperature and hence induce a crossover to Fermi liquid behavior. Because the Lorentzian density of states is automatically self consistent, these crossovers would lead to the same arguments in scaling functions for physical properties that occur in the impurity limit. Specifically, the crossover temperature is proportional to the square of either applied spin or channel fields. Non-trivial self consistency in infinite dimensions (due to, e.g., a starting Gaussian density of states) will not modify the fixed point structure of the effective impurity problem but will generically lead to self-consistent modification of the *next-leading* critical behavior. Thus, for example, we would not expect the zero temperature amplitude of the t-matrix to be modified in the particle-hole symmetric case, but we may well expect the T, H dependent corrections to be modified. This appears to be the case as we argue below for the magnetoresistance.

This unusual behavior may be traced back directly to the behavior of the single particle t-matrix at the Fermi energy, which is purely imaginary and half the unitarity limit. As discussed in Sec. 8.3, this calculation indicates that: (i) the application of a field which couples linearly to the spin degrees of freedom or a field which couples linearly to the channel degrees of freedom will induce a crossover to the Fermi liquid state, (ii) the residual scattering may be understood as corresponding to "spin-disorder" scattering off the degenerate two-channel Kondo clouds. In the absence of a phase transition which

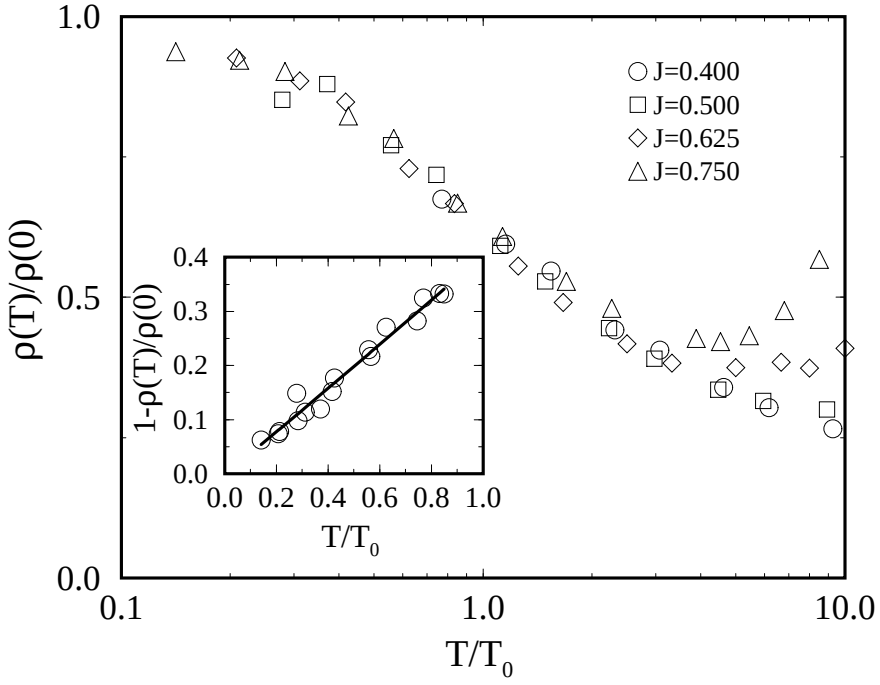

Figure 116: Resistivity of the two-channel Kondo lattice in infinite spatial dimensions at half filling. The four different curves are four different J values as indicated. The best fit to the lower temperature data is with a linear in T behavior, as indicated in the inset. From Jarrell, Pang, Cox, and Luk [1996].

either orders the moments or induces superconductivity, there must be a residual resistivity analogous to that of Gd metal above its Curie point (Cox and Jarrell [1996]).

Since the Lorentzian density of states has unphysically long tails in energy and hence infinite moments in powers of the frequency, this result understandably met some skepticism in the community. Accordingly, a study with a more physical density of states was required to convincingly prove the result.

Quantum Monte Carlo (QMC) studies with a nearest neighbor tight binding model (with a Gaussian DOS) were first carried out by Jarrell *et al.* [1996a], and these studies reached the same conclusion as for the Lorentzian density of states: the resistivity at the Fermi energy is finite, along with the density of states, which develops a cusp at $T \to 0$. Resistivity calculations from this work (at half-filling) are displayed in Fig. 116 (note the scaling behavior for curves computed with different exchange coupling values $\mathcal{J}$; note also that J of Jarrell *et al.* [1996a] corresponds to $\mathcal{J}$ here). The QMC code was based upon the Hirsch-Fye algorithm (Hirsch and Fye [1986]) as modified by Fye [1986] for the Kondo model. Calculation of real frequency properties was carried out with the maximum entropy method for analytically continuing imaginary time data to real frequencies. It should be noted that the low temperature resistivity appears linear in T to an excellent approximation, which is in reasonable agreement with experiments on a number of materials. In the temperature range covered by the QMC, the resistivity appears to monotonically increase with decreasing temperature. There are reasons to believe that this may shift, at least at lower temperatures, away from half-filling. We discuss this point further below.

Corollary results include:

(i) A residual entropy (at half filling) of $(R/2)\ln 2$ per site. This implies that the same "spin-disorder" scattering interpretation of the preceding paragraphs holds in this more physical case as well.

(ii) An absent Drude peak in the optical conductivity at low temperatures (there is a "charge fluctuation"

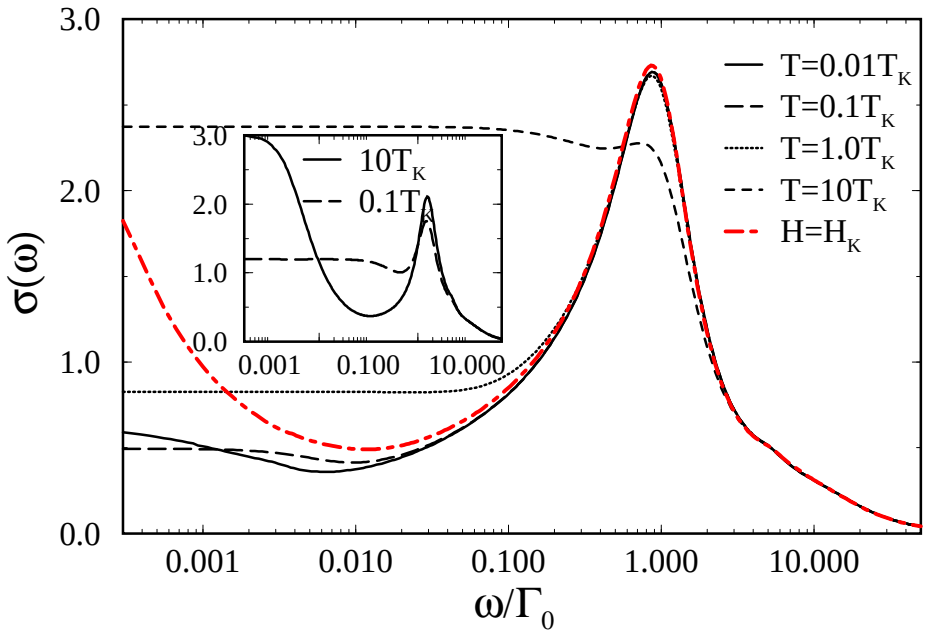

Figure 117: Conductivity of the two-channel Anderson lattice in infinite dimensions in zero and applied magnetic field. The model parameters assure a mapping of the effective impurity model to a Kondo model. Application of a magnetic field restores a Drude like peak. From Anders, Jarrell, and Cox [1997].

peak at energies of the order of $\mathcal{J}$) (Fig. 117). These results for zero field appear to be in excellent agreement with the optical conductivity data for UBe_{13} (Degeorgi [1997]).
(iii) The occupancy function $n(\epsilon_{\vec{k}}, T)$ saturates to a temperature independent *non-step function* form at low T, with a width fixed by the scattering rate of the conduction electrons.
(iv) a finite imaginary part to the conduction electron self energy which immediately implies (through Kramers'-Kronig analysis) that the real part has a *positive* slope in the vicinity of the Fermi energy. This in turn implies that the "mass enhancement" $1-\partial Re\Sigma/\partial\omega|_0$ can be less than one and possibly negative. Taken together with (iii) above, we see that Fermi liquid theory has broken down very severely for this lattice system. (Note that this breakdown implies the usual Fermi liquid relation between specific heat and mass enhancement also breaks down, so heavy fermion behavior is not excluded.)

In addition to these interesting features, the lattice calculations reveal a "coherent enhancement" of the Kondo scale over the impurity limit. Roughly, it is found numerically that $T_0^{latt} \approx E_F(T_0^{imp}/E_F)^{1/\sqrt{\pi}}$. The QMC was unable to reach temperatures below $\simeq 0.1T_0^{latt}$ due to a combination of the familiar fermion sign problem and the L^3 scaling of running time with the number of time slices L.

Magnetoresistance of the Two-Channel Kondo lattice

Anders *et al.* [1996] have studied the magnetoresistance of the two-channel Kondo lattice in infinite dimensions. This is a difficult problem to solve with the QMC approach, particularly at low temperatures of order $\mu_B H/k_B$ where the magnetic field H induces pronounced effects. Accordingly, Anders *et al.* [1996] opted for the Non-Crossing Approximation (NCA) to solve the effective impurity model. As argued in Sec. 5, the NCA provides a reliable method for calculating properties of the overcompensated multichannel impurity models, in particular giving exactly the right critical exponents for all $SU(M) \otimes SU(N)$ models, and providing amplitudes correct to within 7% for the resistivity and residual entropy of the two-channel spin 1/2 model ($N = M = 2$). The NCA is not well suited to a Fermi liquid regime, but does correctly describe the crossover region of the multichannel model in applied spin and channel

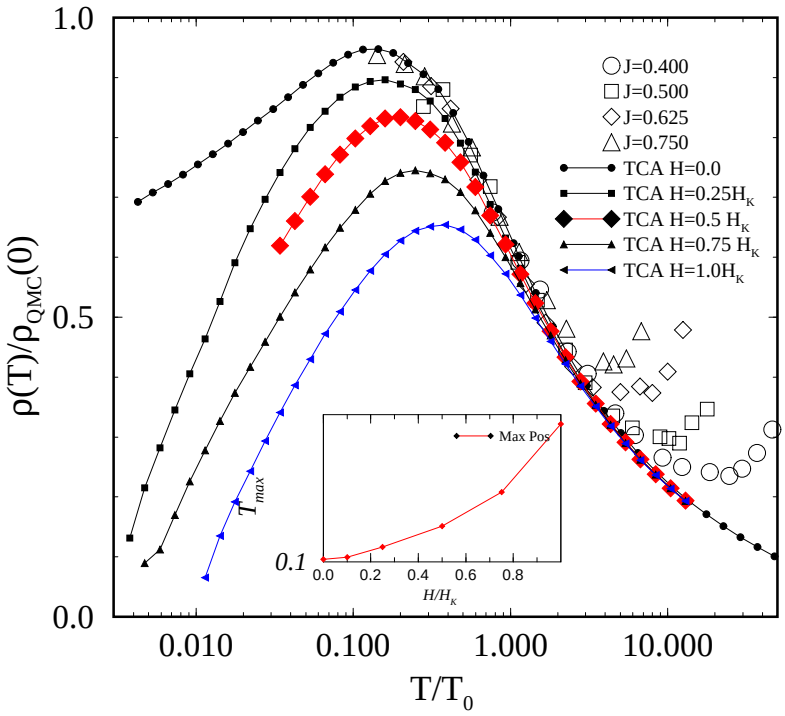

Figure 118: Magnetoresistance of the two-channel Anderson lattice in infinite dimensions in the Kondo regime. Application of a field reduces the residual resistivity driving the system towards Fermi liquid behavior. The points are from the quantum Monte Carlo data of Jarrell *et al.* [1996] and Fig. 116. From Anders, Jarrell, and Cox [1997].

fields, as discussed in Sec. 5.

The NCA approach actually solves the two-channel Anderson lattice model, in which a ground configuration "spin" doublet hybridizes through a quartet of conduction states (possessing spin and channel indices) with an excited configuration "channel" doublet. This corresponds to the lattice generalization of the 3-7-8 model of Eq. (2.2.20). The restriction to two configurations assures that particle-hole symmetry is broken, equivalent to moving away from half-filling in the pure Kondo lattice case.

The NCA results for the magnetoresistance are shown in Fig. 117 First, focussing on the $H = 0$ curve, it is clear that it agrees well with the QMC results in the region above $\simeq 0.1T_0$. Below this an interesting dip in the resistivity arises. This is attributed by Anders *et al.* [1996] to the breaking of particle-hole symmetry by the NCA together with the self-consistent development of a downward cusp. The resistivity still extrapolates to a finite value as $T \to 0$.

In applied field H, the resistivity drops dramatically, and in fact, the extrapolated resistivity is negative. This is taken as a sign that a crossover to a Fermi liquid is being induced, since the T^2 curvature of the Fermi liquid resistivity would lead to a negative intercept for a linearly extrapolation from the crossover regime. The magnetoresistance obeys an approximate scaling form, $[\rho(T,H) - \rho(T,0)]/\rho(T,0) \approx f[H/(T + .006T_0)^{.39}]$, where $f(x)$ is a monotonic decreasing function of x. Concommitant with this resistivity drop is the inducement of a Drude like feature in the optical conductivity near zero frequency and well below the charge transfer peak. Hence, as argued for the Lorentzian case, a return to Fermi liquid behavior in applied spin field is strongly suggested. However, the approach to this Fermi liquid fixed point is significantly different in *quantitative* detail from the analysis of the Lorentzian case, due to the effects of lattice self consistency in infinite spatial dimensions.

9.4 Pairing Effects

In this subsection, we examine the possibility of pairing generated by the local moment fluctuations of the two-channel Kondo model. The idea is intuitively clear as noted long ago by Cox [1990] (see also Cox and Jarrell [1996]). Namely, if one examines the basic renormalization group picture of Fig. 48, it is clear that at each length scale, the effective impurity at the core has a pair of electrons in a spin triplet, channel spin singlet state. In a first study using conformal theory, Ludwig and Affleck [1991] were unable to find evidence for such a triplet pairing correlation and rather found an unusual singularity in the channel for spin singlet, channel-spin singlet, *odd-in-radial-parity*. Because the *odd-in-radial-parity* does not readily translate into a local pair correlation in a realistic model, it remained unclear whether local pairing correlations could plausibly arise in the two-channel Kondo impurity model.

The simplistic picture of triplet pairing is not totally wrong, as first clarified by Emery and Kivelson [1992] using their Abelian bosonization method. The resolution lies in the understanding that the triplet pair is in *correlation* with the local moment spin at the core of the RG picture. This unusual pair field/spin correlation is then a net spin singlet (i.e., it transforms as a scalar under the $SU(2)$ rotations of the total spin of the system). As such, it can mix with other spin-singlet, channel-spin singlet operators which also possess charge ± 2. The complete spectrum of such pair operators with singular susceptiblities was worked out in detail by Ludwig and Affleck [1994] using conformal field theory. The primary viable candidate for such an operator is an *odd-frequency* pairing state, which, put another way, has a node in the relative time coordinate of the electron pair. This possibility of odd-frequency pairing has independently received considerable attention as a candidate for novel superconductivity in real materials (Balatzky and Abrahams [1992]; Balatzky *et al.* [1994]; Coleman, Miranda, and Tsvelik [1993,1994]; Heid [1996]; Heid *et al.* [1995,1996]; Jarrell, Pang, and Cox [1997]).

Given a mechanism for generating strong local pairing correlations for a single impurity, one is tempted to view this result as a kind of Cooper problem in real space for the lattice. Namely, assuming the correct interpretation of the strong local pair correlations to be the formation of a single pair about the impurity at $T = 0$, it is tempting to speculate that a lattice of two-channel Kondo sites may produce a superconductor provided the pairs are able to move coherently from site-to-site. Evidence for just such a superconductor has been found in the extreme limits of one-dimension (Zachar, Kivelson, and Emery [1996]) and infinite dimensions (Jarrell, Pang, and Cox [1997]; Cox and Jarrell [1996]).

Among the unusual properties of such an odd-frequency superconductor are that:
(i) the anomalous Green's function has no equal time expectation value and thus the gap function itself is *not* a suitable order parameter;
(ii) zone center (zero center-of-mass momentum) pairing is apparently at best *metastable* (Coleman, Miranda, and Tsvelik [1993,1994]; Heid *et al.* [1995,1996]; Heid [1996]) though this point remains controversial (Balatzky *et al* [1994]);
(iii) zone boundary (finite center-of-mass momentum) pairing is apparently stable (Coleman, Miranda, and Tsvelik [1993,1994]; Heid *et al.* [1995,1996]; Jarrell, Pang, and Cox [1997]);
(iv) the excitations of this system may be spectacularly unusual (one treatment predicts a gapless branch of Majorana or "real fermions" in the ordered state which has zero charge and spin at the Fermi energy but contributes to the specific heat–see Coleman, Miranda, and Tsvelik [1993,1994]);
(v) the superconductivity is intrinsically intertwined with the local non-Fermi liquid behavior in the lattice.

The plan of this subsection is to first review the impurity results for a diverging local pair field susceptibility (Sec. 9.4.1). Then we'll review a Pairing symmetry analysis useful for constructing phenomenological theories in the heavy fermion materials. This analysis not only gives the local symmetry of the pair wave functions but with the assumption of "negative pair hopping" consistent with the staggered pairing of item (iii) in the preceding paragraph identifies which point(s) in the Brillouin zone are likely for the center-of-mass momentum. In Sec.9.4.3 we will overview the status of understanding on odd-frequency pairing independent of the two-channel Kondo model. Finally, in section 9.4.4 we will describe the microscopic evidence for pairing in the two-channel Kondo lattice from studies in one- and

infinite-dimensions.

9.4.1 Overview of Odd-in-frequency Pairing

In this subsection we shall overview the salient features of odd-in-frequency pairing which are relevant to the subsequent discussion for the two-channel Kondo lattice. In order, we shall discuss: (1) Pauli Principle arguments allowing for odd-in-frequency pairs; (2) phenomenology for a non-singular pairing interaction; (3) equivalence of odd-in-frequency pairs to appropriately defined even-frequency and composite pair fields; (4) the likely instability of odd-in-frequency pairs with zero center-of-mass momentum; (5) the possible connection of composite pairs to Majorana fermions and 3-body fermionic bound states; (6) Evidence for odd-in-frequency pairing in other models.

(1) Pauli Principle Arguments allowing Odd-in-frequency Pairs.
The odd-in-frequency idea was first introduced by Berezinskii [1974] and later elucidated by Balatsky and Abrahams [1992]. Berezinskii was interested in unusual pairing possibilities for superfluid ^{3}He. The basic idea is simple. If we for the moment suppress channel degrees of freedom, a pair field operator at position $\vec{r}$ and imaginary time τ will, prior to any explicit symmetrization, have the form

$$P_{\mu\nu}(\vec{r},\tau) = \psi_\mu(\vec{r},\tau)\psi_\nu(0,0) \tag{9.4.1}$$

where μ,ν are spin indices. The conventional Pauli principle analysis suggests that we can identify allowed pairing symmetries by considering spatial parity P_R and "spin parity" P_S which is the sign of the pair wave function under exchange of the spin labels. This clearly gives the standard results that for $P_R = +$, corresponding to relative pair angular momentum $\ell = 0, 2, 4...$ for the pair, we must have $P_S = -$, or a spin singlet, and for $P_R = -$ corresponding to pair angular momentum $\ell = 1, 3, 5...$ we must have $P_S = +$ or a spin triplet pair.

Berezinskii [1974] noted that there is no reason to focus exclusively on spatial parity in considering the Pauli principle. Rather, we can also augment the conventional discussion with the notion of temporal parity P_T (sign under the exchange of the imaginary or Euclidean time argument). Note that application of temporal parity in Euclidean time is *not* the same as time reversal, a point of easy confusion. This notion is particularly apt for the two-channel Kondo impurity model given the conformal invariance at the fixed point: the real radial coordinate and the Euclidean temporal coordinate are equivalent, so there should be no practical difference between spatial and temporal parity in this sense. Odd temporal parity immediately translates to odd-in-(Matsubara)frequency pairs in exactly the same way that odd spatial parity translates to pair wave functions in momentum space which are odd under $\vec{k} \to -\vec{k}$.

With the new possibility of temporal parity, two new symmetry classes are opened up for pairing of electrons with spin 1/2. The P_T=+ case was already covered. For $P_T = -$, we may have spin singlet pairs ($P_S = -$) with *odd* angular momentum $\ell = 1, 3, 5....$ ($P_R = -$), or spin triplet pairs ($P_S = +1$) with *even* angular momentum $\ell = 0, 2, 4....$

The addition of the channel degree of freedom in the two-channel Kondo model generalizes this further. We can then discuss the possibility of oddness under channel exchange or P_{CH}, the "channel parity." The list of possible pair fields is as follows:

$P_R = +$,P_T=+,$P_S = +$,$P_{CH} = -$ (ℓ even,spin triplet,channel singlet);
$P_R = +$,P_T=+,$P_S = -$,$P_{CH} = +$ (ℓ even,spin singlet,channel triplet);
$P_R = -$,P_T=+,$P_S = +$,$P_{CH} = +$ (ℓ odd,spin triplet,channel triplet);
$P_R = -$,P_T=+,$P_S = -$,$P_{CH} = -$ (ℓ odd,spin singlet,channel singlet);
$P_R = +$,P_T=-,$P_S = -$,$P_{CH} = -$ (ℓ even,spin singlet,channel singlet);
$P_R = +$,P_T=-,$P_S = +$,$P_{CH} = +$ (ℓ even,spin triplet,channel triplet);
$P_R = -$,P_T=-,$P_S = -$,$P_{CH} = +$ (ℓ odd,spin singlet,channel triplet);

$P_R = -$,P_T=-,$P_S = +$,$P_{CH} = -$ (ℓ odd,spin triplet,channel singlet).

The odd-in-frequency pair field has an unusual property relative to an even-in-frequency pair field: it can have no equal time expectation value, and thus cannot by itself serve as an order parameter field. To see this, consider the case with no channel degrees of freedom which is a spin singlet, and thus we have the following anomalous Green's function in $\vec{k}, \omega$ space (repeated indices are summed):

$$F(\vec{k},\omega) = i\sigma^{(2)}_{\mu\nu} \int d^3r \int_0^\beta d\tau e^{i\vec{k}\cdot\vec{r}-\omega\tau} < T_\tau \psi_\mu(\vec{r},\tau)\psi_\nu(0,0) > \quad . \tag{9.4.1}$$

The Pauli matrix in front antisymmetrizes the pair amplitude. The numerator of this anomalous Green's function is, of course, just the "gap function" $\Delta(\vec{k},\omega)$, specifically

$$F(\vec{k},\omega) = -\frac{\Delta(\vec{k},\omega)}{\omega^2 + \epsilon_k^2 + \Delta(\vec{k},\omega)\Delta^*(\vec{k},-\omega)} = \frac{\Delta(\vec{k},\omega)}{\omega^2 + \epsilon_k^2 - |\Delta(\vec{k},\omega)|^2} \tag{9.4.2}$$

where we used the odd-in-frequency property to simplify the denominator and neglected the normal self energy contribution for simplicity. For an even in frequency superconductor, the squared gap term in the denominator enters with a positive sign. Since the denominator is even in frequency, we can see that the numerator must be odd in frequency given the assumed odd-in-frequency behavior of F. Now, if we invert the Fourier transform to find $\Delta(\vec{k},0)$ we see that

$$\Delta(\vec{k},0) = \frac{1}{\beta}\sum_{omega} e^{i\omega\tau}\Delta(\vec{k},\omega)|_{\tau=0} = 0 \tag{9.4.3}$$

which indicates that the gap function itself cannot serve as a suitable order parameter and rather some moment of the gap function with frequency is an appropriate order parameter.

For example, consider $d\Delta(\vec{k},\tau)/d\tau$. The time derivative operation is explicitly odd-in-temporal parity, cancelling the odd-in-temporal parity of the gap function. The derivative explicitly pulls down a factor of ω in the summand of Eq. (9.4.3) which allows the sum to be non-vanishing for $\tau \to 0$. This insertion of a time derivative is analogous to the insertion of a spatial form factor in the case of p- or d-wave pairing for $P_T = +$.

(2) Phenomenology for a non-singular pairing interaction.

Balatsky and Abrahams [1992], Abrahams [1992], Abrahams it et al. [1993], Balatsky *et al.* [1994], and Abrahams *et al.* [1995] have considered extensively the phenomenology of an odd-in-frequency superconductor which has a non-singular pairing interaction. Abrahams [1992] in particular considers a simple interaction form allowing for both s and p-wave pairs which is separable in incoming and outgoing electron energies and momenta

$$V_{\vec{k},\vec{k}'}(\omega_n,\omega_n') = -2\frac{\omega_n\omega_n'}{N(0)\Omega_c^2}[\lambda_0 + 3\lambda_1(\vec{k}\cdot\vec{k}')] \tag{9.4.4}$$

where Ω_c is a cutoff frequency for th mediating Boson (all interaction strength is assumed to die above the cutoff) and λ_0, λ_1 are assumed to be positive. Note that this interaction *can only be generated dynamically* so that there is practically no simple way to derive odd-frequency pairing from a mean field Hamiltonian in the spirit of the BCS approximation and Bogulubov theory.

With this simple interaction form, Abrahams [1992] shows that the Eliashberg equations can admit a solution with off-diagonal long range order in the p-wave channel between two temperatures $T_c^+ > T_c^-$. The condition for achieving superconductivity depends upon the relative strengths of the couplings λ_0 (which enters the normal self energy and therebye determines mass renormalization of the couplings and dynamical pairbreaking) and λ_1. Specifically, to develop p-wave spin singlet pairing requires $\lambda_1 > \lambda_0 + 1/4$, while to have a re-entrant normal phase ($T_c^- > 0$) requires $\lambda_1 < 1 + \lambda_0$. Perhaps

the most important aspect of these requirements is that the renormalization of the interaction strength by the normal self energy requires a critical coupling strength of the net attractive interaction to produce the odd-frequency pairing. In contrast, for a net attractive interaction even-in-frequency pairing can occur for arbitrarily small interaction strength. This result for odd-frequency pairing appears to be generically true for models with non-singular interactions.

Abrahams *et al.* [1993] consider the specific model examples of phonon mediated pairing and an effective interaction generated by the random phase approximation (RPA) for the Hubbard model. In the case of phonon mediated pairing, while an attractive odd-frequency interaction may appear, it cannot satisfy the constraints required to produce a superconducting transition at a finite temperature. In contrast, the RPA model interaction for the Hubbard model can produce an odd-frequency transition. They further argue that because of the pseudo-gap (away from the central coherent quasiparticle band) between the Mott-Hubbard sidebands, that $\partial\Sigma(\omega_n)/\partial\omega_n > 0$ over the majority of the energy range of the electronic fluctuations responsible for pairing. This allows for the renormalization factor $\lambda_0 \approx 0$ which makes odd-in-frequency pairing more plausible.

(3) Connection to Even-Frequency and Composite Pair Fields

One of the intriguing aspects of odd-frequency pairing is that the pair field can linearly mix with other operators containing even frequency pair fields of different symmetry. This fact was first noticed by Emery and Kivelson [1992] for the two-channel Kondo model. To illustrate the idea, we will restrict our attentions to this model.

With the notation introduced above, consider the pair field $P_{0;0}^{R+,T-}(\vec{R},\tau)$ given by

$$P_{0;0}^{R+,T-}(\vec{R},\tau) = \sigma_{\mu\nu}^{(2)}\sigma_{\alpha\beta}^{(2)}\Psi_{\mu\alpha}(\vec{R},\tau)\frac{\partial}{\partial\tau}\Psi_{\nu\beta}(\vec{R},\tau) \tag{9.4.4}$$

with Einstein summation convention implicit on the spin indices μ,ν and channel indices α,β. This operator creates a single odd-frequency pair at position $\vec{R}$ and Euclidean time τ. The point made by Emery and Kivelson [1992] is that the time derivative may be explicitly carried out through the commutator with the Hamiltonian of the fermion pair field operator.

For definiteness, let us model the kinetic energy of the electrons through a nearest neighbor tight-binding Hamiltonian, so that for a two-channel Kondo hypercubic lattice model we have

$$\mathcal{H} = -t\sum_{\vec{R},\vec{\delta},\mu,\alpha}\Psi_{\mu\alpha}^{\dagger}(\vec{R}+\delta)\Psi_{\mu\nu}(\vec{R}) + \frac{J}{2}\sum_{\vec{R}\mu\nu\alpha}\vec{S}_I(\vec{R})\cdot\vec{\sigma}_{\mu\nu}\Psi_{\mu\alpha}^{\dagger}(\vec{R})\Psi_{\nu\alpha}(\vec{R}) \tag{9.4.5}$$

where we assume the nearest neighbor vectors $\vec{\delta}$ are only positively directed. Given $(\partial\Psi/\partial\tau) = [\Psi,\mathcal{H}]$, the explicit evaluation of the time derivative in Eq. (9.4.4) gives

$$P_{0,0}^{R+,T-}(\vec{R},\tau) = -2tP_{0,0}^{R-,T+}(\vec{R},\tau) + 4J\vec{S}_I(\vec{R},\tau)\cdot\vec{P}_{1;0}^{R+,T+}(\vec{R},\tau) \tag{9.4.6}$$

where $P_{0;0}^{R-,T+}$ is an *odd-radial-parity, even-frequency* pair field given by

$$\begin{aligned} P_{0;0}^{R-,T+}(\vec{R},\tau) = \sum_{\vec{\delta}}[&\Psi_{\uparrow,+}(\vec{R},\tau)\Psi_{\downarrow,-}(\vec{R}+\vec{\delta},\tau) - \Psi_{\downarrow,+})(\vec{R},\tau)\Psi_{\uparrow,-}(\vec{R}+\vec{\delta},\tau) \\ &+ \Psi_{\downarrow,-}(\vec{R},\tau)\Psi_{\uparrow,+}(\vec{R}+\vec{\delta},\tau) - \Psi_{\uparrow,-}(\vec{R},\tau)\Psi_{\downarrow,+}(\vec{R}+\vec{\delta},\tau)] \quad , \end{aligned} \tag{9.4.7}$$

and $\vec{P}_{1;0}^{R+,T+}$ is a *spin-triplet even-parity, even-frequency* pair field with components

$$P_{1,1;0}^{R+,T+}(\vec{R},\tau) = \Psi_{\uparrow,+}(\vec{R},\tau)\Psi_{\uparrow,-}(\vec{R},\tau) \quad , \tag{9.4.8.a}$$

$$P_{1,-1;0}^{R+,T+}(\vec{R},\tau) = \Psi_{\downarrow,+}(\vec{R},\tau)\Psi_{\downarrow,-}(\vec{R},\tau) \quad , \tag{9.4.8.b}$$

and

$$P^{R+,T+}_{1,0;0}(\vec{R},\tau) = [\Psi_{\uparrow,+}(\vec{R},\tau)\Psi_{\downarrow,-}(\vec{R},\tau) + \Psi_{\downarrow,+}(\vec{R},\tau)\Psi_{\uparrow,-}(\vec{R},\tau)] \quad . \tag{9.4.8.c}$$

Eq. (9.4.7) describes a very peculiar pairing field, first suggested by Ludwig and Affleck [1991] (see also Ludwig and Affleck [1994]) about which a few words are in order. If one applies the full spatial parity operator to it, one discovers it is even in parity. Indeed, the closest construction to this field for the single channel Kondo model is the "extended s-wave pair field" which has the form

$$\sum_{\vec{\delta}} [\Psi_{\uparrow}(\vec{R},\tau)\Psi_{\downarrow}(\vec{R}+\vec{\delta},\tau) - \Psi_{\downarrow}(\vec{R},\tau)\Psi_{\uparrow}(\vec{R}+\vec{\delta},\tau)] \quad .$$

This field is both even in parity and even under exchange of sites $\vec{R}, \vec{R}+\vec{\delta}$. In fact, it is easy to demonstrate that the two operations are not distinct. However, for the field of Eq. (9.4.7), spatial inversion *does not* correspond to the exchange of sites, for which the field is manifestly odd. What is true is the following: if we understand that the combination of annihilation operators summed upon $\vec{\delta}$ for a given spin and channel destroys an "s-wave" symmetric (full crystal symmetry) electron state in the first shell of atoms about the indexed site $\vec{R}$, the operation of site exchange corresponds to the inversion operation about the midpoint of the one sided chain formed by applying the Lanczos tri-diagonalization procedure to the reference site. Namely, consider the effective one-dimensional chain first discussed by Wilson [1975] (*viz.*, Sec. 4.1). When considering the two-channel model, the inversion operator applied to the pair field of (9.4.7) (with inversion measured about the midpoint between the origin and the first Wilson "site" or "onion-skin shell") is precisely the same operator as site exchange. It is *not* however the full 3D parity operator. Indeed, discretizing the continuum form of Ludwig and Affleck [1991,1994] yields precisely the same result.

Overall, this connection of the odd-frequency pair field to the odd-radial-parity and composite pair fields is a rather remarkable result. Even though we are dealing with the bare Hamiltonian, and not that of the low temperature excitations about the fixed point, Eqs. (9.4.6-8) hint at the outcome of the conformal field theory. Namely, the even-parity, odd-frequency pair field linearly mixes with an even-frequency, odd-radial-parity pair field. This is an explicit real space reflection of the approximate conformal invariance of the free-fermion Hamiltonian for points on opposite sides of the Fermi surface. This follows since the tight binding Hamiltonian, linearized about the Fermi energy, will indeed resemble a light-cone Hamiltonian for points on opposite sides of the Fermi energy, with the Fermi velocity equal to the speed of light. Hence, spatial and temporal parity are seen to be equivalent operations on the pair fields. Also, the dot-product of the spin triplet field with the local moment indicates that the interactions with the local moments will produce composite pair fields as candidate order parameters which are "bound states" of the spin with the triplet pairs. The mixing with the odd-frequency is symmetry allowed since the inner product of the triplet field with the local moment operator produces an object that is a scalar under spin rotations. This result for the composite field of course has a beautiful correspondence to the NRG pictures of the two-channel Kondo fixed point, where at each length scale a core spin is correlated with a triplet conduction pair. Indeed, as argued in Sec. 6.1, the leading irrelevant operator about the two-channel fixed point continues to have the form of the interaction term in Eq. (9.4.3) with S_I replaced by the conformal primary spin field Φ_s.

We note that to the extent the effective electron-electron interactions remain local in position space, it is perhaps unlikely that the odd-radial-parity pair field will be the first to condense. The reason is that unlike the odd-frequency field which requires only a local attractive interaction for condensation, coupling to this field will require an interaction that is extended at least over a lattice constant–an extended discussion will appear later in Sec. 9.4.2 where it is noted that the odd-radial-parity field is rigorously excluded from condensation on the infinite dimensional two-channel (hypercubic) lattice. However, this point should be explored in greater detail numerically.

It appears overall, then, from the impurity model, that the likely candidate for an observable pairing correlation in the two-channel Kondo model is an odd-frequency, even-parity, spin-singlet,

channel-singlet pair field, or equivalently, a composite field consisting of a local moment bound to an even-frequency, even-parity, spin-triplet, channel singlet.

(4) Apparent Instability of Odd-Frequency Pairing for $\vec{q}$=0 Pairs.

Two theoretical works point the the possibility that odd-frequency pairing is actually unstable for pairs with zero center of mass momentum q, at least to the extent that a the solutions reside within Eliashberg-Migdal theory, i.e., the vertex corrections in the self energies and conductivity are negligible.

The most straightforward analysis is put forward by Coleman, Miranda, and Tsvelik [1993], who estimate the superfluid density close to T_c for an assumed $q = 0$ odd-frequency transition. The general form of the superfluid density or inverse penetration depth for $q = 0$ pairs close to T_c *in the absence of vertex corrections to the conductivity* is (suppressing momentum and other dependencies of the gap function)

$$\rho_s \sim \frac{1}{\lambda^2} \sim \sum_{\omega_n} \frac{\Delta(\omega)\Delta^*(-\omega)}{|\omega_n|^3} \tag{9.4.9}$$

where Δ is the gap function. For even-frequency pairing, this is positive definite. For odd-frequency pairing, it is negative definite. The interpretation of this result is straightforward: ρ_s is proportional to the curvature of the free energy with respect to the order parameter at $\vec{q}$=0 (or, in position space in the center of mass coordinates, to the coefficient of the gradient terms in the free energy). $\rho_s(q = 0) < 0$ simply implies that the uniform phase solution of the free energy is not stable. It does not rule out odd-frequency pairing. Another loophole in this conclusion is that the denominator is modified to $(\omega_n^2 - |\Delta(\omega_n)|^2)^{3/2}$ for finite Δ. If a discontinuous transition to finite Δ occurred with $|\Delta(\omega_n)| > |omega_n|$ for at least a few values of n, then $\rho_s(q = 0) > 0$ would be possible (Heid [1995]).

Heid [1995] pointed out another difficulty with $q = 0$ odd-frequency pairs as treated within Eliashberg theory. Employing minimal assumptions, he was able to show that within Eliashberg theory you cannot simultaneously lower the free energy and find a solution to the self consistency equations for $q = 0$ odd-frequency pairs. This means practically that the Eliashberg solutions are extrema but rather *maxima* of the free energy and not minima. Within a simple model, there appear to be no such restrictions on pairs with finite center of mass momenta (Heid [1995]).

The physical interpretation suggested by Coleman, Miranda, and Tsvelik [1993, 1994,1995] is that the phase of the odd-frequency pairs is staggered at the atomic level. This conclusion is model dependent, since strictly speaking the above mentioned instability only implies finite q pairing is favored, not necessarily zone boundary pairing.

Balatsky *et al.* [1994] and Abrahams *et al.* [1995] note that in the composite operator picture, the leading contribution to the anomalous conductivity diagram does in fact have a vertex correction. The leading order diagram is displayed in Fig. 119. The interaction is proportional to the local moment susceptibility. This diagram contributes *positively* to the $q = 0$ superfluid density. Hence, the possibility remains that in moving beyond Eliashberg-Migdal theory to include vertex corrections that $q = 0$ pairs may be stabilized.

(5) Connection to Three-body Bound States and Majorana Fermions.

Coleman, Miranda, and Tsvelik [1995] have noted on rather general grounds that odd-frequency pairing can result from the formation of "anomalous three body" bound states amongst fermions. This intriguing possibility rests on the potential to form Majorana fermion bound states. Because the Majorana fermions have constant squared amplitudes, it becomes possible to develop anomalous expectation values to three body Majorana bound states.

As a concrete example, Coleman, Miranda, and Tsvelik [1995] follow their earlier work (Coleman, Miranda, and Tsvelik [1993,1994]) and focus on a mean field theory for the single channel Kondo lattice.

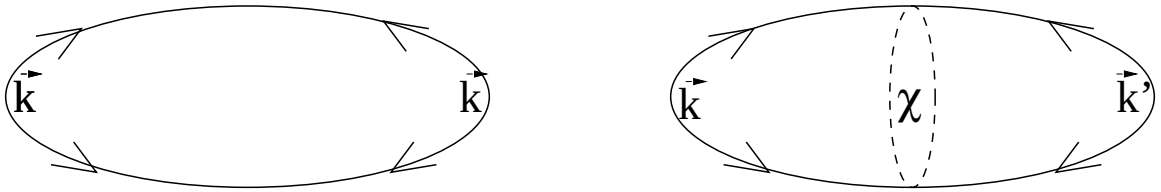

Figure 119: Leading order diagrams for the Meissner "stiffness" for odd-frequency superconductors. The Meissner stiffness, or "superfluid density" is proportional to this anomalous diagram of the electrical conductivity. The first diagram (at left) includes only renormalized anomalous propagators, and, as argued by Coleman, Miranda, and Tsvelik [1994] gives a negative superfluid density or Meissner stiffness for an odd-frequency superconductor with $\vec{q} = 0$ center of mass momentum. The second (at right) is the vertex correction discussed by Balatsky *et al.* [1994] and Abrahams *et al.* [1995] which is argued to enforce a positive sign to the Meissner stiffness for $\vec{q} = 0$ center of mass momentum pairing in which the composite order parameter representation is used. The dashed bubble appearing as a vertex is a spin susceptibility. Note that this diagram at right is ineffective (vanishes) for a purely local moment driven interaction, because the different momentum sums integrate to zero.

At a given site $\vec{R}$, the interaction term in the Hamiltonian takes the form

$$\mathcal{H}_K(\vec{R}) = \frac{J}{2}\vec{S}_I(\vec{R}) \cdot \sigma_{\mu\nu}\Psi^\dagger_\mu(\vec{R})\Psi_\nu(\vec{R}) \tag{9.4.10}$$

$$= const. \quad - J\xi^\dagger_\nu(\vec{R})\xi_\nu(\vec{R})$$

where the spinor field ξ is defined by

$$\xi_\nu(\vec{R}) = \vec{S}_I(\vec{R}) \cdot \sigma_{\mu\nu}\Psi_\mu(\vec{R}) \quad . \tag{9.4.11}$$

If we represent the local moment by a pseudo-fermion, we can see that ξ represents a composite field of three fermions. To produce a mean field theory, Coleman, Miranda, and Tsvelik [1995] make the ansatz that

$$-J\xi_\nu(\vec{R},\tau) = 2V_\nu(\vec{R})\hat{\phi}(\vec{R},\tau) + \ fluctuations \tag{9.4.12}$$

where V_ν is a c-number spinor field that serves as the mean field three body amplitude, and $\hat{\phi}$ is a Majorana fermion field.

The above transformation of the interaction term and mean field Ansatz do not immediately permit an approximate model solution. However, it is easy to show that the operators $\eta^a(\vec{R},\tau) = 2S^a_I(\vec{R},\tau)\hat{\phi}(\vec{R},\tau)$ obey the canonical anticommutation relation $\{\eta^a(\vec{R}), \eta^b(\vec{R}')\} = \delta_{ab}\delta_{RR'}$, and further, $(\eta^a)^2 = 1/2$, so the η^a are Majorana fermions. With the mean field Ansatz, this converts the interaction term on a given site into

$$\mathcal{H}_{K,MF}(\vec{R}) = [\Psi^\dagger_\mu(\vec{R})(\vec{\sigma}_{\mu\nu} \cdot \vec{\eta}(\vec{R}))V_\nu(\vec{R}) + h.c.] + \frac{2V^\dagger_\nu(\vec{R})V_\nu(\vec{R})}{J} \quad . \tag{9.4.13}$$

This mean field Hamiltonian hybridizes the three branches of Majorana fermions η^a with three of four Majorana fermion branches of the conduction electron fields. The unhybridized Majorana fermion remains so in the superconducting state, leaving a linear spectrum of excitations. Coleman, Miranda, and Tsvelik [1993,1994,1995] put forward the intriguing speculation that this corresponds to the observed linear specific heat coefficients below T_c in some heavy fermion superconductors.

Because the Majorana fermions are admixtures of electron and hole operators, the full solution breaks $U(1)$ gauge symmetry, i.e., it is a superconducting state. The energy is lowest for $V_\nu(\vec{R}) \sim \exp[i\vec{Q} \cdot \vec{R}/2]$, with $\vec{Q} = [\pi, \pi, \pi]/a$ in three dimensions. This is the phase of a single anomalous

three body fermion field–this implies that the phase of an anomalous Majorana pair is staggered, i.e., alternates with a periodicity determined by $\vec{Q}$ itself.

The presence of the Majorana field implies that because the Green's function of the η fields in the frequency domain goes as ω^{-1}, the gap function $\Delta(\omega) \sim V^2/\omega$. Namely, the gap function is *singular*. Although Coleman, Miranda, and Tsvelik [1993,1994,1995] do not construct an explicit realization of the effective fermionic interaction which can generate this anomalous gap function, one can infer that is must be an interaction which is singular in the incoming and outgoing relative frequencies of the pair.

The singular pairing amplitude implies that the usual BCS coherence factors have an unusual form in the superconducting state. Specifically, the gapless Majorana excitations have vanishing charge and spin at the Fermi energy. This implies that the vanishing matrix element will induce power law behavior in nuclear relaxation and ultrasound as observed in the heavy fermion systems, but leave open the possibility of non-vanishing linear specific heat coefficients and electronic Lorentz numbers in the superconducting state.

(6) Evidence for Odd-Frequency Pairing Correlations in Other Models

The mean field theory of Coleman, Miranda, and Tsvelik [1993,1994,1995] suggests that a natural model in which to look for odd-frequency pairing states is the single channel Kondo lattice model, or the closely related single channel Anderson lattice model. Unfortunately, searches in $d = \infty$ fail to produce any evidence for pairing in the Anderson lattice model except possibly at unphysically low fillings for the conduction band (Jarrell [1995,1997]). It must be emphasized that a possible reason the correlations are missed in this case is that in the spin singlet sector, the odd-frequency pair fields must have odd-parity, and hence live only at order $1/d$. In the spin triplet sector, it is possible in principle to have an order $(1/d)^0$ contribution in principle, but in practice, the Pauli principle will tend to legislate against this, favoring at least d-wave pairs which are again of order $1/d$. Zachar, Emery, and Kivelson have identified a special parameter region of the one-dimensional Kondo lattice model in which a spin gap develops as an example of where staggered, odd-frequency, spin-singlet pairing correlations are enhanced. In this region, the physics maps to a special version of two-channel Kondo lattice model because of the absence of back-scattering enforced by the spin gap. It remains to be seen whether these correlations can be made to survive in $d > 1$.

A possible understanding of this discrepancy between the $d = \infty$ results and the Majorana mean field theory lies in the nature of the differing fixed point physics between the one-channel and two-channel Kondo models. The mean field theory depends crucially on a decoupling of the spin-dependent interaction term of the single-channel model and assumes that this term is dominant in the low energy scale physics. However, for sufficiently large J, which suppresses antiferromagnetism and enhances the Kondo physics, the single channel model is described by a collection of Kondo singlets which become mobile away from half filling. Hence, the leading irrelevant operator about the low energy fixed point are not likely to be of the exchange interaction form required in the Majorana mean field theory. On the other hand, in the two-channel Kondo lattice the leading irrelevant operator about the paramagnetic fixed point (which is a collection of two-channel impurity fixed points), at least in $d = \infty$, is in fact of the exchange interaction form. Hence, while the single channel model on this basis does not look like a candidate for odd-frequency pairing, the two-channel Kondo lattice looks rather promising. As detailed in Sec. 9.4.4, in $d = \infty$ at least, this possibility of odd-frequency pairing in the two-channel Kondo lattice is in fact realized.

Bulut, Scalapino, and White [1994] have demonstrated that the pairing vertex of the Hubbard model in two-dimensions calculated from Quantum Monte Carlo has maximum eigenvalues for pair amplitudes corresponding to even-frequency d-wave singlet pairs, and odd-frequency, p-wave singlet pairs. However, there is no indication of either eigenvalue reaching unity for the temperature range studied, which would indicate a superconducting transition.

9.4.2 Local Pair Field Susceptibility

The possibility of a truly divergent pair field susceptibility in the two-channel Kondo model was first worked out by Ludwig and Affleck [1991,1994] using conformal field theory. The actual calculation of the pair field susceptibilities within the conformal theory is a *tour de force* in the formalism. We shall not discuss the details of these calculations here but rather summarize and overview the resulting physical picture.

To see the possibility of a diverging pair field susceptibility, it is helpful to recall our discussion of the scaling dimensions of possible operators discussed in Sec. 6.1.2.b. For a pair field operator with charge $Q = \pm 2$, spin $S = 0$, and channel spin $S_{ch} = 0$, the scaling dimension is $Q^2/8 + S(S+1)/4 + S_{ch}(S_{ch}+1)/4 = 1/2$. This implies that the corresponding local pair field susceptibility must have a logarithmic divergence as $T \to 0$.

However, the antisymmetry in spin and channel degrees of freedom requires that we antisymmetrize in some other variable to satisfy the Pauli principle. Let us denote the pair field operators by capital $P^{R\lambda,T\gamma}_{S;S_{ch}}$, where $\lambda = \pm, \gamma = \pm$ and the R, T refer to spatial and temporal parity. The Pauli principle requires that the product $P_R P_T P_S P_{ch} = -1$ where P_R is spatial parity, P_T is temporal parity, P_S is spin parity (symmetry under spin exchange), and P_{ch} is channel parity (symmetry under channel exchange). The first guess implemented by Ludwig and Affleck [1991] was to choose a pair field of the conduction electrons *odd* in the one dimensional spatial coordinate about the origin. Specifically, they chose to effect this by inserting a spatial derivative into the pair field operator (using the notation of Sec. 6.1.1) as given by

$$P^{R-,T+}_{0;0}(r,\tau) = \epsilon_{\mu\nu}\epsilon_{\alpha\beta} c_{\mu\alpha}(r,\tau)\frac{\partial}{\partial r} c_{\nu\beta}(r,\tau) = 2ik_F \Psi_{L\mu\alpha}(r,\tau)\Psi_{R\nu\beta}(r,\tau)\epsilon_{\mu\nu}\epsilon_{\alpha\beta} \tag{9.4.14}$$

which shows that the radial parity gets translated into antisymmetry under exchange of left and right fields. Note that $\epsilon_{ij} = i\sigma^{(2)}_{ij}$ is the two-dimensional antisymmetric matrix, and that we have employed Einstein summation convention in the above equation. Ludwig and Affleck [1991,1994] then showed that this operator does indeed give a local susceptibility which is log divergent.

However, there is a physical problem with this particular operator when reconnected to the full three dimensional physics. When discretized, this operator corresponds the amplitude of the spin-singlet, channel-singlet pair field operator described by Eq. (9.4.7). At the local level, because the operator is off-site, the on-site irreducible vertex will allow no coupling. If we consider the extension to the two-channel Kondo lattice, as considered in Fig. 120, Fourier transformation gives a form factor of $\sum_{i=1}^{d} \cos[(k_i + Q_i)a]$ for pairs with CM momentum $\vec{Q}$. Because the irreducible vertex function, which enters the bound part of the pair field susceptibility, is purely local in either the impurity limit or lattice limit, the momenta sums on either side of the lowest order "bound" correction are independent, and the integral of the cosine sum vanishes. We note that the argument hinges in detail upon the assumption of momentum independent exchange or hybridization vertices on-site–it is conceivable that non-zero contributions may arise from inclusion of a more realistic momentum dependence to the hybridization, but these would be likely smaller in magnitude than the purely on-site contribution of the odd-frequency pair field. More numerical work is in order to assess the importance of this pair field in these more realistic circumstances.

One corollary which is, in retrospect, obvious is that one may equally well insert a time derivative as a space derivative into the singlet pair field operator in view of the conformal invariance of the fixed point and the ensuing space-time equivalence. This procedure completely circumvents the problems with the radial derivative mentioned above. This time derivative pair field operator is

$$P^{R+,T-}_{0;0} = \epsilon_{\mu\nu}\epsilon_{\alpha\beta} c_{\mu\alpha}(r,\tau)\frac{\partial}{\partial \tau} c_{\nu\beta}(r,\tau) \quad . \tag{9.4.15}$$

Ludwig and Affleck [1994] considered this field as well as the composite operator which linearly mixes with this time derivative field as discussed in the previous subsection and below.

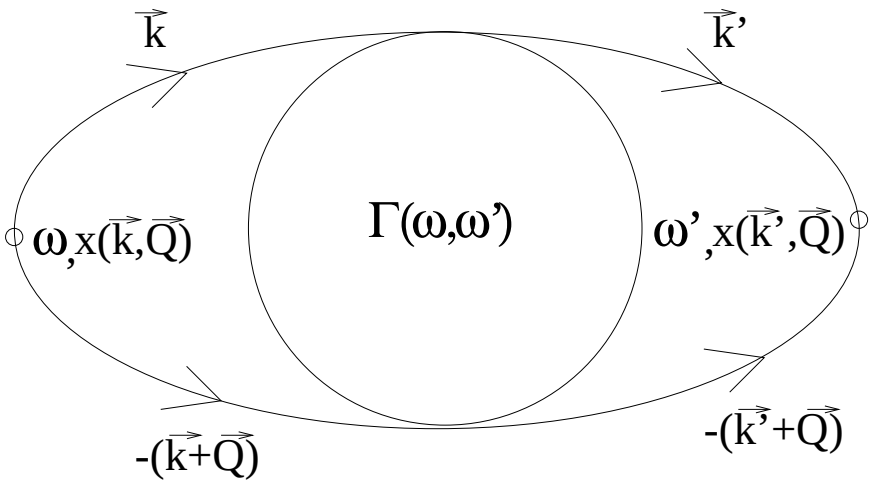

Figure 120: Inefficacy of odd-radial-parity pairing for a local pairing interaction and presumed momentum independent hybridization/exchange between conduction electrons and local electrons. This Feynman diagram represents a contribution to either the full lattice pairing susceptibility for pairs with center of mass momentum $\vec{Q}$ in the local approximation or $d = \infty$ limit, or a term in the local pairing susceptibility for the impurity. This local susceptibility is acquired by summing over $\vec{Q}$. Similar to the conductivity diagram of Fig. 114, the locality of the interaction together with the $x(\vec{k}, \vec{Q}) = \sum_i \cos[(k_i + Q_i)a]$ dependence of the vertices guarantees that this contribution must vanish. This term wou

However, the first consideration of the equivalent composite operator field was by Emery and Kivelson [1992,1994] using the Abelian bosonization approach, which we turn to next. Emery and Kivelson first considered the composite operator formed from the dot product of the local moment spin with the three components of the spin triplet pair field $P^{R+,T+}_{1,m;0}$ where $m = \pm 1, 0$ indexes the spin component. As discussed in the previous subsection and by Emery and Kivelson [1994], this is equivalent Because the starting model breaks the $SU(2)$ spin symmetry to a $U(1)$ symmetry about the z-axis, it is sufficient to consider the composite operator (evaluated at the origin now where $\psi_{L\mu\alpha} = \psi_{R\mu\alpha}$)

$$\tilde{P} = \tau^z P^{R+,T+}_{1,0;0} = -i\hat{a}\hat{b}[\psi_{L,\uparrow,+}\psi_{L,\downarrow,-} + \psi_{L,\downarrow,+}\psi_{L,\uparrow,-}] \tag{9.4.16}$$

$$= -i\hat{a}\hat{b}\psi_c(\psi_{sf} + \psi^\dagger_{sf})$$

where we are using the notation of Sec. 6.2.1. Recall that $\hat{a}$ is the de-coupled local Majorana fermion of the impurity spin field, $\hat{b}$ is the local Majorana degree of freedom which couples to the conduction electrons, ψ_c is the charge fermion degree of freedom obtained from refermionization of the charge boson field, and ψ_{sf} is the spin-flavor fermion field which is obtained from refermionization of the spin-flavor boson field.

The calculation of the pair field susceptibility associated with $\tilde{P}$ is given by the expression

$$\chi_{\tilde{P}\tilde{P}}(T) = \int_0^\beta < \tilde{P}(\tau)\tilde{P}^\dagger(0) > \quad . \tag{9.4.17}$$

Emery and Kivelson argue that the leading singular term of the correlation function in the above integral goes as 1τ for large times. The argument goes as follows: first, for positive times, the Green's function of the $\hat{a}$ field $G_a(\tau)$ is just constant, i.e., we can just view $\hat{a}$ as a constant of the motion (*c.f.* Eq. (6.2.28)). Second, because the combination $\hat{b}(\psi_{sf} + \psi^\dagger_{sf})$ is precisely the combination that enters the effective resonant level Hamiltonian of Eq. (6.2.19), we may view this too as a constant of the motion and extract it from the expectation value. A more precise way of putting this is that when we perform the possible Wick contractions, because of the special character of Majorana fermions this factor is an

allowed contraction. A corresponding contraction for complex fermion fields would generally not be possible (except in a superconducting state). Contraction of $\hat{b}(\tau)(\psi_{sf}+\psi^{\dagger}_{sf})(\tau)$ with $\hat{b}(0)(\psi_{sf}+\psi^{\dagger}_{sf})(0)$ will generate subleading singular corrections to $\chi_{\tilde{P}\tilde{P}}$. Finally, the remaining Green's function is just the charge fermion Green's function which behaves as $1/\tau$ for long times and so generates a log divergence.

We can evaluate $\chi_{\tilde{P},\tilde{P}}$ more precisely using the Green's functions of Sec. 6.2.2 and App. IV, and it is illuminating to do so. First, denote $\psi_{sf}+\psi^{\dagger}_{sf}=\chi_{sf}$ and put $\tilde{V}=iJ_x/\sqrt{\pi a}$ in Eq. (6.2.19) (this is the effective hybridization between $\hat{b}$ and χ_{sf}. Then the expectation value

$$(9.4.18) \qquad < \hat{b}\chi_{sf} >= - < \chi_{sf}\hat{b} >= \frac{\tilde{V}}{\beta N_s}\sum_k \sum_n \frac{1}{i\omega_n - v_F k}\frac{1}{i\omega_n + i\Gamma sgn\omega_n}$$

where $\omega_n = 2\pi(n+1/2)/\beta$ is a Fermion Matusubara frequency. Recall that $\Gamma = \pi N(0)\tilde{V}^2/2$ is the resonant level width, which is one kind of local Kondo scale in the approach. It is straightforward to evaluate this sum and obtain

$$(9.4.19) \qquad < \hat{b}\chi_{sf} > \approx \frac{[N(0)\tilde{V}]}{2}\ln[\frac{D}{\Gamma}]$$

where $N(0)/2 = 1/(4\pi v_F)$ is the Fermi level DOS of the χ_{sf} fields, and $D=2v_F$ is the bandwidth (cut-off) of the linear dispersion relation. Putting this together and using $G_c(\tau)\approx G_s(\tau)\approx 1/[\beta D\sin(\pi\tau/\beta)]$ we obtain

$$(9.4.20) \qquad \chi_{\tilde{P}\tilde{P}}(T) \approx \frac{1}{2\pi D}[\frac{N(0)|\tilde{V}|^2}{4}]\ln^2(\frac{D}{\Gamma})\ln(\frac{D}{T})$$

$$\approx \frac{1}{2\pi D}\frac{\Gamma}{D}\ln^2(\frac{D}{\Gamma})\ln(\frac{D}{T}) \quad .$$

Given that Γ measures the Kondo scale, the interesting point to notice about this susceptibility is that while it is log divergent, it is very small! The effective energy denominator is not T_K as appears in the log divergent spin susceptibility but rather D^2/T_K which is huge! Hence, at the impurity level, this is a terrifically small effect, only presumably visible at very, very low temperatures. In fact, Quantum Monte Carlo studies on the two-channel impurity model failed to reveal any hints of a logarithmic divergence (Pang and Jarrell [1995]). Nevertheless, as discussed in Sec. 9.4.4, a possibility for odd-frequency pairing does emerge in the lattice.

We close this subsection by noting that the local pairing vertex can be evaluated within the NCA discussed in Sec. 5. This program has been carried out by Cox and Ruckenstein [1997]. The diagram is shown in Fig. 121. Prior to a translation to the full physical subspace, the interaction strength for pairs with zero center of mass energy is manifestly antisymmetric in the exchange of either incoming or outgoing frequencies at low frequencies. The explicit asymptotic form valid for $|\omega|, |\omega'| << T_0$ is

$$(9.4.21) \qquad I(\omega,\omega') \approx -sgn(\omega)sgn(\omega')\frac{1}{8N(0)^2}\frac{1}{|\omega_>|}F(\pi/2,\frac{|\omega_<|}{|\omega_>|})$$

where F is the complete elliptic integral of the first kind, and $\omega_{>,<}$ are determined from the min, max of $|\omega|, |\omega'|$. It is clear that this interaction form is singular and non-separable in the incoming and outgoing frequencies. To translate back to three dimensions in the heavy fermion case requires multiplication on the left by factors of $Y_{3m}(\hat{k})Y^*_{3m'}(\hat{k})$ where $\hat{k}$ is the direction of incoming momentum and on the right by corresponding factors in $\hat{k}'$,the direction of the outgoing momentum. The momentum dependence arising from this may allow for some small contribution to the odd-radial-parity pair field discussed by Ludwig and Affleck [1991,1994], but a test of this requires explicit numerical calculations for a more realistic model.

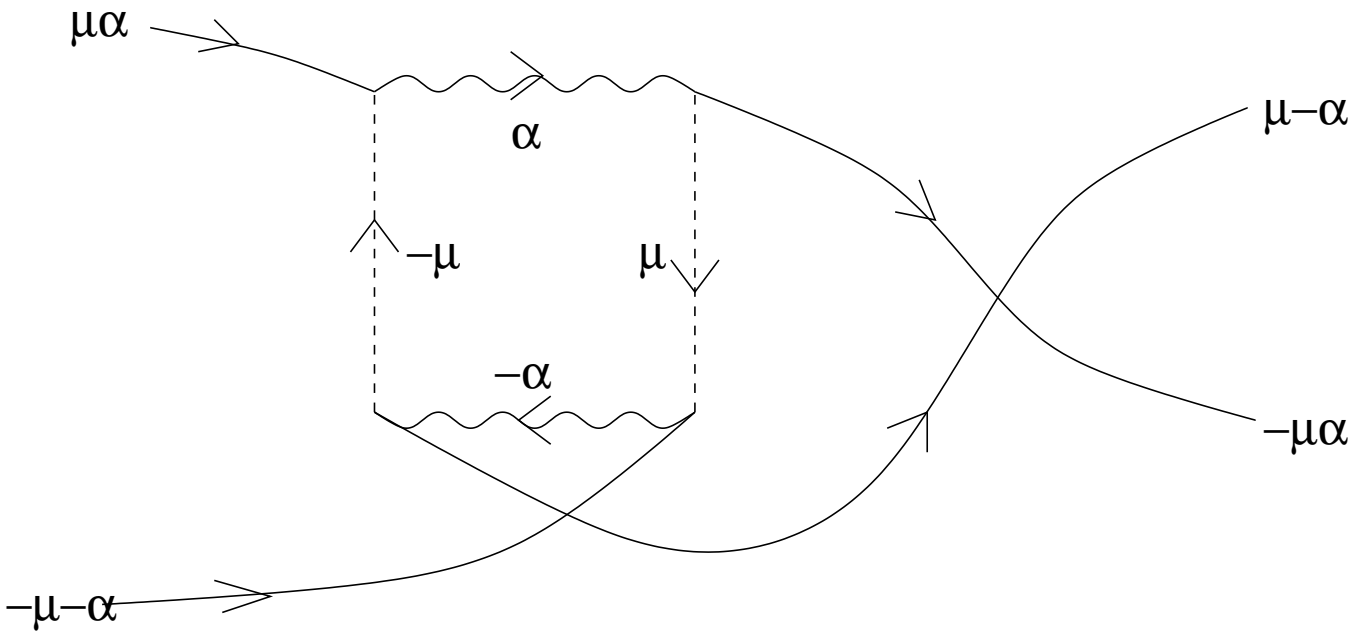

Figure 121: On-site interaction vertex from the NCA for the two-channel Anderson model in the Kondo limit. Each wavy line is an excited configuration propagator, carrying the channel index α, each dashed line a ground configuration propagator carrying the spin index μ. Solid lines are external conduction legs, put in for illustrative purposes.

Ion	**Group**	P_{00}	ν
U^{4+}	O	$\Gamma_2 \sim (x^2-y^2)(y^2-z^2)(z^2-x^2)$	2
Ce^{3+}	O	$\Gamma_2 \sim (x^2-y^2)(y^2-z^2)(z^2-x^2)$	1
U^{4+}	D_6	$\Gamma_2 \sim (x^3-3xy^2)(y^3-3yx^2)$	2
Ce^{3+}	D_6	$\Gamma_2 \sim (x^3-3xy^2)(y^3-3yx^2)$	3
U^{4+}	D_4	$\Gamma_2 \sim xy(x^2-y^2)$	3

Table 15: Symmetry of local spin-singlet, channel-singlet pair fields (P_{00}) and dimensionality ν of P_{00} space due to exchange anisotropy. From Cox and Ludwig [1997].

9.4.3 Pairing Symmetry Analysis

By identifying the physical correspondence of the spin and channel indices of the spin-singlet, channel-singlet pairs discussed in the previous subsection, one can identify the actual symmetry such pair correlations would display in a real material assuming that the two-channel Kondo model serves as an appropriate starting point. This information can then provide a useful input to phenomenological studies of odd-in-frequency pairing.

In the case of the Heavy Fermion materials, this symmetry analysis has been carried out by Cox and Ludwig [1997] for the two-channel model in the allowed symmetry groups as discussed in Sec. 2.2.4. We shall only briefly describe the method and results here, which are summarized in Table 15.

The logic is that regardless of whether the local pseudo-spin is magnetic or quadrupolar, one pair of conduction labels will be a magnetic pseudo-spin determined by the vector space of a doublet irrep of the double point group at the impurity site, and one pair of indices will be orbital/quadrupolar determined by a doublet irrep of the ordinary point group at the impurity site. On physical grounds, by analogy to the spin 1/2 problem, the magnetic pseudo-spin singlet should always transform as A_{1g},

i.e., have the full symmetry of the underlying group. This is indeed the case as explicitly verified from the tables of Koster *et al.* [1963]. On the other hand,the orbital singlet must change sign under any operations which interchange the orbitals, and these are indeed effected by ordinary point group transformations. The only viable candidate is the pseudo-scalar irrep, present for any point group (apart from triclinic) and notated by A_{2g}. As in the case of the magnetic pseudo-spin, it can be explicitly verified that this result for the orbital singlet holds for the cubic, hexagonal, and tetragonal point groups of interest. As a result, transformation properties of the overall singlet pair irrep under the local point group operations must be $A_{1g} \otimes A_{2g} = A_{2g}$.

The A_{2g} irrep generically must be composed of high order angular momentum states about the local moment site. For example, in cubic symmetry $A_{2g} \sim [x^2 - y^2][y^2 - z^2][z^2 - x^2]$ which minimally derives from $l = 6$ or i-wave pairs! Similarly, in hexagonaly symmetry, the A_{2g} state transforms as $(x^3 - 3xy^2)(y^3 - 3yx^3) \sim \sin[6\theta]$ where $\theta = \tan^{-1}[y/x]$, which is also of minimal i-wave character. Finally, in tetragonal symmetry, $A_{2g} \sim xy(x^2 - y^2)$ which is minimally of g wave character. We note that should such pair correlations drive a superconducting instability in the lattice, it is unclear how the complex nodal structure of the pair wave functions *locally* will affect the excitation spectrum. A complete theory of this must await a microscopic approach to the odd-in-frequency pairing state found (at least in $d = \infty$) for the two-channel Kondo lattice.

We close this section by noting that inroads on Ginsburg-Landau phenomenology of odd-in-frequency staggered superconductors can be made with the above result and an assumed "negative pair hopping" in real space consistent with the suggestion that the pairs prefer zone boundary momenta. With the local pair symmetry and with the negative pair hopping assumption, one can uniquely identify likely zone boundary momenta as free energy minima, and construct unique GL theories for all the heavy fermion superconductors. This program is in fact underway, initiated by the work of Heid *et al.* [1995,1996,1997] and Martisovits and Cox [1997]. A review of the phenomenology is beyond the scope of this article, but perhaps the most interesting features to emerge are:
1) For the frustrated hcp lattice of UPt_3, a degenerate *space group* irrep is favored which, in the presence of an ordered antiferromagnetic state, can fully account for the complex $H - vs. - T$ phase diagram of this material (Heid *et al.*, [1995,1996,1997]). In contrast, while a degenerage space group irrep is also favored for the 1-2-3 materials (UM_2Al_3, M=Pd,Ni) which have a simple hexagonal structure, there can be no degeneracy lifting coupling of induced (by a magnetic moment) or applied strain to the superconducting order parameter to all orders in the strain (Martisovits and Cox [1997]). This is consistent with the simple single phase diagrams observed for these materials.
2) In the two cases so far examined the presence of time reversal symmetry breaking can induce microcurrents and thus additional staggered magnetic moments in the material (Heid *et al.* [1996,1997]; Martisovits and Cox [1997]). For relative real phases between order parameter components, an induced charge density wave is possible. Observation of such induced staggered order would provide a spectacular confirmation of the staggered pairing hypothesis.

Finally, we note that superconductivity induced by the TLS Kondo effect has been suggested as a possibilty for A15 materials (T. Matsuura and K. Miyake [1986]; K. Miyake, T. Matsuura, and C.M. Varma [1989]; K. Miyake [1996]) and the cuprate superconductors (N.M. Plakida, V.L. Aksenov, and S.L. Drechsler [1987]; J.R. Hardy and J.W. Flocken [1988]; A.M. Tsvelik [1989]). Depending upon the nature of the anharmonic double well, a similar symmetry analysis should be possible for these models as well.

9.4.4 Superconductivity in the two-channel Kondo lattice

$d = \infty$ Limit

Given the residual entropy and correlated residual resistivity found in the two-channel Kondo lattice model in infinite dimensions by Jarrell *et al.* [1996,1997], it is natural to assume that in the absence of external symmetry breaking fields (c.f. Anders, Jarrell, and Cox [1997]) that the system

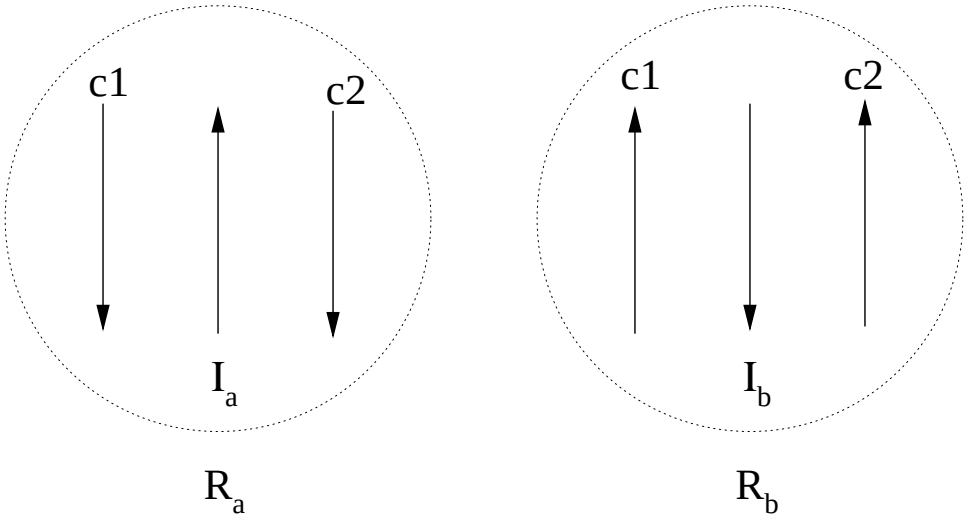

Figure 122: Screening clouds about adjacent two-channel Kondo sites in the lattice for strong coupling $J \geq E_F$, near half filling of each channel. The overall spins are antialigned because the Pauli principle prevents hopping for conduction electrons of equal spin, which gives rise to a superexchange $\sim (t^*)^2/J$.

will be driven to some spontaneous symmetry breaking to remove the residual entropy. Just such a possibility is found by Jarrell, Pang, and Cox [1997a,b], as we shall describe in this section.

Following Jarrell, Pang, and Cox [1997a,b], we note that in at least two regions of the phase diagram, there are very natural candidates for this symmetry breaking identified from the strong coupling limit ($J >> t$).

First, near half filling (unit occupancy of each channel) antiferromagnetism is certainly a favorable possibility. To see this, examine Fig. 122 which shows adjoining two-channel Kondo clouds in the strong coupling limit. The overall spin of the clouds is anti-aligned because of superexchange– by hopping an electron from channel one on site a to channel one on site b to form virtual singlets, followed by a subsequent hop of the original site b electron to site a, we see that the overall energy can be lowered by a factor $J_{eff} \simeq 4t^2/J > 0$. The positivity of this effective exchange assures that the coupling is antiferromagnetic. As usual, the Pauli principle favors antiparallel spin coupling in such a superexchange process.

Second, near quarter (half an electron per spin per channel) filling at strong coupling, in the absence of electron- electron interactions, it is favorable to form Kondo spin singlets at each site rather than two-channel spin doublets at every other site. The former gives an energy of $-3J/4$ per site, while the latter gives an energy of $-J/2$ per site. The addition of on-site interactions between electrons will further stabilize this state, while the addition of intersite density-density electrons will presumably help destabilize the singlets on every site. Neglecting interactions, we see that because the spin singlets are of necessity channel doublets, that there is an intrinsic degeneracy in the problem which the system would like to remove. Fig. 123 illustrates how this can occur via channel superexchange, in which a channel one electron at site a hops to site b to form a trivial local moment spin doublet at site a and a two-channel screened spin doublet at site b. The original channel 2 electron at b then hops to a. The energy lowering in the process is of order $J^{ch}_{eff} \simeq 4t^2/J$. The positivity of this effective exchange indicates that an antiferromagnetic pattern of channel spin is favored near quarter filling.

A priori, there is no reason to anticipate a substantial limitation of the boundaries of spin and channel ordering as a function of filling n, though experience with other models (the Hubbard model and Anderson lattice model, for example) suggest that the boundaries ought to be rather close to half(quarter) filling for spin(channel) ordering. If this is the case, the third law of thermodynamics would again bias us to look for some other kind of ordering in the intermediate fillings. Based upon the outlook of strong odd-frequency pairing correlations from the impurity model,it is natural to consider

Figure 123: Illustration of channel superexchange near quarter filling in the two-channel Kondo lattice for strong coupling. At quarter filling, singlets on every site are energetically favored over doublets on every other site. However, hopping is blocked for spins on adjacent sites in the same channel, while it is not blocked for spins in opposite channels. Hence, a channel superexchange of order $(t^*)^2/J$ results.

an instability to an odd-frequency superconducting phase.

Most of these above expectations are born out in the calculations of the phase diagram of the $d = \infty$ two-channel Kondo lattice model as studied by Jarrell, Pang, and Cox [1997a,b] with the same Quantum Monte Carlo method discussed in Sec. 9.3.2 in the work of Jarrell *et al.* [1996,1997]. The exception is that no strong evidence for channel spin ordering is found in the vicinity of quarter filling, though it may represent a possible secondary phase transition at very low temperatures.

To hunt for instabilities of the spin, channel, and pairing degrees of freedom, the corresponding susceptibilities were evaluated by Jarrell, Pang, and Cox [1996,1997]. These are shown in Fig. 124. The resulting phase diagram is shown in Fig. 125. The remarkable features resulting from this study are:
1) The antiferromagnetism persists for a rather large range away from half filling, and is commensurate except very close to the critical value of the filling where it becomes incommensurate. The antiferromagnetic transition temperature is a function of the bare coupling J, and for arbitrary fillings and coupling strengths, a combination of RKKY and superexchange couplings determine the overall transition temperature. It was not possible numerically to go to sufficiently large couplings to detect the $1/J$ behavior anticipated above.
2) The antiferromagnetism is peculiarly weak on two counts: a) only a very small singularity is observed in the total bulk staggered magnetic susceptiblity (it is quite strong in the local-moment-only contribution to the bulk susceptibility, and so Jarrell, Pang, and Cox [1997a,b] employed this to accurately identify the antiferromagnetic transition and critical behavior), and b) to within numerical accuracy, this singularity is characterized by a non-universal J dependent critical exponent $\gamma < 1$.
3) The line of temperatures T^* represents a *lower bound* on a *first order* superconducting transition to an odd-in-frequency pairing state in which the conduction electrons pair into spin-singlets, channel-singlets, and the pair wave function possesses even spatial parity. The specific value of T^* is determined by where the pair field susceptibility P_S in this channel *changes sign* as a function of temperature. As argued below, this must correspond to a lower bound for a first order phase transition.
4) The pair field susceptibility is computed for pairs with arbitrary center of mass momentum within the Brillouin zone. To within numerical accuracy, the temperature T^* at which $P_S(\vec{q})$ changes sign is identical for all $\vec{q}$ values. As argued later in this subsection, this is an artifact of infinite dimensions which will likely be removed at finite d in favor of a zone-boundary center of mass momentum for the pairs.
5) Quite remarkably, the temperature T^* goes as $C(J)T_0^{latt}$ where T_0^{latt} is the lattice Kondo tempera-

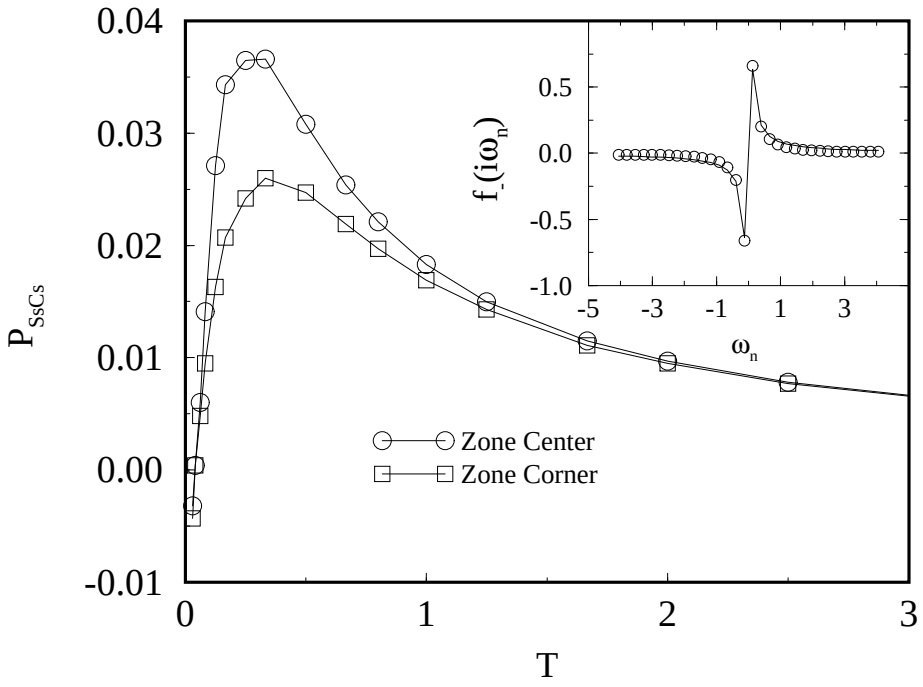

Figure 124: Pair field susceptibilities for the spin singlet, channel singlet, odd frequency (even parity) pairing channel in infinite dimensions. Susceptibilities for all momenta in the Brillouin zone go through zero at the same temperature, and, as argued in the text, this gives rise to a first order transition. From Jarrell, Pang, and Cox [1997].

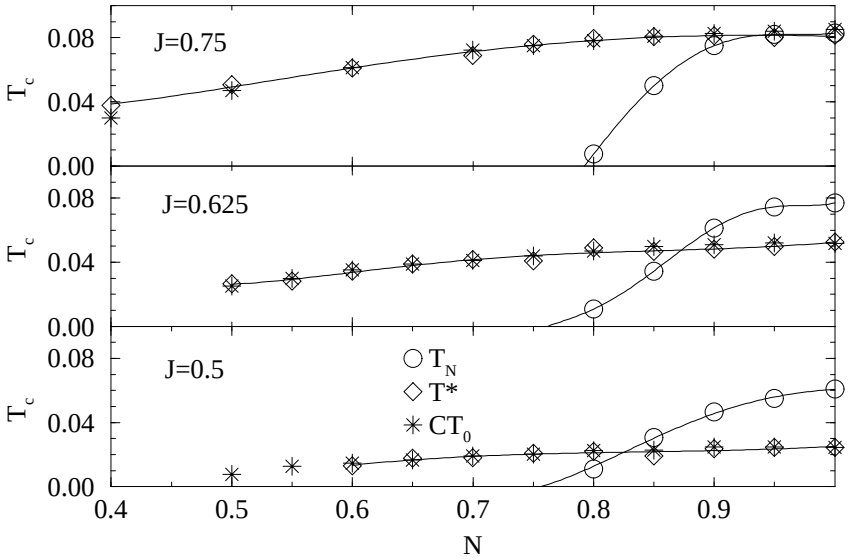

Figure 125: Phase diagram of the two-channel Kondo lattice in infinite dimensions. From Jarrell, Pang, and Cox [1997].

ture determined from a fit of the local susceptibility in the local moment channel to the single impurity results for each value of n, J. The prefactor $C(J) \approx 0.5$ is a weakly J dependent number. Since T_0^{latt} signifies the energy scale for formation of local *non-Fermi liquid* physics, this suggests an interpretation of the superconducting instability in terms of pairs best understood in real space and strongly associated to the non-Fermi liquid formation. This point of view is sharpened by the observation for at least $J < t$ that T^* is close to the temperature at which $Z = 1 - \partial Re\Sigma(\omega)/\partial\omega|_0$ changes sign, where Σ is the conduction electron self energy. In a conventional Fermi liquid, Z represents the dynamical mass enhancement of the quasiparticles. A negative value of Z certainly indicates a complete breakdown of the quasiparticle concept.

6) Though an examination of the staggered channel susceptibility with no coupling to pairing or spin degrees of freedom does indicate a narrow region about quarter filling where ordering is possible, the transition temperature for such ordering is very small compared to T^*, and so Jarrell, Pang, and Cox [1997a,b] focus instead upon the magnetic and superconducting order.

7) The frequency dependent form factor of the spin-singlet channel-singlet pair field which was found from the maximum eigenvector of the pairing kernel is singular in ω–it goes as $1/\omega$, in precise agreement with the result of Coleman, Miranda, and Tsvelik [1993,1994] obtained in a Majorana fermion mean field theory of the ordinary Kondo lattice. While this has a finite overlap with a pair field possessing a regular form factor in frequency (e.g., going as ω), the result suggests that it is necessary to have a singular interaction vertex to induce the pairing. This further suggests that the physical order parameter, while possessing an admixture of the time derivative pair field (which produces a form factor linear in ω in the frequency domain), is predominantly composed of more complicated non-local time operations in the time domain.

To further understand the results and motivation behind the numerical study, it is convenient to consider the problem from the point of view of Ginsburg-Landau (GL) mean field theory, though the numerical findings of Jarrell, Pang, and Cox [1997a,b] are more general than what is provided by this limited theoretical framework. The following presentation follows completely the more extensive work of Jarrell and Pruschke [1996], and Jarrell *et al.* [1997].

Consider the bulk free energy functional for a general scalar order parameter $O(T)$. It is given by

$$\mathcal{F}[O] \approx \frac{O^2(T)}{2\chi_O^{(1)}(T)} + bO^4(T) + cO^6(T) + ... \tag{9.4.22}$$

where $\chi_O^{(1)}$ is the static linear susceptibility corresponding to the order parameter O–for example, for antiferromagnetism it is the linear response coefficient relating the induced staggered magnetization to an applied staggered field. Of course, Eq. (9.4.22) is simplified in that if the order parameter is not a scalar we must generally add more terms. Also, if the order parameter admits a cubic invariant (like volume) we need to include odd powers. However, the above form is sufficient for our purposes. In the study for spin and channel ordering, Jarrell, Pang and Cox [1997a,b] found it sufficient to hunt for divergences in the staggered spin and channel susceptibilities. As discussed above, just such divergences were found. This common scenario is represented graphically in Fig. 126.

Now, in terms of GL theory, the order parameter undergoes a second order transition when the coefficient of the quadratic term vanishes. This clearly implies that $\chi_O^{(1)}(T)$ must diverge. GL theory of course admits the possibility of first order transitions. The customary scenarios require either: (i) that the order parameter admit a third order invariant as happens for isostructural phase transitions or quadrupolar ordering, or (ii) the fourth order term changes sign from positive to negative while the second order and sixth order terms remain positive. This is the situation in which a mean field theory of tri-critical points becomes possible. These scenarios are represented graphically in Fig. 127.

Another rather unusual possibility signifies the presence of a first order transition (Jarrell and Pruschke [1996]; Jarrell *et al.* [1997]): if $\chi_O^{(1)}(T)$ itself changes sign at a temperature T^*. Clearly, such

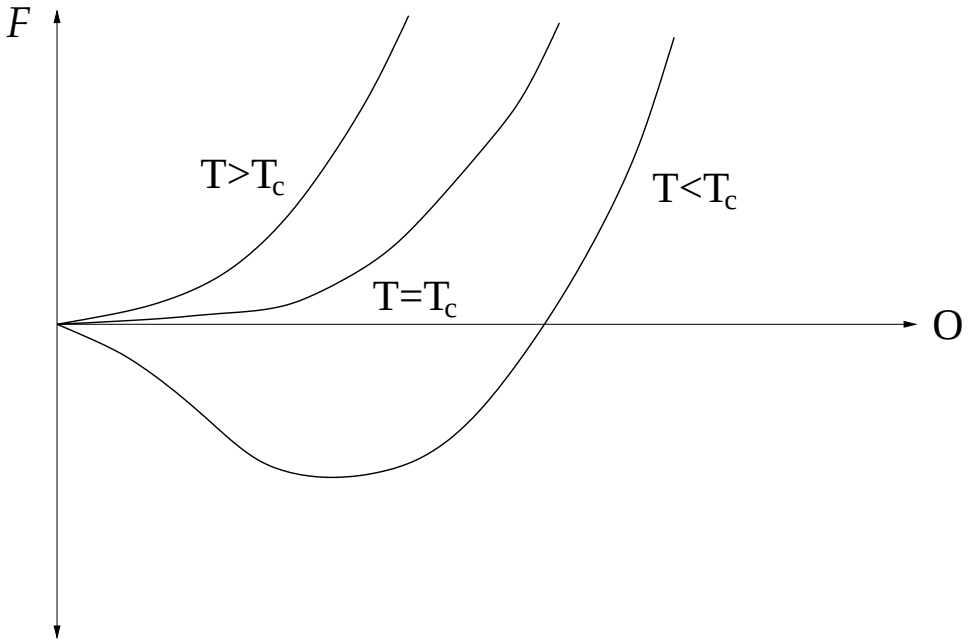

Figure 126: Usual Landau scenario for a second order transition. Sketched is the free energy $\mathcal{F}$ as a function of the order parameter O. At $T > T_c$, there is a quadratic curvature upwards. For $T = T_c$, the free energy is quartic in the order parameter. For $T < T_c$, the free energy has a quadratic curvature downwards. As a result, a stable minimum at finite O arises continuously from zero order parameter as the temperature is lowered.

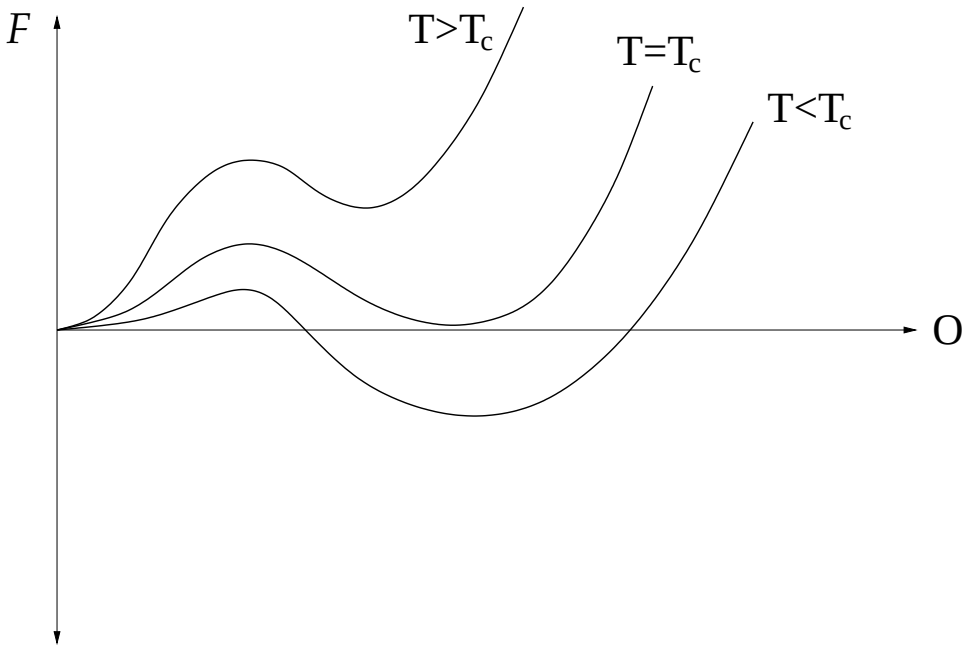

Figure 127: Usual first order transition scenarios. These are either driven by the presence of a third order term (as occurs for liquid crystals, quadrupolar, or structural transitions), or by a change of sign of the fourth order term in the Landau free energy. In either case, the transition occurs when a metastable state is lowered through a degeneracy point with the zero order parameter minimum at a critical temperature T_c. Below T_c the metastable state becomes fully stable.

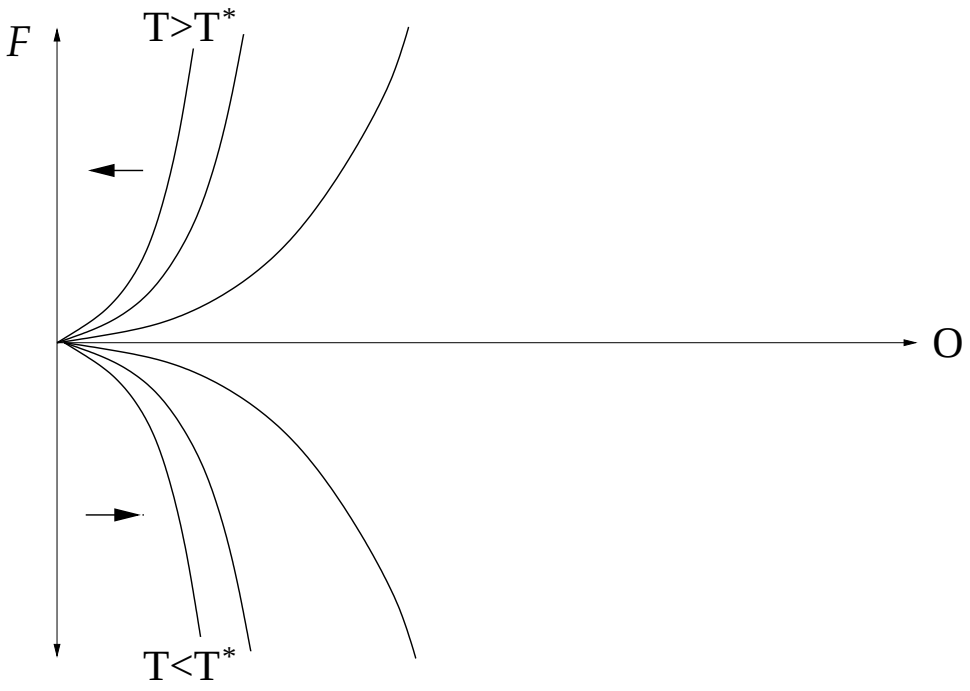

Figure 128: Anomalous first order transition scenario for odd-frequency pairing in the two-channel Kondo lattice. Given the finding of a sign change to the pair field susceptibility at a temperature T^*, and noting that the order parameter susceptibility is the inverse of the free energy curvature at the origin ($O = 0$), we see that the low O curves "pile up" on approach to T^* at which point the free energy has infinite curvature at the origin. Immediately below T^*, the free energy has *negative* infinite curvature, and clearly stability requires a minimum at a finite value of O. The only consistent way to make this happen is for there to be a minimum at finite O above T^*, implying that T^* is a lower bound for the first order transition temperature.

a sign change represents a thermodynamic instability. This scenario is displayed in Fig. 128. As can be seen, above T^*, a minimum at $O = 0$ is clearly present, while below T^*, a minimum at finite O is present. Because these cannot be smoothly connected, we infer that the transition must be discontinuous. Of course, if $\chi_O^{(1)}$ passes through zero, the very assumption of a Taylor's expansion in powers of O for $\mathcal{F}[O]$ breaks down. One approach to remedy this problem is to apply a *gedanken* external field h_O conjugate to O and work in the Legendre transformed free energy $\mathcal{A}[h_O] = \mathcal{F} - h_O O$. By using

$$\mathcal{A}[h_O] \approx -\frac{\chi_O^{(1)}}{2} h_O^2 - \frac{\chi_O^{(3)}}{4!} O^4 - \frac{\chi^{(5)}}{6!} O^6 + ... \tag{9.4.23}$$

where $\chi^{(i)}$is the i-th order non-linear susceptibility, for $h_O \to 0$, one can systematically invert $\mathcal{A}$ to obtain $\mathcal{F}$. The point is that clearly $\mathcal{A}$ is the sensible starting point free energy when $\chi_O^{(1)} \to 0$.

Now, consider first the case $\chi_O^{(3)} < 0$. This gives the usual situation that the GL free energy is stabilized by the fourth order terms, as it is straightforward to show that for $O \to 0$, that $\beta \approx -\chi_O^{(3)}/[24(\chi_O^{(1)})^4] > 0$. However, for $\chi_O^{(1)} \to 0$, this expansion clearly breaks down. Evaluation right at T^* where the linear susceptibility vanishes gives

$$\mathcal{F}[O] \approx -\frac{\chi_O^{(3)}}{4!} h_O^4 + h_O O + ... \tag{9.4.24}$$

$$= \frac{\chi_O^{(3)}}{8} \left(\frac{6O}{|\chi_O^{(3)}|}\right)^{4/3} + ...$$

which is manifestly negative. Stabilization must occur from the sixth order and higher terms in the free energy. Because this energy is already negative at T^*, we infer as claimed that a transition to a finite value of O must have occurred at a temperature above T^*.

For $\chi_O^{(3)} > 0$, we cannot give quite so explicit a proof of this fact. However, we note that when the non-linear susceptibility is positive, the fourth order GL term in O is negative, which indicates the presence of a free energy minimum at finite values of O. Taken together with the observation that the free energy must be negative for infinitesimal values of $T^* - T > 0, O$, then we infer that again a transition to finite O must have occurred above T^*.

Finally, we return to the question of $1/d$ effects upon this phase transition. As mentioned in item (4) above in the discussion of the results for the phase diagram, this transition in $d = \infty$ does not distinguish between different center-of-mass momenta for the Cooper pairs. We expect this to change when $d < \infty$. The argument is as follows. The superfluid density or stiffness can be read off as the coefficient of the diamagnetic term in the electrical conductivity. This results from the anomalous diagram shown in Fig. 119(a). In a systematic $1/d$ expansion, as mentioned in Sec. 9.3.3, the conductivity itself is of order $1/d$. The locality of the self energy implies that correct to this order one can omit any vertex corrections from the conductivity. This implies that the conductivity has precisely the bubble form assumed in the argument of Coleman, Miranda, and Tsvelik [1993,1994] to infer that the superfluid density/stiffness at the zone center is *negative* for an odd-frequency superconductor, while it is *positive* at the zone boundary. Hence, it appears likely that the restoration of a superfluid density at finite d will lift the degeneracy between different $\vec{q}$ (center-of-mass momentum of Cooper pairs) and thus induce a staggered pairing state. While it cannot be ruled out that vertex corrections will modify this result (Balatsky *et al.* [1994], Abrahams *et al.* [1995]), to the extent the leading order (in $1/d$) term determines the sign of the superfluid stiffness, it seems unlikely that the vertex corrections will modify this conclusion.

In closing this subsection, it is worth noting that this unusual pairing must be described by physics which goes beyond Eliashberg-Migdal theory in the local dynamics (in that the local spin fluctuations mediating the pairing must be self consistently adjusted) but not in the intersite dynamics. Hence, it should be possible to develop a kind of real space Eliashberg theory (Jarrell *et al.* [1997]) to understand the physics of this model in the superconducting state. It will of course be important to develop a theory of a finite order parameter to properly identify the location of the first order transition and to assess the impact of the antiferromagnetism on the superconducting transition.

Jarrell, Pang, and Cox [1997a,b] have noted that the possibility of coexisting superconductivity with predominantly commensurate antiferromagnetism along with the anomalous normal state properties makes the two-channel model a leading candidate to explain the heavy fermion superconductors. It should be noted that the observed superconducting transition in these materials appears to be second order. Detailed numerical studies are required to assess whether finite dimensionality effects induce a second order transition or whether a sufficiently weak first order transition can be found to bring this fascinating state more into alignment with experiment.

One-Dimensional Diluted Kondo Lattice

Zachar, Kivelson, and Emery [1996] have studied a single channel Kondo lattice in one dimension with Abelian bosonization techniques. Dilution requires that the spacing between local moments be significantly larger than the spacing between atoms yielding the conduction electrons. The model is soluble in the anisotropic limit analogous to that of Toulouse for the single channel impurity model. Specifically, $J_z = \pi v_F$ must be taken to obtain a soluble model.

In this limit for incommensurate filling of the conduction band, there is an antiferromagnetically ordered ground state in *transformed spin variables* and a gap to spin excitations of $\Delta_s \sim v_F[cJ_\perp/v_F]^{2/3}$ where c is the local moment density. By transformed spin variables we mean $\tilde{\tau}^x(j) = U^\dagger(j)\tau^x(j)U(j)$ where $\tau^x(j)$ is the local moment spin (x-component) at site j and $U(j) = \exp[-i\sqrt{2\pi}\sum_j \tau_j^z \theta_s(r_j)]$ is a

stringlike operator that effects a unitary rotation of the system. θ_s is a "spinlike" bosonic momentum variable introduced through the transformations

$$\Psi^{\dagger}_{\lambda,\sigma}(x) \sim \exp[i\sqrt{\pi}(\theta_\sigma(x) + \lambda\phi_\sigma(x)) + i\lambda k_F x] \tag{9.4.25}$$

where $\lambda = \pm$ is the left moving (+) or right moving (-) index and $\sigma = \uparrow, \downarrow$ is the spin index. The fields θ_σ("momentum") and ϕ_σ("coordinate") are canonically conjugate. The field $\theta_s = [\theta_\uparrow - \theta_\downarrow]/\sqrt{2}$. Note that the physical spin variables are disordered by virtue of the excitation gap, and thus have an exponential decay in real space. Diluteness of the local moment array is self consistently determined by requiring that the spin correlation length v_F/Δ_s is large compared to the inter-impurity spacing.

The free fermi gas in one dimension would have spin, charge, and pair correlations which decay as x^{-2} for large distance x. If it is found that one has correlation functions decaying as $x^{-\alpha}$ for $\alpha < 1$, one can have an indication from the one-dimensional model that there is an enhancement of the ordering tendencies. Zachar, Kivelson, and Emergy find just such enhancement for $2k_F$ ordering of the conduction charge and of the composite spin field $\Psi^{\dagger}_{L\downarrow}\Psi_{R\uparrow}\tau^x$ where Ψ are conduction fields either of left (L) or right (R) moving character and τ^x is the local spin operator. They also find enhanced ordering tendencies for the staggered singlet superconducting field $(-1)^j\Psi^{\dagger}_{L\uparrow}(j)\Psi^{\dagger}_{R\downarrow}(j)$ and the staggered composite field $(-1)^j\Psi^{\dagger}_{L\downarrow}(j)\Psi^{\dagger}_{R\downarrow}(j)\tau^x(j)$, which, as argued earlier, should mix linearly with the staggered singlet spin field. Because L, R act as channel indices here, the staggered singlet spin field is completely analogous to that of the two-channel model. Satisfying the Pauli principle requires odd-in-frequency pairing. This remarkable folding down of the one-channel model in one-dimension to an effective two-channel model is possible because the spin gap stabilizes backscattering terms to zero. It is unclear from the study how generic the spin gap is away from the soluble points, and this is obviously something to be explored further.

Subsequent to the work of Zachar, Kivelson, and Emery [1996], Coleman *et al.* [1997] have suggested that a novel two-channel pairing state can be bootstrapped out of a superficially one-channel lattice when electrons of differing local angular momentum (but the same parity) couple to a given local-moment site.

10 Conclusions and Directions

We have shown in this review that in order to arrive at exotic Kondo states which display non-Fermi liquid fixed points the minimal generalization of the single channel Kondo model is via the addition of channel or flavor quantum numbers to the conduction electrons. The two-channel spin 1/2 Kondo model obtained in this way has been shown to describe a great variety of physical phenomena from disparate areas of condensed matter physics, such as amorphous metals, nanometer scale point contact devices, certain rare earth and transition metal ions in metals (some of which become exotic superconductors at full concentration of the ions), and quantum dots in the Coulomb blockade regime. In particular, it is apparent that *any* time a local pseudo-spin degree of freedom is non-magnetic, a mapping to a two-channel Kondo model is possible in which the channel degree of freedom is the magnetic spin or time reversal index of the conduction electrons, guaranteed to be degenerate in the absence of magnetic field by Kramers' theorem. Given this broad variety of possibilities, we can only anticipate that new models and experimental systems will be discovered for which a mapping to a model with a non-Fermi liquid fixed point will be on solid ground.

We have stressed that the most likely *physical* route to a non-Fermi liquid Kondo fixed point is through the two-channel spin 1/2 Kondo model. However, other intriguing possibilities exist for stable fixed points involving a large effective impurity spin (Zaránd [1996], Moustakas and Fisher [1997]) or unstable fixed points with a large effective conduction spin either for TLS Kondo sites or rare earth/actinide ions (Fabrizio and Gogolin [1994]; Fabrizio and Zaránd [1996]; Kim and Cox [1996]; Sengupta and Kim [1996]; Kim, Cox, and Oliveira [1997]).

On theoretical grounds, the two-channel Kondo model itself is very well understood. On the high temperature side, the multiplicative renormalizatin group (Sec. 3) provides a solid indication of which sectors of parameter space in the model are needed to describe various physical phenomena (valid for $T \geq T_K$, T_K the Kondo temperature). Knowing the relevant sector of parameter space, one is guided to the low temperature regime where a variety of powerful methods are available to characterize the physics. Asymptotically, at low temperatures, conformal field theory and Abelian bosonization may be brought to bear (Sec. 6) (valid for $T << T_K$). The numerical renormalization group (Sec. 4) and the Bethe-Ansatz method (Sec. 7) may be employed to fully characterize the crossover from low to high temperatures provided the model is sufficiently simple (e.g., no excited crystal field states) and the temperature range of interest is far from the band edges. With these methods it is, however, difficult (though not impossible) to obtain dynamical properties. The non-crossing approximation provides an excellent way to study these models in thermodynamic, transport, and spectral properties over all temperature ranges including a variety of interesting physical phenomena (especially realistic electronic structure inputs and excited multiplet states) while being limited practically to the rare earth and actinide ions.

These methods all predict universality in physical properties and are heavily intertwined, in that, for example, the conformal theory must *assume* a fixed point, and have that assumption confirmed by matching to finite size spectra from say the NRG or Bethe-Ansatz approaches. Once such a comparison is made, one may confidently employ the predictions of the conformal theory for, say, a $T^{1/2}$ low temperature behavior in the resistivity. The non-crossing approximation is strictly controlled only for large spin degeneracy N, and its very successful application to the problem for $N = M = 2$, where M is the channel degeneracy, is justified *a posteriori* by a comparison of the critical exponents, amplitudes such as the zero temperature resistivity and entropy, and temperature dependent thermodynamics to exact results such as arise from the Bethe-Ansatz and CFT. In this way, one has confidence in using the NCA to calculate the full temperature dependence of quantities such as the thermopower, electrical resistivity, and van Vleck susceptibility, which are accessed either not at all or in limited ways by the other methods.

Experimentally, there is growing evidence that the TLS interacting with electrons in metals can be described by the two-channel Kondo model. However, further studies are required to answer certain

critical questions, such as:
→ How does the TLS form in metallic glasses, mesoscopic devices, and interfaces?
→ Why are there so many TLS with small asymmetry, for example, in the case of nanoscale point contact devices?
→ What is the role of the complete set of excited states in the TLS?
→ What is the effect of static impurities in the metallic host on the orbitals and spherical waves of the conduction electrons and how does that affect the orbital screening phenomenon about the TLS?

Considering the physics of TLS is not only of interest for establishing the existence and relevance of the two-channel Kondo problem, but also for understanding the signals present in many mesoscopic samples, devices, and interfaces, and thus is highly relevant to the ongoing technological developments in nanoscale physics.

Concerning the possibility of two-channel Kondo physics for heavy fermion alloy systems, it must be said that an impressive body of evidence argues for understanding of many systems in terms of the two-channel Kondo effect. A complete verification of the behavior has not proven possible for any one system however, usually due to: (i) unusual behavior of transport coefficients such as the resistivity and thermopower which do not appear reconcilable with the simple two-channel Kondo model, (ii) unusual thermodynamic scaling in applied magnetic field, or (iii) history dependent freezing effects associated with spin glass physics. However, the clear observation of single ion scaling phenomena in $Y_{1-x}(Th_{1-y},U_y)_xPd_3$, $Th_{1-x}U_xRu_2Si_2$, $Th_{1-x}U_xPd_2Si_2$, $Th_{1-x}U_xM_2Al_3$, $Th_{1-x}U_xBe_{13}$, and, partially, in $La_{1-x}Ce_xCu_2Si_2$ suggests that further experimental studies on very well characterized crystals are worthwhile. In the case of the U based systems, single crystal ultrasound and non-linear susceptibility measurements are worthwhile to directly probe the non-Kramers' ground state. On the theory side, the effects of excited crystal field levels and other physics beyond the simplest two-channel model must be further investigated to assess whether the unusual behavior in transport coefficients may be reconciled with the observations. Also on the experimental side, the recent discovery of anomalous Pr based systems for possibly studying the quadrupolar Kondo effect (Yatskar *et al.* [1996]) worthwhile to examine further, particularly by doping on the Pr sublattice with La to search for dilute quadrupolar Kondo systems where a known non-Kramers' ground state on the ion of interest is assured. Another extremely interesting theoretical question inspired by experiment (Aliev *et al.* [1995a,b]) is to study the situation of extreme mixed valence between two degenerate configurations (c.f., 108).

Perhaps the most wide open and exciting opportunidies for experimental and theoretical research on the rare earth and actinide based multi-channel Kondo candidates are in the periodic compounds such as UBe_{13}, $CeCu_2Si_2$, and $PrInAg_2$. Two of these are exotic superconductors. Investigations of the two-channel Kondo lattice in infinite spatial dimensions yield a non-Fermi liquid normal state and either superconducting or antiferromagnetic ground states (with possible coexistence) (Jarrell *et al.* [1996]; Jarrell, Pang, and Cox [1997]; Anders, Jarrell, and Cox [1997]). The normal state properties have a good correspondence to UBe_{13}, while the superconductivity that is found is *odd* in frequency and proceeds via a very novel first order transition. It is important to further examine whether this transition is robust upon passing to finite spatial dimension (where indications are that finite center of mass Cooper pairs will be favored), what the effects of intersite magnetic correlations are upon the normal state non-Fermi liquid behavior, and what the effects are of the inexactness of channel degeneracy (for the magnetic two-channel lattice) or spin degeneracy (for the quadrupolar two-channel lattice) of the conduction states. Moreover, complete studies of the ordered phases are necessary to characterize the degree of coexistence vs. competition for the magnetic and superconducting order. Studies for a one dimensional model of the single channel Kondo lattice which effectively maps to the two-channel lattice in certain limits also support enhanced staggered odd-frequency pair correlations (Zachar, Emery, and Kivelson [1996]). Because this is the first model Hamiltonian for which odd-frequency pairing is definitively observed, it is important to further develop the phenomenological consequences of this unusual theoretical result. For example, what are the low temperature excitations and how do they manifest in thermodynamics and transport? What happens to Josephson tunneling and Andreev reflection? Some of these questions

have been partially answered (see for example Coleman, Miranda, and Tsvelik [1994], Heid *et al.* [1995]) but clearly much work remains.

It is clear that this is a field which has blossomed extensively in recent years, and for which there remains a promising future for theorists and experimentalists with an Edisonian spirit.

If this does not satisfy the reader, then he/she must go to hell experiencing hectic non-Fermi liquid behavior with non-vanishing entropy in marked contrast to heaven where single channel physics presides with peace ensured by a singlet ground state and Fermi liquid excitation spectrum. Thanks to free will, the choice belongs to the reader.

11 Acknowledgements

This work would not have been possible without the assistance of many of our colleagues. We especially want to thank I. Affleck, F. Aliev, N. Andrei, P. Fazekas, T. Giamarchi, J. Kroha, A.W.W. Ludwig, J. von Delft, and G. Zaránd for carefully reading portions (or all) of the manuscript. We also wish to thank R. Buhrman, V. Emery, B. Jones, S. Kivelson, and D.C. Ralph, and J.W. Wilkins for many useful discussions. D.L. Cox wishes to thank his many collaborators and colleagues over the years for shaping his views on this field, especially M.B. Maple, C.L. Seaman, J.W. Allen, M. Jarrell, F. Steglich, H.R. Ott, H. Pang, F. Anders, T.S. Kim, J. Han, E. Kim, A. Schiller, L. Oliveira, V. Libero, H.R. Krishna-murthy, P. Coleman, A. Tsvelik, R. Heid, V. Martisovits, Y. Bazaliy, and M. Makivic. We are especially indebted to F. (King) Anders for his substantial help in preparing this document, and to K. Hartlein for preparing most of the figures which appear here. We acknowledge the hospitality of the Institute of Theoretical Physics at the University of California, Santa Barbara, where a portion of this work was carried out during the workshop on Non-Fermi Liquid Metals in 1996, and the group of Prof. P. Erdös at the University of Lausanne, Switzerland, where a portion of this paper was written in the spring of 1996. The research efforts of D.L. Cox have been supported by the US Department of Energy, Office of Basic Energy Sciences, Division of Materials Research (normal state properties) and by the US National Science Foundation under DMR-9420920 (superconducting properties). A. Zawadowski has been supported by Grants OTKA T-021228/1996 and OTKA T-024005/1997 from the Government of Hungary. Both authors acknowledge the generous support of Grant No. 587 of the American-Hungarian joint research fund.

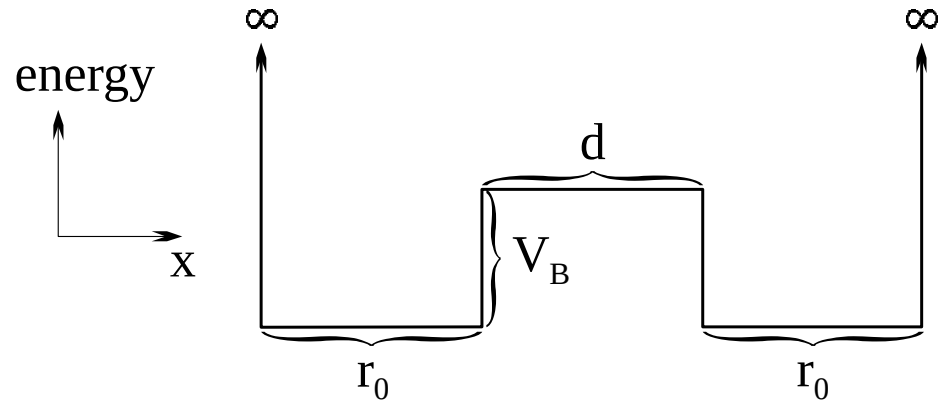

Figure 129: Double square well model potential for TLS Kondo effect.

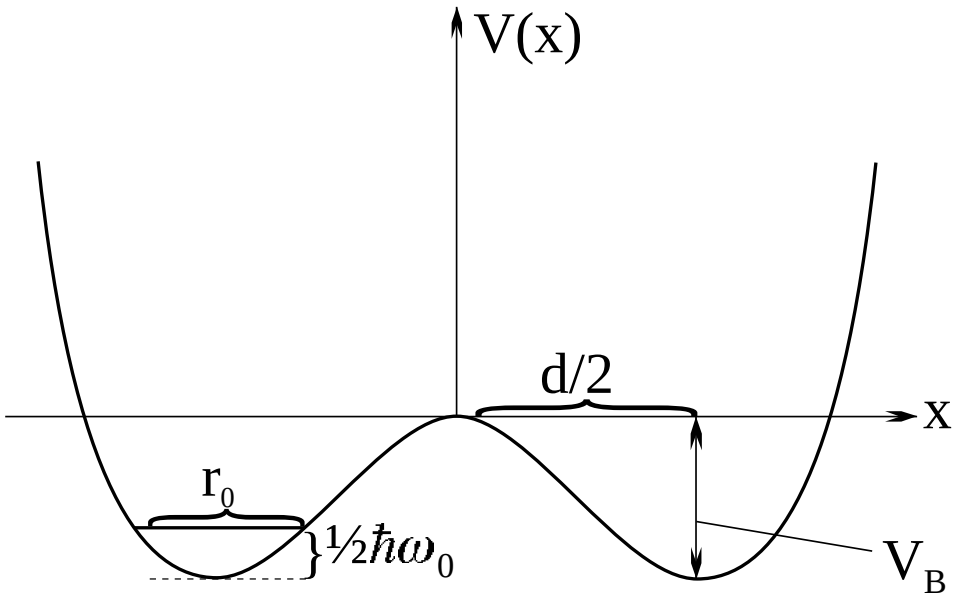

Figure 130: Quartic anharmonic well model for TLS Kondo effect.

Appendix I: Model Calculations of Δ^x, V^x.

In this appendix, we will summarize two model calculations of Δ^x, V^x which provide quantitative justification to the simple theory of Sec. 2.1.3. The examples will follow from exact treatment of the square barrier problem displayed in Fig. 129, and the quartic anharmonic potential problem of Fig. 130, where the non-orthogonal wave functions associated with each well will be taken to be approximately of harmonic oscillator (Gaussian) form.

The general prescription is as follows: We shall only treat the spatial dependence along the axis of the TLS, assuming for convenience a symmetric model so that parity is a good eigenvalue. Denote the lowest two eigenfunctions of the double well as $\phi_\pm(z)$ where the subscript is the parity level. The parity wave functions are delocalized over the double well. Define orthogonalized combinations of wave functions for each side (right R or left L) by

$$\phi_{R,L}(x) = \frac{1}{\sqrt{2}}[\phi_+(x) \pm \phi_-(x)] \quad . \tag{A.1.1}$$

The spontaneous tunneling rate Δ^x is the splitting between the two states of definite parity, which is

equal to the matrix element of the *total* Hamiltonian between the localized states. That is,

$$(A.1.2) \qquad \Delta^x = E_- - E_+ =< -|H|- > - < +|H|+ >= -2 < L|H|R > \quad .$$

The assisted tunneling matrix element may be estimated by directly computing the matrix element of the electron-ion coupling taking the state $L \to R$, i.e.,

$$(A.1.3) \qquad V^x_{\vec{k},\vec{k}'} = -2 < \vec{k}, L|H_{el-ion}|\vec{k}', R >$$

$$= -2U(\vec{k}' - \vec{k}) \int dx(\exp[i(\vec{k} - \vec{k}') \cdot \hat{x}] - \cos[(k'_x - k_x)(d/2)])\phi_L(x)\phi_R(x) \quad .$$

The subtraction procedure is the same as discussed in the section on the TLS Hamiltonian. We shall use Eqs. (A.1.2,3) in estimating the parameters.

The above approach is equivalent to the derivation based upon the Feynman-Hellman theorem developed by Ngai *et al* [1967] for estimating tunneling matrix elements.

Square Barrier Model. Here the atomic wave functions feel an infinite barrier at $x = \pm(d/2 + r_0)$, and a square barrier of height V_B for $-d/2 < x < d/2$. Following Ngai *et al.* [1967], it is straightforward to find the wave functions $\phi_\pm(x)$ from direct solution of the Schrödinger equation subject to the boundary conditions

$$(A.1.4.a) \qquad \phi_\pm(\pm(d/2 + r_0)) = 0 \quad ,$$

$$(A.1.4.b) \qquad \phi_\pm(\pm|(d/2)^+|) = \phi_\pm(\pm|(d/2)^-|)$$

where the superscript indicates whether the limit is taken from the right (+) or left (-), and

$$(A.1.4.c) \qquad \frac{d}{dx}\phi_\pm(\pm|(d/2)^+|) = \frac{d}{dx}\phi_\pm(\pm|(d/2)^-|) \quad .$$

Given the eigenvalues $E_\pm$ and wavenumbers $k_\pm = \sqrt{2ME_\pm}/\hbar$ and $q_\pm = \sqrt{2M(V_B - E_\pm)}/\hbar$, we take the *Ansatz*

$$(A.1.5) \qquad \phi_\pm(x) = \begin{array}{c} A_\pm \exp[ik_\pm x] \pm exp[-ik_\pm x] d/2 \le x \le d/2 + r_0 \\ \frac{B_\pm}{2}(\exp[q_\pm x] \pm \exp[-q_\pm x]) - d/2 \le x \le d/2 \\ \pm A_\pm \exp[-ik_\pm x] + exp[ik_\pm x] - (d/2 + r_0) \le x \le -d/2 \end{array} \quad .$$

This yields the eigenvalue conditions,

$$(A.1.6.a) \qquad k_+ r_0 + \tan^{-1}(\frac{k_+}{q_+} coth[q_+ d/2]) = \pi$$

and

$$(A.1.6.a) \qquad k_- r_0 + \tan^{-1}(\frac{k_-}{q_-} tanh[q_- d/2]) = \pi$$

the wave function coefficients

$$(A.1.7) \qquad A_\pm = \mp \exp[-2ik_\pm(r_0 + d/2)]$$

and

$$(A.1.8) \qquad B_\pm = \mp 2i(\frac{k_\pm}{q_\pm}) \frac{\cos(k_\pm r_0) \exp[-ik_\pm(r_0 + d/2)]}{(\exp[q_\pm d/2] \mp \exp[-q_\pm d/2])} \quad .$$

We are interested in the limit of large barrier height, so that $q_\pm \approx \sqrt{2MV_B}/\hbar = q_0$, and to leading order $k_\pm \approx k_0 = \pi/r_0$, and the overall normalization coefficient of the even and odd parity wave functions is $1/r_0$. We denote the energy $E_0 = \hbar^2 k_0^2/2M$ by $\hbar\omega_0$, and the Gamow factor $\lambda = q_0 d$.

Retaining terms only to leading exponential order, we find that the tunneling rate Δ^x is given by

$$\Delta^x = E^- - E^+ \approx \hbar\omega_0(\frac{2d}{r_0})\frac{e^{-\lambda}}{\lambda} \quad . \tag{A.1.9}$$

Using Eq. (A.1.3) and performing the expansion for small $(k_x - k'_x)d = \Delta k_x d$, we find that to leading exponential order the assisted tunneling matrix element is given by

$$\begin{aligned} V^x_{\vec{k},\vec{k}'} &\approx \frac{\hbar\omega_0 e^{-\lambda}}{12}(\frac{d}{r_0})(\Delta k_x d)^2(\frac{U(\vec{k}-\vec{k}')}{V_B}) \\ &= \Delta^x[\frac{\lambda}{24}(\Delta k_x d)^2(\frac{U(\vec{k}'-\vec{k})}{V_B})] \end{aligned} \tag{A.1.10}$$

which agrees with the heuristic derivation given in Sec. 2.1.

Atom in a potential with quartic anharmonicity We take the potential energy to have the form

$$V(x) = -\alpha x^2 + \beta x^4 \tag{A.1.11}$$

with $\alpha, \beta > 0$. We identify the barrier width $d/2$ with the potential minima, *viz.*

$$(\frac{d}{2})^2 = \frac{\alpha}{2\beta} \quad , \tag{A.1.12}$$

the barrier height V_B with the depth of the two wells

$$V_B = \frac{\alpha^2}{4\beta} = \frac{1}{2}\alpha(\frac{d}{2})^2 \quad , \tag{A.1.13}$$

and the oscillator energy $\hbar\omega_0$ with the natural frequency of harmonic oscillations in the well minima, so that

$$\hbar\omega_0 = \sqrt{\frac{2\alpha}{M}} \quad . \tag{A.1.15}$$

We assume the wave functions $\phi^0_{L,R}(x)$ to orthogonalization have the Gaussian form

$$\phi^0_{L,R}(x) \approx \frac{1}{\pi^{1/4} r_0^{1/2}} \exp(-\frac{(x \pm d/2)^2}{2r_0^2}) \tag{A.1.16}$$

where the oscillator length r_0 is given by

$$r_0^4 = \frac{\hbar^2}{2M\alpha} \quad . \tag{A.1.17}$$

These wave functions have the overlap

$$S = \int dx \phi^0_L(x)\phi^0_R(x) = \exp(-\frac{d^2}{4r_0^2}) = e^{-\lambda} \tag{A.1.18}$$

which defines the Gamow factor $\lambda = d^2/4r_0^2$ in this model. When we orthogonalize, we obtain the wave functions

$$\phi_{L,R}(x) \approx \phi^0_{L,R}(x) - \frac{S}{2}\phi^0_{R,L}(x) \tag{A.1.19}$$

which is correct to leading order in $\exp(-\lambda)$.

With these approximately orthogonal orbitals, one can show exactly that in the expectation value specified by Eq. (A.1.2), only the quartic potential term and the kinetic energy of the orthogonalized pieces survives, so that

$$(A.1.20) \qquad \Delta^x = -2 < L|H|R > \approx \hbar\omega_0 e^{-\lambda}[1 + \mathcal{O}(\frac{1}{\lambda})] \quad .$$

Similar considerations applied to Eq. (A.1.3) yield the estimate for V^x that

$$(A.1.21) \qquad V^x \approx \Delta^x[\frac{\lambda}{16}\frac{U(\vec{k}' - \vec{k})}{V_B}(\Delta k_x d)^2][1 + \mathcal{O}(\frac{1}{\lambda})] \quad .$$

The use of the orthogonalized orbitals also justifies the use of $\delta\rho(\vec{r}) = \rho(\vec{r}) - (\rho(d/2) + \rho(-d/2))/2$. The argument is simple: by plugging $\rho(\vec{r})$ into (A.1.3) and using the orthogonalized orbitals given by Eq. (A.1.19), one finds that

$$(A.1.22) \qquad < L|\rho(x)|R > \approx \int dx \phi_L^0(x)\phi_R^0(x)[\rho(x) - \frac{1}{2}(< L|\rho|L > + < R|\rho|R >)] \quad .$$

Assuming the oscillators to be well localized on the scale of density variation ($\sim k_F^{-1}$) so that $< L, R|\rho|L, R > \approx \rho(\mp d/2)$, we see that the factor in braces is precisely $\delta\rho(x)$.

Hence, in two cases we find results for V^x estimated from the formulation of wave functions of orthogonal orbitals which agree to within factors of order unity with the Scalapino and Marcus formulation of the theory.

Appendix II: Local representation for electrons in the TLS problem

In the most simple model for the TLS Kondo effect, the electrons are scattered by the tunneling atoms in an s-wave channel assuming that the center of the coordinate system is the center of the atom (for a discussion of the more general case, see Vladár and Zawadowski [1983a]). In the case of the TLS the scattering contributes to different angular momentum channels if the mean position of the atom is chosen as the center of the coordinate system. In this case, the wave functions used earlier are not orthogonal. Therefore it is useful to introduce states which are even (e) and odd (o) about the center of the tunneling system as has been done earlier in the two-impurity Kondo problem (Krishna-murthy, Jayaprakash, and Wilkins [1980]) and in the TLS Kondo problem by Moustakis and Fisher [1995]. We shall follow the latter description here.

The non-interacting Hamiltonian used by Moustakis and Fisher [1995] is

$$(A.2.1) \qquad \mathcal{H}_0 = \Delta_0(d_1^\dagger d_2 + d_2^\dagger d_1) + \sum_\sigma \int \frac{d\vec{k}}{(2\pi)^3}\epsilon_k c_{\vec{k}\sigma}^\dagger c_{\vec{k}\sigma}$$

where $d_i^\dagger$ creates the tunneling atom at position $\vec{R}_i$, Δ_0 is the spontaneous hopping matrix element, and the last term describes the conduction band. The operators are assumed to obey continuum commutation relations. Turning on an interaction between electrons and the TLS which does not include assisted tunneling we have the coupling

$$(A.2.2) \qquad \mathcal{H}_1 = \frac{V}{N_s}\sum_{\sigma,i}\int\int \frac{d\vec{k}}{(2\pi)^3}\frac{d\vec{k}'}{(2\pi)^3}e^{-i(\vec{k}-\vec{k}')\cdot\vec{R}_i}c_{\vec{k}\sigma}^\dagger c_{\vec{k}'\sigma}d_i^\dagger d_i$$

where V is the strength of the s-wave scattering off of the atom at either site. Measuring $\vec{R}_1, \vec{R}_2$ from the midpoint of the TLS, we see that $\vec{R}_1 = \vec{R}/2$, $\vec{R}_2 = -\vec{R}/2$, where $\vec{R}$ is the distance between the impurities.

We now introduce a new representation in which

$$\int \frac{d\vec{k}}{(2\pi)^3} e^{\pm i\vec{k}\cdot\vec{R}/2} c_{\vec{k},\sigma} = \int \frac{dk}{2\pi} c_{\pm,k,\sigma} \tag{A.2.3}$$

which defines $\tilde{c}_{\pm,k,\sigma}$. Note that the operators $\tilde{c}_{\pm,k,\sigma}$ are not orthogonal at this point. We can properly introduce now odd and even electron operators which are correctly normalized as

$$c_{ek\sigma} = \frac{1}{\sqrt{N_e}}[c_{+,k,\sigma} + c_{-,k,\sigma}] \quad , \tag{A.2.4.a}$$

$$c_{ok\sigma} = \frac{1}{\sqrt{N_o}}[c_{+,k,\sigma} - c_{-,k,\sigma}] \tag{A.2.4.b}$$

with

$$N_e(k) = \frac{2k^2}{\pi^2}[1 + \frac{\sin kR}{kR}] \tag{A.2.5.a}$$

and

$$N_o(k) = \frac{2k^2}{\pi^2}[1 - \frac{\sin kR}{kR}] \quad . \tag{A.2.5.b}$$

With this definition, and $\alpha = e, o$,

$$\{c_{\alpha,k,\sigma}, c^{\dagger}_{\alpha',k',\sigma'}\} = 2\pi\delta(k-k')\delta_{\alpha,\alpha'}\delta_{\sigma,\sigma'} \quad . \tag{A.2.6}$$

With this definition, we can introduce properly orthogonal left and right conduction operators as

$$c_{1k\sigma} = \frac{1}{\sqrt{2}}[c_{e,k,\sigma} + c_{o,k,\sigma}] \tag{A.2.7.a}$$

and

$$c_{2k\sigma} = \frac{1}{\sqrt{2}}[c_{e,k,\sigma} - c_{o,k,\sigma}] \quad . \tag{A.2.7.b}$$

Note that this definition of conduction basis is completely general for a two-center problem and may thus be applied to the two-impurity Kondo model as well.

We now return to rewrite the interaction Hamiltonian of Eq. (A.2.2). In terms of the e, o basis we have

$$\mathcal{H}_1 = \sum_{\sigma} \int\int \frac{dk}{2\pi}\frac{dk'}{2\pi}[V_1(c^{\dagger}_{e,k,\sigma}c_{e,k',\sigma} + c^{\dagger}_{o,k,\sigma}c_{o,k',\sigma}) + V_2(c^{\dagger}_{e,k,\sigma}c_{e,k',\sigma} - c^{\dagger}_{o,k,\sigma}c_{o,k',\sigma})$$

$$+V_3[(c^{\dagger}_{e,k,\sigma}c_{o,k',\sigma} + c^{\dagger}_{o,k,\sigma}c_{e,k',\sigma})(d^{\dagger}_1 d_1 - d_2^{dagger} d_2)] \tag{A.2.8}$$

where we take $d^{\dagger}_1 d_1 + d_2^{dagger} d_2 = 1$ (appropriate to the restricted Hilbert space) and

$$V_1 = \pi N(0) V \quad , \tag{A.2.9}$$

$$V_2 = \pi N(0) V \frac{\sin k_F R}{k_F R} \quad , \tag{A.2.10}$$

and

$$V_3 = \pi N(0) V \sqrt{1 - (\frac{\sin k_F R}{k_F R})^2} \quad . \tag{A.2.11}$$

This completes the derivation of the Moustakis and Fisher [1995] hamiltonian displayed in Eq. (3.5.12) (recall that $\sigma^z = d_1^\dagger d_1 - d_2^\dagger d_2$).

Finally, we mention that in Eqs. (A.2.9) and (A.2.10), an averaged atomic potential can be subtracted (i.e., a uniform background).

Appendix III: NCA Treatment of Spin and Channel Magnetization in the $SU(N) \otimes SU(M)$ Multi-channel Model

We wish to pull out the singular low field dependence of the spin magnetization when $\gamma \geq 1$ and the channel spin magnetization when $\gamma \leq 1$. Our treatment follows the calculations of susceptibilities in Bickers [1987], Sec. V.B.3. We shall present a more detailed argument for the spin magnetization; the details for the channel spin magnetization will be similar. Our notation follows Sec. 5.1. The strategy is to develop and utilize an expression for the ground state energy as an integral over d_b where the integrand contains only factors of g_f viewed as depending on d_b through inversion of the constant of integration relation (5.1.17). In applied field, g_f will carry all the explicit field dependence and an expression for the magnetization may be obtained. The field is assumed to enter through the Zeeman energy $H_Z = -\sum_\sigma \mu H_{sp} \sigma$ where σ runs between $-J = (N-1)/2$ to J.

First, we extend the NCA differential equations in the applied spin field. Now g_f acquires a σ dependence so the equations are

$$\frac{dg_{f\sigma}}{d\omega} = -1 - \frac{\gamma \tilde{\Gamma}}{\pi d_b} \tag{A.3.1.a}$$

and

$$\frac{dd_b}{d\omega} = -1 - \frac{\tilde{\Gamma}}{\pi N} \sum_\sigma \frac{1}{g_{f\sigma}} \tag{A.3.1.b}$$

subject to the boundary conditions

$$d_b(-D) = D, \quad g_{f\sigma}(-D) = D + \epsilon_f - \mu \sigma H_{sp} \quad . \tag{A.3.2}$$

It is easy to see that we may write

$$g_{f\sigma} = g_{fJ} + (J - \sigma)\mu H_{sp} = g_{fJ} + m\tilde{H}_{sp} \tag{A.3.3}$$

where $m = J - \sigma$ and $\tilde{H}_{sp} = \mu H_{sp}$. In consequence, the integration constant relation between d_b, g_{fJ} is

$$g_{fJ} + \frac{\tilde{\Gamma}}{N\pi} \sum_m \ln(\frac{g_{fJ} + m\tilde{H}_{sp}}{D}) + \mathcal{C} = d_b + \frac{\gamma \tilde{\Gamma}}{\pi} \ln(\frac{d_b}{D}) \tag{A.3.4}$$

from which we infer $\mathcal{C} = -\tilde{\epsilon}_f + J\tilde{H}_{sp}$ by evaluation at $-D$.

In principle, Eq. (A.2.4) allows us to solve for g_{fJ} as a function of d_b, or vice versa. This gives a route to integrate the differential equations of Eq. (A.2.1.a,b). We find

$$\omega = -d_b + \int_D^{d_b} dx \frac{S_1(x)}{1 + S_1(x)} \tag{A.3.5}$$

with

$$S_j(x) = \frac{\tilde{\Gamma}}{N\pi} \sum_m \frac{1}{(g_{fJ}(x) + m\tilde{H}_{sp})^j} \quad . \tag{A.3.6}$$

The x in the integrand is expressing the dependence of g_{fJ} on d_b. At the threshold which is also the ground state energy, d_b vanishes. Hence

$$E_0 = -\int_0^D dx \frac{S_1(x)}{1 + S_1(x)} \tag{A.3.7}$$

where the field dependence enters now only through g_{fJ} in the integrand. Hence, we need a knowledge of $\partial g_{fJ}/\partial \tilde{H}_{sp}$. From Eq. (A.2.4), holding d_b fixed and differentiating with respect to $\tilde{H}_{sp}$, we see that

$$\frac{\partial g_{fJ}}{\partial \tilde{H}_{sp}} = -\frac{J + S_1'}{1 + S_1} \tag{A.3.8}$$

where

$$S_j' = \frac{\tilde{\Gamma}}{N\pi} \sum_m \frac{m}{(g_{fJ} + m\tilde{H}_{sp})^j} \quad . \tag{A.3.9}$$

Putting the above relations together, we obtain the spin magnetization from

$$M_{sp} = -\frac{\partial E_0}{\partial \tilde{H}_{sp}} = \int_0^D dx \frac{[S_2(x)(S_1'(x) + J) - S_2'(x)(1 + S_1(x))]}{(1 + S_1(x))^3} \quad . \tag{A.3.10}$$

Our goal is to simply pull out the low field dependence on $\tilde{H}_{sp}$. Hence we may evaluate the above equation assuming g_f is above the crossover value, but still in the the low energy regime so that $\tilde{H}_{sp} \leq g_f << T_0$. This imposes an infrared cutoff on the integral determined by the relation between g_f and d_b of $x_c \approx (\tilde{\Gamma}/\pi)(\tilde{H}_{sp}/T_0)^{1/\gamma}$ in view of Eq. (5.1.18). The upper cutoff is specified by the maximal value of d_b in the low temperature regime which is $\tilde{\Gamma}/\pi$. It is straightforward to show that for small $\tilde{H}_{sp}$,

$$[S_2(J + S_1') - S_2'(1 + S_1)] \approx (\frac{\tilde{\Gamma}}{\pi})^2 \frac{1}{g_f^4} J(J+1)/3\tilde{H}_{sp} \tag{A.3.11}$$

and since for $\tilde{H}_{sp} < g_f << T_0$, $1 + S_1 \approx \tilde{\Gamma}/\pi g_f$ we see that

$$M_{sp} \approx \frac{\pi J(J+1)\tilde{H}_{sp}}{3\tilde{\Gamma}} \int_{x_c(\tilde{H}_{sp})}^{\tilde{\Gamma}/\pi} \frac{dx}{g_f(x)} \tag{A.3.12}$$

$$= \frac{J(J+1)}{3} (\frac{\tilde{H}_{sp}}{T_0}) \frac{1}{\gamma - 1} [(\frac{\tilde{H}_{sp}}{T_0})^{1/\gamma - 1} - 1] \quad .$$

For $\gamma > 1$, we see then that $M_{sp} \sim (\tilde{H}_{sp}/T_0)^{1/\gamma}$; for $\gamma = 1$, $M_{sp} \sim (\tilde{H}_{sp}/T_0) \ln(T_0/\tilde{H}_{sp})$. For $\gamma < 1$, M_{sp} is linear in $\tilde{H}_{sp}$ at low fields corresponding to the finite value of $\chi_{sp}(0)$.

We may follow analogous reasoning to obtain the channel spin magnetization $M_{ch} = -(\partial E_0/\partial \tilde{H}_{ch})$ in applied channel field which couples linearly to the channel states. The result is that for $\gamma < 1$, $M_{ch} \sim (\pi T_0/\tilde{\Gamma})(\pi \tilde{H}_{ch}/\tilde{\Gamma})^{\gamma}$, for $\gamma = 1$, $M_{ch} \sim (\pi T_0/\tilde{\Gamma})(\pi \tilde{H}_{ch}/\tilde{\Gamma}) \ln(\tilde{\Gamma}/\pi \tilde{H}_{ch})$, and for $\gamma > 1$, M_{ch} simply varies linearly in the applied field corresponding to the finite value for $\chi_{ch}(0)$. The prefactor of $(\pi T_0/\tilde{\Gamma}) = W_{ch}$ reflects the need to virtually excite to the channel configuration to polarize the channel spin.

Appendix IV: Green's Functions in the Abelian Bosonization Approach to the Two-Channel Kondo Model

In this appendix we briefly review the derivation of the Green's functions in the Abelian Bosonization approach to the two-channel Kondo lattice. Of interest are the Green's functions for the Majorana $\hat{b}$ field and for the ψ_{sf} field.

Because the effective resonant level model of Eq. (6.2.19) only couples the combination $\psi_{sf}+\psi_{sf}^{\dagger}$ to $\hat{b}$, it is convenient to decompose the ψ_{sf} field into two real Majorana fields,

$$(A.4.1) \qquad \hat{\chi}_{sf} = \frac{1}{\sqrt{2}}(\psi_{sf} + \psi_{sf}^{\dagger}),\ \hat{\lambda}_{sf} = \frac{1}{i\sqrt{2}}(\psi_{sf}^{\dagger} - \psi_{sf}) \quad .$$

The λ_{sf} field decouples from the problem. The remaining resonant level model may be solved by equation of motion methods. Define the Green's functions

$$(A.3.2.a) \qquad G_b(\tau) = - < T_\tau \hat{b}(\tau)\hat{b}(0) > \quad ,$$

$$(A.4.2.b) \qquad G_{bk}(\tau) = - < T_\tau \hat{b}(\tau)\hat{\chi}_{sf,k}(0) > \quad ,$$

$$(A.4.2.c) \qquad G_{kb}(\tau) = - < T_\tau \hat{\chi}_{sf,k}(\tau)\hat{b}(0) > \quad ,$$

and

$$(A.4.2.d) \qquad G_{kk'}(\tau) = - < T_\tau \hat{\chi}_{sf,k}(\tau)\hat{\chi}_{sf,k'}(0) > \quad ,$$

where $\hat{\chi}_{sf,k}$ is the Fourier transformed Majorana field in momentum space.

The equations of motion in Matusubara frequency space read

$$(A.4.3.a) \qquad i\omega_n G_b = 1 + \frac{\tilde{V}}{\sqrt{N_s}} \sum_k G_{kb} \quad ,$$

$$(A.4.3.b) \qquad (i\omega_n - \epsilon_k) G_{kb} = \frac{\tilde{V}^*}{\sqrt{N_s}} G_{bb} \quad ,$$

$$(A.4.3.c) \qquad i\omega_n G_{bk'} = \frac{\tilde{V}}{\sqrt{N_s}} \sum_{k''} G_{k''k'} \quad ,$$

and

$$(A.4.3.d) \qquad (i\omega_n - \epsilon_k) G_{kk'} = \delta_{kk'} + \frac{V^*}{\sqrt{N_s}} G_{bk'} \quad ,$$

where $\tilde{V} = iJ\sqrt{2/\pi a}$ is the effective mixing matrix element between $\hat{b}, \hat{\chi}_{sf}$, and ϵ_k is the energy of the ψ_{sf} fermions.

It is now straightforward to solve these equations for the separate Green's functions, and we find

$$(A.4.4.a) \qquad G_b = \frac{1}{i\omega_n + i\Gamma sgn\omega_n} \quad ,$$

$$(A.4.4.b) \qquad G_{kb} = \frac{\tilde{V}^*}{\sqrt{N_s}} \frac{1}{(i\omega_n - \epsilon_k)(i\omega_n + i\Gamma sgn\omega_n)} = \frac{\tilde{V}^*}{\tilde{V}} G_{bk} \quad ,$$

and

$$(A.4.4.c) \qquad G_{kk'} = \frac{\delta_{kk'}}{i\omega_n - \epsilon_k} + \frac{|\tilde{V}|^2}{N_s} \frac{1}{(i\omega_n - \epsilon_k)(i\omega_n + i\Gamma sgn\omega_n)(i\omega_n - \epsilon_{k'})} \quad .$$

This completes the derivation.

12 References

Abrahams, E., 1992, J. Phys. Chem. Sol **53**, 1487.
Abrahams, E., A.V. Balatsky, J.R. Schrieffer, and P.B. Allen, 1993, Phys. Rev. B**47**, 513.
Abrahams, E., A.V. Balatsky, J.R. Schrieffer, and D.J. Scalapino, 1995, Phys. Rev. B**52**, 1271 (erratum, B**52**, 15649).
Abrikosov, A.A., 1965, Physics **2**, 5.
Abrikosov, A.A. and A.A. Migdal, 1970, J. Low Temp. Phys. **3**, 519.
Affleck, I., 1990a, Nuc. Phys. B**336**, 517.
Affleck, I., 1990b, in *Fields, Strings, and Critical Phenomena*, eds. C. Itzykson, H. Saleur, and J.-B. Zuber (North-Holland, Amsterdam), p. 563.
Affleck, I., 1993, Proceedings of 1993 Taniguchi Symposium (cond-mat/9311054).
Affleck, I., 1995, Lecture Notes from 1995 Polish Summer School on Theoretical Physics, Acta Physica Polonica B**26**, 1869.
Affleck, I., and A.W.W. Ludwig, 1991a, Nuc. Phys. B**352**, 849.
Affleck, I., and A.W.W. Ludwig, 1991b, Nuc. Phys. B**360**, 641.
Affleck, I., and A.W.W. Ludwig, 1991c, Phys. Rev. Lett. **67**, 161.
Affleck, I., and A.W.W. Ludwig, 1992, Phys. Rev. Lett., **68**, 1046.
Affleck, I., and A.W.W. Ludwig, 1993, Phys. Rev. B **48**, 7297.
Affleck, I., A.W.W. Ludwig, and B.A. Jones, 1995, Phys. Rev. B**52**, 9528.
Affleck, I., A.W.W. Ludwig, H.-B. Pang, and D.L. Cox, 1992, Phys. Rev. B**45**, 7918.
Akimenko, A.I., and V.A. Gadimenko, 1993, Sol. St. Comm. **87**, 925.
Aliev, F.G., 1984, Sov. Phys. Sol. St. **26**, 682.
Aliev, F.G., S. Vieira, R. Villar, H.P. van der Menlen, K. Bakker, A.V. Andreev, 1993, JETP Lett **58**, 762 (Sov. Phys. ZhETP, Pisma **58**, 814).
Aliev, F.G., H. El. Mfarrej, S. Vieira, P. Villar, 1994, Solid State Comm.**91**, p.775.
Aliev, F.G., S Vieira, R. Villar, J.L. Martinez, C.L. Seaman, 1995a, Physica B **206-207**, p.454.
Aliev, F.G., H. El. Mfarrej, S. Vieiera, R. Villar, and J.L. Martinez, 1995b, Europhysics Letters **32**, 765.
Aliev, F.G., H. El. Mfarrej, S. Vieira, and R. Villar, 1996a, Physica B**223&224**, 464.
Aliev, F.G., S. Vieira, R. Villar, and J.L. Martinez, 1996b, Physica B**223&224**, 475.
Aliev, F.G., H. El. Mfarrej, S. Vieira, and R. Villar, 1996c, Europhysics Lett. **34**, 605.
Allen, J.W., 1991, Physica B**171**, 175.
Allen, J.W., L.Z. Liu, R.O. Anderson, C.L. Seaman, M.B. Maple, Y. Dalichaouch, J.-S. Kang, M. Torakachvili, M.A. Lopez de la Torre, 1993, Physica B**186-188**, 307.
Altschüler, D., M. Bauer, and C. Itzykson, 1990, Comm. Math. Phys. **132**, 349.
Altshuler, B.L., and A.G. Aronov, 1985, in *Electron-Electron Interactions in Disordered Systems*, eds. A.L. Efros and M. Pollak (North-Holland, New York), p. 1.
Amara, M, D. Finsterbusch, B. Luy, B. Luthi, and H.R. Ott, 1995, Phys. Rev. B**51**, 16407.
Amit, D.J., Y.Y. Goldshmidt, and G. Grinstein, 1980, J. Phys. A**13**, 585.
Amitsuka, H., T. Hidano, T. Honma, H. Mitamura, and T. Sakakibara, 1993, Physica B**186-188** , 337.
Amitsuka, H., and T. Sakakibara, 1994, J. Phys. Soc. Jap. **63**, 736.
Amitsuka, H., T. Shimamoto, T. Honma, and T. Sakakibara, 1995, Physica B**206-207**, 461.
Anders, F., 1995a, Physica B**206& 207**, 177.
Anders, F., 1995b, J. Phys. Cond. Matt. **7**, 2801.
Anders, F., and N. Grewe, 1994, Europhysics Letters **26**, 551.
Anders, F., M. Jarrell, and D.L. Cox, 1997, Phys. Rev. Lett. **78**, 2000.
Anderson, P.W., 1950, Phys. Rev. **79**, 350.
Anderson, P.W., 1961, Phys. Rev. **124**, 41.
Anderson, P.W., 1967, Phys. Rev. Lett. **18**, 1049.

Anderson, P.W., 1970, J. Phys. C. **3**, 2346.
Anderson, P.W., 1981, in *Valence Fluctuations in Solids*, eds. L.M. Falikov, W. Hanke, and M.B. Maple (North-Holland, Amsterdam), p. 451.
Anderson, P.W., B.I. Halperin, and C.M. Varma, 1971, Philos. Mag. **25**, 1.
Anderson, P.W., and C.C. Yu, Proc. Intl. School of Physics "Enrico Fermi", eds. F. Bassani *et al.* (North-Holland, Amsterdam, 1985), p. 767.
Anderson, P.W., G. Yuval, and D.R. Hamann, 1970, Phys. Rev. B**1**, 4464.
Andraka, B., 1994a, Phys. Rev. B **49**, 3589.
Andraka, B., 1994b, Phys. Rev. B**49**, 348.
Andraka, B. and A.M. Tsvelik, 1991, Phys. Rev. Lett. **67**, 2886.
Andraka, B., and G.R. Stewart, 1994, Phys. Rev. B**49**, 12359.
Andrei, N., 1980, Phys. Rev. Lett. **45**, 379.
Andrei, N., 1982, Phys. Letters **87A**, 299.
Andrei, N., 1995, unpublished.
Andrei, N. and C. Destri, 1984, Phys. Rev. Lett. **52**, 364.
Andrei, N., and A. Jerez, 1995, Phys. Rev. Lett. **74**, 4507 (1995).
Andrei, N., K. Furuya, and J.H. Lowenstein, 1983, Rev. Mod. Phys. **55**, 331.
Appelbaum, J.A., and L.Y.L. Shen, 1972, Phys. Rev. B**5**, 544.
Aronson, M.C., J.D. Thompson, J.L. Smith, Z. Fisk, and M.W. McElfresh, 1989, Phys. Rev. Lett. **63** 2311.
Aronson, M.C., R. Osborn, R.A. Robinson, J.W. Lynn, R. Chau, C.L. Seaman, and M.B. Maple, 1995, Phys. Rev. Lett. **75**, 725.
Auerbach, A. and K. Levin, 1986, Phys. Rev. Lett. **57**, 877.
Baeriswyl, D., P. Horsch, and K. Maki, 1988, Phys. Rev. Lett. **60**, 70.
Balatsky, A.V., and E. Abrahams, 1992, Phys. Rev. B**45**, 13125.
Balatsky, A.V., E. Abrahams, D.J. Scalapino, and J.R. Schrieffer, 1994, Physica B**199&200**, 363.
Balkashin, O.P., R.J.P. Keijsers, H. van Kempen, Yu. A. Koleshnichenko, and O.I. Shklyarevskii, 1997, preprint.
Bander, M., 1976, Phys. Rev. D**13**, 1566.
Barnes, S.E., 1976, J. Phys. F**6**, 1375.
Barnes, S.E., 1988, Phys. Rev. B**37**, 3671.
Berezinskii, V.L., 1974, JETP Lett. **20**, 287 (ZhETP Pisma **20**, 628).
Bermon, S., and C.K. So, 1978, Phys. Rev. Lett. **40**, 53.
Bernal, O.O., D.E. MacLaughlin, H.G. Lukefahr, and B. Andraka, 1995, Phys. Rev. Lett. **75**, 2023.
Bickers, N.E., 1987, Rev. Mod. Phys. **59**, 845.
Bickers, N.E., D.L. Cox, and J.W. Wilkins, 1987, Phys. Rev. B**36**, 2036.
Black, J.L., 1981, in *Metallic Glasses*, eds. H.J. Güntherodt and H. Beck (Springer, New York), p. 167.
Black, J.L., and B.L. Györffy, 1978, Phys. Rev. Lett. **41**, 1595.
Black, J.L., B.L. Györffy, and J. Jäckle, 1979, Philos. Mag. B**40**, 331.
Black, J.L. K. Vladár , and A. Zawadowski, 1982, Phys. Rev. B**26**, 1559.
Broholm, C., H. Lin, P.T. Matthews, T.E. Mason, W.J.L. Buyers, M.F. Collins, A.A. Menovsky, J.A. Mydosh, J.K. Kjems, 1992, Phys. Rev. B**42**, 12809.
Bulla, R., and A.C. Hewson, 1997, preprint (cond-mat/9701152).
Bulla, R., A.C. Hewson, and G.-M. Zhang, 1997, preprint (cond-mat/9704024).
Burin, A.L., and Yu. Kagan, 1996, JETP **82**, 159 (Zh. Eksp. Teor. Fiz. **109**, 299).
Buschinger, B., C. Geibel, and F. Steglich, 1996, unpublished.
Buyers, W.J.L., A.F. Murray, T.M. Holden, E.C. Svensson, P. de V. Du Plessis, G.H. Lander, O. Vogt, 1980, Physica **102B**, 291.
Caldeira, A.O. and A.J. Leggett, 1981, Phys. Rev. Lett. **46**, 211.
Caldeira, A.O. and A.J. Leggett, 1983, Ann. Phys. (NY) **149**, 374.

Cardy, J.L., 1984, Nuc. Phys. B**240**, 514.
Cardy, J.L., 1986a, Nuc. Phys. B**270**, 186.
Cardy, J.L., 1986b, Nuc. Phys. B**275**, 200.
Chandra, P., A.P. Ramirez, P. Coleman, E. Brüch, A.A. Menovsky, Z. Fisk, and E. Bucher, 1994, Physica B**199&200**, 426.
Chattopadhyay, A., and M. Jarrell, 1996, to be published in Phys. Rev. B (Rap. Comm.) (cond-mat/9609238).
Chun, K. and N.O. Birge, 1993, Phys. Rev. B**48** 11500.
Clarke, D., T. Giamarchi, and B. Shraiman, 1993, Phys. Rev. B**48**, 7070.
Cochrane, R.W., R. Harris, J.O. Strom-Olsen, and M.J. Zuckerman, 1975, Phys. Rev. Lett. **35**, 676.
Coleman, P., 1983, Phys. Rev. B**28**, 5255.
Coleman, P., 1984, Phys. Rev. B**29**, 3035.
Coleman, P., 1987, Phys. Rev. B**35**, 5072.
Coleman, P., and A.J. Schofield, 1995, Phys. Rev. Lett. **75**, 2184.
Coleman, P., L. Ioffe, and A.M. Tsvelik, 1995, Phys. Rev. B**52**, 6611.
Coleman, P., E. Miranda, and A.M. Tsvelik, 1993, Phys. Rev. Lett. **70**, 2960.
Coleman, P., E. Miranda, and A.M. Tsvelik, 1994, Phys. Rev. B**49**, 8955.
Coleman, P., E. Miranda, and A.M. Tsvelik, 1995, Phys. Rev. Lett. **74**, 1653.
Coleman, P., A. Georges, and A.M. Tsvelik, 1997, J. Phys. Cond. Matt. **9**, 345.
Coleman, P., A.M. Tsvelik, N. Andrei, and H.Y. Kee, 1997, preprint (cond-matt/9707002).
Coqblin, B. and J.R. Schrieffer, 1969, Phys. Rev. **185**, 847.
Costi, T.A., P. Schmitteckert, J. Kroha, and P. Wölfle, 1994, Phys. Rev. Lett. **73**, 1275.
Costi, T.A., J. Kroha, and P. Wolfle, 1996, Phys. Rev. B**53**, 1850.
Cox, D.L, 1987a, Phys. Rev. B**35**, 4561.
Cox, D.L., 1987b, Phys. Rev. Lett. **59**, 1240.
Cox, D.L., 1987c, Phys. Rev. Lett. **58**, 2730.
Cox, D.L., 1987d, in **Proceedings of the 5th International Conference on Valence Fluctuations**, eds. S. Malik and K. Gupta (Plenum, New York) p. 553.
Cox, D.L., 1988a), Physica C**153**, 1642.
Cox, D.L., 1988b), J. Mag. Mag. Mat. **76/77**, 53.
Cox, D.L., 1990, preprint, unpublished.
Cox, D.L., 1993, Physica B **186-188**, 312.
Cox, D.L., 1996, Physica B **223&224**, 453.
Cox, D.L., and A. Ruckenstein, 1993, Phys. Rev. Lett.**71**, 1613.
Cox, D.L., and M. Makivic, 1994, Physica B**199&200**, 391.
Cox, D.L, and A.W.W. Ludwig, 1997, to be published.
Cox, D.L., and M.B. Maple, 1995, Physics Today **48**, 32.
Cox, D.L., K. Kim, and A.W.W. Ludwig, 1997, unpublished.
Cox, D.L., 1996, Physica B**223&224**, 453.
Cox, D.L., and M. Jarrell, 1996, J. Phys. Cond. Matt. **8**, 9825.
Cragg, D.M. and P.Lloyd, 1978, J. Phys. C **11**, L597.
Cragg, D.M., P. Lloyd, and P. Nozières , 1980, J. Phys. C**13**, 803.
Cruz, L., P. Phillips, and A.H. Castro-Neto, 1995, Europhysics Lett. **29**, 389.
Dai, P., H.A. Mook, C.L. Seaman, M.B. Maple, and J.P. Koster, 1995, Phys. Rev. Lett. **75**, 1202.
de Haas, W.J., J. de Boer, and G.J. van den Berg, 1933/34, Physica **1**, 1115.
DeGeorgi, L., and H.R. Ott, 1996, J. Phys. Cond. Matt. **8**, 9901.
DeGeorgi, L., 1997, private communication.
Delft, J. von, D.C. Ralph, R.A. Buhrman, A.W.W. Ludwig, and V. Ambegaokar, 1997a, submitted to Annals of Physics (cond-mat/9702048).
Delft, J. von, A.W.W. Ludwig, and V. Ambegaokar, 1997b, submitted to Annals of Physics (cond-

mat/9702049).
Delft, J. von, and G. Zaránd , 1997, preprint.
Desgranges, H.-U., 1985, J. Phys. C**18**, 5481.
Dobrosavljevic, V., T. Kirkpatrick, G. Kotliar, 1992, Phys. Rev. Lett. **6**, 1113.
Emery, V.J., and S.A. Kivelson, 1992, Phys. Rev. B**46**, 10812.
Emery, V.J., and S.A. Kivelson, 1993, Physica **209C**, 597.
Emery, V.J. and S.A. Kivelson, 1993, Phys. Rev. Lett. **71**, 3701.
Emery, V.J., and S.A. Kivelson, 1994, in **Fundamental Problems in Statistical Mechanics, VII**, eds. H. van Beijeren and M.E. Ernst (North-Holland-Elsevier, Amsterdam) pp. 1-26.
Endo, T., and T. Kino, 1988, J. Phys. F**18**, 2203.
Esquinazi, P., H.M. Ritter, H. Neckel, G. Weiss, and S. Hunklinger, 1986, Z. Phys. B**64**, 81.
Esquinazi, P., R. König, and F. Pobell, 1992, Z. Phys. B**87**, 305.
Fabrizio, M. and A.O. Gogolin, 1994, Phys. Rev. B**50**, 17732.
Fabrizio, M. and G. Zaránd , 1996, Phys. Rev. B**54**, 10008.
Fabrizio, M., A.O. Gogolin, and P. Nozières , 1995a, Phys. Rev. Lett. **74**, 4503.
Fabrizio, M., A.O. Gogolin, and P. Nozières , 1995b, Phys. Rev. B**51**, 16088.
Falci, G., G. Schön, and G. Zimányi , 1995, Phys. Rev. Lett. **74**, 3257.
Fendley, P., 1993, Phys. Rev. Lett. **71**, 2485.
Fowler, M. , and A. Zawadowski , 1971, Sol. St. Comm. **9**, 471.
Fradkin, E., 1991, **Field Theories of Condensed Matter Systems**, (Addison Wesley, Cambridge, MA)
Friedel, J., 1952, Philos. Mag. **43**, 153.
Fujimoto, S., N. Kawakami, and S.K. Yang, 1996, J. Phys. Korea **29**, 136.
Fulde, P., 1978, in **Handbook on the Physics and Chemistry of the Rare Earths, Vol. II**, eds. K.A. Gschneidner and L. Eyring (Elsevier, Amsterdam), Ch. 17.
Fye, R.M., 1994, Phys. Rev. Lett.**72**, 916.
Fye, R.M., and J.E. Hirsch, 1989, Phys. Rev. B**40**, 4780.
Gammel, J.T. and D.K. Campbell, 1988, Phys. Rev. Lett. **60**, 71.
Gan, J., 1995a, Phys. Rev. B**51**, 8287.
Gan, J., 1995b, Phys. Rev. Lett. **74**, 2583.
Gan. J, N. Andrei, and P. Coleman, 1993, Phys. Rev. Lett. **70**, 686.
Gaudin, M., 1967, Phys. Lett. A**24**, 55.
Georges, A., and A.M. Sengupta, 1995, Phys. Rev. Lett. **74**, 2808.
Georges, A., G. Kotliar, and Q. Si, 1992, Int. J. Mod. Phys. **6**, 705 .
Georges, A., G. Kotliar, W. Krauth, and M. Rozenberg, 1996, Rev. Mod. Phys. **68**, 13.
Giamarchi, T., and H.J. Schulz, 1988, Phys. Rev. B**37**, 325.
988, Phys. Rev. B**37**, 325.
Giamarchi, T., C.M. Varma, A.E. Ruckenstein, and P. Nozières , 1993, Phys. Rev. Lett. **70**, 3967.
Giordano, N. in **Mesoscopic Phenomena in Solids**, 1991, eds. B.L. Altshuler, P.A. Lee, and R.A. Webb (Elsevier Science, Amsterdam), p. 131.
Gogolin, A.O., 1996, Phys. Rev. B**53**, R5990.
Golden, J.M., and B.I. Halperin, 1996a, Phys. Rev. B**53**, 3893.
Golden, J.M., and B.I. Halperin, 1996b, Phys. Rev. B**54**, 16757.
Golding, B., J.E. Graebner, A.B. Kane, and J.L. Black, 1978, Phys. Rev. Lett. **41**, 1487.
Golding, B., N.M. Zimmerman, and S.N. Coppersmith, 1992, Phys. Rev. Lett. **68**, 998.
Gorymychin, E.A. and R. Osborne, 1994, Phys. Rev. B**47**, 14280.
Graebner, J.E., B. Golding, R.J. Schutz, F.S.L. Chu, and H.S. Chen, 1978, Phys. Rev. Lett. **39**, 1480.
Gregory, S., 1992, Phys. Rev. Lett. **68**, 2070.
Grewe, N., 1983, Z. Physik B**53**, 271.
Grewe, N., 1984, Sol. St. Comm. **50**, 19.

Grewe, N. and H. Keiter, 1981, Phys. Rev. B**24**, 4420.
Grewe, N., and T. Pruschke, 1985, Z. Phys. B**60**, 311.
Grewe, N., and F. Steglich, 1991, in *Handbook of the Physics and Chemistry of the Rare Earths, Vol. 14*, eds. K.A. Gschneidner Jr. and L.L. Eyring (Elsevier, Amsterdam), p. 343.
Grüner, G., 1974, Adv. in Phys. **23**, 941.
Gunnarsson, O. and K. Schönhammer, 1983, Phys. Rev. Lett. **50**, 604.
Gunnarsson, O. and K. Schönhammer, 1984, Phys. Rev. B**28**, 4315.
Haldane, F.D.M., 1981, J. Phys. C **14**, 2585.
Hamann, D.R., 1970, Phys. Rev. B**2**, 1373.
Hamermesh, M., 1962, *Group Theory in Physics* (Addison-Wesley, Reading, Mass.), pp. 161-181.
Han, J., 1994, private communication.
Heid, R., 1995, Z. Phys. B**99**, 15.
Heid, R., Ya.B. Bazaliy, V. Martisovits, and D.L. Cox, 1995, Phys. Rev. Lett. **74**, 2571.
Heid, R., Ya. B. Bazaliy, V. Martisovits, and D.L. Cox, 1996, Physica B**223&224**, 33.
Herbst, J.F. and J.W. Wilkins, 1987, in **Handbook on the Chemistry and Physics of the Rare Earths, Vol. 10**, eds. K. A. Gschneidner and L. Eyring (Elsevier, Amsterdam), p.321.
Hettler, M.H., J. Kroha, and S. Hershfield, 1994, Phys. Rev. Lett. **73**, 1967.
Hewson, A.C., 1993, **The Kondo Problem to Heavy Fermions** (Cambridge Press, Cambridge UK).
Hirsch, J., 1983, Phys. Rev. B**28**, 4059.
Hirsch, J., 1989, Phys. Lett. **138**A, 83.
Hirsch, J., and R.M. Fye, 1986, Phys. Rev. Lett. **56**, 2521.
Hirst, L.L, 1970, Phys. Kondens. Matt. **10**, 255.
Hirst, L.L., 1978, Adv. in Physics. **27**, 231.
Horn, S., E. Holland-Moritz, M. Loewenhaupt, F. Steglich, H. Scheuer, A. Benoit, and J. Flouquet, 1981, Phys. Rev. B**32**, 3260.
Hubbard, J., 1963, J. Proc. Roy. Soc. (London) **276**, 238.
Hunklinger, S., and W. Arnold, 1976, in *Physical Acoustics*, eds. W.P. Mason and R.N. Thurston (Academic, New York), v. 12, p. 1555.
Inagaki, S., 1979, Prog. Th. Phys. **62**, 1441.
Ingersent, K., B.A. Jones, and J.W. Wilkins, 1992, Phys. Rev. Lett. **69**, 2594.
K. Ingersent, and B.A. Jones 1994, Physica B**199&200**, 402 .
Ishiguro, T., H. Kaneko, Y. Nogami, H. Ishimoto, H. Nishiyama, J. Tsukamoto, A. Takahashi, M. Yamaura, T. Hagiwara, and K. Sato, 1992, Phys. Rev. Lett. **69**, 660.
Jaccard, D., 1992, Phys. Lett. A**163**, 475.
Jansen, A.G.M., A.P. van Gelder, and P. Wyder, 1980, J. Phys. C**13**, 6073.
Jarrell, M., 1995, Phys. Rev. B**51**, 7429.
Jarrell, M., and T. Pruschke, 1996, private communication.
Jarrell, M., H.-B. Pang, D.L. Cox, and K.-H. Luk, 1996, Phys. Rev. Lett. **77**, 1612.
Jarrell, M., *et al.*, 1997, unpublished.
Jarrell, M., H.-B. Pang, and D.L. Cox, 1997, Phys. Rev. Lett. **78**, 1996.
Jarrell, M., H.-B. Pang, D.L. Cox, F. Anders, and A. Chattopadhyay, 1996c, Physica B **230-232**, 557.
Jerez, A., 1995, private communication (unpublished).
Jones, B.A., 1988, Ph.D. dissertation (Cornell Univ., unpublished).
Jones, B.A., and C.M. Varma, 1987, Phys. Rev. Lett. **58**, 843.
Jones, B.A., C.M. Varma, and J.W. Wilkins, 1988, Phys. Rev. Lett. **61**, 125.
Kac, V.G., and K. Peterson, 1984, Adv. Math **53**, 125.
Jones, B.A., and K. Ingersent, 1994, Physica B**199&200**, 411.
Han, J., 1995, private communication.
Kagan, Yu. and N.V. Prokof'ev, 1986, Zh. Eksp. Teor. Fiz. **90**, 2176 [Sov. Phys. JETP **63**, 1276 (1987(a))].

Kagan, Yu. and N.V. Prokof'ev, 1987, Zh. Eksp. Teor. Fiz. **93**, 366 [Sov. Phys. JETP **66**, 211 (1987(b))].
Kagan, Yu. and N.V. Prokof'ev, 1989, Zh. Eksp. Teor. Fiz. **96**, 1473 [Sov. Phys. JETP **69**, 836 (1989)].
Kagan, Yu. and N.V. Prokof'ev, 1992, in **Quantum Tunneling in Condensed Matter**, eds. Yu. Kagan and A.J. Leggett (Elsevier, Amsterdam), p. 37.
Kästner, J., H.J. Schink, and E.F. Wasserman, 1981, Sol. St. Comm. **33**, 527.
Katayama, S., and K. Murase, 1980, Sol. St. Comm. **36**, 707.
Katayama, S., S. Maekawa, H. Fukuyama, 1987, J. Phys. Soc. Jap. **56**, 697.
Keiter, H. and J.C. Kimball, 1971, Int. J. Magn. **1**, 233.
Keijsers, R.J., O.J. Shklyarevskii, and H. van Kempen, 1995, Phys. Rev. B**51**, 5628.
Keijsers, R.J., O.J. Shklyarevskii, and H. van Kempen, 1996, Phys. Rev. Lett. **77**, 3411.
Kim, E., T.-S. Kim, J. Han, M. Makivic, and D.L. Cox, 1995, to be published.
Kim, J.S., B. Andraka, C.S. Jee, S.B. Roy, and G.R. Stewart, 1990, Phys. Rev. B**41**, 11073.
Kim, J.S., B. Andraka, and G.R. Stewart, 1992, Phys. Rev. B**45**, 12081.
Kim, T.-S., 1994, private communication.
Kim, T.-S., 1995, Ph.D. dissertation (The Ohio State University, unpublished).
Kim, T.-S., and D.L. Cox, 1995, Phys. Rev. Lett. **75**, 1622.
Kim, T.-S., and D.L. Cox, 1996, Phys. Rev. B**54**, 6494.
Kim, T.-S. and D.L. Cox, 1997, to be published in Phys. Rev. B, (cond-mat/9508129).
Kim, T.-S., L.N. Oliveira, and D.L. Cox, 1997, to be published in Phys. Rev. B (cond-mat/9606095).
Kim, W.W.,J. S. Kim, B. Andraka, and G. R. Stewart, 1993, Phys. Rev. B**47**, 12403.
Kivelson, S., W.P. Su, J.R. Schrieffer, and A.J. Heeger, 1987, Phys. Rev. Lett. **58**, 1899.
Kondo, J., 1964, Prog. Theor. Phys. **32**, 37.
Kondo, J., 1976a, Physica **84B**, 40.
Kondo, J., 1976b, Physica **84B**, 207.
Kondo, J., 1984a, Physica **123B**, 175.
Kondo, J., 1984b, Physica **126B**, 377.
Kondo, J., 1985, Physica **132B**, 303.
Kondo, J., 1986, Hyperfine Interactions **31**, 117 (1986).
Koster, G.F., J.O. Dimmock, R.G. Wheeler, and H. Statz, 1963, *Properties of the Thirty-Two Point Groups* (M.I.T. Press, Cambridge, Mass.).
Kotliar, G., E. Abrahams, A.E. Ruckenstein, C.M. Varma, P.B. Littlewood and S. Schmitt-Rink, 1991, Europhysics Lett. **15**, 655.
Kozub, V.I., 1995, private communication.
Kozub, V.I. and I.O. Kulik, 1986, Zh. Eksp. Teor. Fiz. **91**, 2243 (Sov. Phys. JETP **64**, 1332 (1986)).
Krishna-murthy, H.R., J.W. Wilkins, and K.G. Wilson, 1980a, Phys. Rev. B**21**, 1003.
Krishna-murthy, H.R., J.W. Wilkins, and K.G. Wilson, 1980b, Phys. Rev. B**21**, 1044.
Kroha, J., P.J. Hirschfeld, K.A. Muttalib, and P. Wolfle, 1992, Sol. St. Comm. **83**, 1003.
Kroha, J., P. Wolfle, and T.A. Costi, 1997, Phys. Rev. Lett. **79**, 261 (1997).
Kuramoto, Y., 1983, Z. Phys. B**53**, 37.
Kuramoto, Y. and H. Kojima, 1984, Z. Phys. B**57**, 95.
Kuramoto, Y., and E. Müller-Hartmann, J. Mag. Magn. Mat. **52**, 122.
Kusunose, H., and K. Miyake, 1996, J. Phys. Soc. Jap. **65**, 3032.
Lang, J.K., Y. Baer, and P.A. Cox, 1981, J. Phys. F**11**, 121.
Langreth, D.C., 1966, Phys. Rev. **150**, 516.
Lasjaunias, J.C., and A. Ravex, 1983, J. Phys. F**13**, L101.
Lee, P.A., and T.V. Ramakrishnan, 1985, Rev. Mod. Phys. **57**, 289.
Lea, K.R., M.J.M. Leask, and W.P. Wolf, 1962, J. Phys. Chem. Solids **23**, 1381.
Leggett, A.J., S. Chakravarty, A.T. Dorsey, M.P.A. Fisher, A. Garg, and W. Zwerger, 1987, Rev. Mod.

Phys. **59**, 1.
Liu, L.Z., J.W. Allen, C.L. Seaman, M.B. Maple, Y. Dalichaouch, J.-S. Kang, M.S. Torikachvili, and M.A. Lopez de la Torre, 1992, Phys. Rev. Lett. **68**, 1034.
Livermore, C., C.H. Crouch, R.M. Westervelt, K.L. Campman, and A.C. Gossard, 1996, Science **274**, 1332.
Lloyd, P., A.W. Mirtschin, and D.M. Cragg, 1981, J. Phys. A. **14**, 659.
Löhneysen, M. Platte, W. Sander, H. J. Schink, G.V. Minigerode, and K. Samwer, 1980, J. Physique **41**, C8-745.
Ludwig, A.W.W., 1994a, Int. J. Mod. Phys. B**8**, 347.
Ludwig, A.W.W., 1994b, Physica B**199-200**, 406.
Ludwig, A.W.W. and I. Affleck, 1991, Phys. Rev. Lett. **67**, 3160.
Ludwig, A.W.W., and I. Affleck, 1994, Nucl. Phys. B**428**, 545.
Luk, K.-H., 1992, Ph.D. dissertation (The Ohio State University, unpublished).
Luk, K.-H., M. Jarrell, and D.L. Cox, 1994, Phys. Rev. B**49**, 16066.
Luke, G., 1995, private communication.
MacLaughlin, D.E., O.O. Bernal, and H.G. Lukefahr, 1996, J. Phys. Cond. Matt. **8**, 9855.
Maekawa, S., S. Takahashi, and M. Tachiki, 1984, J. Phys. Soc. Jap. **53**, 702.
Maekawa, S., S. Takahashi, S. Kashiba, and M. Tachiki, 1985, J. Phys. Soc. Jpn. **54**, 1955.
Mahan, G.D., 1990, **Many Particle Physics (Second Edition)** (Plenum, New York).
Maldacena, J.M., and A.W.W. Ludwig, 1996, to be published in Nuc. Phys. B. (cond-mat/9502109).
Maple, M.B., C.L. Seaman, D.A. Gajewski, Y. Dalichaouch, V.B. Barbetta, M.C. deAndrade, H.A. Mook, H.G. Lukefahr, O.U. Bernal, and D.E. MacLaughlin, 1994, J. Low. Temp. Phys. **94**, 225.
Maple, M.B., R.P. Dickey, J. herrmann, M.C. de Andrade, E.J. Freeman, D.A. Gajewski, and R. Chau, 1996, J. Phys. Cond. Matt. **8**, 9773.
Marumoto, K., T. Takeuchi, and Y. Miyako, 1996, Phys. Rev. B**54**, 12194.
Matsuura, T., and K. Miyake, 1986a, J. Phys. Soc. Jap. **55**, 29.
Matsuura, T., and K. Miyake, 1986b, J. Phys. Soc. Jap. **55**, 610.
Matveev, K.A., 1991, Sov. Phys. JETP **72**, 892 [Zh. Eksp. Teor. Fiz. **99**, 1598].
Matveev, K.A., 1995, Phys. Rev. B**51**, 1743.
Matveev, K.A., L.I. Glazman, and H.U. Baranger, 1996a, Phys. Rev. B**53**, 1034.
Matveev, K.A., L.I. Glazman, and H.U. Baranger, 1996b, Phys. Rev. B**54**, 5637.
McElfresh, M.W., M.B. Maple, J.O. Willis, D. Schiferl, J.L. Smith, Z. Fisk, and and D.L. Cox, 1993, Phys. Rev. B**48**, 10395.
McEwen, K., M.J. Bull, and R.S. Eccleston, 1995, Physica B**206&207**, 112.
Menge, B., and E. Müller-Hartmann, 1988, Z. Phys. B**73**, 225.
Metzner, W., and D Vollhardt, 1989, Phys. Rev. Lett. **62**, 324.
Mezei, F. and A. Zawadowski , 1971, Phys. Rev. B**3**, 3127.
Mihály, L. and A. Zawadowski , 1978, J. Phys. Lett. **39**, L-483.
Miranda, E., V. Dobrosavljevíc, and G. Kotliar, 1996, J. Phys. Cond. Matt. **8**, 9871.
Miranda, E., V. Dobrosavljevíc, and G. Kotliar, 1997, Phys. Rev. Lett. **78**, 290.
Mirtschin, A.W., 1986, Ph.D. Dissertation, University of Monash (unpublished).
Mirtschin, A.W., and P. Lloyd, 1984, J. Phys. C**17**, 5399.
Millis, A.J. and P.A. Lee, 1987, Phys. Rev. B**35**, 3394 (1987).
Molenkamp, L.W., K. Flensberg, and M. Kemerink, 1995, Phys. Rev. Lett. **75**, 23.
Mook, H., C.L. Seaman, M.B. Maple, M.A. Lopez de la Torre, D.L. Cox, M. Makivic, 1993, Physica B**186-188**, 341.
Morin, P., and D. Schmitt, 1981, Phys. Rev. B**23**, 5936.
Moustakas, A. and D. Fisher, 1995, Phys. Rev. B**51**, 6908.
Moustakas, A., and D. Fisher, 1996, Phys. Rev. B**53**, 4300.
Moustakas, A., and D. Fisher, 1997, preprint (cond-mat/9607208).

Müller-Hartmann, E., 1984, Z. Phys. B**57**, 281.
Müller-Hartmann, E., 1989, Z. Phys. B **74**, 507.
Muramatsu, A. and F. Guinea, 1986, Phys. Rev. Lett. **57**, 2337.
Newns, D.M. and N. Read, 1987, Adv. in Phys. **36**, 799.
Ngai, K.S., J.A. Appelbaum, M.H. Cohen, and J.C. Phillips, 1967, Phys. Rev. **163**, 352.
Niksch, M., W. Assmus, B. Lüthi, H.R. Ott, and J.K. Kjems, 1982, Helv. Phys. Acta **55**, 688.
Nozières , P., 1969, unpublished.
Nozières , P., 1974, J. Low Temp. Phys. **17**, 31.
Nozières, P. and A. Blandin, 1980, J. Phys. (Paris) **41**, 193.
Nozières, P. and C.T. De Dominicis, 1969, Phys. Rev. **178**, 1097.
Nozières , P., J. Gavoret, and B. Roulet, 1968, Phys. Rev. **178**, 1084.
Nunes, A.C., J.W. Rasul, and G.A. Gehring, 1986, J. Phys. C**19**, 1017.
Ott, H.R., 1987, Prog. Low. Temp. Phys. **6**, 215.
Pang, H.-B., 1992, Ph.D. dissertation (The Ohio State University, unpublished).
Pang, H.-B., 1994, Phys. Rev. Lett. **73**, 2736.
Pang, H.-B., and D.L. Cox, 1991, Phys. Rev. B**44**, 9454.
Parcollet, O., and A. Georges, 1997, preprint (cond-mat/9707337).
Pasquier, C., U. Meirav, F.I.B. Williams, D.C. Glattli, Y. Jin, and B. Etienne, 1993, Phys. Rev. Lett. **70**, 69.
Penc, K., and A. Zawadowski , 1994, Phys. Rev. B**50**, 10578.
Phillips, W.A., 1972, J. Low Temp. Phys. **7**, 351.
Pruschke, Th., 1989, Ph.D. Dissertation, Technische Hochschule, Darmstadt, Germany (unpublished).
Pruschke, Th., D.L. Cox, and M. Jarrell, 1993, Phys. Rev. B**47**, 3553.
Pruschke, Th., M. Jarrell and J.K. Freericks, 1995, Adv. in Phys. **44**, 187.
Ralls, K.S., and R.A. Buhrman, 1988, Phys. Rev. Lett. **60**, 2434.
Ralls, K.S., and R.A. Buhrman, 1991, Phys. Rev. B**44**, 5800.
Ralph, D.C., 1993, Ph.D. Dissertation (Cornell University, unpublished).
Ralph, D.C., and R.A. Buhrman, 1992, Phys. Rev. Lett. **69**, 2118.
Ralph, D.C., and R.A. Buhrman, 1995, Phys. Rev. B**51**, 3554.
Ralph, D.C., A.W.W. Ludwig, J. von Delft, and R.A. Buhrman, 1994, Phys. Rev. Lett. **72**, 1064.
Ralph, D.C., A.W.W. Ludwig, J. von Delft, and R.A. Buhrman, 1995, Phys. Rev. Lett. **75**, 770 (1995).
Ramakrishnan, T.V., 1981, in *Valence Fluctuations in Solids*, eds. L.M. Falikov, W. Hanke, and M.B. Maple (North-Holland, Amsterdam), p. 13.
Ramakrishnan, T.V., 1988, J. Mag. Mag. Mat. **76&77**, 657.
Ramakrishnan, T.V. and K. Sur, 1982, Phys. Rev. B**26**, 1798.
Ramirez, A.P., P. Chandra, P. Coleman, Z. Fisk, J.L. Smith, and H.R. Ott, 1994, Phys. Rev. Lett. **73**, 3018.
Read, N., K. Dharamvir, J.W. Rasul, and D.M. Newns, 1986, J. Phys. C**19**, 1597.
Read, N. and D.M. Newns, 1983, J. Phys. C**16**, 3273.
Roulet, B., J. Gavoret, and P. Nozières , 1968, Phys. Rev. **178**, 1072.
Rudin, S., 1983, Phys. Rev. B**28**, 4825.
Sacramento, P.D. and P.Schlottmann, 1989, Phys. Lett. A**142**, 245.
Sacramento, P.D. and P.Schlottmann, 1991, Phys. Rev. B**43**, 13294.
Sakai, O., Y. Shimizu, N. Kaneko, 1993, Physica B**186-188**, 323.
Scalapino, D.J. and P. Marcus, 1967, Phys. Rev. Lett. **18**, 459.
Schiller, A., and S. Hershfield, 1995, Phys. Rev. B**51**, 12896.
Schiller, A., and S. Hershfield, 1997, preprint.
Schlottmann, P., 1978, J. Phys. **C6**, 1486.
Schlottmann, P. and P.D. Sacramento, 1993, Adv. Physics **42**, 641.
Schofield, A.J., 1997, Phys. Rev. B**55**, 5627.

Schrieffer, J.R., 1967, J. Appl. Phys. **38**, 1143.
Schrieffer, J.R. and P.A. Wolff, 1966, Phys. Rev. **149**, 491.
Seaman, C.L., M.B. Maple, B.W. Lee, S. Ghamaty, M.S. Torikachvilli, J.-S. Kang, L.Z. Liu, J.W. Allen, and D.L. Cox, 1991, Phys. Rev. Lett. **67**, 2882.
Seaman, C.L., M.B. Maple, B.W. Lee, S. Ghamaty, M.S. Torikachvilli, J.-S. Kang, L.Z. Liu, J.W. Allen, and D.L. Cox, 1992, J. Alloys and Compounds **181**, 327.
Seaman, C.L. and M.B. Maple, 1994, Physica B**199&200**, 396.
Sengupta, A.M., and A. Georges, 1994, Phys. Rev. B**49**, 10020.
Sengupta, A.M., and Y.B. Kim, 1996, Phys. Rev. B**54**, 14918.
Sereni, J., G. Nieva, J.G. Huber, E. Braun, F. Oster, E. Bruch, B. Roden, D. Wohlleben, 1986, J. Mag. Mag. Mat. **63&64**, 597.
Sethna, J., 1981, Phys. Rev. B**24**, 698.
Shiba, H., 1970, Prog. Theor. Phys. **43**, 601.
Silva, J.B., W.L.C. Lima, W.C. Oliveira, J.L.N. Mello, L.N. Oliveira, and J.W. Wilkins, 1996, Phys. Rev. Lett. **76**, 275.
Slichter, C.P., 1989, *Principles of Magnetic Resonance, 3rd Edition* (Springer-Verlag, Berlin), pp. 486-497.
Smolyarenko, I.E., and N.S. Wingreen, 1997, private communication.
Sólyom, J., 1974, J. Phys. F. **4**, 2269.
Sólyom, J., 1979, Adv. in Phys. **28**, 201 (1979).
Sólyom, J. and A. Zawadowski, 1974, J. Phys. F. **4**, 2269.
Takano, S., Y. Kumashiro, and K. Tsuji, 1984, J. Phys. Soc. Japan **53**, 4309.
Steglich, F., 1996, private communication.
Steglich, F., P. Gegenwort, C. Geibel, R. Helfrich, P. Hellmann, M. Lang, A. Link, R. Modler, G. Sparn, N. Büttgen, and A. Loidl, 1996, Physica B**223&224**, 1.
Tahvildar-Zadeh, A.N., M. Jarrell, and J.K. Freericks, 1997, Phys. Rev B**55**, 3332.
Tanabe, Y. and K. Ohtaka, 1986, Phys. Rev. B**34**, 3763.
Tinkham, M., 1964, *Group Theory and Quantum Mechanics*, (McGraw-Hill, New York).
Toulouse, G., 1970, Phys. Rev. B**2**, 270.
Trees, B., 1993, Ph.D. Dissertation (The Ohio State University, unpublished).
Trees, B., 1995, Phys. Rev. B**51**, 470.
Trees, B., and D.L. Cox, 1994, Phys. Rev. B**49**, 16066.
Tsvelik, A.M., 1985, J. Phys. C. **18**, 159.
Tsvelik, A.M., 1988, Pis'ma Zh. Eksp. Teor. Fiz. **48**, 502 [Sov. Phys. JETP Tsvelik, A.M., 1990, J. Phys. Cond. Matt. **2**, 2833.
Tsvelik, A.M. and P.B. Wiegman, 1984, Z. Phys. B**54**, 201.
Tsvelik, A.M., and P.B. Wiegman, 1985, J. Stat. Phys. **38**, 125.
Upadhyay, S.K., R.N. Louie, and R. A. Buhrman, 1997, to be published.
van der Vaart, N.C., A.J. Johnson, L.P. Kouwenhoven, D.J. Maas, W. de Jong, M.P. de Ruyter van Steveninck, A. van der Enden, C.J.P.M. Harmans, and C.T. Foxon, 1993, Physica B**189**, 99.
Varma, C.M., P.B. Littlewood, S. Schmitt-Rink, E. Abrahams, and A.E. Ruckenstein, 1989, Phys. Rev. Lett. **63**, 1996.
Verlinde, E., 1988, Nuc. Phys. **B300**, 360.
Vladár , K., 1991, Phys. Rev. B**44**, 1019.
Vladár , K., 1993, Prog. Th. Phys. **90**, 43.
Vladár , K. and A. Zawadowski , 1983a, Phys. Rev. B**28**, 1564.
Vladár , K. and A. Zawadowski , 1983b, Phys. Rev. B**28**, 1582.
Vladár , K. and A. Zawadowski , 1983c, Phys. Rev. B**28**, 1596.
Vladár , K., A. Zawadowski , and G.T. Zimányi , 1988a, Phys. Rev. B**37**, 2001.
Vladár , K., A. Zawadowski , and G.T. Zimányi , 1988b, Phys. Rev. B**37**, 2015.

Vladár , K. and G.T. Zimányi , 1985, J. Phys. C**18**, 3755.
Waugh, F.R., M.J. Berry, D.J. Mar, R.M. Westervelt, K.I. Campman, and A.C. Gossard, 1995, Phys. Rev. Lett. **75**, 705.
Waugh, F.R., M.J. Berry, C.H. Crouch, D.J. Mar, R.M. Westervelt, K.I. Campman, and A.C. Gossard, 1996, Phys. Rev. B**53**, 1413.
Wiegman, P.B., 1980, Zh. Eksp. Teor. Fiz. Pis'ma Red. **32**, 392 (JETP Lett. **1**, 364).
Wiegman, P.B. and A.M. Finkelshtein, 1978, Zh. Eksp. Teor. Fiz. **75**, 204 [Sov. Phys. JETP **48**, 102 (1979)].
Wiegman, P.B. and A.M. Tsvelik, 1983a, Pis'ma Zh. Exp. Teor. Fiz. **38**, 489 [JETP Lett. **38**, 591.]
Wiegman, P.B., and A.M. Tsvelik, 1983b, Advances in Physics **32**, 453.
Wilson, K.G., 1973, in *Collective Properties of Physical Systems, Nobel Symposium 24* (Academic Press, New York), p. 68.
Wilson, K.G., 1975, Rev. Mod. Phys. **47**, 773.
Wingreen, N., B.S. Altshuler, and Y. Meir, 1995, Phys. Rev. Lett. **75**, 769.
Winzer, K., 1975, Sol. St. Comm. **16**, 521.
Wyatt, A.F.G., 1964, Phys. Rev. Lett. **13**, 401.
Yafet, Y., C.M. Varma, and B.A. Jones, 1985, Phys. Rev. B**23**, 3171.
K. Yamada, Kei Yosida, and K. Hanzawa, 1984, Prog. Th. Phys. **71**, 450.
Yang, C.N., 1967, Phys. Rev. Lett. **19**, 1312.
Yanson, I.K. and O.I. Shklyarevskii, 1986, Fiz. Nizk. Temp. **12**, 899 [Sov. J. Low. Temp. Phys. **12**, 509 (1986).]
Yanson, I.K., V.V. Fisun, A.V. Khotkevich, R. Hesper, J.M. Kraus, J.A. Mydosh, and J.M. van Ruitenbeek, 1994, Soviet Phys. Low Temp. Phys. **20**, 836 (Fiz. Nizk. Temp. **20**, 1062).
Yanson, I.K., V.V. Fisun, R. Hesper, A.V. Khotkevich, J.M. Kraus, J.A. Mydosh, and J.M. van Ruitenbeck, 1995, Phys. Rev. Lett. **74**, 302.
Yatskar, A., W.P. Beyermann, R. Movshovich, and P.C. Canfield, 1996, Phys. Rev. Lett. **77**, 3637.
Ye, Jinwu, 1996a, Phys. Rev. Lett. **77**, 3224.
Ye, Jinwu, 1996b, submitted to Phys. Rev. B (cond-mat/9609058)
Ye, Jinwu, 1996c, preprint (cond-mat/9612029).
Ye, Jinwu, 1996d, preprint (cond-mat/9609057).
Ye, Jinwu, 1996e, preprint (cond-mat/9609076).
Yoshimori, A., 1976, Prog. Th. Phys. **55**, 67.
Yosida, K., and A. Yoshimori, 1973, in *Magnetism*, ed. H.Suhl (Academic, New York), Vol. V., p. 253.
Yu, C.C., and P.W. Anderson, 1984, Phys. Rev. B**29**, 6165.
Yu, C.C., and A. V. Granato, 1985, Phys. Rev. B**32**, 4793.
Yu, C.C., and A.J. Leggett, 1989, Comm. Cond. Mat. Phys. **14**, 231.
Yuval, G. and P.W. Anderson, 1970, Phys. Rev. B**1**, 1522.
Zachar, O., S.A. Kivelson, and V.J. Emery, 1996, Phys. Rev. Lett. **77**, 1342.
Zaránd , G.,1993, Sol. St. Communications **86**, 413.
Zaránd , G., 1995, Phys. Rev. B**51**, 273.
Zaránd , G., 1996, Phys. Rev. Lett. **77**, 3609.
Zaránd , G., and L. Udvardi, 1996a, Physica B **218**, 68.
Zaránd , G., and L. Udvardi, 1996b, preprint (cond-mat/9605063).
Zaránd , G., and K. Vladár , 1996, Phys. Rev. Lett. **76**, 2133.
Zaránd , G., and A. Zawadowski , 1994a, Phys. Rev. Lett. **72**, 542.
Zaránd , G., and A. Zawadowski , 1994b, Phys. Rev. B**50**, 392.
Zaránd , G., and A. Zawadowski , 1995, Physica B **218**, 60.
Zaránd , G., J. van Delft, and A. Zawadowski , 1997, preprint (submitted to Phys. Rev. Lett. [Comm.]).
Zimányi , G.T., K. Vladár , and A. Zawadowski , 1987, Phys. Rev. B**36**, 3186.
Zawadowski , A., 1970 (unpublished).

Zawadowski , A., 1974, *Collective Properties of Physical Systems, Nobel Symposium 24*, (Academic Press, New York), p. 76.
Zawadowski , A., 1980, Phys. Rev. Lett. **45**, 211.
Zawadowski , A. and K. Vladár , 1980, Sol. St. Comm. **35**, 217.
Zawadowski , A. , 1987, Phys. Rev. Lett. **59**, 469.
Zawadowski , A., 1989(a), Phys. Rev. B**39**, 4682.
Zawadowski , A., 1989(b), Sol. St. Comm. **70**, 439.
Zawadowski , A., 1989(c), Phys. Scr. T**27**, 66.
Zawadowski , A. and M. Fowler, 1970, in *Proc. 12th International Conf. on Low Temp. Phys.*, (Science Council of Japan), p. 324.
Zawadowski , A. and P. Fazekas, 1970, J. Appl. Phys. **41**, 1155.
Zawadowski, A., K. Penc, and G.T. Zimányi , 1991, Prog. Th. Phys. Supp. **106**, 11.
Zawadowski, A. and K. Vladár , 1992, in "Quantum Tunneling in Condensed Media," eds. Yu. Kagan and A.J. Leggett (Elsevier, Amsterdam), p. 427.
Zawadowski , A., and G. Zimányi , 1985, Phys. Rev. B**32**, 1373.
Zawadowski , A., G. Zaránd , P. Nozières , K. Vladár , and G. Zimányi , 1997, preprint.
Zimmerman, N.M., B. Golding, and W.H. Haemmerle, 1992, Phys. Rev. Lett. **67**, 1322.
Zhang, F.C. and T.K. Lee, 1983, Phys. Rev. B**28**, 33.
Zhang, F.C. and T.K. Lee, 1984, Phys. Rev. B**30**, 1556.
Zhang, G., A.C. Hewson, and R. Bulla, 1997, preprint (cond-mat/9705199).
Zhang, S. and P.M. Levy, 1989, Phys. Rev. Lett. **62**, 78.
Zhang, S.C., 1990, Phys. Rev. Lett. **65**, 120.
Zhang, X.Y., 1994, Physica B**199&200**, 445.